Title

The Cellular and Developmental Biology of Wing Scales: Two Genera of Structurally-Colored Butterflies Provide Mechanisms for Evolution of Color Diversity

Author

Null, Ryan W

Publication Date

2017

Peer reviewed|Thesis/dissertation

The Cellular and Developmental Biology of Wing Scales: Two Genera of Structurally-Colored Butterflies Provide Mechanisms for Evolution of Color Diversity

By

Ryan W Null

A dissertation submitted in partial satisfaction of the

requirements for the degree of

Doctor of Philosophy

in

Molecular and Cell Biology

in the

Graduate Division

of the

University of California, Berkeley

Committee in charge:

Professor Nipam H Patel, Chair
Professor David G Drubin
Professor Daniel S Rokhsar
Professor Rosemary G Gillespie

Spring 2017

Abstract

The Cellular and Developmental Biology of Wing Scales: Two Genera of Structurally-Colored Butterflies Provide Mechanisms for Evolution of Color Diversity

By

Ryan W Null

Doctor of Philosophy in Molecular and Cell Biology

University of California, Berkeley

Professor Nipam H Patel, Chair

The coloration of butterflies and moths, Lepidoptera, has been an important force in biological inquiry, providing among the first supporting evidence for biogeography, Darwinian evolution, and models of morphogen diffusion. In nature, color patterns have evolved that aid species' navigation of many ecological interactions via crypsis, warning coloration, mate signaling, and the multiple forms of mimicry, which often lean heavily upon color to achieve their effect.

Butterflies and moths as a whole have evolved the ability to produce all of the colors visible by humans, as well as into the UV range. As is true for most animals, the repertoire of pigments available for use in Lepidoptera is actually rather restricted – by and large limited to long-wavelength colors red, orange, and yellow, as well as, black and brown pigments. To expand into the short wavelength (violet, blue and green), Leps have repeatedly resorted to manufacturing photonically-active nanostructures. These harness physical properties of light to create the impression of color in an observer without having to manufacture a pigment. Despite knowledge of butterfly structural coloration for centuries, intense study has only taken off following the advent of the electron microscope, and despite interest, studies have been largely limited to descriptive studies and physical estimations of their function.

I have undertaken efforts to understand the developmental and cellular underpinnings of structural coloration in butterflies. In the work presented here I have furthered the understanding of the field with a particular focus on how pigments modulate the diverse structural colors of 2 genera – the *Morpho* genus of the neotropics and the *Achillides* sub-genus of *Papilio* found throughout Oceania, East, and South Asia. In addition, I have addressed how scale ultrastructure is constructed in the developing pupa from a cell biological perspective. These studies have come hand-in-hand with the improvement of live-imaging techniques, which I argue, will be indispensable for future studies on scale development. What has emerged, is the suggestion that the Actin cytoskeleton, is essential for ultrastructural formation of scales including the modulation of nanostructure profiles. What's more, I have shown that melanin is deployed to tune the saturation of structural color reflections and, in at least one case, to tune the hue of a multilayer-based structural color.

Graphical Abstract

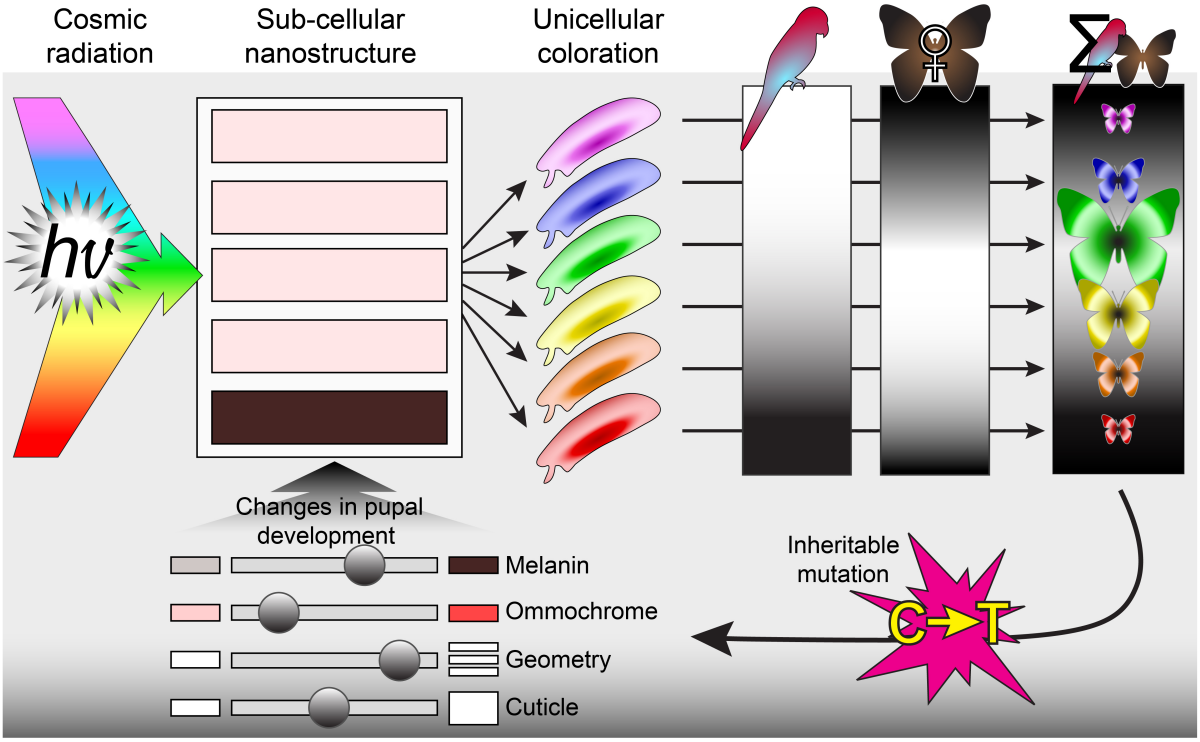

Spectral filters comprised of nanostructures and pigments are built during scale morphogenesis and influence the color production of unicellular epithelial projections known as scales. A variety of colors are theoretically possible by altering the pigment, geometry, and composition of spectral filters, but owing to the importance of coloration at the population and community level (such as evading predation and attraction of mates) the genetic programs involved in their construction are likely pruned by selection and drift, leading to biases in structural color prevalence. Through inherited mutations, new alleles in genes controlling pigments and nanostructure construction (such as number and thickness of nanostructure layers) will be born, allowing for further refinement and tuning of colors. Over time, changes in predation and mate preference, as well as other environmental shifts and random drift are likely to occur, altering the parameters by which nanostructures are evaluated, and allowing for novel colors to evolve. Thus, photonic interference filters, born during pupal development, encoded by a multitude of factors, can be selected upon at the population and community level leading to novel colors, and eventually populations and species. **Cosmic radiation –** The spectrum of light visible in a particular niche. **Sub-cellular nanostructure –** a hypothetical multilayer nanostructure built within a scale cell that produces color based on its geometry, chitin composition/thickness, and various pigments. **Unicellular coloration –** The diversity of possible scale colors at the individual and population levels if variation of nanostructure and pigmentation is allowed. The pattern produced by many scales on a wing creates the overall appearance of a butterfly. **Bird symbol –** Hypothetical pressure from predation on a particular color of butterfly due to its particular nanostructure/pigment combination; gradient indicates increasing detriment of a color on survival of a butterfly with that color. **Brown female butterfly symbol –** Hypothetical mate-preference pressure based for males of a particular color due to that organisms' particular scale coloration (owed to nanostructure and pigment combination); within the gradient, white represents a highly preferred color, black is highly ignored. **Sigma –** Combined pressures on a butterfly to be a color not conspicuous to a predator and preferred by a mate. Colored butterflies' sizes represent the prevalence of a color morph given the combined community-level pressures. **Inherited mutations** –Germline mutations inherited by the subsequent generation produce novel alleles that influence the "position" of phenotypic "sliders" influencing the developmental and cytological parameters of a scale's nanostructure and pigmentation. These lead to novel colors being produced in the scales of the next generation.

Table of Contents

List of Figures

Chapter 1: Introduction

Chapter 2: Melanization is Necessary for High Saturation of Structural Blue in Morpho Butterflies

Chapter 3: Modulation of the Actin Cytoskeleton and Pigmentation as Sources of Evolutionary Diversity in the *Papilio* Sub-Genus *Achillides*

Introduction to the Work

In this dissertation I will present the findings of my doctoral research on the developmental and cellular biology of structural coloration in butterflies. What follows are five main chapters, beginning with an introduction summarizing the current state of the field and ending with a look forward to the future of the field. These chapters bookend 3 chapters of my original work. In addition, the reader will find 4 appendices with supporting information for the main text, including data from 2 surveys (Appendices 1 & 2), genetic information for constructs built and a cloned gene (Appendix 3), and finally the code (and an explanation of) software developed for image analysis (Appendix 4). I hope the reader finds some excitement within these data, as they were breathtaking to discover.

Here now is a summary of each chapter:

Chapter 1: I present the reader with a summary of the current state of research. Given the very broad reach between nearly-instantaneous photonic behavior and the geologically time-scales of ecological population divergence, I've touched upon the extremes briefly while trying to focus upon how unicellular development may unite the two.

Chapter 2: In the second chapter I argue that the *Morpho* genus has diversified over time in part or as a consequence of utilizing melanin to increase the saturation of their blue coloration. Further, I suggest that the change in melanin type and/or level is involved in the differences between and within naturally occurring species. I have harnessed a live imaging technique developed in the 1980's to culture pupal wings *ex vivo* to visualize *Morpho peleides* pupal wing disks prior to pigmentation. In so doing, I have been able to modulate specific steps in the melanin enzymatic pathway, inhibiting and rescuing the production of black pigments and, simultaneously, the level of blue saturation. Through *in vivo* injection of drugs preventing or promoting melanization I have been able to see deviations from the wild type blue saturation in the predicted manner. Together these data are compared to a survey of pigmentation and structural saturation in existing Morphos representing between species variation, within species variation, and within individual variation of blue saturation. I conclude that pigments may, in fact, literally underpin the change in apparent blue coloration across this genus.

Chapter 3: In the third chapter, I investigate the formation of a nanostructure and its pigmentation in a species of *Achillides* butterfly, *Papilio palinurus*. Development of nanostructures are hard to study as they are smaller than the diffraction limit of light microscopes, requiring study via electron microscopy. *Achillides* species use internal multilayers to produce structural color, which are beyond the diffraction limit, however, some species also mold their multilayer into a 3-dimensional shape that harnesses structural coloration's angle dependence to produce multiple reflected colors. This 3-dimensionality in *P. palinurus* looks like a parabolic reflector, which I affectionately refer to as a dimple. The results of a survey of the close relatives of *P. palinurus* demonstrated that not all species have this dimple ultrastructure and that the shape of

the multilayer falls out along the suggested clades within the *Achillides*. In earlier work, scale ultrastructure has been suggested to be defined in large part by F-actin dynamics. When I investigated two species of *Achillides* pupae (*P. palinurus* and *P. ulysses)* I found this was also true. Interestingly, *P. palinurus* cover scales appeared to undergo a dramatic rearrangement from longitudinally arranged F-actin to a hexagonally packed actin structure along the scale's upper lamina. These hexagons of F-actin delimited local invaginations of the plasma membrane in roughly parabolic shape. It appears that *P. ulysses* begins with a similar hexagonal shape that gets contracted across its width to narrow the hexagons into boxes that also resemble the adult structure. Though drug treatments to disrupt actin were inconclusive, I did find several animals with red-shifted coloration and disrupted dimple formation. At least one red-shifted animal also showed a change in internal multilayer order.

Also investigated in the third chapter was an anomalous, unilateral blue-shifted phenotype that appeared in adults emerging from injected pupae of *P. palinurus.* It did not matter what was injected, as multiple drug treatments and even control injections all gave a similar phenotype, so I attribute the blue shift to an injection trauma response. These blue-shifted damage phenotypes were often correlated with a decreased dark pigmentation. Investigation of pigmentation levels between damaged and wild type scales agreed with this observation. Knowing pigment can be removed in a pigment dependent manner I tried to bleach the wings (to remove melanin) and to extract, via acidified MeOH, ommochromes (known to be in Papilionid wings and to absorb blue wavelengths). Surprisingly the bleaching resulted in a red-shift while the ommochrome extraction led to a blue-shift. The ommochrome extraction method ended up creating damage to structural elements in a control, and the change in absorbance profile of MeOH-treated *palinurus* wings did not match perfectly the expected absorbance profile upon modeling, leaving the ommochrome contribution possible but inconclusive. Injection of melanin inhibitor into developing pupae resulted in blue shifted adults – a contradiction with the bleaching but in agreement with the damage reduction of pigment. Comparison of the bleached wing's absorbance to known pigments in *Drosophila* suggested that the pigment was a melanin that was damaged and unable to absorb red wavelengths – the likely source of red shift. The remaining blue shift of melanin reduction remained a mystery. Measurement of wild type internal multilayers from TEM micrographs showed that the multilayer was not comprised of uniform chitin and air layers, instead the multilayer was chirped (decreasing in size as one moved toward the adwing surface). Moreover, there was an increased electron density in these lower thinner laminae. When I compared this to damage induced blue scales and melanin inhibitor injected scales I saw similar layer thicknesses but a decrease in electron density. What I conclude from these experiments is that the melanin based pigment is limited to the thinnest layers providing saturation and eliminating their blue shifted contribution from the reflection. Prevention of melanin formation by damage or inhibition results in a decrease in saturation (as seen in the *Morphos*) but also unmasks the lower laminae allowing their reflection to be included in the color reflection. Comparison to wild type *P. blumei*, which has similar greens and blues, shows that there is also be a decrease in pigmentation in the blue scales of the tails. This suggests that a chirped multilayer may be conducive to the selective tuning of reflected coloration simply through pigmentation modulation – and this may be a mechanism, in coordination with

actin based alteration to the scale's ultrastructure, by which the *Achillides* have altered their coloration over their evolutionary history.

Chapter 4: In the fourth chapter, I report some of my efforts to live image scale development and argue that the Indian Meal Moth, *Plodia interpunctella,* may be an ideal species for undertaking investigations of scale development. *Plodia* is a Pyralid moth and a pest species. The latter point comes with the benefits of low maintenance, willingness to be reared in high densities, and high fecundity lacking in most butterfly species. The former point comes with the benefit that they feature beautiful scales and similar anatomy to butterflies. Though lacking in structural color, the mysteries of the nanostructure construction processes would benefit highly from working out general scale development, which is lacking. In addition to having scales, *Plodia* feature a frenulum, a hook that connects the fore and hindwings during flight, and this structure is composed of many independent bristles fused together by ECM. Together with its large size, the frenulum could be a great canary in the coalmine for scale defects when performing genetic manipulations/screens. Also in this chapter, I detail efforts to build genetically encoded live imaging constructs and to introduce them into developing cells. I combine this work with two techniques that eliminate the presence of the opaque pupal cuticle and allow visualization of the developing pupal wing disk and its scales. These technological advances will be highly beneficial for pushing further into our understanding of unicellular morphogenesis and scale development.

Chapter 5: In the final chapter, I describe what still needs to be done. There is a great bit of work still that can be informed by study in and comparison to *Drosophila.* In addition, I outline the experiments that still need to be done in the *Morphos* and *Achillides*, before resting on the exciting future of live imaging of scales *in vivo.*

Acknowledgements

The scope of this project is beyond the abilities of any single person's ability. I am indebted to a great number of individuals and institutions for their thoughts, comments, time, skills, and encouragement. This includes a number of high school and undergraduate students who volunteered their time on various projects including Anthony Gilbert, Hwei Ee Tan, Jerry Lo, Jessica Poon, Jose Breton-Arias, Julian Kimura, Alexis Krup, Lauren Matsuno, Lisa Chuong, Madhu Joshi, Maria Pizzano, Marylin Rowswell, Mia Salans, Mrinal Sinha, Yuriko Kishi, and Zach Null. My co-graduate students in the Patel lab, Aaron Pomerantz, Angela Kaczmarczyk, April Dinwiddie, Dennis Sun, Erin Jarvis, Heather Bruce, Jaap van Krugten, Kyle DeMarr, and Rachel Thayer. The gracious post docs who made themselves open and available for science discussions and more including Arnaud Martin, Chris Winchell, and Jacques Bothma. The labs who were generous in helping me further my investigations in particular Erin Brandt in Damien Elias' lab, Lewis Bartlett in Mike Boots' lab, Matthew Norstad in Hernan Garcia's lab, as well as the Daane and Mills labs, who allowed me to use their quarantine facility. In addition, I want to acknowledge Reena Zalpuri, Guangwei Min, and Kent McDonald at the EML, AJ Gubser, Naima Azgui, Frances Allen, and Paul Lin in the QB3 imaging facility, the DNA Sequencing Facility, and the fine folks in the Cell Culture Facility for their experience and access to their equipment. Significant progress was made during my time in Woods Hole, Massachusetts the summers of 2013-2015 thanks to the staff and faculty running the Embryology course including Matt Ronshaugen, Louie Kerr, Alejandro Sanchez-Alvarado, and Richard Behringer. Of course, I also owe a thank you to the students of the Embryology course, including the one closest to my heart, Duygu Ozpolat, for without whom I would not have developed into half the scientist or human I am today. The kind people and classmates of the 2015 QBio class at UCSB inspired a fascination with quantitative biology, physics, and how biology could be truly engineered. They were also the same people who saw me through a turning point in my life and I wish them the best in their lives and careers. I want to thank my friends, classmates, and sometimes commiserators, Andy Navarrete and Kevin Tsui for their support and camaraderie over the course of our time at Berkeley. To Al Moolick, who may have literally saved my life by introducing me to strength training, his was the class that I have learned the most from. I would like to thank my family for their love and support from the beginning of grad school through the hard parts and to the end. No acknowledgement would be complete without a tip of my hat to the GAO who bent over backwards to be helpful. My rotation mentors Nicole King and Craig Miller made the choice to join Nipam's lab a challenge. I want to thank the Cal Academy, Spine Films, and KQED's Deep Look for producing beautiful films based on our work. Lastly, I am grateful to my thesis committee David Drubin, Rosie Gillespie, and Dan Rokhsar for their helpful comments and guidance, which paled only in comparison to Nipam, from whom I learned about science, butterflies, development, and sports. His guidance has been indispensable; I have grown tremendously as a scientist and as a person with his help. Thank you all.

Chapter 1
Introduction and Background

1.1 Introduction

An organism's coloration is often directly tied to its survival and reproductive success. Lepidopterans, butterflies and moths, are among the most popular insect groups with the public. This is in no small part due to the diversity of glorious patterns and bright colors found on the nearly 200,000 species contained in the group. While much of the scientific study has focused on how color patterns are made, it is the scales (unicellular, epithelial cell projections), which are ultimately responsible for the colors displayed.

When executing a particular pattern, cells across the pupal wing tissue interpret developmental signals and deploy different pigmentation pathways accordingly. The juxtaposition of differently colored scales thus determines the pattern observed at the macroscopic level. With few exceptions, Lepidopteran pigments are only able to access red, orange, yellow, black, and brown regions of the color palette. To achieve the short-wavelength colors of the spectrum (such as violets, blues, and greens), many independent Lepidopteran lineages have evolved color production through the purely physical mechanism of photonic interference – or structural color. This phenomenon is made possible by, often elaborate, sub-cellular patterning of the scales' exoskeleton built with such extreme precision (on the order of 100nm) that it manipulates incident light, resulting in particular colors being intensified, while the rest are cancelled out. It is in this way that the majority of violets, blues, and greens are produced in butterflies and moths.

Developmentally, the ability to produce 100nm structures is complicated by both the number of scales per wing and the short duration of time most organisms stay in the pupa. For instance, *Morpho peleides*, a bright blue butterfly, has about 10,000 scales per square centimeter, with ~8cm^2 per wing being blue. Each blue *Morpho* scale has an average of 50 ridges where structural color is produced, and each ridge can have up to 6 lamellae contributing to coloration at any one location on a ridge. Thus the mindboggling reality comes into focus that each butterfly must make 100nm structures nearly 100 million times in order to appear blue! By analogy, if we arbitrarily adjust our size scale such that 100nm is equivalent to 100mm, a butterfly must build 320,000 cells the size of the TransAmerica Pyramid building (260um=260m) with the accuracy equivalent to a coffee cup (100nm=10cm) over an area 2x the size of the entire San Francisco peninsula (8cm^2/dorsal wing surface =800km^2 – or – ½ of one SF peninsula at 1600km^2) in the matter of a week and a half (Fig1.1)! If the organism's nanostructures deviate from very tight tolerances (±10nm), the reflected light will be biased to another color with likely effects on ecological interactions.

Examples from many structurally colored groups of butterflies suggest that while the nanostructures are faithfully inherited from generation to generation, they remain evolutionarily and developmentally labile, with closely related species often having different colors or saturation levels (Fig1.2). Taken together we reach a stunning

conclusion: that the evolution of morphogenesis of single cells at the nanoscopic level is responsible for changes in perceived color of an individual, which is in turn responsible for many of the complex interactions butterflies and moths have with predators and conspecifics. In other words, sub-micron morphogenetic processes in cells of an individual, resulting in novel photonic behavior, may directly drive evolution of populations at a geological timescale.

Here, I will briefly touch on patterning of the wing pattern before focusing on a few aspects of scale biology including what physicists have uncovered about structural coloration in Lepidoptera, the known developmental patterning of scales, and likely cell biological mechanisms leading to the requisite repeating nanoscale structures responsible for some of the most brilliant and vivid colors in nature.

1.2 Ecological importance of coloration

As organisms that have placed considerable weight on visual information for understanding our world, humans have paid attention to color occurring in the natural world. Given the diversity of organisms in the natural world and the long periods of time that life has had the opportunity to drift and adapt upon it, it should be unsurprising that life has woven color deeply into its complex interactions.

Individual organisms have to navigate through countless encounters on a daily basis within their ecosystem. From quorum sensing two-component systems in bacteria to the 5-sense human experience we are most familiar with, organisms have evolved to be efficient information integrating machines (1). Most bilaterian animals are born with or develop visual senses during their lifetime. While color vision is not ubiquitous, it is common and hence, often plays an important role in interpreting the world. From what we know there are 3 main pressures driving the majority of color-information in ecological interactions. 1) The avoidance of predation, 2) the need to eat, and 3) the drive to mate and reproduce.

Strategies have emerged among communities of species that result from each of these pressures. For instance, the avoidance of predation has selected for organisms with remarkable camouflage to hide from predators such as the *Kallima* genus of butterflies, leafy sea dragons, katydids, Membracid bugs, and stick insects. Camouflage can also be less elaborate drab coloration as is often seen on birds, small mammals, and moths (such as Kettlewell's melanic *Biston* moths) or the white coats of arctic hares.

Counterintuitively, organisms can also avoid predation by being brightly colored with highly contrasting colors. This coloration is often correlated with the organism being a potential prey item and having the ability to inflict illness or injury upon the potential predator. Known as aposematism or warning coloration, such color patterns make their wearer highly conspicuous, in essence advertising their ability to poison, bite, sting, or otherwise maim. Examples of aposematism include the bright black and yellow of yellow

jacket wasps, the beautiful coloration of poison dart frogs, the red, black, and yellow banding of coral snakes, and the orange and black of Monarchs.

Aposematism requires selective pressures from predators trying to eat dangerous individuals and learning not to attack a particular pattern through surviving highly unpleasant interactions. This learning paradigm can create pressures that drive evolution among other dangerous organisms to convergent color patterns, known as Mullerian mimicry, best known from the *Heliconius* species. In the *Heliconius* mimicry rings, multiple butterfly species in geologically close quarters share predators that drive selection in all species toward a single phenotype (2–4). This is thought to benefit the predator as it only has to learn a single pattern, while the individual butterfly species can share the burdens of predator learning trials.

In some cases aposematic coloration of a dangerous species can result in collateral selection upon otherwise harmless species with no noxious defense. This selection likewise leads to a convergent color pattern that “lies” to predators about the danger of eating a harmless organism (5). Known as Batesian mimicry, this type of color signaling is famous among the corn snake mimics of coral snakes, bee-mimicking robber flies, the snake-mimicking caterpillars of some *Papilio* species, and Bates’ own Ithomiine-mimicking *Dismorphia* butterflies.

Of course, some of the same tricks some species use to avoid predation have been employed by predators themselves to hide from their prey. Particularly cryptic patterns that are common among ambush predators which can be as simple as the dorsal grey and ventral white of Great White sharks, and as elaborate as cuticle reticulations and color variegation of the Indian Rose mantis, Ambush bugs of the Phymatidae family, and the carnivorous *Eupithecia* caterpillars of Hawaii (6).

Beyond the need to eat or keep from being eaten, color plays important roles in mediating the interactions between conspecifics. Sexual dimorphism accounts for some of nature’s most spectacular color patterns, such as the difference between the sexes of the Bluefin Nothos (*Nothobranchius rachovii*) fish, mandarin ducks, and *Ornithoptera* butterflies (Fig1.2). According to the so called “good genes” hypothesis, sexual dimorphism arises from a pressure put on males by females choosing more extreme phenotypes, which often makes males more conspicuous than the female, and as a result increases their likelihood of being predated upon or making it more challenging to survive otherwise. Thus, males surviving to adulthood must carry high quality gene complements, which when mated with will benefit the female’s offspring.

Given the complex nature of community relationships, it is not surprising that color patterns can be flexible to accommodate situations. Polyphenisms can provide seasonal variation to meet the needs of an organism across temporally differing environmental contexts. Many male birds for instance will molt into sexual color feather colors during the breeding season while being drab otherwise. Peacocks, as an example, drop their tail feathers after breeding season. While butterflies cannot change their coloration within an

individual, generations eclosing during different seasons can have seasonal coloration variation. One such example is *Junonia coenia*, which has redder ventral coloring during the wet season generation and tan ventral color during the summer generation when brush is dry and dead (7,8).

In an extreme example of combinatorial color pattern paradigms, some butterflies have sex-limited Batesian mimicry where the female will mimic an unpalatable model and the male will not – such as *Papilio dardanus* and *Papilio polytes*. In this twist on sexual selection, males must bare waving a palatable flag while the female hides, not in drab colors, but in faux-warning coloration (9–13).

Finally, while it is easy to dive headlong into the adaptive values of color and power of selection, it would be a disservice to the reader not to acknowledge that biological color may simply be the result of contingency, drift, or the adaptation of a system for one purpose that subsequently produced color indirectly. For example, the differences in the color of green algae and plants, brown algae, and red algae represent different mechanisms of performing the same function: absorbing light energy for conversion to chemical energy (14,15). Carotenoids and bacteriochlorophylls provide a purple hue to some bacteria, but only as a consequence of utilizing longer wavelength light to pump protons across the membrane for assisting in electron transfer chain (16). Examples exist too of more exotic structural colors that have no obvious adaptive function such as the rainbow reflections of ctenophore ciliary combs, where color is the consequence of light diffracting from the close-packed cilia constituting the swimming combs.

In sum, coloration has likely been evolved by a handful of pressures into some of the most dumbfounding visual stimuli in nature. Crypsis, aposematism, mimicry, sexual dimorphism, and polyphenisms have emerged as ways of aiding survival and reproduction in animals. So, in studying further how animals manifest their coloration, we stand to learn more about evolution and the diversification of life itself.

1.2.1 Wing patterns drive species diversity

There is little doubt that the seemingly endless wing patterns displayed by the many lineages within Lepidoptera, moths and butterflies, has been a key to their popularity among the public, collectors, and scientists alike. Indeed, even after spending decades in extremely biodiverse tropical locations naturalists like Alfred Russell Wallace seemed resistant to becoming jaded to their beauty: Wallace remarked upon first capturing the spectacularly fire-orange birdwing, *Ornithoptera croesus,*

> *On taking it out of my net and opening the glorious wings, my heart began to beat violently, the blood rushed to my head, and I felt much more like fainting than I have done when in apprehension of immediate death* (17)*.*

Moths and butterflies (also affectionately known as Leps), together are a monophyletic group with nearly 200,000 described species, increasing at a rate of about 1,000 per year.

Kristensen et al. suggest that there may be as many as 24 synapomorphies for the Lepidopteran lineage with the eponymous “densely scaled wings” included as one (18). Butterflies (Rhopalocera) are a monophyletic group of day-flying moths with clubbed antennae comprised of 6 families (Hesperiidae, Papilionidae, Pieridae, Nymphalidae, Lycaenidae, and Riodinidae) with close to 20,000 described species.

Lepidoptera is sister to the hairy-winged Trichoptera, which together form a clade that is sister to the Diptera (in which *Drosophila melanogaster* resides). Unlike Dipterans that have 1 pair of wings covered in small, hair-like projections, both Lepidoptera and Trichoptera have 2 pairs of wings that are covered in large, chitinized remnants of sensory organ precursor (SOP) derived cells (18–20).

As holometabolous insects, the Lepidoptera are indirect developers with egg, larval, pupal, and adult life stages. Similar to *Drosophila melanogaster*, Lep larvae have internal imaginal discs that will become the adult wings following a dramatic maturation during the pupal stage. It is during the metamorphic pupal stage when the wings’ color patterns are largely established through the specification, construction and, often, pigmentation of large, unicellular epithelial outgrowths known as scale cells. Following eclosion of the adult from the pupa, the soft, wet wings expand to their full size via hydraulic pressure applied by the hemolymph (much like expanding sails on a boat) and harden to their final shape in a few hours. Once formed, scales and wings are both considered dead tissues which cannot be repatterned, nor regenerated.

Wing patterns are akin to a tile mosaic, and each butterfly manifests their particular pattern by juxtaposing many independently colored scales on a 2 dimensional matrix as such, the pattern of the wing is effectively a color matrix like that of a tiff image. While there are species where the patterns exhibited by an individual are somewhat random (the black stripes of the sunset moth, *Chrysiridia rhipheus,* for instance), by and large patterns are remarkably similar between individuals and generations. Complexity, therefore, should not be mistaken for randomness, as is perhaps best observed in the wings of the *Brahmaea* moth genus, which display remarkable complexity that is highly ordered and exhibits perfect symmetry across left and right wings. Moreover, between individuals of the same species, patterns stretch and shrink with the variation in wing size, suggesting that even though tightly regulated, the pattern “knows” how to form itself and can be dynamically adapted to the size of its canvas. Taking this fidelity to even more impressive heights, it is common for species to display polymorphic or polyphenic patterns, often associated with mimicry or seasonal variation. These additional patterns remain faithful to their own pattern and evidence has been collected that suggests that these alternate patterns can be caused by alleles at a single locus (13,21,22).

Together, the fidelity to a pattern seen between individuals and generations suggests control of patterns by inheritable genetic influences. Conversely, the existence of polymorphisms, polyphenisms, and even the great diversity of patterns that exist throughout all Lepidopteran lineages suggest that patterns are mutable. Through several

continuing lines of research, that this is in fact a reality. Briefly summarized, the emerging concepts of genetic control of wing patterns are:

1) **Low-level control of pattern elements occurs via redeployed developmental pathways**
   Work on the eyespot of several Nymphalid butterfly species has shown a correlation between the pigmentation of the concentric elements in an eyespot and pupal expression of developmental genes such as *distal-less, spalt,* and *engrailed* in identical patterns prior to pigmentation (23). Ectopic eyespots can be induced by wing damage or transplantation of eyespot foci early in pupation, these are hypothesized to be *wnt* based damage responses functioning secondarily as a pattern organizer (24–26)*. wntA* and *optix* have been implicated for controlling many color patterns as well, with *wntA* in particular seemingly important for defining pattern boundaries within the wing (27–29). These patterning signals may be combinatorial in some instances, as evidenced by the additive bar patterns shown by lab-hybridization of *Heliconius cydno* and *H. melpomene* that phenocopied the double bar pattern of *H. heurippa* (30).

2) **Polymorphism is driven by large-effect alleles expressed in large domains**
   Studies done on *Papilio dardanus* and *Papilio polytes*, which feature females that mimic multiple distasteful models, have demonstrated that alleles of *engrailed/invected* and *sex lethal,* respectively, are master control genes deciding what pattern any particular female will display (24–26). Similarly, alleles of the gene *cortex* determine patterns within multiple *Heliconius* species, *Bicyclus anynana, Biston betullaria,* and *Bombyx mori* (31,32). The exact mechanism by which alleles of these genes produce different patterns is unclear, whether they change the interpretation of patterning signals common to all morphs, or if they completely change the signals produced between morphs.

What is clear from the literature is that developmental genes are redeployed in patterning wings, and that some genes like *engrailed* may have many roles at both high and low-level specification. Secondly, with the exception of *cortex,* which has an unclear function in Lepidoptera, all of the genes implicated in pattern formation are components of signaling pathways or are transcription factors. Perhaps this is unsurprising, given that the ultimate effect is a change in the juxtaposition of differentially colored scales.

1.2.2 Scale color determination drives wing pattern diversity

In the adult, scales are the dead, chitinous remnant of a large, unicellular wing epithelial projection, which are born, specialized, and die all within the pupal stage. The decision of neighboring scales to produce any given color is what defines the color pattern, and as

such, it is the response of the developing scale cell to the various patterning inputs produced by the wing that will manifest the pattern. How a scale enacts a program to produce a color can ultimately be as simple as turning on an enzymatic pathway to produce a pigment, or as complex as to require precise tuning of cytological elements during scale morphogenesis so as to create an optically-active nanostructure. The latter method leads to wavelength specific enhancement through photonic manipulation. While pigments and structural colors are often thought of as mutually exclusive, hints that the some genes deciding scale pigmentation may also influence the cuticular super-structure came from Larry Gilbert et al. in 1988 – in addition to suggesting that structure may modify the appearance of a pigmented scale type (33).

Just as wing patterns themselves are inherited and mutable, evidence suggests that scale morphologies may also be inherited and mutable. Studies on *Ornithoptera* structural coloration have suggested that both structures and pigments have evolved between species to produce the range of colors displayed by males (Fig1.2) (34,35). Helen Ghiradella proposed that gyroid structures evolved from internal lamina of the Urania-type, speculating an evolutionary role for the smooth endoplasmic reticulum in the transition (36). Comparisons of Cattleheart structural scales suggested a similar but parallel evolutionary transition in Papilionids (37,38). Changes in scale profile and multilayer thickness have been noted between closely related species *Papilio ulysses, blumei, peranthus, and palinurus,* which are also associated with gross color changes and retroreflection production (39–41). Scale morphology was also recently utilized in resolving the phylogenetic relationships of the species within the *Morpho* genus, suggesting that scale morphology mutability has some relationship to speciation (42).

1.3 Sources of biologically derived color

It is necessary to stress the functional difference of pigments and nanostructures as well as their ontogenetic origins to understand how they can be modified over the course of evolution. To explain how pigments and nanostructures differ it is first important to discuss what color actually is from a physical perspective.

1.3.1 Light and color

Light is a form of electromagnetic radiation, having properties that are both wave-like and particular in nature. A light particle is known as a photon. Photons are discrete packets of energy with characteristically oscillating electric and magnetic fields. The amount of energy a photon carries determines how quickly its electric and magnetic fields oscillate, which in turn define its wavelength. Since all photons in a vacuum travel at the same speed, the speed of light, their wavelength is a function of how energetic the photon is. The higher a photon's energy, the faster the oscillation, the shorter its wavelength, and – if within the visible spectrum of the organism observing it – the more violet the light appears. Conversely, the lower the energy, the slower the oscillation, the longer the wavelength, and the more red the light appears. Furthermore, these linguistic color categories (e.g. Blue, Red, Green) are at their most fundamental, simply differences in

how fast a photon's electric and magnetic fields oscillate. A particular "blue" photon, for instance, will oscillate once every 450nm traveled, whereas a particular "red" photon oscillates slower, at once every 700nm. These oscillation distances are critical for our understanding of the physics of a butterfly's structural color.

1.3.2 Pigmentary versus structural color

A pigment is a molecule whose particular arrangement of atomic bonds define how it can absorb energy. When a light source containing an even mixture of all wavelengths (white light) is directed upon a pigment, the photons interact with the pigment molecules causing resonation of atomic bonds and resulting in some or all of their energy being absorbed. Those photons that cannot be absorbed are either reflected or reradiated at a longer wavelength (fluorescence). The characteristic profile of absorbance of a molecule provides the color for the object containing it; for instance, chlorophylls A and B are poor at absorbing green and hence a plant appears green.

In contrast, non-white structural color results from the interaction of white light with an object which has 2 characteristics: 1) the object must be made of a material with a refractive index that is different from the ambient medium (the speed of light changes when entering/exiting the material) and 2) must have a geometry that is non-random in some way (although this is not always obvious). Everyday examples include the rainbows produced by oil films on water and in soap bubbles (known as thin-films) and the colors seen on the underside of a CD (caused by a diffraction grating). In most biogenic cases, structural color is produced by repeating structures with dimensions and spacing on the order of 100nm. Simply put, a pigment is a molecule that absorbs light, leaving what the remainder as the color we see. While structural colors in biology, tend to be regularly ordered, super-molecular sized reflectors that bias reflections towards a wavelength without absorption.

Structural colors have evolved many times within the Lepidopteran lineage, and exist in all bilaterian superphyla, including Humans where blue and green irises arise from structural coloration as do some skin patches such as blue nevi and portwine birthmarks (43–45). Structural colors may have arisen in animals to compensate for the rarity of violet, blue, and green pigment evolution. Thus their evolution allows for the access of more of the visible spectrum – something that has been applied to camouflage, signaling, aposematism, and mimicry among the butterflies (46–53). Interestingly, there exist a few common ultrastructural elaborations allowing scales to create structural colors, often evolving *de novo* in independent lineages (37,40,46,54–56).

The physics of how structural color works has been a topic of discussion that dates back to the birth of optics. Newton's famous prism experiments, reported in his 1704 tome "Opticks", showed that colors existed within white light and could be separated at interfaces of materials with different properties and postulated structural color as the source of peacock colors. It was about 200 years later that the idea of a physical separation of colors could be the cause of colors found in the biosphere, Lord Rayleigh

offering a hypothesis about birds, insects, and bivalves (57–59). In the first decade of the 20th century, C.W. Mason expounded on this hypothesis while providing an entertaining account of structural colors in insects and birds, complete with withering dismissals of his contemporaries' hypotheses and very clever experiments of his own, which are still the investigative tools all physicists use when studying structural color by today (60–64). Since the invention of the electron microscope, there have been a flurry of investigations that began to pick up steam in the 1970's, exploding during the 1990's continuing to expand today. With the 300 year history of experimentation with the properties of light, it should not be surprising that there exists an immense optics literature.

1.3.3 Pigment and structural color

In addition to exploring how structural colors in nature work, the diversity of structures, and how best to recreate nanostructures for industrial processes, many authors have remarked or noticed the close relationship photonic element containing cells have with pigments.

Purple for instance, is a non-spectral color, that is, it is a mixture of wavelengths that approximates violet (a spectral color). In nature purples are often created by overlaying red pigments with blue structures (65). Similarly, some greens are produced by an organism juxtaposing a yellow pigment over a blue structure, as in the case of the Budgerigar parrots, where blue-green structural color lies over a strongly blue-absorbing yellow pigment. This results in the subtraction of much of the blue from the blue green reflectance leaving the green portion of the reflectance intact (66).

In most explored cases, it is a dark, broadly absorbing pigment that is found associated with a photonic element; often this pigment is assumed to be melanin, but rarely are there rigorous tests of the fact (34,38,46,51,65–83). Theoretically, a black pigment absorbs uniformly across the visible spectrum. When paired with a nanostructure (which can only bias the reflectance toward a wavelength), the pigment uniformly removes across the spectrum. The bias provided by the structure creates a signal which cannot be removed by the pigment entirely, though the vast majority of other stray photons are. As a result, the peak wavelength reflected by the nanostructure is all that remains (Fig2.1).

In stark contrast, structurally assisted absorption also has been demonstrated to exist. In the example published (84) a velvety black portion of *Papilio ulysses* was examined in comparison with a less black region on the same wing. In air, the velvet black scales were demonstrated to be more absorbing than the lustrous black scales. However, when the scales were submerged in refractive index matching liquid the velvet black scales were actually less absorbing than the lustrous black suggesting that in fact the velvet black scales contained *less* pigment than the lustrous scales. Further it suggested that the enhancing effect on absorption was provided by the scale's morphology. Upon examination of the scale super-structure it was found that the scale had been produced in such a way as to channel the light to the inside of the scale where black pigment could absorb it. In addition, the structure promotes light's reflection toward the ridges on initial

incidence. The ridges have small grooves which in this case are thought to act like the corneal anti-reflection arrays on many insect eyes. The grooves reduce the reflectivity of the ridge by having created an alternating amplitude, which is a less efficient reflector. By forcing multiple reflections and reducing reflection efficiency, the light has to travel through more pigment and has greater opportunity to be absorbed. It is unknown if this improves the heat absorption of the tropically distributed *P. ulysses.* However, it is not hard to imagine that this mechanism could be utilized by melanistic forms of butterflies found in temperate climes.

The field of biological structural color has focused mostly upon the most colorful of organisms currently found on earth – the birds and the Lepidoptera (moths and butterflies). As a result, the reported structures may represent a biased section of how life has managed to explore structural coloration. Nevertheless, it should be noted that the many of the following structures have evolved independently in disparate lineages of life, suggesting that even if ascertainment biases prevail, there is some universality that exists in those structures that are known. I will address some of these nanostructures from a morphological standpoint accepting the physical mechanism of color production as a given. For a more in depth discussion, I refer the reader to several excellent reviews of biogenic structural color including Shuichi Kinoshita's extremely thorough book which tabulates all known studies of structural color in Lepidoptera and birds up to its publication (85).

1.4 Common themes where biology harnesses physics

In order for structural color to be manifested in an organism, that organism must obey the laws of physics that allow the color to be made. As such, an exploration of the themes common to all described versions of structural color, will lead to a fruitful discussion of how to approach the fascinating problems inherent in biological structural color.

In most structural color found in nature, constructive and destructive interference are utilized to bias the reflection of white light into appearing a color. One effective way to do this is to organize disorganized photons so that reflections of some photons have their wavelengths in phase with other photons of the same wavelength (constructive interference) and the rest of the photons of different wavelengths fall out of phase. This type of organization is dictated by 2 main components, the geometry of a nanostructure (most often, its thickness), and a contrast in how slowly light travels through the medium (its refractive index) of the nanostructure (typically chitin or keratin) when compared with the speed of light in its ambient material (usually air or water).

1.4.1 Contrast in refractive indices

All structural color heretofore described in biology is dependent upon diffraction. Diffraction of light within a medium is described by Snell's law as the ratio of the angle of a beam of light in two media is equal to the inverse of the ratio of the speed that light travels in those media:

$$\frac{\sin\theta_{medium}}{\sin\theta_{incident}} = \frac{N_{incident}}{N_{medium}}$$

In the simplest case, a thin film reflector, this bend in the direction of light ($\sin\theta_{medium}$) directs light to take a new direction within the medium. Once light reaches the lower boundary of the thin film and the ambient, it is partially reflected. When the light reaches the upper interface of the thin film and the ambient, it bends back according to Snell's law (Fig1.3A). Here it can interact with the reflection of the incident light and will have traveled a longer distance than the reflection (Fig1.3B) equal to

$$Path\ length\ difference = thickness_{medium} * 2N_{medium}\cos\theta_{medium}$$

Using Snell's Law, this can be rearranged into terms of the angle of incidence and refractive index contrast:

$$PLD = 2 * thickness_{medium} * N_{medium}\cos(\sin^{-1}(\sin\theta_{incident} * \frac{N_{ambient}}{N_{medium}})$$

For incident white light (light including all wavelengths), whatever photons have a wavelength equal to an integer multiple, m, of this path length difference will experience complete interference. Those photons that are non-integer multiples of the path length difference will experience partial interference.

We can predict what wavelengths will experience completely constructive interference by the following equation:

$$\lambda_{enhanced} = PLD/(m - \frac{1}{2})$$

The subtraction of ½ accounts for a phase shift that occurs in reflected photons traveling from a medium of a low refractive index to a high refractive index – in other words, at the time of entering the film (Fig1.3C).

Similarly, we can predict what wavelengths will experience completely destructive interference by the following equation:

$$\lambda_{destroyed} = PLD/m$$

Importantly, it becomes obvious that refractive index contrast is a necessary aspect of structural color production. This means simply that light changes speed as it enters and exits a medium such as chitin. If light doesn't change speed as it passes from one medium to another, it will not change direction nor will light reflect off the interface of the ambient and structural media. Without a change in reflection and direction structural color will not be made. This fact is still a preferred method of demonstrating a color is structural in nature since Mason suggested it in 1923 (60). Mason suggested that by immersing an object of interest in a liquid with a refractive index matching the refractive index of the object's material, say chitin. If the object makes color in a structural manner the liquid will eliminate the refractive index contrast, and subsequently the reflection and refraction of the light abolishing the color. If on the other hand the object is colored by a pigment, the

submergence in refractive index matching oil will make no difference to the color as the pigment uses absorptive properties of its chemical bonds to create color.

The contrast of refractive indices is ultimately dictated by the nanostructure's composition (chitin, keratin, cellulose, etc.) and that of the medium surrounding the nanostructure – air or hemolymph for butterflies, air for birds, water for aquatic species, cytosol for iridocytes of fish, squid, spiders, or reptiles.

1.4.2 Geometry of a nanostructure

The geometry of a nanostructure is also highlighted in the thin film case. Critical to understanding the path length difference was knowing how far apart the upper and lower interface of the thin film were (Fig1.3B). Only in this way could we calculate the distance traveled within the film. Further, Snell's Law tells us that the direction a photon will travel within the medium is dictated in part by the angle the photon is traveling with respect to the surface of the thin film when it enters it. In terms of butterflies, a thin film often makes up the lower face of a scale (Figs1.4, 2.3, 2.4, 2.10, 2.11, and 4.20).

If a person watches a butterfly with structural color as it flaps its wings, one will often see remarkable iridescence – a change in color – as the wings move. This is a direct consequence of Snell's law on the preferred wavelength constructively interfered as the incident light changes its angle relative to the photonic structures of the moving wing. An example of iridescence is given in Fig1.5, albeit the butterfly uses an internal multilayer, not a thin film to produce its color.

1.5 Classes of common biological nanostructures

While not all butterfly structures are thin films, the majority are related to elaborated versions of thin films and, hence, share physical characteristics with this simplest form. Briefly I will summarize the major classes of photonic nanostructures found in nature and provide an intuitive account of their function. The mathematics for the majority are understood and described, however understanding the mathematics is beyond the purview of this description.

1.5.1 Thin films

As just described, thin films are the simplest of all structural reflectors. We are familiar with thin-film-produced color from seeing the swirling rainbow reflected from oil on the surface of a puddle after a rain, or the hypnotic dancing of colors in a soap bubble on a summer day. As the name suggests, a thin film is just this, a single film of material that is only a few tenths of a micron thick. When the film is in a medium of lower refractive index, some of the white light reflects off of the film's surface, while some enters into the film, reflecting some more light off the back side of the layer before the remainder passes through. Upon reuniting on the outside of the bubble, the two reflections have traveled different distances through the bubble. In this moment the color is born. When the light entered the film, its electrical and magnetic oscillations were in step. But once the light splits up at the surface of the film that lock step is broken, and the light that travels into

the film emerges again after following a route with a length dependent upon the thickness of the film, the material properties of the film (most importantly the refractive index), and the angle at which the light approached the film from initially. There is nothing to prevent the two reflections from being in register again except the path they took within the film which forces some colors to fall in register with the first reflection's oscillations, and others to fall out of register with the first. This is simply an effect of the ratios created by different photons' wavelength relative to the length of the path taken through the thin film. When two photons' oscillation peaks and troughs fall into register, they act as if they are the sum of their individual amplitudes – thus appearing brighter – while the opposite occurs for those that are out of register – the two amplitudes negating each other and appearing dimmer. This is referred to as constructive interference or destructive interference respectively. One of the most critical distinctions between structural color and pigmentary color is thusly illustrated, for structural color no light is absorbed by the medium, instead the light is selectively made to appear dimmer or brighter through interference.

Though simple, thin films have been a surprisingly rare structure to find deployed in butterflies for coloration purposes. However, they are commonly found making the lower surfaces of scales hidden under pigments. A few butterflies have been described to use this mechanism for their primary coloration including the *Junonia* genus and some Morphos (see Chapter 2 and Fig4.19 and Fig4.20) (51,81,86,87). Outside of butterflies, the violet-green structural color of pigeons and doves is derived from a thin film that has a thickness sufficient to create two peaks ("m" in the equation above) that are violet and green (88,89).

1.5.2 Multilayers

Multilayers, also known as Bragg reflectors, are a play on the thin film that serves to improve reflection efficiency. As the name implies, a multilayer stacks several thin films such that the planes of the films are parallel (Fig1.4 inset). To get into the mechanics of a multilayer, it is important to bring into focus another property of any material through which light travels – the extinction coefficient. The extinction coefficient gives a sense of how well the material absorbs light that passes through it. In the present structural color literature, there are only rarely discussions or measurements of the extinction coefficient – however, it remains an important concept to understanding how color is produced. In biological structural color the extinction coefficient is often quite low within structured elements. This means that in the case of thin-films, much of the incident light will pass through the thin film into whatever lays behind the structure, and not reflected away from the animal. As a result, a single thin film is rather inefficient for producing color. Nature's solution has been the repeated evolution of multilayers (34,41,73,78,79,82,90–97). Each layer in a multilayer reflects a little bit more of the incident light that has passed through the layer above it, adding to the overall color reflected. The rules still apply to ensuring constructive interference of a particular color – all of the independent reflections have to remain in phase for any given color to be amplified. Thus, it is not just critical that the thicknesses of the layers are consistent, but also the spaces between the layers must be

consistent. Of course for every rule in biology, there are counter examples; in this case, there have been examples of chirped multilayers described. In chirped multilayers, the spacing between layers and/or the thickness of layers is variable (79,98). If sufficiently variable, all colors are reflected without bias and produce an effect of metallic silver. Perhaps unsurprisingly given the diversity of organisms employing this type structure, there are many ways of building a multilayer despite the strict requirements. For instance, the two most common structures within butterflies and moths, Morpho–type reflectors (Fig1.4 inset) and Urania-type reflectors (Fig1.4 internal yellow structure), are at face value entirely different structures but behave physically in the same way. One of the more interesting varieties of Urania-type structure is that seen in the *Achillides* subgenus of the *Papilio* butterflies (Chapter 3). Within this group there exists a clade of butterflies which have learned to warp their internal multilayers from flat into parabolic reflectors and in so doing have created a remarkable dual color reflector without changing the spacing within the multilayer (Fig3.1). This instead relies upon the difference created by changing the angle of incidence of the light upon different areas within the reflector.

1.5.3 Diffraction gratings

Diffraction gratings have been more rarely described within the biological literature. Diffraction gratings appear in some ways like a multilayer, an array of regularly spaced, regularly thick elements. Whereas a Bragg reflector stacks thin-films perpendicularly to the direction of light propagation (the Z axis), a diffraction grating rotates the stack so that the elements themselves are standing parallel with the light propagation (the X or Y-axis). It should not be a surprise then that the math describing what color will be produced by a grating is quite similar to that for a thin film. In effect, the bending of light incident upon many of these rulings spreads the wavelengths present within the light resulting in discrete viewing positions that receive a single color amplified relative to the rest of the spectrum. The color produced by a grating is thus obviously prone to be highly angle-dependent, examples described in nature have corrected for this by shaping the elements of their gratings – referred to as blazing – and allows for the grating to be selectively reflective. Examples given in the literature include fine rulings on the surface of butterfly scales, repeatedly upturned distal ends of scales across a large area of a butterfly wing, ctenophores, and squid reflectins sculpt the surface of iridiphores into gratings (99–102).

1.5.4 Gyroid/3D photonic crystals

Diffraction gratings and Bragg reflectors are commonly classified as one dimensional crystalline reflectors as the elements resulting in color repeat in a single axis, X, Y, or Z. More exotic crystals also exist but operate in ways that are not so easy to intuit. As the structures are so elaborate, it is hard to imagine that they could be easily evolved. However butterflies have evolved just such a structure, known as a gyroid, at least three times independently to create color in *Teinopalpus*, *Parides*, and the Lycaenid *Mitoura* and *Callophrys* genera (37,103,104). The physics underlying how color production is managed in a gyroid is more akin to a fiber optic cable or filter than to thin film constructive interference. The spacing and geometry of a gyroid crystal permits only certain

wavelengths to be propagated through the crystal, this in effect purifies the spectrum that passes through it. In the closely related butterflies *Callophrys* and *Mitoura* many gyroid crystals fill the distal tip of each ventral scale (46). The tuning of this structure has been such that it only permits blue and yellow light to emerge, resulting in a color mixing stimulus that appears green to our eyes. Gyroids are less sensitive to iridescence, but do result in strong angularity of their reflectance. As a mechanism to cope with this *Callophrys* and *Mitoura* butterflies seed multiple crystals within each scale oriented randomly with respect to one another, and ensuring that the angle at which they are viewed doesn't impact the color they are seen to be.

1.5.5 Quasi-ordered/Tyndall scatterers

The most controversial of structural elements are those that have been classically described as producing color by Tyndall scattering. Nearly the entirety of the fantastically clever report produced by CW Mason on the blue of birds focused on demonstrating how bird barbs behaved in accord with Tyndall scattering (60). The mechanism has been attributed to butterflies, birds, dragonflies, and Vervet monkey scrota as well (61,64,105). In effect, Tyndall scattering, like that of the Rayleigh scattering that gives the sky its blue hue, acts by the differential interaction of the wavelengths of light with molecules. In Rayleigh, the more energetic violet and blue wavelengths are scattered by their interaction with the dipoles of molecules, but the long wavelength end of the spectrum fails to have such an interaction. The blue we see during the day is produced thusly, and the orange and reds of a sunset occur when the sun is in a different position relative to the earth's surface, meaning that its blue has already been filtered out when the light arrives at our eyes. Tyndall behaves similarly albeit with larger molecules than Rayleigh, and therefore thought to be biologically relevant. In recent years however, work done across many clades of life by Rick Prum's lab has waged war on this hypothesis. The argument of Prum's work suggests a form of constructive interference producing structure that has gone unnoticed because of the lack of an obvious periodicity. Thus far the remarkable property of all of the structures is their regularity, and as has been mentioned, when that regularity breaks down (such as in a chirped multilayer) the structure fails to bias its reflection to one color. In quasi-ordered structures, Prum and colleagues, argue for a cryptic periodicity of elements such as melanosomes, successfully demonstrating its existence through Fourier transform (92,106–108). As evidence accumulates it may change the interpretation of the observations currently reported as supporting Tyndall reflection within the literature.

1.6 Common problems of using structural color in biology

The evolution of structural coloration comes with many challenges. 1) Pigments have distinct enzymatic pathways made of a few genes – they are reliable to make the same color scale to scale and generation to generation; structural colors require extremely tight tolerances (~10s of nanometers) and are likely to employ many cellular components to

achieve the final geometry (109) 2) pigments look the same color from all angles; structural colors often exhibit iridescence as a result of a change in the way light travels through a structure at the different angles of incidence occurring during motion (Fig1.5) (110), 3) pigmentary colors are highly saturated (pure) as a result of the narrow number of wavelengths reflected following absorption; structural colors often employ interference to create color. As such, in structural coloration some wavelengths are enhanced while the rest are reduced – but critically, most nanostructures themselves cannot absorb light, meaning that reflections are biased toward a color but are at low saturation on their own. As a result, most nanostructures found in nature tend to be associated with dark pigments, which are suggested to aid in increasing saturation (34,38,41,46,51,65–83).

As discussed previously, color has evolved important roles in intra- and interspecific communication. There lies in these associations, a subtle but powerful inference when considering aposematism (warning coloration), mimicry, or sexual coloration: for information and signals to be sent and received efficiently, everyone involved has to speak the same visual language. One necessary component of speaking the same language is fidelity of an individual to the informative colors (111,112). Though it is true that the evolution of novel color patterns suggests that this fidelity is not necessary over geological time scales, for any interaction within a single generation the individuals within a sufficiently large population will likely be constrained to maintain color fidelity.

It is in this requirement for fidelity that much of the problems can be imagined to exist for structural color. As mentioned, all of the prevalent forms of structural color in biology require at least one broad surface of ~100nm in thickness, and most require the coordination of 3-10 ~100nm thick surfaces oriented with a regular spacing between them at a similar distance.

To give a sense of the fidelity problem we will use an example of how precise and accurate a Morpho butterfly must be to appear blue (Fig1.1). The source of the blue color admired in species like *Morpho cypris* and *Morpho godartii didius* is found on the surface of their scales in ridge-derived multilayers (Fig1.5 inset, Fig2.3P,P'). The structural elements exist as overlapping finger-like projections, called lamellae, from the surface of the scale cell, having dimensions that are ~100nm in diameter, and 3um to 20um in length. A given ridge along the scale is composed of a consistent number of fingers in height, 3-10 in number, determined by the species and scale type. The ridges run the full length of the scale, ~275um, and exist across the width of the scale, ~75um, at a regular interval that is again species and scale type dependent (between ~150nm-1.5um). Depending upon the species of the butterfly, a single surface of a wing will have ~10,000 scales/cm^2. With no formal mathematics, it is plain to see the immensity of the problem in reproducing several 100nm structures on every one of the ~50 ridges across each of the ~300,000 scales with ~10nm accuracy so as to produce a single color. If we assume there is a purifying selection for the blue color, (reasonable given the large number of blue morpho species), then this intricate construction must also occur on every organism in a population, every generation or else it will likely result in death or failure to mate.

Another core issue when relying upon structural color for amplifying any particular color stems from the aforementioned iridescence that most structures show as the angular relationship between the structure and the incident light changes (Fig1.5). Should the light and structure be positioned differently relative to one another, the color amplified from it will change – clearly a problem if an organism were to employ structural color for crypsis or aposematic signaling.

Lastly, a common problem with structural color comes from the fact that all of the mechanisms described merely enhance one color of light relative to the others; they do not remove the others from the reflected light as pigments do. This requires additional measures to ensure that the reflected structural color is pure enough to be perceived as a saturated color rather than a diluted hue-biased white (see Chapters 2 and 3, and Fig2.1 and Fig3.30).

Though evidence strongly suggests species and populations of butterflies evolve novel coloration by fine tuning nanostructure details and pigments of their scales, the cellular and developmental origins of the exquisite precision and accuracy across the diversity of documented scale morphologies has largely been left untouched. This is a consequence of many practical challenges including:

1) Scale development occurs within the confines of a typically opaque pupa

2) Aside from late pigmentation, there has been no success in culturing wing tissue *ex vivo*

3) There are no available wing tissue-specific enhancers and few genetic tools are available to make developmental manipulations of the wing

4) RNAi is widely considered to be non-functional in scales without challenging methodology

and

5) bristle development in *Drosophila* (a homologous system) is still poorly understood and not always directly applicable (i.e. morphogenesis processes dependent upon bristle:neuron interactions (Fig1.6)) (113–116).

I believe these to be mainly technological barriers awaiting to be overcome. Once accessible, scale morphogenesis will be a critically important frontier for understanding how butterflies make color and more generally, how cells accomplish morphogenetically complex and rigidly-defined structures.

1.7 Summary of scale development

With all that has been studied in the physical “how” of structural color there remains a wide gulf in our understanding of the developmental “how” of even basic pigmented scale

morphogenesis occurs, let alone the morphogenesis of highly complex, structurally-colored scales like those of *Callophrys*.

1.7.1 Evolutionary origin of scales

Scales' ubiquity among Lepidoptera suggests the evolution of this cell type was beneficial for the success and diversity of the order. Given the complexity and variety found among Lepidopteran scale morphologies, understanding the origin of the cell type and its prototypical development should provide a foothold for further inquiry. Several lines of evidence suggest that scales have arisen as a modification of mechanoreceptor organs. Given that the hard, acellular exoskeleton prevents direct sensory stimulation via the ectoderm (as in soft-bodied animals), mechanoreceptors have likely evolved in the arthropod lineage to provide touch sensation (117). The developmental origins of mechanoreceptors have perhaps been best studied in *Drosophila* macro- and microchaetes. Both of these mechanoreceptors follow similar developmental programs differing mostly in number and ultimate size. Macro- and microchaetes are specified as a Sensory Organ Precursor cell (SOP) on the fly notum during metamorphosis, undergoing a stereotyped division and development that ultimately leads to the organ which is comprised of 4 cells: an externally oriented bristle (trichogen), a socket holding the bristle (tormogen), as well as a neuron which is triggered by movement of the bristle and a sheath cell covering the neuron. A fifth cell is produced but undergoes apoptosis. The location of the SOPs is determined by overlapping domains of transcription factor expression as well as a subsequent battle among the epithelial cells via Delta and Notch signaling leading to expression of the genes a*chaete* and *scute* (together symbolized as *As-c*) within the cell which will become the SOP (118,119). Although flies also have hairs covering their wings, these are unlikely to be homologous with Lepidopteran scales as they form as a result of non-canonical Wnt/PCP signaling directing a localized actin outgrowth from each wing cell and not through an SOP intermediary (120).

Studies have shown that butterfly and moth scales undergo a set of similar stereotyped divisions leading to a socket and scale, while apoptosis prunes the neural lineage of Lepidopteran SOPs, removing a sensory function (121). There has also been demonstration of conserved *As-c* mRNA expression in butterfly SOPs, further arguing homology with sensory organs (122). Moreover, the surface striations (ridges and troughs) of developing butterfly scales and fly bristles show correspondingly similar F-actin association and sensitivity to F-actin perturbation (123,124) (Fig1.6).

Flies (Diptera) and Lepidoptera are close relatives within the insect phylogeny. Lepidoptera is the sister order to the caddisflies (Trichoptera) which together are sister to the Diptera. As *Drosophila* bristles are limited to the body and not found on the wings, one would expect that if Lepidopteran scales were homologous that at some point in the lineage leading to Leps, an expansion of the SOPs must have occurred at the expense of wing hairs. Indeed, this seems to be exactly what has happened, as observation of the Trichoptera shows mechanosensory-like bristles covering the wings, and in at least one Trichopteran there has even been the conversion of these bristles into scales (20).

Taken together, evidence of gene expression, developmental similarity, and phylogenetics suggests that Lepidopteran scales have likely evolved from mechanosensory organs. Further, it suggests that it is fair to make inferences and predictions from the work done on *Drosophila* macro- and microchaetes.

Albeit analogous, *Drosophila* wing hairs and denticle belts, *C. elegans* alae and hypodermal cells *vis-à-vis* the cuticle, and perhaps even plant plastid and vertebrate photoreceptor outer segments and neurons, all represent important morphogenesis systems for the fine and elaborate structures found in many Lepidopteran scales.

1.7.2 Scale anatomy and axes

The basic anatomy of a fully-formed Lepidopteran scale has been summarized by Ghiradella and others (125). In short, a scale is a flattened sac roughly paddle shaped, with an upper surface and a lower surface, variably discussed as upper and lower laminae or ab- and adwing surfaces (Fig1.4). The lower lamina is rarely modified, typically remaining quite flat and functioning in many cases as a thin-film reflector (51,81,86,87). By contrast, the upper lamina is often highly modified, nearly always featuring ridges running the length of the scale with uniform lateral spacing across the scale. The ridges are often formed of a stack of finger-like projections known as lamellae, the precise number, spacing and details of ridges vary from species-to-species and are a common source of structural color. Ridges are connected laterally to one another by crossribs, which are commonly (though not always) perpendicular to the ridges. Thus, the ridges and crossribs form the edges of a lattice, the space between which can be solid – preventing the view of the lumen – or windowed (fenestrated) – allowing one to view into the lumen of the scale. Connecting the upper and lower laminae within the lumen of the scale are struts known as trabeculae. The lumen can also contain many elaborate structures such as multilayers, gyroids, and quasi-ordered structures (as discussed earlier and seen in Fig1.4). The scale inserts into the wing via a petiole through a pore created by the remnant of the socket (Fig1.4).

As an example of unicellular morphogenesis, there are few rivals to the scale. Scales have multiple symmetry axes (Fig1.4). I will define them in relation to their developmental origin with some aid from their final position on the adult wing as we believe this will help discussion of the cellular processes likely to be involved.

The adult scale inserts proximally (nearer the insect's body) and extends distally toward the lateral edge of the wing. Thus in the adult, scales' long axis orient perpendicular to the anteroposterior axis. However, in the developing pupa, what will become the distally located end of the scale is actually the apical projection of the cell. So I will define the long axis of the scale, along which the ridges run, as the apicobasal axis of the scale. In the adult the upper lamina of the scale (abwing) is oriented away from the wing (dorsal on the dorsal surface, and ventral on the ventral surface) with the lower lamina (adwing) apposed to the wing membrane (ventral on the dorsal surface, and dorsal on the ventral surface). However, when we consider the developmental origins, with the long axis

defined as apicobasal, the future upper lamina will always form on the proximal side of the scale, and the future lower lamina always is oriented toward the distal edge of the wing. This orientation forms regardless of whether the scale is found on the dorsal or ventral face of the wing. By rearranging the axes in this relationship, immediate candidates emerge for the control of scale development, namely apical targeting of exocytosis and cytoskeletal processes influencing outgrowth and non-canonical Wnt/Planar Cell Polarity (Wnt/PCP) pathways influencing the upper and lower laminae differences.

1.7.3 Developmental origin of scales

The wings of a Lepidopteran are specified during the embryonic stage, existing within the body of the caterpillar as imaginal discs. Upon pupation, the imaginal discs are everted to the external surface of the animal where proliferation, patterning, and differentiation of SOPs occurs within the first 14% of pupal development (124,126). It is in these early hours of development that Notch and Delta signaling are thought to be involved in specifying the SOP and eventually trichogen and tormogen fate following *As-c* expression within the SOP (122,127–129). Following specification of the trichogen/tormogen at about 21% pupal development, the scale begins as a small bud pushing on the apical surface of the trichogen cell membrane in an actin-associated manner (126). The socket (the cell body of which sits distally to the position of the trichogen cell body), forms arms that wrap around the bud, meeting on the proximal side of the trichogen projection (124,126). The interface of the emerging scale and socket at this early stage are highly enriched in β-Catenin staining suggesting the presence of adherens junctions (124). Subsequently, apical outgrowth of the scale proceeds with thick, apicobasally-oriented, plasma-membrane-apposed microfibrils of F-actin form at regular lateral spacing relative to each other, between which the plasma membrane buckles outward initiating the development of the longitudinal ridge (54,124,126). A second population of F-actin forms within the scale's lumen closer to the distal side of the scale – this presumably will aid the scale in orienting its apical tip toward the wing's distal edge and may play a role in the differentiation of the upper and lower laminae (124). Elongation of the scale continues until the final length is achieved, at which the scale begins to flatten, perhaps in conjunction with a change in the behavior of the microtubules (Fig5.1) (36,126). Fine external and internal structure elaboration occurs during this time just prior to chitin deposition which may involve endocytosis/exocytosis pathways as well as the endoplasmic reticulum (36,126,130). Once the cuticle is secreted, it holds the ultrastructure of the scale in place eliminating the need for the structural F-actin components which subsequently breakdown (124). Pigmentation occurs last, and in all observed species follows a predictable series of pigment synthesis with ommochromes and pterins preceding melanin just prior to the adult's emergence from the pupa first (131–135).

Given the apparent homology between Lepidopteran scales and the well-studied *Drosophila* bristles, we will look to what is known about bristle morphogenesis to seek answers about how a scale may be made and modified.

Bristle mutants were among the very first mutations isolated by Thomas Hunt Morgan and Calvin Bridges (136). However, it wasn't until nearly 50 years later until the first hints of their molecular function was teased out (137). Forked (*f*) and Singed (*sn*) were shown to be actin cross linking proteins which functioned in bristles to help maintain the large bundles of actin found at the membrane along the length of the bristle (137–139). Mutants of *singed* and *forked* lead to morphological defects in the adult bristle including reduction in length, random curvature, and irregular fluting (138). Internally, the large hexagonally packed bundles of actin at the membrane surface become smaller and irregularly packed. However, even in *sn/f* double mutants, actin filaments still associate at the membrane in approximately even spacing (137,138,140). Moreover, they retain an asymmetry in distribution seen in wild type bristles, with larger bundles closer to the posterior face of the bristle and smaller bundles accumulating at the anterior face of the bristles. Together, this is suggestive that the cross-sectional size of a bristle is mediated by actin cross-linkers and has influence upon the length, structural integrity, and fluting of a bristle, but that these cross-linkers are not necessary for actin association or spacing on the membrane, nor in the asymmetric distribution of bundle size along the A/P axis of the bristle.

Butterfly scales also show a distribution of actin bundle thickness along the proximodistal axis of the scale (Fig1.6) (54,124,126). No known mutants have been recovered in actin crosslinking proteins in Lepidoptera, however some butterflies have been found that have severely reduced scale sizes with disorganized ridges such as the cover scales of *Morpho rhetenor* and *M. cypris* (see Appendix 2), and heat-shocks of *Vanessa urticae* pupae were demonstrated to produce highly disorganized ridges similar to mutations in capping protein within *Drosophila* bristles (141).

Joji Otaki's lab has shown that the wild type ultrastructure development of *Junonia orithya* can be perturbed by treatment of pupae with Thapsigargin, a small molecule causing the loss of ER calcium stores poisoning (142). In another study, the mutation of *Junonia coenia*'s Tyrosine hydroxylase in eggs leads to loss of pigmentation in adult scales as well as disrupted ultrastructure (77). These two experiments are among the only published data manipulating structurally colored scales during their development. In both studies, it is likely that proper cuticle formation is disrupted leading to ultrastructural defects and loss of coloration. The phenotype associated with Thapsigargin treatment is potentially exciting but given the broad impacts of shutting down ER function, they could simply be the result of making very sick scales incapable of properly developing.

1.8 Some possible cell biology underlying the construction of nanostructures

There may be no more discipline uniting structure in all of biology than the scale. It is a cipher of cell biology that links macroevolution and population structure with multicellular

development, unicellular development, materials science, and photonics. Even among its most pedestrian forms, the scale is a cell type that seemingly harnesses every conceivable cellular process to construct magnificent edifices in miniature. They are cathedrals of biology which quite literally transcend their own individual birth and death to manipulate light and emit pheromones at the minute extreme for a plethora of purposes: camouflaging with cryptic patterns, conveying information (or lying about) distastefulness to predators, provide defense from sticky spider webs, enticing mates, and generally modulating complex population and community interactions at the ecological extreme. In no uncertain terms, the scale is the unit by which Lepidoptera color patterns are defined, manifest, and manipulated. It would seem likely that the eventual progression of study of pattern manipulation will lead researchers toward how the patterning genetics influence the cell biology of the scales displaying the pattern. Understanding the biology of scale development and the diversity therein will almost certainly provide entirely new insights into what a cell can do, how genetics influence material properties, and the boundaries interfacing active and self-assembly with the genome of the individual and evolutionary processes within a population. And perhaps eventually we will be able to take these lessons and apply them to create industrial processes which are, by definition, biocompatible and biodegradable.

For all the work that has been done to explain the diversity of color patterns, there has been only a single causative mutation described that influences structural color (77). Largely this dearth of evidence is a result of a few practical challenges which I have mentioned earlier. In addition, there are the following issues to contend with: 1) the species that are ideal for lab rearing and species that have interesting structural colors rarely have overlapped. One that does have structural color, the Common Buckeye (*Junonia coenia*), has small patches of structural color that are likely thin-film in origin. If one is interested in the Morpho-type, Urania-type, or gyroids, buckeyes do not offer obvious inroads. The fact that structurally colored butterflies have not been intensively studied may merely be a consequence of the bulk of research institutions being based in North America and Europe where there are fewer species with structural color compared with the tropics and neotropics. 2) While lab-reared species do have homologous scale components to structurally colored species (ridges, for instance), nanostructures are by definition smaller than what is resolvable by light microscopy, requiring electron microscopy to observe changes. So, a forward or reverse genetics project to look for genes important for, say, ridge structure in commonly used lab butterflies would require screening by electron microscopy, which is not particularly efficient in time or expense. 3) In most non-model studies, it is helpful to lean on the observations made in the homologous tissues of a model species. Butterfly scales being homologous structures to *Drosophila* Sensory Organs is a boon. However, the development of macrochaetes is actually relatively poorly understood even in *Drosophila.* It was only recently, since 2010, that more in depth observations of microtubule dynamics have been analyzed in *Drosophila* (143–147). Given that these basic studies are just now being done in *Drosophila* means that butterfly research may actually aid *Drosophila,* as often as the other way around. 4) Traditional forward genetics will be difficult, if not impossible, with current technologies in Lepidoptera. The average Lepidopteran has a haploid chromosome number of 31, and maintaining lines of butterflies is difficult. Creating and maintaining the tools useful for forward genetics, like balancer chromosomes, is unlikely

to be undertaken. Many groups have tried to get around these limitations by using genomics-based analyses to make statistical associations between phenotypes of inbred organisms and their genomes (52,134,148,149). To date, this has led to the identification of upstream effectors like patterning genes (*wnt*) or transcription factors (*optix, doublesex, invected*) likely due to the fact that they have large effects on phenotype. These approaches have given some insight into proximal mechanisms (myosin), however the interpretations have been controversial and require more study (150,151). 5) Scale development occurs within the pupa. The cuticle of the pupa is often heavily pigmented and distorts the transmission of light. If one wants to ascertain how a particular cell biological system influences the final nanostructure being able to live-image development is arguably the best way to do so. 6) Lastly, even though the revolution occurring in genome-editing allows for the targeted mutation of candidate genes in Leps, candidates have to be carefully chosen so as pleiotropy can be avoided (77,152). Destroying many cell biologically important genes will kill the animal well before the pupal stage preventing the ability to obtain phenotypes relevant to scale development. Published accounts target genes only required for wing patterning or use a high level of mosaicism to avoid pleiotropy. Reliance upon mosaicism is useful for highly visible phenotypes like whole wing color pattern defects, but genes influencing scale substructure will still require EM visualization for determining effects.

Despite the limitations presented by current technology there are frontiers that have been advanced by Drosophilists (see Appendix 1 for analysis of one broadly reaching RNAi screen). Some of those areas I will summarize here, with more specific thoughts explored throughout the rest of the text and the future directions.

1.8.1 Actin and Microtubules

Actin and alpha-Tubulin/beta-Tubulin are polymerizing proteins found in every eukaryote that have been examined for their presence and are the constituent proteins of microfilaments and microtubules respectively. The roles of these proteins are numerous including cell morphogenesis and shape maintenance, cellular motion, organelle and vesicular trafficking, cellular protrusions and endocytosis, chromosomal segregation and cytokinesis, muscle and myocyte contraction, ciliary beating and much more. Actin exists as a monomer (also known as G-Actin or globular Actin), and is an ATPase with a “pointed, minus-end” and a “barbed, plus-end”. In filamentous form (F-Actin), ATP-bound monomers assemble more quickly at the growing filament’s barbed end, shortly thereafter the intrinsic ATPase activity will convert ATP to ADP creating a conformation change in the protein that generates stresses in the filament ADP-bound monomers within F-Actin are more likely to dissociate from the minus-end, but there exists a vast variety of accessory proteins that interact with Actin (both G- and F- forms) to modify its polymerizing/depolymerizing activity, which includes internal severing.

F-actin dynamics have been examined extensively in *Drosophila* sensory bristles and are critical for normal patterning and development. Interestingly, it has been frequently noted that alleles of actin (and tubulin) associated proteins have defects that manifest only in larger chaetae (144,153–155). Given that size of chaetae is determined by ploidy levels,

it seems likely that absolute levels of expression are important for normal development. In other words, it seems that haploinsufficiency is often copy number dependent and not as simply defined as being normal at 50% of functional genomic copies.

Likewise, F-Actin appears critical for butterfly scale development (54,124,126). I expand upon work done by Dinwiddie et al. (124) in Chapter 3 of this manuscript, but still more work is needed.

As for Tubulin, it has recently emerged that tubulin-dependent localization of Ik2 leads to many defects in *Drosophila* bristles, some of which produce vaguely scale-like phenotypes (144,145,156). Moreover, Ik2 may influence the activity of F-Actin bundling proteins needed for normal phenotypes, suggesting that microtubules are required for actin to form properly (156).

Very little has been done in butterflies to examine the role of tubulin, though in the future directions I present some preliminary evidence for a functional role of tubulin in gross morphogenesis of scales (Fig5.1).

1.8.2 Fine structure and ZP domain proteins

Part and parcel with a structurally-colored scale's ability to make color is its finely sculptured chitin ultrastructure. The fine tuning of the chitin ultrastructure has been suggested to be a source of color diversity (34,35,40,41,157,158). Though chitin is certainly important in most insect exoskeletons, it is apparent that chitin does not act alone in creating the exoskeleton. In fact, there are examples such as the praying mantis ootheca (a protective egg case) where chitin is entirely absent, instead entirely composed of self-organizing proteins (159). When considering the fine reticulations and structure seen in butterfly scales it is important to recognize that the shape of the hardened cuticle is templated from the plasma membrane. Indeed, even the swirling gyroid's 3-dimensional crystal found within the lumen of some butterfly scales is thought to be templated by internalized-yet-topologically-external membrane (130). Having discussed how actin-based mechanisms may drive gross morphological development, and how purely physical reactions to forces can be the source of regularity, a third morphogenetic source that remains poorly understood seems to straddle the realm of protein-based active mechanisms and purely physical mechanisms, perhaps uniting the two. While there are a handful of proteins known to influence the shape of the various membranes within a cell, here we will consider the role of a family of proteins which have been shown to have great importance on the morphogenesis of cuticle from the extracellular space: zona pellucida domain-containing proteins.

Originally discovered as the constituent proteins of mammalian oocyte extracellular matrix, zona pellucida (ZP) genes have been described throughout Bilateria and Cnidaria, perhaps suggesting its evolution as a key innovation in Eumetazoan identity (160). The ZP domain itself is a cysteine-rich polymerization domain which provide stability and allow filaments of homo- and heterodimers to form, respectively. In addition, the canonical mouse ZP1, ZP2, and ZP3 proteins all feature N-terminal secretion signal peptides, C-

terminal transmembrane domain, and a furin cleavage site between the transmembrane domain and the rest of the protein, which is thought to free the rest of the protein from the membrane. In the oocyte ZP2 and ZP3 form filaments which are crosslinked by ZP1 and the protein mass surrounds the oocyte controlling sperm entry and preventing polyspermy. The ZPs of mammalian oocytes have been suggested as one half of the lock-and-key mechanism which ensures only intra-specific fertilization and that mutation of ZPs may allow for prezygotic isolation barriers between diverging populations. These observations suggest that even external to the cell, ZP domain proteins have dynamic functions (161,162).This itself doesn't necessarily translate directly to butterflies and structural color, but does suggest that evolution of a single protein is sufficient to direct ultrastructural changes great enough to alter function.

Closer to the topic at hand, are several stories emerging within the last decade from the dissection of exoskeletal morphogenesis in *C. elegans* and *Drosophila melanogaster*. *C. elegans* cuticles feature medially-located ridges running the length of the animal known as alae, which are thought to aid the animal's locomotion(163). Further, alae are morphologically life-stage-specific with cross-sections characteristic of that molt: L1, dauer, and adults feature unique morphologies (164). Recent forward genetic screens have identified several ZPs as constituents of the cuticle: Cut-1,Cut-3,Cut-4,Cut-5, and Cut-6 (163). This work included a genetic dissection of these proteins by RNAi led to the conclusion that the ZPs worked in a combinatorial fashion dictated by stage specific expression to create alae with particular morphologies.

Several studies in *Drosophila* have come to similar conclusions. Studies on wing, wing hair, tracheal, and denticle development have all implicated the importance of ZPs for normal morphogenesis (165–170). Most exciting among these is the 2010 publication of Fernandes et al., which examined in detail the role of ZPs in the morphogenesis of larval denticles and found that no fewer than 8 ZPs participated in sculpting the hook-like shape of the denticle. Denticles themselves are of varying size, but on average are triangular extrusions of the cuticle with a base of ~3.5um and height ~2.2um, with fine structures such as the hook defined with dimensions on the order of 100nm. Interestingly, the loss of any particular ZP influenced the shape of the hook in a spatially restricted manner, for instance only influencing the tip of the denticle, or its base. What is more, the authors found that expression of a chimeric ZP (one where its ZP domain had been swapped for another ZP domain) alone was insufficient to rescue loss of the wild type ZP protein, at best giving partial rescue of the mutant phenotype. While the authors do not show images of their domain swapping experiments (thus making interpretation of phenotype a challenge) this hints at several interesting ideas pertinent to butterfly structural color evolution. 1) ZPs have programmed spatial information 2) ZP domains alone do not dictate their spatial localization or function but rely upon the other domains in their sequence as well, and perhaps most interestingly, 3) if we consider the domain swapping experiments as not a partial rescue, but instead as a novel phenotype that could arise naturally through domain shuffling, the exploration of phenotypic space through fine ultrastructural sculpting may merely be a domain modification away. There are 19 genes on Flybase annotated as containing a ZP domain (release FB2016_05, October 2016).

The evidence present in the *Drosophila* literature suggests that ZPs act to connect the chitinous ECM to the plasma membrane. Thin section TEMs of denticles mutant for the ZP proteins Dusky-like (Dyl), Miniature (M), Trynity (Tyn), and Zye (Zye), all show separation of the plasma membrane from the ECM(165). Similarly, mutant embryos for ZP genes *dusky* (dy) and *piopio* (pio) have tracheal development defects, which are similar to mutants affecting chitin secretion like *kkv*, a chitin synthase, suggesting that ZPs connect the plasma membrane to the chitin exoskeleton (166). Loss of *dyl* also produces shrivelled wing hairs and phenocopies loss of *Rab11*, a small GTPase that marks recycling endosomes, and is transported by Nuclear Fallout (a dynein adaptor) and Dynein (168). Lastly, *pio* was implicated by transcriptomic analysis in butterflies as differentially expressed between areas of different colors in *Heliconius* (134), which were shown decades ago to also vary in ultrastructural phenotype (33) perhaps being suggestive of a role in scale morphogenesis. In sum, ZPs play roles in multiple epidermal organs with unique structures, with particular morphogenetic sculpting likely driven by combinatorial expression of multiple ZPs, the repertoire of which may be expanded by duplication and domain swapping, with its ultimate effects derived by connecting the plasma membrane to the exoskeleton.

1.8.3 Organelles, internal membranes, and cnidocytes

Internal membranes, like those in the rod outer segment of vertebrate photoreceptors and the thylakoid membranes of chloroplasts, are have not evolved for color production, but serve to increase internal surface area for the specialized light collecting proteins of their respective structures. It is hard not to look at these structures and not imagine how a similar process could be useful for creating the internal multilayers of Urania-type scales. In some plants that grow in highly shaded niches there has been the evolution of just such a structure from their chloroplasts. Termed iridoplasts, the spacing of the chloroplasts are built and spaced in such a way as to reflect light (90,171–173). While it is unlikely that a homologous method is employed within butterflies (which conspicuously lack chloroplasts) assembly of such internal membrane structures may still prove informative when chasing the roots of internal multilayers.

In a sea of dumb-foundingly periodic structures, the gyroid is certainly Neptune. As a 3-dimensional photonic crystal, gyroids feature regular repeats in all three dimensions. Moreover, the gyroid forms within the lumen of the developing scale rather than on the scale surface, the domain where actin and ZP domains seem to function most prominently. Gyroids have evolved in multiple lineages of butterflies (as well as in beetles and birds). A common observation is that species with gyroids often emerge from clades with internal multilayers. This of course leads the observer to wonder if, even with the complexity of the structure, whether the repeatedly-evolved gyroid is not necessarily a large evolutionary leap, but a transition from another structure. In support of this are results from an unlikely source – materials science.

Polymers are macromolecules made of repeated sub-units. DNA, RNA, polypeptides, chitin, cellulose and many lipids are the familiar biogenic polymers. Polymers have emergent physical and chemical properties that are derived from the building blocks

within. Secondary, Tertiary, Quaternary structures in proteins, enzymatic activity, ribozyme activity, solubility, etc. are emergent properties of any given polymer. It is not hard to imagine that different polymers provide different functions. In the realm of block copolymers, multiple polymers with different chemical and physical properties are covalently bound to one another forcing their association. Depending upon the properties of the containing system, these copolymers adopt differing volumetric configurations. In Knoll et al.'s 2002 paper, the authors constrain thin films of polystyrene-polybutadiene-polystyrene copolymer by varying film thickness in space (174). The resulting configuration of the copolymer at the lowest concentration was to adopt a pillar form (perhaps not unlike trabeculae), with increasing thickness the copolymer became a multi-laminar morphology (strikingly similar to that seen in scales with internal multilayers), and at highest thickness the laminae gave way to 3-dimensionally reticulating crystals. It is not hard to imagine a biogenic copolymer. Glycocalyxes, long polymers of glycosylation attached to proteins and lipid moieties at the plasma membrane, can be enormous. If a long filamentous protein, or even a lipid, were to be glycosylated, the result could function as such a copolymer in theory. This is one physical model which suggests that, if true for biology, perhaps the view of self-assembling or partially-templated nanostructures promoted by some is accurate. Perhaps all biology and genetics are doing is to achieve the correct physical conditions for spontaneous assembly.

When Ghiradella investigated gyroid formation in butterflies, she was of the opinion that a simple lamina to gyroid transition would be the mechanism, citing the fact that some species produce individuals with gyroids on the ventral wing face and use laminae on the dorsal face (36). As sure as she was that she would find a simple transition between multilayer and gyroid, the exploration of two species developing scales via TEM thin sections of pupal scales, showed that biology would not be so accommodating. While both the developing gyroid scales and laminar scales appeared very similar through early development, their development diverged significantly post-day 7 (36).

The ideas proposed by Ghiradella were elaborated upon by Prum's group through modeling based on Ghiradella's original micrographs. They came to the conclusion that the smooth endoplasmic reticulum itself formed a second gyroid interlocking with the future photonic crystal as support! Is it possible that the plasma membrane and its chitin secretion that will be the gyroid, are actually templated by/simply slaves to, the morphology of the cell's secretion machinery? Is it possible that the secretion machinery and the plasma membrane form a kind of block copolymer perhaps through a linking protein?

Despite the advances associated with understanding how gyroids form, even the basic biology remains poorly understood. For instance, in the species studied, the gyroids form at the apical-most tip of the scale. The nucleus, and presumably the ER, exists at the opposite end of the scale through the narrow aperture created by the socket ~300um away. Though not impossible, it is challenging to imagine that the SER extends from the nucleus, up through the constriction by the socket, to the distal most portion of the scale

where only there, does it form the gyroid structure. While it is generally considered the ER which tubulates and contorts, there is at least one known example where another component of the secretion machinery forms highly elongated and elaborate structures.

Cnidarian cnidocytes are spiritual muse of butterfly scales. Cnidocytes are the stinging cells of cnidarians (jellyfish, coral, anemones, Siphonophores, etc.), those which are used by the organism to ensnare and envenomate prey and deter predators. As unicellular morphogenesis is concerned, cnidocytes are produced by stem cells called cnidoblasts, where after post-Golgi vesicles fuse into a giant vesicle (175). Cnidocyte firing owes to selective mechanical and chemical inputs triggering intense osmotic pressure within the vesicle, propelling the contents into the prey or predator. In order to withstand that pressure, one of the earliest events in morphogenesis is the accumulation of reinforcing, disulfide-crosslinked minicollagens and cysteine rich protein NOWA along the interior of the vesicle (176–178). Continued addition of small vesicles to a single end of the vesicle in coordination with microtubules leads to tubulation of the giant vesicle to several cell diameters in length. Invagination of the tubule within the giant vesicle follows, where it coils within to fit. In TEMs of developing vesicles, the packed tubule has a chiral triskelion cross-section with the arm lengths on the order of 100nm. Eventually, the cnidocyst grows so large within the cytoplasm that it displaces much of the machinery of the cell into a small corner. It is clear from the work on the cnidocyte that a non-ER organelle can grow large, complex and finely structured (179). This underlines the necessity of cell biological approaches to dissecting the cellular origins of butterfly scale nanostructures such as the gyroid and multilayer.

1.8.4 Membrane gerrymandering by Rab GTPases

Rab proteins are a large family of Ras small GTPases. They mediate interactions of sub-cellular membrane domains by regulating activity of docking and fusion proteins such as SNAREs (180). *Drosophila* has 27-33 Rabs, with Rab5, Rab6, Rab11, and Rab35 having demonstrated roles in the morphogenesis of fly bristles (168,181–184). It is logical that membrane compartment identity and trafficking need to be tightly regulated in cells.

Rab6, also known as *warthog (wrt)*, was initially discovered in *Drosophila* as an enhancer of eye phenotypes in Notch mutants (184). Rab6 is highly conserved among Eukaryotes, and evidence from yeast and mammalian cells suggested a role in modulating Golgi to Trans-Golgi network (TGN) vesicle trafficking (185,186). Further work showed that both hypomorphic and null allele clones produced stunted macrochaetes with weakly defined ridges with variable severity. Phenotypes were occasionally seen in a cell-non-autonomous fashion whereby *wrt/wrt* mutant bristles at the edge of clones displayed minor phenotypes (184). Interestingly the expression of a constitutively active wrt^{Q71L} allele in an otherwise wild type background, gave novel split or bent bristle phenotypes with no ridge defects. The authors also claimed that only in clones with null alleles did microchaetes gave phenotypes, otherwise all *wrt* phenotypes were limited to ocelli, notum, and scutellar bristles.

warthog represents and interesting candidate for butterfly structural color development for several reasons. One postulated reason for the synthetic effect of *Notch* and *warthog* is that the Notch product is a cell surface receptor that requires furin-protease-mediated cleavage to be functional. Thus Rab6's involvement in shuttling cargoes between the Golgi and TGN could represent a breakdown in Notch transport both to the appropriate cellular surface and/or to the appropriate domain for proteolytic cleavage (187–190). While it was suggested that the influence of *warthog* on bristle development was made in a non-cell-autonomous manner, the variety of phenotypes as well as fact that large bristles were preferentially impacted by the loss (something seen in cell-autonomous actin phenotypes), suggests that it also has a cell-autonomous role. It is not hard to imagine that cell-autonomous defects in Golgi to TGN trafficking would be likely in a cell which must grow 300um in 24 hours. Also, it is tempting to speculate that ZP domain proteins may be similarly affected by Rab6 loss, given that they, like Notch, have furin-protease sites and are cell surface proteins. Finally, when considering structures such as internal multi-layers and 3-D photonic crystals, the secretory pathway is a strong candidate. While the TEM studies by Ghiradella (expounded upon by Prum) mentioned before have suggested ER as a prime candidate for photonic crystal construction, as discussed, the TGN is the progenitor of the large, tubulated, and highly-complex nematocysts of cnidarians (36,104,130). As such, it would be interesting to explore *warthog* orthologs in scales of photonic crystal generating species.

One can easily imagine that Rab proteins hold a key to reorganizing cellular membrane compartments involved in nanostructure morphogenesis. In defining compartment identity, the cell defines where enzymes, structural components, secreted macromolecules, etc. are sent and maintained.

1.8.5 Photoperiodism and structural color

The night-day cycle and seasonal variation are environmental changes born from the passage of earth through its daily revolution about its axis and the overall orbit of earth around the sun, respectively. Given that these rotations create changes in local surface energy flux provided by the solar radiation both diel and seasonal variation result in marked changes in temperature and light. As ectotherms and prey items, Lepidoptera have differentially adapted to these patterns to take advantage of the warmth and brightness of the day or the cover of darkness.

Insects as a whole have evolved circadian clocks which provide synchronization to the 24hr cycle of the earth. One of the interesting observations made in multiple species of insects is that chitin deposition alters in its orientation depending on the time of day (191,192). Further, recent evidence of the manipulation of circadian clock transcripts suggests that they also feed into certain aspects of seasonal cycles (193). The exoskeleton of insects is quite similar in principle to fiberglass. Chitin, a polymer of the disaccharide (B1->4) N-Acetylglucosamine, is secreted from the apical plasma membrane of epithelial cells. ~20 individual strands of chitin arrange into a "crystallite" fiber through intermolecular hydrogen bonds (194). The crystallites are encased in

various protein matrices depending on the region and function of the body part. Together the chitin and its matrix are referred to as the cuticle. In most cases following a molt, an insect will continue to secrete cuticle in a layered way. While chitin crystallites in any given layer are aligned in parallel, in successive layers they may be laid down in parallel or at predictable rotation angles within the plane of the secretion (forming a pattern called a helicoid). When this process was observed in locust legs, Neville et al. found a correlation between this secretion pattern and the circadian rhythm where during the day, successive layers of chitin are laid down in parallel, but when switched to dark, the pattern became helicoidal (195). He was able to demonstrate that this was a locally controlled switch in locusts, as blinding the eyes and ocelli of the locust produced no change from normal, but painting over a region of the cuticle to prevent light stimulation at the site of deposition was capable of altering the pattern and switched to an entirely helicoidal deposition (195).

This is particularly interesting for structural coloration as the elytra in some beetles utilize a cholesteric chitin deposition to create a multilayer with circularly polarizing activity (196). Would this necessarily play a role in scale development? It is unclear if light could penetrate deeply enough into the cuticle to drive such a deposition, but perhaps the same mechanism of deposition could be genetically entrained on some other cycle separate from direct stimulation.

1.9 Potential mechanisms for creating regularity

Biological morphogenesis mechanisms are remarkable in their ability to be robustly capable of reproducing forms. Ask any Sierra Club member that comes across poison ivy how they knew not to touch it and they will tell you it was the shape and clustering of the plant's leaves. (Arguably, it's the same robust morphogenesis coupled to biochemistry that has made the cannabis leaf an iconographic representation of counterculture.) Despite this robustness, close analysis of the accuracy of the symmetry in a face or across multiple *Drosophila* wings shows that it is, at best, limited to (the still impressive) width of a cell ~5um in the latter (197). However, variation on the order of 5um is still far too large for structural color to be reproducible in most instances.

In the puddles of rainy days, oil-slick thin films swirl in randomized rainbows, pinwheeling like animated novelty lollipops for the simple reason that the oil has no control over its thickness – quite unlike butterflies using the same optical tricks. It is rare to think of nature as morphologically exacting – computers, automobiles, and any other product that requires very precise tolerances do not use the reaction-diffusion systems that biology uses to make its products. Among artists, shapes that are soft and without symmetry are classified as "organic", suggesting they've arisen from nature's palette. Even among biologists, there is a sense that life is robust precisely because it must overcome being and existing in a sloppy, unpredictable amalgam of too-many-moving-parts – this is a far cry from the industrialized perfectionism of welding robots and CNC milling machines. But, held implicitly in the equations for producing structural colors is the thrilling concept that there must be regularity and uniformity in the nanostructure's composition and morphology for a color to be made. And therefore, there must be mechanisms that allow

nature, sloppy in tooth and claw, to regiment itself into building regular structures, at regular intervals, with uniform material properties. I will explore some of these ideas here.

1.9.1 Secretion clocks

As mentioned previously, the majority of materials providing refractive index contrast are sugar polymers secreted by epithelial cells. Multi-layer and thin-film structures are therefore the product of secretion. In addition, multi-layers must alternate their secreted films with a layer of a contrasting material. Since the thicknesses of these two types of layers should remain constant for color production, a reasonable hypothesis for their creation is the idea of a deposition clock. A few examples from the literature highlight the possibility for such a mechanism existing. The chelicerae of one Jumping Spider (Salticidae) have green structural color (198). TEM imaging of the chelicerae's cross section indicated that there were 85 layers of alternating high and low index of refraction materials. Modeling of a structure using the thicknesses of the high and low refractive index layers suggested that there should be nearly 100% reflectance from a multilayer with that many elements. Upon adding a term for extinction coefficient, the multilayer modeled, reproduced the observed spectrum with only 10 layers. In addition, more layers provided no additional reflection because light was absorbed completely before reaching further into the chelicera (198). It is therefore reasonable to assume that since additional layers provide nothing more to the reflection, they either exist for improving rigidity and robustness to the stresses of prey envenomation or are merely a byproduct of cellular response during the chitin secretion cycle.

1.9.2 Bio-block-copolymers

Mentioned earlier, block copolymers are comprised of physically tethered polymers with incompatible physicochemical properties. Experiments have shown that boundary conditions can force the adoption of different morphologies to reduce the amount of entropy in the system. These morphologies include pillars, laminae, and gyroid structures like those seen in many butterflies. A biological block-copolymer could explain how gyroids are often found in butterflies with internal multilayer baring relatives.

1.9.3 Molecular rulers

A molecular (or protein) ruler is a molecule that provides spatial information to the cell that uses it – best demonstrated, in my opinion, by modifications to the "ruler's" length that result in subsequent and proportional shifts in the cellular details reliant upon the molecule. For the purposes of this discussion, I use this strict definition of molecular ruler in order to separate out those molecules that provide spatial information from those that only provide function with some particular domain length (i.e. ROCK2 (199)). The best example to date of a molecular ruler is the *Chlamydomonas* flagellar complex composed of FAP59 and FAP172. These proteins interact directly with one another and the microtubule doublet through several coiled-coil domains regulating the periodicity of dynein arms as well as accessibility of the radial spoke proteins that connect circumferential microtubule doublets to the central doublet (200). Loss of either FAP leads to immobile flagella and increased periodicity of radial spoke assemblies/loss of dynein arm binding. The key experiment was to show that duplication of coiled-coil sub-domains led to predictable increases in protein length and in turn shifted the periodicity of radial

spokes from 96nm in wild type to 128nm or 120nm depending on the domain that was duplicated. The immediately important observation in this is that proteins exist that can determine cellular architecture on length scales relevant to structural color, and that these through modification (here duplication) can produce shifts in the periodicity. Whether, such a mechanism will bear out in biological color remains to be seen, but it certainly represents a mechanism worth keeping in mind during experiments.

1.9.4 Elastic buckling

One of the earliest attempts at explaining how regularity could come about was Helen Ghiradella's 1974 hypothesis of the scale ridges arising from elastic buckling in the plasma membrane (54). Buckling occurs when a stress is applied to a material that responds to the stress by bending perpendicularly to the direction of the force. Pulling on a rubber glove will cause it to wrinkle out of the plane of the latex creating a sine wave in the plane. The sine wave will propagate evenly across the plane of the latex and as such, buckling can be thought of as a purely passive physical consequence leading to regularly spaced peaks and valleys. A similar buckling concept has been demonstrated for the morphogenesis of the villi chicken gut (201).

1.9.5 Genetic control of the physical properties of the scale

Many of the ideas I have presented rely upon the material properties of the cell and the cell membrane (i.e. buckling morphogenesis). This makes it tempting to simply point to physics and thermodynamics as what decides how the nanostructures producing a structural color form – not genetics. As a geneticist, however, I contend that since in the short-term, structural color remains constant from generation to generation – that is, it is the blue of a Morpho species is inherited – it is reasonable to assume that there must be some genetic encoding for the nanostructure. Even if it were proven to be true that the regularity of a nanostructure was entirely driven by passive assembly, it would be foolish to ignore the genetics of the organism. The physics-only viewpoint fails to recognize that the material constituency of the plasma membrane is dictated by the organism's genetics. For example, the level of cholesterol in the plasma membrane may determine the bending rigidity of the membrane, and so determine the extent of buckling and the spacing of the nanostructure (202–204). Moreover, the behavior of the actin cytoskeleton is also highly cell type specific (inner ear hair cells vs. macrophage for example) and can influence the physical properties of membranes (205). Given that both the membrane and actin appear to be important to nanostructure development, and that alleles in proteins can modulate actin dynamics and lipid metabolism, it seems reasonable to assert the idea that even purely physical mechanisms of nanostructure development will be genetically encoded.

1.10 Summary

Throughout the dissertation, I have sought to draw a line between the photonic properties of an organism and how this influences the evolution of populations via color. This thread finds its fulcrum in the cell biology of a large unicellular epithelial projection known as a scale. The repeated evolution of structural coloration within independent lineages of butterflies and the diversification of structural color between species is full of fascinating

biological questions. From this point forward I will present evidence that pigmentation is as crucial for structural color as the structure itself. Saturation and hue derived from a nanostructure are mutable via pigment manipulation alone. I also demonstrate that F-actin dynamics are responsible for the formation of some structures and perhaps manifest changes between species. Lastly I share some of the steps I and others have made toward making real-time live imaging of butterfly scales during their development, as well as my thoughts on what are open questions waiting to be answered.

Figure 1.1 The scale of nanostructures and scales

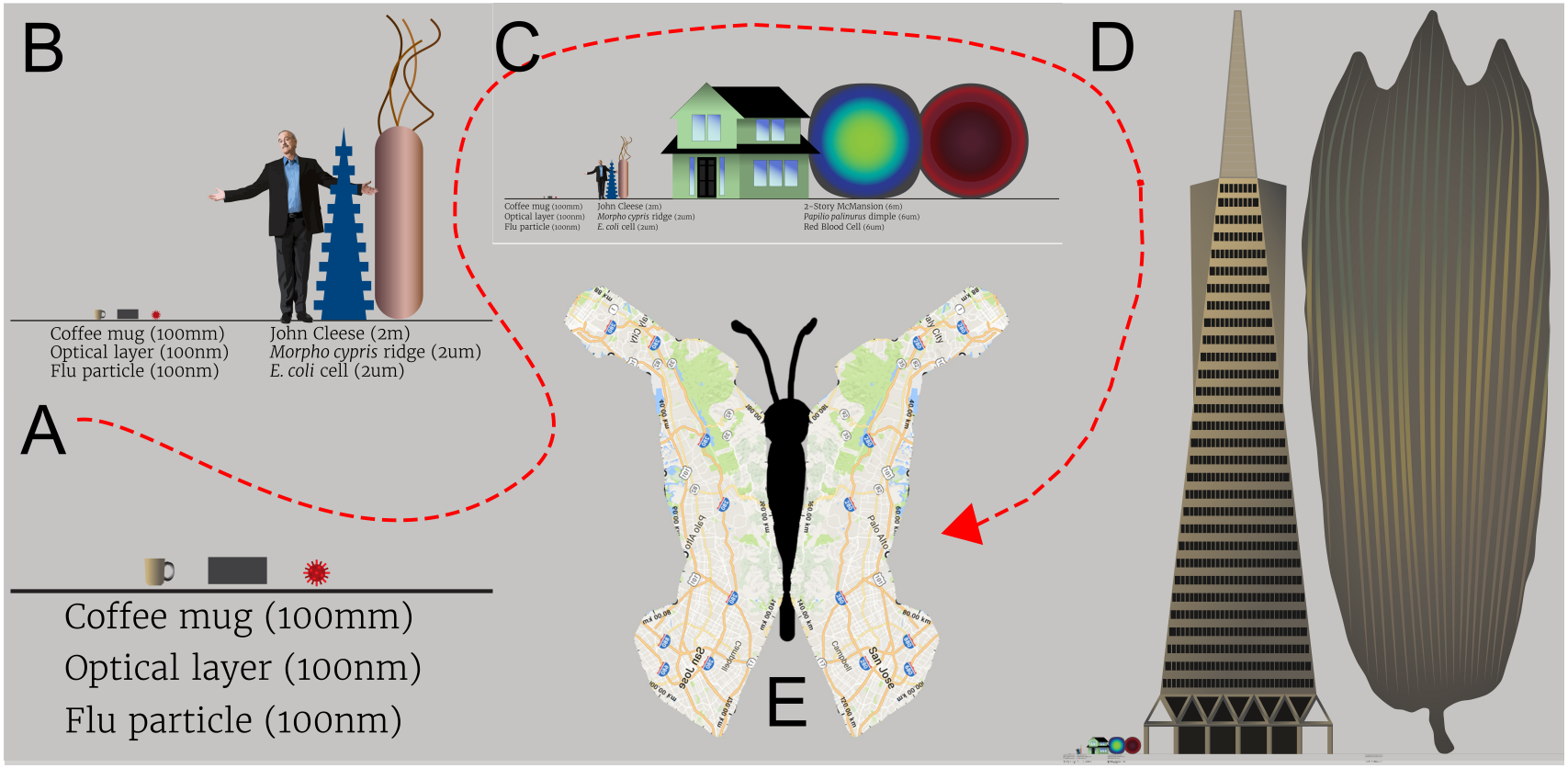

This diagram gives a sense of scale for the small size of photonic nanostructures and the large size of the scale cells that carry them. **A** Nanostructures in most butterflies are about 100nm thick – the diameter of a flu virus particle. If we establish a conversion that sets a nanometer equal to a millimeter, then a 100nm optical component is about the size of a coffee cup's height ~10cm. **B** maintaining this conversion, a typical 2um tall multilayer (such as is found on the surface of a Morpho) is about the size of a tall man at 2m. **C** The distance across a parabolic reflector found on *Papilio palinurus* or *Papilio ulysses* at 5um is as tall as a 2 story house ~5m **D** At this scale, a typical unicellular adult scale cell is 260um (compare this to a red blood cell at 5um or an E. coli at 2um) about the size of a skyscraper like the TransAmerica Pyramid (260m). **E** Finally, when an optical layer is the size of a coffee cup, the surface area of a typical butterfly is about 6400km^2 counting dorsal and ventral surfaces – about 4 times the size of the San Francisco peninsula.

Figure 1.2 Diversity of color patterns among *Ornithoptera* males derives in part from structural differences

The *Ornithoptera* offer an interesting example of how evolution of sub-cellular organization within unicellular scale nanostructures and pigmentation can result in changes in photonic interference that in turn influence ecological interactions. Given the island specific structural coloration and obvious sexual color pattern differences (males on left of upper panel, females on right) it is tempting to speculate a few means of speciation. 1) Males with coloration distinct from an ancestral population may land on a new island and select for females who prefer that color. Or *vice versa* 2) females with preferences differing from the ancestral population may pull male coloration away from the ancestral population. In hypothetical, a mix of selection and drift acting upon genetic elements determining cellular development result in shifts of photonic interference and ultimate result in the birth of new species. **Top** composites of males and females of several species and their location within the Indonesian archipelago. From left: *O. croesus*, *O. aesecus, O. goliath, O. priamus,* and *O. urvillianus*. **Bottom** Images of scales from the males of *O. urvillianus* (blue), *O. aesecus* (aqua), *O. priamus* (green), *and O. croesus* (orange). Scale bar 250um.

Figure 1.3
Refractive index contrast and geometry in a simple thin film produce structural color

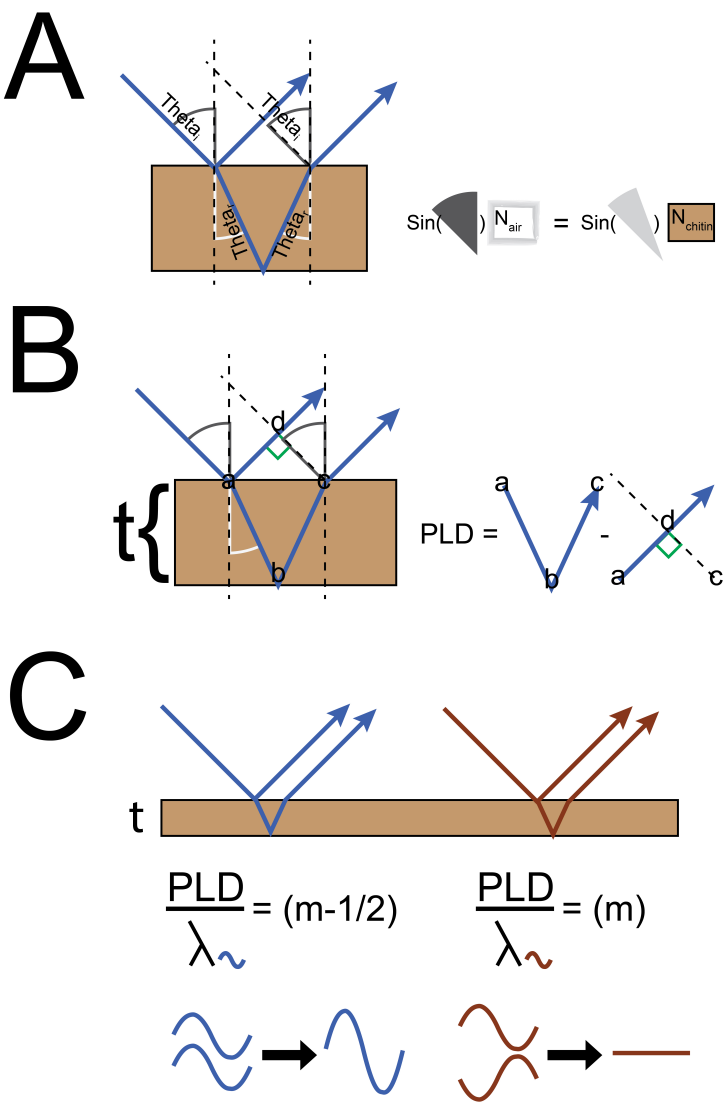

A The contrast in refractive index (N) between a hypothetical chitin thin film and surrounding air bends incident light. We can predict this angle using Snell's law:

$$\sin\theta_{incident} * N_{incident} = \sin\theta_{medium} * N_{medium}$$

B Knowing thickness of the film (t) and the angle an incident beam travels through the thin film (θ_{medium}) allows us to calculate the path length difference (PLD) traveled by the beam by subtracting the reflected beam's path (AD) from the refracted beam's path (ABC) at a point (D) in the reflected beam normal to where the refracted beam emerges (C) from the thin film. **C** Incident light of different colors (blue vs. red rays) will interfere differently as a function of their wavelengths when angle of incidence, thin film thickness, and refractive index contrast are held constant. If the PLD is an integer multiple of the wavelength, the interfering photons will be perfectly out-of-phase and deconstructively interfere **(red sine waves and straight line)**. If the ratio of the PLD and wavelength considered is equal to an integer minus one-half, the photons are perfectly in phase and will constructively interfere, amplifying their apparent strength **(Blue sine waves)**. In this way incident white light gets biased in its apparent coloration despite all wavelengths interacting with a single structure of a fixed thickness.

Figure 1.4 Orientation to scales and their nanostructures

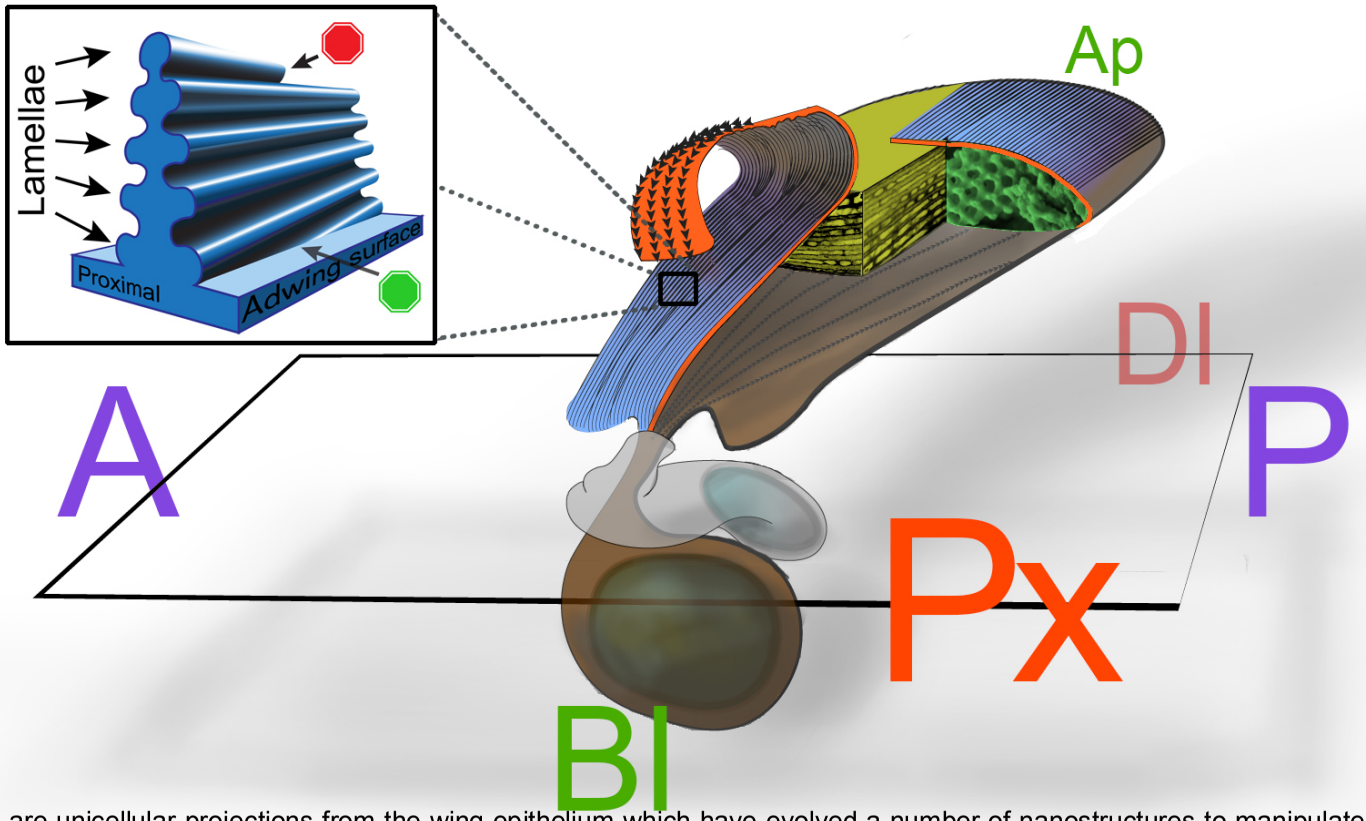

Scales are unicellular projections from the wing epithelium which have evolved a number of nanostructures to manipulate light reflection (blue upper surface represents Morpho-type ridge based multilayers (see inset), yellow multilayer represents Urania-type internal multilayer, and Green SEM inside scale represents 3D photonic crystals like gyroids). **Inset –** Morpho-type reflectors are made of layers of lamellae that emerge at an angle relative to the surface of the scale and so start and stop in various positions along the length of the ridge (**green and red octagons**). In cross-section, Morpho-type reflectors often appear like Christmas trees. Scales also have axes of symmetry that are variously described through the literature. I use a combination that is based in relation to the axes of the wing and the developing scale. An adult scale extends from the proximal to the distal margin of the wing; developmentally the tip of the scale is an apical outgrowth from the wing epithelium. As such I will refer to the tip of the scale as apical (**Green Ap**), and regions closer to the wing surface as relatively more basal **(Green BI)**. If one were to stand a scale perpendicular to the wing, it would have its flat faces (ab and adwing) pointing toward the proximal or distal aspect of the wing **(Red Px&DI)**, respectively. This suggests that differences in upper and lower lamina may derive from differences in proximodistal specification – the PCP pathway. Finally, when these axes are set, the width of the scale falls along the anteroposterior axis **(purple A&P)** of the wing.

Figure 1.5 Demonstration of angle dependence in structural coloration

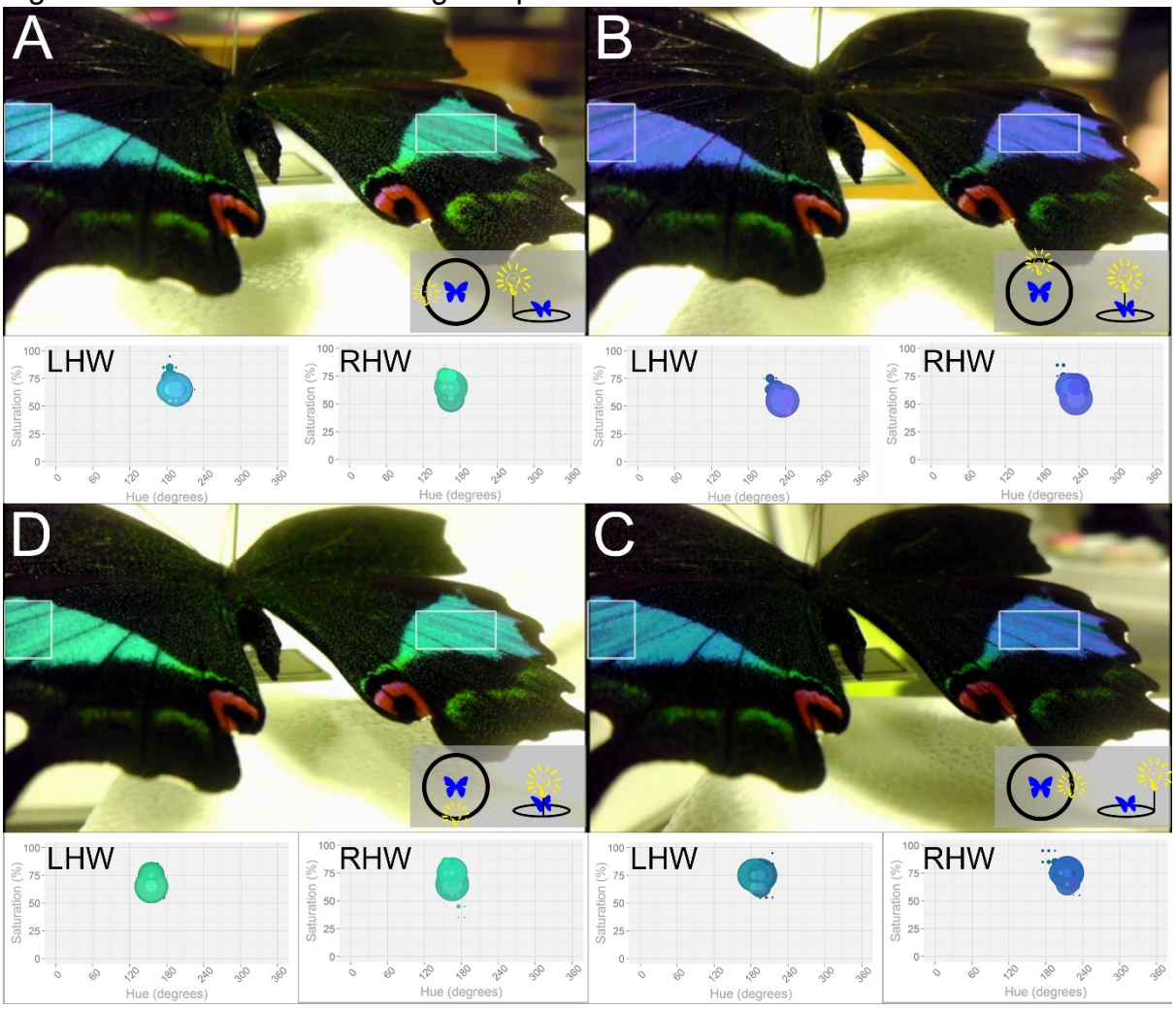

Frames of a movie depiciting the iridescence of *Papilio karna* as incident light changes position relative to the butterfly and the camera. Indicators in the lower right corner of the picture show the relation of the light source to the butterfly. White boxes on the hindwing demarcate regions of interest (ROI) upon which color information was extracted and plotted in each of the graphs below the image. These graphs indicate the left hindwing (LHW) or right hindwing (RHW) ROI. Graphs plot color upon a cartesian coordinate system using degrees of hue on the X axis, saturation of the hue on the Y axis, and prevalence via bubble size. The color of the bubble corresponds to the color plotted. **A –** light comes from the left, **B –** light comes from the anterior side of the butterfly, **C –** Light comes from the right, **D –** light comes from posterior side

Figure 1.6 *Drosophila* chaetae: a hypothesis generator for butterfly scales

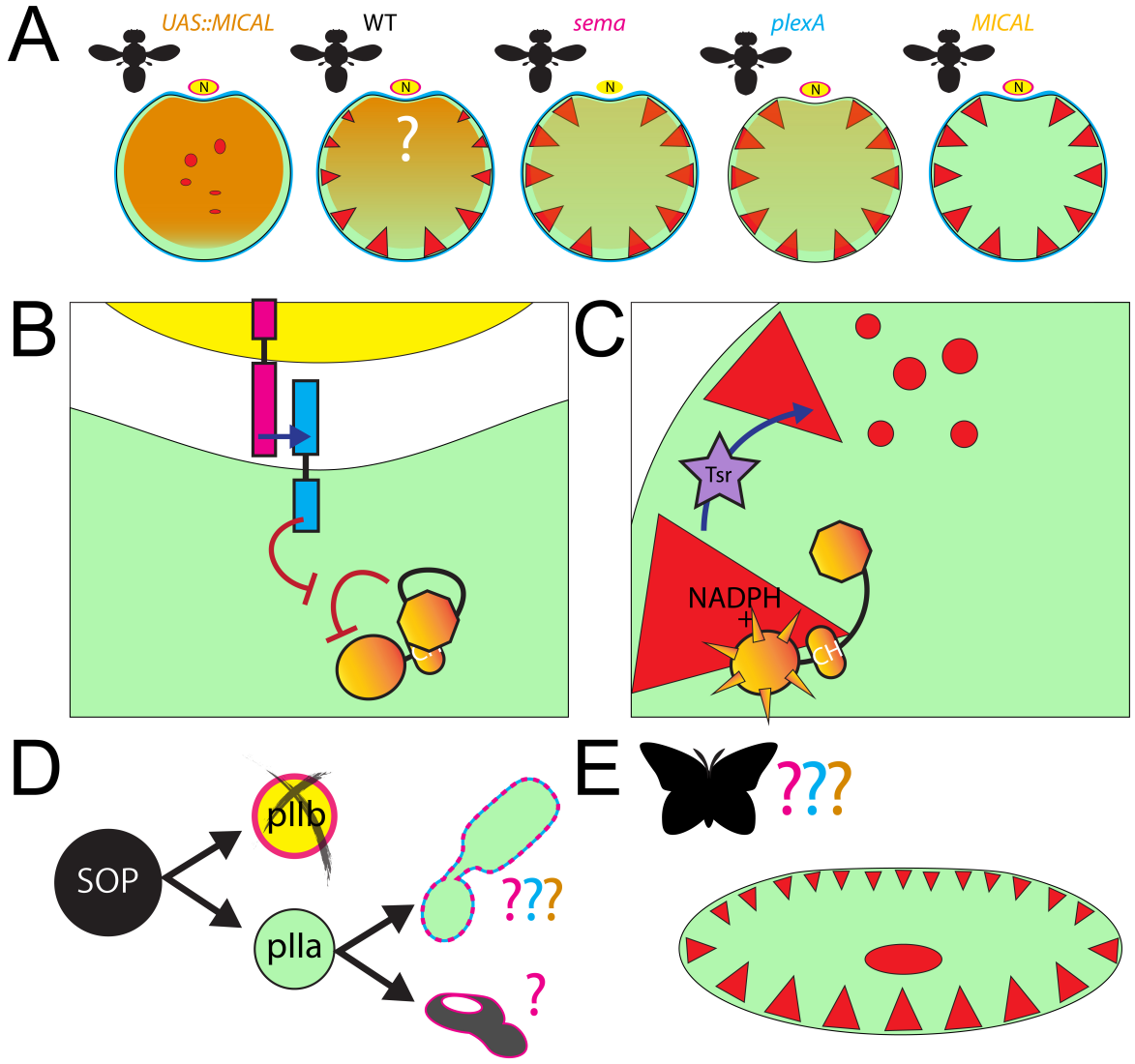

Drosophila bristles are homologous structures to butterfly scales with many similarities and differences. Using existing studies done on bristles may illuminate developmental questions in butterflies with direct relevance to structural coloration. **A** Genetic screens and manipulations in *Drosophila* bristles have identified the non-canonical redox protein MICAL (**orange**) as being important for asymmetry in the size of actin bundles **(red triangles)** around the circumference of *Drosophila* bristles (**seafoam circle**). This asymmetry has been suggested as a driving force for the curvature of the bristle and requires Semaphorin (**pink**) signaling from the associated nerve cell **N** via PlexinA (**blue**). **B** Semaphorin signaling received from nerve cell via PlexA protein relieves autoinhibition of MICAL within the bristle. **C** Activated MICAL (**spiky orange**) directly oxidizes a methionine residue within the actin protein leading to destabilization in concert with Twinstar (**lavender star**) activity. **D** In *Drosophila* the destabilization occurs in a gradient that is highest near the neuron. However in Lepidoptera, the pIIb lineage leading to the neuron dies prior to the specification of the neuron. **E** Despite the death of the neuron butterflies still show a decreased actin bundle diameter on the proximal (abwing) surface. One is left with the question of how or if a similar Sema/PlexA/MICAL pathway exists (**colored question marks**) in scales or if the difference is merely a consequence of proximodistal patterning. Alternatively the socket (**D - dark grey with pink**) expresses Sema in leps, replacing the neuron as a signaling center.

Chapter 2

Melanization is Necessary for High Saturation of Structural Blue in Morpho Butterflies

2.1 Introduction

Interest in the origins of species is a common source of inspiration among biologists and the public alike. Darwin, Wallace, Muller, and Bates all drew evidence for evolution from the many color patterns of butterflies during the years surrounding the publication of Darwin's treatise on the subject (4,5,17,206,207).Since the modern synthesis, Lepidoptera have remained influential in understanding evolutionary mechanisms, largely by focusing on wing pigmentation (13,23,28,30,208–214). Given the large number of species, the diversity of conspicuous color patterns, and the biogeographical relationship of those color patterns with butterfly species/populations, it is no surprise Leps have been important to evolutionary studies.

Lepidopteran wing patterns are made by the juxtaposition thousands of individually-colored, extensively modified, wing epithelial cells known as scales. This suggests that for a butterfly wing to display a color, its scales must produce that color. Therefore, a thorough understanding of how color evolves in Lepidoptera requires focus on how scales produce color at a cellular level.

Pigments are often considered to be the source of animal coloration and for the most part are enzymatically produced by proteins coded in the genome or taken up from the diet (109). However, it is rare to find animal pigments that reflect short wavelength colors like blue, green, or violet – butterflies included. The majority of butterfly pigments are limited to black, brown, orange, yellow, red, and UV reflective, with occasional exception (109,215,216). The vast majority of violet, blue, and green butterflies owe their color to nanostructures built on the scales (43,110). Mechanistically, most nanostructures produce color by regimenting the phases of photons with similar wavelengths, creating constructive interference of some wavelengths and destructive interference in others (85,217,218). But destructive interference does not eliminate the reflected photons, instead it reduces their apparent intensity – biasing the reflection of white light toward an apparent hue. This is in contrast to a pigment that selectively absorbs photons based on their wavelengths – eliminating their reflection. Because structural colors are biased towards a color but still include photons of all wavelengths, structural colors are inherently less saturated than a pigment-based color.

It has been observed in histological sectioning and electron microscopy that organisms employing structural colors often deploy pigments or pigmented cells in close proximity to nanostructures. A multitude of studies suggest that organisms combine structural elements with dark pigments to enhance the saturation of their structures (34,38,51,65–79,81,82,216). When structures without underlying pigments have been studied, there has been a demonstrable peak of reflectance intensity according to the geometry of the associated nanostructure, as well as a baseline reflectance across the remainder of the

visible spectrum (75). By combining nanostructures and pigments animals receive benefits of both: the nanostructures selectively enhance particular wavelengths that are otherwise inaccessible by pigments, while the dark pigments absorb the majority of the nanostructure's baseline reflectance (Fig2.1). Yet, with few exceptions, no biologically relevant manipulation of pigmentation has been undertaken in structurally colored organisms (77).

Morpho species have been repeatedly suggested to use melanin to enhance the saturation of their structural blues, yet to date no direct manipulation of melanization has been undertaken (42,109,219,220). Morphos thus seem particularly suited for examining the role of melanin in structurally colored butterflies: the genus is well studied with an ever improving phylogeny, dead specimen are valued by collectors, living specimen are raised for display in butterfly houses, and principally important, among the species there are many shades of blue, as well as green, orange, and many white or nearly white forms. The presence of white species was particularly important to us as Yoshioka and Kinoshita have shown that the white bands of *Morpho cypris* were due to a lack of pigmentation (Fig2.1) (75). Moreover, the positions of the white species within the phylogeny suggest 1) they have likely arisen independently, 2) that it is a fairly simple transition from colored to white, and 3) that comparison of white species would highlight the biological commonalities/unique features they share. I hypothesized that exploring the biological mechanisms influencing the nanostructure/pigment interface in Morphos would provide a window into how pigments actually enhance structural coloration.

2.2 Methods

2.2.1 Low magnification imaging

Images of whole forewings were taken by scanning forewings from dead, dried museum specimen on an Epson Perfection V500 Flatbed scanner at high resolution (>1200 pixels/inch) in the presence of a DGK Digital Kolor Kard for color balancing. Close-up views of intact wings showing scales were taken on a Spot 15.2 64 MP Shifting Pixel Camera (Diagnostic Instruments, Inc.) attached to Zeiss Axiophot Compound microscope with a 10X objective. A 360 degree rotating stage allowed us to rotate the specimen relative to a fiber optic lamp with an approximate 45 degree angle of incidence. Single scale reflectance and transmittance images were taken at 20X on the same set up using the microscope's own light paths rather than the fiber optic. Single scales were removed from regions of interest by paint brush or flame-polished glass needle and were mounted on glass slides. Reflected microscopy took place without a coverslip, directly imaging the scales with light arriving at normal incidence. Images shown are focus stacked in Helicon Focus with the settings B,8,4. Transmission images were achieved by covering the scales with Zeiss F355 Immersion oil (n=1.518) and covering with a coverslip; these are not focus stacked. Pupal wing imaging for manipulations was done on a Zeiss LUMAR V.12 connected to a JenOptik ProgRes C14 plus camera or a Leica M80 dissecting scope attached to a Leica MC170 HD camera. The phenotypic series of eclosed animals was taken using a Canon D7000 with an AF Micro Nikkor 60mm lens attached to a RPS Studio CS-920 copy rail. Though imaged under the same conditions and settings, three images were stitched in Adobe Photoshop to capture the whole series.

2.2.2 Scanning Electron Microscopy

Museum specimen were prepared for SEM by cutting regions of interest out with a razor blade. To ensure solid conductance, the ventral surface scales were removed from this region by pressing it onto double stick tape and lifting away. The now naked wing membrane was then adhered to an aluminum stub via double sided carbon tape (both Ted Pella). For scales from *ex vivo* cultured wings, scales were removed from regions of interest using a fire-polished glass needle and placed onto stubs with carbon tape. For images of the color producing ridges, scales were broken using a sharpened tungsten probe. Following preparation, stubs were sputter coated with 10nm of gold and imaged using an FEI Quanta 3D FEG FIB scanning electron microscope.

2.2.3 Spectrophotometry

All spectrophotometry was performed using an Ocean Optics Flame microspectrophotometer (MSP) in reflected mode or transmission mode, which produced useful information for 870 unique wavelengths between 400 and 700nm. All spectra were the result of 10 averaged sequentially captured spectra and were set to a boxcar of 5 for smoothing purposes. For whole wing reflected spectrophotometry, the MSP was attached to a Leica M205 FA dissecting scope with lighting applied via fiber optic at a 45 degree angle of incidence and an azimuthal angle perpendicular to the long axis of the scales. White balancing was done on $BaSO_4$. For spectra shown, I relate the relative reflectance for ease of comparison. This was calculated by finding the maximum value in a spectrum and then dividing the all values across the spectrum by the maximum value and multiplying by 100. For transmission measurements, the MSP was attached to the Zeiss Axiophot with light applied normally from below. An area with dimensions 80umX80um, falling entirely within the scale, was sampled. The MSP was continually calibrated on regions of the sample without scales present. Spectra obtained were the average of 10 sequentially captured spectra, with a boxcar of 5. Absorbance spectra were calculated from these spectra by applying the transformation: $Abs=2-\log_{10}(Transmission)$. For bar plot comparisons of average absorbance, I first averaged the spectra of all samples considered, then I summed all values of absorbance across the averaged spectrum to create a single metric of comparison. And finally, I divided this sum but the number of unique wavelengths measured (870) to arrive at the average absorbance per wavelength. In all measurements, time of integration was set to the recommended 55,000-58,000 photon counts suggested by the manufacturers.

2.2.4 Image analysis

To obtain quantitative data from our images where MSP was not feasible, I wrote custom Python scripts inspired by Vijay Pandurangan's analysis of movie posters (221). I have graphically summarized the script in Fig2.13. In short, images were cropped to regions of interest (ROI) in Photoshop, which were then fed to the program. The software extracted hue, saturation, and value data from each pixel and, to allow easier visualization/quantification, binned the pixel's H,S,V into one of 36 hue categories, 10 saturation categories, and 10 value categories – reducing all possible input colors to one of 3600 colors. Running counts of binned pixel color data were tallied and a CSV file was output for each ROI. These data were then wrangled in R to produce plots and statistics.

2.2.5 Pupae

Pupae of *Morpho helenor peleides* were purchased from London Pupae Supplies (Denver, Colorado), maintained under ambient dark:light cycles at room temperature, and misted daily with tap water. As they were received as pupae I had no knowledge of when the animals pupated. For all *ex vivo* and *in vivo* experiments I tried to coordinate their ages by using pupae only after the eyes had pigmented. This was reliably the first body part to pigment and thus I could have some confidence that the animals were preparing to pigment elsewhere; more precise control was not possible.

2.2.6 Ex vivo *culture*

Based on results from Koch and Nijhout, I found that culturing in 3mL of 1X Grace's Medium (GIBCO) supplemented with 1X Antibiotic/Antimycotic (Sigma-Aldrich) and 2%(v/v) Fetal Bovine Serum (GIBCO) in a 35mm Falcon 353001 Tissue Culture dish reliably allowed for pigmentation (113,222–224). I refer to this as our standard (STD) medium. Dissection of pupae proceeded following eye pigmentation and took place in 1XPBS. I found that *M. peleides* rapidly, extensively, and non-specifically melanized in response to dissection. In order to reduce the non-specific immune melanization, the pupal wings were transferred into a dish of STD medium supplemented with 400uM phenylthiourea (PTU) (Sigma-Aldrich) for 20-30min. This eliminated immune melanization but had little impact upon scale specific melanization. For time lapse, multiple condition/inhibitor-rescue, and spatiotemporal experiments, STD medium was supplemented, as indicated, with stock solutions to a final concentration of 100uM 3-Iodo-Tyrosine (Sigma-Aldrich), 5mM L-Tyrosine (Sigma-Aldrich), 5mM L-DOPA (Sigma-Aldrich), and/or 5mM Dopamine (DA) (Sigma-Aldrich).

For spatial restriction experiments, TuffTag masks (Diversified Biotech) were patterned with a marker and cut using a scalpel. The wing was placed in medium and the mask submerged sticky side toward the wing. The mask was held in place using the lid from a 5mL snap-cap tube (Falcon) with the center removed (resulting in a donut shape). DA or L-DOPA were added to the medium and mixed thoroughly. To ensure the region of the mask opening received access to the drug, following mixing I pipetted medium into the region through the hole in the lid. Wings were incubated overnight.

For temporal control experiments, thin strips of Parafilm "M" (Bemis) were cut using scissors. As Parafilm would not stick to the dish following addition of the medium, I placed strips of cut Parafilm into the dry dish parallel to one another, and attached one end of the strips to the dish by applying pressure. Next, the wing was removed from the STD+PTU medium and quickly blotted dry on a Kimwipe (Kimberly-Clark) to remove excess medium. The wing was positioned under the Parafilm and the other end of the strips were adhered to the dish. Immediately 3mL of STD medium were applied to the dish before the wing could dry out. The medium was then supplemented with L-DOPA or DA as previously described.

With the exception of the TuffTag masked wings, all *ex vivo* cultured wings were kept at room temperature on a rocker set to 60RPM. At the end of the experiments, wings were washed several times in 1XPBS and then in diH_2O before being allowed to air dry thoroughly.

2.2.7 In vivo *injections*

I estimated the average volume of *M. peleides* pupae to be about 2mL. From previous experiments I found that pupae can tolerate injection volumes between 1/500th and 1/1000th the pupal volume (124). Accordingly, I prepared stock concentrations of 3IT and DA for 1000X dilution. When pupae had reached the black-eyed stage I injected 20uL of these stock solutions using a 26Ga ½ inch needle (Becton Dickinson) at the pupal cuticle suture between the 1st abdominal segment and metathoriacic segment on the dorsal side. Pupae were segregated based on what was injected and hung up to eclose. Following eclosion, animals were sacrificed and stored in glassine envelopes (BioQuip).

2.3 Results

2.3.1 Terminology and Survey

Throughout the paper I will use the scale anatomical terminology set forth by Ghiradella and Giraldo; I refer to observation of scales as abwing (developmentally proximal) if analyzing the side pointed away from the wing membrane, and adwing (developmentally distal) for the surface that faces the wing membrane (Fig1.5) (65,110). Lastly, I use the convention of cover and ground to describe the two types of scales that lie in adjacent rows on the wing. The former lie above the latter, and in Morphos the former tend to be transparent, sometimes being referred to as “glass scales” (225). Occasionally, the cover scales are greatly reduced, as in *M. rhetenor* and *M. cypris,* and do not cover the ground scales (see Appendix 2) (42).

Focusing at the scale level, I began by surveying regions from the adult wings of 16 *Morpho* species and 2 outgroup butterflies, *Antirrhea philoctetes avernus* (a member of the sister genus to *Morpho*) and *Appias sylvia* (Pieridae). In order to get a sense of pigment’s role in saturating structural color, I wanted to know what pigments and nanostructures were found in our specimen. I chose to use SEM to visualize the nanostructures, reflected light spectrophotometry to measure the colors being reflected, and single-scale transmission measurements in immersion oil (n=1.518) to assay for pigmentation level and absorbance profile.

The survey provided a great deal of information that I will not discuss in full (the summary of the survey is found in Fig2.10 with raw data found in Appendix 2). Rather, I have chosen to present three vignettes that are most instructive of pigment’s role vis-à-vis the structural elements. Further, these vignettes show that saturation variation coincides with pigment variation at three levels of ecological importance: the individual, within a single species, and between closely related species.

2.3.2 Within an individual: combinatorial method of pigmentation to blue variation

Morpho marcus major demonstrates the correlation of pigmentation with structural color at the individual level nicely. I found three regions of varying blue saturation: white, light blue, and dark blue (Fig2.2A,B). When I looked at single scales from these three regions I found that in all regions, both cover and ground scales had structures and reflected blue from their abwing sides (Fig2.2C-N’). What distinguished the regions seemed only to be pigmentation levels: the white region had pigment in neither the cover nor ground scales (Fig2.2D’,E’ & O,O’- black line), the light blue region had pigmentation only in its ground

scales (Fig2.2H',I' & O,O'- light blue line), and the dark blue region had pigment in both the cover and ground scales (Fig2.2L',M' & O,O'- dark blue line). Importantly, the level of pigmentation was nearly indistinguishable in all pigmented scales regardless of the region's color. When I removed only the cover scales from the light blue region, the uncovered ground scales produced a quality of blue indistinguishable from the dark blue region (Appendix 2). When I viewed the scales from the adwing side I found that all pigmented scales appeared gold, while unpigmented scales were bluish (Fig2.10, Appendix 2). Members of the *Deyrollia* sub-genus, to which *Morpho marcus* belongs, have been remarked upon because they have unique railroad track-like ridges made from a single lamella (42,86,219). Cassildé et al. remarked that they believed the majority of color came from the stacking of multiple scales in this clade rather than from the ridges (42). While I am unable to falsify this hypothesis, I believe that the lower lamina functions as a thin-film reflector based upon the peaks I see only in white and light blue regions (the only regions where the lower lamina can produce a reflection visible from the abwing surface). The shift in saturation between the white and light blue regions is likely a result of a combination of the saturated blue produced by the ground scales' multilayer with the reflection produced in the cover scales' multilayer and/or stacking. Further, I believe our data scales suggest that the ridges do function as a multilayer as evidenced by the blue color reflected by the adwing surface of pigmented scales. In these scales, the effects of stacking would be negligible due to their high absorbance and the attenuation of lower lamina reflections. From these observations I concluded that *M. marcus* utilizes a combinatorial strategy of dark pigment in a spatially-restricted manner across a field of cover and ground scales featuring more-or-less homogeneous structural elements to create multiple shades of blue.

2.3.3 Within-species variation: continuous variation in concentration and ventral pigmentation contribute to structural saturation variation

In our second vignette, I have focused on the multiple shades of blue found within *Morpho godartii* sub-species: the dark blue *M. g. didius* (Fig2.3A), the intermediate *M. g. assarpai* – dark form (Fig2.3F), and the pale blue *M. g. assarpai* – light form (Fig2.3K). As I saw in *M. marcus*, the three shades were indistinguishable in nanostructure morphology (Fig2P-R'). It was only when I began to look at transmission spectra that I found differences. All three specimen lacked pigmentation in the cover scales (Fig2.3C',H',M',T), something originally seen in *M. g. didius* by Vukusic et al. (225). I hypothesized that I would see a decreasing concentration of pigmentation present in the ground scales correlating with the decreasing saturation of blue exhibited by the specimen. I was then surprised to find that while *M. g. didius* did in fact have the most pigment (Fig2.3D',T'-dark blue line), the two forms of *M. g. assarpai was* indistinguishable (Fig2.3I',N',T'-light blue and black lines). It was only when I then assayed the pigmentation levels of the ventral scales that I found the light form of *M. g. assarpai* was significantly less absorbent than the dark form (Fig2.3E,E',J,J',O,O',U,U'). This was in agreement with modelling done by Yoshioka and Kinoshita that suggested pigmentation in either the dorsal or ventral scales would be sufficient to improve saturation of structural coloration (75). While their focus on *M. cypris's* did not include a direct test of their model, as no regions of *M. cypris* with white dorsal scales and dark ventral scales were tested, I believe that these data provide supporting evidence.

2.3.4 Between-species variation: More than one way to skin a former caterpillar

In the last vignette, I compared three closely allied species: the prominently blue *Morpho helenor peleides* (Fig2.4A,P- dark blue line), a white morpho with a decidedly blue sheen, *Morpho epistrophus catenarius* (Fig2.4E,P – light blue line), and the purely white *Morpho polyphemus* (Fig2.4I,P – black line). Until recently, there has been some speculation that *M. polyphemus* and *M. epistrophus+M. iphitus* were sister groups, but their isolated geographic distribution of Mexico and Atlantic forests of Brazil respectively, left a great puzzle to be solved (219,226). Alternatively, it was possible that these were independently evolved phenotypes. I believed that in comparing the three species that some light could be thrown into how these white phenotypes have evolved.

As expected from the previous findings, the cover and ground scales from both white species were lacking in pigments (Fig2.4G'',H'',K'',L'' & Q,Q' – light blue and black lines). In *M. h. peleides* (Fig2.4C'',D'' & Q,Q' – dark blue lines) I found that the cover scales were clear and the ground scales contained pigments in agreement with both Cassildé et al. and Ding et al. (42,227). Further, when I visualized the structures of *M. h. peleides*, I found that both cover and scale had multi-lamellar ridges, though with fewer lamellae per ridge than the *godartii* specimen (Fig2.4M,M'). I found that *M. e. catenarius* also had multi-lamellar ridges on both cover and ground scales (Fig2.4N,N'), though significantly reduced in lamellae/ridge. This was in contrast to *M. polyphemus* which still had ridges but showed nothing resembling a multilayer (Fig2.4O,O'). On the whole, the *M. polyphemus* scale was reminiscent of the strictly pigment-based, distal black scales found on *M. h. peleides* (Appendix 2).

When I looked at the ab- and adwing appearance of the species, I found that *M. h. peleides* cover scales had a distinct blue sheen when seen from either side (Fig2.4C,C'), in contrast to the ground scales that showed a dark saturated blue when viewed from the abwing surface (Fig2.4D), and a gradient of orange, blue and violet when viewed from the adwing side (Fig2.4D'). The adwing colors cannot be seen from the abwing side suggesting that they are attenuated by the internal deposit of pigments. This is similar to many other species' pigmented scales which had adwing colors that were different than the color of the region they originated in suggesting that internal pigmentation serves broadly to inhibit lower lamina reflections (Fig2.10, Appendix 2). The cover and ground scales of *M. e. catenarius* were similar in shape and reflection to that of *M. h. peleides'* cover scales (Fig2.4G,G',H,H'). While I cannot rule out the influence of the reduced multilayer on *M. catenarius* as a source of coloration, it appeared to us as though the color emanated evenly from the lower lamina. In either case, it would seem that the blue sheen seen on the wings of *M. catenarius* is thus due to the lack of pigmentation desaturating the reflection from either or both the ridges and lower lamina. This is in contrast to *M. polyphemus* cover and ground scales, which have an adwing reflectance similar to that of the non-structurally colored black scales and the blue ground scales of *M. h. peleides*: an obvious orange, blue, and violet constituency (Fig2.4K,K',L,L'). Together, *M. polyphemus'* flat reflectance profile is likely due to the lack of multilayer reflectors but the possession of a multi-colored lower lamina, which is similar to what has been described in white scales of the butterfly *Argyrophorus argenteus* (228).

Together I hypothesize from this analysis that *M. polyphemus* and *M. epistropus+M. iphitus* were born from independent origins of white. The lineage leading to *M. e. catenarius* likely lost pigmentation, desaturating the structural color of its ancestor. Though it has retained a multilayer and a blue lower lamina it is possible that the lack of pigment is leading to the gradual degeneration of the multilayer, as indicated by its smaller number of lamellae per ridge compared with the majority of blue Morphos. In the lineage leading to *M. polyphemus* it seems that the ridge multilayer was lost entirely. Moreover, given its similarity to unstructured, pigmented scales on *M. h. peleides* (Appendix 2), one hypothesis is that the patterning and differentiation programs for a "non-structural scale" program has been expanded while pigmentation has been lost.

2.3.5 Pigmentation manipulation in living organisms

I, as others have suggested, was convinced of the importance of pigmentation to structural color saturation, and felt that direct manipulation of pigmentation pathways could provide an understanding of how the structural variation I saw in the survey could be manifested. Several predictions fall out of the survey: 1) a single structure should be sufficient to produce many shades of a color 2) spatial control of pigment may be sufficient to produce structural color variation 3) varying levels of pigment alone should be sufficient to produce multiple shades of a color and 4) pigments may purify a structural color by isolating the reflection of the lower lamina of a scale from the abwing view. Manipulations of pigments in living tissues have been performed in butterflies previously by several groups, however no groups have sought to use the techniques to approach these questions about structural color (113,223). Fortunately, *M. h. peleides* is commercially raised for display in butterfly houses and living pupae are readily available for experimentation.

2.3.6 Ex vivo *culture of pupal discs suggests melanin is the pigment and necessary for blue coloration*

To start, I wanted to ensure that I could reproduce the *ex vivo* pigmentation results previously demonstrated by Koch and Nijhout, and to positively confirm that melanin is the dark pigment as is commonly believed. This latter point I believed was important as other pigments are known to be capable of producing a dark brown color, such as ommochromes (which likely make up the reds, oranges, and perhaps yellows of Morphos) (Fig3.19) (109). Case-in-point, as people have actually started to investigate the molecular basis of spider pigmentation, genetic evidence mounted on the side of ommochromes until recently, when advanced spectroscopy suggests melanins (229). I decided that determining the type of pigment used by the Morphos was a critical point to make.

I approached this by culturing *M. h. peleides* pupal wings *ex vivo* in dishes containing Grace's medium supplemented with 2%FBS and antibiotic (STD Medium) just before the onset of body pigmentation (cued off of the onset of eye pigmentation). I found that pupal wings cultured in STD medium slowly melanized with a concurrent appearance of structural blue (Fig2.6A Left Kymo,F). Wings treated in the same way but supplemented with the immediate precursor to melanin, dopamine (DA), pigmented and became blue in <1/3 the time as wings without the dopamine (Fig2.6A Right Kymo,G).

I wanted to further confirm melanin as the pigment and so I cultured pupal wings *ex vivo* with and without melanin inhibitors and with or without melanin precursors. I chose the Tyrosine Hydroxylase (TH) inhibitor 3-Iodo-Tyrosine (3IT) to disrupt the melanization process. 3IT disrupts the melanin synthesis pathway at the first step, the conversion of L-tyrosine to L-DOPA (230,231). Therefore, I expected that if melanin was the pigment, and if it was necessary for structural saturation, wings cultured in the presence of 3IT would fail to pigment and fail to turn blue. Moreover, I expected that wings supplemented with L-DOPA or DA in the presence of 3IT would rescue the block. This is what I found.

In non-3IT supplemented cultures of wings from the same animal but cultured in different conditions, all wings pigmented and turned blue (STD n=6, STD+Tyrosine n=6, STD+DOPA n=6, STD+DA n=6). Those supplemented with DA pigmented/turned blue first, followed by DOPA, then Tyrosine and STD medium alone (Fig2.5A). Conversely, in 3IT incubated cultures I found that wings never pigmented/turned blue unless supplemented by L-DOPA or DA (Fig2.5C) (STD+3IT n=8, STD+Tyr n=8, STD+DOPA n=8, STD+DA n=4). Critically, regions that are typically white spots along the margin of the forewings remain white (Fig2.5A,C forewings; compare with Fig2.4A), suggesting that pigmentation was a specific and cell-autonomous activity of the scales. I further analyzed the pigmentation of scales from 3 experiments and found that in blue regions, ground scales were the only scales to pigment, and only if 3IT was absent or if 3IT and L-DOPA or DA were present (Fig2.5B,D right most columns, Fig2.5G). In regions that were black, both cover and ground scales pigment when conditions allow blue regions to pigment (Fig2.5B,D left two columns). I was able to analyze structures of scales from wings and found that the overlapping lamellae constituting the Morpho-type reflector appeared unaffected. However, I found some instances of 3IT treated scales without rescue having a collapse of the ridge, as if the Christmas tree had been felled (Fig2.12). As I show later, this phenomenon seemed to be limited to *ex vivo* experiments, but perhaps hints at a developmental importance for Tyrosine metabolism in structure integrity. In sum, these data confirm the long held suspicion that melanin is the pigment present in Morphos. Moreover, through the direct manipulation of pigmentation in a region known to be structurally blue, I show conclusively that presence of melanin is necessary for structural purity.

2.3.7 Spatially restricted melanization leads to restricted saturation within a wing

Though the previous experiments suggest that pigmentation is necessary for color saturation, it was theoretically possible (considering the felled-tree phenotype) that the inhibitor was damaging other processes where the Iodinated-Tyrosine was incorporated. I sought to eliminate the need for 3IT addition by creating a physical block that limited the access of a small region of a wing to the medium. I was able to do this by anchoring a TuffTag mask over the pre-pigmented wing and then adding DA to the medium (Fig2.7A-C') (n=8). The mask precluded the DA from reaching the underlying scales preventing their melanization, this was confirmed by assessing the absorbance of the scales from 5 experiments (Fig2.7J).

To get a sense of how structural coloration was affected by this treatment I adjusted the angle of lighting incident upon the treated wings. In so doing, I was able to illuminate the structures in both DA exposed and DA naïve regions (Fig2.7C'), and by analyzing regions

of interest (ROI) I was able to conclude that, indeed, the colors were of the same hue but differed in their saturation (Fig2.7D-E). There was clearly structural color being produced when single scales were imaged in reflected light, though there appeared to be some subtle change in color particularly between the ground scales (Fig2.7G,I). Again, while the lamellae of the ridges appeared normal, there was evidence for felling of the ridge in both exposed and non-exposed regions. This seems to suggest that it is not pigmentation that is required for ridge integrity but could instead be due to the conditions of the culture or during preparation for SEM. Moreover, as the blue color clearly exists in the samples, I believe this suggests that the structures were still functional during our assays. In total, this provides evidence that a scale can produce multiple shades of structural color by varying the pigmentation underneath a nanostructure. Further, these data recapitulate the within-individual variation of *M. marcus* and the previously studied *M. cypris*.

2.3.8 Temporal restricted DA access produces graded saturation variation

It was apparent that spatial restriction of pro-melanization factors could modulate the saturation of color reflected. The I data collected from *M. marcus, M. polyphemus, M. epistrophus, M. peleides* and that previously seen in *M. cypris* suggested that pigment could influence apparent color in a binary way – either it was present and a region appeared saturated or it was absent and was desaturated (75). Our data from the sub-species of *M. godartii* suggested that a more subtle graded effect on saturation could be possible by reducing, but not eliminating entirely, melanin levels. As it is understood that melanization is an enzymatic process with temporal accumulation, I reasoned that both enzymatic kinetics and reaction time could influence structural color saturation (77,222,224,232–242). Given that I could control access of the wing to pro-melanin factors with a simple physical barrier, I hypothesized that I could control when multiple regions of an ex vivo cultured wing melanized, and in turn I hypothesized that regions with varied levels of melanin would have accordingly varied levels of structural blue saturation.

In these experiments I made the barrier from Parafilm as it allowed better control over small regions of the wing. I cut small thin strips and affixed them to the culture dish, belting the wing down in place. I filled the dish with STD+DA medium and allowed the wing to begin pigmenting for a couple of hours. Then one-by-one I removed one Parafilm strip an hour, allowing the previously unexposed scales below to access the DA in the medium (Fig.2.8A-F). I was able to image the adjacent regions of the same wing with varying times of exposure, and found that regions that were darker had correspondingly more saturated blues (Fig.2.8F',F'' & G-H'') (n=8). Subsequently, I quantified the differences of pigment in cover and ground scales within the same wing and I found that pigment quantity varied only in the ground scales and absorbance increased directly with time of exposure (Fig2.8I-N). I also found that ground scales appeared less saturated in blue color when viewed from the abwing surface if they were from regions of less melanization time (Fig.2.8J-M 3rd column). It appears that there is not a uniform blue reflection in the ground scales. I take this to suggest a combination of ridge collapse and lower lamina reflection as a causative factor in the reduced saturation. Cover scales on the other hand, qualitatively appeared identical and all showed uniform structural blue reflectance.

I take these results to suggest that temporal modulation of the melanization pathway is sufficient to modulate the saturation of structural colors. While I demonstrate that variation in pigmentation can be produced temporally, one can imagine the same outcome produced by reduction in enzyme kinetics for proteins like Tyrosine Hydroxylase or DOPA Decarboxylase. It is possible then that alleles of melanization genes altering their temporal expression, activation, or enzymatic kinetics could be causative of the structural color variation seen in *M. godartii*.

2.3.9 In vivo *injection of melanization modulators produce a "phenotypic" series of structural saturation*

Finally, I was curious to know if it is possible to recreate any of the findings of our previous experiments *in vivo.* Since I had been able to modulate melanization with both pro- and contra- pigmentation factors *ex vivo,* I reasoned that these same molecules (DA and 3IT) could be effective *in vivo*. Further, I hypothesized that varying concentrations of inhibitor should create a gradation of color saturation by influencing the extent of melanization. Accordingly, I injected 20uL of 3IT (20mM, 60mM, 100mM, or 140mM) or 500mM of DA into pupae with pigmented eyes and allowed them to eclose (n=3,3,5,6, and 3, respectively). Examples of eclosed adults are shown in Fig2.9A. As expected the darkest animals were those injected with DA and these subsequently appear more saturated (though I did not attempt to quantitate this). Animals injected with 3IT varied in pigment from roughly equivalent to wild type to very pale blue, providing evidence that enzymatic rate decreases are feasible mechanisms for structural color evolution. While our palest animals were 140mM 3IT injected animals (Fig2.9B), there was not a perfectly linear change in pigmentation with the other concentrations. I attribute this to the fact that I had no control over age and that pupal volume varied despite receiving the same dosages. It was not uncommon for animals receiving the most concentrated dosage of 3IT to fail to eclose, dying within the pupa and arguing this dosage as an upper limit for modulation. Those 140mM treated animals that did eclose, often had crippled fore and hindwings, an example can be seen in Fig2.9B at the distal-posterior corner. I chose to focus the rest of the analysis on the most striking knockdown I achieved, seen in Fig2.9B. Ground scales from this animal showed a taco-like phenotype, folding along their length (Fig2.9G') but retained their nanostructures and color production (Fig2.9E,F,G,G',H,H'). The taco-ing of scales along their length reminded me of observations made by Wilts et al. when looking into *Parides lysander* and the deformities seen in scales where *pale* had been targeted by CRISPR/Cas9 *pale* (38,77). Despite this whole scale warping, I saw no felled ridges as I had observed *ex vivo*. When compared to wild type *M. h. peleides* full-wing reflectance or ground scale pigmentation/absorbance, 140mM 3IT injected animals were less saturated and less pigmented (Fig2.9C,I-K). This level of pigmentation was still greater than what I was able to achieve in *ex vivo* knockdowns. It is possible that the amount of knockdown permissive of eclosion is less than that which creates felled ridges *ex vivo* and, hence, why I do not observe this phenotype with *in vivo* injections. Given the death I saw with high concentration injections, I imagine that the lack of Tyrosine metabolism created by the drug has additional epistatic effects, including the decreased production of NBAD, necessary for sclerotization and for the neurotransmitter levels of DA and the downstream catecholamines.

2.3.10 Recapitulation of Morpho saturation variation with industrially-produced paints

Given that the phenotypes I produced were based on basic physical principles of light, however biologically-derived, I felt the greatest test of the idea would be to mimic the variation using a non-biological system. I created an image in Adobe Illustrator with defined values of blacks that were spatially separated (Fig2.12A) and then bought acrylic clear paint and mixed in a silica-based blue-colored thin film pigment. This structural blue was painted over the LaserJet printed greyscale image (Fig2.12A'). The unpainted and painted images were scanned, ROI chosen (Fig2.12 boxes), and image analysis performed (Fig2.12 graphs). As expected, regions of increasing value in the greyscale defined areas of higher saturation blue when painted over. This lends strong evidence to the idea that pigment level can determine hue saturation, even when the structure is identical across the object.

2.4 Discussion

The field of biogenic structural coloration has provided a fascinating look into the surprising diversity of ways life has evolved to meet a need of color production. The widespread lack of short wavelength pigments has led many lineages to evolve the elegant and varied solutions of interference based colors (92,243–246). The intrinsic nature of structural color however, is a game of biasing the appearance of white light, not of absorbance. As a result, it has been widely observed that organisms deploy pigments to regions of structural color. Physical studies to date have provided strong evidence that these pigments are used to aid the purification of the spectra reflected (68,70,72,78). In some cases pigments can be used to eliminate parts of the spectrum as in Budgerigars that utilize a yellow pigment that specifically absorbs blue wavelengths changing blue-green feathers toward a purely green color, and in some cases adding wavelengths to create non-spectral colors as seen in Queen Purple Tip butterflies where a blue structure is placed over red pigments (65,66). This latter type of non-spectral color is likely more common than commonly thought as UV structures are commonly deployed in the Pierid butterflies over yellow pigments likely creating a non-spectral color that human's cannot see and have no name for (49,246). Most commonly though are structures laid over broadly absorbing pigments for the purpose of purifying the colors amplified by the nanostructures. In some cases there has been good reason to name these pigments as melanin since they occur within melanocytes and melanocyte loss leads to desaturation of the color reflected (68,247). In most studies of butterfly structural color this broadly colored pigment is suggested to be melanin, which is reasonable given its demonstrated prominence in butterfly wings (42,109,218). In agreement with past studies, I found the repeated presence of a dark pigment correlated with saturated structural blues and conspicuous reduction of saturation in regions that were white or pale blue. This theme repeated at multiple levels of ecological importance: in individuals, within a species, and between species. Given the recurrent nature of the covariation between pigment and blue saturation, it seemed reasonable to hypothesize that alleles modulating pigment biosynthesis could result in novel color phenotypes in individuals that may propagate through time to eventual speciation.

To approach this I aimed to recapitulate the natural pigment variation, which first required an understanding of what pigment was being deployed. The survey showed that this dark

pigment was broadly absorbing across the visible spectrum, consistent with descriptions of melanin. However, despite the affirmations present in the literature, it remained to be demonstrated definitively that this pigment is melanin in the Morphos. One reason I believed this to be important was because the long-held belief that the dark colors of spiders were all ommochromes and yet when further tests were done, the evidence suggested them to be melanins instead (229). Moreover, even across the *Morpho* species, some organisms within the *Morpho* sub-genera *Iphamedeia* and *Laurschwartzia* contain conspicuous orange pigments that I found to be MeOH soluble (data not shown) and which have been shown to be ommochromes in other Nymphalids (7,81,109,134,248). Between the spider data and the observations of orange Morphos, I thought that direct evidence of melanization in Morphos would be an important to obtain.

By utilizing commercially available *M. h. peleides*, which has had the physical basis of color previously described, I was able to make manipulations *in vivo* and *ex vivo* that melanin is indeed the dark color pigment of at least this species (227). Moreover, I was able to show that modulating the activity of *M. h. peleides*' tyrosine metabolism is sufficient to reduce pigmentation levels and simultaneously the saturation of the overlying structural colors. I further provide evidence with the TuffTag experiment that spatial regulation of pigmentation is sufficient to drive structural color saturation tuning. Given the research done on the patterning of color in *Heliconius* where a single gene, WntA, has been demonstrated to regulate the size and shape of melanin pigmentation, I believe that a similar mechanism is likely to have evolved within *Morpho* species, such as *Morpho cypris* and *M. rhetenor*, to produce large regions of desaturated structural blue (28,29). I have also provided evidence from the Parafilm, *in vivo,* and painting experiments that modulation of time of pigment onset, enzymatic activity, and overall pigment level are sufficient mechanisms for tuning the appearance of structural colors. In all cases, between organisms of a single species, within an individual, and printed black levels on paper, I provide evidence that a single structure is sufficient to produce multiple shades of blue.

Results from the *ex vivo* experiments suggest that one possible mechanism melanin aids structural purity is through the isolation of the multilayers from the often non-blue lower laminae of wild type ground scales (Fig2.11). I was struck by the color similarity of the lower laminae from wild type ground scales of *M. h. peleides*' with those of *M. polyphemus*. While other differences were clearly involved in the spectral reflectance difference, when I knocked down pigmentation in *M. h. peleides* I often still saw the structural colors of the lower lamina suggesting that the lower lamina could be contributing to broad-spectrum, low-saturation reflectance. I also saw occasional collapse of ground scale ridges in *ex vivo* cultured wings. Though when and why this occurred is unclear, it is possibly due to the inhibition of pigmentation or sclerotization. This needs further study, but if in fact due to pigmentation/sclerotization, could represent the first pathway implicated in the construction of a multilayer nanostructure in butterflies.

From the results of our survey and of our manipulations, I am enthusiastic about repeatedly finding similar variation at multiple ecological-levels, as it suggests parallel evolution of color pattern by one mechanism: ground scale based pigment deposition levels. Further, it implies a potential origin for the variability species with structural colors. It is easy to imagine a novel allele controlling pigmentation arising in an individual, which

fixes in a population subsequently sufficiently isolated as to birth a new species. Species origination could therefore theoretically occur in structurally colored lineages without the manipulation of the structure itself.

I am left with a couple of questions to which I can only speculate. The first is, why do cover scales not suffer phenotypic effects like the taco-ing noticed in the *in vivo* experiments or the collapse of ridges? I suspect one of two scenarios 1) the cover scales of *M. h. peleides* aren't ever pigmented, arguing that they may not need TH to be structurally sound, or 2) by the time I make experiments, the cover scales are done developing and do not experience any effects simply because they cannot be affected. I tend to believe the latter, but have no evidence for or against either scenario. A possible means of addressing this would be to target *pale* as Zhang et al. have done in the lab rat species (77). I've cloned *M. h. peleides' pale* from pupal cDNA (SeqA3.7), so experiments targeting it just need to be designed and carried out to test this.

Secondly, since high levels of TH inhibition (afforded by high concentrations of 3IT) lead to death, but not to white butterflies, is TH modulation relevant to how white Morphos come about? I imagine that in pale blue Morphos with low pigment levels, like *M. godartii assarpai*, Tyrosine Hydroxylase or DDC modulation could be a plausible mechanism. Previous results suggest that sensitivity to hormonal signals, decreased enzyme kinetics, and down regulating expression levels are all means of altering pigmentation (235,247–251). In scales that are truly pigmentless, like the white of *M. theseus*, portions of *M. hecuba, M. epistrophus,* and *M. polyphemus*, or the highly desaturated blues of *M. sulkowskyi, M. cypris, M. rhetenor*, and *M. marcus*, it is more reasonable to imagine that DA and L-DOPA are shunted into alternative pathways like NBAD sclerotin by the product of genes like *ebony* (77,235,252). In these species I would speculate that a lesion in *ebony* or the increased expression of the counteracting *tan* would force these white species to be pigmented and possibly transform the phenotype of a butterfly like *M. sulkowskyi* into that of the closely-related, brilliantly blue *M. zephyritis* (77,233,235,250,253–255).

One final implication of these experiments is that the methods provide an ability to answer a question that has been frequently discussed in the literature: the refractive index of scale chitin and melanin *in situ* (82,217,256,257). By the methods described here, I imagine that it should be possible to measure the levels of pigmentation and the corresponding refractive indices of scales that come from the same wing and thus share everything else in common. Further, I believe these methods provide a framework by which many of the pigments proposed to influence structural color in the literature can be directly tested.

2.5 Conclusions

In sum, these results suggest that many of the color forms found within *Morpho* and, indeed in other structurally colored groups, could originate with mutations in genes that do not necessarily affect the structure itself. For the first time in a structurally colored butterfly I demonstrate that melanin is a tunable resource that may allow for the large diversity of patterns and species the Lepidoptera are known.

2.6 Relevant appendices:

Spectrophotometry data for whole wing reflection readings and single scale transmission readings, images used for image analysis, and data from the survey can be found in Appendix 2.

Custom Python software used for analyzing images can be found in Appendix 4 and at the GitHub repository: https://github.com/rnull13/MorphosAndMelanin/ and utilizes the Python library PIL v. 1.1.7-14 found at: http://www.pythonware.com/products/pil/.

The sequence to *M. h. peleides pale* and an alignment of its translation with other Lepidopteran *pale* sequences can be found in appendix 3, sequences 7 and 8, respectively.

Figure 2.1 Dark pigment underlies the difference in structural saturation

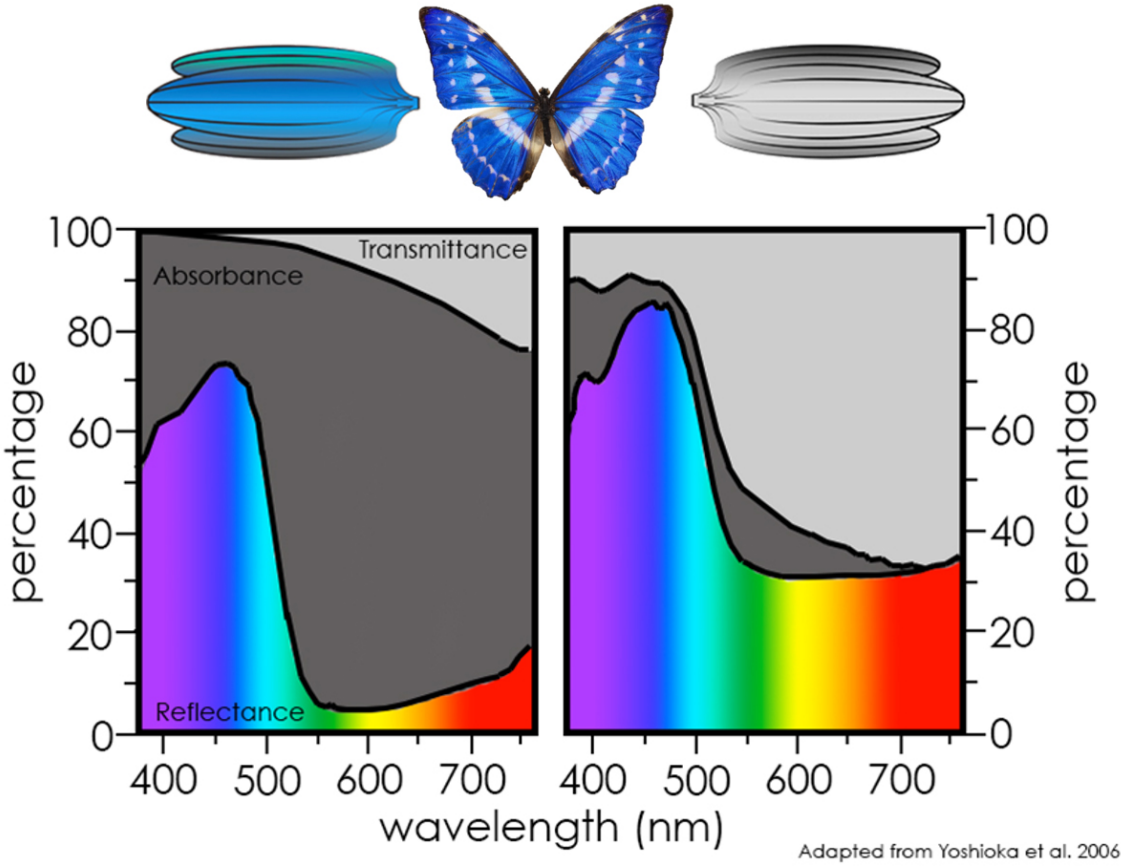

Yoshioka and Kinoshita have suggested that a dark pigment is the main difference between structurally blue and white bands in *Morpho cypris*. The high absorbance of blue scales correlates with low reflectance in the long wavelengths. While white scales show a similar reflectance spectrum, the low amount of absorbance correlates with overall higher reflectance across the spectrum. As a result, the blue scales reflect a purer blue than the white despite having identical structural elements. Figure adapted from Yoshioka and Kinoshita 2006 (75)

Figure 2.2 Characterization of the many blues within an individual

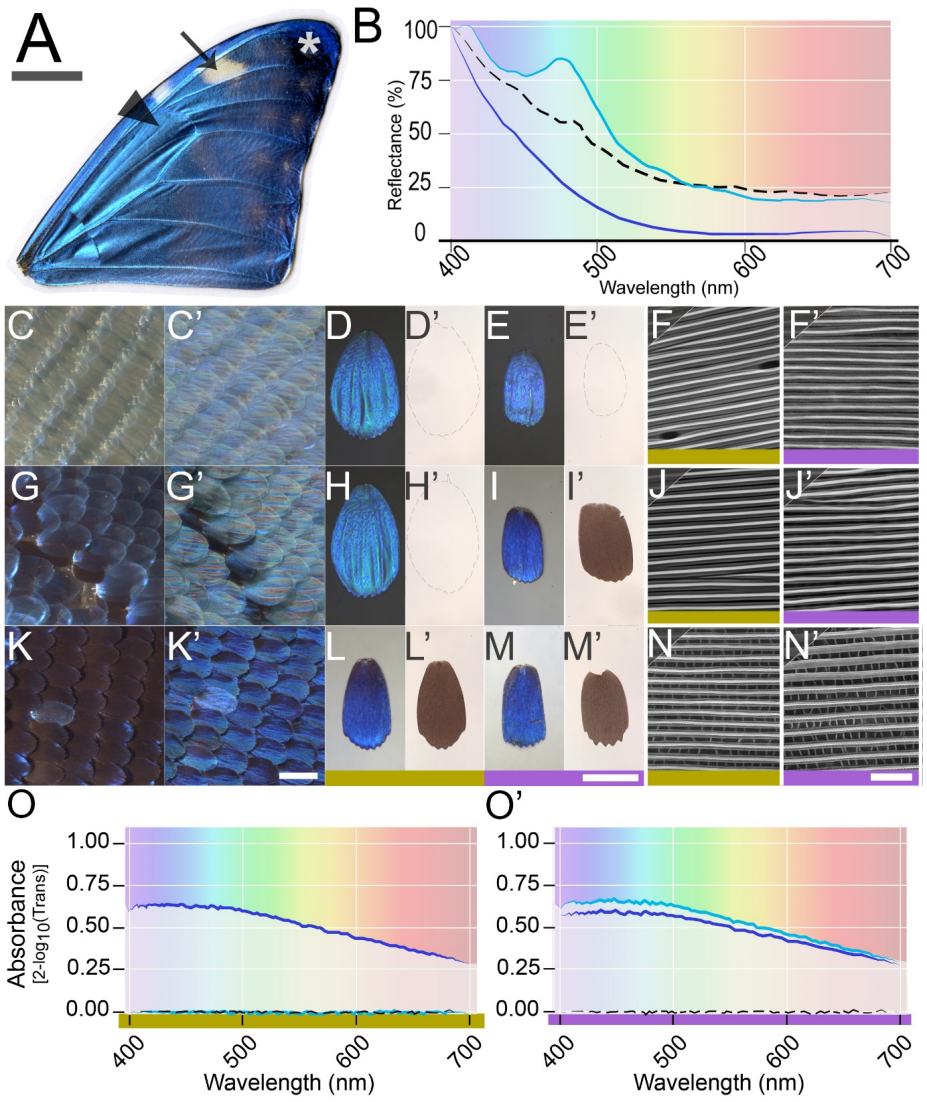

A View of dorsal forewing from *Morpho marcus*. Arrow indicates analyzed white region, arrowhead: main blue region, asterisk: dark blue. Scale bar 1cm. **B** Normalized whole-wing reflection spectra for white region (dashed black line), main blue (cyan), and dark blue region (dark blue). **C-F'** visualization of scales in white region. **G-J'** visualization of scales in main blue region. **K-N'** visualization of scales in dark blue region. **C,G,K** Reflected light microscopy of indicated regions lit from the left to highlight differences in pigmentation. **C',G',K'** The same regions lit from the top (90 degree rotation) showing differences in appearance when color is apparent. Scale bar 150um. **D,H,L** Single cover scales from each region shown in reflected light microscopy lit normally. **D',H',L'** Single cover scales from each region placed in immersion oil to eliminate structural color production, and imaged by transmission to highlight differences in pigmentation. **E,I,M and E',I',M'** are ground scales treated in the same way as D,H,L and D',H',L' respectively. Scale bar corresponds to D's, H's, L's, E's, I's, and M's 100um. **Dotted line** in D',E',H' shows the outline of the scales which are nearly invisible in immersion oil. **Yellow bar** indicates these are cover scales, **purple** that these are ground scales. The same color scheme will be applied throughout all figures to orient the reader. **F,J,N** SEM images of the cover scale ridges – considered to be the source of Morpho blues. **F',J',N'** SEM micrographs of the ground scale ridges. Scale bar 2um. **O,O'** Average absorbance spectra for 3 scales in immersion oil; cover in O, ground in O'. Color scheme is maintained from B.

Figure 2.3 Characterization of the many blues between populations of a species

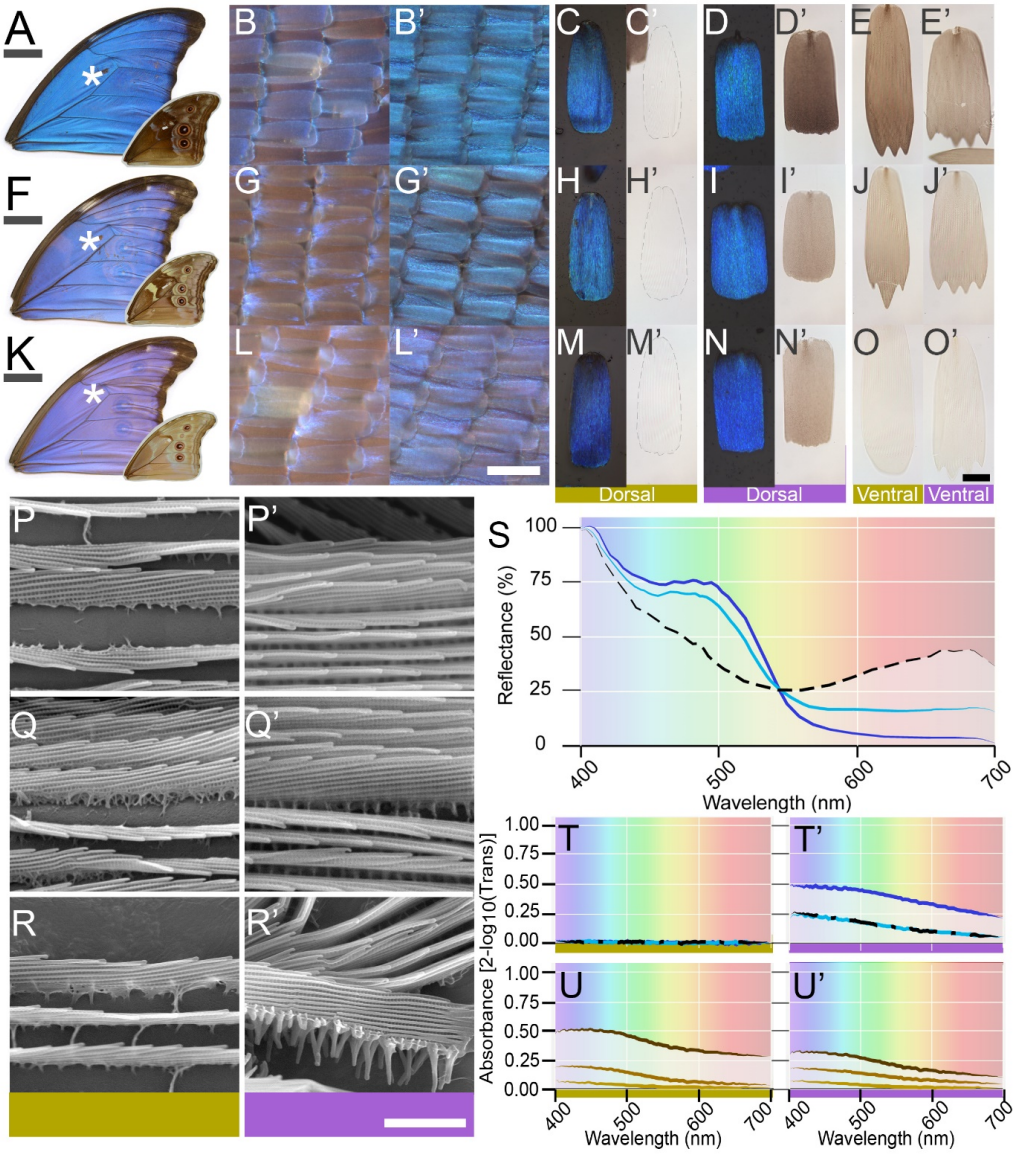

A-E',P,P' *Morpho godartii didius*. **F-J',Q,Q'** *M. g. assarpai* (dark form) **K-O',R,R'** *M. g. assarpai* (light form). **A,F,K** Dorsal views of forewings showing variation in blue, inset are the ventral views of the same wings showcasing variation in ventral pigmentation. Scale bars reference dorsal wings, 1.5cm. **Asterisk** indicates regions imaged in subsequent figures. **B,G,L and B',G',L'** as in fig.1 these show close ups of indicated regions lit from left and top, respectively to highlight pigment and structural variation. Scale bar 150um. **C,H,M and C',H',M'** single scale reflectance and transmittance of dorsal cover scales. **D,I,N and D'I'N' M'** single scale reflectance and transmittance of dorsal ground scales. **E,J,O and E',J',O'** are single scale transmittance images of ventral scales, cover and ground respectively, corresponding to the same region as imaged on the dorsal surface highlighting pigmentation differences on the ventral surface. Scale bar 50um corresponding to all single scale images shown. **P,Q,R and P',Q',R'** SEM micrographs of color producing ridges; cover and ground respectively. Scale bar 2um. **S** Normalized whole-wing reflectance in area marked by asterisks. Dark blue – *didius*, cyan – dark form *assarpai*, black dashed line – light form *assarpai*. **T,T'** Average absorbance spectrum of 3 cover and 3 ground scales, respectively, taken from the dorsal surface in immersion oil. Color scheme retained from S. **U,U'** Average absorbance spectrum of 3 cover and ground scales, respectively, taken from the ventral surface in immersion oil.

Figure 2.4 Characterization of the blue and whites between closely-related species

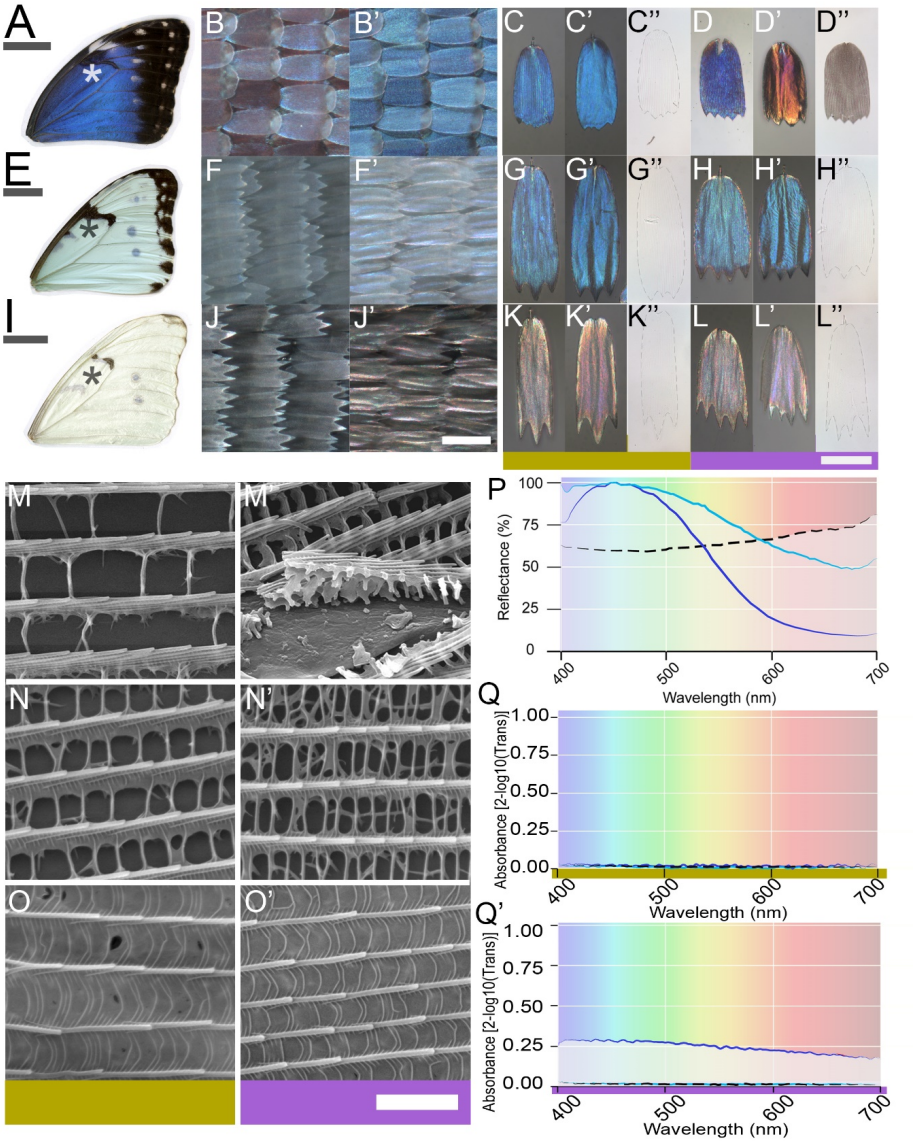

A-D'',M,M' *Morpho helenor peleides*. **E-H'',N,N'** *M. epistrophus catenarius* **I-L'',O,O'** *M. polyphemus* **A,E,I** Dorsal views of forewings showing variation in color. Scale bars 1.5cm. **Asterisk** indicates regions imaged in subsequent figures. **B,F,J and B',F',J'** as in previous figs these show close ups of indicated regions lit from left and top, respectively to highlight pigment and structural variation. Scale bar 150um. **C,G,K and C',G',K'** single scale reflectance of dorsal cover scales. The former are abwing views (as seen when looking at the wing), the latter adwing (from the "under side") highlighting that structural color in cover scales is largely thin film based. **C'',G'',K''** are cover scales placed in immersion oil and imaged in transmission. **D,H,L and D'H'L'** single scale reflectance dorsal ground scales again in ab and adwing views. The orange color of *M. h. peleides* thin film suggests that the blue color is derived from its ridges. **D'',H'',L''** ground scales in transmission to show pigment differences. Scale bar 100um, corresponding to all single scale images shown. **M,N,O and M',N',O'** SEM micrographs of ridges; cover and ground respectively. M' from a broken ground scale showing ridge in profile. Scale bar 2um. **P** Normalized whole-wing reflectance in area marked by asterisks. Dark blue – *peleides*, cyan – *catenarius*, black dashed line – *polyphemus*. **Q,Q'** Average absorbance spectrum of 3 cover and 3 ground scales, respectively, taken from the dorsal surface in immersion oil. Color scheme retained from P.

Figure 2.5 Inhibition and rescue of melanization inhibits and rescues structural blue

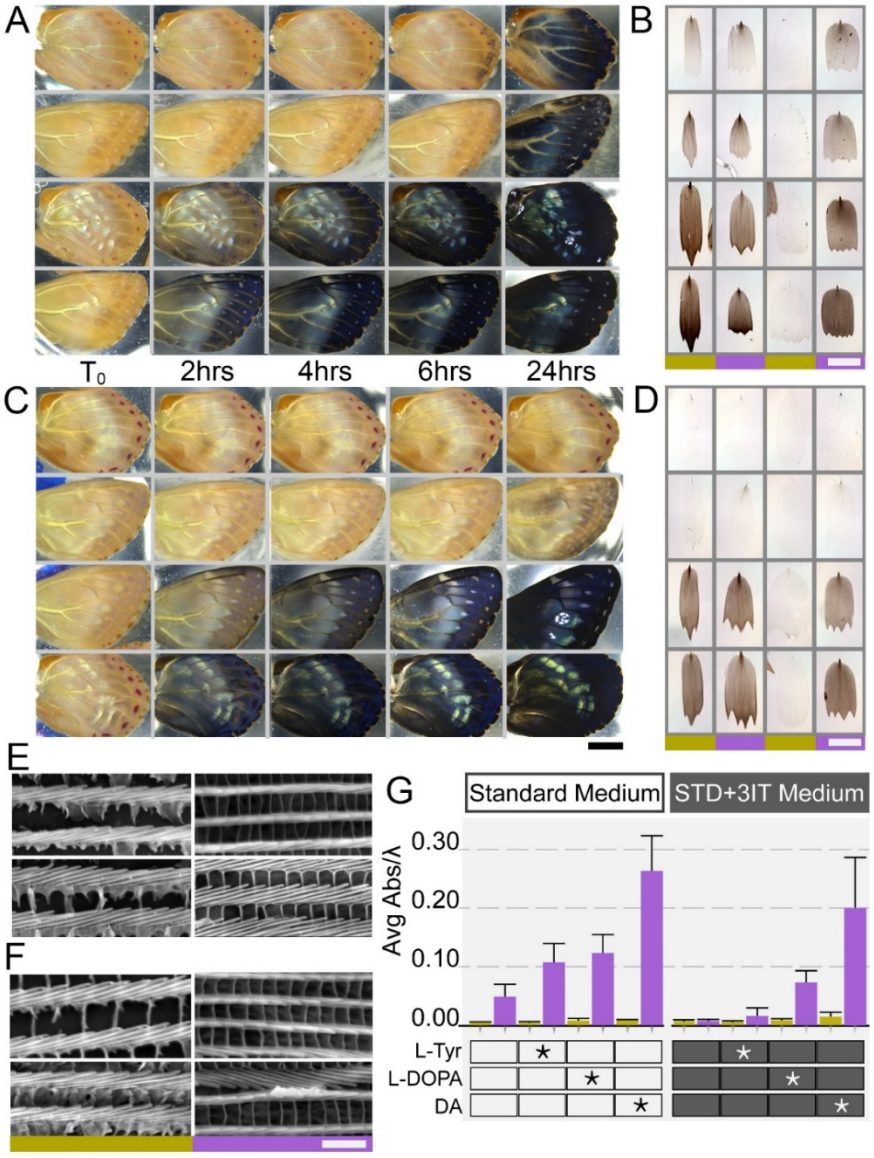

A,C Incubation of *M. h. peleides* pupal wings in absence and presence of 100uM 3-Iodo-Tyrosine (3IT), respectively. Each panel shows 4 wings from the same animal cultured simultaneously in different conditions, Top to bottom: STD alone, STD+5mM L-Tyr, STD+5mM L-DOPA, STD+5mM DA. Left to right shows progression of pigmentation and blue emergence through time. For the sake of comparison, the bottom wings have been mirrored in A, and the top two wings in C. Scale bar 5mm. **B,D** Single scales in immersion oil imaged in transmission from wings cultured as in A and C respectively. For each row, the left two scales are from the distal black region, and the right two from the blue area. Cover and ground scales are indicated as in previous figures by yellow and purple bars. Scale bars 100um. **E** SEM images of ridges from scales cultured in STD medium; upper images without 3IT, lower with. Left images are cover scales, Right images are ground. Scale same as F. **F** Same as E except now cultured with 5mM L-DOPA. Scale bar 2um. **G** Comparison of absorbance by single scales, ground (purple) and cover (yellow), for all conditions. For each bar, absorbance spectra for 3 scales were taken from 3 different experiments; n=9 for all. To give a simple statistic for comparison, we averaged the 9 spectra, then averaged all values across the 870 wavelengths (between 400-700nm) of the resulting average, producing an average absorbance per wavelength of the 9 scales. Error bars are SD. Unless otherwise stated, all further bar graphs of absorbance are calculated in the same way.

Figure 2.6 Structural blue appears faster in *ex vivo* pupal wing disc cultures when melanin-promoter present

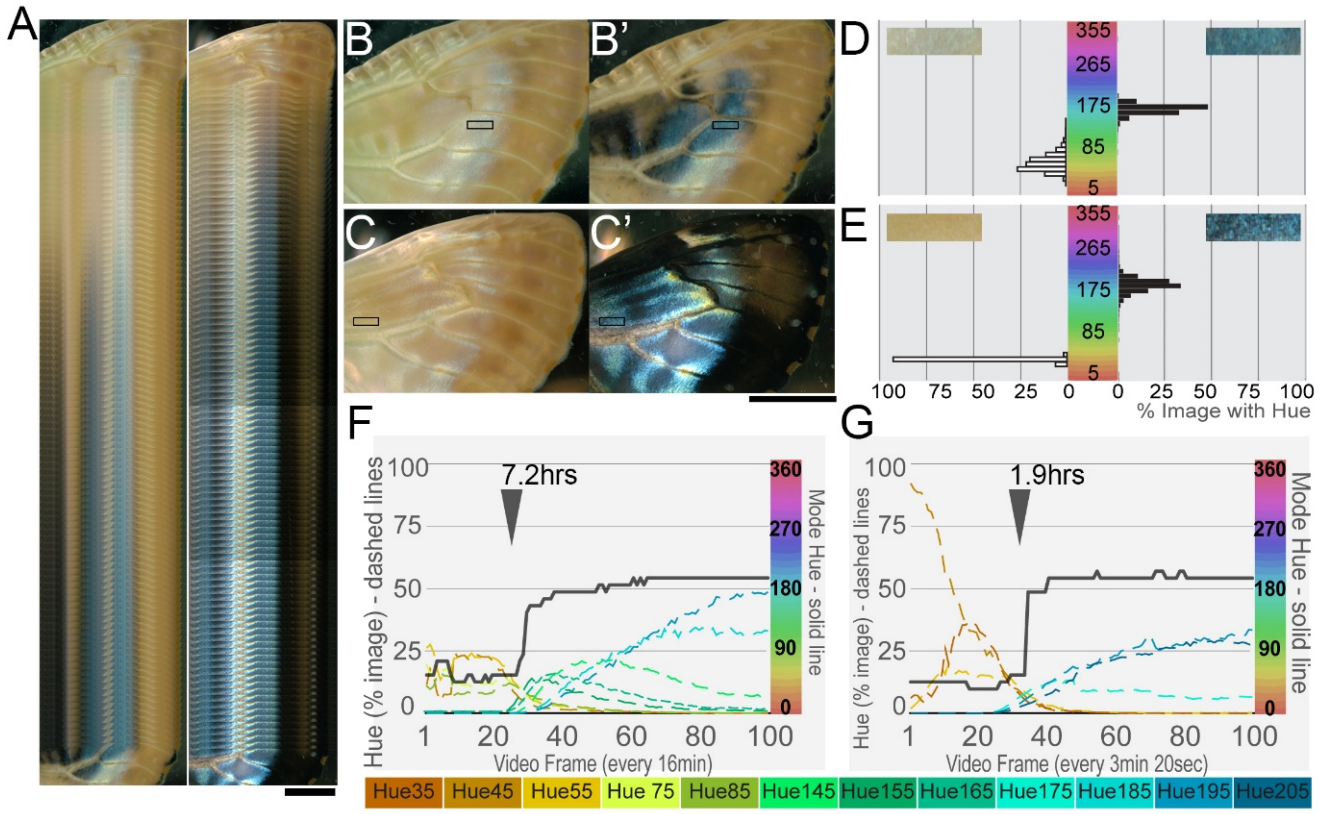

A Kymographs from time lapses of ex vivo cultured *M. h. peleides* pupal wing discs. Left kymograph is in the STD medium, time between slices 16min; right in STD+DA, each slice every 3min 20sec. Scale bar 5mm. **B,B'** First and last frames of STD time lapse (26.4hrs elapsed), box indicates region of interest (ROI) for subsequent data analysis in D and F. **C,C'** First and last frame of time lapse from STD+DA incubated wing (5.5hrs elapsed), boxes indicate ROI for E and G. Scale bar 5mm. Wings imaged in this way fail to completely pigment, this is in contrast to wings kept on a rocker and not continuously imaged. We believe this to be a matter of stagnation and oxygen permeation. **D** 7900 pixels in the ROI from first and last frames of STD culture were analyzed using custom software (see Methods section). Distributions for hue in the first frame ROI are shown on the left (white bars) and the distributions for the last frame shown on the right (black bars). Vertical axis indicates hue, horizontal axis (positive in both directions) indicates percent of pixels in ROI with that hue. **E** Same as D but for STD+DA culture. **Inset** show ROIs analyzed. **F** Using the same ROI indicated previously in B,B', a frame-by-frame analysis across the whole kymograph. Plot shows mode hue (black solid line – right axis) and, for all hues that are the mode for at least one frame, the percent of pixels in ROI represented by that hue (colored lines – left axis). **Arrowhead** indicates the time at which blue pixels out number brown. **G** Same as F but for the ROI in C,C' across the emergence of the wing in STD+DA as seen in right kymograph of A. Color of dashed lines corresponds to **the legend at the bottom of the figure** and indicates the hue represented.

Figure 2.7 Spatial restriction of DA to cultured wings recapitulates within individual variation of blueness

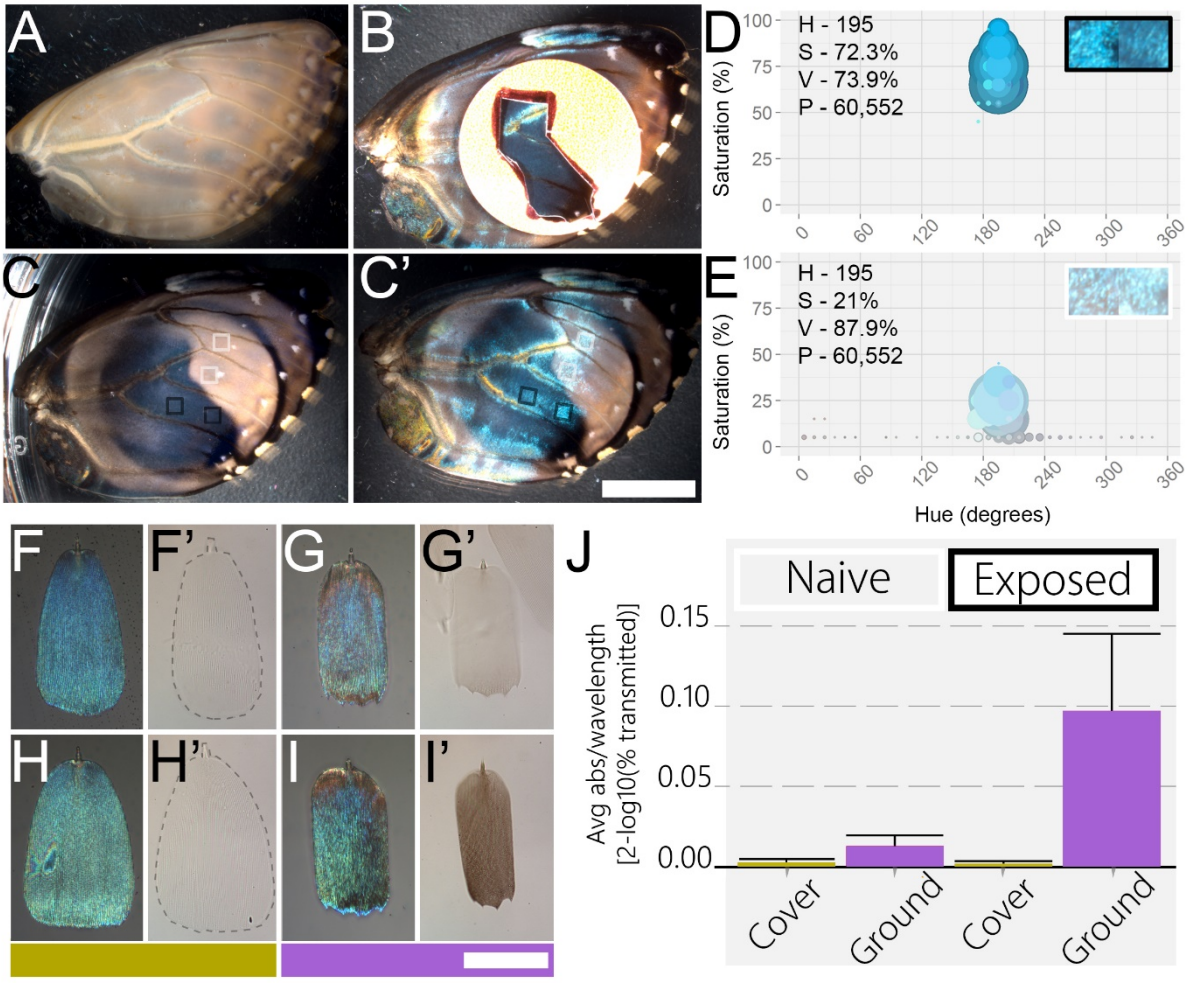

A A freshly dissected *M. h. peleides* pupal forewing just beginning melanization **B** The same wing 19hrs after culture in STD+DA medium. The TuffTag mask used to occlude the wing from DA exposure can be seen with a California-shaped hole cut to allow exposure. **C,C'** the same wing with the TuffTag mask removed. C is lit obliquely from the right highlighting pigmentation differences, C' is lit obliquely from the left to show how structural blue is affected. **White boxes** in C,C' show regions of interest (ROI) of the DA naïve region; **black boxes:** ROI of DA exposed region. Scale bar 5mm. **D** Bubble plot analysis (see Methods, Supplement) of the DA exposed ROI shown in C'. X-axis is hue, Y-axis saturation, concentric bubbles of varying darkness indicate HSV color combinations centered at the same hue and saturation, observable area is equal to number of pixels. **Inset** shows ROI considered. **Legend** H=mode hue, S = average saturation of all pixels, V = average value of all pixels, P = number of pixels analyzed. **E** Bubble plot of DA naive ROI shown in C'. **F-G'** Cover and ground scales for DA naïve regions in reflected and transmitted light. **H-I'** The same as F-G' but taken from DA exposed region. Scale bar - 100um **J** A plot similar to Fig4G comparing the averaged absorbance of 3 cover and e ground scales in DA naïve and exposed regions taken from 5 experiments; n=15 each.

Figure 2.8 Temporal control of DA exposure *ex vivo* recapitulates variation seen within and between species

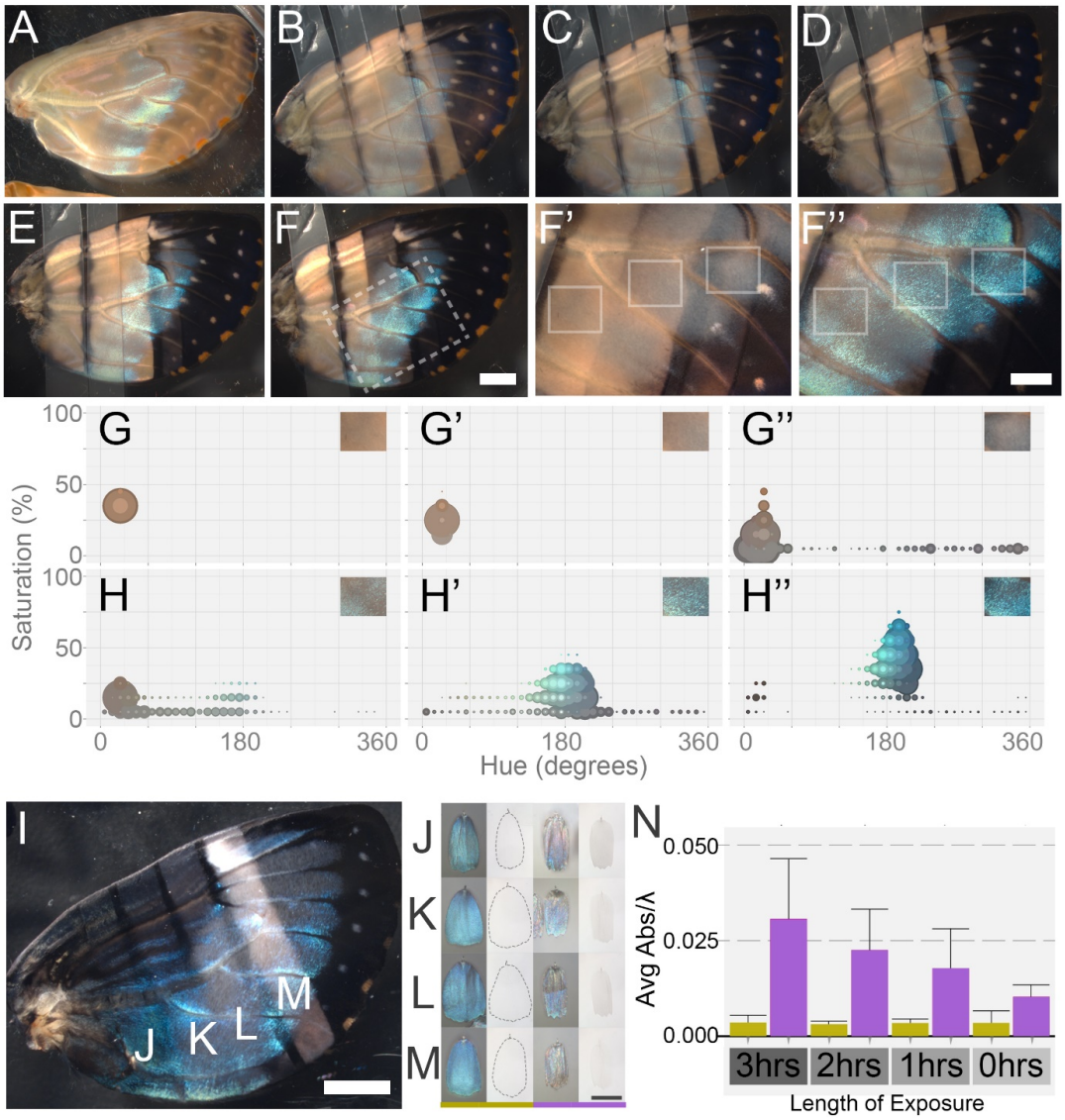

A A freshly dissected pupal disc. **B-F** 1hr time intervals of the same wing cultured in STD+DA. Strips of Parafilm were placed over the wing prior to incubation in the medium. Starting at hour 3 (D), one strip was removed per hour allowing access to previously occluded scales. All images lit from left. **Dashed Box** in F corresponds to the region shown in F' and F''. Scale bar in F is 3mm and is the same for A-F. **F',F''** Three stripes with 0, 1, and 2hrs of DA exposure from left to right. F' lit from right, F'' from left. Boxes in F' are ROI for G-G'', boxes in F'' are ROI for bubble plots in H-H''. Scale bar is 1.5mm. **G-G'' and H-H''** Bubble plot analysis of ROI from F' and F'' respectively – inset indicates specific ROI measured. Plotting performed the same as in figure 4. **I** Another wing cultured in the same way as A-F, after 7hrs of incubation. J-M correspond to regions measured for single scale analysis. J 3hrs incubation, K 2hrs, L 1hr, M freshly removed. Scale bar 3mm. **J-M** Rows across feature scales from regions indicated in I. As in other figures cover and ground are indicated by yellow and purple bars with reflected light to the left, transmission to right in each. Dashed lines indicate boundaries of nearly invisible cover scales in transmission. Scale bar 100um. **N** Comparison of average absorbance for 4 regions per wing with different DA exposure time. Each bar is the average of 3 scales from 3 experiments; n=9 each. Error bars are SD.

Figure 2.9 *In vivo* injection of 3IT produces a range of phenotypes recapitulating within and between species blue variations

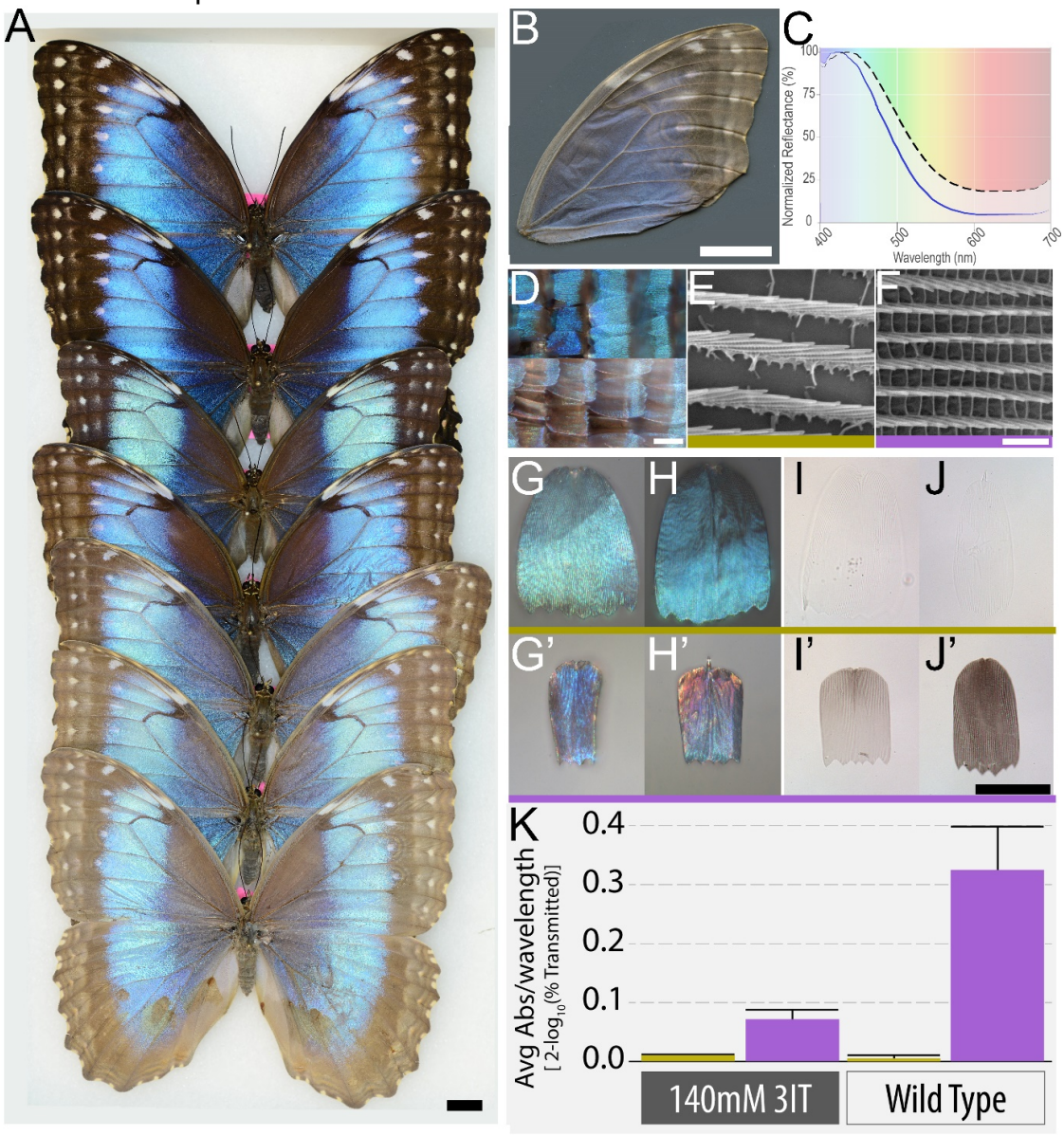

A Range of blue phenotypes in butterflies eclosed from manipulated pupae. Top to bottom: 1) 20uL 500mM DA, 2) 20uL 500mM DA, 3) Uninjected WT, 4) 20uL 20mM 3IT, 5) 20uL 100mM 3IT, 6) 20uL 100mM 3IT, 7) 20uL 60mM 3IT. Scale bar 1cm **B** Forewing from the palest eclosed butterfly, 20uL 140mM injected animal – unmountable due to crippled hindwings. Scale bar 1.5cm. **C** Relative reflected light spectrum of intact wing blue areas. Wild type *M. h. peleides* in blue, wing from B hatched black line. **D** Reflected light image of wing from B. Upper half was imaged with light oriented from top of image, bottom half from the left of the image. Scale bar 100um. **E,F** SEM images of the ridges of cover and ground scales respectively from B. Scale bar 2um. **G,G'** Reflected light images of abwing surface of cover and ground scales. G' shows characteristic taco-ing of ground scale along its length. **H,H'** Adwing reflected light images of cover and ground scales. **I,I'** Transmission in immersion oil of dorsal blue cover and ground scales from B. **J,J'** Transmission images of cover and ground scales from dorsal blue region of a wild type *M. h. peleides.* Scale bar 100um. **K** Average absorbance bar chart comparing scales from the blue regions of manipulated and wild type butterflies: 3 cover and 3 ground scales from the animal in B and 3 cover and 3 ground scales from 3 wild type animals; n=3 for each 3IT bar, n=9 for each WT bar. Error bars are SD.

Figure 2.10 Summary of data collected in survey of Morphos

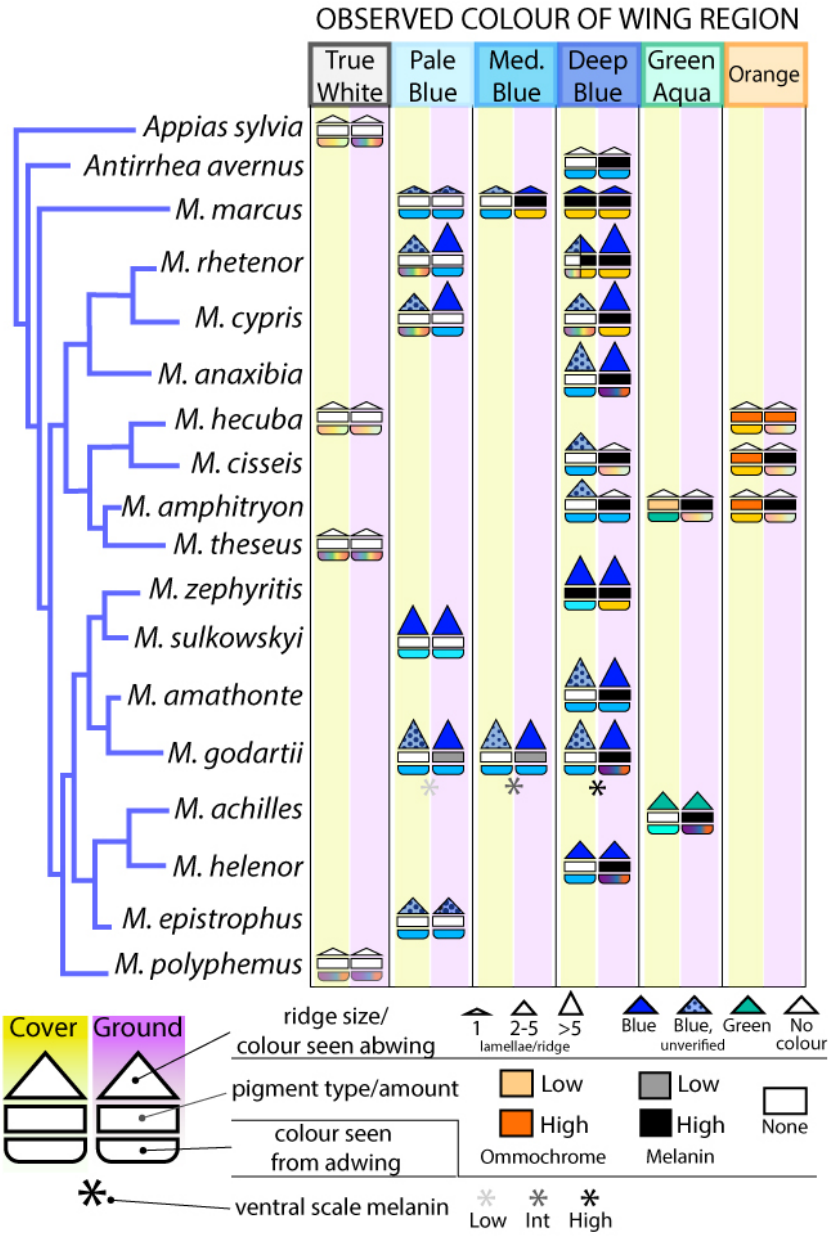

For the reader's ease I have summarized our findings when surveying the SEM, reflectance, and transmittance data. The original data can be accessed in Appendix 2. Phylogenetic relationships from the tree produced by Chazot et al. are summarized on the left (219). Data for each species are organized by regions of color on the wing (**across the top of the figure**). Each color is then broken in to cover and ground columns (**yellow and purple respectively**) representing data from cover and ground scales. As discussed, relevant elements to manufacturing color in morphos are ridges, pigmentation, and the lower lamina's thin film reflectance. Here I have indicated what each of these components contributes, where the triangle size indicates number of lamellae in a ridge and its color representing the reflected color of the ridges where it is possible to discern. In many instances, the reflection from the lower lamina overpowered the reflection of the ridges, and though SEMs generally showed no major differences from ground scales, we interpret this to suggest that the ridges do produce blue but do not have conclusive evidence. The rectangle's color indicates type and concentration of pigment within the scale. The rounded rectangle at the bottom of each set indicates the color of the thin film.

Figure 2.11 Importance of melanin for insulating abwing reflectance from lower lamina

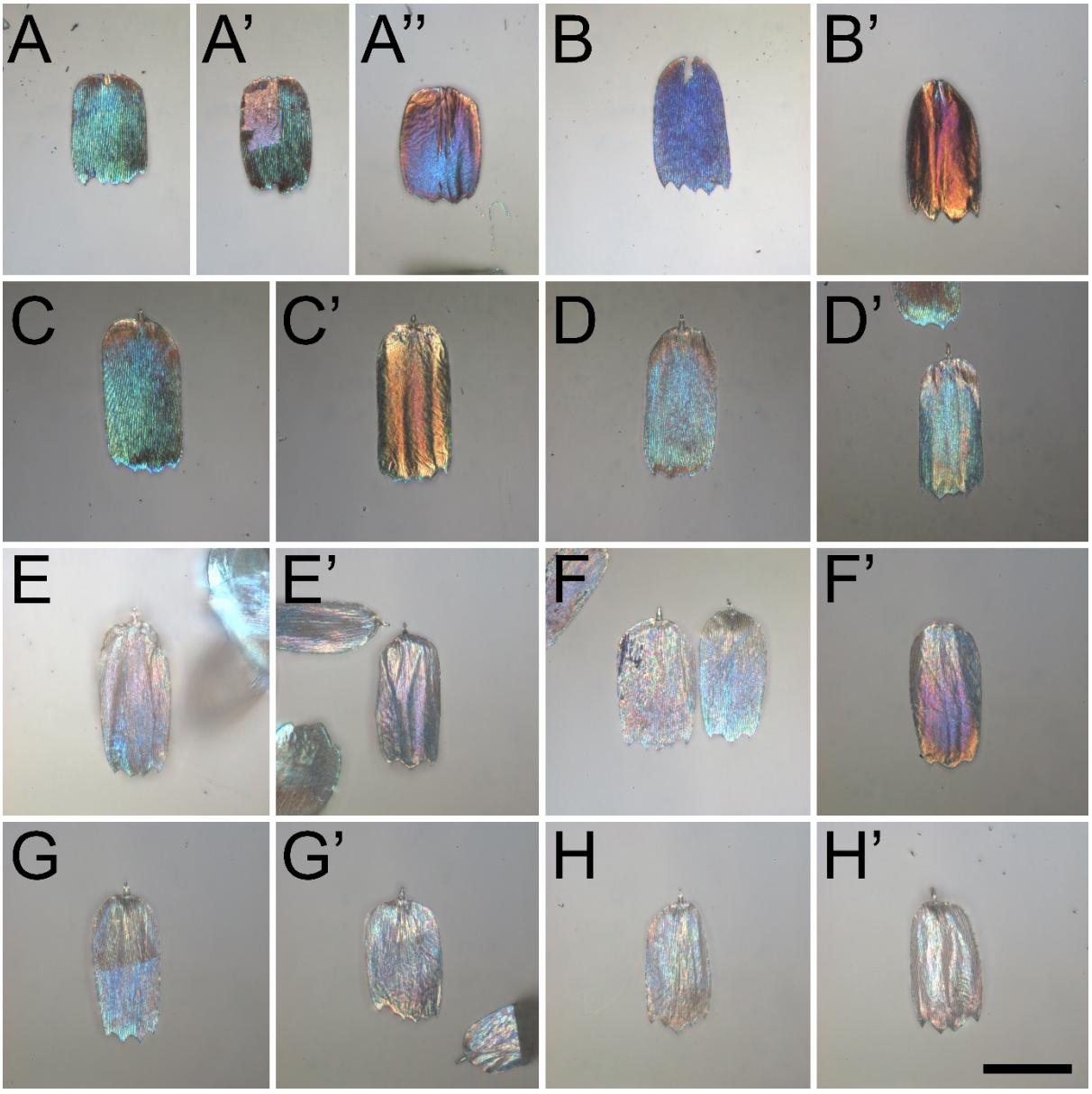

A Ground scale of *Morpho achilles* seen in reflectance from abwing side – ridges produce green color. **A'** Ground scale from same animal seen from abwing side, where ridges with melanin have been partially stripped away. The thin film's coloration can now be seen. **A''** The reflectance of *M. achilles'* ground scale when viewed from abwing surface. **B,B'** Morpho peleides' ground scale in ab- and adwing views, respectively. The distinct coloration of the adwing surface is not seen in the abwing view. **C-D'** Scales taken from the same *M. peleides ex vivo* dopamine masking pupal wing culture experiment. **C,C'** Ab- and adwing views of grounds scales in a dopamine exposed region showing isolation of the orange/magenta lower lamina color from the dorsal ridge colors. **D,D'** Ab- and adwing views of ground scales taken from a dopamine naïve region of the same wing. The orange regions of D' can be seen shining through the ridges.

Figure 2.12 Ridge collapse may contribute to decreased saturation

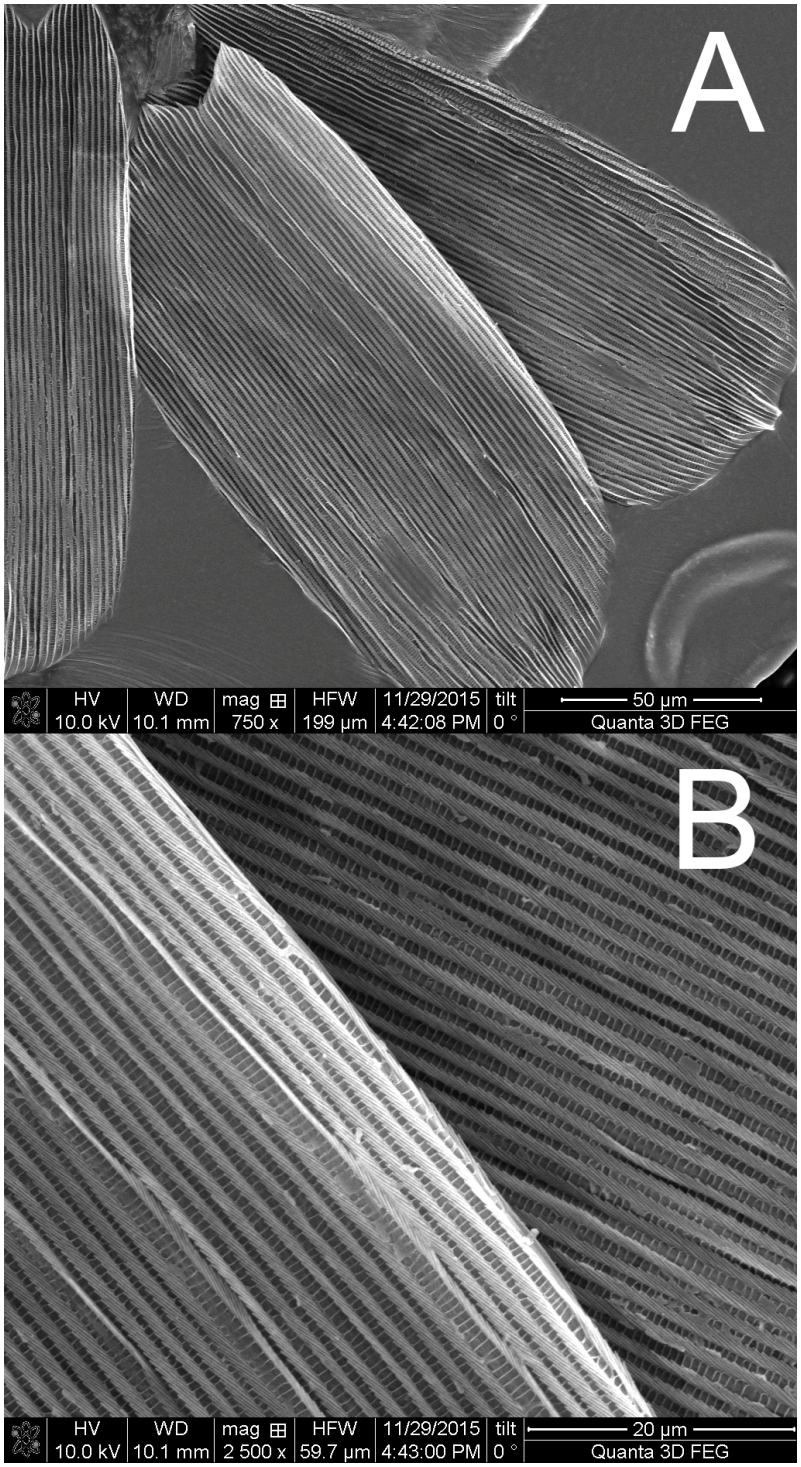

A,B – SEM images at different magnifications showing ground scales taken from a wing incubated ex vivo with standard medium + 3IT. Ridges collapse on their side in these conditions (even though *in vivo* injections do not have this phenotype). This may result in a decrease in saturation by eliminating the multilayer's effect on reflectance spectrum.

Figure 2.13 Recapitulation of findings with iridescent paints

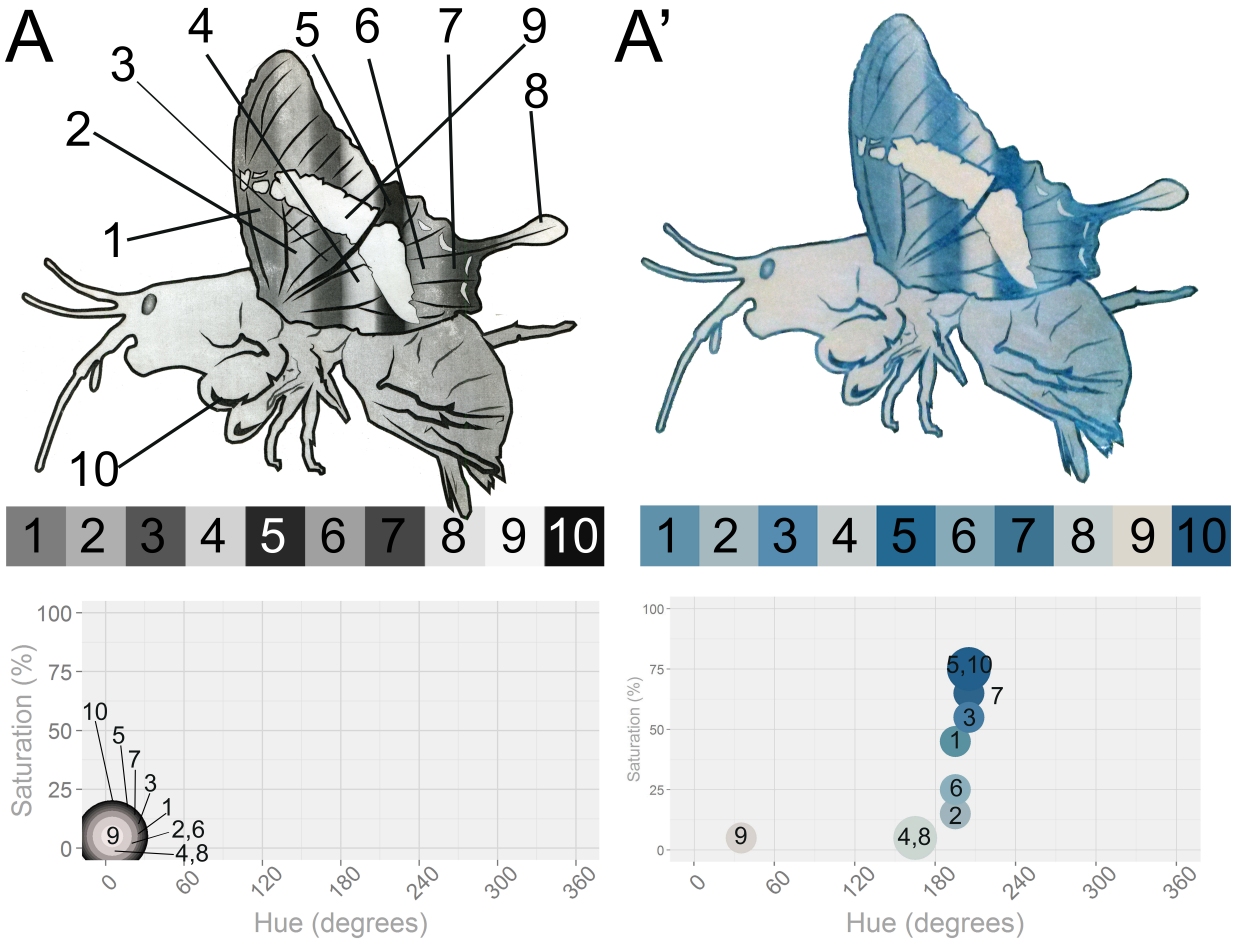

I tested the generalizability of pigmentation's effect upon apparent saturation from structural origins by printing an image on an HP Laserjet with defined darkness levels we set upon illustration **(A - top)**. This was then painted over using a blue silica-based thin-film structural pigment in a clear acrylic paint **(A' - top)**. Images of the illustration before and after being painted with iridescent paint were captured, then regions of interest were point sampled (**numbers A**, same positions **A'**) and subjected to image analysis **(numbered boxes and plots)**. As expected areas of darker toner were correlated with areas of more saturated structural blue despite the same structure/paint being used to create the blue. Some colors/values have merged (e.g. values 4,8) owing to their close absolute value being parsed by the algorithm into a single bin of value or saturation.

Chapter 3
Modulation of the Actin Cytoskeleton and Pigmentation as Sources of Evolutionary Diversity in the *Papilio* Sub-Genus *Achillides*

3.1 Introduction

The color of an organism informs many ecologically-relevant inter- and intraspecific interactions, which can be cunningly deceptive or powerfully conspicuous. An organism must be capable of making colors regardless of whether it employs coloration to hide (crypsis), to show off (sexual display), to warn would-be predators of poison or venom risk (aposematism), to lie (Batesian mimicry), or to share the burden of aposematic learning trials (Müllerian mimicry). To this end, butterflies have evolved the ability to make melanins (black and browns), ommochromes (browns, reds, yellows), and yellow pigments such as pterins and papiliochromes. By and large, pigmentary coloration in butterflies is limited to long wavelengths with few exceptions (215,216,258). So to exploit hues of green, blue, or violet, butterflies have evolutionarily leveraged physics resulting in structural colors reflected from chitinous nanostructures.

One clade of butterflies exhibiting a diversity of structural color is the *Achillides* sub-genus of *Papilio* swallowtails. A monophyletic clade of approximately 25-30 species, the *Achillides* sub-genus is predicted to have originated in Indonesia 15-20Ma and has a current range spreading across India and Northern China, the archipelagoes of Southeast Asia, Northern Australia, and New Caledonia (259). Among the *Achillides* species, individuals display a spectral sampling of colors in a species specific manner that can range from indigo to yellow-green. Spectral variation is seen at multiple ecological levels: from individuals of *P. krishna* displaying yellow-green, green, aqua, and blue patterns on one wing, to the within species variation exemplified by the polymorphic blue (spring) or green (summer) forms of *P. maackii* based on the season of the individual's eclosion, and the clear differences seen between sister-species like *P. pericles's* blue and *P. neumoegeni's* yellow-green (Fig3.12).

The diversity of scales found across Lepidoptera as a whole suggests that despite being a common feature of butterflies and moths, there are many degrees of freedom associated with their manufacture. Pigmentation has received much of the attention, but ultrastructural variation abounds as well (43,92,110). Nearly 30 years ago, evidence was garnered by comparing scales from races of *Heliconius* species to hybridized individuals and led to the conclusion that master control genes dictating color fate may also control ultrastructure and produce subtle optical effects when viewed from afar (33). Evidence for changes in optically-active nanostructures over time between closely related species has been demonstrated before from studies performed on several genera including *Morpho, Ornithoptera, Parides,* as well as *Achillides* (34,38,39,41,220,260). In the case

of the latter it was found that the *Achillides* use a *Urania*-type internal multilayer to produce their coloration. In addition, when compared to the relatively flat multilayers of *Chrysiridia,* the *Achillides* multilayer can exhibit comparatively high levels of curvature (41,47,157,261). Interestingly, in the green regions of the closely related *Achillides* species *P. palinurus* and *P. blumei*, there is a parabolic profile to the multilayer which results in dual color reflections – yellow-green and blue. In the more distantly related *Achillides* species *P. ulysses* the profile of the multilayer is squared off and boxy allowing only a single reflection to take place – a blue color (39,41). This example highlights the importance of controlling not just the ~100nm layers of the multilayer, but the morphogenesis of the scale's ultrastructure at the micron resolution as well (Fig3.1).

Understanding how subcellular morphogenesis may result in a multilayer's formation and curvature will be important to make sense of how butterfly structures are produced and evolve over time to make novel coloration. Some work has been done on the basic biology of scales, including early studies on moths and butterfly scale development, including heat shock perturbations that gave rise to altered ultrastructure development, particularly in the orientation of ridges, though with little understanding of the molecular and cytological factors involved (121,141). Further, a TEM-based developmental series for the non-structurally colored scales of the moth, *Ephestia kuhniella,* highlighted potential roles of microfilaments and microtubules, as well as providing strong evidence for the homology of scales and fly macrochaetes (126,137). More recently, the tools of molecular biology have aided the coarse-grained analysis of normal and perturbed butterfly scale development, with the conclusion that F-Actin dynamics participate in growth and ridge ultrastructural morphogenesis (124).

Given that structural color arises from finely sculpted structures on and within butterfly scales, and that structural color can vary within and between species, it stands to reason that variation at a genetic level may lead to differences in scale development and ultimately to what colors a butterfly can produce. Yet despite having been studied for nearly a century, we still know little about the cell biology or specific players involved in scale development. Outside of a descriptive paper on *Colias eurytheme*'s Morpho-type UV reflectors, one on the development of gyroids in *Mitoura grynea*, and a paper utilizing Thapsigargin that resulted in loss of structural color in *Junonia orithya*, the cell biology leading to nanostructures have been relatively neglected (36,142,246). This lack of study has been in part owed to the reliance on TEM and SEM micrographs of scales required to visualize nanostructures making living tissue unavailable for study, and partly for the majority of studies being optical in nature and thus outside the sphere of biological inquiry.

Here, I harnessed the fact that *Papilio palinurus* modifies its scale ultrastructure into large 5-10um parabolic ultrastructures to create dual reflections from a single internal multilayer. I hypothesized that perturbation of cellular components aiding the formation of the ultrastructure would result in changes to the dual reflection properties accordingly. Further, given the published observations in *Drosophila, Ephestia*, and *Vanessa*, I predicted that F-Actin dynamics may play a role in ultrastructure formation. With the help

of several undergraduate researchers, I have characterized the F-Actin dynamics in developing *P. palinurus*, finding that F-Actin does indeed prefigure the parabolic ultrastructure. Subsequently, I have tried to interfere with normal dynamics by injecting developing pupae with F-Actin inhibitors and characterizing emerged adults. While there have been no phenotypes unique to drug treatment, it appears that both parabolic ultrastructure and multilayer formation are separably perturbable – both resulting in color shifts. When compared to the ultrastructure of other *Achillides* species (Fig3.12), the observed morphological variation seen in *P. palinurus* dimples is remarkably similar. This suggests that alleles exist within populations of *P. palinurus* that may have become fixed within these *Achillides* species. Lastly, following the observation of damage-related color phenotypes, I asked whether pigmentation variation can contribute to structural color variation by manipulating wild type *P. palinurus* pigmentation, finding that, unlike in Morphos, pigment manipulations lead to hue variation in addition to the expected loss of saturation (Chapter 2). The origin of this hue shift appears to be the unmasking of sub-sections of *P. palinurus'* narrow-band chirped multilayer. Despite wide discussion of the role of dark pigments in enhancing structural saturation, this method of tuning hue, to my knowledge, has not been noted before in insects.

In sum, I have direct evidence of two modifiable cellular processes, cellular morphogenesis and pigmentation, that have independent potential to result in novel structural coloration – suggesting that modification of the actin cytoskeleton or pigmentation maybe ideal candidates for investigation in other structurally colored species.

3.2 Methods

3.2.1 Pupae and Drosophila

Pupae of *Papilio palinurus, Papilio ulysses, Papilio nireus, and Morpho helenor peleides* were purchased from LPS, LLC. (Denver, Colorado), maintained under ambient dark:light cycles at room temperature, and misted daily with tap water. As they were received as pupae we had no knowledge of when the animals pupated. For pigmentation experiments in Morphos I tried to coordinate their ages by using pupae only after the eyes had pigmented. This was challenging in the *Papilio* species that have opaque cuticles. For *P. palinurus* the pupal cuticle covering the wings (normally green or tan) gradually turns purple as they begin to lay down melanin, while this is later than ideal it is somewhat helpful.

For measurements of *Drosophila* abdomen pigments, I obtained a few flies of the Oregon R wild type stock from Hernan Garcia's lab. They were euthanized in EtOH, then they abdomens removed, fileted, and cleaned with forceps. They were immersed in Zeiss F355 immersion oil to remove the influence of the remaining fat body and the cuticle. A #1.5 coverslip held them in place for imaging.

3.2.2 Low magnification imaging

To image large regions of butterfly wings, butterflies were humidified and mounted or wings were disarticulated from the body. Samples were imaged on a Keyence VHX-5000 with a 20-200x lens; the microscope also performed the focus stacking and stitching. For the images comparing wild type and red-shifted whole mount butterflies, a Canon D7000 with an AF Micro Nikkor 60mm lens attached to a RPS Studio CS-920 copy rail.

Single scales were removed from wings using a fire polished glass needle pulled on a Sutter flaming brown needle puller. Scales were transferred to clean glass slides. Reflected light microscopy was performed on a Zeiss Axiophot with a 20x objective and zoom magnification at 4x. White balancing was performed on BaSO4. Image exposures were taken to minimize overexposure and were maintained for all images of the same type (abwing, adwing, ground). Transmitted light images were captured by submerging single scales in a drop of Zeiss F355 immersion oil (n=1.518) and covered with a 1.5 coverslip using the same microscope and objective. White balance was set on a region with no scales and exposure was set to not underexpose or overexpose the image, with all samples treated the same. Z stacks were captured manually using a on a Spot 15.2 64 Mp Shifting Pixel Camera (Diagonstic Instruments, Inc.) and were digitally focus stacked in Helicon Focus using method B with radius of 18 and smoothing set to 1.

3.2.3 Scanning electron microscopy

Single scales were pulled from specimen of interest with fire polished needle and placed directly onto double sided carbon tape previously mounted to a 1” aluminum stub (both Ted Pella). Following preparation, stubs were sputter coated with 10nm of gold and imaged using an FEI Quanta 3D FEG FIB scanning electron microscope with 10kV potential, 3nA current, and a 30um aperture.

3.2.4 Transmission electron microscopy

Day 1

Single scales were removed from dead dried wings and fixed for 2 hours at room temperature on a rocker in 2% glutaraldehyde in 0.1M Sodium Cacodylate buffer with 0.01% Tween-20 after being centrifuged at 13kXg for 10min. After fixation the samples were stored overnight at 4c in the same medium.

Day 2

A 10 minute wash in cacodylate buffer followed and then samples were embedded in 2% low melt agar suspended in water. Following solidification on ice, the agar-embedded samples were carved into smaller pieces to improve diffusion and washed twice more in 0.1M Sodium Cacodylate buffer for 10 minutes each. Post fixation was performed by treatment with cold 1% OsO_4 and 1.6% Potassium Ferrocyanide in 0.1M Sodium Cacodylate buffer for 30 min rocking at room temperature and 30 minutes on ice in foil covered tubes. 3 5minute 0.1M Sodium Cacodylate buffer washes followed to remove the

OsO_4. A graded acetone series followed: 35%, 50%, 70%, 75%, 95%, 100%, 100%, 100%. With each step equilibrating for 10 minutes at room temperature. Epon resin was prepared by mixing 23.5g Eponate 12, 12.5g DDSA, and 14g NMA (BDMA accelerant was added on Day 3 to the remainder of resin not used for infiltration). Infiltration was performed using 1 hour steps through an Epon/Acetone graded series of 25/75% Epon/Acetone, 50/50% Epon/Acetone, 75/25% Epon/Acetone. A 30 minute 100% Epon incubation, followed by a fluid change for more 100% Epon incubated for 10 minutes, then the sample was moved into a new tube with more 100% Epon and incubated for 15 minutes. A final change for 100% Epon followed and the samples were incubated overnight on a tube rotisserie.

Day 3

The unaccelerated Epon resin was replaced for Epon containing BDMA and allowed to equilibrate for 30 minutes on the rotisserie. This was exchanged for more accelerated resin and allowed to equilibrate on the rotisserie for 3.5 hours. Samples were moved to molds with gas evacuated Epon with BDMA then heat cured at 60C overnight.

Day 4

Cured samples were triaged for orientation then 70nm thin sections were prepared using a Reichert-Jung Ultracut E microtome with a Diatome Ultra 45 diamond knife. Sections were floated on water and compression relieved with brief exposure to chloroform before being mounted on copper grids. Imaging took place on a Phillips FEI Tecnai12 TEM at 120kV potential. Uranyl Acetate and Lead Citrate staining were not performed and did not appear to be necessary for good contrast.

3.2.5 Staining and laser scanning confocal microscopy

Pupal wing tissue was fixed 20-30 minutes at room temperature in PIPES, EGTA, $MgSO_4$ (PEM) buffer with 3.7% formaldehyde. Samples were then moved to 1XPBS+0.1% Triton-X 100 (PT) with 1:200 dilution of Alexa555-Phalloidin and 1:700 Alexa647-WGA for >12 hours. Generally speaking, the longer the incubation the better the staining. Following incubation, samples were washed for a minute 3x with PT, and another 3x for 20 minutes. Samples were then incubated >12hours at 4C in 50% Glycerol:PBS with 1ug/mL DAPI to stain the nuclei. The samples were then replaced with 70% Glycerol:PBS and mounted for imaging.

For antibody stains, tissue was fixed similarly and then incubated with PT+5% Normal Goat or Donkey Serum for 1 hour. Directly-labeled primary antibody Alexa647-goat-anti-HRP was added at a dilution of 1:200 and allowed to incubate overnight. No secondary was necessary so following a 3x5min, 3x20min PT wash schedule, samples were incubated >12hours at 4C in 50% Glycerol:PBS with 1ug/mL DAPI to stain the nuclei. The samples were then replaced with 70% Glycerol:PBS and mounted for imaging.

Stained specimen were imaged using a Zeiss LSM700 LASER scanning confocal microscope with 20x, 40x, and 63x objectives and 1au pinhole. For ultrastructure analysis

of adult scales, it was found that mounting single scales from regions of interest dry on a microscope slide, imaging it on the reflected light scope as mentioned previously, then covering it with #1.5 glass coverslip, and imaging on the LSM700 with a 40X lens optimized for water immersion using the DAPI filter set, provided the clearest images while preventing movement during the operation.

3.2.6 Spectrophotometry

Absorbance measurements were taken on the same Zeiss AxioPhot configured to perform transmission microscopy. Measurements were taken using an Ocean Optics Flame microspectrophotometer with a 900ms integration time, averaged over 10 measurements and with boxcar set to 5. New blanking was done on every sample to eliminate mounting effects on the measurement. In all measurements, time of integration was set to the recommended 55,000-58,000 photon counts suggested by the manufacturers.

3.2.7 In vivo *injections*

1mM stock of Cytochalasin D, 100uM stock of Latrunculin A, or 1mM Blebbistatin were prepared by adding 0.22um syringe-filtered DMSO to powder. Stock of 140mM 3-Iodo-L-Tyrosine made by diluting powder in H2O which was acidified dropwise with HCl until all powder was suspended. Stocks were maintained at -20C. Dilutions were made in either 1xPBS or Grace's medium to achieve desired concentration; stocks were made to be used at $1/100^{th}$ stock concentration. 15-20uL injections were made at the left hand dorsal thoracic-abdominal boundary with a 26g hypodermic needle.

3.2.8 Chlorine gas and acidified MeOH treatments

Chlorine gas exposure - In a fume hood, wild type wings were placed dorsal side up on an aluminum can support within a deep glass Petri dish. A piece of Parafilm was laid within the lid to serve as a gasket to prevent leaks. To the deep well dish, I added 15mL of house hold bleach at full strength, then when ready to start the reaction, approximately 2mL of concentrated HCl was added to the bleach. The vessel was immediately sealed and remained so for 45 minutes. At the end, the lid was propped ajar to allow the fumes to dissipate. Wings were then removed and imaged.

Acidified MeOH extraction - Samples were submerged dorsal side up in a mixture of 250uL 15% HCl in 10mL 100% MeOH and then rocked in petri dish for 20hrs at 35rpm at room temperature. Samples were removed from the mixture and washed several times in MilliQ H2O then allowed to dry.

3.2.9 Composites of reflected light and SEM or Confocal images

In order to make a composite image of color information with structural information better achieved on the Confocal or SEM, we had to image the same scale on both microscopes. Once this was achieved we could merge the two data sets. The imaging was performed

as previously outlined with high density Z-stacks taken on the confocal to improve Z-axis resolution.

For merging with the confocal data, each confocal Z stack was first made into a Z-projection for alignment purposes with the color image. Once aligned the confocal stack was exported to individual Z-planes which were segmented and used as masks to extract local color information from the color image. Once completed for every Z-position, these colorized images were recombined into a single Z-stack and 3D images were taken. All of these steps were done in Adobe Photoshop and ImageJ.

For combining color and SEM data, a much simpler process was done consisting of loading the color and SEM image into Adobe Photoshop as separate layers, aligning the images, and screening the layers over one another.

3.2.10 Image analysis

Regions of interest (ROI) were defined in images and then color information was extracted using the algorithm found in appendix 4 (Script A4.1). For hue distributions, the sum of all pixels with a binned hue was found using R, then plotted using the R library ggplot2.

Transmission plots were derived from microspectrophotometer absorbance data by converting each wavelength's absorbance using the equation T=10^-(Abs-2) and plotted using ggplot2.

3.3 Results

Papilio palinurus scales have longitudinal ridges running their length. These are intersected at perpendicular angles by crossribs spaced 5-10um apart, with crossribs in adjacent rows of ridges not necessarily falling into register – suggesting a row-by-row autonomy of crossrib specification. The result is that the abwing surface of the scale is separated into an imperfect grid of roughly square intersections of ridges and crossribs (Fig3.12K). Within any single square, the surface becomes concave – parabolic in cross-section (41,262) – as if a loose piece of fabric was supported by a square frame at its edges. The parabolic concavity of the surface is required for the production of the dual blue and yellow reflections of the internal multilayer (Fig3.1) (262). While no studies have focused upon the developmental process of any *Achillides,* we hypothesized that the basic morphology would heavily rely upon F-Actin dynamics based upon previous studies in butterflies, moths, and *Drosophila* (54,124,126,137,138,140,263–265).

As developing pupae will not demonstrate structural or pigmentary coloration until near the time of eclosion, we first examined a number of adult specimen and identified landmarks on the hindwing which always corresponded to green regions – the distal tip of the discal cell. In so doing, we had a reliable location to be confident that we were looking at scales that were fated to be structurally colored (Fig3.2). The distal discal cell is also structurally-colored in other commercially raised *Achillides* species *P. blumei* and

P. ulysses, making it an ideal location for analysis in comparative developmental studies (Fig3.3). In contrast, the tails of *P. palinurus* and *P. ulysses* rarely have any structurally colored scales, whereas *P. blumei* has blue scales with morphology closer to that of *P. palinurus'* and its own green scales – yet they display colors closer to that of *P. ulysses.*

3.3.1 Description of Actin dynamics in structurally colored scales of P. palinurus

Owing to importing permit restrictions, we were unable to maintain a full lifecycle – I received all animals as pupae. Though this is an obvious limitation on being able to rigidly assign an age to specimen, I believe that we can more or less assign a relative chronological age to specimen based upon what has been previously detailed in the literature. Through a combination of phalloidin (Ph) staining to mark F-Actin and fluorescently labeled wheat germ agglutinin (WGA) to label chitin and GlcNAc glycosylated proteins, we examined a large number of scales from the green bands of *P. palinurus* pupal discs with confocal microscopy. In the youngest specimen, we found that future green scales appear no different than unspecialized butterfly scales – roughly balloon-shaped with lots of small actin rods fanning out from the pedicel to the apical tip of the scale (Fig.3.4A-B). Next, scales obtain a slightly squared tip with an average of 25 longitudinal F-Actin rods across the abwing surface (Fig3.4C). Development continues leading to a loss of about half of the abwing F-Actin cables, without a change in the thickness of the scales (Fig3.4D). It is unclear if the reduction occurs by fusion or break down of cables. Moreover it is unclear how the scale directs the changes to every other cable. After this selective reduction in F-Actin rods, the remaining rods appear to thicken and roughen (as a fraying rope) (Fig3.4E). It is at this point in time that WGA staining begins to light up puncta between the remaining thickened F-Actin rods. The WGA puncta colocalize with small patches of phalloidin stain – though it is unclear whether there is a causal relationship between the two stains (Fig3.4E F-Actin vs. GlcNAc). Next we found in the same regions where the actin/WGA puncta were, discrete rings of F-Actin connected by thin fibers of F-Actin reminiscent of textbook models of uncoiled DNA during replication (Fig3.7). These rings appear to become hexagonally packed F-Actin concentric with the developing parabolic reflectors, which can be seen by WGA stain overlay (Fig3.4F). Interestingly, this conversion of longitudinal to circular to hexagonal F-Actin is limited to the abwing surface only – the adwing surface retains its longitudinal array of F-Actin (Fig3.6). During the conversion it also appears that the aspect ratio of the scale changes from long and narrow to a stockier, short and wide (Fig3.4A-D vs. Fig3.4E-F).

3.3.2 P. palinurus *Actin-dynamics inhibitor injections*

Given the apparent importance of dynamic F-Actin for these scales, I hypothesized that interfering with the dynamics would interfere with ultrastructure development and perhaps shift the apparent color. Specifically, I suspected that, since the parabolic shape is most critical for producing the retroreflected blue coloration, alteration of the shape would abolish the blue retroreflection resulting in a red-shifted butterfly. I injected pupae with 10uM Cytochalasin D (CytoD) (final concentration in the butterfly) and allowed them to

eclose, then characterized their color and scale morphology. As predicted, I recovered many red-shifted animals following treatment when compared to wild type dimples (Fig3.8-3.10). The degree to which animals were red-shifted varied as one might expect given the lack of control over when we injected relative to any individual's developmental progress (Fig3.9). In the most severe red-shifted individuals the typically jungle green bands became distinctly greenish-yellow with distal margin chevrons moving from yellow-green to orange (Fig3.8B). Also occurring occasionally, we found that the bands became more specular in reflectivity than wild type, appearing metallic.

Closer examination of the scales with reflected light microscopy revealed a multitude of changes including distinctly disorganized dimples, dimples which appeared to be split in half, loss of retroreflection, squaring of the normal circular profile, loss of dimples in the proximal region of the scale, and a red-shifting of both the retroreflected blues as well as the central green (Fig3.9 and Fig3.10). To further characterize how the ultrastructure may influence reflection we pulled scales from the treated samples and examined them with SEM. Where in wild type animals crossribs and ridges created a regular lattice (Fig3.10A,A'), in treated animals the crossribs (and occasionally the ridges) were often disorganized and failed to create the perpendicular lattice (Fig3.10B and D). As a result the normal parabolic profile of the dimples, became warped and contributed to a loss of the retroreflection as revealed when we overlaid the reflected light with the SEM images (Fig3.10B',D').

When we examined uninjected specimen from museum collections, we found that these phenotypes exist at roughly the same frequency (Fig3.11). It is hard to say with confidence whether the phenotypes we found in our injected animals are recapitulating natural mutants or whether the drug treatments were simply ineffectual - the latter seems more likely as treatment with Latrunculin A did not result in additional or stronger phenotypes over a range of concentrations. Despite this, there is still a likely connection between dimple morphology change and the hue change whether caused by drugs or not.

While disorganization of dimple morphology can easily account for red-shifts attributed to the loss of retroreflected blues, the red-shifting of the central green or retroreflected blue likely lie in changes made to the internal multilayer (Fig3.8B and Fig3.10C). To examine if this was the case we performed TEM on scales from treated animals to quantify if there were changes to the multilayer's chitin and air dimensions (Fig3.12). Measurements of TEM thin sections suggest that the red shifted scale did show an increase in thickness relative to the wild type, as well as having very disorganized lower laminae (Fig3.13 and Fig 3.14).

3.3.3 Achillides *sub-genus ultrastructure survey*

Having found that alteration to the ultrastructure and nanostructure of the scale and production a multitude of colors was possible, we were curious if there were any analogous phenotypes in other *Achillides* species. To address the reflected light

coloration of wings from ~30 specimen representing most of the *Achillides* species was documented. Also leveraged was the fact that the dimple ultrastructure is large enough to visualize using light microscopy (5-10um) so high density confocal stacks of the scales were made using the autofluorescence of chitin in the near UV to visualize. These were then compared with photographs of the same scales to again get a sense of how the morphology contributes to coloration and finally this data was aligned to the most recent *Achillides* phylogeny (259). Excitingly, several phenotypes emerging from the Actin manipulations and museum specimen closely correspond to existing phenotypes in our survey, including serpentine reflectance created by incomplete crossrib formation and boxy, squared-off structures (Fig3.10C and 3.10D vs. Fig3.15E,F,H,L,P). Interestingly, when placed on the phylogeny dimple shape and retroreflection presence/absence fall out in monophyletic groupings (Fig3.16). Further, one parsimonious explanation for the evolution of dimple morphology places the *P. palinurus*-like dimple as ancestral to all other dimple morphologies (Fig3.16B).

3.3.4 Comparison to Papilio ulysses *Actin dynamics*

To address this, we were examined the development of a few *P. ulysses* pupae. While we are less capable of assigning age than in *P. palinurus,* the scales of *P. ulysses* have a hexagonal F-Actin arrangement reminiscent of *P. palinurus,* attaining a squared-off rectangular pattern (Fig3.17A-F). While inconclusive, it is likely that the hexagonal morphology precedes the rectangular because the adult structure is squared off (Fig3.15P). This data supports the hypothesis proposed earlier that a circular dimple structure, like *P. palinurus's,* is representative of the ancestral *Achillides* dimple (Fig3.16B). In this scenario, the ancestral *Achillides* scale development would have possessed the hexagonal arrangement actin arrangement seen in Fig3.4F, which later was modified into to a boxy structure like in *P. ulysses*, and the serpentine structures of species like *P. paris* (Fig3.15L). This latter point being supported by the observed variation presented in Figures 3.10 and 3.11.

3.3.5 Blue-shifted damage phenotype and pigmentation in P. palinurus

In the course of performing small molecule injections, I regularly found *P. palinurus* individuals emerging with distinctly blue patches where green was expected (Fig3.18). Given that the substance injected never seemed to matter (DMSO, LatA, CytoD, Heparin) and that the blue was often associated with an area of reduced pigmentation on the ventral surface, I suspect that this is merely an effect of injection trauma, not the substance injected.

Though I found that pigment reduction in Morphos only resulted in a loss of saturation not a hue shift (Chapter 2), I wanted to ensure that pigment manipulation wasn't the cause of this blue shift. To this end, I treated wings of two dead wild type adults with chlorine gas, which breaks down the melanin polymer. To my surprise this resulted in not a blue shift nor a simple desaturation, but a desaturated wing with a red shift (Fig3.19). I hypothesized that underlying pigments in the scales may have changed color, as has been suggested

in dragonflies and geckos, which could be the ultimate source of the red shift (72,266). When I examined single scale reflection and pigmentation, this did seem to hold true as dark black/brown pigments in both cover and ground scales became lighter and reddened (Fig3.20A,B vs. Fig3.20A',B' and Fig3.20C,C'-green lines vs Fig3.20C,C'-yellow green lines).

Given that the red-shifted result of Chlorine treatment was attributable shift in pigment absorbance, I wanted to further test the unlikely possibility that pigmentation loss was causing the hue shift seen in Fig3.18. Since, I was able to manipulate Morpho melanization with 3-Iodo-Tyrosine (3IT) (Fig2.9), I made the same manipulation in *P. palinurus*. Again surprisingly, there was a visible hue shift in addition to the desaturation – however this too was blue like the damage phenotype, albeit global in effect as expected of a small molecule (Fig3.18C-C'').

3.3.6 Characterization of pigment in P. palinurus *cover scales*

On examining the absorbance of single scales pulled from both damage blues and 3IT treated butterflies, the blue shifted damage phenotypes look like simple decreases in the level of pigmentation, as read out by an increase in transmission across the spectrum that maintains the same slope as the wild type (Fig3.21D-green lines vs blue). However, the 3IT treatment (while still decreasing overall absorbance) also shows a change in slope, with an increase in red absorbance relative to blue absorbance when compared to wild type (Fig3.21D-turquoise line). This could suggest that there is more than a single pigment and that 3IT can only reduce the presence of a single component (melanin) leaving a blue bias. Moreover, 3IT impacts the ground scale far more than the cover scale, suggesting that the two scale types have differential types of pigmentation (turquoise lines Fig3.21D'vsD).

It has been shown in many Papilionid butterflies that ommochromes play an important role in wing coloration, and given the possibility that a second pigment existed in the wings we performed an acidified MeOH extraction on a disartiulated adult wild type wing (34,51,56,74). This treatment resulted in a strong blue shift, surprisingly however, when we examined the absorption of single scales we saw a similar shift in absorption as in the Cl_2 treated animals (decrease in red absorbance) (Fig3.19 and Fig3.20-blue line). Given that there was clearly a blue shift in reflected light, this suggests that the Acidified MeOH may have extracted some pigment, but may have caused damage to the wing. To ask whether this was merely a damage effect and if the procedure was working correctly, I performed the same extraction on the hindwing of *Morpho peleides*. *Morphos* use an external multilayer to create blue and so should control for damage associated with the treatment, they have ommochromes both dorsally and ventrally, but these ommochromes do not overlap with the structural elements so there is less concern for confounding a color shift in the blue region with merely pigmentation loss. When we investigated treated wings we found that there were areas where red pigments were strongly depleted (Fig3.22DI$_{Chevron}$). This was qualitatively obvious just by examination, but in yellow regions this was less obvious (Fig3.22VI$_{eyespot}$). Indeed single scale examination showed that red

scales were strongly depleted of pigments but yellow scales hardly at all (Fig3.22-Transmittance). The yellow scales also showed a spectrum similar to bleached *P. palinurus* scales (Fig3.20A',B',C,C'). It is quite clear that the Acid MeOH can damage scale ultrastructures, as is clear from the twisted husk of the red scales and the red-shift of the Morpho blue structures.

To characterize the yellow pigments of Morpho and bleached *P. palinurus* I examined the abdominal cuticle of OregonR *Drosophila melanogaster* adults, which have known pigments thanks to genetic manipulations (Fig3.23) (235). After measurement, I could conclude that the region of the abdomen that has yellow pigment (known to be Beta-alanyl dopamine melanin) has absorbance that is very similar to the morpho's yellow eyespot annulus, while its dark brown dopamine melanin stripe matches closely to *P. palinurus*'s cover scale.

As mentioned before, we did see a blue shift in *P. palinurus* following MeOH exposure, so it was formally possible that there were two pigments in the cover scales. In other Papilionids, papiliochrome is a common pigment, and it has strong blue absorbance so we imaged *Papilio nireus* scales, which have been described as containing papiliochrome II (Fig3.24) (56,73). One expectation would be that extraction of papiliochrome from *P. palinurus* would eliminate its blue absorbance and allow for blue reflections to contaminate the green of the wild type producing a blue shift. I modeled this by empirically combining weighted portions of absorbance profiles from dopamine melanin scales and that of *P. nireus's* papiliochrome II profile (Fig3.24D dark blue line). Despite attempts to find a close fit, I was unable to create a tight fitting curve to the wild type *P. palinurus* cover scale absorbance profile. This could reflect the absence of an ommochrome in wild type scale or it may be that papiliochrome II is the wrong ommochrome.

I looked further into this possibility by dissecting pupae at various time points following structural development. At a point when the wings became opaque, which signals chitin deposition, scales in the region that will eventually be green produce a dilute greenish structural color (Fig3.25A,A'). In most described butterflies, including a Papilionid, pigmentation productions is sequential with ommochromes preceding melanization, with the notable exception of *Vanessa cardui* where it was observed that melanin came in first (131–135). In pupal wings without evidence of melanization, a strong yellow-orange pigment was present in non-structural patches along the distal margin (arrowheads Fig3.25B,C), along the future main green stripe and peppered through the region distal to this. Upon closer inspection, the pigmented scales are the structurally colored scales (Fig3.25B'). This pigment appeared prior to melanization, which I was able to show was a global phenomenon by incubating a wing at a similar stage to B in Grace's medium supplemented with L-DOPA to promote melanization. Over the course of ~3 hours the wing pigmented fully with a dark black pigment, while the structurally colored region went from yellow-green to emerald green (Fig3.25C,D). More investigation needs to be done including spectrophotometry of the pupal scales.

In sum, it is possible, though not conclusive, that *P. palinurus* utilizes 2 pigments in its wings, melanin, and possibly an ommochrome, perhaps xanthommatin.

3.3.7 TEM analysis of blue shifted scales in relation to pigment localization

We next prepared the scales from a damage induced blue region and from the 3IT individual for TEM to ascertain if changes to multilayer or electron density occurred relative to wild type. It was unclear whether the blue shifted scales would have changes to the multilayer or not. In wild type animals, it has been shown and we confirmed, that there is a substantial difference in electron density between upper and lower laminae of the multilayer (Figs 3.12,3.13,3.26) (41). This has been speculated as being a difference in pigmentation by Vukusic et al. but not shown conclusively (41). These lower laminar layers are also thinner than the upper lamina (Fig3.13, Fig3.14). As a consequence it is possible in the blue shifted animals, that a loss of pigment could unmask thinner layers that are likely of a thickness that is biased to reflect bluer wavelengths. Alternatively, it is possible that the multilayer layer requires pigmentation or sclerotization (such as NADA melanin or N-Beta-alanyldopamine) to achieve its wild type dimensions. This is not out of the question as we have noted structurally weakened Morpho scales following 3IT treatment (Chapter 2), and Zhang et al. noticed a similar weakening of scales in *Junonia* following mutation of *tyrosine hydroxylase* (77). Densitometry measurements of our collected TEM images suggested that there was less electron density in both the 3IT and damage blue scales when compared to those of the wild type (Fig3.26). Whereas it was qualitatively obvious that there was a thickening of laminae in red-shifted scales, in the blue shifted scales there was not an obvious thinning. One exception to this was what appeared to be the collapse of the lowest layer in the 3IT-treated dimples. It remains to be seen whether this is an artefact of the sectioning or if it is a genuine result of 3IT knockdown (Fig3.26).

3.3.8 Pigment changes in other structurally-colored Achillides

If we accept that pigmentation changes, both red shifts in pigment transmission and unmasking of thinner laminae by melanin loss, it is reasonable to imagine that pigmentation level/type could produce hue shifts between naturally occurring *Achillides* species. Therefore, we examined the pigmentation of scales from naturally occurring species with structural color variation similar to what we observed in our manipulated *P. palinurus* specimen. *P. blumei fruhstorferi* has a green band similar to *P. palinurus* but also has structural blue tails with coloration similar to our damage phenotype (Fig3.27A). *P. peranthus* has structural green that varies with subspecies between what we observe in wild type and bleached/manipulated *P. palinurus – P. peranthus transiens* and *P.p. kangeanus* respectively (Fig3.27B and C). When we examined the single scale from these species, we found that the blue tails of *P. blumei* did have less pigmentation than the green band as in the damage and 3IT specimen, but *P. peranthus kangeanus* had less pigmentation than *P. p. transiens,* which was not expected given the results of the Cl_2 exposed specimen (Fig3.28). However, if loss of pigment in *P. palinurus* and *P. blumei* result in blue shifts, then perhaps it is reasonable to imagine that a gain of pigment could

result in a red-shift (Fig3.30E). I believe these data represent the exciting possibility that, unlike Morphos (Chapter 2), pigmentation changes in at least some of the *Achillides* may be sufficient for, not just saturation changes but also changes in hue thanks to the masking/unmasking of portions of the chirped multilayer.

3.4 Discussion

Color has evolved to be an important part of ecological interactions within and between species. However, for many organisms pigmentation does not allow full access to the visible spectrum. This is the case in most butterflies and moths, which have instead evolved the ability to produce colors through physical manipulation of light. A great deal of research has gone into understanding how the physics of a multitude of nanostructural solutions produce their color. For a number of reasons though, little has been done to investigate how an organism generates their structures during metamorphosis.

The majority of nanostructures in butterflies falls into one of 4 categories: 1) thin-films – typically the scale lower lamina, 2) Morpho-type (elaborated ridge) multilayers, 3) Urania-type (internal lumen) multilayers, and 4) 3-D photonic crystals (typically gyroids). Investigation of nanostructure morphogenesis has been done largely by Helen Ghiradella through TEM of developing pupae. Her study on the development of *Colias eurytheme*, a UV reflecting butterfly with Morpho-type reflectors, noted a relationship with F-Actin bundles similar to what had been seen for non-Morpho-type ridges (54,124,126). Her study on the development of Urania-type multilayers and 3-D photonic crystals found a series of internal membrane-bound compartments where the eventual chitin lattices would be, but could divine little else with any certainty (36). There has not been much done since 1989 to understand more about development: one paper, using Ghiradella's own data, argued that the adult gyroid forms from 2 intertwining organelles (the SER and plasma membrane) that support one another until the chitin can be deposited in the finalized scale (130). While this was a step forward, they produced no new primary data, made no biological manipulations, provided no actual evidence for the cytologic origin of the organelles, and did not provide any direct insight for the mechanical aspects of how organelles would produce such a structure – all of which are clearly important for understanding how an organism evolves nanostructures. Another paper sought more detailed understanding of scale cell development, focusing on F-Actin dynamics in a descriptive manner and also making manipulations of said dynamics through small molecule inhibitors (124). While there was a clear importance for actin in creating normal scale morphology, this study was not done in structurally colored organisms, and so allows only for speculation as to how such manipulations could affect nanostructures. Here I have provided the first evidence to suggest that F-Actin dynamics are critically important for the construction of structural elements and further I hypothesize that F-Actin dynamic modulation may be an important source of evolutionary diversification among structurally colored organisms. Understanding how butterflies reproducibly build nanostructures from organic tissue represents a new frontier for biology, which is often thought of as messy and imprecise. In addition, I've harnessed knowledge about

pigmentation genetics and damage response phenotypes to peek inside a novel phenomenon whereby pigmentation associated with the chirped multilayer tunes hue and saturation by eliminating reflection from layers that provide blue-shifted coloration. This work represents a further step into understanding how butterfly scales alter their structural color over time, which is important for illuminating processes of phenotypic diversification and ultimately speciation from a uniquely unicellular perspective.

The *Achillides* sub-genus of *Papilio* is an advantageous group to examine cell biology contributing to structural coloration for several reasons: 1) there is a recent molecular phylogeny that provides a framework for understanding the relationship of most species, 2) there are working hypotheses for how the species produce color, 3) one of the important components of their structural color is the scale's ultrastructure which is believed to be largely defined by actin in other systems, 4) the ultrastructural components are large enough to see with standard light microscopes in comparison to the nanostructrures, which require EM, allowing for quick triage of phenotypes, and 5) there are several species commercially raised and easily available. *Papilio palinurus* is a butterfly featuring a distinct jungle green stripe that has a 2 component structural origin. Though ultimately owing to a Urania-type internal multilayer, the green color of *P. palinurus* is actually a spatially averaged color synthesis stimulus (how halftone works in newspapers) produced by the combination of blue and yellow reflections. The production of 2 colors is achieved by the scale actually leveraging angle dependent wavelength reflectance – typically what causes iridescence. By warping the multilayer into discreet 5-10um parabolic reflectors, the edges of the reflector sit at approximately 45-60 degrees and thus are optimal for blue reflection, but more importantly the round shape means that a reflection from one side is reflected to the opposite side where it is re-reflected out toward the source (retroreflection). The retroreflected blue thus directly depends upon the ultrastructural curvature of the scale multilayer.

Given the proven and hypothesized importance of actin in producing anatomical structures in scales and beyond, we began our investigation by performing a time series of phalloidin stains in *P. palinurus* scale development. Although we could not objectively define chronological order, we have produced a reasonable approximation of the development of structurally colored scales of *P. palinurus.*

It appears that *P. palinurus* scales produce a hexagonally packed array of F-Actin on their adwing surface where each hexagon defines the boundary with a forming dimple. It is unclear whether the multilayer has already been formed at this point in development. A multitude of possibilities for how a hexagonal array could arise were considered including partial bundling of adjacent straight fibers via Forked/Singed, Arp2/3 dependent branching, and even deformation of a quadrilateral array into a hexagonal array by applying forces at the edges. However, instead I found evidence that suggests localized specification of circular F-Actin, which may grow until contacting nearest neighbors. This is perhaps best analogized to what occurs during cellularization of the *Drosophila* syncytial oocyte and it is hence tempting to hypothesize a redeployment of the embryonic

program (267–270). If this was indeed true, one would have to replace the critical positioning information of the oocyte nuclei with some other signal in the scales. While I cannot define how spacing is established, I have found evidence for the presence of positional information in the regions where circular F-Actin will appear through WGA stains (Fig3.5). I believe these WGA puncta to be GlcNAc glycosylations rather than localized chitin secretion due to the finding of similar puncta when stained with anti-HRP antibodies, which have been demonstrated to bind α1,3-fucosyl glycosylation events (Fig3.5) (271). How the cell produces such regularity remains unresolved but that such potential centers exist provides a plausible source of circular F-Actin inception (Fig3.29).

I wanted to functionally test the role of F-Actin in *P. palinurus'* scale development. Studies in both fly bristles and butterfly scales have utilized the F-Actin capping small molecule Cytochalasin D to interfere with its dynamics (124,272). Further, mutational anaylsis of proteins affecting actin polymerization in fly bristles has produced strong evidence for a delicate balance being required for normal morphogenesis (154,273,274). Several of the phenotypes in flies appear similar to phenotypes induced in butterfly scales by heat shock arguing that there may be a similar process required for scales (141). Many color shifted adults emerged following injection of CytoD into developing pupae. Upon analysis of whole wing and single scale color and morphology, we found that there were discernable and correlated changes. I first focused upon those butterflies where there was a red-shift in overall color relative to wild type and found that there was not one single change that explained any given organism's color change. Rather there were a handful of changes, including the expected loss of retroreflection due to misshapen dimples: simply put, a loss of retroflection is a loss of blue, and hence alters the perceived color towards the red. In others I found that while ultrastructural morphology was largely maintained, the most apparent source of color shift was due to changes in both central and retroreflected colors towards the red. This type of change was a surprise as it suggests that the internal multilayer has been changed, indicating a potential role of F-Actin in establishing multilayer dimensions. The particular balance of color shift and loss of retroreflection was different from sample to sample, a fact which suggests the two are separable developmentally – a logical assumption given the diversity of colors within naturally occurring species sharing identical ultrastructures.

Upon surveying many wild type animals in museum collection specimen, I found similar phenotypes to what we noted in our CytoD injected animals. Failure to find similar phenotypes in Latrunculin A injected animals (another actin depolymerizing drug) made me question whether CytoD injection was actually causative of the phenotypes (which are unquestionably deviations from wild type).

Taken together these morphological data in combination with F-Actin description in *P. ulysses* and the survey of ultrastructures throughout the *Achillides*, leads to a hypothesis that the circular ultrastructure is an ancestral phenotype which was subsequently altered in multiple lineages to produce a wide diversity of structures with different reflection properties and hues.

Owing to the repeated appearance of blue-shifted wing regions correlating with depigmentation following injection of animals (irrespective of what was injected), I focused on trying to understand if pigments alone could be responsible for this color shift. Manipulations of adult wings (Cl_2 gas and acidified MeOH) aimed to remove pigments known to be in butterfly wings. Unlike what I had seen in the loss of pigmentation in damaged blue regions, the destruction of pigments by chlorine gas gave the wing a red shift. This was surprising as red shifts in structural color are typically associated with the increase in thickness of an optical layer – something unlikely from the destructive nature of chlorine gas. Since it was known that some pigments can shift according to redox state, I had a look at the absorbance profile of these bleached scales (72,266). Here I found that the pigments failed to absorb long wavelengths when compared to wild type. This absorbance profile looked remarkably similar to the absorbance profiles of *Drosophila* NBAD melanin and a MeOH-unextractable yellow pigment in yellow scales of *Morpho peleides's* eyespot. It seems reasonable that the red-shift found from chlorine bleaching *P. palinurus* wings is owed to pigmentation change, not to multilayer defect. When looking at 2 of the most red-shifted butterflies emerging from the CytoD injections, one of them had pigmentation absorbance similar to the NBAD melanin – arguing that it may simply be a pigment change (data not shown). The other red-shifted animal appeared to have adwing reflectance defects however, suggesting an actual structural defect. This was confirmed by TEM imaging of the inside of scales from this butterfly, where the multilayer was clearly disorganized and had thickened laminae relative to wild type, but did not show any difference in electron density relative to wild type (suggested to be pigment).

Adult wings treated with acidified MeOH gave a blue shifted coloration. This led to the hypothesis that in addition to melanin, *P. palinurus* may use an ommochrome in its cover scales. This possibility was tested by imaging a papilionid with scales known to utilize papiliochrome II, *Papilio nireus.* Papiliochrome II has a yellowish color which is likely due to its very strong absorbance of short wavelengths. It seemed more reasonable that extraction of a blue-absorbing pigment via acidified MeOH would result in a bluer-looking wing. However, I was unable to confirm this directly, and empirical attempts to match the absorbance of a wild type *P. palinurus* cover scale by combining varying levels of melanin absorbance and papiliochrome absorbance were unsuccessful. I also asked whether the harsh conditions of the acidified MeOH exposure alone could be responsible for color shifts. To do this I used a structurally colored Blue Morpho hindwing. The Morpho hindwing was ideal because it uses a multilayer to create its blue color, and has ommochromes in unstructured regions which provide positive confirmation for ommochrome extraction. While the ommochrome extraction was successful in this control, I did notice color change in the structural regions of the wing as well. Given that *Morpho peleides* does not use an ommochrome in the blue regions, this suggests that the medium itself is damaging to the structures and may in its own right lead to the color shift seen in the wing of *P. palinurus* treated in this manner. On the other hand, observation of wing discs from developing *P. palinurus* prior to melanin onset suggests that a yellow-orange pigment is selectively deposited in the structurally colored scales

though I did not analyze the absorbance of these scales arguing for the presence of a second pigment.

While the presence of a second pigment remains debatable, between observations of the absorbance of single scales pulled from damaged blue regions and those taken from the wing of a butterfly treated with 3IT, it seems likely that melanin is present in the ground and cover scales of *P. palinurus.* This likelihood is compounded by similarity of the absorbance profiles with those of known pigments from *Drosophila melanogaster* abdomen. Moreover, the low level of electron density in lower lamina of damaged and 3IT treated butterfly scales (suspected to be pigment) differentiated them from the highly dense lower laminae of wild type butterfly scales. A similar difference in absorbance spectra was noted between the green and blue scales of the closely related *P. blumei*, suggesting that the reduction in at least melanin presence may be a mechanism used to tune coloration in naturally occurring species.

Biologically constructed structural coloration presents fascinating ontogenetic puzzles. The tight tolerances required to make a color face to face with comparatively large surface areas of a scale and a large number of scale replicates is a level of control that is rather unfathomable for a biological (read: messy) system. Yet, there must exist a rigid and robust determination of said morphology as the failure to maintain those tight tolerances is sufficient to produce deviation in colors, which could impact the ecological interaction it is meant to mediate. Paradoxically, we know from evolutionary comparisons that closely related species, such as the *Achillides*, that color does change overtime, suggesting that morphological variation may be selected upon or may be fixed by drift.

Here I, with significant help from several others, have found 2 mechanisms that appear to be robust to perturbation and highly accurate, while still representing potential sources of variation and novel coloration (Fig3.31). The actin cytoskeleton is essential for normal scale development, in *Drosophila* bristles it plays a similar role, and in *Drosophila* embryos it is necessary for cellularization of the syncytial blastoderm. I have described a process that bears remarkable morphological similarity to cellularization in *Drosophila* embryos being deployed to cause shallow invaginations of the cell surface of a butterfly scale (268,270). While I am uncertain as to the nature of some observed perturbations found in treated and wild caught adults, those perturbations logically fit with disruptions to the proper formation of a set of ring-like cortical actin structures. I suggest that those disruptions mirror some of the naturally occurring ultrastructural variation that defines entire clades within the *Achillides,* and perhaps aid in the construction or destruction of retroreflectors within these groups.

Secondly, I have presented data that suggests that at least one pigment is present in *P. palinurus*, that pigment is a melanin, and it not only serves to improve structural color saturation (as we've shown in Morphos) but also masks thinner layers of the chirped multilayer that creates the structural reflections. This is an exciting finding as chirped multilayers have been thought of as great ways to make broad band reflectors capable of making silvery mirrored finishes. In this case however, the chirped multilayer spans a

narrow range of thicknesses, which from this data, maintain the reflector itself in a blue-green ballpark. The neat trick that *P. palinurus* seems to have has evolved, is to spatially restrict its melanization to lower, thinner laminae. Given that the wild type proves this spatial restriction is possible, it is exciting to imagine that spatial restriction is also mutable. If so, it is fathomable that the birth of a given allele could alter the spatial restriction of pigment to more or fewer laminae in the chirped multilayer. In so doing, pigmentation alone could alter both the saturation and the preferred reflected hue – a situation that is not seen in the Morphos. In a cursory look into *P. blumei,* this did seem to be a mechanism by which hue could be altered.

Finally, from the observational differences of scale morphology and color across the three commercially available *Achillides* species (*P. palinurus, ulysses*, and *blumei*), one expects that comparison of tails and discal cell development may provide a handle for separating the contributing factors controlling and manifesting pigmentation, multilayer, and ultrastructural morphogenesis differences.

3.5 Conclusions

Here I have investigated the morphological origins of an ultrastructural warping in a Urania-type internal multilayer and found F-Actin dynamics delimit the boundaries of a parabolic reflector. Though inconclusive, phenotypes emerging in the test population, samples of a closely related species, and in wild caught specimen both have ultrastructural phenotypes that reduce retroreflection. Investigation of *P. palinurus* specimen with structural color shifts in both the central reflection and the annulus of the reflectors, has shown disarray in the internal laminae predicted by the general color shift of the reflections. Prompted by anomalous pigment defects has led to the observation that melanin deposition in subsets of the chirped multilayer's chitin laminae may provide a mechanism for tuning the reflected color by eliminating reflectance from those layers encrusted by pigment. This pigmentation simultaneously purifies the structural reflection from the unpigmented layers as predicted from the results seen in Chapter 2 and elsewhere. The cursory investigation of other species with slight hue shifts also suggests that pigments may be responsible. I believe that the evolution of actin dynamics and pigmentation levels represent generalized mechanisms for hue and saturation tuning in the *Achillides.*

Figure 3.1
P. palinurus vs. *P. ulysses* structure and optical properties

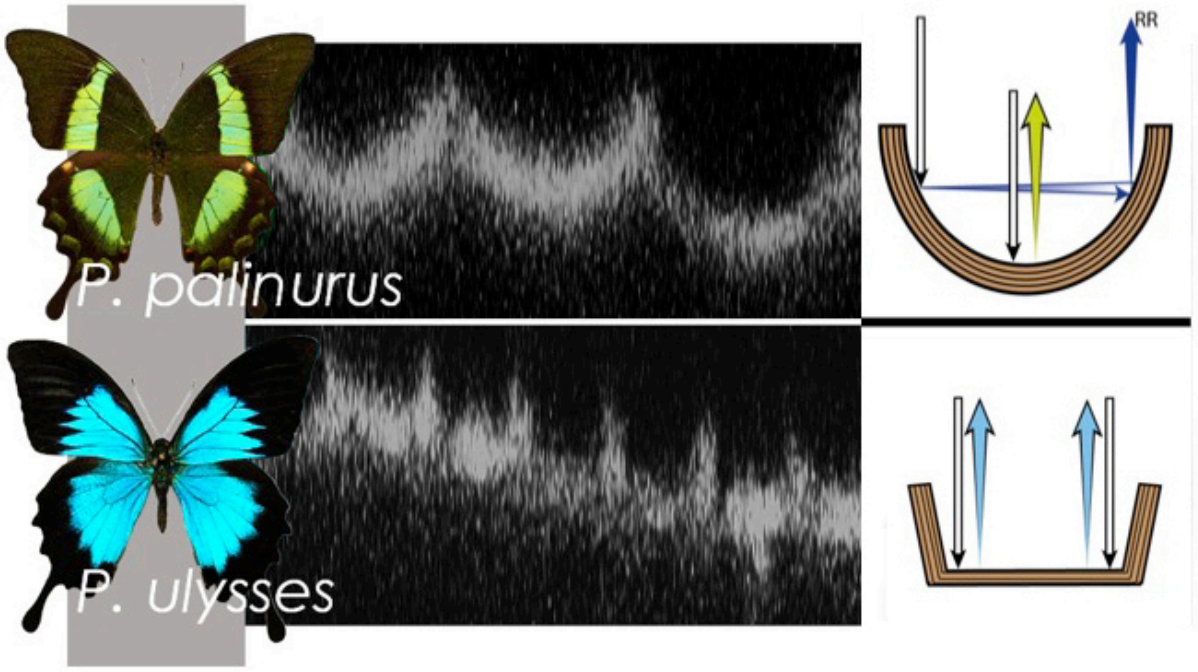

Papilio palinurus and *P. ulysses* are two species of *Achillides* with different modalities of structural color. While both utilize internal multilayers for color production, there are significant differences in the spacing and ultrastructure. *P. palinurus* uses thicker laminae shaped into parabolic dimples and *P. ulysses* uses thinner spacing with a boxy cross-section. The ultrastructural differences are seen clearly in the black and white images, which are XZ projections of adult structurally colored scales taken by scanning laser confocal microscopy. The shape of the ultrastructure determines the ability of the scale to produce 2 differently colored reflections in *P. palinurus* (blue and yellow arrows in schematic on right). Together these dual reflections result in the observed green color of *P. palinurus* seen on the left by an optical effect called a spatially-averaged color-synthesis stimulus. The square profile of the ultrastructure in *P. ulysses* does not allow dual reflections, resulting in a single reflected blue color. The size of *Achillides* ultrastructures is large enough to visualize without electron microscopy. Confocal stacks taken by Alexis Krup.

Figure 3.2
Identifying areas consistently containing or lacking structural scales in *P. palinurus*

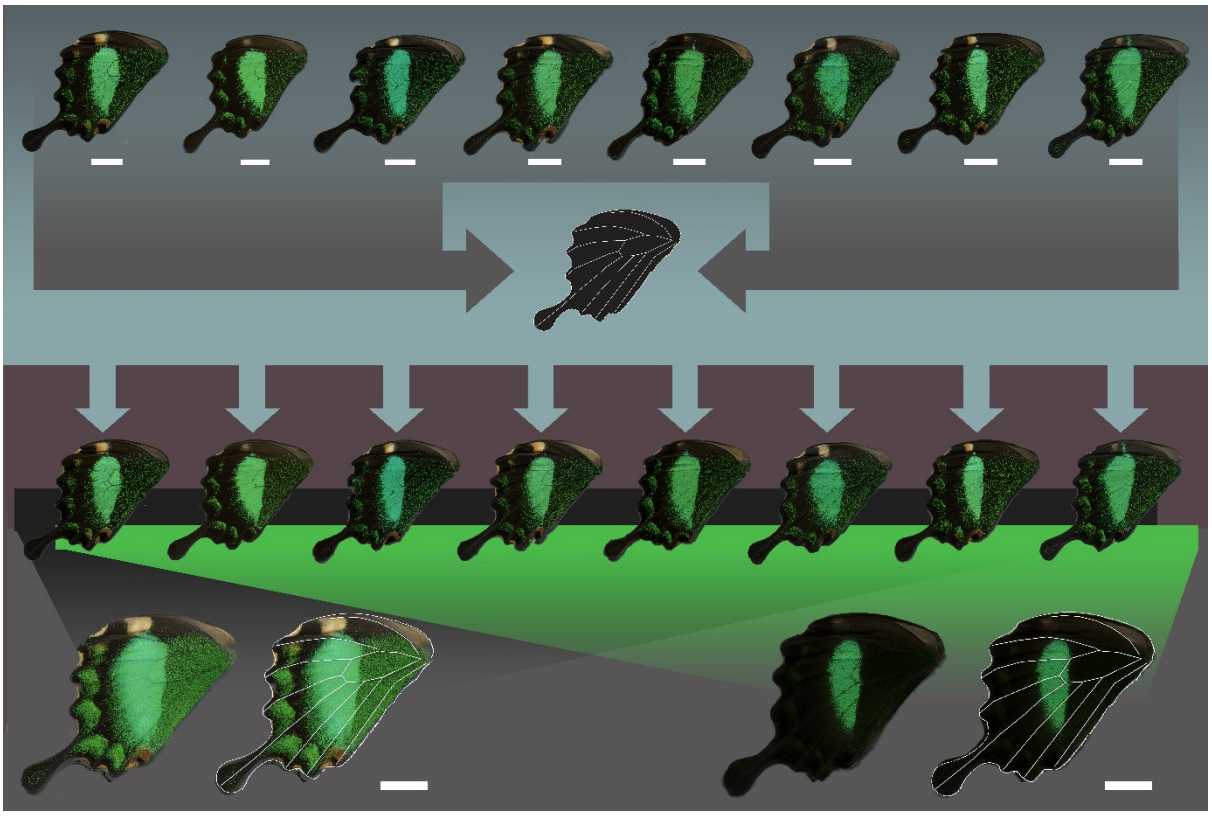

In order to find regions in pupal discs with structural colored scales prior to being morphologically distinct, we scanned hindwings of several individuals (**top row**), and fit them to a standardized wing shape by using puppet warp in Adobe Photoshop to align the veins and perimeter of each individual wing with the master (**second row**). Then by overlaying all standardized wings we could identify regions that never have green scales (**dark areas bottom row left side**) and those which always have green regions (**green areas bottom row right side**). Since wing veins are set early in the pupal wing, green regions and black regions can be identified by using veins as landmarks prior to structural color production or even prior to morphological differences between developing scale types.

Figure 3.3
Identifying conserved spatial domains of structural coloration across species

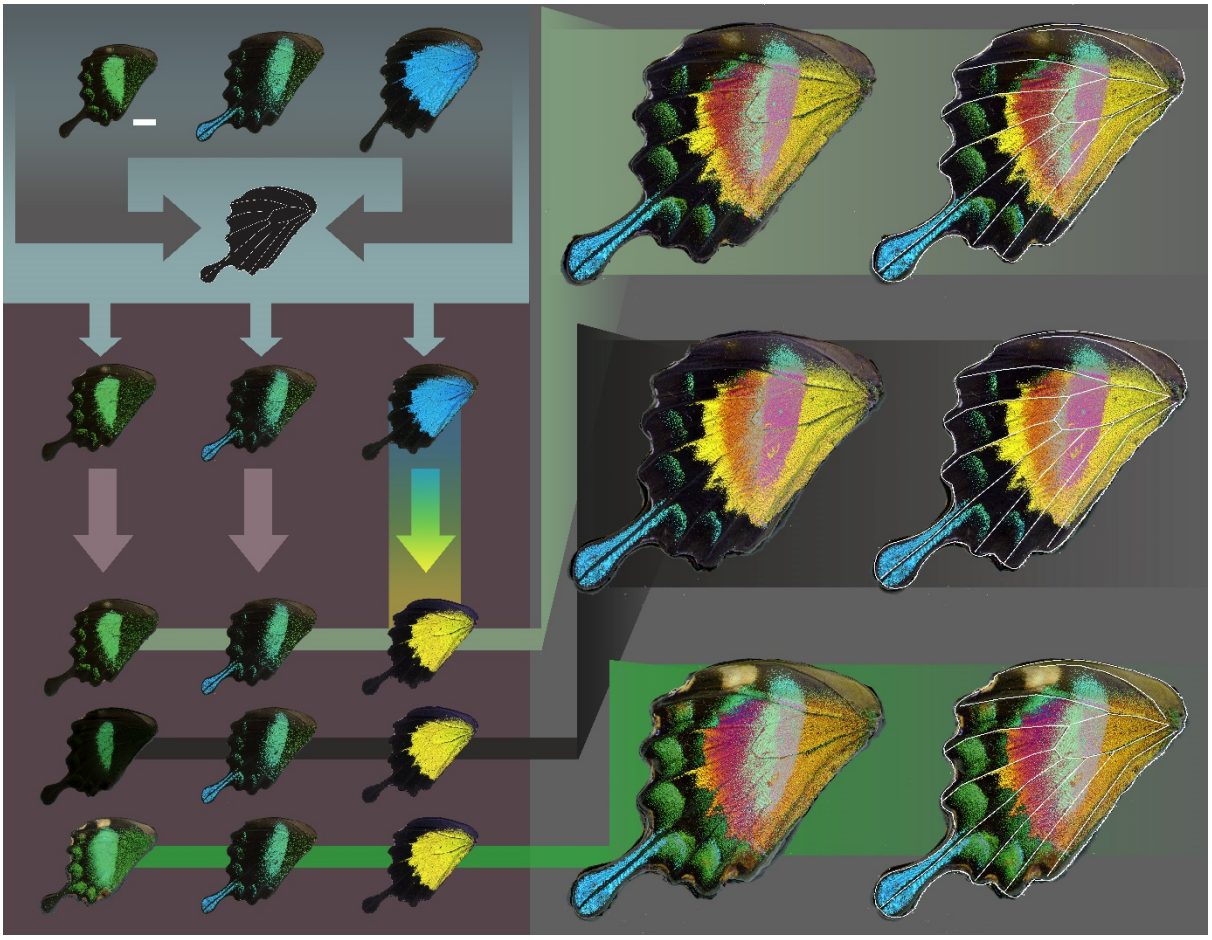

Using a similar work flow to the previous figure, we took hindwings from commercially raised *Achillides* species*, P. palinurus, P. blumei,* and *P. ulysses,* and fit them to a standardized wing (**left side, top row**). Next, we arbitrarily changed the hue of *P. ulysses* from blue to yellow (**left side, middle row**), so that we could obtain regions of distinct coloration when we overlaid the three species (**bottom row, left side & right side**). By combining the conserved green and black maps of *P. palinurus* from the previous figure, we could identify spatial domains with conserved structural presence across the three species with different levels of confidence. **Right side, Top row** – any given single *palinurus* may give a broad domain of conserved structural presence (**mint green**) with the other species. **Right side, middle row** – the area that is always green in *palinurus* significantly reduces the overlap across all three species to a narrow band aligned with the distal discal cell (this represents the highest confidence location). **Right side, bottom row** – utilizing the *palinurus* map of conserved black regions serves to demonstrate where overlap could potentially happen and is thus the lowest confidence region of overlap but the broadest spatial domain of green. Even though the broadest, only the distal 20% of the discal cell shows overlap across all species.

Figure 3.4
Actin stains of developing *P. palinurus* structural scales

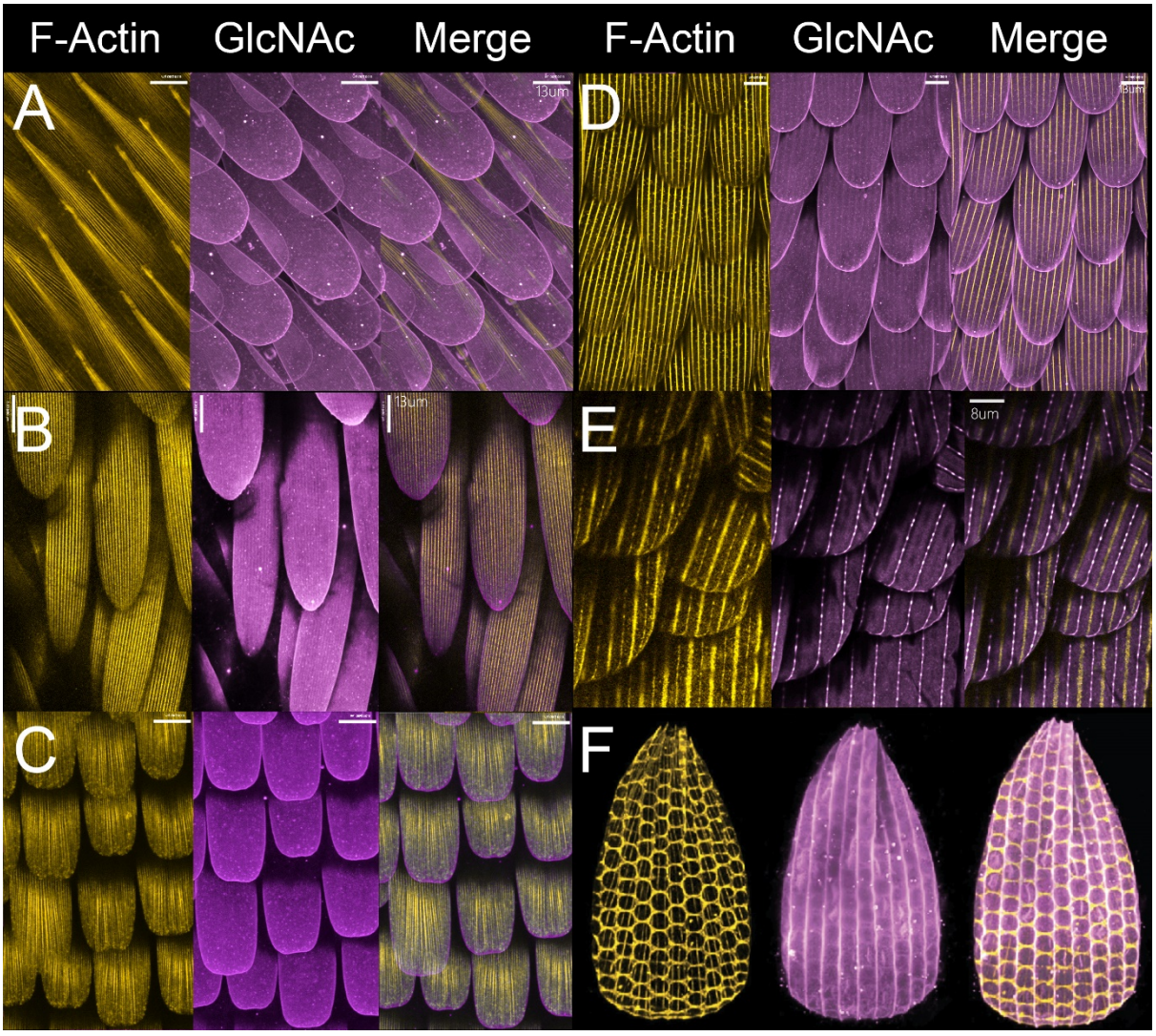

A time series of phalloidin and WGA stains of *P. palinurus* wing discs from multiple individuals imaged via Laser Scanning Confocal Microscopy and temporally ordered to our best knowledge. **A-C** – Earliest buds we found look similar to typical early scales in terms of actin and WGA staining. **D** – Upper lamina's Actin becomes more broadly spaced and thicker than typical scales. **E** – In between thick actin small puncta of Actin staining co-occurs with bright spots of WGA staining (see Figure 3.5 for details). **F** – F-Actin completely rearranged into regular hexagons, each surrounding a nascent dimple as seen in WGA stain (puncta have disappeared). WGA indicates GlcNAc residues which comprise chitin as well as forms the backbone of membrane protein glycosylation.

Figure 3.5
Glycosylation stains suggest membrane protein may be involved in Actin formation

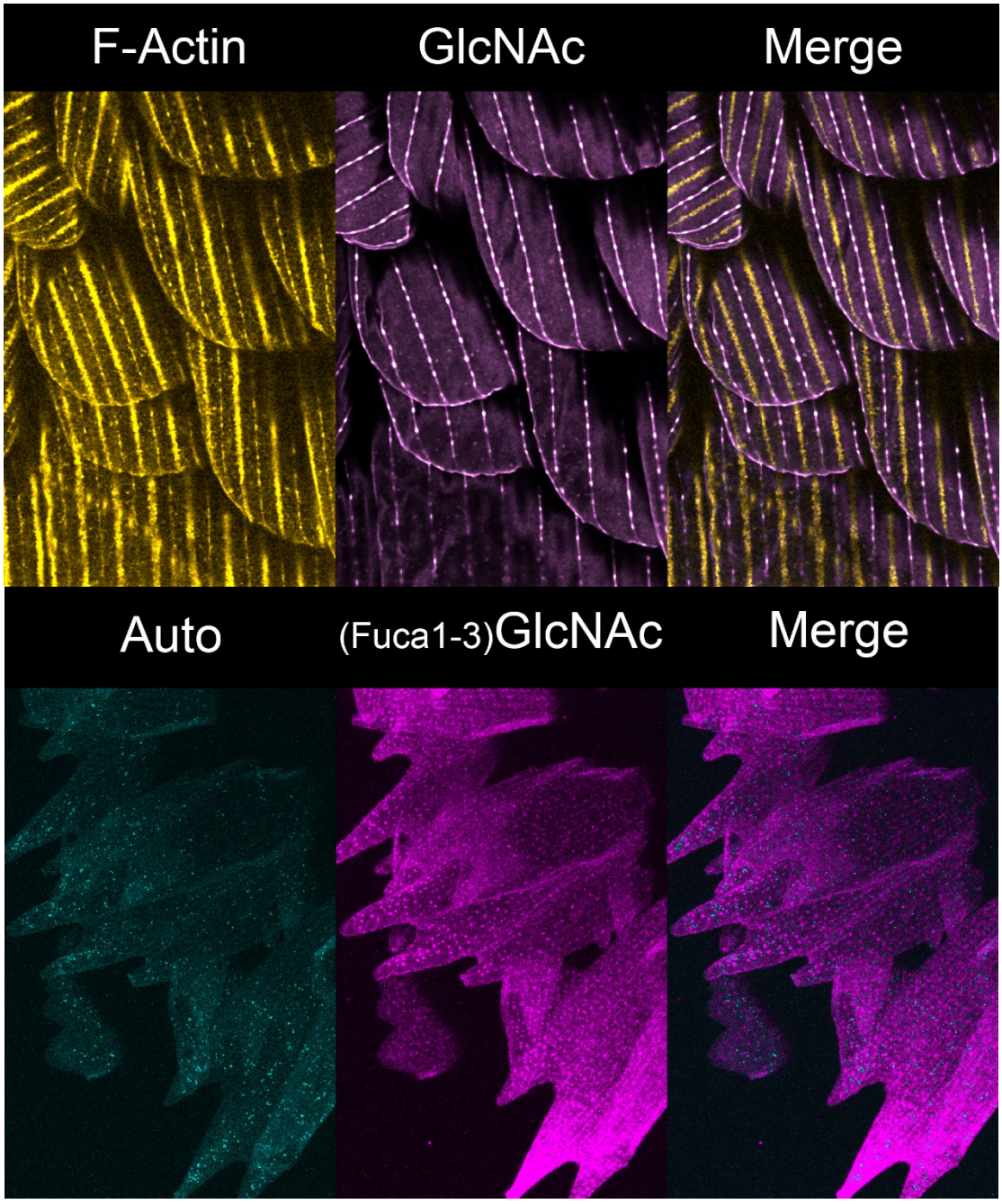

Top - Prior to the presence of circular actin in *P. palinurus* scales, alternating thick and thin actin can be found. The thin actin bundles has a punctate appearance that colocalizes with WGA staining for GlcNAc (both a subunit of chitin and a common protein glycosylation residue). **Bottom -** Arguing for a conserved membrane bound protein, staining developing *Junonia coenia* pupal discs (bottom row) with the Goat anti-HRP antibody (marking $\alpha 1,3$-Fucosyl-GlcNAc, a glycosylation found on membrane proteins) results in similar punctate staining. In flies, Sb is an actin associated, glycosylated membrane protein important for bristle morphogenesis – and so may be playing a role in the formation of circular actin in *P. palinurus* (275–277).

Figure 3.6
Lower lamina Actin has different morphology from upper lamina Actin

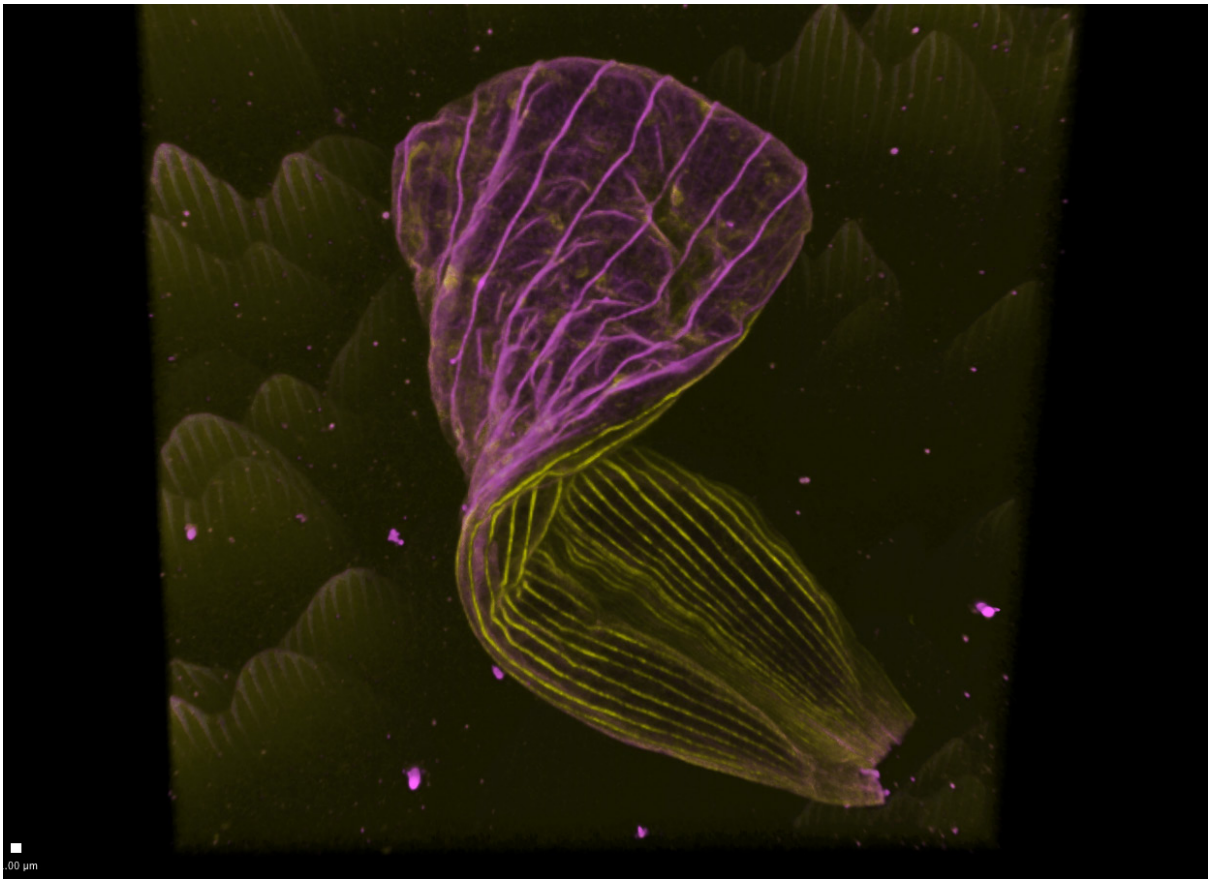

Phalloidin stain (yellow) of a structurally colored *P. palinurus* scale which has curled over on itself shows the lower lamina (bottom half) with longitudinal actin bundles. The upper lamina (top half of image) shows stronger Chitin Binding Protein (pink). The sample is a similar stage as the hexagonally-patterned scales seen in Figure 3.4.

Figure 3.7
Sample showing small circular F-Actin in between large bundles

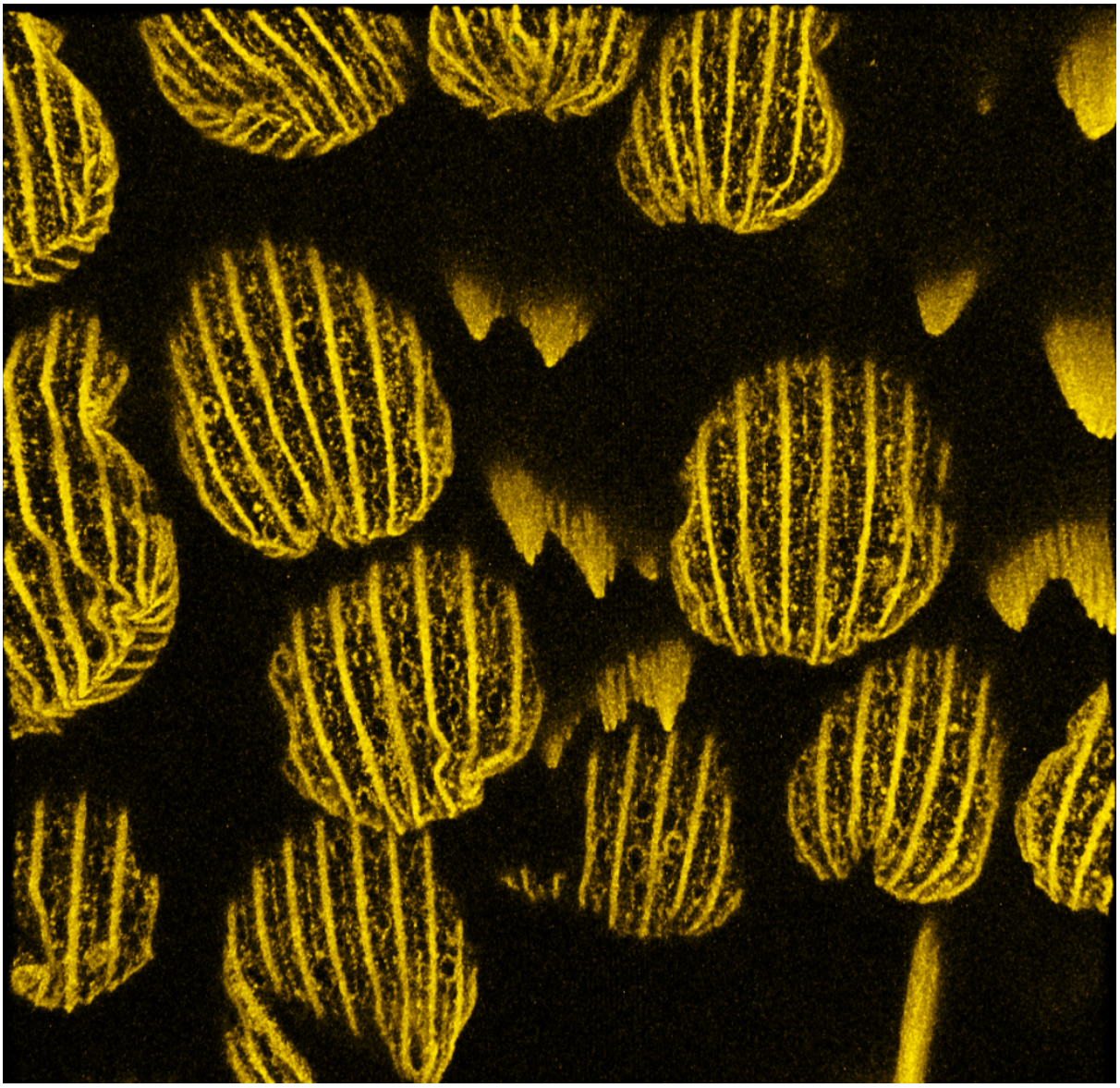

Confocal stack of developing *P. palinurus* structurally colored scales demonstrating the presence of small circular F-Actin in between the thicker bundles of Actin. We believe these represent the first step in the formation of the scale's hexagonal pattern. This particular animal had been injected with 15uL 10uM Blebbistatin leaving open the possibility that Myosin plays a role in the formation of the hexagonal pattern. Although it is possible, if not likely, that we have simply caught this process in the act and this stain does not show any effect of the drug treatment.

Figure 3.8
Red shift relative to Wild Type following injection of CytochalasinD

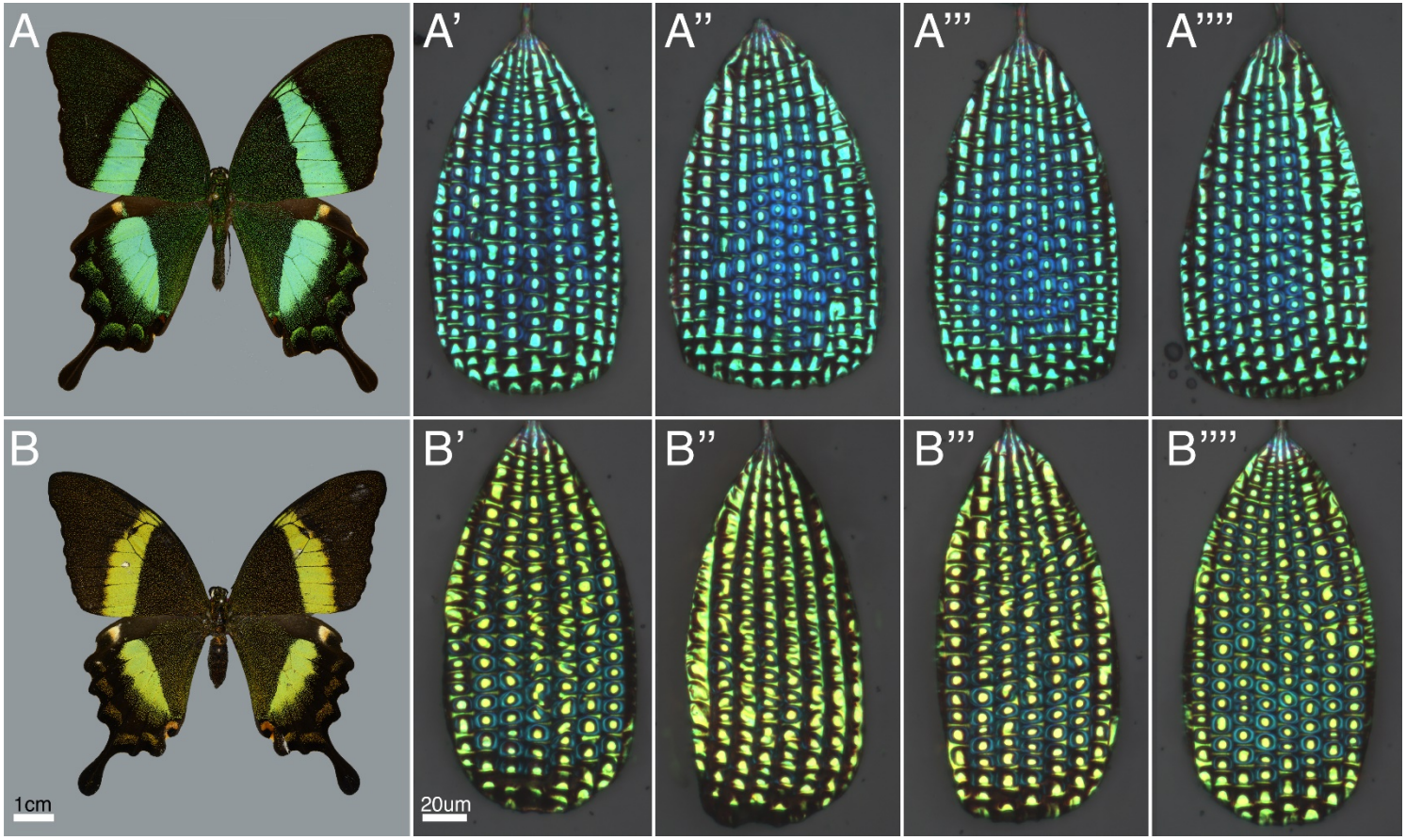

An example of an organism showing a strong red-shifted coloration (B) relative to wild type (A). Upon close examination of individual scales (A'-A'''',B'-B'''') one finds evidence of how red-shifts occur. The change in color of both the dimple and annuli points to a multilayer change, while the loss of regularity in dimple shape, inhibits the retroreflection that is prominent in wild type samples.

Figure 3.9 Distribution of wing color in treated *P. palinurus* with perturbed scale morphologies

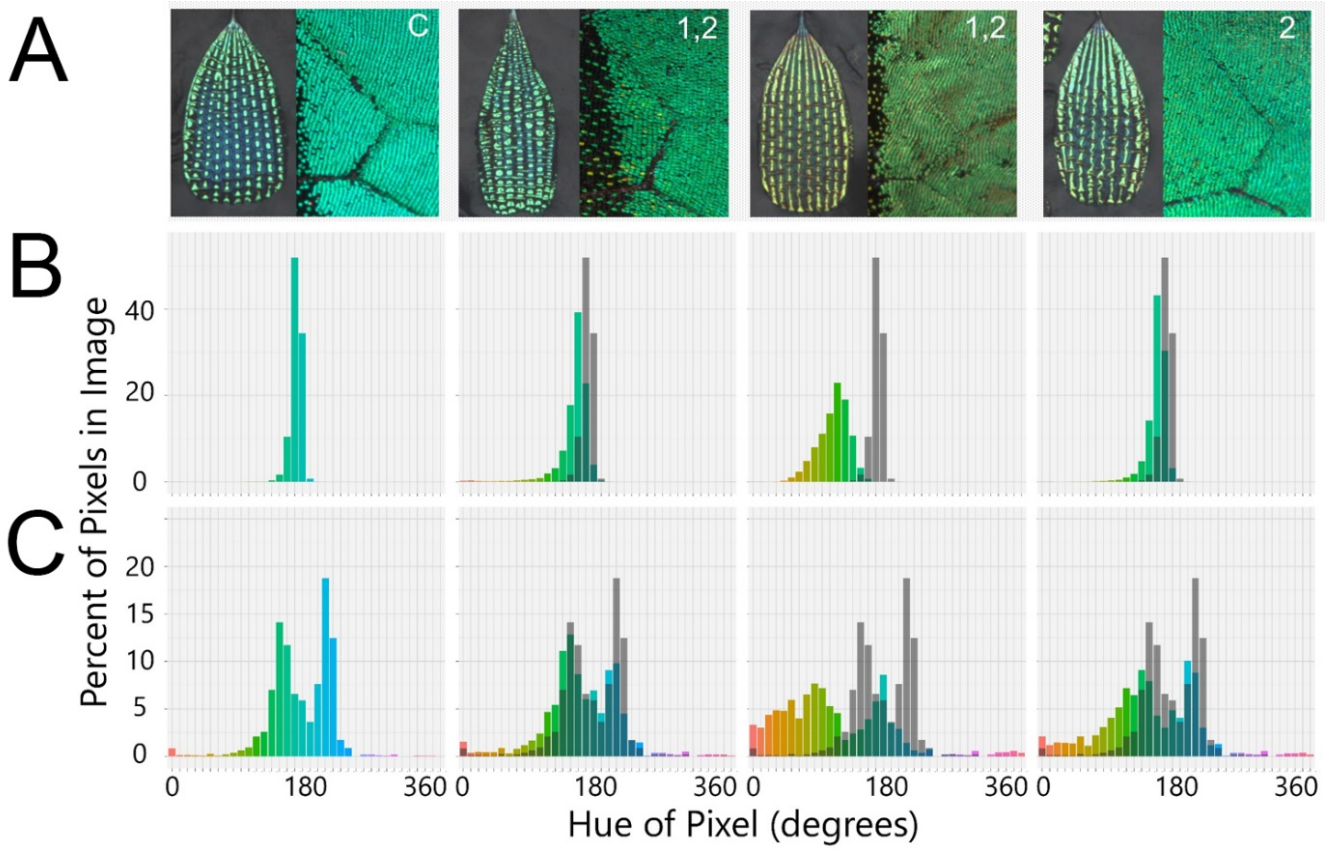

Quantification of color from several red-shifted animals all treated with CytoD. A – Images of single scales (left) and hindwing discal cell (right). B – Quantification of pixels with any given hue from the discal cell giving an estimated apparent color. C – Quantification of pixels with a given hue from the single scale showing actual reflection character of the scale. 1st column – Control, 2nd and 3rd – animals receiving 2 injections 24hrs apart, 4th Animal injected only on the second day. Grey distributions are the wild type for comparison.

Figure 3.10
Ultrastructural phenotypes of red-shifted structurally colored scales

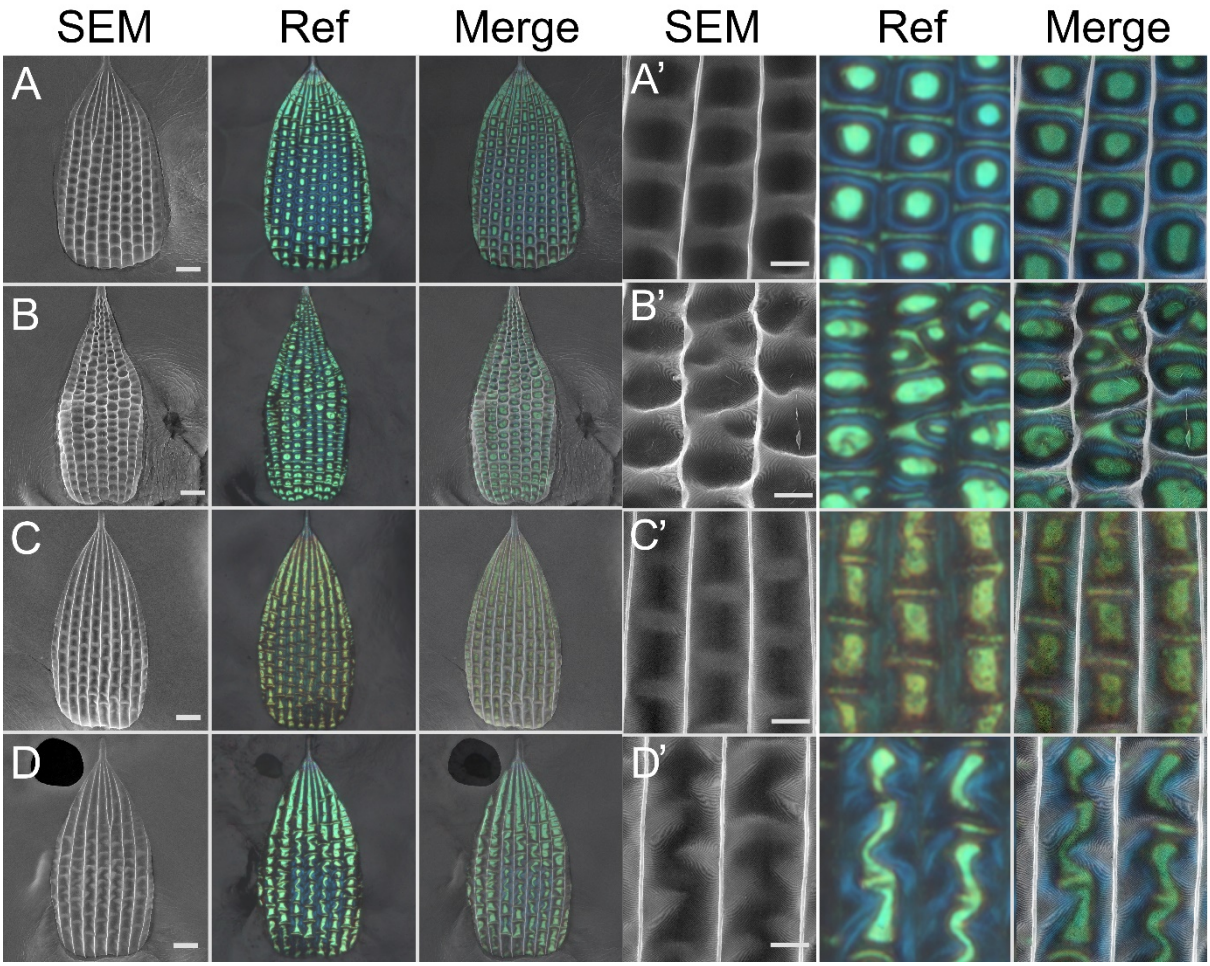

SEM imaging of red-shifted butterflies from figure 3.9. (**SEM**) can be combined with reflected light microscope images (**REF**) to detail how ultrastructural morphology influences color and the red shift (**Merge**). Scales taken from the same animals as in the previous figure. **A,A'**- Control, **B,B'** and **C,C'** dual injected CytoD animals, **D,D'** animal injected on second day only. **B,B'** has lost control of regularly shaped and spaced dimples resulting in expanded green reflection at cost of blue. **C,C'** – Animal has red shifted reflection in centers and annuli suggesting multilayer defect, but the dimples are also squarer than normal resulting in a boxy shape lacking retroreflection from the cross ribs. **D,D'** – Again dimples are lost now rarely ever forming complete cross ribs, instead featuring serpentine shaped, continuous troughs, with retroreflection occurring incompletely, and only along the length.

Figure 3.11
Museum specimen of *P. palinurus (daedalus)* with dimple deformities

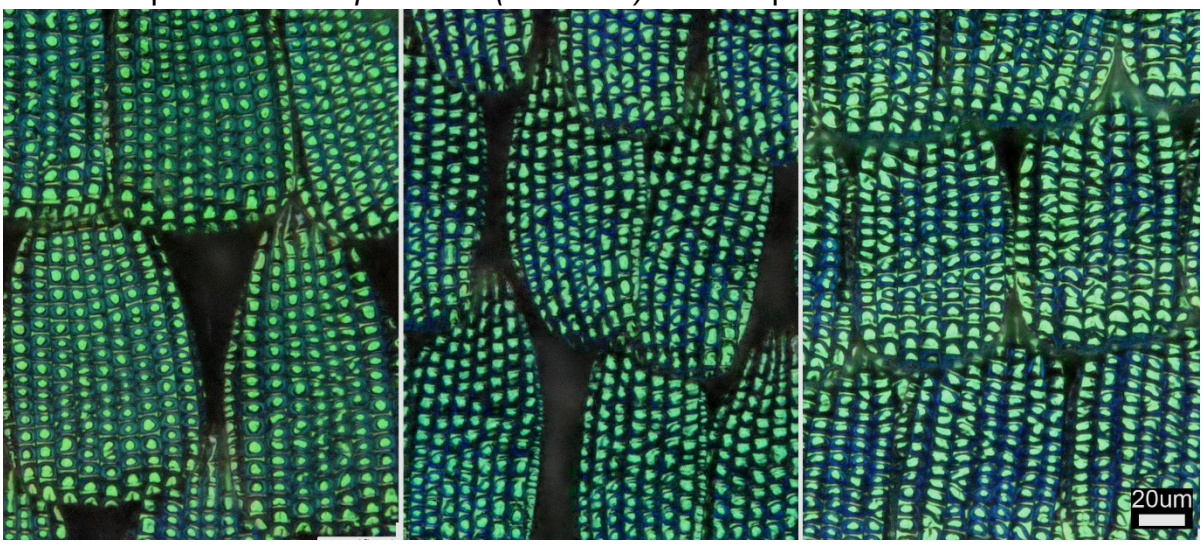

Scales from three wild caught *P. palinurus (daedalus)* individuals with similar ultrastructural phenotypes to those in CytoD treated butterflies (Fig3.10B).

Figure 3.12 TEM of wild type and red-shifted scales

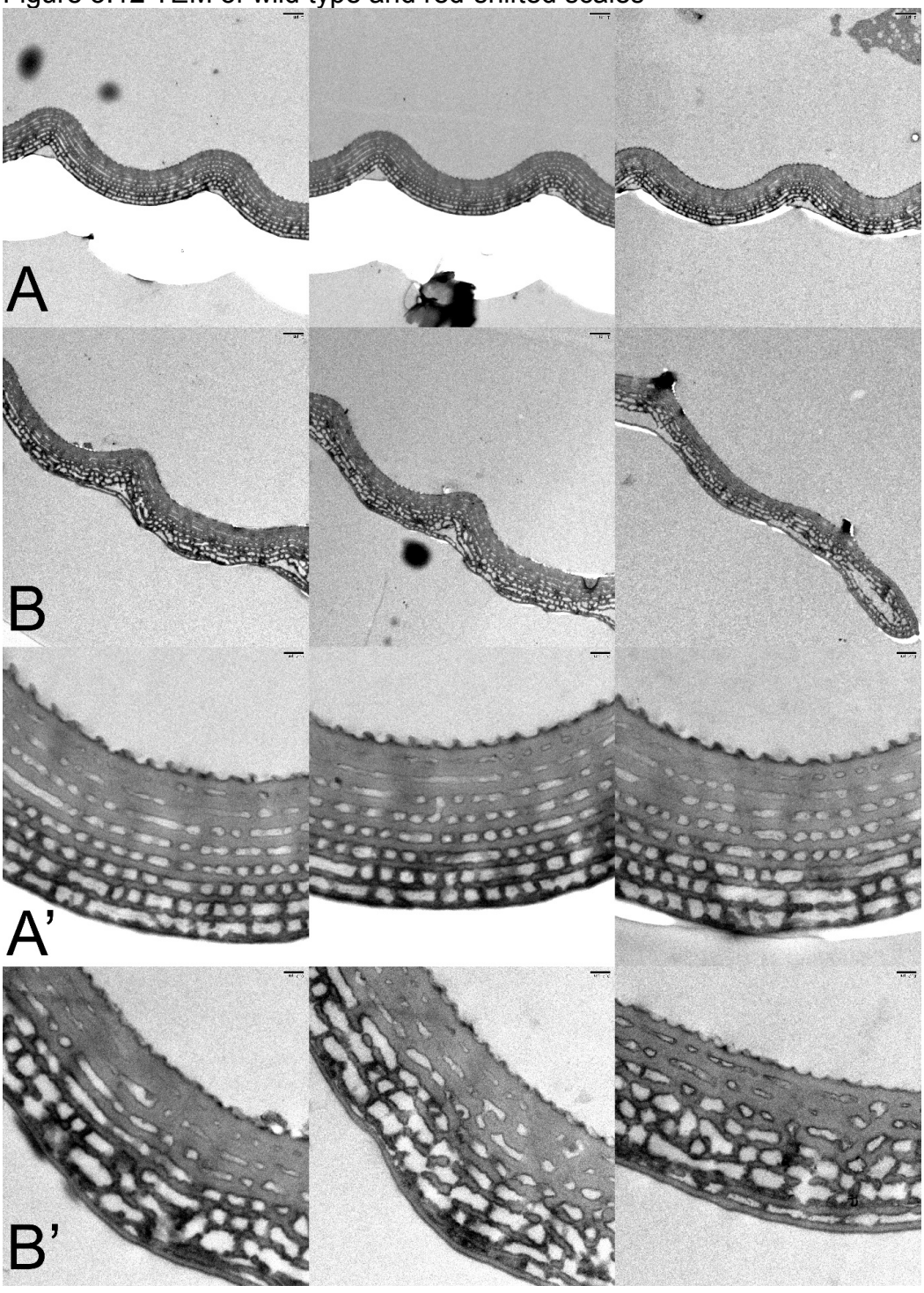

70nm thin sections of wild type (**A,A’**) and red-shifted scales (**B,B’**) cut longitudinally. Internal structures are regular with decreasing thickness in wild type scales (A’), while they are irregular in the lower laminae of the red-shifted animals (B’). As Vukusic noted in 2001, we also see higher electron density in the lower laminae of the multilayers of both wild type and red-shifted animals (41). Red-shifted scales from the same animal in Fig3.9 (3rd Column) and Fig3.10C. Abwing surface is up, Adwing surface is down. Scale bar 1um in A,B; 200nm in A’,B’.

Figure 3.13
Examination of wild type and red-shifted scale multilayer thickness and order

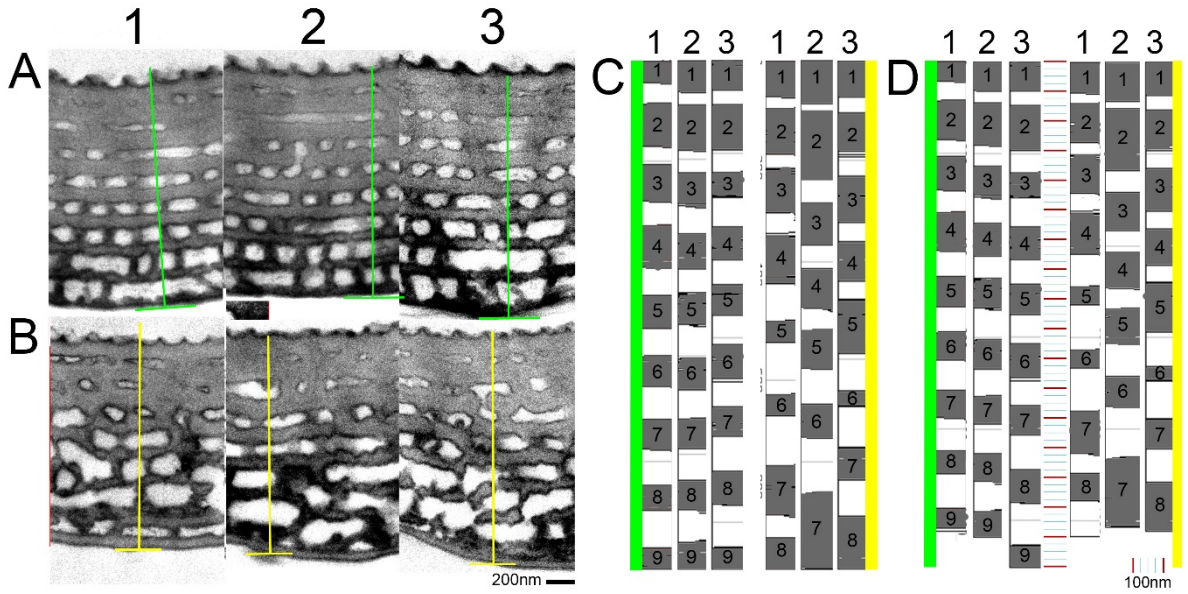

Quantification of layer thickness from TEM thin sections of WT (**A,C$_{green}$,D$_{green}$**) and Red shifted scales from Fig3.12 **(B,C$_{yellow}$,D$_{yellow}$)**. Line traces from each of 3 samples **(1,2,3)** were made perpendicular to the abwing surface along the colored lines in **A,B** after manual segmentation in ImageJ. Line trace intensities were converted into schematics in **C,D** – Grey boxes indicate chitin layers, white space indicate air spaces. **C –** All line traces were normalized to have the same length. This allows us to observe overall pattern and thickness irrespective of irregularities in the sectioning process. **C$_{green}$(1,2,3) -** Wild type sections have highly regular and similar patterns of layering, whereas red-shifted animals (**C$_{yellow}$(1,2,3)**) have irregular numbers of layers, irregular spacing, and irregular thicknesses. In **D,** the same line scans are kept to their actual scaling relative to one another – measurements of their dimensions are indicated by the ruler in between the wild type and red-shifted samples (distance between 2 red lines is 100nm). One interesting finding is that red-shifted samples are often missing one or more chitin laminae. It is important to recognize that due to sample prep, sample may have shrunk making direct conversion of nm-thickness-to-color hard to achieve other than to say one sample is thicker and thus more red-shifted relative to another.

Figure 3.14
Quantitative comparison of laminae thicknesses between wild type and red-shifted samples

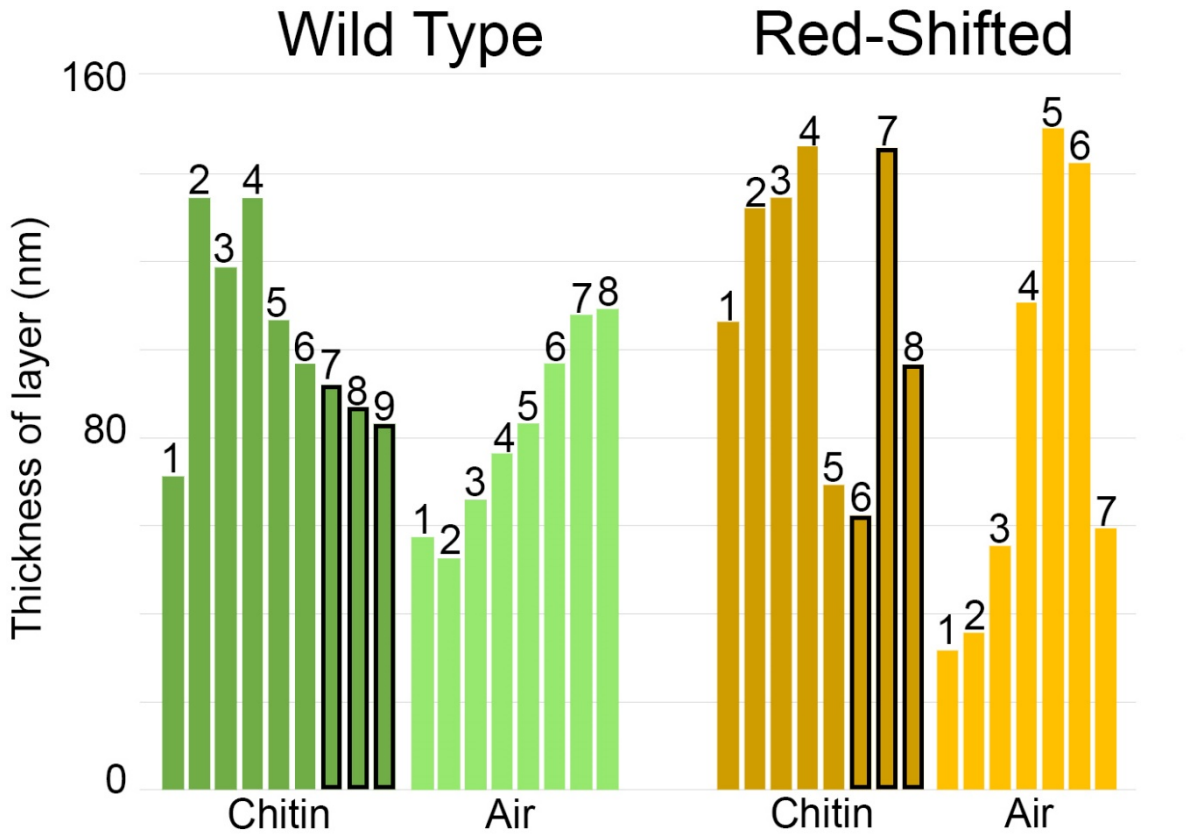

Barplot of chitin and air layer thicknesses from abwing to adwing (layer numbers indicate chitin layers increasing in the direction from the abwing toward the adwing surface and are the same used in Figure 3.13C & D). Plots show data from samples A#1 and B#1 in Figure 3.13. In addition to an overall larger thickness in the red-shifted animal, the decreasing thickness of the chitin layer-to-layer seen in the wild type is lost in the red-shifted animal. Electron dense chitin layers seen in Figure3.12 are indicated by black borders.

Figure 3.15 Survey of *Achillides* species shows a diversity of structural elements

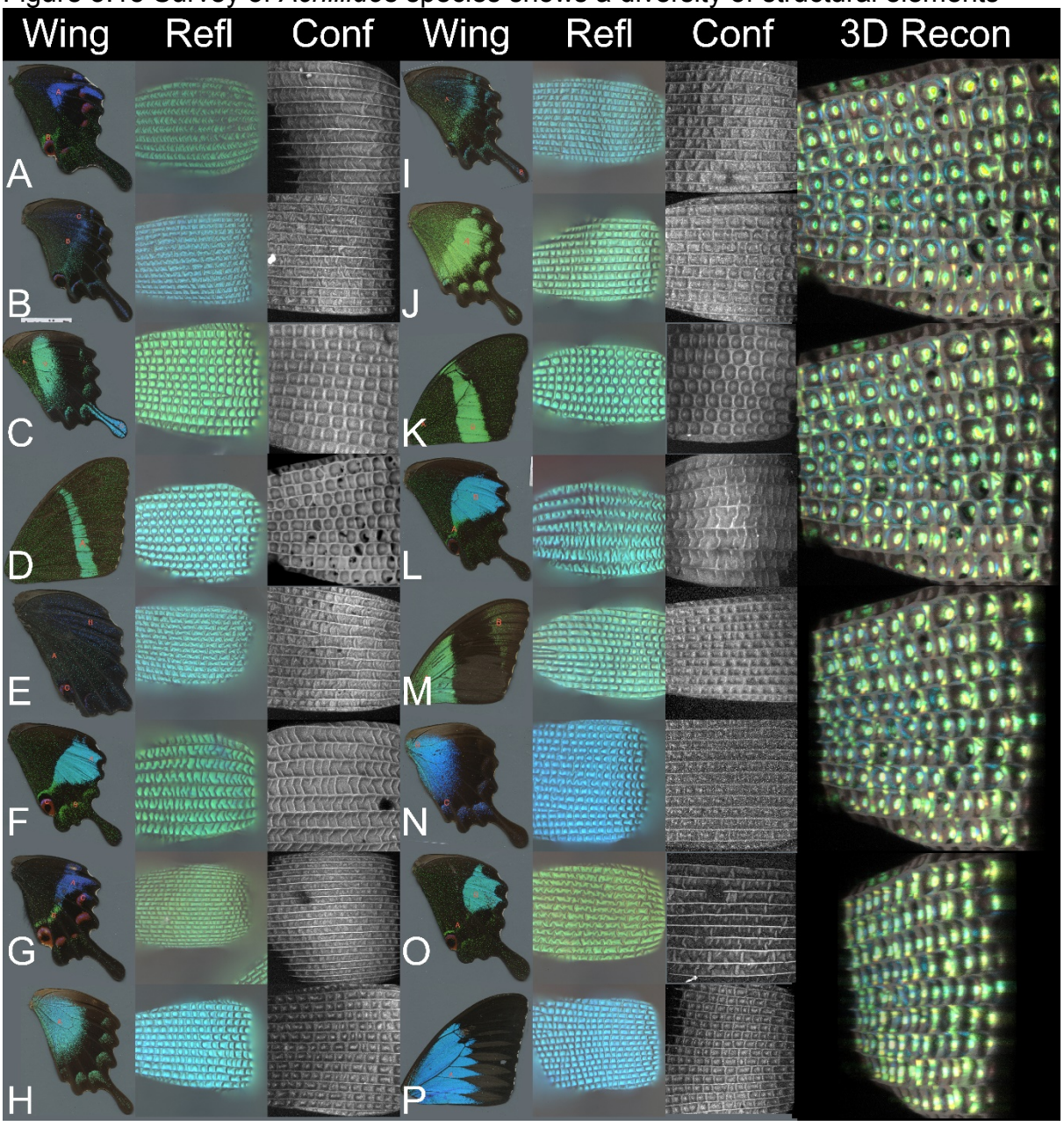

Representative images of the diversity of color and structure across the *Achillides.* Images of wings, single scales in reflected light (**Refl**), and confocal stacks of single scales (**conf**) for the majority of *Achillides* species. **3D Recon** - Projecting the reflected light image onto a confocal stack of the same scale allows us to make a 3D map of color localization, which we can rotate *in silico*, as shown here with a scale from *P. crino,* to achieve a sense of how ultrastructure dictates structural color reflections. **A** – *P. arcturus,* **B** - *P. bianor,* **C** - *P. blumei,* **D** - *P. crino,* **E** - *P. dodsi,* **F** - *P. karna,* **G** – *P. Krishna,* **H** - *P. lorquinianus,* **I** - *P. maackii,* **J** - *P. neumoegeni,* **K** - *P. palinurus,* **L** - *P. paris,* **M** - *P. peranthus,* **N** - *P. pericles,* **O** - *P. polyctor,* **P** - *P. ulysses.* All images collected and processed by Jerry Lo.

Figure 3.16
Condamine's *Achillides* phylogeny with morphological observations from survey

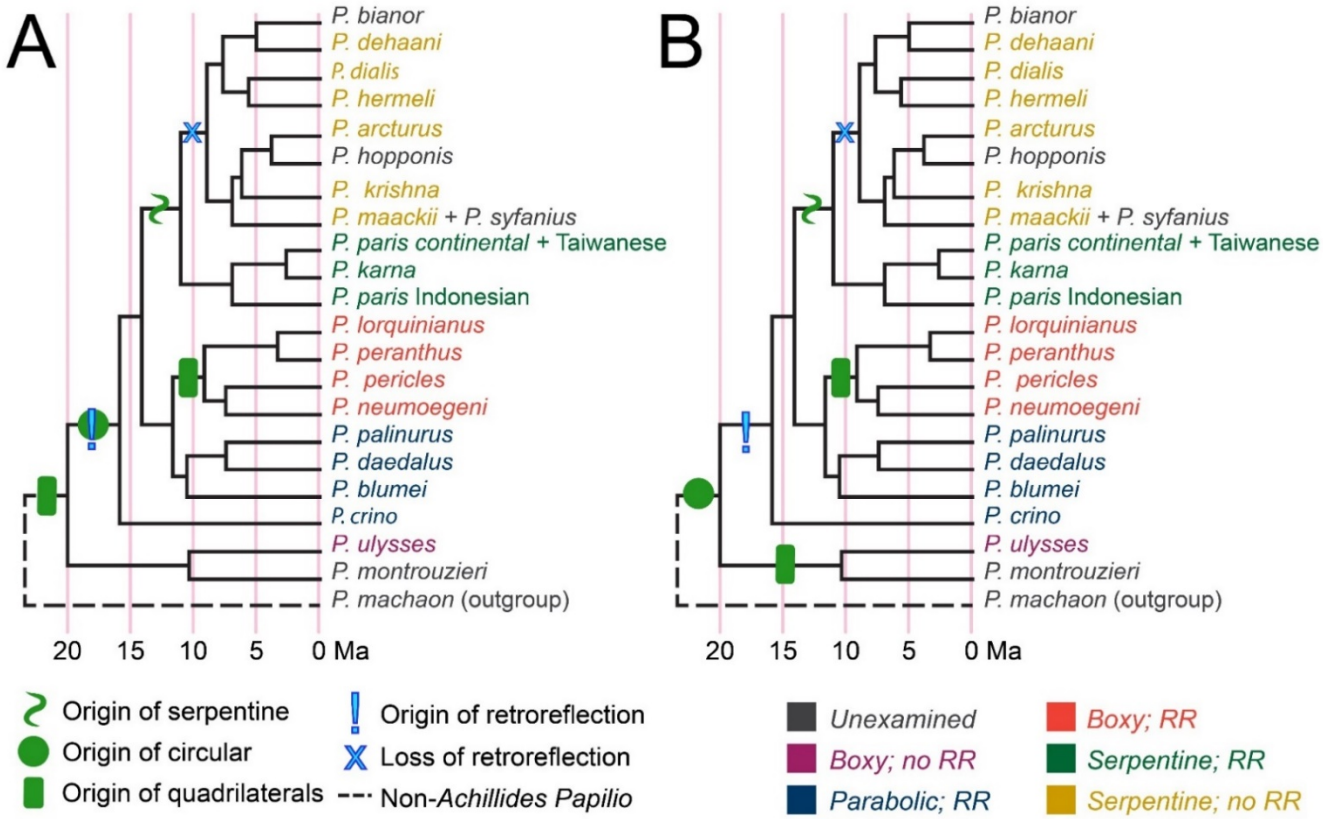

Findings of anatomical survey of *Achillides* structural scales of Figure 3.15 placed on Condamine *et al.* phylogeny. With the exception of *P. crino* scale ultrastructure predicts phylogenetic relationships (structure type indicated by color of species name). Two equally parsimonious hypotheses about origin of structure type emerge from this analysis (A&B). In the first (A), the ur-*Achillides* had boxy shaped dimples without retroreflection, which was maintained in the *ulysses* branch, but subsequently gained retroreflection and a rounded shape that was further modified in individual lineages. In the second (B), the ur-*Achillides* had round dimples, not necessarily producing retroreflection which was gained after the split with the *ulysses* clade. This round shape was secondarily lost in the neumoegeni/pericles/peranthus/lorquinianus lineage while retaining retroreflection.

Figure 3.17
P. ulysses F-Actin suggests a modified, *P. palinurus*-like hexagonal pattern

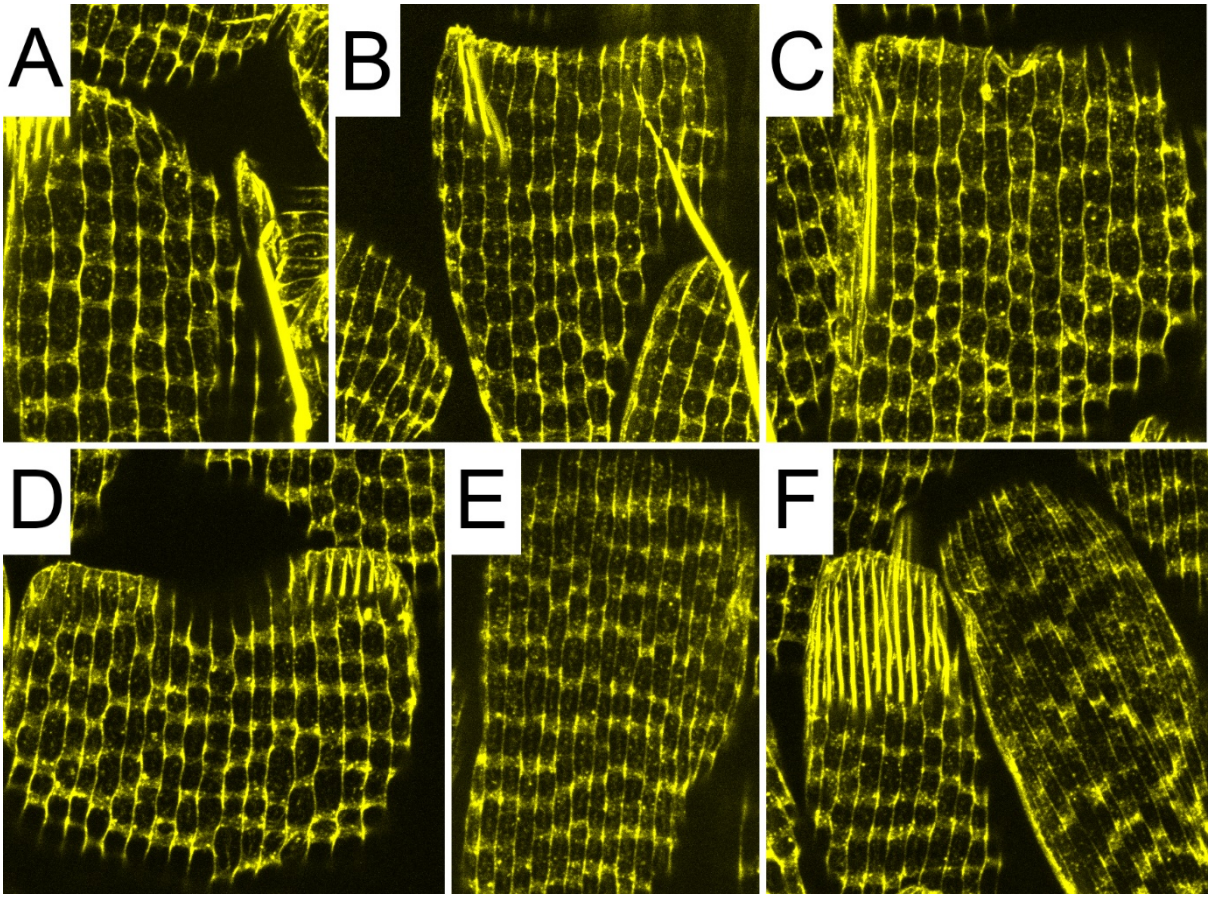

Phalloidin stain of scales on pupal wing discs of *P. ulysses* shown as max projections of confocal stacks. A range of phenotype could be found even on a single wing disc, and given that scales *of P. ulysses* adults are square and boxy similar to those of **E** and **F,** I have laid out the scales in what appears a temporal order from the youngest in **A** to the oldest in **F**. Crossrib staining becomes intensified through the series, suggesting that actin accumulation in the crossrib could be a mechanism of contraction (perhaps like muscle fiber contraction). Interestingly, if this is true, it suggests that the round dimples of *P. palinurus et al.* could be the ancestral phenotype which was further modified by those with boxy profiles as suggested by Fig3.13B. All images to the same scale.

Figure 3.18
Blue shifts from tissue damage or 3IT injection correlate with pigment reduction

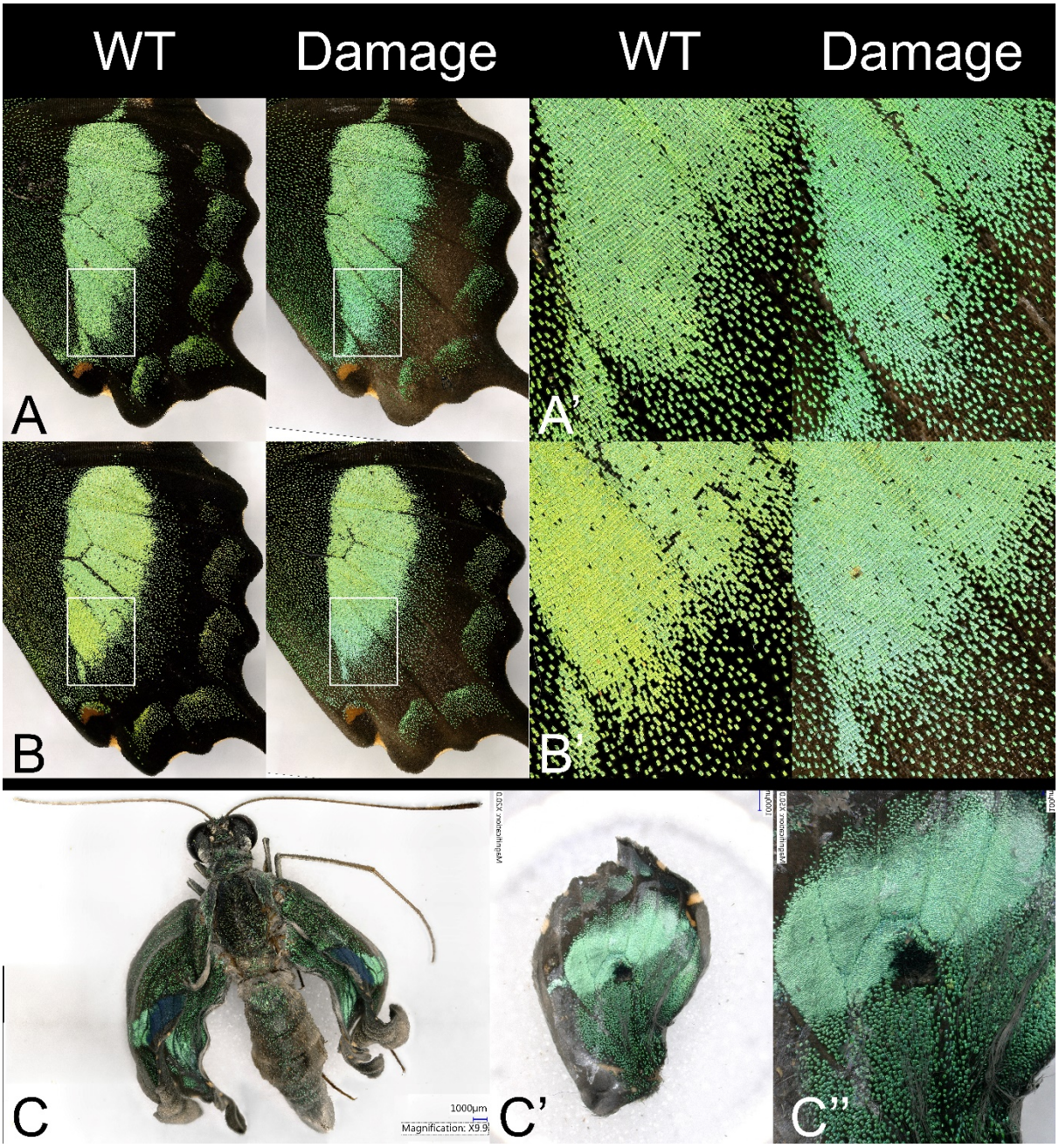

Blue-shifted animals were consistently found irrespective of treatment or control suggesting a damage phenotype. Two examples of unilateral blue-shifts are shown in **A** and **B** (damage images mirrored for ease of comparison). Blue shift most commonly seen on side of injection. **A',B'** close up of area indicated by **white boxes in A,B**. Decrease in pigmentation is apparent in A',B' dark areas, suggesting a role for pigmentation in creating the blue coloration. **C,C',C''** – images of an animal injected with 140mM 3-Iodo-L-Tyrosine to inhibit melanization as in Morphos. Clear loss of pigmentation throughout the body is seen in **C**, and a blue shifted coloration is apparent in a disarticulated hindwing **C',C''**.

Figure 3.19
Effects of chlorine and acidified MeOH treatment on *P. palinurus* wings

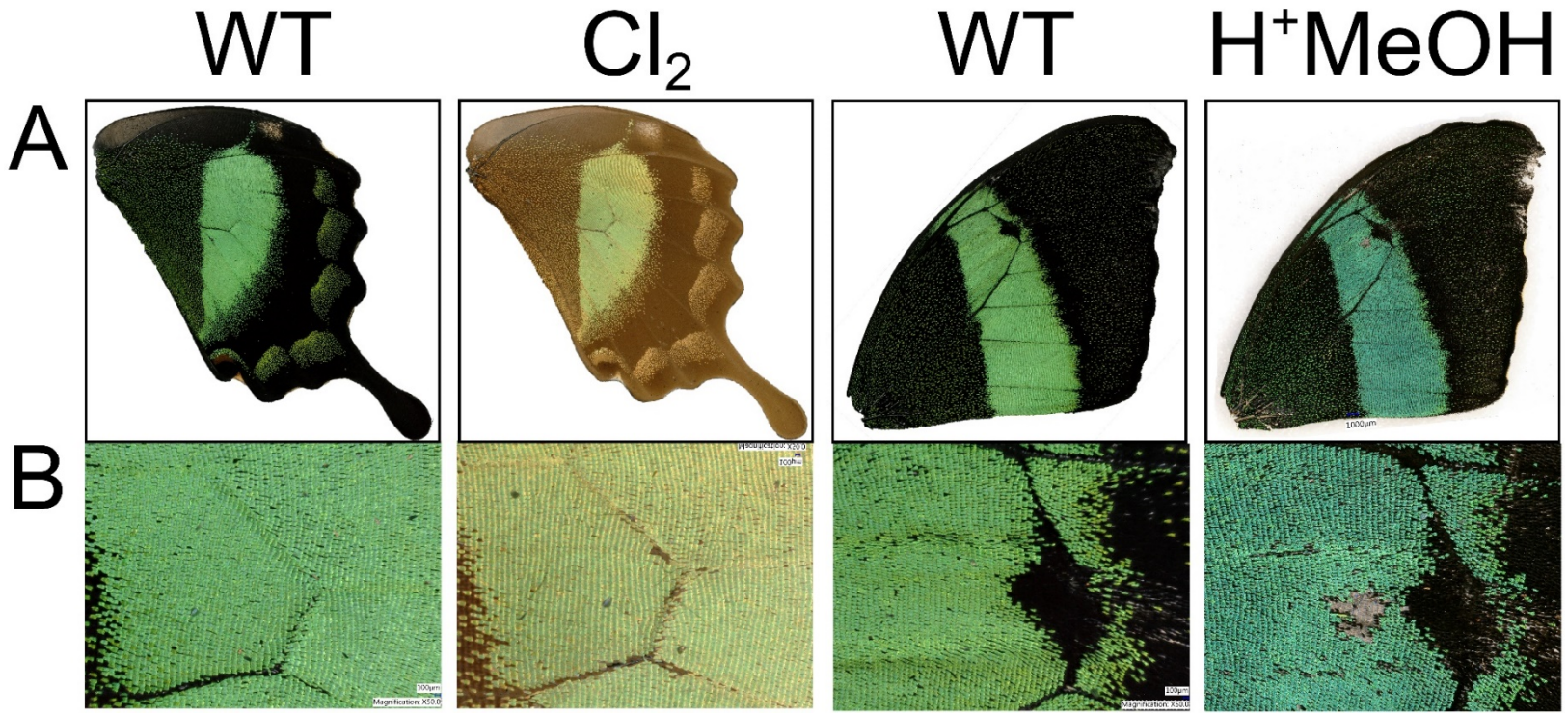

Exposure of wild type hindwings to chlorine gas for 45min results in decrease in darkness and red shift within green areas, while submersion in acidified MeOH for 20hrs results in a blue shift (all wings from same animal). **A** – Dorsal surface of wings, **B** – Close up of discal cell from A. Chlorine and MeOH treated wings mirrored for purposes of comparison with WT.

Figure 3.20 Effects of Cl_2 and acidified MeOH exposure on pigment and color in *P. palinurus* scales

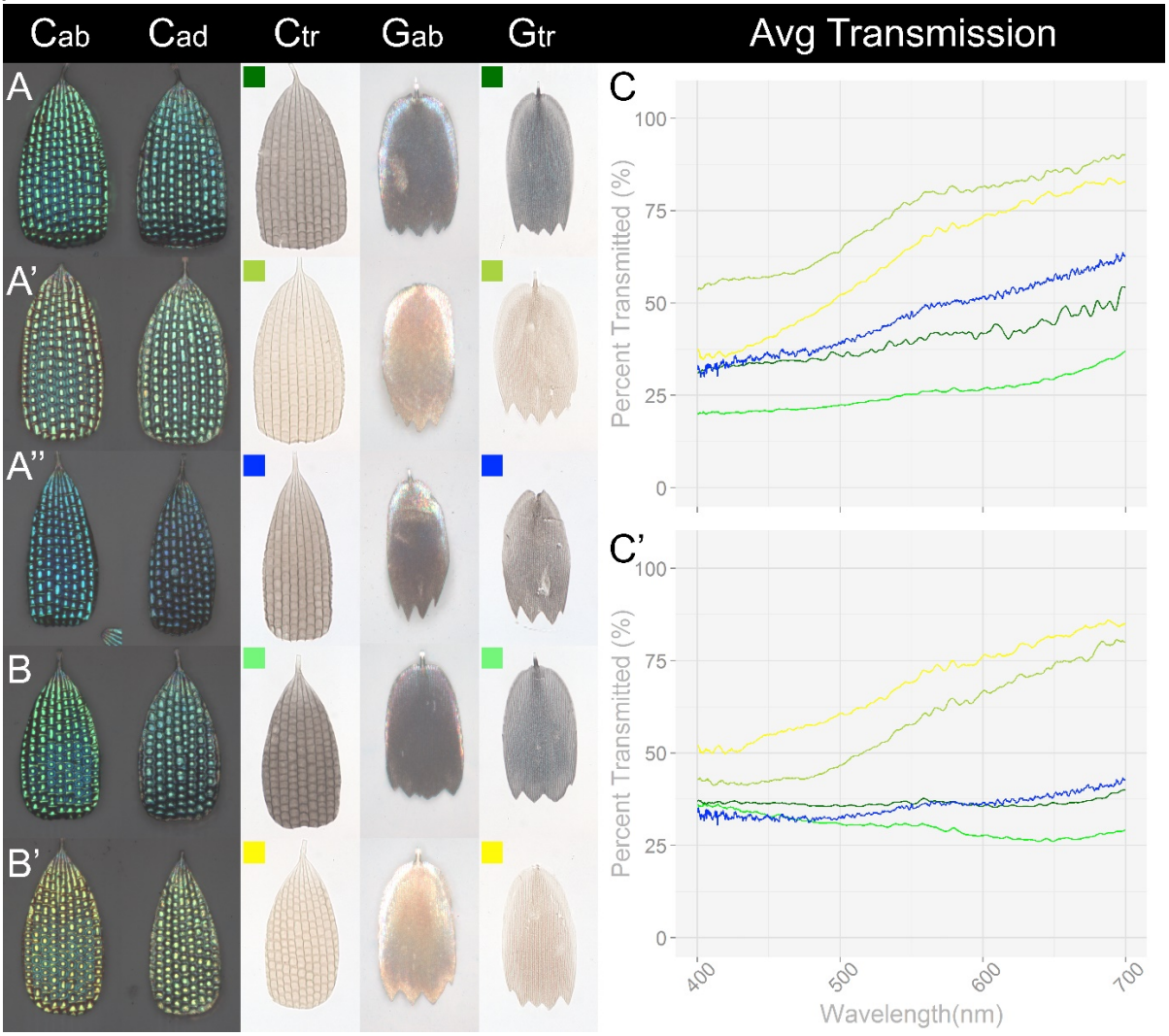

Comparison of WT hindwing *Papilio palinurus* discal cell scales (**A,B**) with bleached scales (**A',B'**) and Acidified MeOH extracted scales (**A''**). All A scales are from same butterfly, while all B scales are from a second butterfly. A distinct redshift occurs in bleached structural scales (A',B'), concurrent with a strong reduction and hue shift in the internal pigments of the cover and ground scales (**Ctr,Gtr**). Cover scale adwing view does not appear different than abwing (**Cad,Cab)** suggesting lower lamina is not contributing to hue shift. **Cab** – Cover scale abwing view in reflected light, **Cad** – Cover scale adwing view in reflected light, **Ctr** – Cover scale immersed in oil viewed in transmitted light, **Gab** – abwing view of ground scales in reflected light, **Gtr** – Ground scale immersed in oil viewed with transmitted light. Exposures of Cab, Cad, Gab are the same; Ctr and Gtr are the same. Images all to the same scale.

Figure 3.21
Pigmentation analysis of blue-shifted damage and 3IT phenotypes

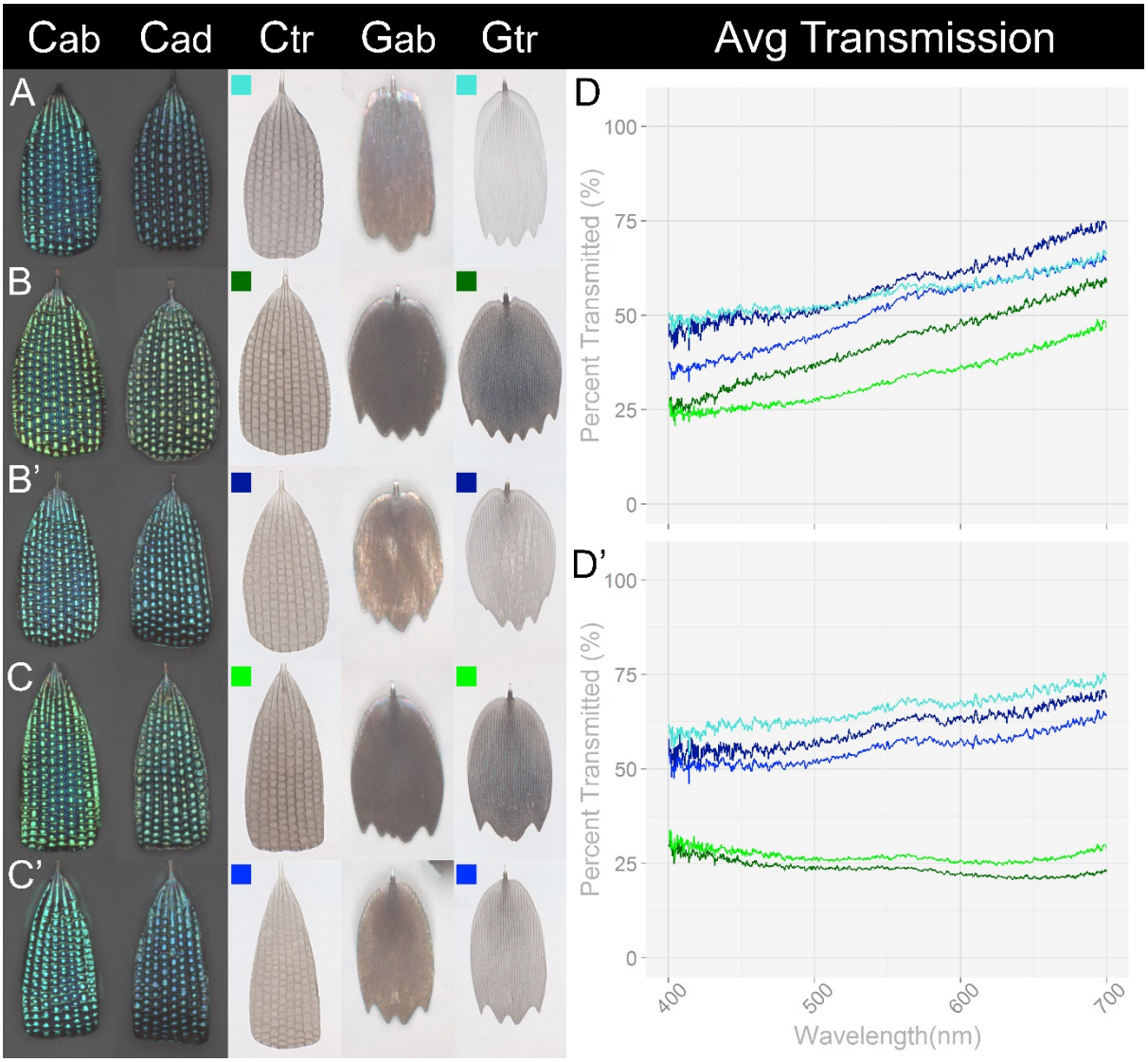

Analysis of pigment characteristics from 3IT blue shifted animal and 2 damage induced blue-shifted animals. A scales from 3IT hindwing, **B,C** scales from wild type wings of 2 animals, **B',C'**- scales from the damaged areas of the same animals. **Cab** – Reflected light images of cover scales viewed from abwing, **Cad** – Reflected light images of cover scales viewed from adwing surface, **Ctr** – Transmitted light images of cover scales immersed in oil to eliminate structural effects. **Gab** – Reflected light images of ground scales viewed from abwing surface. **Gtr** – Transmitted light image of ground scales immersed in oil to eliminate structural effects. **D** – Average transmission spectrum of 3 cover scales, lines colored according to sample indicated by square next to sample's Ctr image. **D'** – Average transmission spectrum of 2 ground scales, lines colored according to sample indicated by square next to sample's Gtr image. Transmission spectra of 3IT clusters with damage phenotypes suggesting damage phenotype is a melanin deficiency. Slope of 3IT cover differs from that of damage and wild type scales suggesting damage may inhibit the production of more than just melanin.

Figure 3.22 Control acidified MeOH ommochrome extraction in *Morpho*

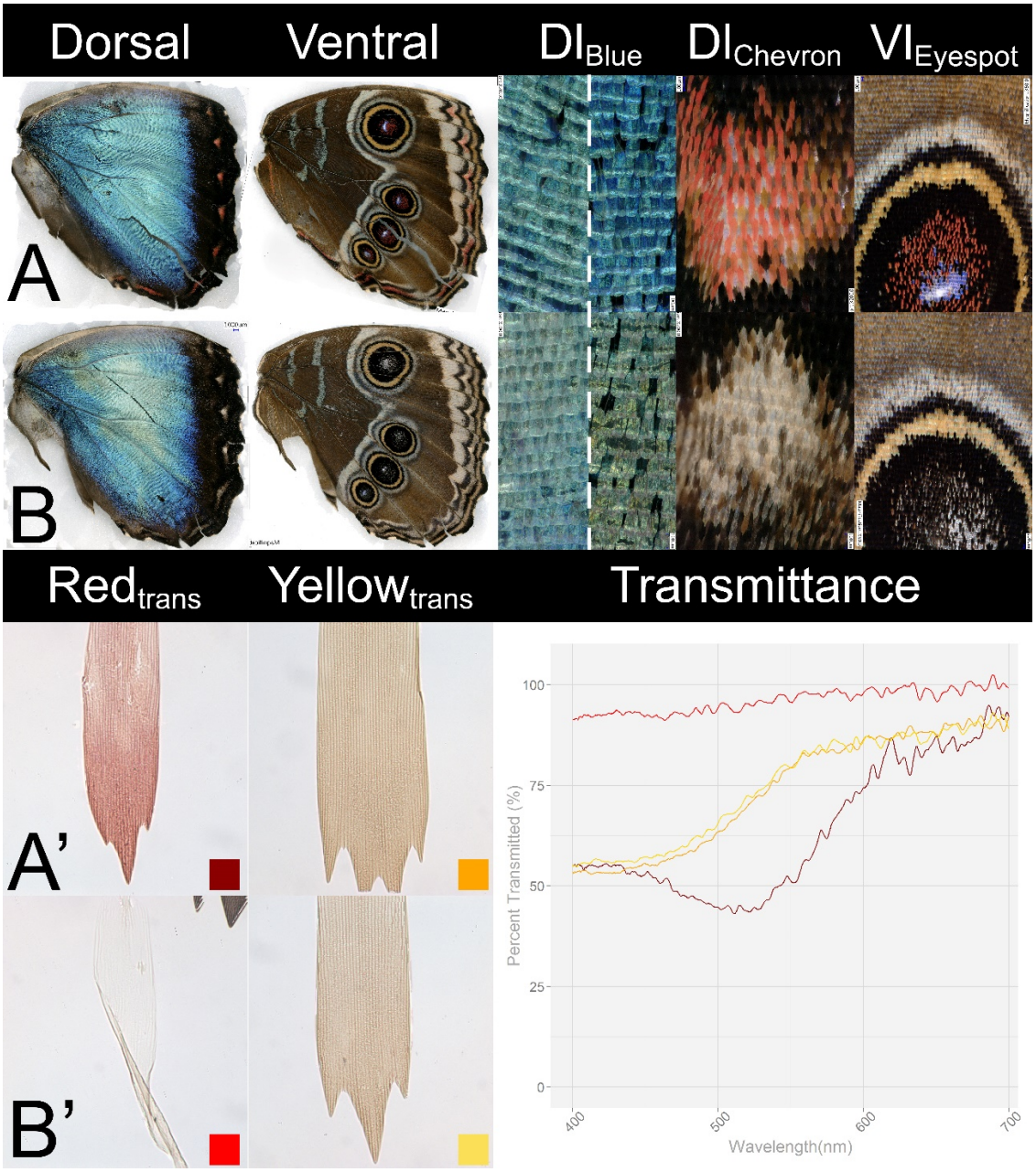

Acidified MeOH can extract ommochromes, but also causes damage to scales. **A –** Row of images from an untreated hindwing. **B –** Row of images from the same areas of the contralateral hindwing following Acidified methanol treatment for 20hrs. (all images mirrored for comparison to A). **A'** – row of images of scales from red and yellow regions of the eyespot of the untreated wing. **B'** – same as A' from treated wing. Transmittance plot shows average curves of three scales from each sample color coordinated with the boxes from A',B'. **DI_{blue}-** two regions of the dorsal blue field, comparable between A,B. **$DI_{chevron}$-** dorsal ommochrome containing pattern element at the distal margin of the wings seen in "Dorsal" column. **$VI_{eyespot}$** – Eyespot region of the ventral wing comparable in both A,B. The reds are clearly lost following treatment, while the yellow does not show much extractability (though its curve is reminiscent of what is seen in the chlorine treated *palinurus*. The treatment does result in scale damage and color change in both red scales and the structural scales.

Figure 3.23 Measurement of known pigmentation from *Drosophila* abdomen

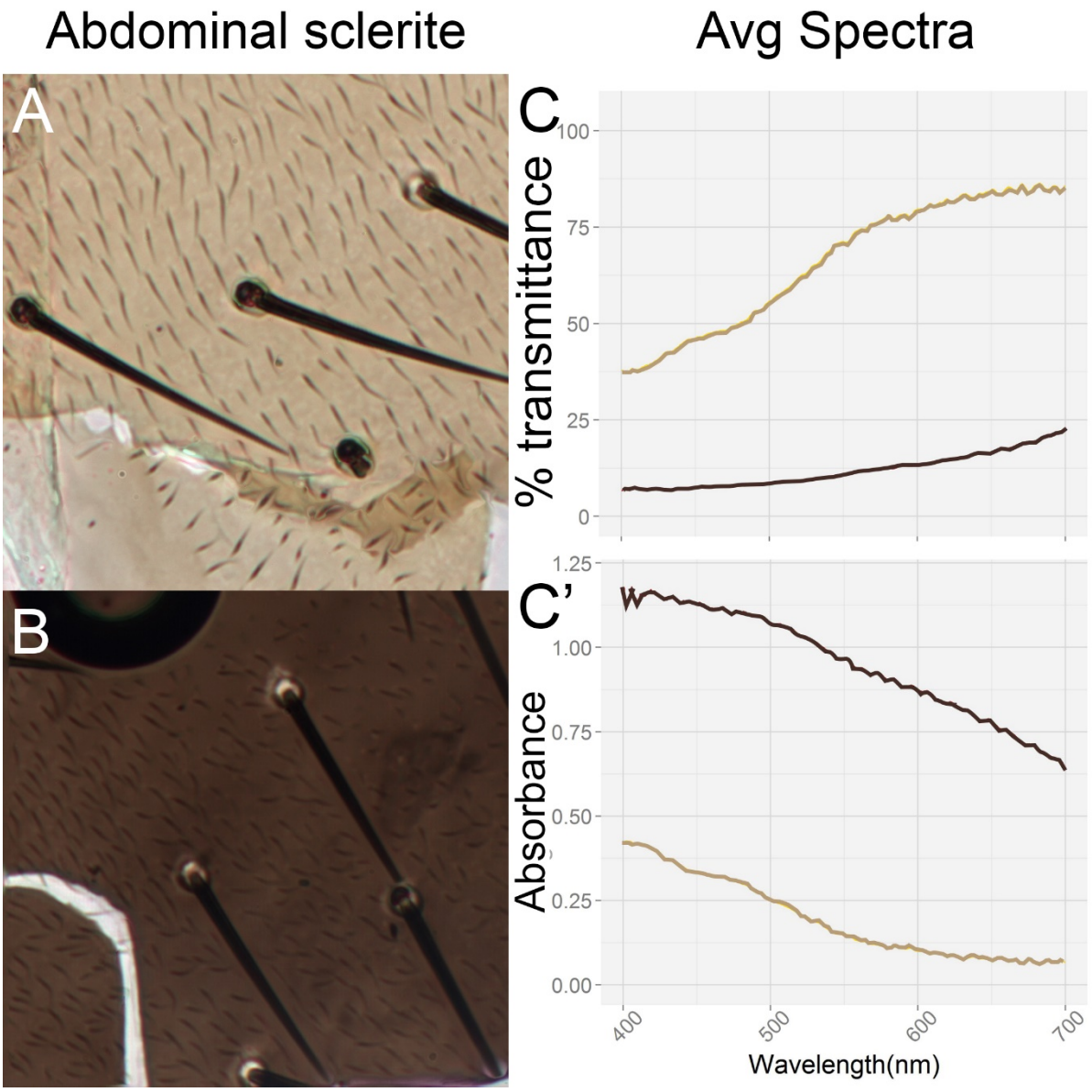

Genetic experiments in *Drosophila* have elucidated the pigmentary nature of the abdominal coloration of adults (235). **A** Beta-alanyl Dopamine-derived melanin (NBAD) from the light colored areas of an adult OregonR *Drosophila*. **B** Dopamine-derived dark brown melanin in the dark bands of the adult abdomen. **C,C'** Average transmittance and absorbance curves calculated from 3 readings each. The NBAD melanin curvature is very similar to the yellow ring of the Morpho, while the dopamine melanin curve looks very similar to the curve of *Papilio palinurus* cover scales.

Figure 3.24 Transmission spectrum of Papiliochrome II in *P. nireus* scales

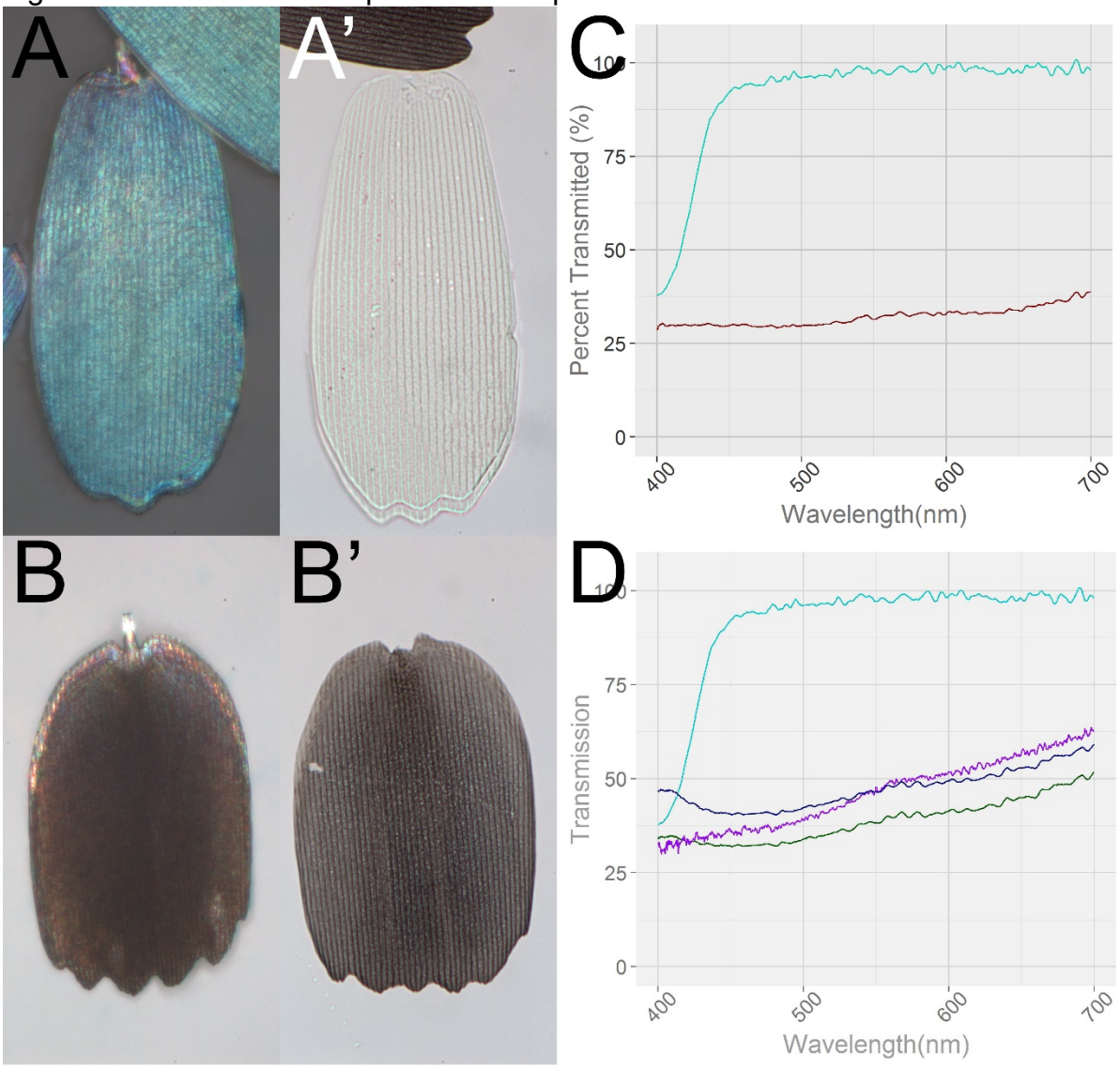

Cover scales from *Papilio nireus* are known to contain Papiliochrome II, an ommochrome which has a strong absorbance in the short wavelengths. **A –** Cover scale of *P. nireus* in reflected light, **A' –** Cover scale immersed in N=1.518 oil and imaged in transmission; note the slight yellow color due to blue absorbance. **B,B'** – Ground scales treated in the same way as A,A'. **C** – Transmission plot of cover (turquoise) and ground scales (brown) from *P. nireus;* the strong short wavelength absorbance of papiliochrome II can be seen between 400-450nm. **D –** Transmission plot as in C, with the green line being the wild type *P. palinurus* cover scale absorbance, purple is the MeOH extracted cover scales from the same animal. The dark blue line models what the transmission spectrum a scale with 85% of the melanin absorbance from the wild type scale (approximating the melanin level of the extracted scale) would transmit if pigment equivalent to 10% of the Papiliochrome II absorbance was removed. This curve does not match the observed (purple) spectrum well.

Figure 3.25 Dissected *P. palinurus* pupal wings suggest second pigment

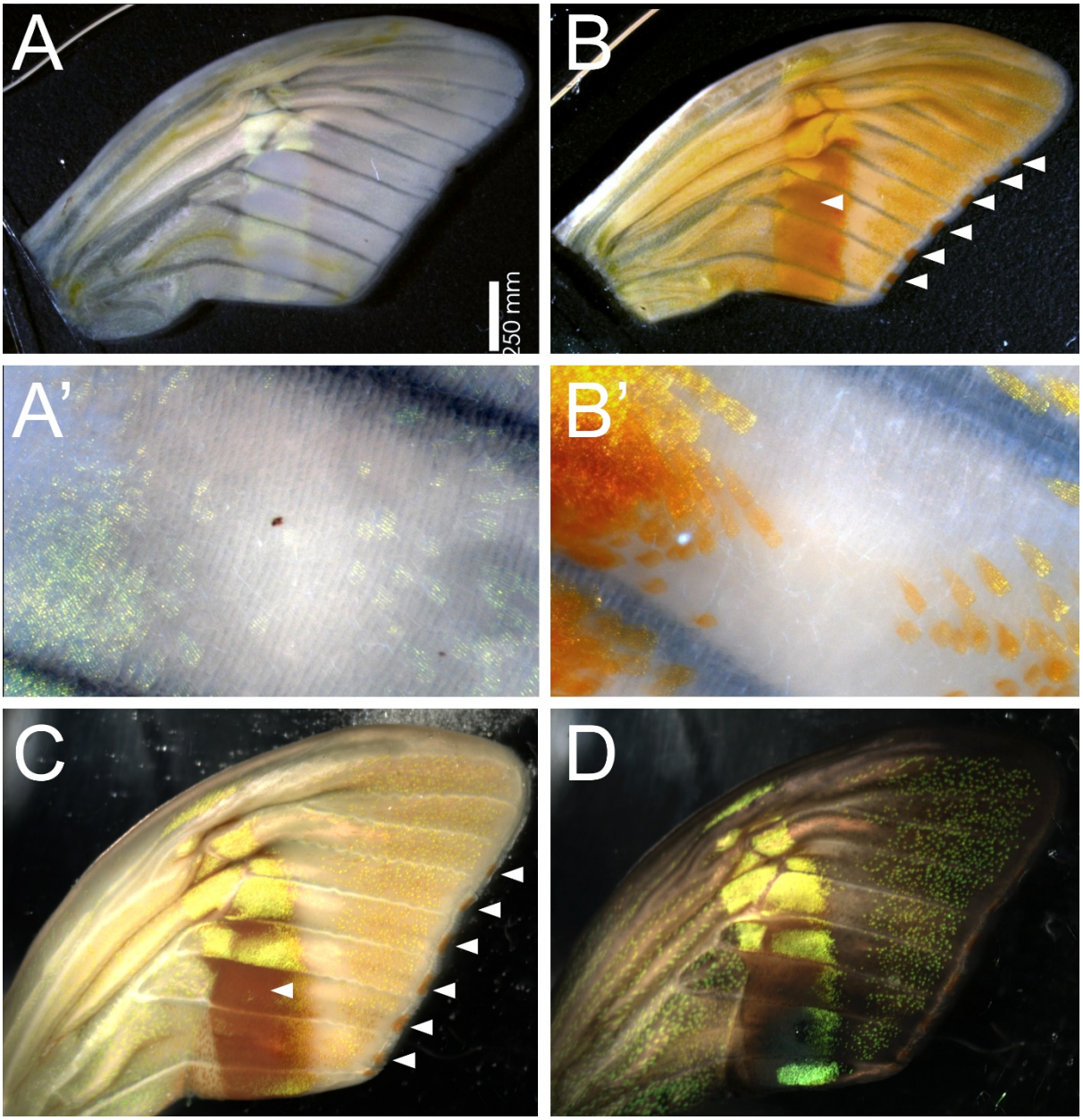

Dissection of pupae from later stage *Papilio palinurus* shows that prior to any pigment deposition scales have reflecting structures (**A,A'**). In older pupae, a yellow-orange pigment gets deposited in select scales including those of the main green band and in discrete patches of unstructurally colored scales along the distal margin (**Arrowheads, B,B'**). Close up views of the distal edge of the structural band (**A',B'**) show the difference between pre-pigmented scales and those following deposition of the yellow-orange pigment. In a test of melanization a wing was removed from a pupa and incubated in Grace's medium supplemented with L-DOPA, as done with the Morphos. Starting from a time point similar to the wing in B, the wing pigments and the color shifts from yellow-green to a deeper emerald green (**C,D**). Time elapsed is 2 hours and 45 minutes.

Figure 3.26 Wild Type scales have more pigment than damaged blue or 3IT scales

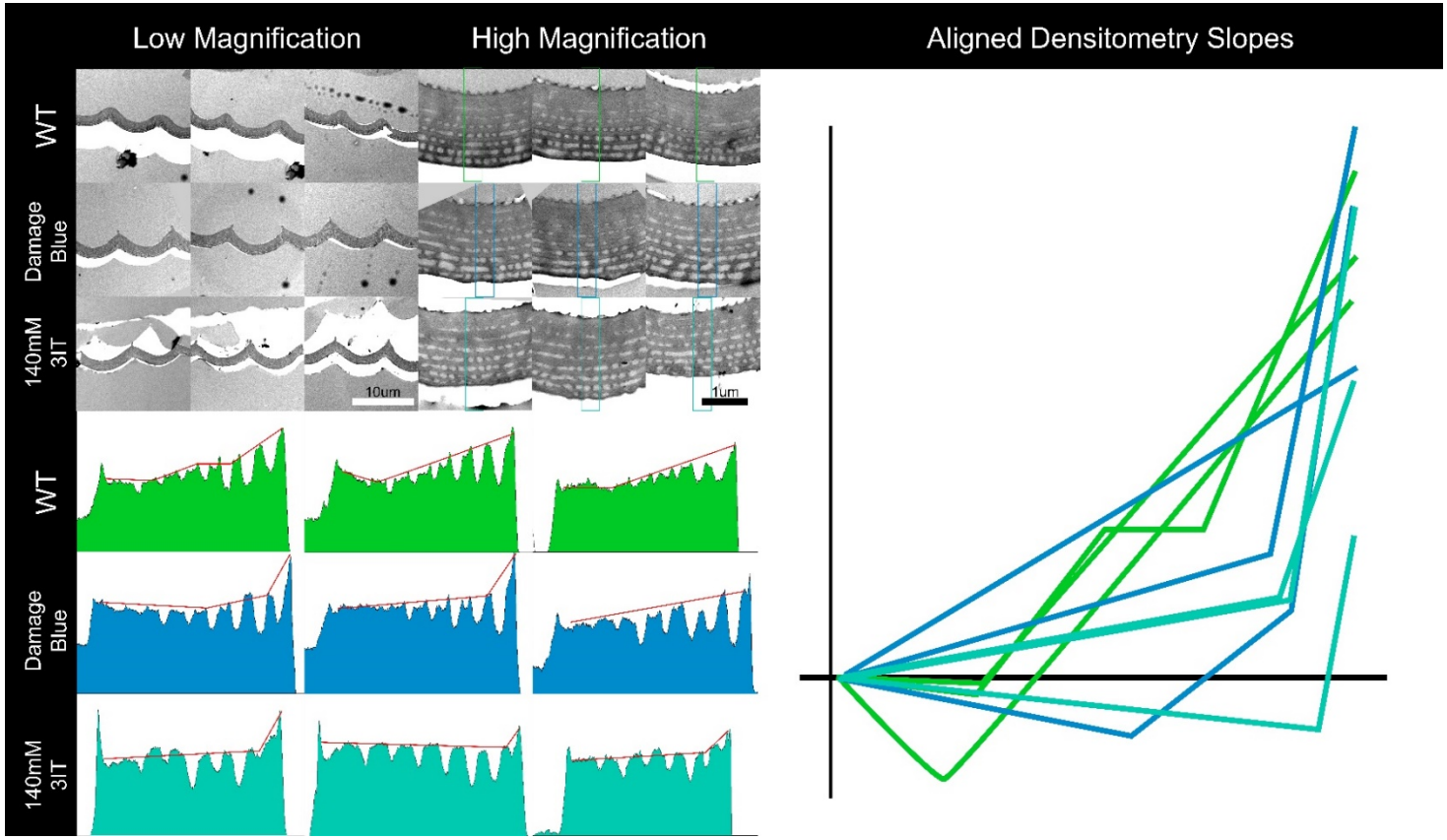

TEM thin sections (~70nm) of scales from wild type scales and blue-shifted counterparts in damaged areas as well as those treated with 3IT. Unlike red-shifted animal, the blue and 3IT treated animals show relatively well organized laminae (though the 3IT scales seem to collapse in their lower lamina, perhaps as an artifact of sectioning). Boxes in High magnification TEMs correspond to ROIs for densitometry readings taken in ImageJ and shown as plots below TEM. Peaks indicate darker regions, while valleys are lighter. X-axis of plots starts at adwing surface of box in TEM (top) and continues to the right indicating increasingly abwing regions (bottom). Thus the increase in slope to the right indicates an increase in darkness in the lower laminae of the scale. Far right plot aligns the slopes at their origin and are color coordinated with the densitometry plots. It is clear that there is a steeper slope in the wild type than most of the blue-shifted scales suggesting higher pigmentation in the former.

Figure 3.27
Hue diversity on naturally occurring *P. peranthus* and *P. blumei* wings

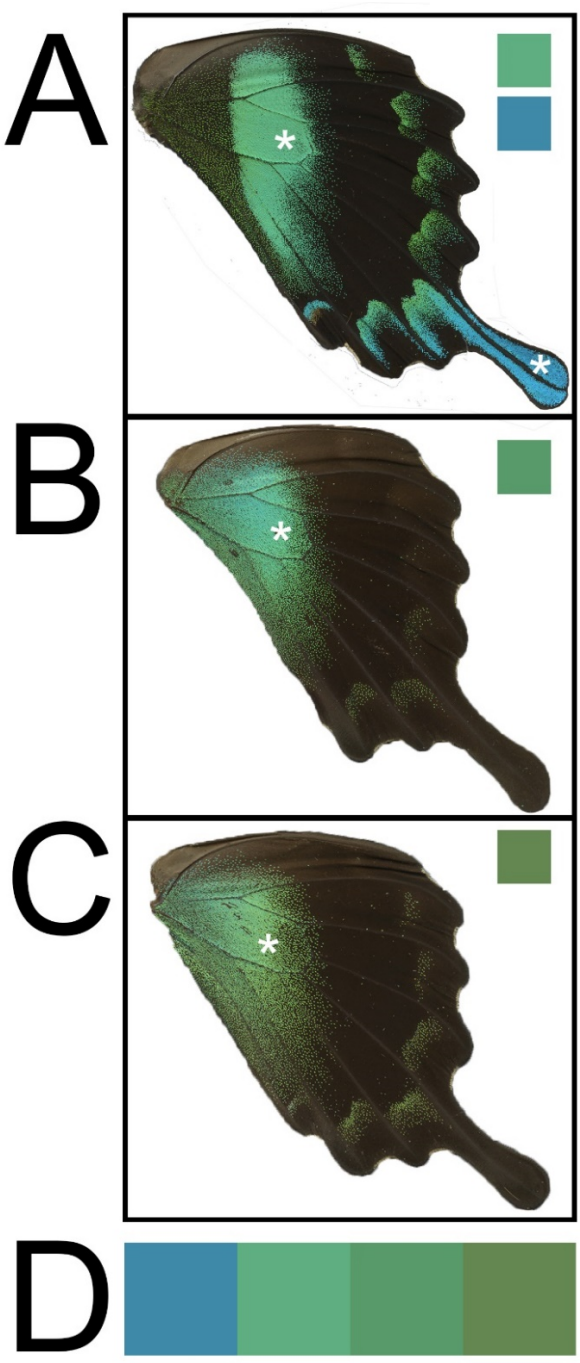

Hue diversity exists naturally in *Achillides* species. *P. blumei fruhstorferi* has mint green and blue hues (**A**), *P. peranthus transiens* (**B**) and *P. peranthus kangeanus* (**C**). Asterisks indicate regions where scales were sampled, and correspond to inset colored boxes, which are 11X11 pixel hue samples of the area. **D** – Alignment of colored boxes for hue comparison. The within-individual and within-species diversity suggests these samples may be insightful for comparison of structure and pigment contributions. Images taken by Jerry Lo.

Figure 3.28
Naturally occurring hue variation vis-à-vis pigments in *P. blumei* and *P. peranthus*

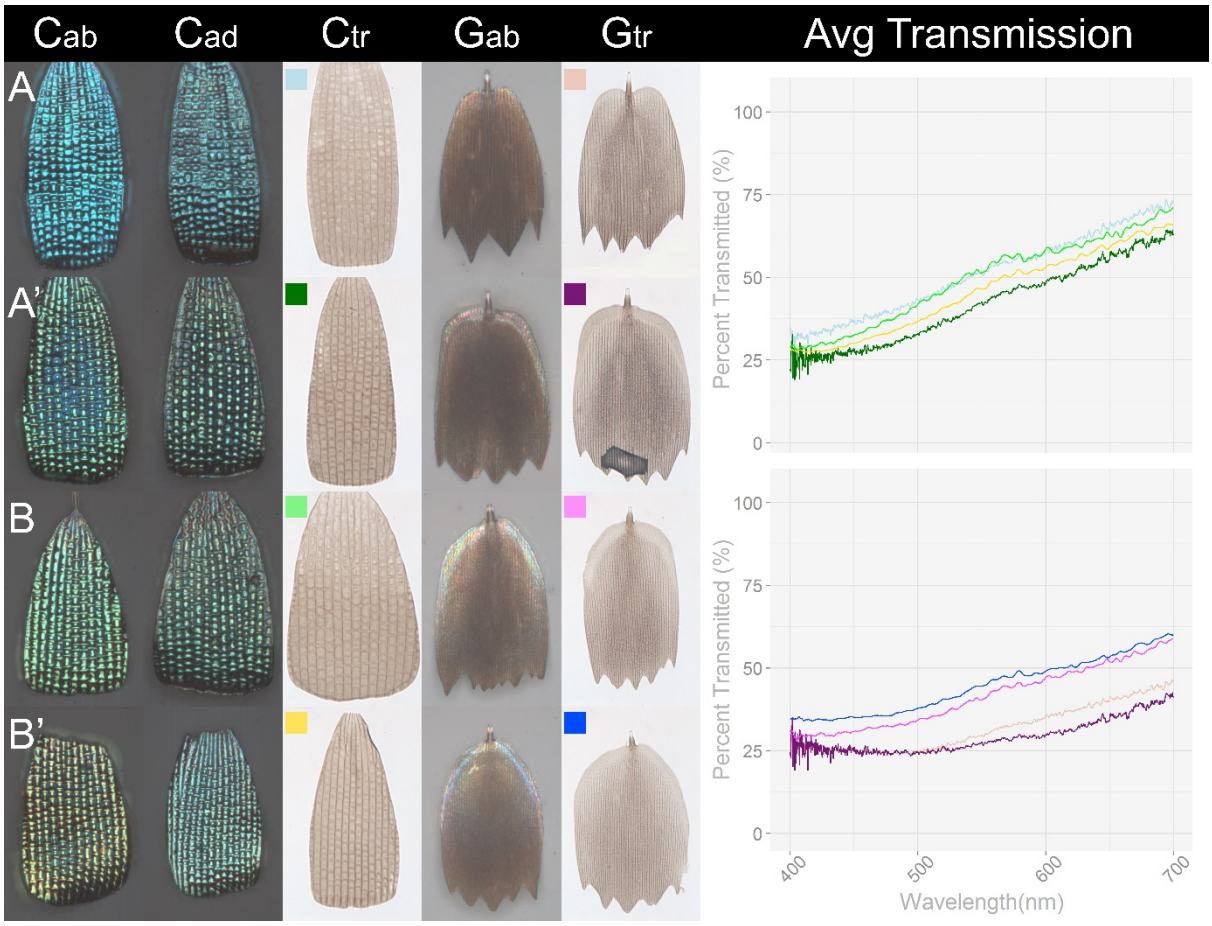

Comparison of WT hindwing scales from discal cell and tail of *P. blumei* (**A,A'**) and between HW discal cell scales of *P. peranthus transiens* (**B**) and *P. p. kangean* (**B'**). Despite the similarity of structural hue variation to Cl_2 manipulations of *P. palinurus* (Figs3.17 & 3.18), there seems to be an inverse correlation between structural reflection and pigment levels between *P. peranthus* subspecies with redder scales having higher absorbance. Suggesting either variation in color depends upon multilayer variation alone or that like *P. palinurus*, the elimination of more blue-biased lamina in *P. p. transiens* than in *kangean*. In support of both hypotheses, *P. peranthus kangean's* cover scales have lower laminae reflections that differ from the abwing (**B' - Cad vs. Cab**). However, the contribution to the overall reflection is likely minimal given the level of pigmentation within the scale (B' – Ctr). *P. blumei*'s blue and green cover scales show considerable differences in absorbance (**Avg Transmission dark green vs. light blue line**) in what may be similar to damage and 3IT compared to wild type *P. palinurus* (Figs 3.15 & 3.16). ***Cab*** – Cover scale abwing view in reflected light, **Cad** – Cover scale adwing view in reflected light, **Ctr** – Cover scale immersed in oil viewed in transmitted light, **Gab** – abwing view of ground scales in reflected light, **Gtr** – Ground scale immersed in oil viewed with transmitted light. Exposures of Cab, Cad, Gab are the same, Ctr and Gtr are the same. All images to the same scale.

Figure 3.29
Model of F-Actin rearrangements in *P. palinurus* and *P. ulysses*

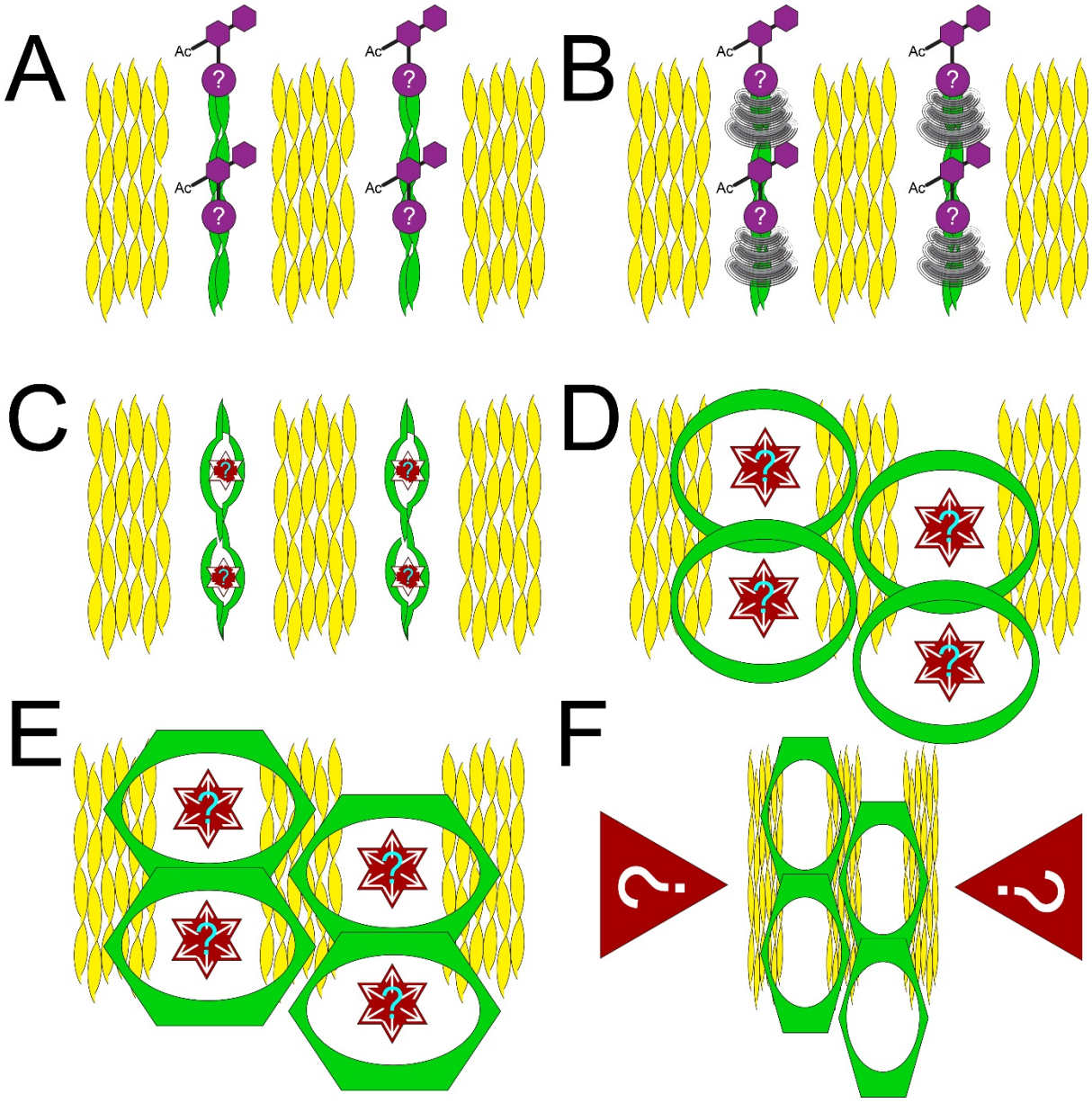

(A) – Alternating thin and thick actin bundles (green and yellow, respectively) exist with an unknown glycosylated protein/protein complex (purple) localized along the thin actin alone **(B)** – An unknown trigger potentially emanating from the puncta of glycosylated proteins, stimulates **(C)** a force (Red stars-of-David) that splits and spreads or otherwise remodels the thin actin into **(D)** large circular actin structures that begin to collide until packing results in (**E**) a hexagonal actin network. **(F)** A third unknown force (red triangles) leads to compression/contraction of the actin perpendicular to the long axis squeezing hexagons in to the boxy shapes seen in *P. ulysses*.

Figure 3.30
Model of melanin based fine tuning of chirped multilayer reflectance mechanism

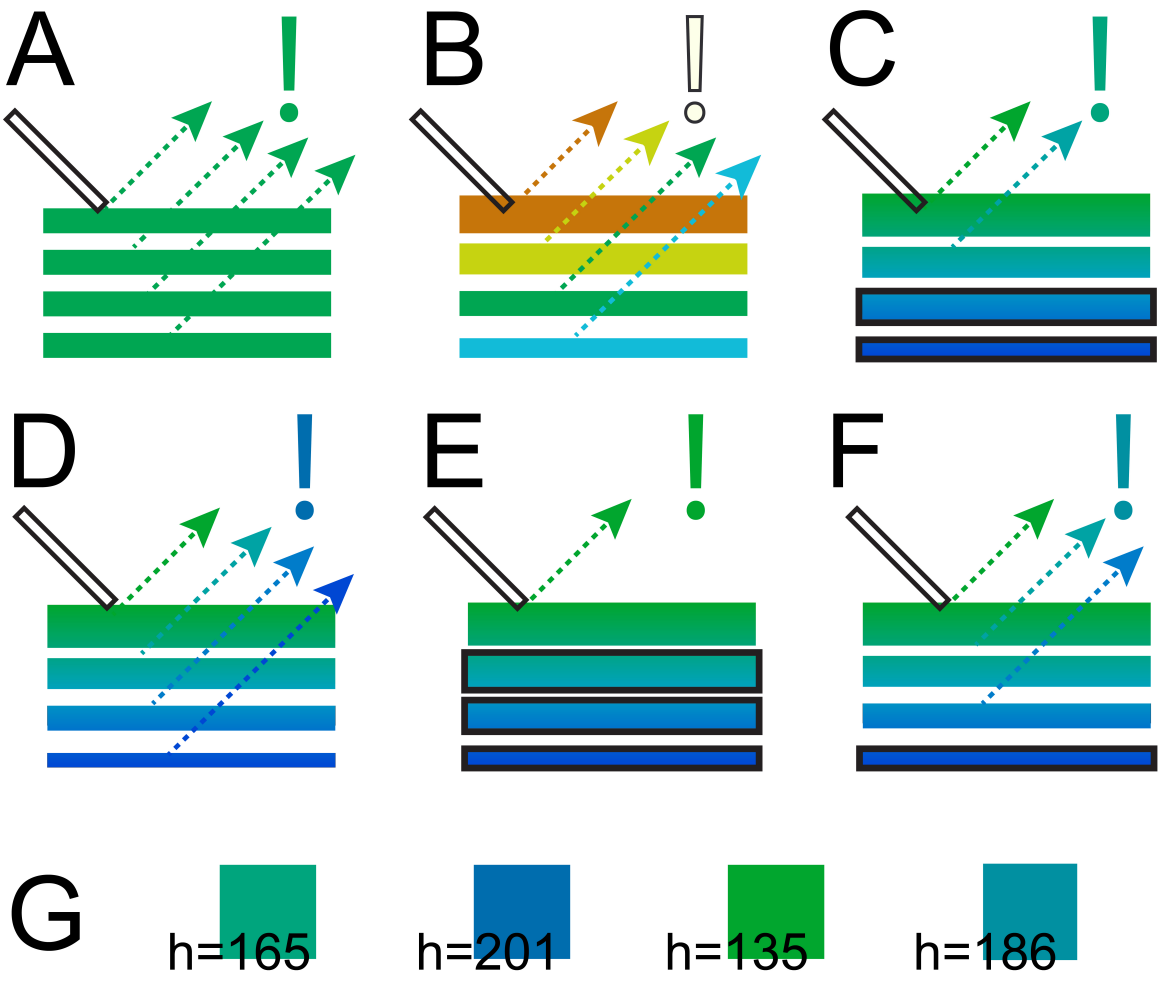

A The simplest multilayer consists of evenly spaced layers of identical composition and thickness (green layers) constructively interfering the same peak wavelength (dashed arrows), resulting in a convergence on a particular wavelength (exclamation point) **B** A chirped multilayer is comprised of layers with changing thicknesses (colored layers) reflecting different peak wavelengths (colored, dashed lines). This hypothetical chirped multilayer reflects across the visible spectrum resulting in a silver/white reflection (white exclamation point). **C** A chirped multilayer that spans only part of the visible spectrum (green to blue boxes), like *P. palinurus.* This example has pigmented its lower two layer (black outline) resulting in reflections only coming from the upper two layers and a green bias to the reflection. **D** This multilayer, is identical to C except it lacks pigmentation in the lower two laminae. As a result, the lower laminae can contribute to the color reflection and blue shift the reflection when compared to C. **E** This multilayer is also identical to C however it has expanded pigmentation to the lower three laminae, eliminating reflection from all but the upper most lamina. This strongly red shifts the reflection compared to C and D. **F** Pigment has been eliminated from all but the lower most lamina resulting in a subtler blue shift than D. It is important to note that D would (like the damage and 3IT injected animals) suffer from low purity of reflection as there is no control on back scatter of light. **G** Comparison of the hypothetical hue shifts from each of the experiments in C-F.

Figure 3.31
Model of interactions between multilayer, actin, and pigment in *P. palinurus*

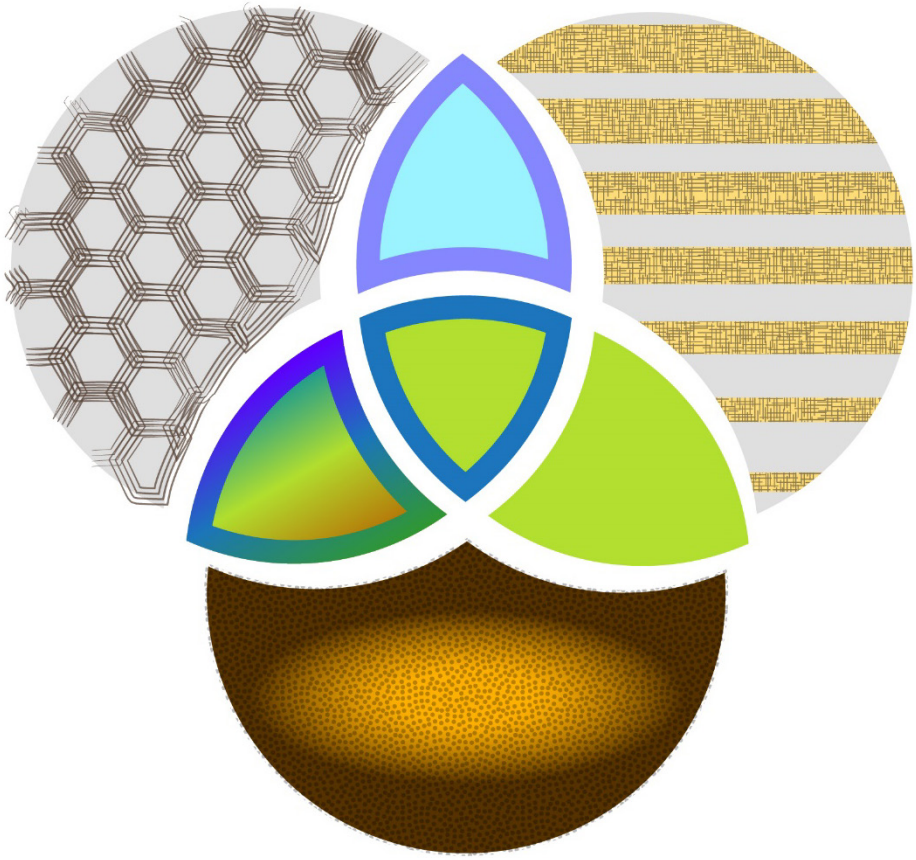

The proper coloration of *P. palinurus's* green stripe requires the interaction of at least three components: Hexagonal F-Actin delimiting dimple shape **(hexagons)**, a chirped internal multilayer **(hatched horizontal bars)**, and a potential ommochrome with dopamine melanin **(stippled orange and brown)**. Actin hexagons define structure of dimple and possibly its profile; modification of this component would lead to a loss of retroreflection and a hue shift toward the red **(green triangle)**. The internal chirped multilayer is what produces structural reflectance, complete loss would lead to the scale appearing brown – modification would lead to a hue shift in both the reflectance from the bottom of the dimple, as well as to the color coming from the retroreflected annulus **(multicolored triangle with multicolored stroke)**. Dopamine melanin appears to be found most heavily in the thinnest, lower laminae serving to increase saturation by preventing backscatter while extinguishing the reflective ability of those thinner laminae. Loss of melanin leads to increased backscatter, reducing saturation, and unmasks the thin laminae of the chirped multilayer allowing for the reflection of blue biased light. The result is a desaturated and blue shifted reflection of the central reflectance and annulus **(blue triangle with dark blue stroke)**. The ommochrome seems to help further extinguish some of the blue reflectance, although it's not clear if it is broadly distributed through the multilayer or localized to particular laminae. Only when these three components properly interact does the saturated reflectance of the wild type green central reflection and blue annulus occur **(center green triangle with blue stroke)**.

Chapter 4

Progress Toward Robust Live Imaging of Scale Development

4.1 Introduction

Development intrinsically represents a coordinated set of events that lead an organism from one state to another over spatial and temporal domains. Most commonly, development is thought of in embryonic terms, whereby a fertilized egg undergoes rounds of division and specialization to form an organism *de novo.* However, post-embryonic development has major implications for most organisms, often revolving around achieving sexual maturity or metamorphosing between life stages. Yet, post-embryonic development is much less well studied, likely in part due to the lack of locomotion, feeding, and organismal behaviors associated with embryos, which are all beneficial qualities when trying to study a developmental process.

The metamorphosis of a larval insect into an adult is one of the most striking morphological changes in living beings. Endopterygotan insects comprise a monophyletic group where the synapomorphy is indirect development through a larval stage, which metamorphoses during the pupal stage into a sexual adult. Both Lepidoptera and flies belong to Endopterygota and have said life cycle. Our understanding of how adult structures come to be (including sexual organs, wings, and butterfly scales), will therefore be focused largely upon the pupal life stage. However, there has been relatively little progress made in understanding the events of metamorphosis in detail when compared with its embryonic development. This is perhaps exemplified by the common misconception that caterpillars turn to soup during the pupal stage only to completely reorganize and emerge as a butterfly (278,279).

In Lepidoptera the wing scales, unicellular epithelial outgrowths that make up the adult's color pattern, are born, grown, specialized, and sclerotized entirely during the pupal stage (109,124,126). Our understanding of how the unicellular developmental processes involved in making scales is therefore entirely tied to pupal development. The majority of studies on scale development have taken a time series approach: attempting to capture snapshots in time, establishing an order in which they occurred, and inferring how processes occur by filling in the blanks (36,124,126). While this approach has produced fundamental knowledge necessary for our understanding, dynamics cannot be easily captured and the number of animals sacrificed is necessarily much larger. In some cases (such as dynamics of F-actin leading to a scale's adwing contours, the development and organization internal laminae and gyroids within scale bodies, and the early cell division patterns of the wing leading to highly organized rows of scales) having a means of live imaging would be vastly superior to the time series method.

The pupal stage has many of the same beneficial qualities for study as an embryo – they move very little, they do not feed, and otherwise have few organismal-level behaviors,

while they do undergo a host of fascinating developmental changes. Unlike embryos, pupae can be very large (on the order of centimeters) and when combined with their sedentary behavior represent easy targets for predation. This has likely been a selective pressure that has resulted in butterfly pupae being heavily sclerotized and pigmented. Despite all of their ideal qualities, this camouflage represents a major barrier for visualization of scale development as it is not possible to image through the pupal cuticle.

Ex vivo culture of pupal wing discs has been attempted but appears to be limited to very late stage pupae just prior to pigmentation (Fig2.5-8, Fig3.22) (113,222–224). As a result this method is useful so long as one is interested in how pigments emerge on a wing, but offers no handle on the vast majority of scale developmental processes. An advance was made by the Otaki lab whereby very fresh pupae (<1hAP) were manipulated to reveal the animals' dorsal hindwings and ventral forewings (232,280). While this did allow for the full visualization of development, the method requires enormous manual dexterity and access to larvae, which is not always easy to accomplish for some species.

In addition to the relative challenge of directly visualizing the developing tissue, there also exists the challenge of having means of gene expression and tissue markers. Given the few labs working on Leps and the propensity for those labs to focus on different species, it means that there are few intensely studied species of leps, which in turn means there are few tools in existence that allow for manipulations *in vivo*. Moreover, unlike *Drosophila* (which are small, fecund, and feature only 4 chromosomes), as a whole Lepidoptera are large, not highly fecund, picky about food source type and quality, and on average have 31 chromosomes. These differences likely account for what has made most Leps not exceedingly lab friendly or useful for the generation of lines/forward genetic studies when compared to *Drosophila*.

Whether or not forward genetics becomes readily adopted in butterflies would be less important if it were more readily possible to develop means of reverse genetics and sub-cellular visualization. CRISPR has recently made its debut in Lepidoptera through embryonic injection (77,152). However, the drawbacks to CRISPR are manifold as they are currently being done. Chiefly, that coding mutations made in embryos with the intent of affecting adult structures (as scales are), often have highly pleiotropic effects particularly when targeting likely candidates for structural color in the cytoskeleton or secretion pathways. Ideally, we will eventually identify enhancers and be able to target those which are scale specific. For most bench species (though *Heliconius* may be our best bet in the short term) this is far off, and may have to be repeated many times in whichever species best satisfies the particular question at hand.

Some progress on expression has been made utilizing electroporation and piggyBac mediated transgenesis, though these were relatively inefficient, which when combined with low fecundity equates to sub-par technology (115,281–283). Too, these studies merely express soluble fluorescent proteins which provide little benefit beyond demonstrating the expression has been successful. On another front, there have been attempts at utilizing dead-end viruses to deliver DNA or RNA to butterflies in order to

achieve expression or knock down (284–287). However, these methods have also failed to catch on, likely in part due to the lengthy screening process and heightened biosafety levels. Even in published studies there remains a dearth of tissue specific, robust enhancer/promoter combos. Most have utilized *Drosophila* heat shock promoters, Baculovirus derived immediate early gene promoters (HR5:IE1), or an Actin promoter (282,288–295).

What emerges in the current state is a list of needs:

1. Improved methods of expression – conditional & robust
2. Improved methods of DNA introduction & integration
3. Means of reverse genetics that avoid as much pleiotropy as possible
4. An easier way of live imaging pupal developmental dynamics
5. A truly lab-friendly organism

Over the course of my time in the lab, I have made attempts at advancing the state of the art with some promising gains.

4.2 Methods

4.2.1 Rearing Plodia

A breeding stock of *Plodia interpunctella* was donated by Lewis Bartlett in Mike Boots' lab. In short, 180g of food stuff (honey, glycerol, cereal, and vitamins) is placed in a Mason jar and 20-30 adults or several hundred eggs. This Mason jar is maintained on a 18:6 light:dark cycle at 18C. The generation time at this temperature is about 5 weeks from egg-to-egg.

4.2.2 Confocal imaging of phalloidin and WGA stains

Pupal wing tissue was fixed 20-30 minutes at room temperature in PIPES, EGTA, and MgSO4 (PEM) buffer with 3.7% formaldehyde. Samples were then moved to 1XPBS+0.1% Triton-X 100 (PT) with 1:200 dilution of Alexa555-Phalloidin and 1:700 Alexa647-WGA for >12 hours. Generally speaking, the longer the incubation the better the staining. Following incubation, samples were washed for a minute 3x with PT, and another 3x for 20 minutes. Samples were then incubated >12hours at 4C in 50% Glycerol:PBS with 1ug/mL DAPI to stain the nuclei. The samples were then replaced with 70% Glycerol:PBS and mounted for imaging. Stained specimen were imaged using a Zeiss LSM700 LASER scanning confocal microscope with 20x, 40x, and 63x objectives and 1au pinhole.

4.2.3 Lipofection of SF9 cells

SF9 cells were prepared to a cell density of 10^5-10^6 cells/mL with glass coverslips provided for their adhesion by the UC Berkeley Cell Culture facility. According to the manufacturer's guidelines, 8uL Cellfectin II (Life Technologies) was diluted in 100uL

Grace's Medium (Gibco), and a microgram of plasmid of interest was also diluted in 100uL Grace's Medium. Plasmids of interest were prepared via a Qiagen MIDIprep kit and were used at 1ug/uL concentration. The two were combined and allowed to incubate for 30 minutes. In a cell culture hood, the old medium was removed from the SF9 cells and replaced with fresh, unsupplemented ESF921 medium (Expression Systems). The 200uL of prepared lipofection medium was then added dropwise and the cells were incubated for 3 hours at 27C. After incubation the medium was removed and replaced with fresh medium supplemented with FBS and antibiotics. Cells were allowed to rest for 48hrs before imaging.

4.2.4 Electroporation of pupae

MIDIprepped plasmids were mixed with MilliQ, 10XPBS, and a small amount of Phenol Red until they were at ~1ug/uL and 1XPBS. Following the Golden method (294), two small holes were made in the wing cuticle (if present) within 0.75 centimeters of each other with a hypodermic needle, careful not to puncture the wing. Next a glass needle with 2uL of the plasmid cocktail was inserted through one of the holes and the contents expelled via Narishige Microinjector. Quickly after injection, a current was passed via platinum electrodes with the negative electrode placed at the injection site, and the positive electrode at the other hole. The current was 6 280 millisecond pulses of 20V with 1s of time between each pulse in a square wave. Pupae were electroporated at various and often unknown ages after pupation. This and the distance between electrodes (Golden recommend within a millimeter) could be an important source of variation in efficiency.

4.2.5 Cannulation of pupae

Following pupation, a very small hole is cut in the forewing cuticle using a #11 scalpel blade. It was critical to avoid cutting deeply and damaging the forewing, this is especially true if the animal is <36hAP while the wing is firmly adhered to the cuticle. After removal of the cuticle, a volume of 40mM PTU was added to the hole such that it was $1/100^{th}$-$1/500^{th}$ of the pupal volume to slow the localized melanization by the immune system. Next, the hole was covered by a piece of cling film with a small, clean fragment of cover glass glued to it (Loctite Go2Glue). Ideally, the cover glass fits within the hole so as to reduce the loss of working distance. The cling film is then glued to the cuticle using the same glue.

4.2.6 Larval forewing imaginal disc removal (Forewingectomy/FWE)

A day or two following the molting to the last larval instar (so the larva is very well fed and still feeding) a larva is placed on a CO_2-emitting flypad and is additionally gassed with CO_2 until it stops fighting. This is often preceded by vomiting and release of bowels. A small incision is made in the T2 segment at a location landmarked by the spiracles on adjacent segments. Just within the cuticle, the forewing imaginal disc lies, and is easily accessed by #5 forceps. Eversion from the cuticle and removal by scission of forceps follows. It is quite common for heavy bleeding to occur, however this does not seem to

influence survivorship. Surgeried animals are moved to individual soufflé cups with generous food rations and allowed to recover. Pupation should occur normally save the production of the forewing and its cuticle.

4.2.7 Live Imaging of pupae from larvae with FWE

It is easiest to prepare an animal for imaging within 1 hour of pupation. While the animal is still soft, one can place it open side down on an EtOH cleaned 24x60 cover slip and apply very gentle pressure to adhere it flat to the glass. Areas of the hindwing peripodial membrane that do not get sealed to the glass will pigment in response to the air. Adding Go2Glue around these areas may help prevent pigmentation (though it will not allow visualization through it). Injections such as Heparin injection can be done following mounting by injecting the exposed surfaces and allowing the blood to carry the drug. Electroporation should be done prior to mounting. Imaging was done on a Zeiss Stemi DRC dissecting Microscope with a SPOT camera or a Zeiss LSM700 LASER scanning confocal microscope. Images were collected every 10 minutes and sub-sampled for analysis and movie making.

4.2.8 Transgenesis preparation and injections

To collect eggs, we move 30-50 adult *Plodia* from the rearing jar into a smaller mason jar with a small amount of dry cereal mix (nothing sticky) and allow them to lay for 2 hours. We then sieve the eggs from the cereal, wash them a few times with MilliQ or DI water, then dry them with a steady, low-pressure air stream. The clean, dry eggs are mounted on a slide with double stick tape and positioned using a fire-polished microinjection needle. *In vitro* transcribed, capped mRNA encoding Tni transposase via T7 or SP6 kit was produced from plasmid containing the coding sequence. 10 parts mRNA were combined with 4 parts of MIDIprepped pBac derived plasmid DNA, and 1 part of Phenol Red. These were microinjected into the eggs within 6 hours of the start of egg collection. Injected eggs were then kept at room temperature and monitored for fungal growth and fluorescence.

4.3 Results

4.3.1 Improved methods of expression & means of reverse genetics that avoid pleiotropy

One of the greatest tools Drosophilists have at their disposal are libraries of tissue specific enhancers to drive expression of constructs in particular locations and/or at particular times. These often take the form as an enhancer trap mediated by P-element insertion of a Gal4 ORF like the *neuralized*:Gal4, which expresses within the SOPs of pupae (among other sites). The level of expression owes to a complicated mixture of regulatory elements and positional effects, but the high-throughput benefits of *Drosophila* allow selection/maintenance of lines with varying characteristics. Combination of tissue specific Gal4 lines with temperature-sensitive Gal80 repressor lines or use of 2 complimentary

split Gal4 lines can provide fine tuning to allow highly targeted conditional expression of constructs (296,297).

As we've discussed, these tools are far from available in Lepidopteran species and currently we rely on promoters that are ubiquitous such as Actin and the HR5:IE1 promoter. At best we can deploy the *Drosophila* HSP70 promoter for temporal control but heat shock may bring about artifacts which could be confounding in a study on scale development (141). In my work I have utilized the HR5:IE1 promoter which expresses very robustly in scale cells as well as in its intended host: SF9 cells that are derived from *Spodoptera frugiperdis* ovary (298). In SF9 cells, I was able to get expression of several fluorescent varieties (GFP, mCherry, mEos3.2) of the transient F-Actin-binding-domain of yeast Abp140p, known as LifeAct, as well as a construct coexpressing histone H2B:RFP and the membrane marker GFP:CAAX via an F2A peptidyl-transferase skip site (Figs4.1 - 4.3) (299,300). Some of these same constructs were also functional in scale cells as described later (Fig4.4).

While I had some success with the viral promoter, this is not without the caveat that there were defects associated with the high level of expression of some constructs (particularly the LifeAct). These correlated with fluorescence level, suggesting that copy number is an important consideration when using the viral promoter (Fig4.2). Perhaps of interest, was that the high expression of LifeAct led to multiple processes, a twisted and bifurcated shape, and general loss of "scaleness" (Fig4.5). This was very similar to a *forked/sn* double mutant bristle in *Drosophila,* suggesting a competition between the LifeAct peptide and actin crosslinkers (301).

If continuing to pursue expression via HR5:IE1, it will likely prove necessary to utilize other means of conditional expression or evaluation. To this end, I have built a LifeAct construct with mEos3.2 – a monomeric photoconvertible mKaede derivative that is used in PALM super-resolution microscopy (302,303). This construct was modified from Addgene plasmid 54696 (a gift of Michael Davidson). I first expressed it in SF9 cells to verify construction and were successfully able to get expression at the cell cortex and to get fluorescent photoconversion from green to red, using standard DAPI channel excitation (Fig4.3). The photoconversion capability will be extremely useful if integrating with broadly expressing promoters like the HR5:IE1 – by regionally photoconverting a small region of expression, one can focus on only those that are photoconverted as a work-around to the ubiquitous expression throughout the tissue. In addition, the utilization of mEos or similar proteins, will allow for super-resolution microscopy to be used in development, which will be necessary for visualizing nanostructures that by definition are beyond the diffraction limit of light. This will be useful not just for actin, but for many sub-cellularly localizing tags like KDEL (ER) or CAAX (plasma membrane).

Another approach to work around non-tissue specific promoters, is to use a broadly expressing promoter, such as HR5:IE1, in combination with optogenetic fusion proteins. Again, I have started building constructs with this approach in mind starting with the photoactivatable Lov:HsaRac1 (Addgene 22027) a gift of Klaus Hahn (304). Lov domains

are steric inhibitors which are relieved from hindrance via a conformation change stimulated by energy imparted by bombarding UV photons – again using the standard DAPI filter set (305). In theory, this set up will allow a multitude of spatiotemporally controlled experiments to be within reach such as:

- Candidate antimorphic/neomorphic allele expression (e.g. controllable dominant negative Lov:*Ik2*^{K41A} or the neomorphic myr:Abp1:Lov) (144,145,306,307)
- Candidate TALEN-derived null clone manufacture (e.g. TALEN$_{(Ik2)}$:Lov)
- Real time visualization of cellular dynamics/kinetics (e.g. unmasking of localization signal) (308,309)
- Modulation of enzymatic activity (e.g. Lov:Rebuf to control Kkv chitin synthase activity and chitin layer thickness) (310)

While we are still in the early days, these technologies seem to be promising in SF9 cells even utilizing the current viral HR5:IE1 promoter. Though further work needs to be done, it seems likely that a combination of photoactivation and photoconversion based strategies will yield many insights until a deep-dive for tissue-specific promoter/enhancer combinations can be attained.

4.3.2 Improved methods of DNA introduction/integration

One of the largest hurdles to clear in regards to dissecting the genetics and cell biology of Lepidopteran scales, is the ability to introduce DNA constructs. Drosophilists have had great success utilizing mainly the P-element and piggyBac transposable elements. Integration of a construct via transposable element allows the construct to be inherited by all descendants of the cell in which it originally integrates. This can be limited to somatic integrations or can be integrated into the germline allowing for subsequent generations to inherit the construct. Alternatively, introduction of non-integrating plasmids can be achieved via microinjection or electroporation. In the latter, an electric current transiently creates pores in the plasma membrane of nearby cells and simultaneously can be used to push negatively charged nucleic acids into these pores. Once the current is removed, the pores close up and the nucleic acids remain trapped inside. Since there is no integration and electroporated plasmids do not contain centromeres, plasmids are diluted and eventually lost through cell divisions. In some situations this temporary means may be better, and, if optimized, may be far more efficient than the low levels of integration that occur in most transposable element systems.

I attempted to use electroporation, based on the examples provided by Golden and Ando (115,294), to introduce various LifeAct constructs expressed using the HR5:IE1 enhancer/promoter in 3 species, *Junonia coenia*, *Vanessa cardui*, and *Papilio palinurus.* I had inconsistent success with both Golden and Ando's protocols but found the latter to work better in my hands. One thing which appeared to perhaps make a difference is when electroporation took place during development. In the most efficient, *Vanessa cardui* pupae were ~36-48hAP, from 20 operated pupae (1ug (500ng of 2 differently colored LifeAct plasmids (each ~4kb))) 17 (85%) were positive for fluorescent protein expression.

It was far commoner for me to electroporate *P. palinurus* and for these to be completely unsuccessful, or have a single animal with expression from a round of ~20 animals. When it worked, the introduced LifeAct gene was expressed and recapitulated the previous phalloidin stains (Fig4.4 vs. Fig3.4). Part of the inefficiency could be attributed to having no control over age of the animals. Through careful and rigorous testing, the effects of pupal age on electroporation efficiency may prove enlightening.

As for transgenesis, I've attempted piggyBac transgenesis, which has many advantages including semi-random introduction at TTAA sites, precise excision, it was originally derived from a Lepidopteran (*Trichoplusia ni*), and it has a demonstrated viability in a range of non-Lepidopteran hosts (311,312). The majority of papers using piggyBac transgenesis use a vector containing the gene of interest and a helper plasmid that encodes the transposase (usually under heat shock promoter) (115,281–283,291). These studies also have reported very low transgenesis rates. I reasoned that injecting the plasmid of interest with *in vitro* transcribed mRNA encoding the transposase would be more efficient, as the heat shock promoter is not the most robust, and the delay of induction of transcription to accumulation of sufficient transposase may be longer than the time the embryo remains as a syncytium. This latter point is important if aiming for a large number of clones or germline integration, as cellularization prevents the widespread access to nuclei afforded by the syncytium. Again here it was hard to evaluate actual transgenesis as no expression was seen after the first larval instar, but I was having fluorescent protein expression in about 5-10% of both *Plodia* embryos and hatched larvae. In most instances fluorescence was limited to large macromeres in embryos and the gut of hatched larvae (Fig4.6, Fig4.7). I was able to confirm this was actually expression of the introduced LifeAct:mEos construct by exposing the organisms to UV light, following which the green fluorescence shifted into a red pattern identical to the original green fluorescence (Fig4.6 top vs. bottom). It remains to be seen whether this was actually transgenic or merely expressing off of the plasmid. In addition we did not see expression similar to what had been reported for the 3XP3 artificial reporter that was also contained on the plasmid (281,282). There have been recent reports of hyperactive piggyBac transposases which have higher activity in both yeast and mammalian cell lines, suggesting they should also be higher in Leps (311). By utilizing a hyperactive piggyBac as an mRNA injection we may be able to push transgenesis to a more efficient state. Alternatively, the hyperactive Tn5 transposase used for ATAC-seq may be adapted for transgenesis use in Leps (313).

4.3.3 Live imaging pupal developmental dynamics

Our understanding of biological processes is inextricably linked to our ability to visualize processes. For every advancement of imaging technology – camera lucida, film, confocal, EM, super-res – biology has advanced in its understanding. The majority of technologies benefit from fixation and staining which improves contrast but may introduce artefacts. Moreover, fixation necessarily results in death which is the antithesis of biological processes. Indeed, as we've encountered with the formation of *Papilio palinurus*'

hexagonal actin arrays (Fig3.4), having a time series still leaves much unresolved. Inspired by the information I was able to pull from the *Morpho* work (Chapter 2) and Otaki's group, I wanted to see if live imaging could be adapted to work in younger animals without the technically challenging and temporally restricted limitations of Iwata's method (232,280).

We first asked if we could simply culture young tissue. Dissected wing discs from *Vanessa* between 1 and 3dAP were cultured in Grace's supplemented with FBS and antibiotics. In a matter of minutes, the tissue would ball up and discolor, in many respects this seemed to be a function of the tracheae tightening like purse strings. We thus set out to ask if adjusting osmolarity was a sufficient means to prohibit this shrinking. We added sugar or water to increase or decrease the tonicity of the medium as well as varied the level of FBS in the medium. In no instance did we find an ideal medium.

We then asked if, despite gross tissue level deformation, scale development proceeded normally. Experiment on fileted fly thoraces provided some support for this idea as macrochaetes seem to develop normally despite the high level of dissection (140,314). Our first experiment was simply to dissect an animal, fix and stain one wing, culture the contralateral wing for a few hours and then fix and stain it. In comparisons of scales from these experiments, it was clear some growth had occurred although the apical tip of the scale appeared to be blown out (Fig4.8). Curious about this result we set up a time lapse to visualize the development of these young *ex vivo* cultures. What we found is that the nascent scales produced large inflated tips while the remainder of the scale was very thin (Fig4.9). This phenotype is very reminiscent of actin defects in bristle development (140,143,145,146,156,263,315). It is unclear how the dissection or culture conditions contribute to a cytoskeletal phenotype, but it was clear that this was not the best method for live imaging.

Next, I attempted to simply cut a window in the pupal cuticle to allow visualization of the underlying tissue. Damage to pupae results in the onset of protective melanization which acts to encase invading microbes or parasites and also serves as a scab to close up the wound (316). The melanization inhibits the ability to perform microscopy as the pigment is too dark and prevalent to allow visualization of features. Inspired by the finding that Morpho blood melanization could be prevented with phenylthiourea (PTU) without obvious effect on the rest of the biology, I added a small amount of PTU (1uL of 40mM PTU/1mL of pupal volume) and closed the wound with a shard of cover glass glued to a piece of saran wrap. This worked remarkably well, with the exception that pupal cuticle thickness was often greater than the working distance of compound objectives >20X. Time lapse using autofluorescence of the tissue allowed for visualization of some of the early SOP dynamics in pupal wings, albeit quite grainy. These matched up quite nicely with the beta-catenin stains of fixed tissue. The benefit of this pupal cannulation technique is that it does not require having larvae, and can be done at any time in the pupal development – we were able to perform the technique on older *P. palinurus* pupae and were able to bookend the pigmentation process (Fig4.10).

One limitation of the cannulation method is that one can only visualize a small region of the wing, so gross pattern visualization is not possible. This is one of the prime benefits of the Iwata methodology, particularly as it will be useful to pair time lapse with transgenics, which can be inherently mosaic and patchy in an unpredictable way (232). As mentioned however, Iwata's method requires quite good dexterity and access to very young pupae – both often in short supply in America. In a serendipitous finding during the 2015 MBL Embryology course, Julian Kimura performed an experiment to see if caterpillars could regenerate lost wing discs. He surgically removed a 5th instar forewing disc only to find on pupation that the pupa lacked the forewing and cuticle providing an unobstructed view of the dorsal hindwing through a thin membrane, presumably the hindwing peripodial membrane (Fig4.11). With time if not protected from the atmosphere, the peripodial membrane of the hindwing pigments and prevents visualization (seen in Fig4.13 and Fig4.14). I've since found that covering or pressing the pupa to cover glass is sufficient to prevent the majority of pigmentation and allow visualization of the full length of development to eclosion. This has been true of every species attempted (*Vanessa cardui, Junonia coenia, Battus philenor*, and *Plodia interpunctella*) suggesting that the majority of Lepidopterans will be amenable to this surgery (Fig4.11-Fig4.13 and Fig4.21). I have also examined whether it is possible to visualize the effects of typical manipulations such as Heparin sulfate injection and found that this too is possible (Fig4.14). Further, one animal I visualized experienced considerable damage but continued to develop suggesting that cautery experiments to induce ectopic eyespots or even focus transplantations should be possible (24,26). Live imaging of scale cells is possible with no additional contrast agents, however it is limited in what can be detailed. So it was exciting when I was able to combine this surgery with the electroporation of LifeAct (SeqA3.2) into the wing to visualize for the first time the actin associated elongation of a nascent scale cell (Fig4.17). In total, this method has huge benefits all around for understanding scale cell development and simply needs advancement in contrast agents to reap insights.

4.3.4 A lab-friendly Lepidopteran

After working with *Morpho peleides* and *Papilio palinurus/ulysses* it was clear that having access to larvae would be a major advantage for our studies. Having access to (at least) the last larval instar allows one to more accurately decide when pupation occurred and thus makes piecing time series together less complicated. Larvae also allow one to make very early pupal manipulations such as Heparin/Dextran Sulfate injections, which must be done within the first 6 or so hours after pupation (24,317). And as described in the methods, it is required to have larvae if one wishes to remove the forewing imaginal disc for easy pupal live imaging later.

After working with *Vanessa* and *Junonia,* for which larvae were available, it was sorely desired to have the ability to easily grow hundreds of larvae in relatively small confines without cannibalism, and without the need for frequent and large food plant harvests. In addition to having larvae I wanted to easily and frequently collect large numbers of eggs

(hundreds per day) for genetic manipulations including CRISPR and transgenesis. This is as much a function of population size as pickiness for laying substrate – both butterfly species are a challenge to raise in large number and require living plant tissue to lay on.

After a short stint using *Galleria mellonella,* we began using *Plodia interpunctella* for our basic biological approaches. Both are Pyrallid moths and are generally considered pests. *Plodia* have an approximately 5 week egg-to-egg lifecycle and can be raised without any maintenance for the duration of their larval instars. Their small size means that hundreds of individuals can be reared in a single Mason jar with less than 200g of food stuff, which is made in large batches and kept frozen until needed. Where *Galleria* requires honeycomb for culture, *Plodia* merely requires grains making it very easy to maintain. Moreover, a *Plodia* genome sequencing project is underway, meaning CRISPR etc. will be easier. It is good to keep *Galleria* in mind though, as it is a larger moth, meaning some manipulations may be easier in this moth species. An important caveat to these moth species is that they have no apparent coherent structural coloration, though *Plodia* do show thin film reflections on the lower lamina and *Galleria* are largely white, which is a broadly reflecting incoherent structural color.

When listing ideal qualities of a lab organism, *Plodia* has the majority of them. An ideal system would also feature a small haploid chromosomal number (n). A small n value facilitates the manufacture and maintenance of balancer chromosome lines that make forward genetics and stock maintenance easy. Unfortunately, unlike *Drosophila* or *C. elegans*, karyotyping suggests that *Plodia* have an n=31, requiring 31 separate balancer chromosomes to be made and maintained (318). It may be worth keeping this in mind as work progresses, and either make a concerted effort to produce balancers in *Plodia*, or to be on the watch for an organism with fewer chromosomes.

Work has just begun in *Plodia,* but already it seems promising for the investigation of basic scale biology – an area that is in desperate need of advancement. Upon obtaining the line I first wanted to ensure that their scales were typical of those that have already been reported in butterflies. Simple phalloidin/WGA stains of developing pupae showed that scales are indeed prototypical and seem to rely heavily on F-Actin cables like their close relative *Ephestia kuhniella* as well as nymphalids that we've studied (Fig4.18) (124,126). Interestingly, along the border of the hindwing, there is an obvious gradient of scale morphology, progressing from scale-like with small apical tridents to less broad scale with more substantial apical tridents to tridents which are very finger like and no scale body of which to speak (Fig4.19). This transition could serve as an important source of information when seeking to understand how bristles become scales or vice versa. Finally, it's also worth mentioning that *Plodia* have a fully developed frenulum (lacking in butterflies), which aides in connecting the fore and hindwings during flight. It was noticed long ago that the frenulum is a composite structure that forms from several independent bristles which fuse together (319). Indeed, we can confirm the presence of many independent bristle structures in the developing frenulum and lots of intervening WGA-positive stain (Fig4.20A,A',B,B'). Accordingly, this structure's formation is likely to depend

heavily upon the interaction of many bristles' extracellular matrix (perhaps via ZP-domain proteins) for fusion – something speculated upon nearly 100 years ago in *Galleria* (319). Thus, thanks to its large size and scale-homologous cellular origins, the frenulum's morphogenesis may serve as a canary in the coal mine for bristle, actin, and/or ECM/ZP-dependent processes in scales.

It will also be important to be able to visualize development, and what seems to be true for all other species we've tested holds in *Plodia.* Larval excision of the forewing imaginal disc leads to a gap in the pupal cuticle that allows visualization of the hindwing pupal disc (Fig4.21C). This is an important advance, as the larvae form silken cocoons prior to pupation so exact timing of pupation is harder to ascertain making the method of Iwata harder to achieve, as time is of the essence with that method and one must be exceptionally delicate in removing soft pupae from the silk (232). It seems likely that application of the forewing removal to manipulated *Plodia* will allow exceptional advances in our understanding of scale development.

In sum, the need for a true bench species of Lepidopteran still exists and it seems a return to the Pyrallid species of yesteryear may be our best current option (121,126,319). The advantages of *Plodia, Ephestia*, and *Galleria* are hard to top – though there may still be room to improve. As a workhorse of basic scale cell biology, the Pyrallids presently offer our best handle on how scales are built from/into the far more studied bristle cell types and from there it is easy to imagine the fine scale adjustments needed for coherent structural color arising.

4.4 Conclusions

Here I've detailed the steps taken to improve our ability to visualize scale development in real time. As much as has been accomplished, it amounts as much to a guide for what I see as a way forward. Largely inspired by the benefits Drosophilists have accrued over a century of work, I foresee a similar approach as an obvious way forward. To this end employing small, fecund Pyralid moths that have *Drosophila*-like characteristics seems like an important first step. Once this has been established, optimizing transpositional transgenesis will provide many benefits including establishment of lines, the ability to start projects such as enhancer trapping, as well as transposition-based mutagenesis studies. In the meantime electroporation based studies may allow rapid evaluation of questions where integration takes time. Both of these technical approaches will continue to benefit from construct testing via cell line transfection of SF9 or SF21 cells given their Lepidopteran origins. Further the utilization of constructs with optogenetic or temperature sensitivity can aid in restricting the effects/avoiding pleiotropy especially as many of the interesting candidates are cytoskeleton associated. Such conditional constructs could utilize known dominant negative alleles from the *Drosophila* literature or employ TALENs (which require no small RNA or RNAPolIII transcription for their deployment) to create genetic clones or possibly inactivate genes after the establishment of scale cells to assay

temporal necessity within the scale. Given our ability to now have visual access to the full development of the dorsal hindwing, and the retain ability to perturb the patterning as demonstrated by Heparin or ectopic eyespot induction – it seems likely that we will be able to ask a wide range of questions about development. Though still needing attention, the steps we've made in live imaging will be important for achieving a deeper understanding of the many facets of cell biology that scales are able to provide. How axis specification, sub-micron patterning, cytoskeletal dynamics, genetic analyses etc. occur in scales are closer than ever. Pushing to improve transgenesis, with conditional and/or tissue specific constructs, in species which are lab friendly while employing cannulation or forewingectomy surgeries will be key to this progression.

4.5 Relevant Appendices

For sequence data of constructs mentioned, see Appendix 3

Figure 4.1 Expression of histone H_2AmCherry:F2A:eGFP:CAAX in SF9 cells

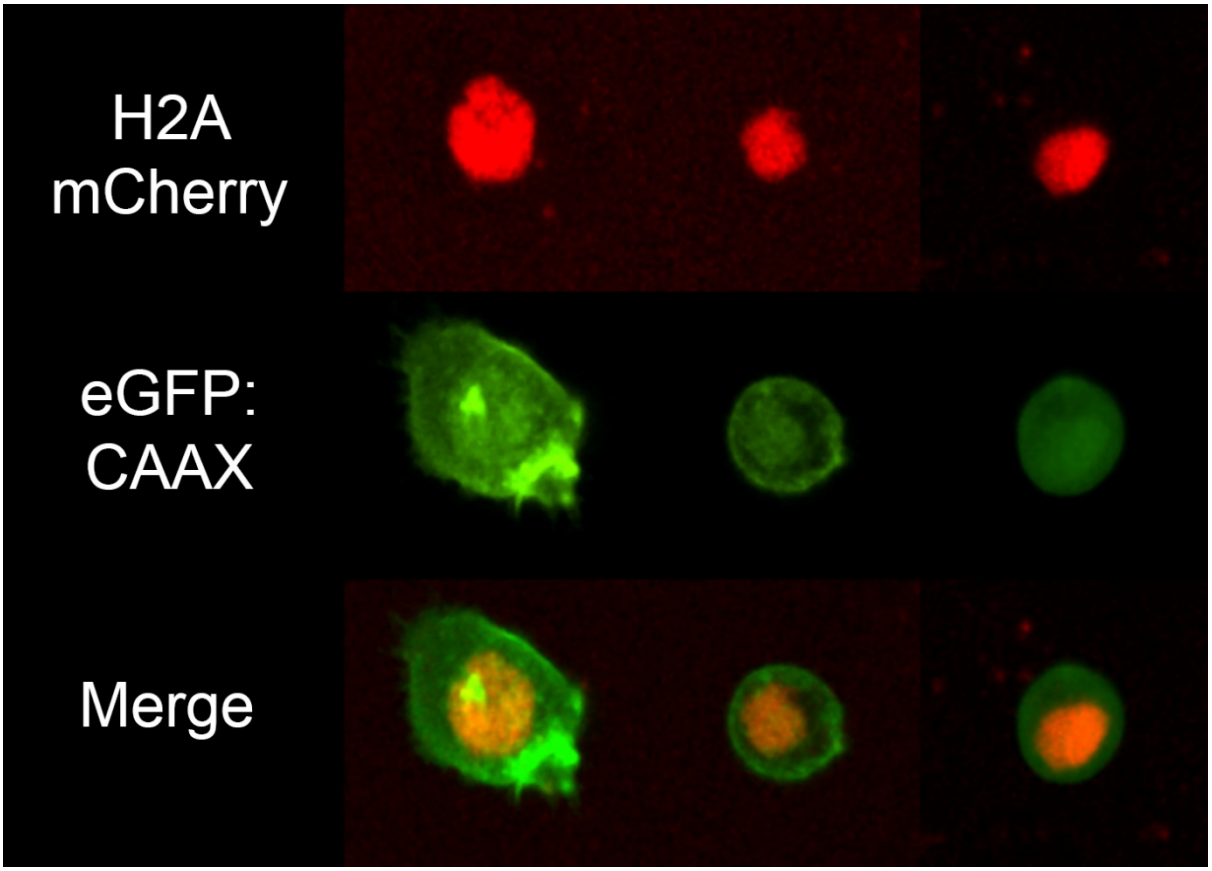

SF9 cells (a cell line derived from the ovary of the moth *Spodoptera frugiperdis*) express proteins from a transfected plasmid pfIErfly[H_2A:mCherry:F2A:eGFP:CAAX] (SeqA3.6). The correct localization of histone mCherry in the nucleus with clean separation from the membrane localized GFP. Use of the F2A ribosomal skip site prevents the peptide bond between a C-terminal Glycine on H_2A:mCherry and an N-terminal Proline on eGFP:CAAX, thus freeing the two peptides from one another despite being encoded by the same mRNA. Perinuclear staining of eGFP:CAAX may result from imperfect skipping efficiency and/or may be due to the ER localization of GFP during CAAX box prenylation. The ability to express multiple fluorescently-tagged peptides from single constructs may be very useful for butterfly work. Images taken with Jose Breton-Arias.

Figure 4.2 Expression of pIEX4:LifeAct:eGFP in SF9 cells

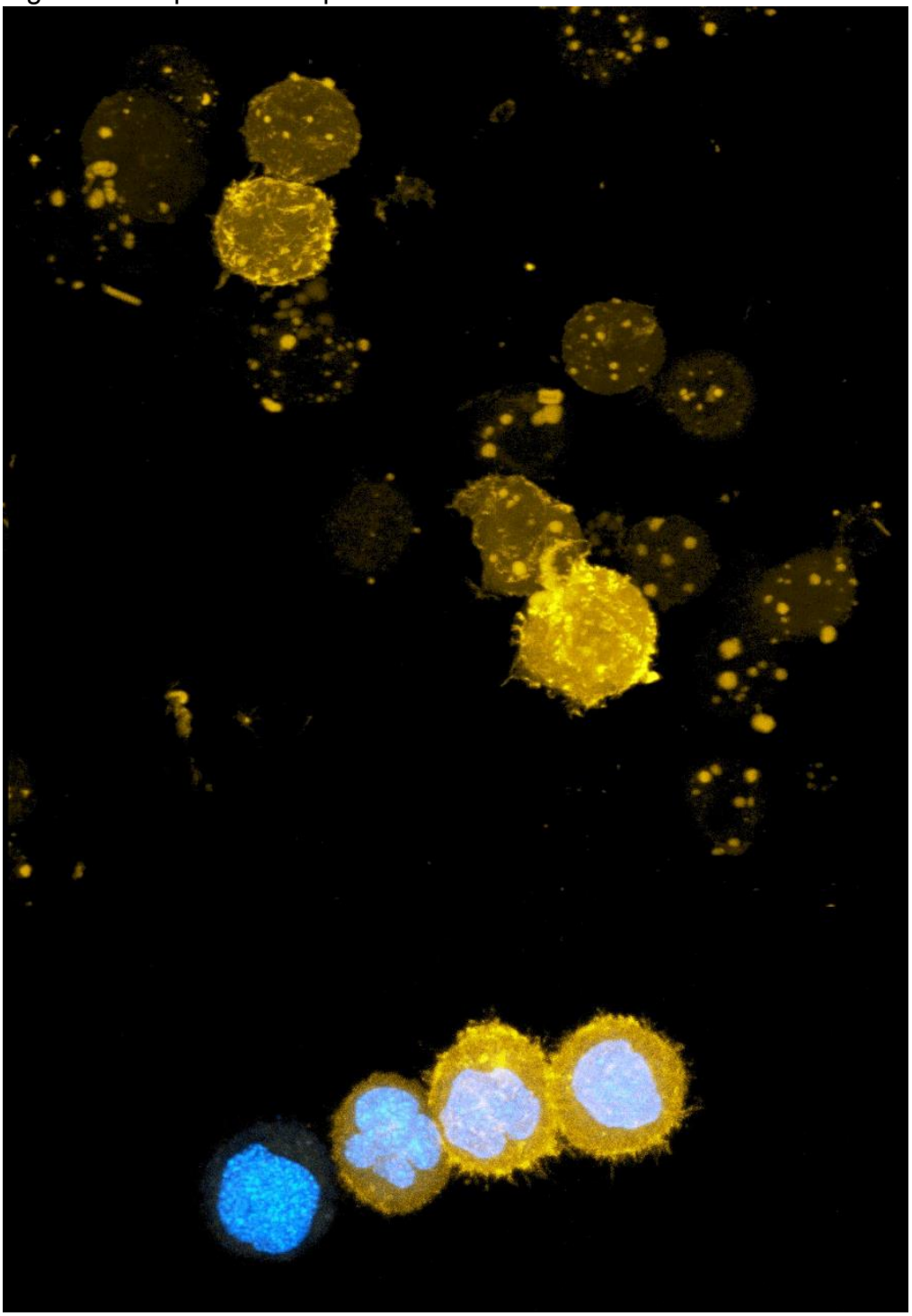

SF9 cells expressing LifeAct:eGFP (yellow) driven from transfected pIEx4 plasmid (SeqA3.1). Thanks to the transient binding of LifeAct peptide to F-Actin, fine details, such as movement of filopodia, can be seen on the surface of the cells. DAPI stain (blue) highlights preferential localization of LifeAct to the cellular cortex, and varying levels of expression can be seen which we interpret as an effect of copy number. Images taken by Jessica Poon.

Figure 4.3 Photoconversion of LifeAct mEos in SF9 cells

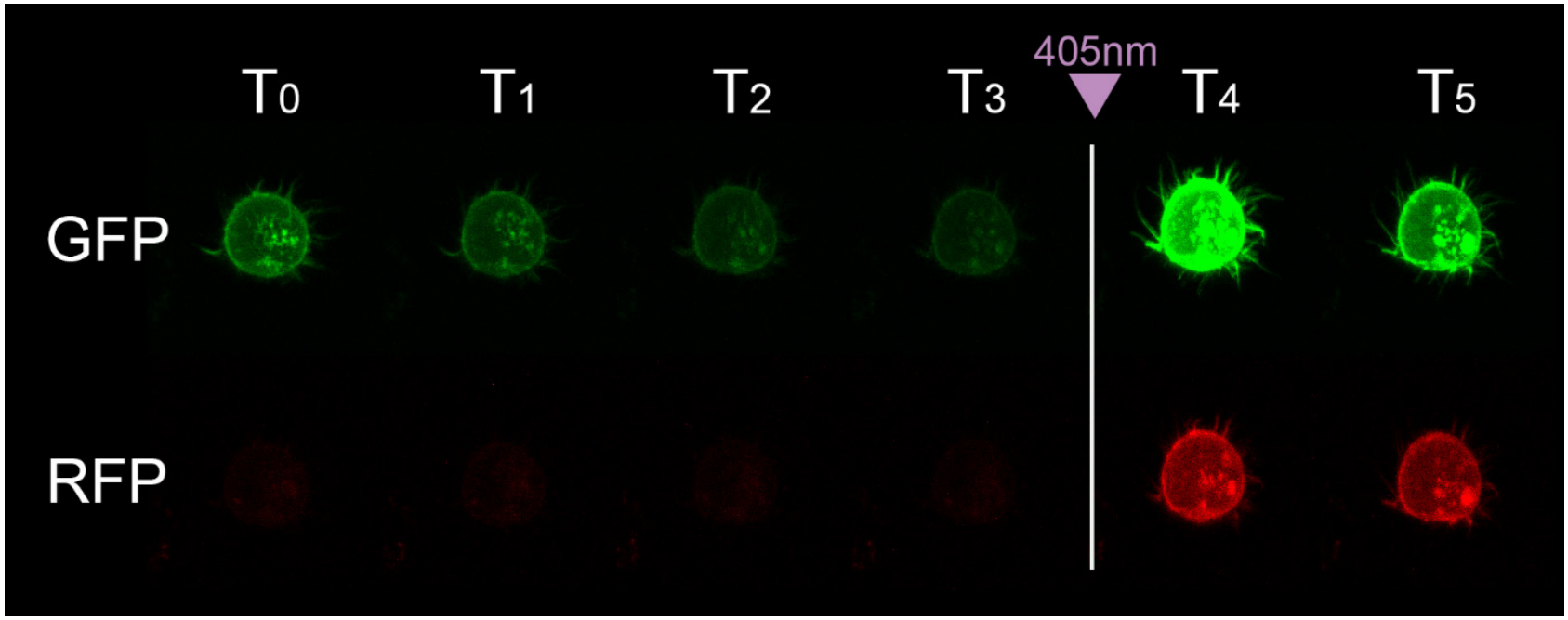

The expression of photoconvertible mEos3.2:LifeAct in SF9 cells via HR5IE1 promoter (SeqA3.5). mEos3.2 is a photoconvertible fluorescent protein derived from mKaede and used in PALM super-resolution microscopy. In the **top panels** we show a time lapse of a cell expressing mEos:LA where expression is largely confined to the green fluorescence channel. Upon stimulation with the DAPI LASER, photoconversion of mEos occurs resulting in red channel fluorescence (**bottom row**) and recovered fluorescence in the green channel. Z stack of cell was captured every minute with a pulse of UV light at the start of the 4th stack (**line/405nmArrowhead)**.

Figure 4.4 pIEX:LifeAct:eGFP in electroporated and fixed butterfly scales

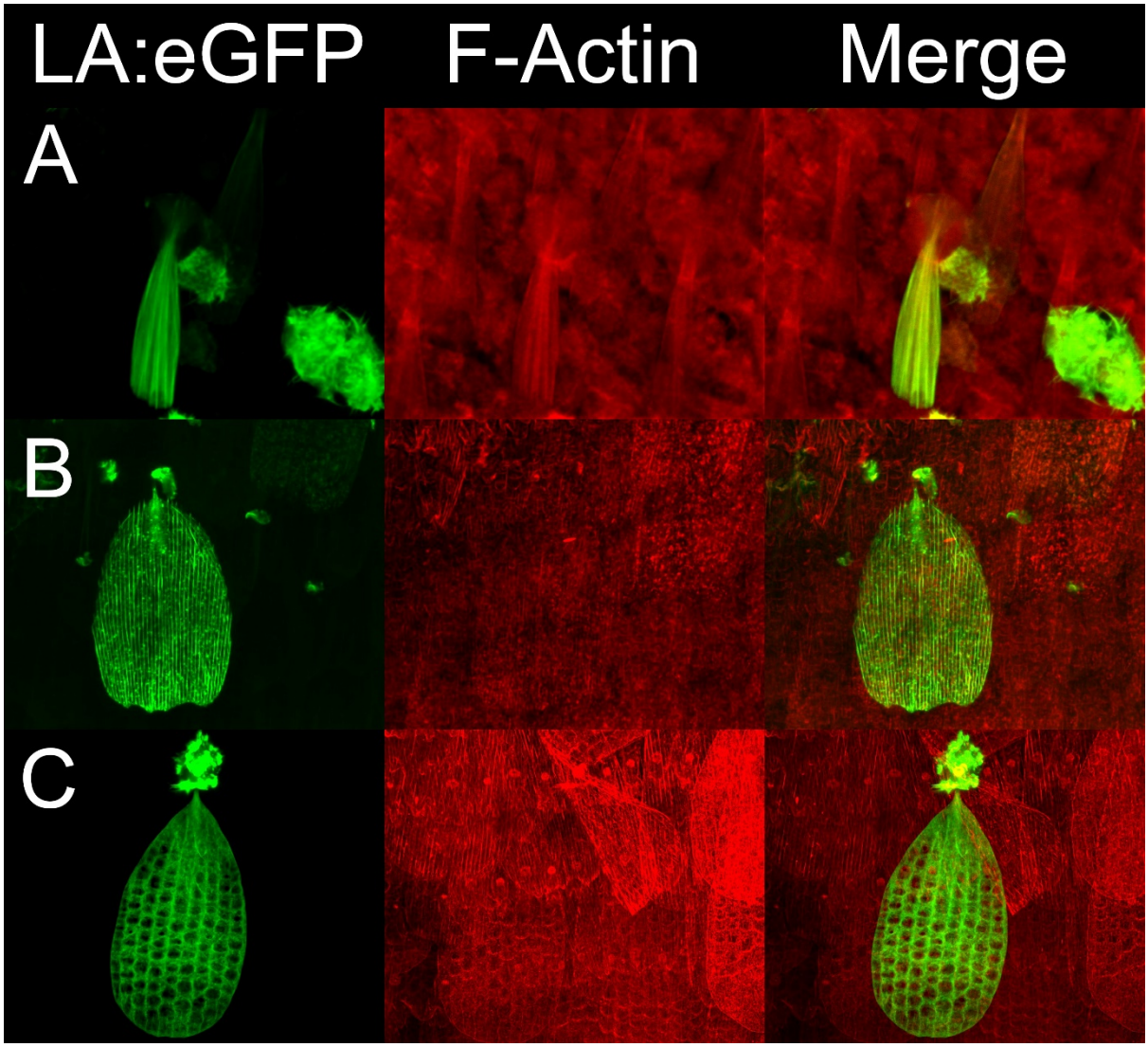

Electroporation of pIEx-4 containing eGFP:LifeAct (SeqA3.1) into pupal wing discs shows F-actin similar to phalloidin stains. Rare scale cells expressing the GFP-tagged F-actin binding domain in *Vanessa cardui* (**A**) and *Papilio palinurus* ground and cover scales (**B,C**). **C** shows remarkable similarity to the hexagonal actin of the phalloidin stain seen in Figure 3.4 with arguably better detail suggesting LifeAct could be a very useful construct for understanding F-Actin dynamics in real time *in vivo*. Electroporation also marks the cell body (bright green ball at base of scale) Electroporated pupae were fixed and stained with phalloidin then imaged via laser scanning confocal microscopy. Images are Z projections of data captured by Jessica Poon.

Figure 4.5 Brightest scales expressing LifeAct have a *f/sn*-like phenotype

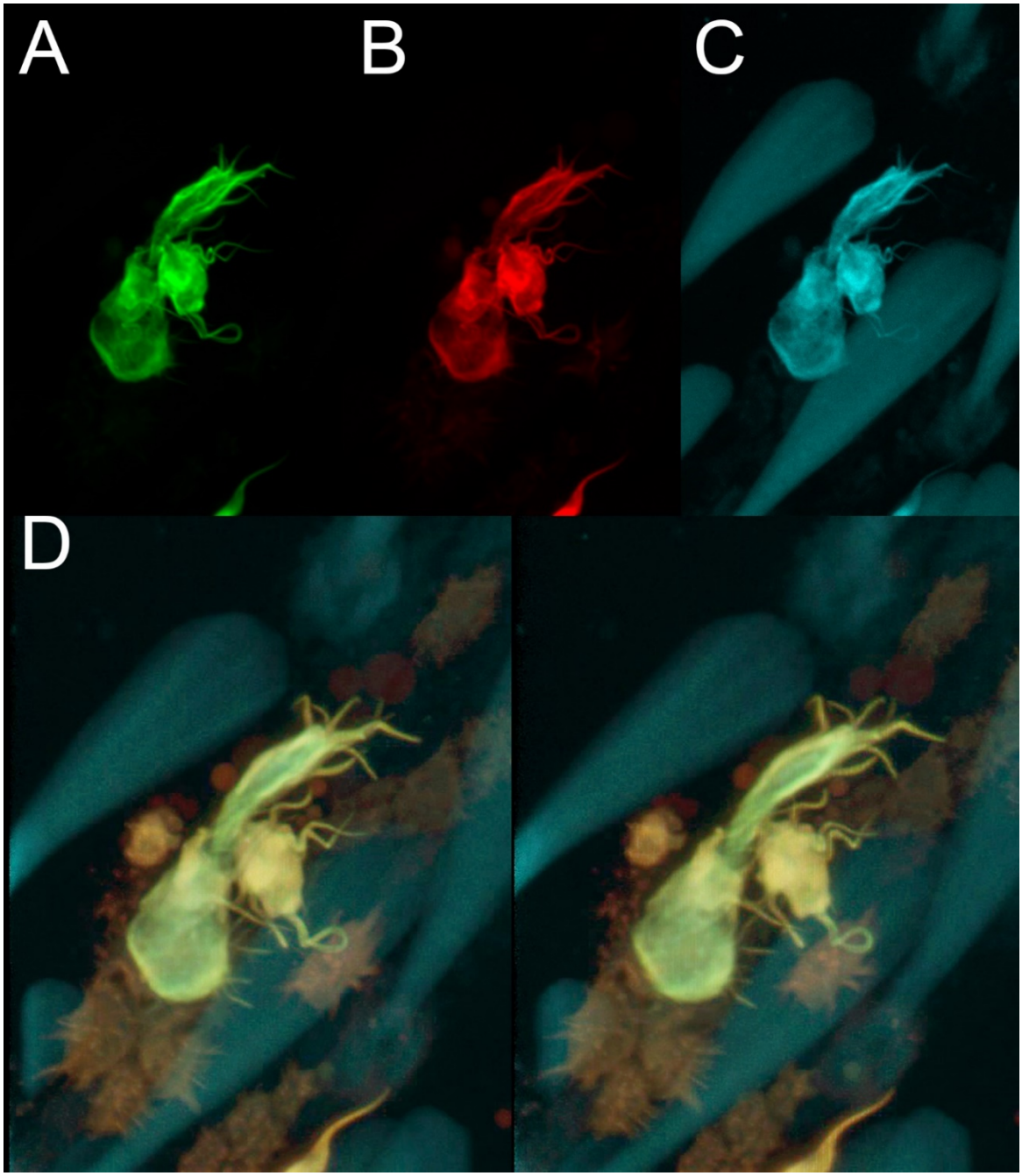

As we noticed in SF9 cells, there are differential levels of expression in electroporated pupal wing scales. Here I co-electroporated LifeAct:eGFP and LifeAct:mCherry encoded on separate pIEx-4 plasmids (Seqs A3.1 & A3.2). On occasion, cells with exceptionally bright fluorescence (such as the one shown), displayed phenotypes similar to loss of *singed* and *forked* in *Drosophila* bristles when compared with wild type scales not expressing the constructs (seen easily in the autofluorescent blue **C**). LifeAct at high concentrations may compete with Forked and/or Singed proteins for access to F-Actin filaments preventing their bundling. **A** LifeAct:eGFP, **B** LifeAct:mCherry, **C** Autofluorescence captured in DAPI channel. **D** Stereoimage of the merge.

Figure 4.6 Expression of mEos3.2:LifeAct in *Plodia* embryos

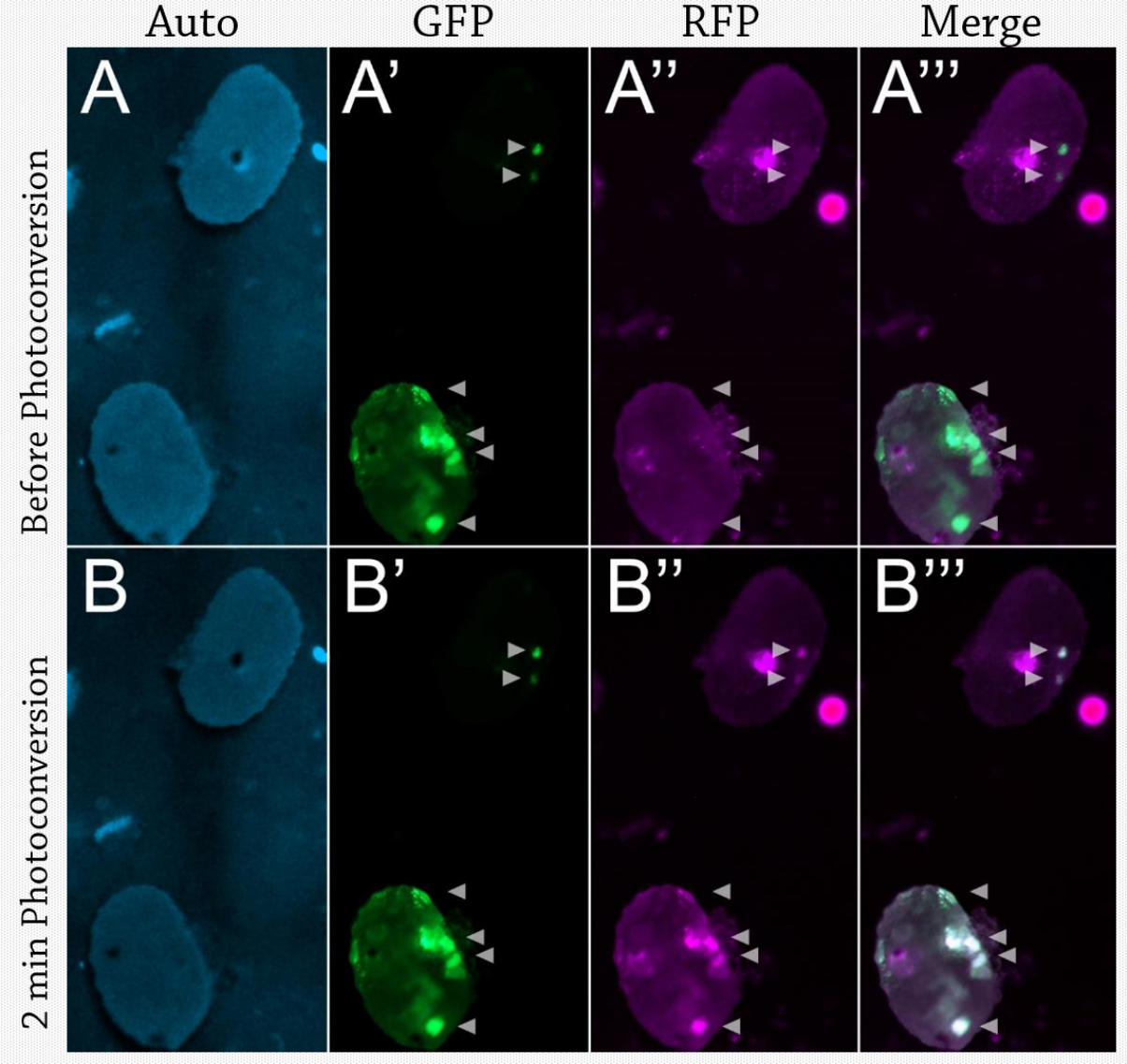

Plodia embryos expressing photoconvertible fluorescent protein (mEos3.2) 48 hours after injection. Injection of pBacIE[3xP3:eGFP;LifeAct:mEos3.2] (SeqA3.5) and *in vitro* transcribed piggyBac transposase mRNA occurred between 2 and 6hrs after egg laying. Before photoconversion (**top row**) large cells within the embryos express a fluorescent protein that is visible only in the GFP channel (**arrowheads GFP vs RFP columns**). Following exposure to UV light (DAPI filter excitation) fluorescence was noted in the RFP channel in all of the locations previously restricted to the GFP channel (**bottom row arrowheads GFP vs RFP**). This is easily understood by comparing the merge panels before and after photoconversion. Bright spots in RFP channel were often seen near injection site (**dark spot in Autofluorescence column**) suggesting that either damage induces autofluorescence or photoconversion of the fluorescent protein. The RFP fluorescing region associated with the injection site shows no photoconversion arguing that it is caused merely by damage and not fluorescent protein expression.

Figure 4.7 Expression and photoconversion of mEos3.2:LifeAct in *Plodia* larvae

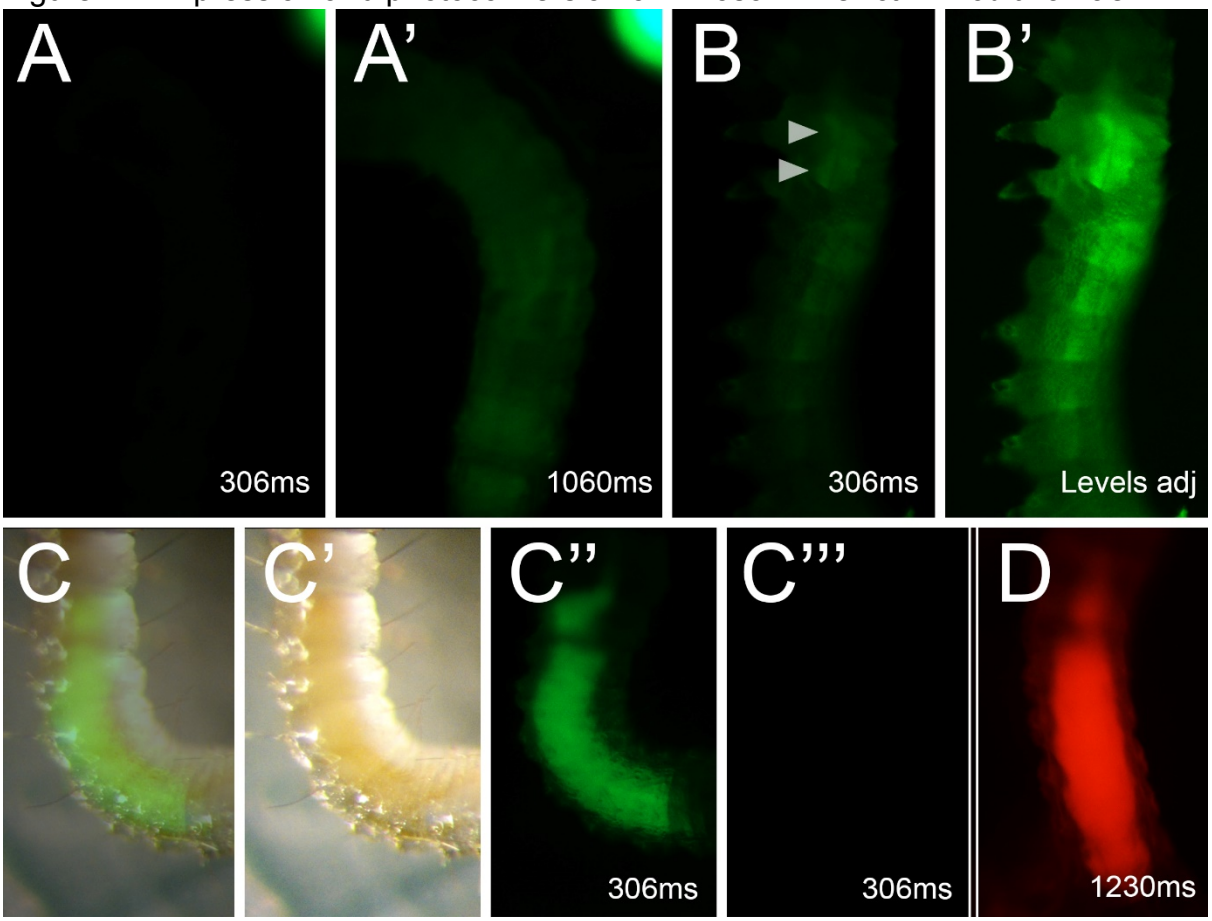

Expression of photoconvertible fluorescent protein in *Plodia* hatchlings 4 days after injection. Injection of pBacIE[3xP3:eGFP;LifeAct:mEos3.2] (SeqA3.5) and *in vitro* transcribed piggyBac transposase mRNA occurred between 2 and 6hrs after egg laying. **A,A'** Non-expressing larvae taken at 2 exposure levels. **B,B'** Expression within larval somatic tissues taken at lower exposure and levels adjusted to show expression. **C-C''** Commonly found gut expression of fluorescence. **C''** Fluorescence in GFP channel, **C'** Brightfield image of larva, **C** Merge. **C'''** Lack of fluorescence in RFP channel. **D** Photoconverted gut fluorescence seen in RFP channel.

Figure 4.8 Phalloidin stain of *ex vivo* pupal wing disc culture before and after

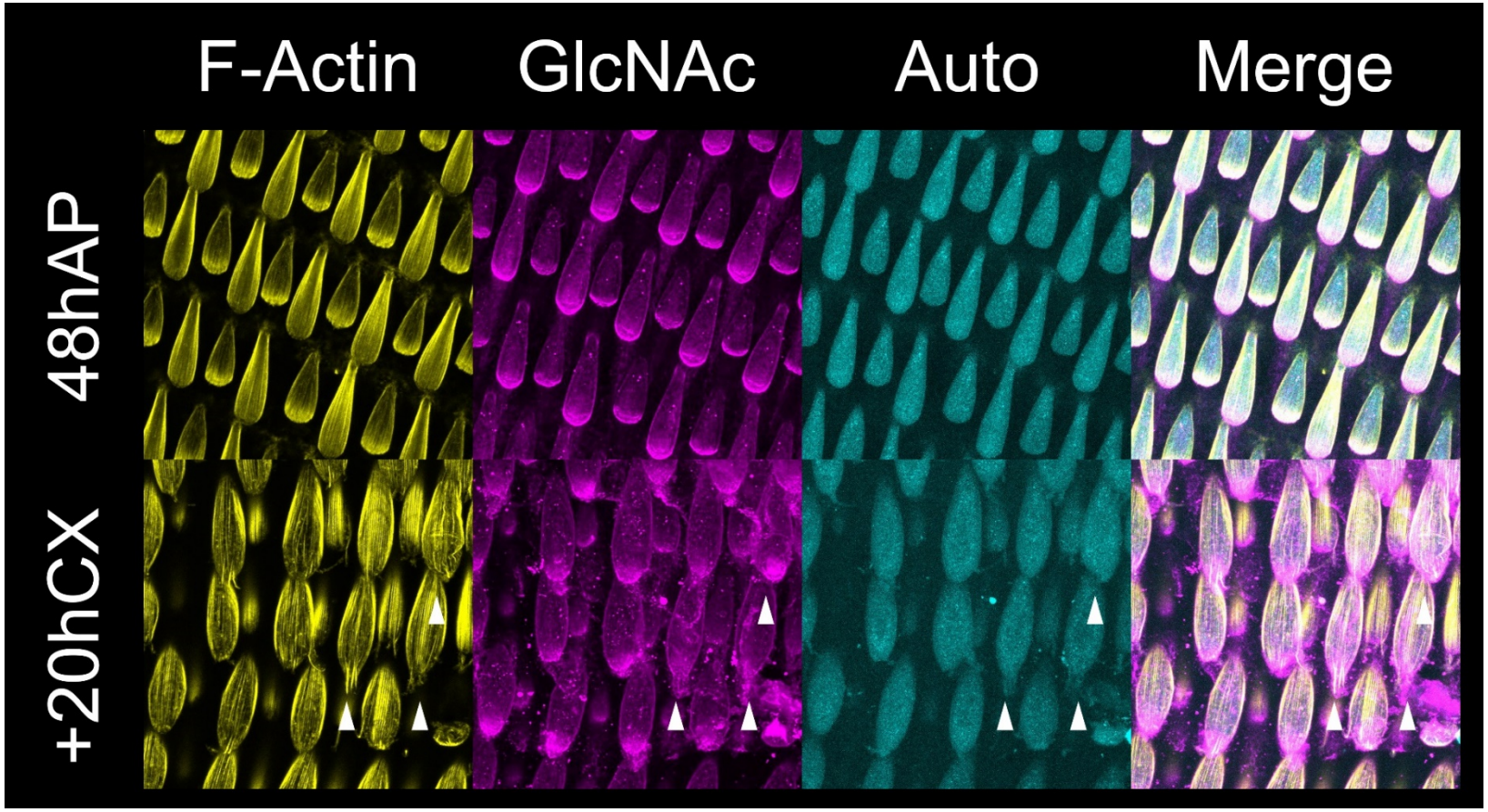

Ex vivo culture of 48hAP *Junonia coenia* pupal wing disc before and after culture suggests that scales grow but ultimately fail to develop properly. **Top row** shows a wing disc from an early pupa fixed immediately following dissection and stained with Phalloidin and WGA. LASER scanning confocal microscopy shows young elongating scale buds. **Lower row** shows wing tissue taken from the same pupa cultured *ex vivo* for 20 hours. While there is some evidence of growth, **arrowheads** show areas of the scales that appear blown out where F-Actin appears to extend beyond the end of the scale. GlcNAc staining also appears disorganized relative to the tissue before.

Figure 4.9 Time lapse of *ex vivo* cultured pupal disc illuminates developmental defects seen in time series

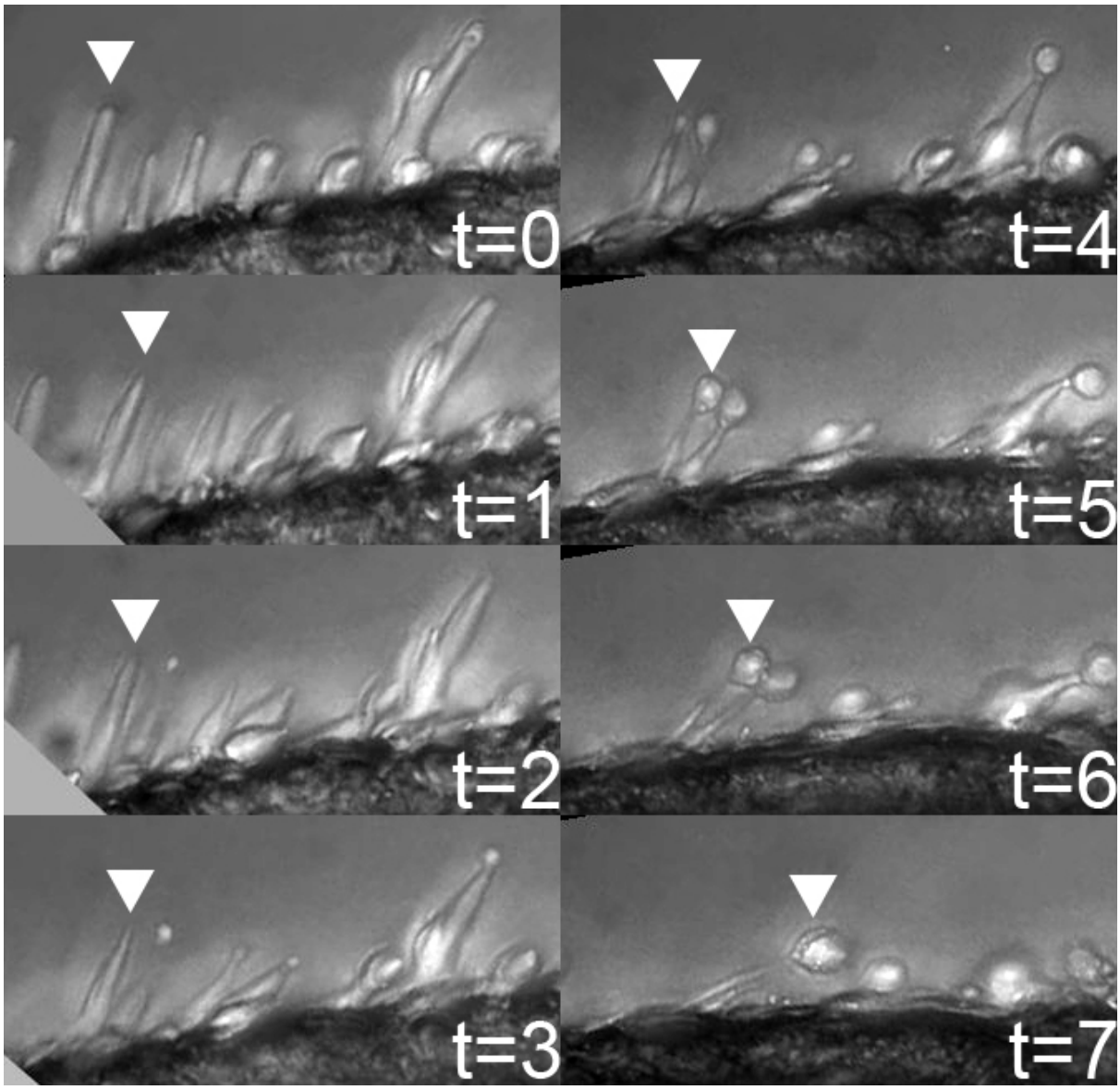

Time lapse of 48hAP *Junonia coenia* wing tissue *ex vivo* cultured with insulin and 20-OH-Ecdysone over 6 1/3 hours. Each frame is the maximum projection of 10 z-slices. **Arrowheads** follow one scale bud and clearly shows the scale tip ballooning as the body thins, possibly explaining the defects seen in Figure 4.12. This phenotype looks similar to defects in *Drosophila* bristles treated with the kinase inhibitor staurosporine and mutants of the cytoskeleton (140,143,145,146,156,263,315). Each frame separated by ~54 minutes. Sample prepared and images taken with Mrinal Sinha.

Figure 4.10 Pupal cannulation of *P. palinurus* before and after pigmentation

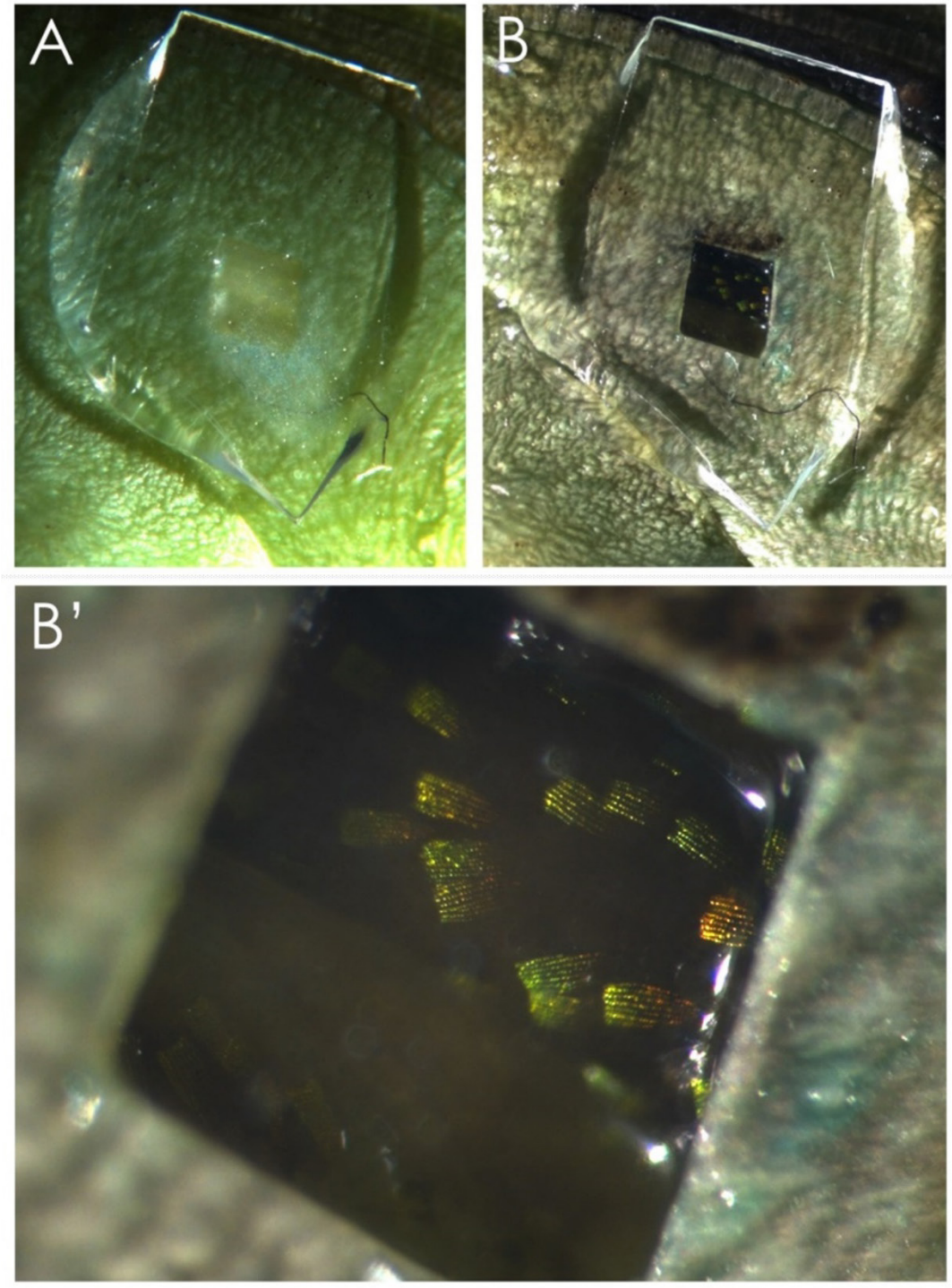

Pupal cannulation of *P. palinurus* allows visualization of pigmentation of dorsal forewing. A small window was cut into the pupal cuticle covering the forewing of *P. palinurus*. A small amount of phenylthiourea was added to the opening to prevent damage response melanization and the window was sealed by a piece of coverslip attached to cling wrap. **A –** Pupa just following cannulation, **B,B' –** Pupa after 48hrs showing pigmentation and structurally colored scales of *P. palinurus* have developed normally. Experiment and imaging done with Jerry Lo.

Figure 4.11 Forewingectomied Nymphalid and Papilionid pupae

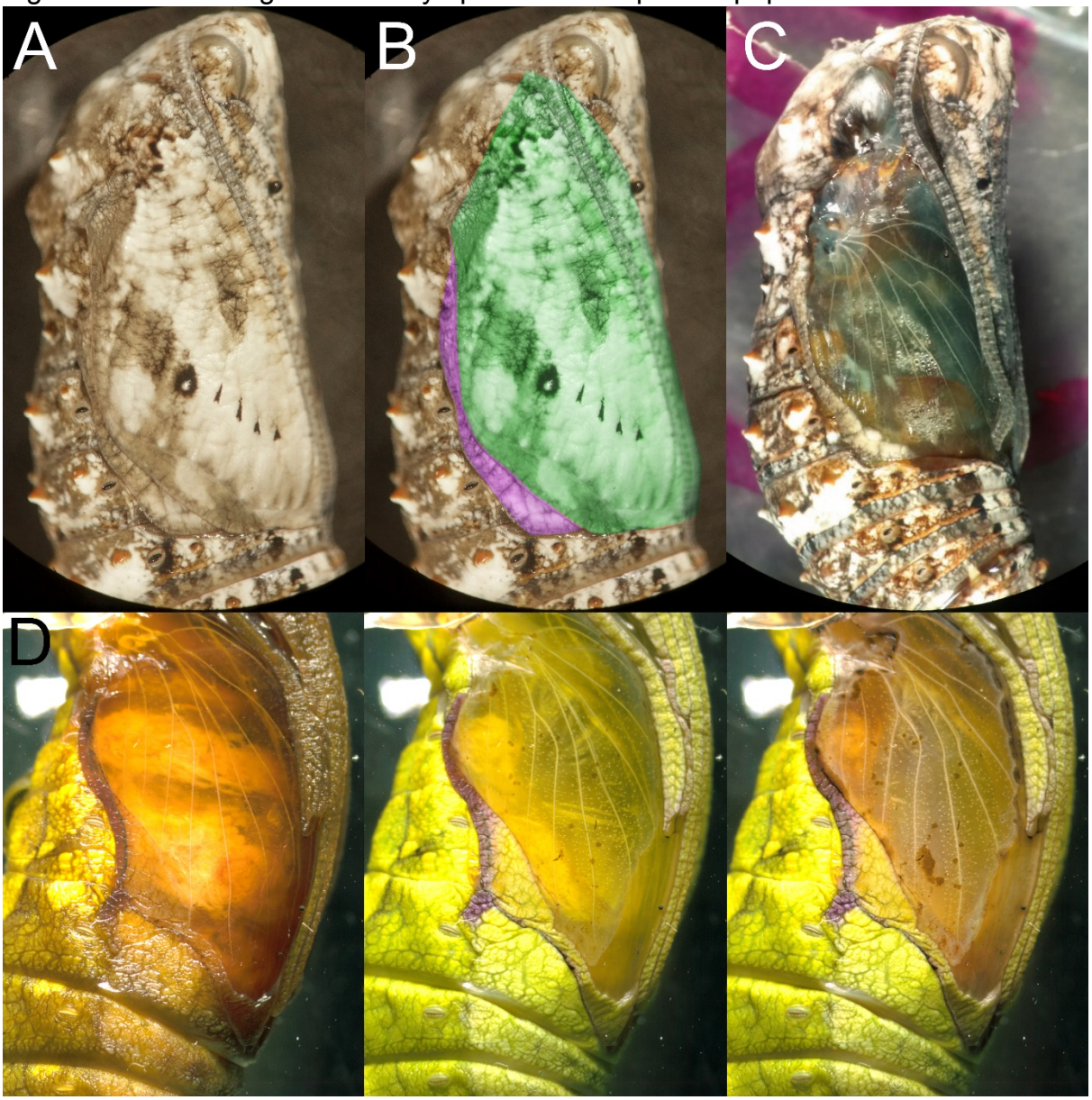

Larval forewing imaginal disc removal (forewingectomy) prevents the formation of a large region of pupal cuticle upon metamorphosis and provides an unobstructed view of the developing hindwing. **A** An unoperated animal (*Junonia coenia*) showing normal pupal cuticle. **B** Contributions of forewing (green) and hindwing (magenta) tissues to pupal cuticle. **C** An operated animal showing the unobstructed view of the hindwing tissue as well as the small amount of cuticle from **B** still present. The latter observation suggests the hindwing cuticle development does not require, nor respond to, where the forewing is, when determining where to form. **D** Frames from early time points in the development of the Papilionid, *Battus philenor*. This, with the successful operation of *Plodia* (Figure 4.4), suggests that this surgery is not limited to Nymphalids. Technique developed with Julian Kimura; *Battus* experiment done with Aaron Pomerantz.

Figure 4.12 Normal development of *Vanessa cardui* following forewingectomy

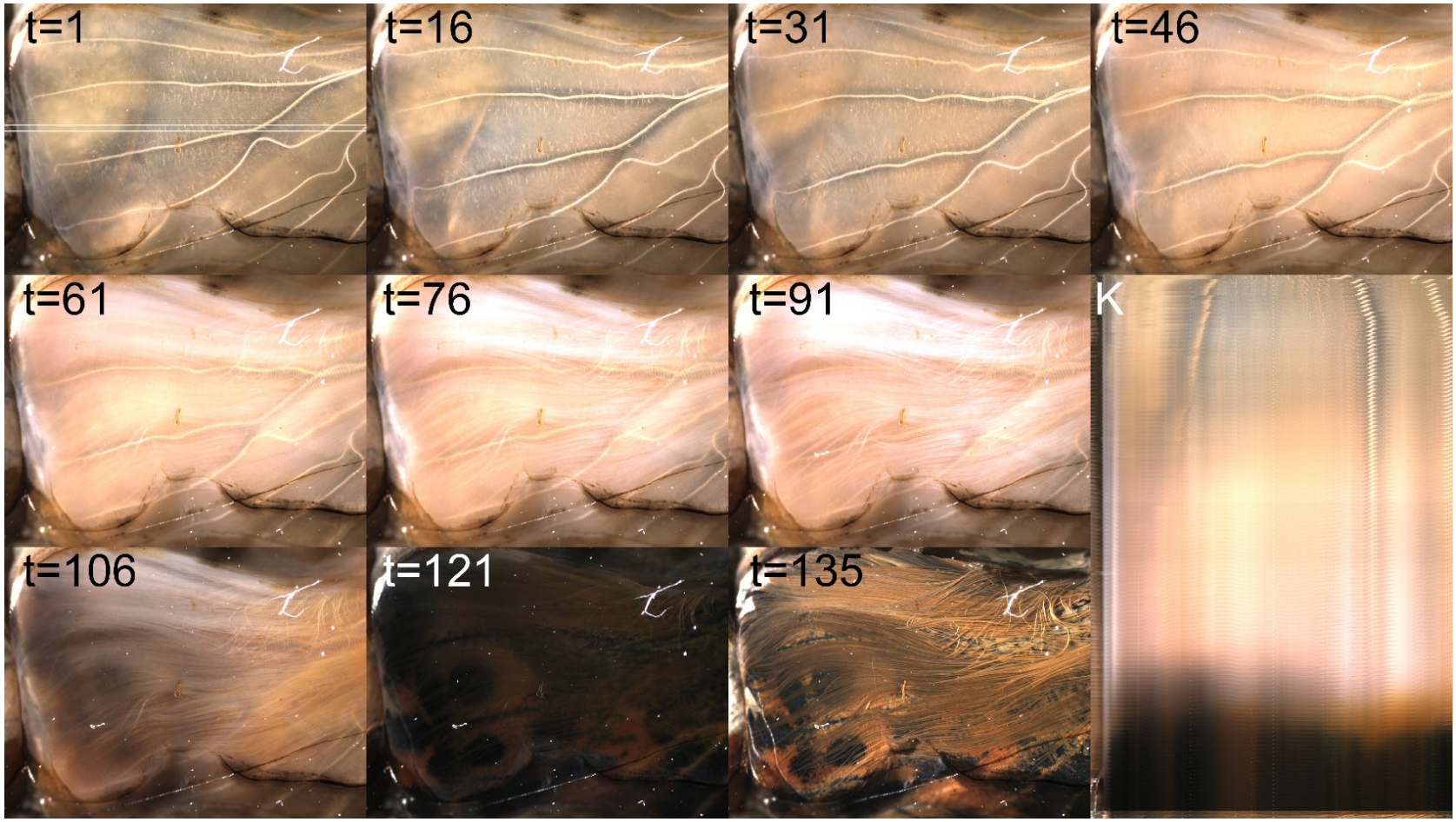

Images taken over the duration of development of an operated *Vanessa cardui* pupa starting ~40hAP and continuing until eclosion, ~111hrs later. Region in **t=1** marked by white box was used to create the kymograph, **K,** containing data from 135 frames. The movement of veins, increase in brightness during chitin secretion, emergence of ommochromes and melanin, and draining of hemolymph just prior to eclosion can be seen in detail. Images captured on Zeiss StemiDRC dissecting scope every 5 minutes, frames here are equivalent to 12 hours and 20 minutes of developmental time with Kymograph slices progressing by 49 minutes and 45 seconds from the previous.

Figure 4.13 Normal development of *Junonia coenia* following forewingectomy

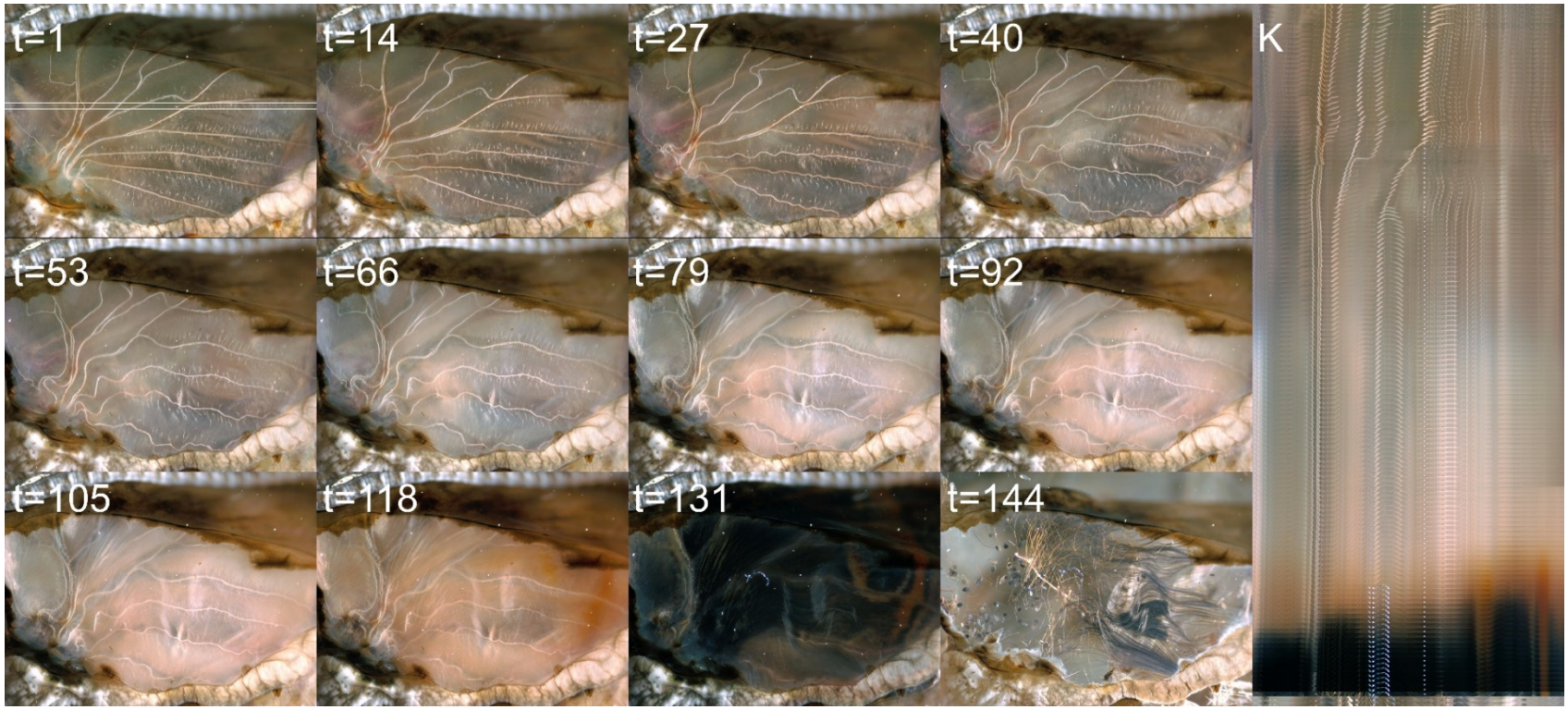

Images taken over the duration of development of an operated *Junonia coenia* pupa starting 45hAP and continuing until eclosion ~191 hours later. Region in **t=1** marked by white box was used to create the kymograph, **K,** from 144 frames. The movement of veins, increase in brightness during chitin secretion, emergence of ommochromes and melanin, and draining of hemolymph just prior to eclosion can be seen in detail. Melanized region at the top of the pupal wing is where a good seal to the coverslip could not be obtained and darkening occurred. Images captured on Zeiss StemiDRC dissecting scope every 5 minutes and subsampled. The time difference between frames here (t=14 to t=27 for instance) is equivalent to 17.5 hours of developmental time. Each slice of Kymograph is equivalent to ~1 hour 20 minutes.

Figure 4.14 Wing pattern differences in animals with FWE and Heparin injection

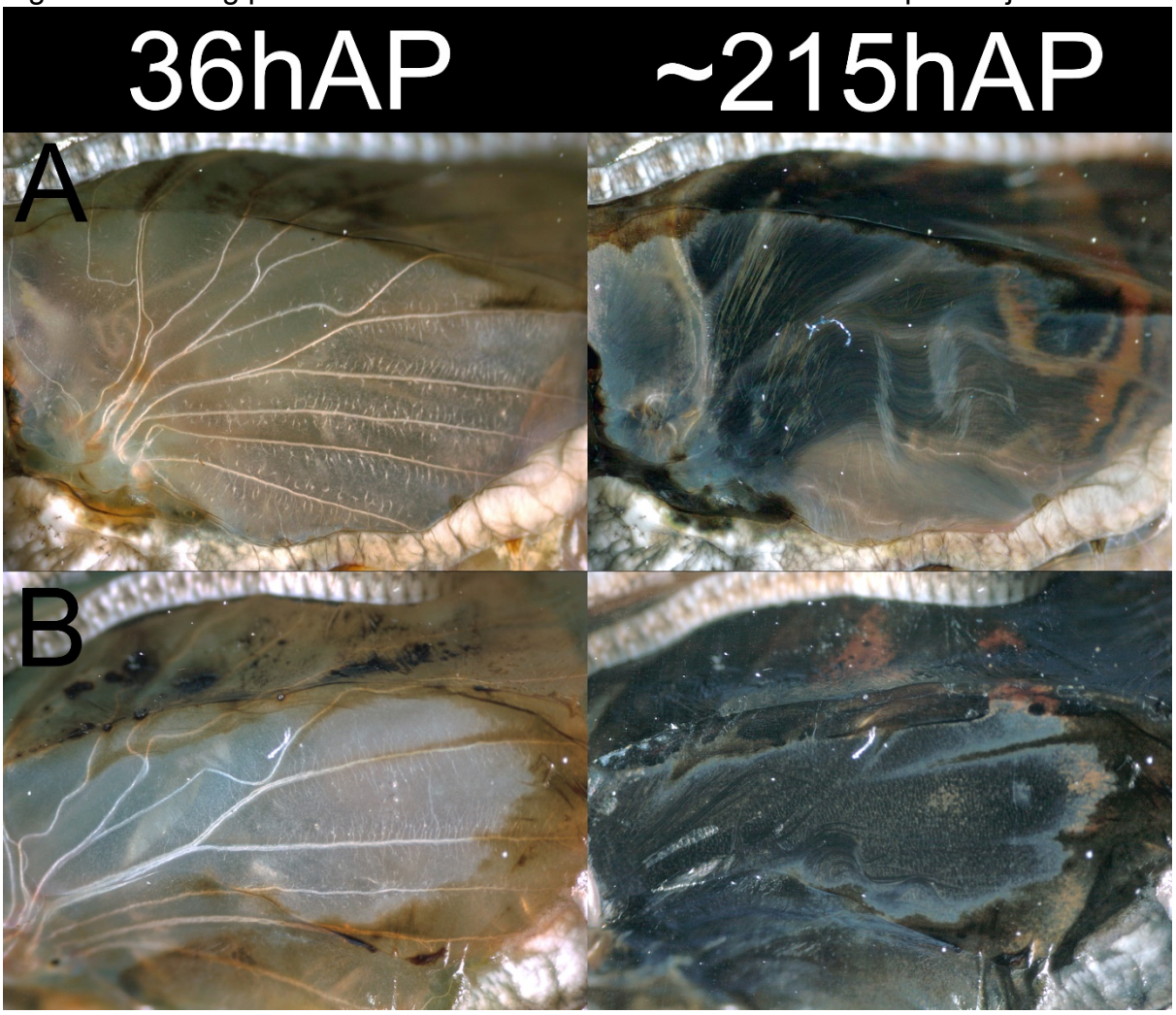

Comparison of *Junonia coenia* pupae following forewingectomy. **A** Wild type pupa at early stage of development and just prior to eclosion. **B** An animal that received an injection of Heparin sulfate 6hAP to perturb the normal color pattern which can be seen on the right just prior to eclosion. This data suggests that the forewingectomy technique can be used in coordination with perturbations to highlight what has heretofore been limited to examination only after eclosion. Melanized regions in the images on the left are areas which didn't seal to the coverslip and resulted in darkening in response to oxygen exposure.

Figure 4.15 Damage and structural color emergence in *J. coenia* following FWE

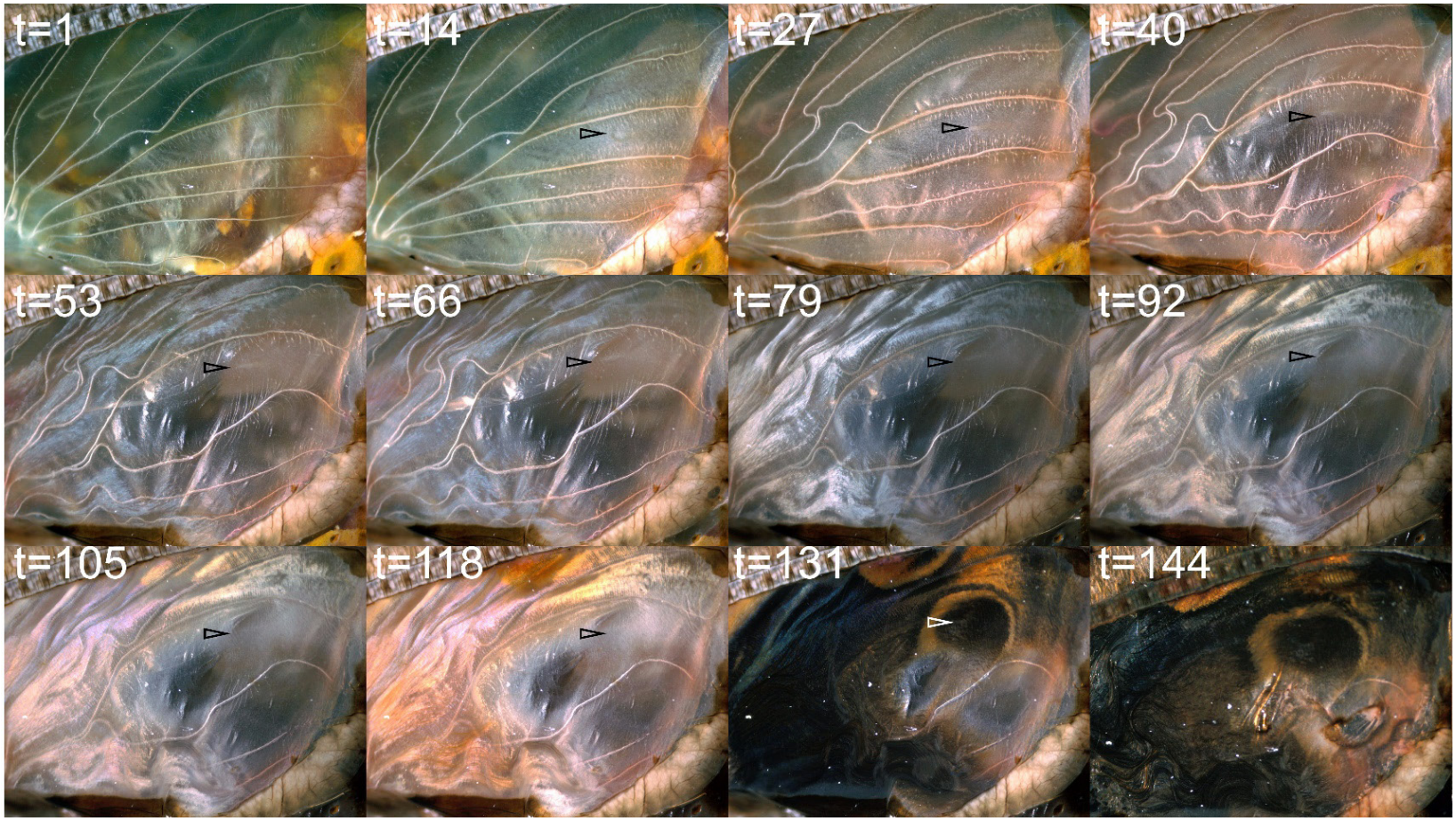

Images taken over the duration of development of an operated *Junonia coenia* pupa starting 12hAP and continuing until pupal development completed ~238hrs later. The animal experienced damage to the wing tissue due to rough mounting, but we can also see the emergence of structural color and follow the posterior eyespot focus (**arrowhead**). The fact that the wing continues to develop normally despite such extensive damage suggests that manipulations like cautery and eyespot focus transplantation should be possible. Images captured on Zeiss StemiDRC dissecting scope every 5 minutes, each frame progresses 21 hours and 40 minutes of real developmental time.

Figure 4.16 Comparison of structural color maturation and thin film of adult scale

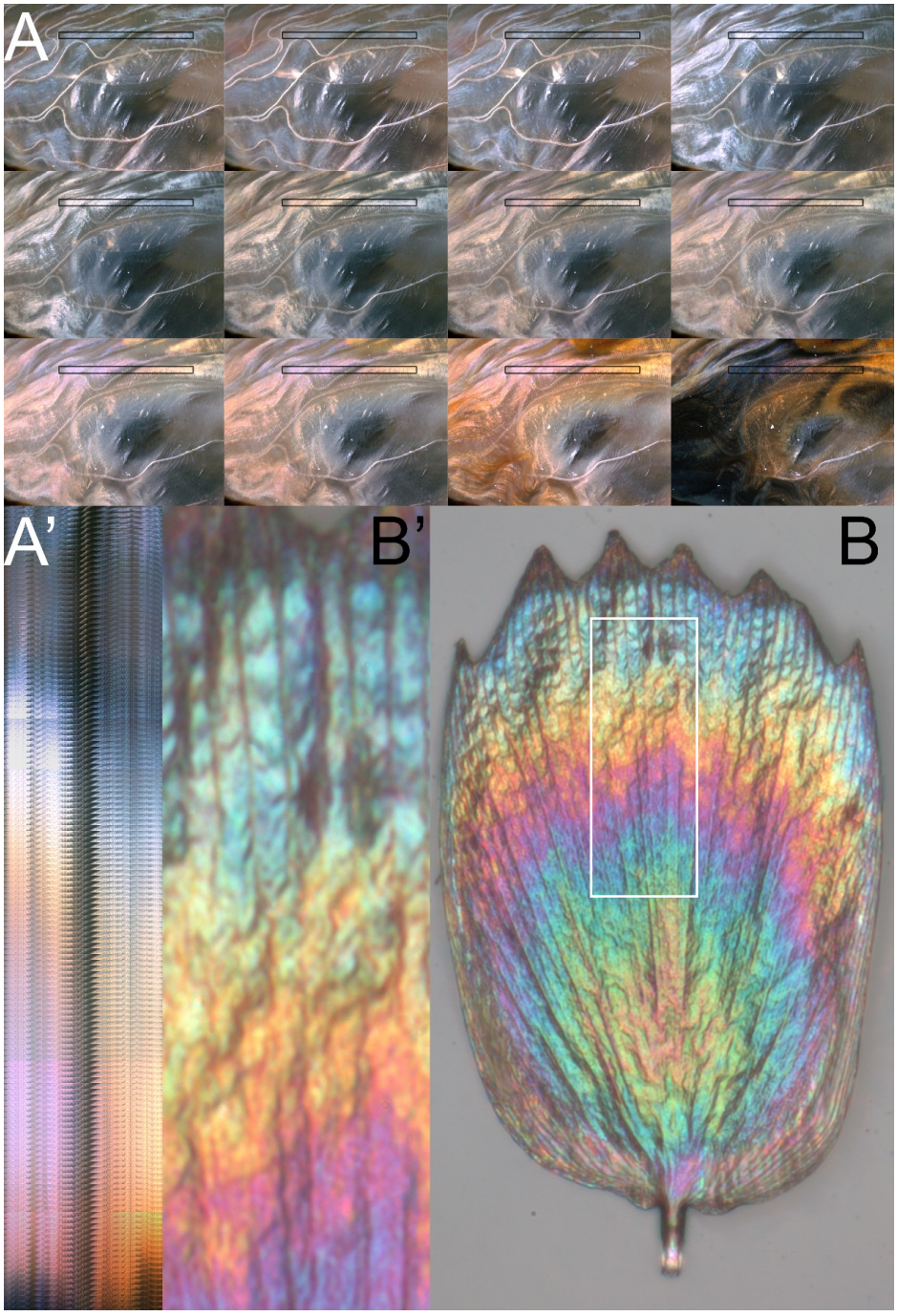

A subsection of the time lapse from Figure 4.15 starting at ~98hAP until 214.25hAP (116.75h elapsed). Here analysis focuses on the emergence of structural color in the scales of the main wing field. The boxes in **A** are used to create the kymograph **A'.** Structural color of *Junonia coenia* is derived from lower lamina thin film reflectance. Thin film thickness determines the observed color, so as thickness increases, presumably by chitin secretion, the color reflected changes. A similar progression of thickness often appears in ground scales when viewed from the adwing surface, as is the case of the ground scale of *Papilio blumei* seen in **B,B'**. Thanks go to Aaron Pomerantz for the inspiration.

Figure 4.17
Scale development in FWE animal electroporated with pIEx:LifeAct:mCherry

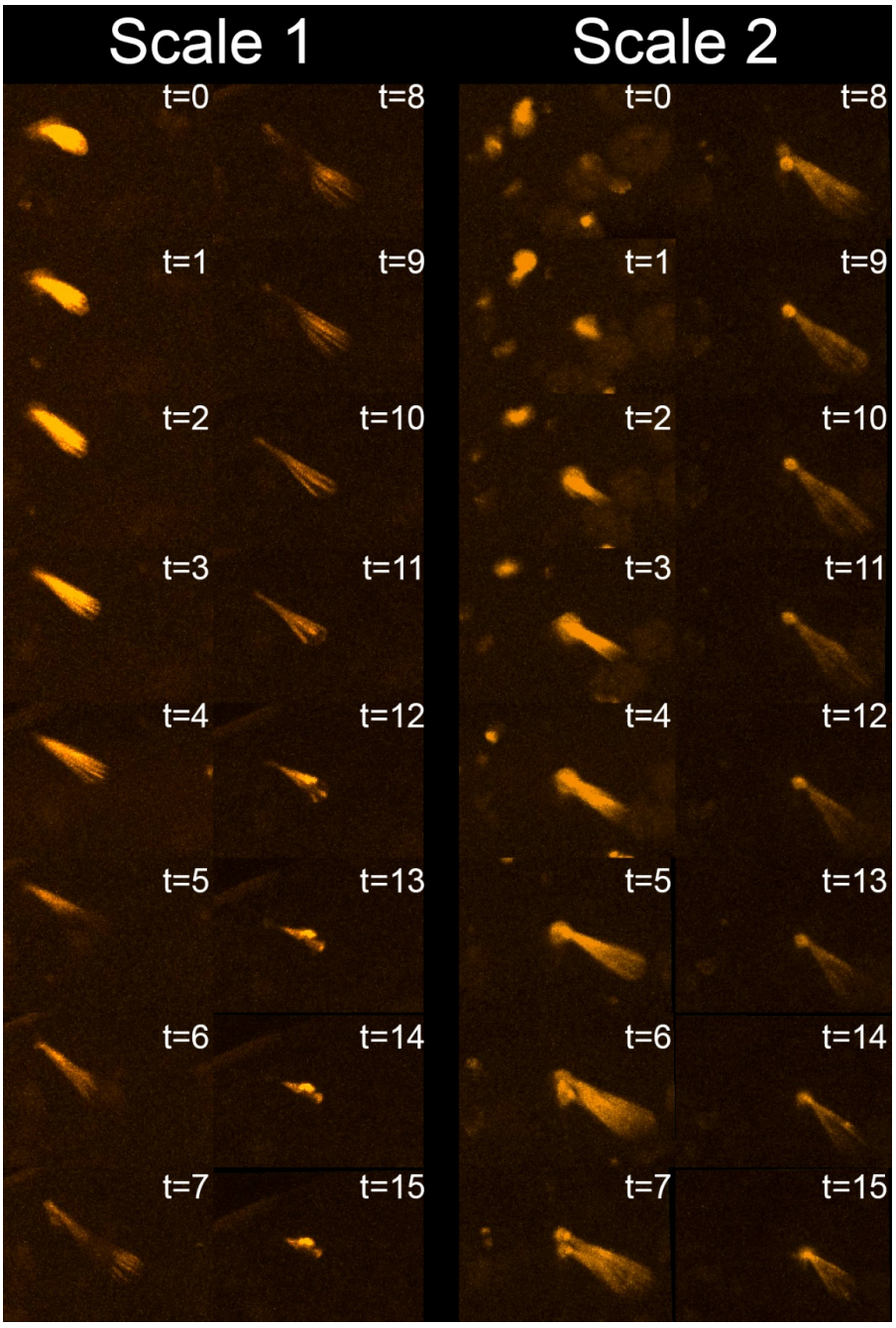

A forewingectomied *Vanessa* pupa electroporated 24hAP following metamorphosis with pIEx-4 containing LifeAct:mCherry (SeqA3.2). The expression by a couple of scales allowed us to follow the extension and retraction of the F-Actin via LASER scanning confocal microscopy time lapse imaged with a 10x objective for working distance starting ~3dAP. The enhanced contrast from the fluorescent protein allows us to follow a single cell despite being found in a field of many. We believe the contraction of the scale was due to dehydration and death of the pupa following extended imaging and not a part of normal development. Time elapsed was ~9 hours.

Figure 4.18 Phalloidin stain of dorsal hindwing scales from *Plodia interpunctella* pupa

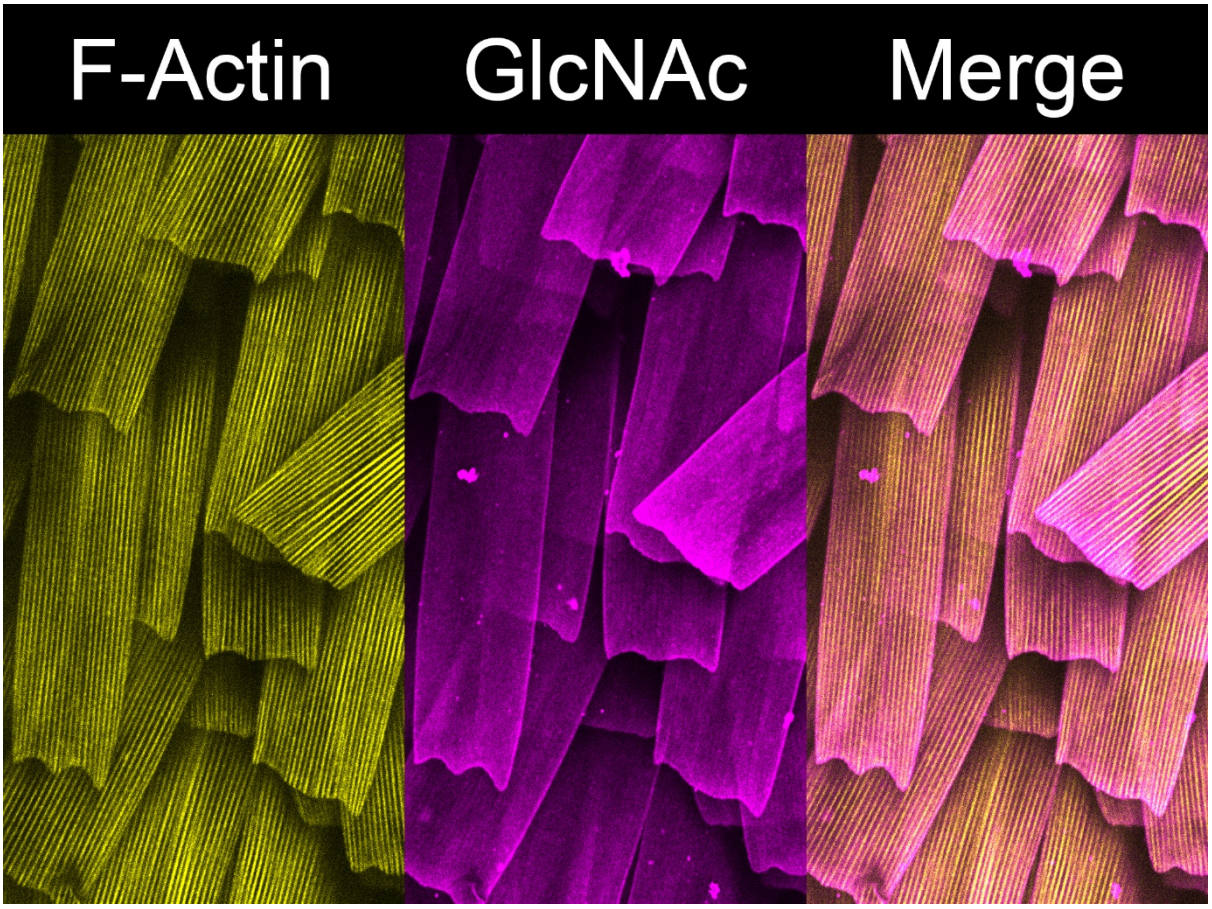

Phalloidin and WGA stain of a *Plodia interpunctella* pupal hindwing disc. F-Actin (**yellow**) and Chitin/glycosylation shown in **magenta** have characteristic butterfly-scale-like phenotype. These scales are found within the main body of the wing away from edges and are remarkably uniform in shape and size.

Figure 4.19 Change of scale shape along distal border of *Plodia* hindwing

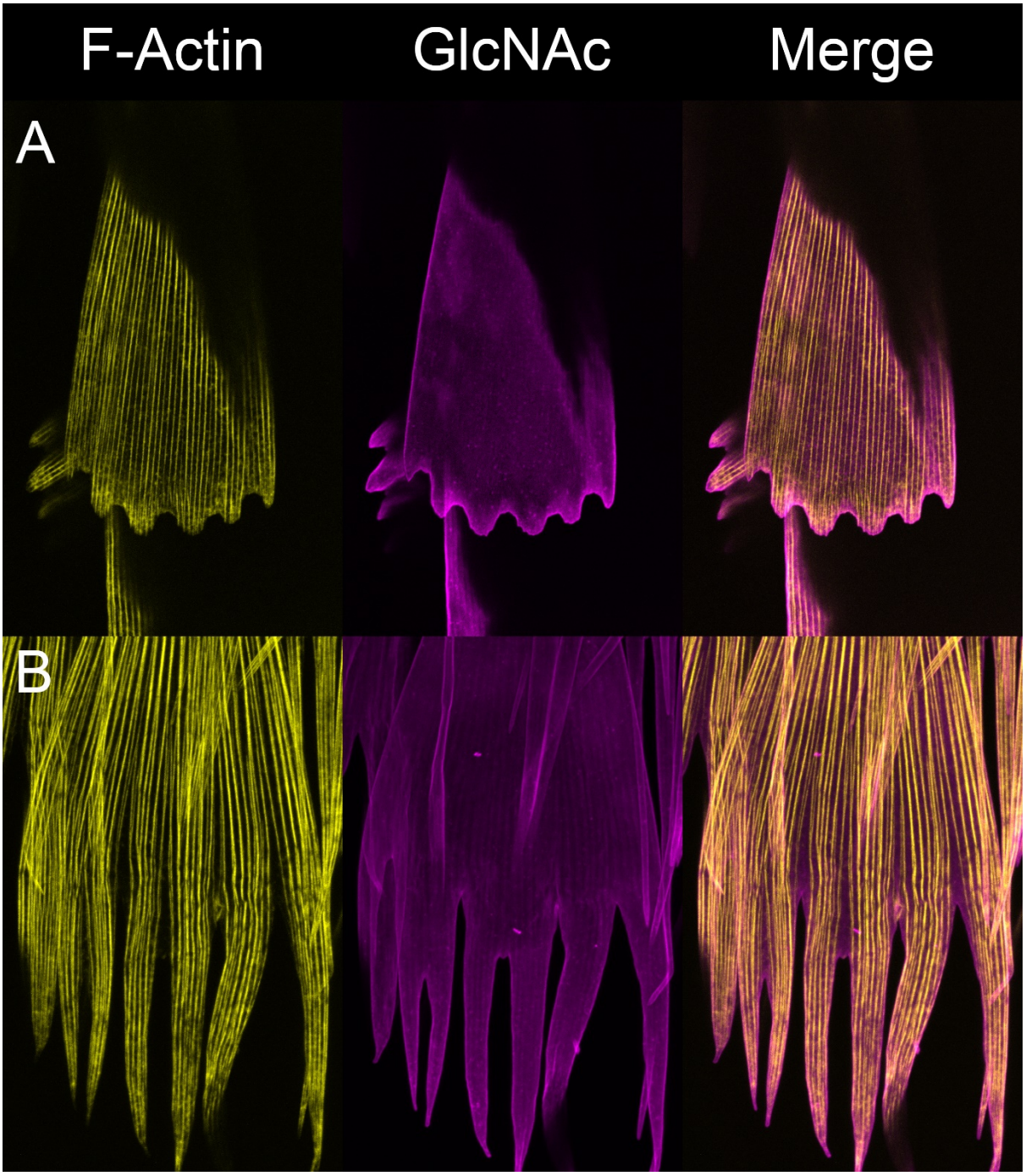

Phalloidin (**yellow**) and WGA (**magenta**) staining of *Plodia interpunctella* pupal wing scales from different locations on the margin of same wing. The distal tip of *Plodia* marginal scales exists as a continuum of phenotypes with some scales exhibiting elongated actin-based protuberances. Understanding of the cytological basis of these protuberances may be informative to the differentiation of a scale from a bristle. **A –** Scale from the distal anterior hindwing margin, **B –** Scale from the Posterior medial hindwing margin.

Figure 4.20
Plodia's frenulum is comprised of many bristle-like cells held together by ECM

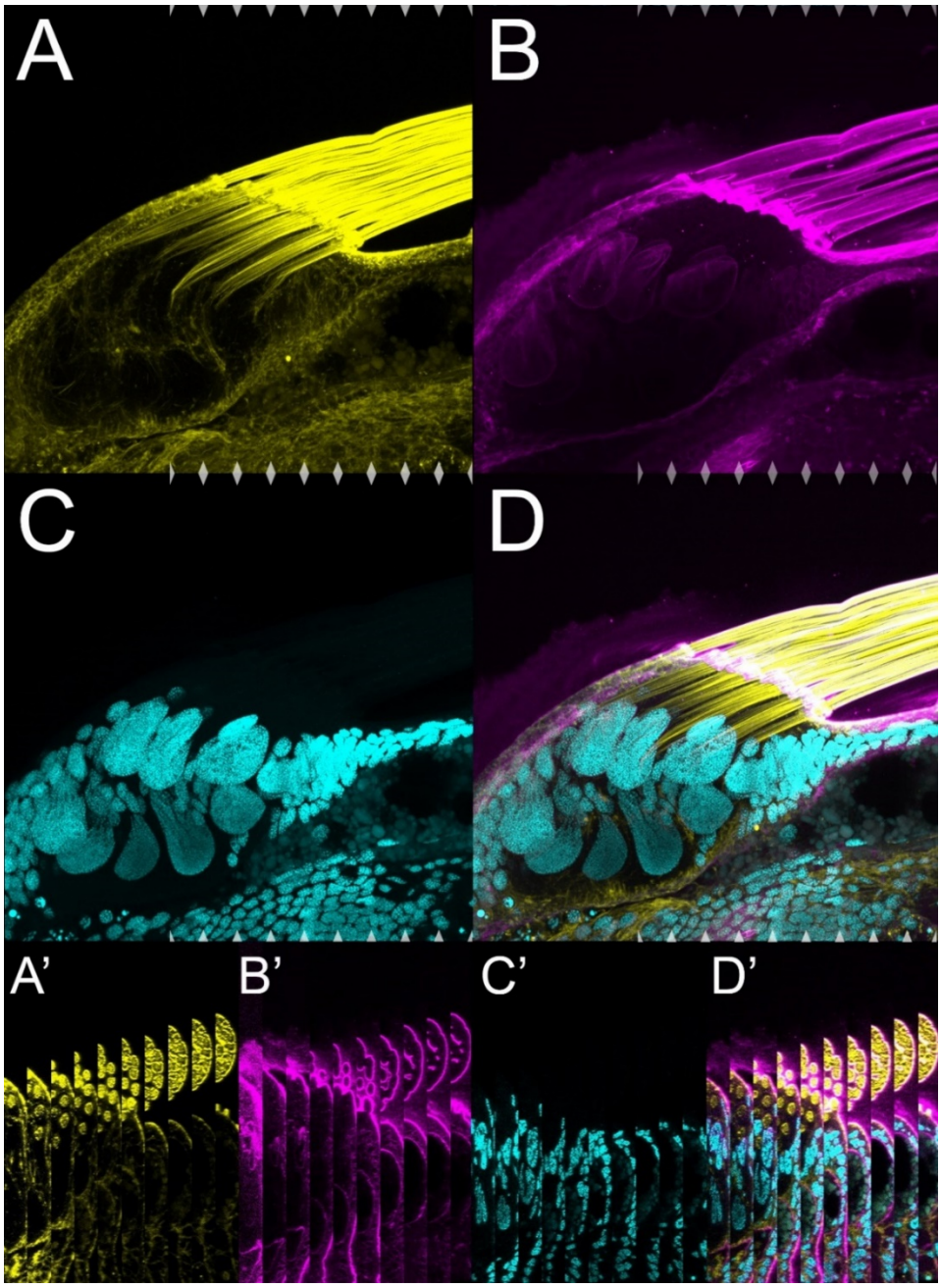

The frenulum mediates coordinated motion of the fore and hindwings in *Plodia* and has SOP-derived developmental origins. **A –** Phalloidin F-Actin stain, **B –** WGA GlcNAc stain, **C –** DAPI DNA stain, **D-** Merge. In **A-D**, the Z-projections are shown from the inside of the frenulum (internal) toward the dorsal surface outside (superficial). **Triangles** in A-D correspond to YZ sections shown in **A'-D'** in order from left-right. YZ sections show the round cross-section of individual bristles and the intervening chitin/ECM. Defects in the proper development of the very large Frenulum may thusly be informative of defects in the development of the smaller scales – whether caused by CRISPR/Cas9, forward mutagenesis, drug treatment, or other manipulations.

Figure 4.21 *Plodia* larvae are amenable to forewing imaginal disc surgery

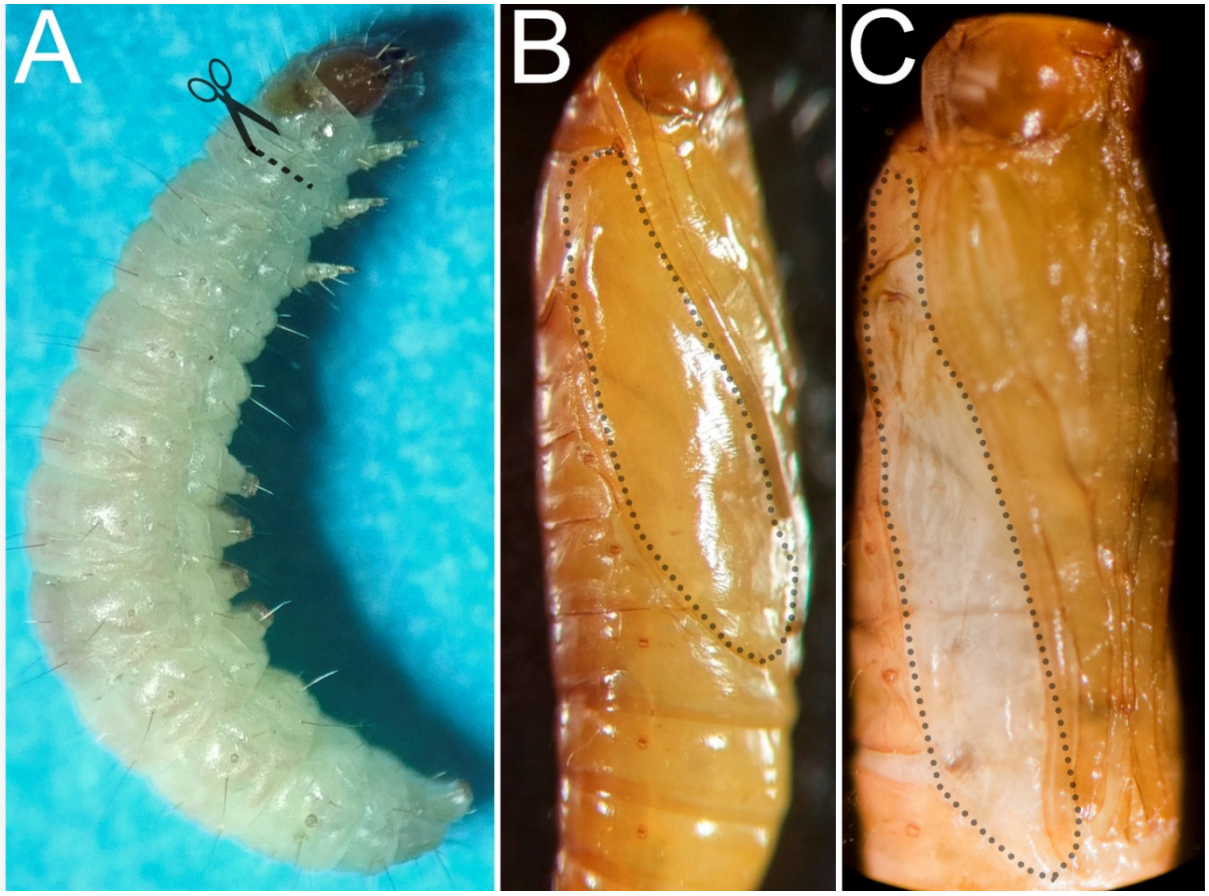

Plodia will prove to be an important Lepidopteran workhorse for many reasons including the ability to perform larval forewing imaginal discectomies (forewingectomy,FWE). **A –** Last instar *Plodia* larva showing the location of incision to remove the larval forewing imaginal disc. **B –** A wild type, unoperated pupa. Dashed line indicates the pupal cuticle secreted by the forewing and/or the forewing's peripodial membrane. **C –** A genetically wild type pupa metamorphosed from an operated larva. The dashed line indicates where the forewing cuticle should be (as in **B**). The surgery reveals the underlying hindwing and will allow for direct visualization of the hindwing's developmental dynamics within.

Chapter 5

Future Directions

5.1 Introduction

As with any project, the questions I have been able to answer have only led to more questions. Here I will address some of the questions I feel are natural out growths of my explorations. I will break the questions down into several categories: 1) What we can learn from *Drosophila* chaetae? 2) What questions remain in *Morpho* with regard to melanization? 3) What remains to be answered for actin and pigmentation's role in the *Achillides?* and 4) Where can the technologies be improved?

5.2 The Role of *Drosophila* Chaetae as a Scale Comparative Model (R*D*CSCM)

Though functionally distinct, several lines of evidence point to a cellular homology between sensory bristles and the scales of butterflies: 1) morphologically both bristles and scales are very large, unicellular structures associated with a basal socket cell, 2) there are marked ontological similarities in the cell divisions leading to scales and sensory bristles, 3) molecular expression similarities in developing scales and bristles such as Notch/Delta and Achaete/Scute and a heavy reliance upon F-Actin cables leading to subsequent surface ridging, as well as 4) evolutionary evidence from the Lepidopteran sister lineage, Trichoptera, where the wings are covered in bristles and in some lineages these have become scale-like. One of the most important realities of this homology is the ability to leverage the copious amount of research done in *Drosophila* to ask meaningful questions about butterfly scales and how they may have evolved structural coloration. In particular, research in *Drosophila* has begun to illuminate 1) how ridges are formed and their spacing, 2) how the coarse and fine scale shape is achieved, and 3) an understanding of cuticle deposition and modification. Though far from complete, there have been emerging trends suggesting that Actin protein complexes, Tubulin protein complexes, Rab GTPases, and Zona Pellucida genes are important and often interact to produce bristles in *Drosophila.*

Lees and Picken described normal development of *Drosophila* bristles in 1945, and detailed the process for a few mutants {Formatting Citation}. In wild type animals kept at 25C, socket and bristle precursors are visible 16hrs after puparium formation (hAPF). Between 18 and 30hAPF the socket and bristle grow in volume and obtain their relative positions in space. About 30hAPF, the bristle begins to grow out from the surface of the pupa's notum. Between 30 and 35hAPF, the nascent bristle grows in diameter and in length, though greater growth is achieved in the width. At 35hAPF the bristle will have achieved its final diameter – since the fully formed bristle will ultimately be roughly cone shaped this diameter will establish the base of the bristle. It is also during this 30-35hAPF

time frame that ridges can first be visualized. The bulk of length (~75% of final) is achieved between 35-41hAPF, with bristle growth terminating at about 45hAPF. (301)

5.2.1 RDCSCM: Overall shape

Butterflies are often large by insect standards with wings that can be 10's of centimeters in size. Given that scales are the major source of wing coloration and are the fundamental modular elements for pattern construction, that the scale has a large surface area aids the organism in covering the vast swaths of wing surface area. Thus having control over cell shape – including the production of flattened cell types – could be highly beneficial. Indeed, it seems one way of making a Lepidopteran wing transparent, is to manipulate the shape of its scales into more hair-like structures (216). How the scale "decides" to be scale-like or bristle-like is therefore likely to reside in control of the cellular developmental processes during the pupal stage and a comparison of scales to *Drosophila* bristles could be enlightening.

Lees and Picken came to the surprising revelation that many genetic mutants resulted in altered overall dimensions of the *Drosophila* bristle, but maintained the internal volume. Mutants of this type included *Stubble/stubbloid, forked,* and *singed* (301). Stubble-stubbloid was characterized later as a transmembrane serine protease with potential influence of normal actin organization and cleavage of the ECM (275). Forked and Singed were later characterized as actin crosslinking proteins critical for the normal elongation of the bristle (138). Together there is the suggestion that cytoplasmic volume is genetically separable from the components involved in forming the shape – namely the actin cytoskeleton and ECM. As a corollary of this, the genetically defined variation in bristle size seen across the fly notum requires the coordination of outgrowth and volumetric components – something also seen in butterflies where size of scales relates to position on the wing and to the DNA content of the scale (320). Ploidy and polyploidization of the growing bristle/scale, therefore, represent a scaling mechanism that could potentially serve to keep the genetic stoichiometry of length and volume. Moreover, the idea introduced by Lees and Picken that control of the volume-to-surface-area (V:SA) ratio is critical for maintaining bristle shape also is fundamentally important to butterflies as their shape is not best represented by an ideal cone and, in fact, changes over the course of development (126). Geometrically speaking, the flattened cross-section of a butterfly scale has a V:SA ratio less than that of a bristle's circular cross-section. Therefore, it stands to reason that there may be a modulation of either (or both) the components leading to cytoplasm proliferation (volume) or membrane manufacture/export (surface area) to create the flattened profiles of scales. In the past decade the contribution of the microtubule cytoskeleton to *Drosophila* bristle development has begun to come into focus and some phenotypes suggest that this may be the case.

The first clues microtubule-related proteins may be important came from clonal analysis of kinesin heavy chain (*khc*), which produced shortened, flattened bristles that

superficially resembled butterfly scales (153). This has since been elaborated upon to a more fleshed-out model that suggests microtubules, oriented in a minus-end out orientation localize Ik2 and Spn-F via Dynein motor proteins to the tip of a growing bristle. In turn, Ik2 phosphorylates itself and Spn-F, leading to a host of downstream effects including regulation of the retrograde transport of the Rab11-positive recycling endosomes via control of the Dynein-binding intermediary, Nuf, dephosphorylation. This same Ik2/Spn-F regulatory pathway controls the secretion of ECM-binding, Zona Pellucida protein Dusky-like (Dyl) (168). Failure of any of these components leads to bristle phenotypes including thinned, shortened bristles. Ik2 has been suggested to also regulate F-actin assembly, making it a potential crossroads for secretion, lengthening, and surface structure.

Interestingly, it appears that at least in some instances, the negative-end-directed, microtubule-motor-protein, Dynein, represents the motor utilized for both antero- and retrograde transport, despite the highly-polarized nature of the microtubules. Mutation of Dynein heavy chain (Dhc) or elements of Dynein light chain (Dlc) produce scale-like flattened architecture as well as causing internalization of F-Actin fibers – similar to what was reported by Dinwiddie et al. in developing Nymphalid butterfly scales (124,147). It would be very exciting to analyze Dynein/Kinesin double mutant bristles in *Drosophila* as one would predict an additive effect that may greatly resemble butterfly scales.

An interesting protein that may help to establish and/or maintain the tubulin and actin cytoskeleton is Skittles. Truncations of *sktl* result in severely bent or warped bristles which mimic *sn* and *chickadee* mutations and hyperproliferation of bristles (321–323). While little else has been done in bristles, in oocytes, *sktl* mutations lead to a loss of proper microtubule polarity and mislocalization of Kinesin and Spn-F (324). This proper localization may depend on αPKC inactivation of the PAR protein, Bazooka, and the mutual antagonism of Par1 and Lgl (324). Together these 4 proteins help establish polarity of the microtubules in the oocyte. αPKC in particular has been suggested to be activated by diacylglyceride, a metabolite of $PI_{4,5}P_2$. Thus, it is possible that Skittles' role in phosphorylation of PI_4P may directly lead to Kinesin/Spn-F mislocalization. Further, Skittles' role as a PI4P-kinase may have a role in localization and modulation of many Actin modulators (325).

From preliminary experiments done during my work in collaboration with Julian Kimura, the distribution of acetylated-tubulin in butterfly scales has dynamic staining from prevalent throughout the scale body from initiation of elongation until ~48hAP at which point acetylated-tubulin staining collapses to a small region near the petiole of the scale (Fig5.1A-G''). This dynamic is disrupted when Taxol is administered to developing pupae, resulting in a stabilization of Acetylated-Tubulin (AcTub) signal throughout the scale and a narrower rounded overall profile (Fig5.1I-I'' vs. Fig5.1H-H''). In her analysis of *Ephestia* scale development, Overton found that major shape changes were correlated with changes to the orientation of the cytoplasmic microtubules (126). Thus it is tempting to suggest that there is a role of the acetylated population of tubulin in maintaining a round

cross section, potentially through the movement of cytoplasmic components. And in flies, loss of Kinesin leads to a similar collapse of AcTub staining concomitant with a flattened scale-like bristle (146).

The heavy reliance of *Drosophila* bristles on the tubulin cytoskeleton and its role in organizing secretion and the actin cytoskeleton make it an ideal candidate for future analysis in butterflies. Preliminary small molecule inhibitor work in butterflies further suggests that tubulin is central in establishing the broad flattened morphology of bristles (Fig5.1). Genetic manipulations utilizing some of the tricks mentioned in Chapter 4, like photoactivatable DN:IK2 or adapting over the proven optogenetic PIP3 kinase to instead be able to induce PIP4 formation (326), could result in important steps forward in understanding the gross developmental differences between bristle and scale morphogenesis.

5.2.2 RDCSCM: Ridge formation

As demonstrated in previous chapters (particularly chapter 2), ridges are longitudinally oriented, regularly spaced chitin processes extending perpendicularly from the abwing surface of most adult Lepidopteran scales (110). Ridges also exist in *Drosophila* adult bristles, evenly spaced around the perimeter of the bristle (301). In both flies and Leps, the ridges may serve a rigidifying function, although they can be lost without consequence to outgrowth (as in *Drosophila* Khc mutants) and, as such, may simply result as a consequence of the developmental processes leading to bristle/scale formation (153). In some butterfly scales, like those of *Morphos*, ridges are modified to produce multilayers that in turn create coloration (54,125,327,328). In other species ridges serve as diffusing elements that help avoid iridescence issues (37,329). The number and density of ridges therefore has an impact upon how intense a structural color can be (260).

Adult fly notum bristles can be coarsely grouped into 2 classes, the smaller, plentiful (~200) microchaetes and the larger, but fewer (22), macrochaetes. The ratio of length:diameter is roughly maintained in both macrochaetes and microchaetes with size correlated to nuclear volume (all are highly polyploid). When ridge number is considered however, one finds a size dependence – absolute number is not maintained. One interpretation of this is that the circumference can be “sensed” either by measuring the circumference directly and spacing ridges via a molecular ruler or, alternatively, through physical means such as elastic buckling that results as a response of the cell by evenly distributing a buckling force. Although examples of molecular rulers exist, the fact that bristles are roughly conical over their length (i.e. with a decreasing radius), it seems unlikely that a ruler of constant length would be producing spacing along the length of the bristle. The molecular rulers described are often coiled-coil proteins which operate on a roughly 100nm span, their use in maintaining rings of actin around the circumference of neurons, for instance, works well because the axon can be approximated as a cylinder with unchanging radius (330). Imagining a similar application to a cone of continuous change in radius is hard to conceptualize with an assumed discreetly sized ruler – though probably not impossible to achieve.

It is simpler to imagine a scheme where buckling of the membrane caused by an imbalance of internal and external forces results in the membrane evenly adopting a sinusoidal perimeter. A mechanism like this has been proposed for the buckling of the trachea, where forces applied by myosin to actin rings acting against the ECM produce buckles in the membrane (331). There are mixed reports on the role of Myosin II (*zipper*) in bristles: Bayer et al., reported it has no impact upon bristle development when lost, suggesting that this is unlikely to be the direct mechanism in bristles (276). However more recently, misexpression of MyoII truncations have been shown to produce split bristles potentially with variable numbers of ridges – though no detailed look at F-Actin was taken (332). All the same, a buckling hypothesis should scale with volume assuming relative forces and membrane properties are maintained. This has been noted by a few early investigators as a potential mechanism – as yet it has been hard to ask directly, though one could imagine adjusting membrane properties by adjusting cholesterol levels, etc. (54,126,333). One would predict that increasing membrane stiffness should reduce the compliance of the membrane to buckling forces and result in a smaller number of ridges.

Developmentally, ridge formation is intimately tied to elongation of the scale and bristle driven by F-Actin dynamics (124,126,137,263). Shortly after elongation begins (~36hAPF in flies), F-Actin can be found at the membrane in areas of positive curvature – and the same can be said for Leps (126,137). Despite being outward bulges of the membrane, it is not the areas containing F-Actin that will become the ridges of the adult. Rather, ridges begin as bulges in the plasma membrane from between adjacent bundles of F-Actin; through serial section of a single microchaete, Tilney showed that while the tip had just begun to add actin to positively curved areas, the base had begun to throw membrane out from between the Actin cables (263). These bulges later are hardened and sculpted when the developing pupa secretes its exoskeleton (124–126,137). This process preserves the shape of the membrane even after the cell itself dies. From studies in *Drosophila* it has become quite clear that the balance of actin crosslinking proteins and many actin polymerization promoters and inhibitors is critical for the formation of a normal number and orientation of ridges. This suggests that it is not just localizing actin to the membrane that is important, but that their organization and maintenance through development is required.

In normal bristle development, following the budding of the bristle, Actin first appears at the cell membrane at regularly-spaced regions of positive curvature around the perimeter of the cell, which likely occur as an elastic buckling process (137). The proteins responsible for this initial assembly are still unknown, as candidates Forked and Fascin can both be lost and F-Actin will appear at the membrane (138,314). Actin bundles appear to be nucleated at the apical (distal) tip of the growing cell and are assembled first by the F-Actin bundling protein forked into a loose array and secondarily are assembled into highly periodic crystalline array by Fascin (encoded by *singed*) (138,140,263,264). The protein Javelin (*jv*) also seems to play a role in bundle maintenance or assembly although still poorly understood. Bundles without Javelin precociously splinter and fragment parallel to the membrane resulting in poorly curved bristles with an inflated, spear-like tip

(315). There is some evidence that Javelin may directly interact with Actin (although it may be localized to the membrane and indirectly interacting) (315). This is quite different from the protein Javelin-like (*jvl*), which despite having a similar overall phenotype, *javelin-like* mutants have an actin bundle phenotype strongly resembling over-expressed Forked protein, with larger-than-wild type, hexagonally-packed Actin bundles (314). This comes as somewhat of a surprise, as in the oocyte Jvl seems not to interact with Actin at all, instead likely creating its oocyte phenotype via mislocalization of Ik2 throughout the cytoplasm (334). Together, this suggests that Jvl may negatively regulate Forked activity, and given the association of Jvl with microtubules, Spn-F, and Ik2, the Actin phenotype may derive from effects on localization of these proteins.

The temporal order of Actin crosslinking assembly seems to be encoded spatially, but the mechanism(s) are still debated. Evidence was presented suggesting that the activity of Rab35 activates Sn (183). This data fit nicely with previous investigations that showed disruption of the Rab35 distribution in Ik2 mutants. However this data has been disputed and unable to be replicated by Otani et al., who remarked that the expression of dominant negative Rab35 used a driver that was expressed in more than the bristle and could be the result of non-cell autonomous activity (156). To be fair, Otani et al. performed RNAi knock-down of Rab35 rather than using DN isoforms meaning that the difference could be in the level of knockdown. All the same, Otani found that Ik2 inhibited PKCα, which in turn phosphorylated Fascin, preventing F-Actin bundle assembly (156). This mechanism however is counter-intuitive as the tip localized Ik2 should inhibit PKCα in the tip leading to active Fascin – but Fascin is not incorporated into bundles at the tip, leading one to question how this interaction produces a normal phenotype. One explanation would be the local dephosphorylation of PKCα in the tip combined with retrograde diffusion of phospho-PKC. Another possibility is that Fascin will be incapable of bundling F-Actin without Forked first being present. There is a demonstrated additive phenotypic effect of *forked* and *ik2*, but not *sn* and *ik2*, suggesting that Forked proteins are unaffected by Ik2 loss. These bundles seem to assemble as roughly 3um-long cables which are assembled tip-to-tip by a process which seems to involve the Arp2/3 complex and Forked (265).

Curiously, among the vast majority of bristle TEM thin-sections, when Actin bundles are found at the membrane they have a slight positive curvature – even in mutants or when the membrane bulges out from between bundles (137,138,140,272,314). Similar data has been described in Lepidopterans as well (54,126). This suggests that whatever is facilitating F-Actin's binding may have a preference for a positively curved membrane surface. Additionally, we can be confident that membrane binding is not due to *forked* or *singed,* as *f;sn* double mutants still accrue F-Actin at the membrane (138,140). What's more, no additional actin accumulates at the membrane when developing *f;sn* double mutant bristles are incubated with the F-Actin stabilizer Jasplakinolide – suggesting that there is an active process associated with bundle accumulation and not a natural proclivity for F-actin to bind them membrane in a concentration based means (314). We can also rule out *javelin* as a membrane recruiter, as in *jv* mutants, premature breakdown within bundles occurs (in a similar process to normal degradation of the bundles in late pupae

or in cycloheximide treated animals), but doesn't seem to inhibit binding to the membrane (315,335) The only instance described in which, Actin is not found at the membrane at all, is in bristles treated with Oakadaic acid (a specific inhibitor of Phosphatase 1 and 2A) (140). This treatment has no effect on packing of bundles, however, with large hexagonally packed F-Actin bundles found in the bristle lumen, suggesting that whatever associates F-Actin to the membrane may also require dephosphorylation or may be inhibited by a molecule that must remain dephosphorylated, but that this effect is separable from the role of *forked*, *singed,* and *javelin* (140).

In the end we are left with the question, what binds F-Actin bundles to the membrane? Since we can rule out *f, sn,* and *jv,* and can be reasonably sure a protein is involved given the Oakadaic acid and jasplakinolide treatments, we are left with possibly positive curvature binding proteins and proteins regulated by phosphorylation (directly or not). Spectrins are a good candidate as they are positive-curvature membrane binding proteins known to interact with Actin from work done in neurons and mammalian red blood cells (330,336,337). Spectrins to date have not been examined in developing bristles and hence are open for interrogation. Additionally, a spectrin-related protein, alpha-Actinin (*actn*), is a known Actin binding protein and has an association near the plasma membrane (337,338). While no dedicated report has looked at alpha-Actinin in the bristle, Mummery-Widmer et al. list *actn* RNAi as having an extreme impact on bristle morphology (Appendix 1) (339). Further, we have collected evidence that alpha-Actinin protein is present in the earliest sprouting buds of butterfly scales (Fig5.2). What's more, *actn1* has been shown to have phosphorylation dependent activity at focal adhesions in cancer cells (340) and reduced Actin binding activity following EGF-mediated phosphorylation in mouse fibroblasts (341). In sum, Spectrins and alpha-Actinin, seem like good candidates for the missing link mediating the connection of Actin to the bristle (and perhaps scale) plasma membrane.

Aside from the potential role of elastic buckling in establishing the pattern of ridges in bristles/scales, it has been shown that reductions in the protein titer of Arp2/3 complex proteins or the Arp2/3 nucleators Abp1 and Scar lead to bristles with an increased number of cuticular ridges in adult bristles, suggesting extra longitudinal F-Actin had formed during development (273,307,342). While providing less resolution than TEM thin-sections, confocal microscopy of phalloidin stained bristles with Arp2/3 deficiency seem to suggest this is true (307). So it seems that beyond the initial establishment of large F-Actin bundles, there is a requirement for Arp2/3 to maintain the arrangement. Several authors have identified transient disorganized populations of F-Actin occurring as "snarls" between established bundles of F-Actin (273,314). These snarls are associated with bulges in the membrane at the tip originally noted in Lees and Pickens descriptive work (301,314). How bulges are made from regions which have negative curvature is unknown. One possibility is represented in the form of Phosphorylated Phosphatidyl-Inositides (PIPs), lipids with large head groups relative to their fatty-acid tails. This means they can be modeled as upside down cones with the vertex equivalent to the tail. A membrane packed with PIPs on the inner leaflet, will experience a lateral pressure that can result in

spontaneous inward (negative) curvature. Further, evidence mounting suggests that the opposite (curvature separating lipid species) is possible if the system is tuned to do so (343). It is hence tempting to imagine that the act of membrane buckling in the early bristle rudiment could dictate where Actin filaments form (positive curvature) but also where Actin snarls form by localizing $PI_{(4)}P$, Skittles, and $PI_{(4,5)}P_2$ (and subsequently Abp1/Scar, Sra-1/Kette/Wasp, the Arp2/3 complex, and new Actin). To date nothing similar has been described in butterflies, though no one has looked closely.

Arp2/3 has also been shown to be in a delicate balance with the Actin plus-end capping-protein *capping protein beta (cpb),* which serves to terminate elongation of a growing filament (273). Where flies transheterozygous for *cpb* normally show complete disarray of ridges (and hence actin), having flies heterozygous for *arp3, arpc4, arpc5,* or *wsp* was sufficient to rescue the disarray (273). In a non-intuitive result *arpc1* actually enhanced the *cpb* phenotype – though structural and biochemical evidence suggests that *arpc1* may prevent spurious activation of the Arp2/3 complex (344). Thus removing *arpc1* may allow for additional activation enhancing the loss of *cpb.* Also unexpectedly, loss of *cpb* components does not seem to manifest in the earliest rudiment of the bristle (no observation of the basal aspect of Arp2/3 complex mutants has been published) – the basal region of the bristles shows no phenotype (154). This suggests that there may be an early non-Arp dependent morphogenetic phase followed by an Arp2/3 dependent phase. What appears to be true however, is that snarls localize to bulges in the membrane between Actin bundles. How this is managed is unclear, as is how the membrane evaginates between bundles in more basal regions where snarls are less prevalent.

What can be hypothesized for future study is that a combination of membrane properties and a balance of internal and external forces determine the buckled state of the membrane. This, in turn may provide sites for Actin nucleation via proteins with a positive-membrane-curvature tropism such as the Spectrin complex proteins or alpha-Actinin. The resulting regions of negative curvature may become enriched in PIPs and serve as nucleation sites for Scar/Wasp mediated Arp2/3 snarls. This, perhaps combined with the crystallization of the adjoining actin bundles during the integration of Sn proteins, may create a reversal of the membrane buckling resulting in the protrusions between adjacent actin bundles which eventually are solidified into ridges. Manipulation of membrane properties should be able to predictably manipulate ridge number, while much of the rest needs to be addressed first in flies by stain/knockdown of alpha-Actinin and positive curvature binding proteins.

5.2.3 RDCSCM: Fine structure

In butterflies with structural coloration, often fine striations and reticulations built on the surface of larger structures (such as ridges) are the ultimate source of color. Structures like these seem to form well after the specification of ridges in *Ephestia* and *Colias* (54,126). Recently it was shown similar structures, though not as elaborate, exist on the surface of adult *Drosophila* macrochaetes (345). This suggests that similar conditions and mechanisms involved in developing scales may exist in *Drosophila.* How these fine

structures form is unclear, though the regular 100nm spacing could imply that buckling or molecular rulers plays a role.

In support of the former, one can consider the cuticle of *C. elegans*. *C. elegans*, like flies and butterflies, is an Ecdysozoan that secretes a cuticle. Being nematodes, *C. elegans* have no appendages and use serpentine motion to move across a substrate. Apparently in aid of their locomotion, regularly spaced ridged rings, annuli, transect the length of the animal and larger, lateral, stage-specific ridging, alae, runs parallel to the length (164,346,347). Annuli are spaced roughly 1um apart in the embryo by an elaborate system that seems to use actin and tubulin rings (like butterfly or fly ridges), which are themselves patterned by underlying muscle (very unlike butterfly and fly ridges) (348–350). Where it becomes an interest to a buckling hypothesis is in Fig2E of Costa et al. in which a TEM thin section of a curled-up *C. elegans* embryo shows the annuli in cross section (348). On the outer edge of the embryo, which has had to lengthen to accommodate the curl, there is no hint of annuli. In contrast, the interior surface of the curve not only has annuli, but there is ~100nm sub-buckling along each of the annulus' surface (348). In this sense, it is tempting to hypothesize a similar phenomenon in structural coloration where level of buckling force could produce variation in the fine structure spacing.

In support of molecular rulers creating 100nm spacing in the cuticle, there is very little evidence outside of *C. elegans* muscle fibers (which could be considered a form of molecular ruler). However, between the FAP proteins of *Chlamydamonas* flagella and the aforementioned neuronal Spectrin/Actin rings, one could imagine a novel and mutable protein which imparts spatial order in the cuticle of butterfly structures yet allows for length adjustment and hence changes in spacing (200,330).

In some instances, merely the thickness of chitin deposition could be evoked as a mechanism for generating diversity of structural color, particularly for thin films (as in Fig4.16). Chitin synthase is encoded by the gene *krotzkopf verkehrt (kkv).* Recently it has been demonstrated that Kkv activity is regulated by the activity of two closely related proteins Rebuf *(reb)* and Expansion *(exp)* (310). Either Exp or Reb are sufficient to stimulate chitin synthesis in tissues where Kkv is usually not active and, individually, are necessary for Kkv activity in tissues of normal expression. In polyphenic, polymorphic, or just closely related species, it is possible to imagine a heterochronic shift in activation of Kkv through Reb or Exp as generating thinned or thickened chitin layers, leading to altered dimensions and peak wavelength reflections (Fig1.3). In examples like the Sunset moth (*Chrysiridia (Urania) rhipheus*), which have a spatial gradient of structural coloration, one could imagine a simple threshold of activation or inactivation of *reb, exp,* or *kkv* as a morphogen readout (62,157,261). Moreover in chirped-multilayers, like those in *P. palinurus* (Fig3.24 and Fig3.30), changes in *exp, reb,* and/or *kkv* activity would be straight forward mechanisms perhaps especially if tied into molecular clock pathways (191,351).

Finally, there is a family of proteins that aids in shaping cells via ECM interactions – the Zona Pellucida genes. Originally identified as contributing to the gate-keeping region

around mammalian oocytes, ZP-domain proteins are membrane bound or secreted, often highly glycosylated, and able to interact with each other or the substrate in specific, combinatorial ways (162). In *C. elegans* it has been demonstrated that a combinatorial presence of the ZP-domain proteins Cut-1, Cut-3, Cut-5 and Cut-6 are responsible for the stage specific morphology of the alae as well as delimiting the boundaries where alae and annuli meet (163). In flies, ZP-proteins have been demonstrated to be involved in aiding the morphogenesis of the wing, the tracheal system, the wing hairs, and larval denticles (165,166,168–170,352). Even in *Heliconius* butterflies, it has been noted that *piopio* (a ZP protein) is differentially regulated between black and red wing regions, which corresponds nicely to the recognition that pigment type correlated with variation in scale ultrastructure (possibly determined by ZPs) (33,134). Between the observations (particularly of Sapio in *C. elegans* and Fernandes in *Drosophila* denticles) and these correlations in butterflies, it is tempting to imagine ZP proteins as generators of much of the cuticular diversity among butterfly scales perhaps even extending to structural origins. In fact, 5 ZP genes (*dpy, m, qsm, nompa,* and *tyn*) have been implicated in *Drosophila* bristle development by Mummery-Widmer's RNAi bristle screen (FigA1.2 - Chitin GO Term breakdown) suggesting this may be a fruitful group to evaluate further, both in flies and leps.

5.2.4 RDCSCM: Cellular Axis Specification

Scales and bristles offer no end to fascinating problems. One interesting question that is typically thought of as a multicellular developmental problem – that of axis specification. Both fly bristles and butterfly scales show asymmetries along their long apico-basal axis as well as in their proximo-distal (superior-inferior/ad-abwing) axes. For instance in flies, there is a progressive reduction in diameter as the bristle grows out, this is in contrast with many butterflies which either continually grow wider or balloon distinctly following their most basal extension. Though touched on in terms of microtubule differences, this is also interesting in some butterflies like *Callophrys rubi,* which have been shown to produce gyroids only in their most apical tips (46). Given the hypotheses of a role for the smooth ER in producing the gyroids, apical trafficking studies of organelles could produce important leads in learning about their development. This has begun in fly bristles with a study on mitochondrial transport which highlighted the role of dynein and the microtubule cytoskeleton but more work on the various organelles is needed particularly in a Lep system (147).

In terms of the proximo-distal asymmetry, flies show a reduction in actin bundle thickness nearer to the superior side and an overall curvature which follows along the proximo-distal axis (137,138,353). In studies of the former, it has been shown that the neuron associated with the proximal (superior) side, signals with Semaforins through PlexinA to the non-canonical redox protein MICAL which degrades F-Actin bundles on the superior surface (Fig1.6) (116). The latter is less well defined, with the authors suggesting that apposition to the pupal case forces a bend, but this is not convincing given that there are hundreds of microchaetes which bend along the P/D axis without ever contacting the pupal case.

Though it is tempting to simply conclude that the neuron determines curvature by weakening the upper surface (which may be true) it cannot be the mechanism by which butterflies achieve their curvature. In butterflies and moths, scales point toward the distal tip of wings and those on the body point toward the posterior of the body. Here too, F-Actin bundles are smaller on the proximal (adwing/superior) surface and often there are specific elaborations on the proximal surface that do not occur on the distal surface, suggesting that the cell "knows" the difference between the two. Unlike flies however, the vast majority of scales never have a neuron to communicate with, as that lineage apoptosis prior to the neuron even being specified (121). It stands to reason that planar cell polarity (PCP) pathways are involved in orienting the scales, and through the specification of proximal versus distal, enough information should be present to create the adwing/abwing asymmetry. In flies, the most downstream component of PCP signaling that dictates where wing hairs may grow is the gene *multiple wing hairs (mwh).* Mwh protein was visualized within bristles within actin bundles but no phenotype was recognized when mutant for *mwh* making it difficult to pinpoint its functional role (if one exists) in bristles (354). Given that PCP has been extensively studied in fly wing hair orientation, it is intuitive to imagine application of the same information to a field of scales (or macrochaetes in the case of Trichopterans) to produce such organization (20). Along these same lines, there is some suggestion that physical forces produced by tension in the wing membrane may be sufficient to aid organization as well, suggesting that the aforementioned ZP domain protein Dumpy may play dual roles in organizing tissues by orienting and establishing superior/inferior axes (352,355).

5.2.5 RDCSCM: Scale reduction, clearwings, and antiglare

Butterflies and moths are best known for their color patterns created by large elaborately colored scales. However, it is worth pointing out that a great number of Leps have created striking wing patterns and colors by doing precisely the opposite – making their scales diminutive. Whether the shrinking of cover scales in the Morpho species *cypris, rhetenor, sulkowskyi,* and *zephyritis* producing intensely metallic and specular reflections or the seemingly elimination of scales or their transmogrification into bristles in clearwing butterflies, these processes may be informed by studies in *Drosophila.*

Obviously understanding of how a bristle becomes a scale would likely inform the reverse process – so microtubule dynamics, as previously discussed, seem highly informative.

Additionally, the size difference between fly macrochaetes and microchaetes has been hypothesized to be a difference in the polyploidy state of the respective cells with macrochaetes completing more rounds of endocycling than microchaetes (123). Given that a similar result has been noted in Lep scales, it would be very interesting to know if forcing a scale to prematurely exit the cell cycle would be sufficient to create a scaled-down scale like what is seen in *Morphos* and *Graphium* (87,216).

As optical physicists have taken an interest in butterflies it has come to bear that optical properties are just reserved for scales. Siddique et al. had a look at the wing surface of

Greta oto, a clearwing butterfly, and found that the surface was covered in randomly arranged micropillars that abolished specular reflectance from the surface reducing glare (356). This is remarkably similar to the antiglare “nipple-arrays” found on the cornea of *Drosophila* eyes, and may be related to the microvilli found in emerging bristles, sockets, and epithelial cells of the fly notum (357–360). While likely operating on a different level, the loss of the gene *shavenoid* was reported to specifically eliminate the hairs from the notum, not impacting the macrochaetes or microchaetes in any way (360). In addition, Lees and Pickens noted that *spineless* (a PAS-bHLH transcription factor)*, hairless* (a notch transcriptional repressor)*, shaven* (the transcription factor Pax2)*,* and *prickly* (which has an unknown molecular function but localizes within the genomic region containing *dysf,* a bHLH transcription factor, involved in tracheal and arista development) all resulted in shrunken or missing bristles, suggesting that there are many crucial transcription factors needed for the execution of the bristle program (301).

In fact, there is more than one way to shave a fly, as a great number of mitochondrial mutations result in miniature bristles (361). As does the gene *miniature* a member of the ZP-domain proteins discussed prior. And the gene aptly named *shavenbaby* may instruct the production of denticle belts through ZP domain protein expression (362). In sum, *Drosophila* chaete may inform us not only on how to form a scale, but how to destroy them.

5.3 Morphos and Melanin

In the Morphos, we were able to leverage understanding of the process of melanization to produce what seems to recapitulate much of the diversity in color we see throughout the *Morpho* genus (and elsewhere). However, due to limitations on life cycle, we were unable to make genetic manipulations to evaluate our hypotheses. For instance, as Zhang et al. have recently shown, there are a handful of genes responsible for the variety of coloration seen in *Vanessa* and *Junonia*, and these are seemingly spatially restricted (77). Moreover, though we were able to force the loss of pigmentation through drugs, we hit the upstream-most enzyme (Tyrosine hydroxylase), which has many pleiotropic effects including the collapse of the cuticle and presumably a down regulation of catecholamines. This pleiotropy argues that *pale* may not be the mechanistic target of pigmentation in naturally occurring populations. It is important therefore to analyze the genetic structure of coding and non-coding melanin genes especially in populations of subspecies with varying pigmentation levels such as *Morpho godartii* or *Morpho rhetenor*. It is also tempting to predict in the latter a role for WntA in the expansion/contraction of white domains, so heparin/dextran sulfate manipulation of young pupae could help inform this. In addition, being able to employ larval surgeries could be beneficial for getting a reproducible sense of pigmentation kinetics, which in *ex vivo* experiments were trickier to get.

Beyond the role of melanin, the *Laurschwartzia* and *Iphamedeia* sub-genera incorporate high levels of orange pigments (presumably ommochromes) into their dorsal surface. Pigment extraction experiments I have done with the orange form of *M. cisseis gahua* and *M. hecuba* resulted in visibly orange pigment extraction when utilizing acidified MeOH – known to extract ommochromes. In naturally occurring specimen the levels of orange can vary conspicuously as best demonstrated by the many forms of *M. cisseis cabrera* which seem to form orange patches in a means remarkably similar to the variation seen in sub-species of *M. rhetenor* and their white spots. In addition, I found that *M. amphitryon* relies heavily upon lower lamina thin-films for its gradients of color in addition to varying levels of orange pigment (Fig2.10 and Appendix 2). Blue scales lacked pigment, green scales had a small amount of pigment, and orange scales were heavily pigmented. Given the examples provided by budgerigars, there may be a similar mechanism being deployed in *M. amphitryon* of blue structural lamina + [low orange pigment] == green overall appearance (66). Manipulation of ommochromes may prove more difficult to perform than melanin. Ommochromes derive from L-Tryptophan, and though effectively undergoing the same enzymatic manipulations (hydroxylation followed by decarboxylation) inhibitors of ommochrome synthesis are not readily available. Thus, genetic manipulation may be necessary to evaluate the effects of ommochromes on structural color.

Lastly, by looking into a species in the sister genus of *Morpho*, *Antirrhea avernus*, we found that the blue color was entirely lower lamina thin-film derived. Combined with the lower lamina derived structural color we saw in the *Deyrollia, Laurschwartzia,* and *Iphamedeia* sub-genera of *Morpho* and what has been acknowledged in *Morpho peleides,* it is tempting to suggest that the ur-*Morpho* lacked structurally colored ridges (86,227). This is obviously an interesting idea considering that the multi-lamellar ridge was named after the *Morphos.* This is harder to test, given it is an event that is in the inaccessible past, however more dense sampling of the outgroups of *Morpho* may highlight whether *Antirrhea avernus* has lost ridges relative to other *Antirrhea* or *Caerolis* species or if all of the outgroups similarly lack structural ridges. More elaborately, if we could pinpoint the developmental mechanisms leading to large robust multi-lamellar ridges in *Morpho*, we could assay the syntenic genomic regions controlling function across the *Morpho* and *Antirrhea* to gather evidence for inherited alleles controlling ridge formation. The distribution of alleles across the genera could inform our understanding of the ancestral state.

5.4 *Achillides*: Actin and pigment

I was able to provide a sense of the actin dynamics that I believe are necessary for the construction of the wild type parabolic reflectors found on *Papilio palinurus* and began to get a sense of how this may be modified to produce the boxy structures found in *Papilio ulysses.* However, in not being able to maintain a full life cycle, our ability to be confident about the age of pupae (and hence when dissections/manipulations occurred) is limited. Further, attempts to manipulate the actin cytoskeleton with small molecules have been at

best inconclusive. This could be in part due to our lack of age control, but given the large number of injected animals over a range of concentrations, it may be possible that the drugs do not gain access to the cytoskeleton. Small molecules like Phalloidin seem to stain weakly in most cells with hexagonal actin perhaps lending credence to an access issue. Still, in order to test the functional importance of actin in structurally colored scales, the ability to manipulate it with confidence will be important. Further, given that hexagonal actin containing scales were rare, it may suggest that the transition from longitudinal actin to hexagonal is a rapid transition. Though we have found some evidence of how this transition occurs, being able to visualize the development in real time will be of great benefit for understanding this process.

In exploring the role of pigments in the structural colored scales of *Papilio palinurus*, I found with some surprise that loss of pigmentation (both in damaged areas of the wing and through 3IT inhibition) created desaturation phenotypes as expected from my Morpho exploration, but also led to a blue shift. When treated with 3IT to block melanization, *P. palinurus* cover scales still show significant absorbance despite the fact that the absorbance profile of wild type *P. palinurus* cover scales approximates that seen in the areas of *Drosophila melanogaster*'s abdomen (known to contain dopamine derived melanin). This may be because I only have examined a single individual, however it is possible that multiple pigments are present such as an ommochrome like xanthommatin. TEM of treated, damaged, and wild type animals revealed that the electron dense lower laminae within wild type *P. palinurus* had decreased electron density in treated and damaged scales suggesting the electron dense regions were indeed pigments. Moreover, the multilayer of *P. palinurus* is actually chirped, with decreasing chitin thickness and increasing airspaces. I believe that in losing the dark pigments, these thinner laminae are able to contribute to the spectrum reflected and are likely to bias the reflectance toward a blue in addition to reducing the apparent saturation. What's more, *P. blumei* shows a similar blue and green coloration as the damaged phenotypes, so it is tempting to imagine that the difference between its colors are pigment derived. It is obvious from these experiments that an exploration of the role of pigmentation in the *Achillides* may provide powerful insights into the evolution of the group's structural color.

5.5 Developing Lepidopteran technologies

In my estimation, there are 3 major factors preventing in depth study of scale biology: 1) a lack of scale-limited expression constructs, 2) the ability to make conditional knockdowns, and 3) the ability to have lines or reliable means of temporary expression. One of the great benefits to fly researchers has been the development of specific expression lines (typically driving the expression of the Gal4 transcription factor). This has allowed cell-type specific expression of any multitude of useful constructs including GFP, RNAi, etc. allowing for in depth analysis of developmental and cell biological processes. In turn, expression constructs have relied heavily upon the development of robust transgenesis protocols including piggyBAC and p-elements. The ability to make

lines which transmit genetic modifications from generation to generation allow for things like enhancer traps to be made and utilized. Intrinsic in making and keeping lines is the need for a highly fecund, small organism that doesn't mind living at high population density. *Drosophila* has been fortunate for just this reason, in addition to having only 4 chromosomes – allowing the production of balancer chromosomes which simplify the task of maintaining mutations and lines without meiotic loss.

At every one of these points, Lepidoptera as a whole suffer greatly. The majority of species are large and sensitive to high population densities with low fecundity, they have a mode haploid chromosomal number of 31, which greatly complicates the ability of maintaining lines even if they could be easily created. The 100 years of *Drosophila* study has also aided those researchers by their concerted effort and cumulative efforts, where butterfly researchers have divided their attention between many models. As a result, there are few tools that have been developed to allow the genetic trickery seen in flies. In addition, models that are more amenable to benchwork (*Bombyx, Ephestia,* or *Plodia* for instance) may lack characters of interest (e.g. structural color) requiring studies to be worked out in one species and then adapted to species with the actual characters of interest.

Towards the end of my tenure, I began working on *Plodia* but did not have sufficient time to develop techniques there – though promising preliminary results were achieved. It seems to me that concerted effort at building and integrating useful expression vectors, with focus on clever constructs that allow for conditional knockdown (optogenetic dominant negatives) and visualization (photoconvertible markers/FPs) is an absolute necessity for understanding scale development. Especially where the gate keepers of nanostructure (Actin/Tubulin/ER/Cuticle) are likely to be highly pleiotropic, embryonic knockout will lead to death far before any phenotype can be ascertained in adult structures like scales. Addressing these deficiencies will improve the state of the field greatly.

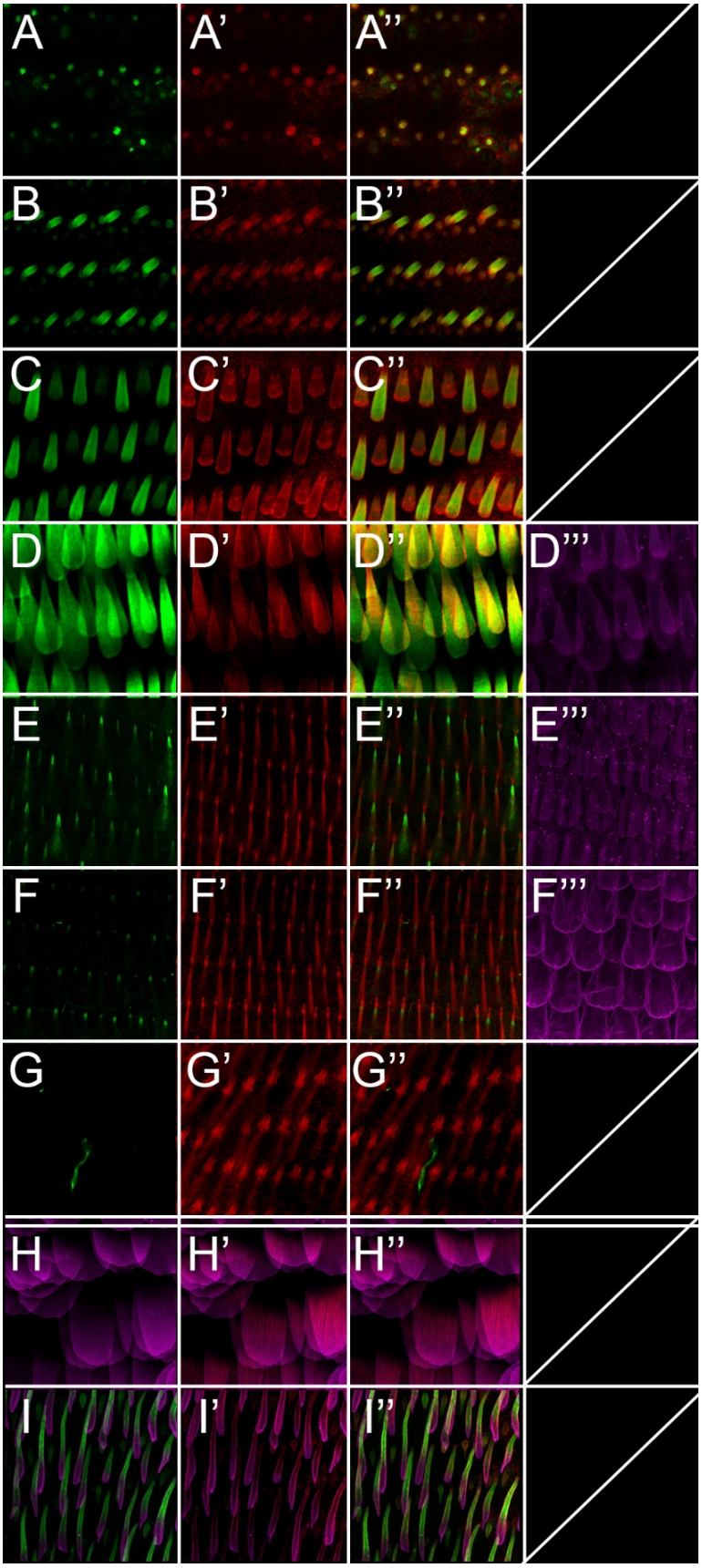

Figure 5.1 Tubulin time series and Taxol treatment suggests important role for microtubules in scale shape

Z projections of confocal stacks. Fluorescent antibody staining of butterfly pupal wing discs. For all, **Green** – anti-Acetylated-Tubulin, **Red** – Phalloidin (F-Actin), **Magenta** – WGA (Chitin/GlcNAc glycosylation).

A-G – untreated pupae, **H** – DMSO injected at 48hAP, stained 96hAP, **I** – 50uM Taxol injected at 48hAP, stained 96hAP

A – 36hAP, **B** – 38hAP,
C – 42hAP, **D** – 48hAP,
E – 54hAP, **F** – 66hAP,
G – 78hAP

Cells are filled with AcTub until at least 48hAP, at which point the expression collapses to the pedicel alone. This collapse is prevented by injecting Taxol just prior to the collapse, and in coordination, the scale takes on a very bristle-like appearance compared to DMSO injected controls.

Data collected in collaboration with Julian Kimura (Duke/Harvard).

Figure 5.2 alpha-Actinin is enriched in developing scale buds in 48hAP *Vanessa cardui* wings

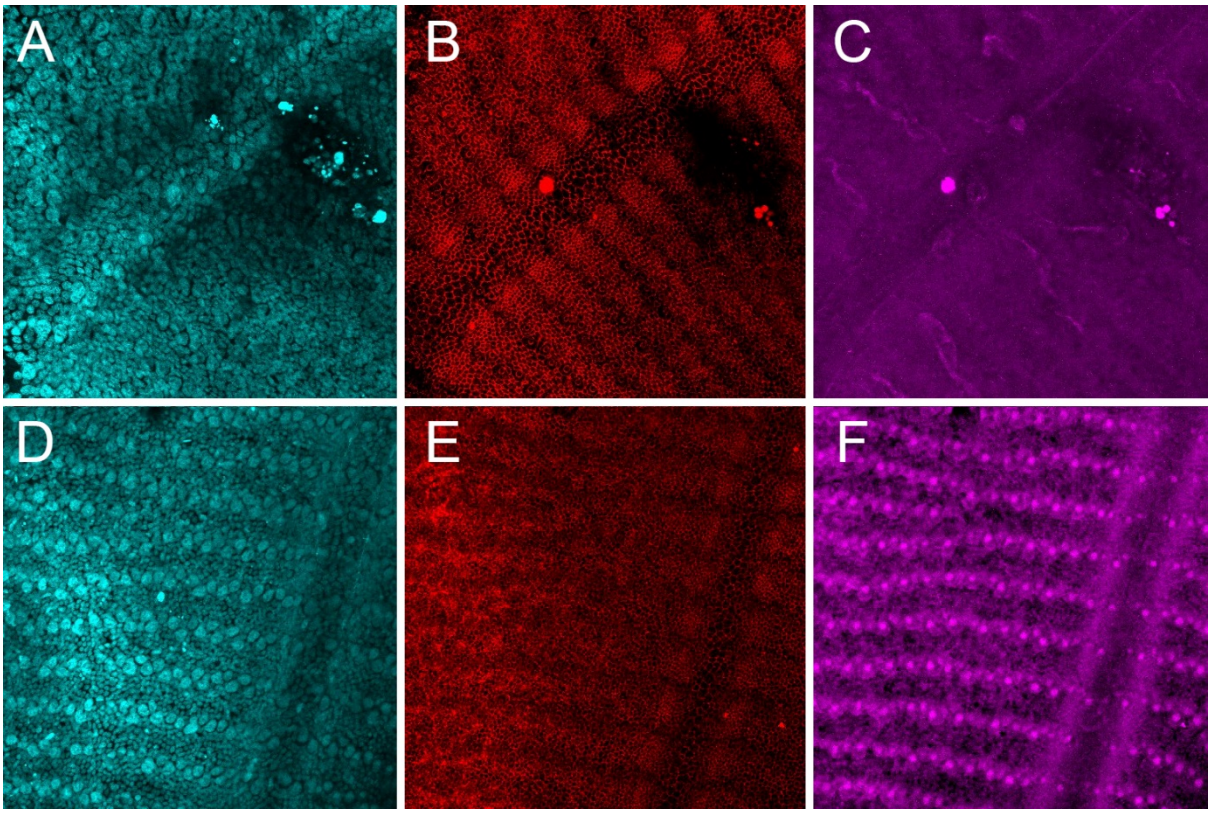

Z projections of confocal stacks. Fluorescent antibody staining of 48h pupal hindwings from *Vanessa cardui.* **A,D** – DAPI stain showing nuclei of the wing epithelium including large scale nuclei. **B,E** rabbit anti-beta Catenin positive control stain, showing outlines of cells in the wing epithelium. **C** – secondary only antibody stain as negative control. **F** – 1:10 rat anti-alpha-Actinin stain marking the protruding scale buds.

References

1. Podgornaia AI, Laub MT. Determinants of specificity in two-component signal transduction. Curr Opin Microbiol. 2013 Apr;16(2):156–62.
2. Kronforst MR, Papa R. The Functional Basis of Wing Patterning in Heliconius Butterflies: The Molecules Behind Mimicry. Genetics. 2015 May 1;200(1):1–19.
3. Joron M, Jiggins CD, Papanicolaou A, McMillan WO. Heliconius wing patterns: an evo-devo model for understanding phenotypic diversity. Heredity (Edinb). 2006 Sep 12;97(3):157–67.
4. Muller F, Meldola R (Translation). Ituna and Thyridia: a remarkable case of mimicry in butterflies. Trans Entomol Soc London. 1879;20–9.
5. Bates HW. The naturalist on the River Amazons, a record of adventures, habits of animals, sketches of Brazilian and Indian life and aspects of nature under the Equator during eleven years of travel. 1st ed. London: J. Murray; 1863.
6. Montgomery S. Carnivorous caterpillars: the behavior, biogeography and conservation of Eupithecia (Lepidoptera: Geometridae) in the Hawaiian Islands. GeoJournal. Kluwer Academic Publishers; 1983;7(6):549–56.
7. Nijhout HF. Ommochrome pigmentation of the linea and rosa seasonal forms of Precis coenia (Lepidoptera: Nymphalidae). Arch Insect Biochem Physiol. 1997;36(3):215–22.
8. Daniels E V, Mooney KA, Reed RD. Seasonal wing colour plasticity varies dramatically between buckeye butterfly populations in different climatic zones. Ecol Entomol. 2012;37(2):155–9.
9. Nijhout HF. Polymorphic mimicry in Papilio dardanus: Mosaic dominance, big effects, and origins. Evol Dev. 2003;5(6):579–92.
10. Clarke CA, Sheppard PM. The Genetics of Papilio Dardanus, Brown. I. Race Cenea from South Africa. Genetics. 1959;44(6):1347–58.
11. Clarke CA, Sheppard PM. The genetics of Papilio dardanus, Brown. II. Races dardanus, polytrophus, meseres, and tibullus. Genetics. 1960;45(4):439–57.
12. Nishikawa H, Iga M, Yamaguchi J, Saito K, Kataoka H, Suzuki Y, et al. Molecular basis of wing coloration in a Batesian mimic butterfly, Papilio polytes. Sci Rep. 2013 Nov 11;3:3184.
13. Kunte K, Zhang W, Tenger-Trolander A, Palmer DH, Martin A, Reed RD, et al. Doublesex Is a Mimicry Supergene. Nature. Nature Publishing Group; 2014;507(7491):229–32.
14. Manning WM, Strain HH. Chlorophyll D, a green pigment of red algae. J Biol Chem. 1943;151(1):1–19.
15. Haxo FT, Blinks LR. PHOTOSYNTHETIC ACTION SPECTRA OF MARINE ALGAE. J Gen Physiol. 1950;33(4).

16. Hu X, Damjanović A, Ritz T, Schulten K. Architecture and mechanism of the light-harvesting apparatus of purple bacteria. Proc Natl Acad Sci U S A. 1998 May 26;95(11):5935–41.

17. Wallace AR. The Malay Archipelago: The land of the orang-utan, and the bird of paradise. A narrative of travel, with sketches of man and nature. 1st ed. Vol. 1 + 2. London: Macmillan; 1869.

18. Kristensen NP, Scoble MJ, Karsholt O. Lepidoptera phylogeny and systematics: the state of inventorying moth and butterfly diversity. Zootaxa. 2007;1668:699–747.

19. Powell JA. Lepidoptera: Moths, Butterflies. Encycl Insects. 2009;559–87.

20. HUXLEY J, BARNARD PC. Wing-scales of Pseudoleptocerus chirindensis Kimmins (Trichoptera: Leptoceridae). Zool J Linn Soc. Blackwell Publishing Ltd; 1988 Mar;92(3):285–312.

21. Thompson MJ, Timmermans MJTN, Jiggins CD, Vogler AP. The evolutionary genetics of highly divergent alleles of the mimicry locus in Papilio dardanus. BMC Evol Biol. 2014 Aug 31;14(1):140.

22. Clark R, Brown SM, Collins SC, Jiggins CD, Heckel DG, Vogler AP. Colour pattern specification in the Mocker swallowtail Papilio dardanus: the transcription factor invected is a candidate for the mimicry locus H. Proc R Soc London B Biol Sci. 2008;275(1639).

23. Brunetti CR, Selegue JE, Monteiro A, French V, Brakefield PM, Carroll SB. The generation and diversification of butterfly eyespot color patterns. Curr Biol. 2001 Oct 16;11(20):1578–85.

24. Nijhout HF. Pattern formation on lepidopteran wings: Determination of an eyespot. Dev Biol. 1980;80(2):267–74.

25. Monteiro A, Brakefield PM, French V. The genetics and development of an eyespot pattern in the butterfly Bicyclus anynana: Response to selection for eyespot shape. Genetics. 1997;146(1):287–94.

26. Nardi JB, Kafatos FC. Polarity and gradients in lepidopteran wing epidermis I. Changes in graft polarity, form, and cell density accompanying transpositions and reorientations. Embryol exp Morph. 1976;36(3):469–87.

27. Martin A, Reed RD. Wnt signaling underlies evolution and development of the butterfly wing pattern symmetry systems. Dev Biol. 2014 Nov 15;395(2):367–78.

28. Martin A, Papa R, Nadeau NJ, Hill RI, Counterman BA, Halder G, et al. Diversification of complex butterfly wing patterns by repeated regulatory evolution of a Wnt ligand. Proc Natl Acad Sci U S A. 2012 Jul 31;109(31):12632–7.

29. Gallant JR, Imhoff VE, Martin A, Savage WK, Chamberlain NL, Pote BL, et al. Ancient homology underlies adaptive mimetic diversity across butterflies. Nat Commun. 2014 Sep 8;5:4817.

30. Mavárez J, Salazar CA, Bermingham E, Salcedo C, Jiggins CD, Linares M. Speciation by hybridization in Heliconius butterflies. Nature. 2006;441(7095):868–71.

31. Nadeau NJ, Pardo-Diaz C, Whibley A, Supple MA, Saenko S V, Wallbank RWR, et al. The gene cortex controls mimicry and crypsis in butterflies and moths. Nature. 2016 Jun 2;534(7605):106–10.

32. Van't Hof AE, Campagne P, Rigden DJ, Yung CJ, Lingley J, Quail MA, et al. The industrial melanism mutation in British peppered moths is a transposable element. Nature. 2016 Jun 2;534(7605):102–5.

33. Gilbert LE, Forrest HS, Schultz TD, Harvey DJ. Correlations of ultrastructure and pigmentation suggest how genes control development of wing scales of Heliconius butterflies. Vol. 26, Journal of Research on the Lepidoptera. 1988. p. 141–60.

34. Wilts BD, Matsushita A, Arikawa K, Stavenga DG. Spectrally tuned structural and pigmentary coloration of birdwing butterfly wing scales. J R Soc Interface. 2015 Oct 6;12(111):20150717.

35. Zhang K, Zhou S, Tang Y, Wang G, Zhou H, Fan T, et al. Polarization-sensitive color in iridescent scales of butterfly Ornithoptera. R Soc Chem. 2014;4:51865–71.

36. Ghiradella H. Structure and Development of Iridescent Butterfly Scales: Lattices and Laminae. J Morphol. 1989;88(202):69–88.

37. Wilts BD, Michielsen K, De Raedt HA, Stavenga DG. Iridescence and spectral filtering of the gyroid-type photonic crystals in Parides sesostris wing scales. Interface Focus. 2012;2(5):681–7.

38. Wilts BD, IJbema N, Stavenga DG. Pigmentary and photonic coloration mechanisms reveal taxonomic relationships of the Cattlehearts (Lepidoptera: Papilionidae: Parides). BMC Evol Biol. 2014;14(1):160.

39. Tam HL, Cheah KW, Goh DTP, Goh JKL. Iridescence and nano-structure differences in Papilio butterflies. Opt Mater Express. 2013;3(8):1087–92.

40. Diao Y-Y, Liu X-Y. Mysterious coloring: structural origin of color mixing for two breeds of Papilio butterflies. Opt Express. 2011;19(10):9232–41.

41. Vukusic P, Sambles R, Lawrence C, Wakely G. Sculpted-multilayer optical effects in two species of Papilio butterfly. Appl Opt. 2001;40(7):1116–25.

42. Cassildé C, Blandin P, Pierre J, Bourgoin T. Phylogeny of the genus Morpho Fabricius, 1807, revisited (Lepidoptera, Nymphalidae). Bull la Soc Entomol Fr. 2010;115(2):225–50.

43. Ingram AL, Parker AR. A review of the diversity and evolution of photonic structures in butterflies, incorporating the work of John Huxley (The Natural History Museum, London from 1961 to 1990). Philos Trans R Soc London B Biol

Sci. 2008;363(1502):2465–80.

44. Mason CW. Blue Eyes. J Phys Chem. 1923 Jan;28(5):498–501.

45. McPhedran RC, Nicorovici NA, McKenzie DR, Botten LC, Parker AR, Rouse GW. The Sea Mouse and the Photonic Crystal. Aust J Chem. CSIRO PUBLISHING; 2001;54(4):241.

46. Michielsen K, De Raedt HA, Stavenga DG. Reflectivity of the gyroid biophotonic crystals in the ventral wing scales of the Green Hairstreak butterfly, Callophrys rubi. J R Soc Interface. 2010 May 6;7(46):765–71.

47. Vukusic P, Sambles JR, Lawrence CR. Colour mixing in wing scales of a butterfly. Nature. 2000;404(6777):457.

48. Penz CM, DeVRIES PJ. Phylogenetic Analysis of Morpho Butterflies (Nymphalidae, Morphinae): Implications for Classification and Natural History. Am Museum Novit. 2002;3374(3374):1–33.

49. Rutowski R., Macedonia J., Morehouse N, Taylor-Taft L. Pterin pigments amplify iridescent ultraviolet signal in males of the orange sulphur butterfly, Colias eurytheme. Proc R Soc B Biol Sci. 2005 Nov 7;272(1578):2329–35.

50. D'Alba L, Saranathan V, Clarke J a, Vinther J a, Prum RO, Shawkey MD. Colour-producing β-keratin nanofibres in blue penguin (Eudyptula minor) feathers. Biol Lett. 2011;7(4):543–6.

51. Stavenga DG, Leertouwer HL, Wilts BD. The colouration toolkit of the Pipevine Swallowtail butterfly, Battus philenor: thin films, papiliochromes, and melanin. J Comp Physiol A Neuroethol Sens Neural Behav Physiol. 2014 Jun 9;200(6):547–61.

52. Kunte K, Shea C, Aardema ML, Scriber JM, Juenger TE, Gilbert LE, et al. Sex Chromosome Mosaicism and Hybrid Speciation among Tiger Swallowtail Butterflies. Moran NA, editor. PLoS Genet. Sinauer Associates; 2011 Sep 8;7(9):e1002274.

53. Kunte K. THE DIVERSITY AND EVOLUTION OF BATESIAN MIMICRY IN PAPILIO SWALLOWTAIL BUTTERFLIES. Evolution (N Y). 2009 Oct;63(10):2707–16.

54. Ghiradella H. Development of ultraviolet-reflecting butterfly scales: How to make an interference filter. J Morphol. 1974;142(4):395–409.

55. Kinoshita S, Yoshioka S, Kawagoe K. Mechanisms of structural colour in the Morpho butterfly: cooperation of regularity and irregularity in an iridescent scale. Proc Biol Sci. 2002;269(1499):1417–21.

56. Wilts BD, Trzeciak TM, Vukusic P, Stavenga DG. Papiliochrome II pigment reduces the angle dependency of structural wing colouration in nireus group papilionids. J Exp Biol . 2012;215(5):796–805.

57. Lord Rayleigh. VII. On the optical character of some brilliant animal colours. Philos Mag Ser 6. 1919;37(217):98–111.

58. Lord Rayleigh. Studies of Iridescent Colour, and the Structure Producing it. II. Mother-of-Pearl. Proc R Soc London Ser A. 1923;102(719):674–7.

59. Lord Rayleigh. The Iridescent Colours of Birds and Insects. Proceedins R Soc London Ser A. 1930;128(808):624–41.

60. Mason CW. Structural Colors in Feathers. I. J Phys Chem. American Chemical Society; 1923;27(3):201–51.

61. Mason CW. Structural Colors in Insects. I. J Phys Chem. American Chemical Society; 1926;30(3):383–95.

62. Mason CW. Structural Colors in Insects. II. J Phys Chem. American Chemical Society; 1927;31(3):321–54.

63. Mason CW. Structural Colors in Insects. III. J Phys Chem. American Chemical Society; 1927;31(12):1856–72.

64. Bancroft WD, Chamot EM, Merritt E, Mason CW. Blue Feathers. Auk. 1923 Apr;40(2):275–300.

65. Giraldo MA, Yoshioka S, Stavenga DG. Far field scattering pattern of differently structured butterfly scales. J Comp Physiol A Neuroethol Sensory, Neural, Behav Physiol. 2008;194(3):201–7.

66. D'Alba L, Kieffer L, Shawkey MD. Relative contributions of pigments and biophotonic nanostructures to natural color production: a case study in budgerigar (Melopsittacus undulatus) feathers. J Exp Biol. 2012;215(8):1272–7.

67. Shawkey MD, Morehouse NI, Vukusic P. A protean palette: colour materials and mixing in birds and butterflies. J R Soc Interface. 2009;6(Suppl 2).

68. Shawkey MD, Hill GE. Significance of a basal melanin layer to production of non-iridescent structural plumage color: evidence from an amelanotic Steller's jay (Cyanocitta stelleri). J Exp Biol. 2006;209(Pt 7):1245–50.

69. Tinbergen J, Wilts BD, Stavenga DG. Spectral tuning of Amazon parrot feather coloration by psittacofulvin pigments and spongy structures. J Exp Biol. 2013;216(23).

70. Mäthger LM, Bell GRR, Kuzirian AM, Allen JJ, Hanlon RT. How does the blue-ringed octopus (Hapalochlaena lunulata) flash its blue rings? J Exp Biol. 2012;215(21).

71. Shawkey MD, Hill GE. Carotenoids need structural colours to shine. Biol Lett. 2005 Jun 22;1(2):121–4.

72. Saenko S V, Teyssier J, van der Marel D, Milinkovitch MC. Precise colocalization of interacting structural and pigmentary elements generates extensive color pattern variation in Phelsuma lizards. BMC Biol. 2013;11(1):105.

73. Trzeciak TM, Wilts BD, Stavenga DG, Vukusic P. Variable multilayer reflection together with long-pass filtering pigment determines the wing coloration of papilionid butterflies of the nireus group. Opt Express. 2012 Apr 9;20(8):8877–90.

74. Stavenga DG, Matsushita A, Arikawa K. Combined pigmentary and structural effects tune wing scale coloration to color vision in the swallowtail butterfly Papilio xuthus. Zool Lett. ???; 2015;1(1):14.

75. Yoshioka S, Kinoshita S. Structural or pigmentary? Origin of the distinctive white stripe on the blue wing of a Morpho butterfly. Proc R Soc B Biol Sci. 2006 Jan 22;273(1583):129–34.

76. Teyssier J, Saenko S V., van der Marel D, Milinkovitch MC, Bartl MH. Photonic crystals cause active colour change in chameleons. Nat Commun. Nature Publishing Group; 2015 Mar 10;6:6368.

77. Zhang L, Martin A, Perry MW, Van Der Burg, Karin R L, Matsuoka Y, et al. Genetic Basis of Melanin Pigmentation in Butterfly Wings. Genetics. 2017;

78. Vignolini S, Rudall PJ, Rowland a. V., Reed A, Moyroud E, Faden RB, et al. Pointillist structural color in Pollia fruit. Proc Natl Acad Sci. 2012;109(39):15712–5.

79. Parker AR, McKenzie DR, Large MCJ. Multilayer reflectors in animals using green and gold beetles as contrasting examples. J Exp Biol. 1998;201(9):1307–13.

80. Siddique RH, Vignolini S, Bartels C, Wacker I, Hölscher H. Colour formation on the wings of the butterfly Hypolimnas salmacis by scale stacking. Sci Rep. Nature Publishing Group; 2016 Nov 2;6:36204.

81. Stavenga DG, Leertouwer HL, Wilts BD. Coloration principles of nymphaline butterflies - thin films, melanin, ommochromes and wing scale stacking. J Exp Biol. 2014;217(12):2171–80.

82. Stavenga DG, Leertouwer HL, Hariyama T, De Raedt HA, Wilts BD. Sexual dichromatism of the damselfly Calopteryx japonica caused by a melanin-chitin multilayer in the male wing veins. PLoS One. 2012;7(11):e49743.

83. Maia R, Caetano JVO, Báo SN, Macedo RH. Iridescent structural colour production in male blue-black grassquit feather barbules: the role of keratin and melanin. J R Soc Interface. The Royal Society; 2009 Apr 6;6 Suppl 2(Suppl 2):S203-11.

84. Vukusic P, Sambles JR, Lawrence CR. Structurally assisted blackness in butterfly scales. Proc R Soc London B Biol Sci. 2004;271(Suppl 4):S237–9.

85. Kinoshita S. Structural colors in the realm of nature. World Scientific. 2008.

86. Giraldo MA, Stavenga DG. Brilliant iridescence of Morpho butterfly wing scales is due to both a thin film lower lamina and a multilayered upper lamina. J Comp Physiol A. 2016 May 12;202(5):381–8.

87. Stavenga DG, Matsushita A, Arikawa K, Leertouwer HL, Wilts BD. Glass scales on the wing of the swordtail butterfly Graphium sarpedon act as thin film polarizing reflectors. J Exp Biol. The Company of Biologists Ltd; 2012 Feb 15;215(Pt 4):657–62.

88. Yoshioka S, Nakamura E, Kinoshita S. Origin of Two-Color Iridescence in Rock Dove's Feather. J Phys Soc Japan. The Physical Society of Japan; 2007 Jan 15;76(1):13801.

89. Yin H, Shi L, Sha J, Li Y, Qin Y, Dong B, et al. Iridescence in the neck feathers of domestic pigeons. Phys Rev E. American Physical Society; 2006 Nov 22;74(5):51916.

90. Jacobs M, Lopez-Garcia M, Phrathep O-P, Lawson T, Oulton R, Whitney HM. Photonic multilayer structure of Begonia chloroplasts enhances photosynthetic efficiency. Nat Plants. Nature Publishing Group; 2016 Oct 24;2(11):16162.

91. IMAFUKU M, KUBOTA HY, INOUYE K. Wing colors based on arrangement of the multilayer structure of wing scales in lycaenid butterflies (Insecta: Lepidoptera). Entomol Sci. Blackwell Publishing Asia; 2012 Oct;15(4):400–7.

92. Prum RO, Quinn T, Torres RH. Anatomically diverse butterfly scales all produce structural colours by coherent scattering. J Exp Biol. 2006;209(Pt 4):748–65.

93. Kinoshita S, Yoshioka S, Fujii Y, Okamoto N. Photophysics of structural color in the Morpho butterflies. Forma-Tokyo-. 2002;17:103–121.

94. Yoshioka S, Matsuhana B, Tanaka S, Inouye Y, Oshima N, Kinoshita S. Mechanism of variable structural colour in the neon tetra: quantitative evaluation of the Venetian blind model. J R Soc Interface. 2011;8(54):56–66.

95. Levy-Lior A, Shimoni E, Schwartz O, Gavish-Regev E, Oron D, Oxford G, et al. Guanine-Based biogenic photonic-crystal arrays in fish and spiders. Adv Funct Mater. 2010;20(2):320–9.

96. Oxford GS, Gillespie RG. Evolution and ecology of spider coloration. Annu Rev Entomol. Annual Reviews; 1998 Jan;43(1):619–43.

97. Oxford GS. Guanine as a colorant in spiders: development, genetics, phylogenetics and ecology. Proc 17th Eur Colloq Arachnol Edinburgh 1997. 1998;121–31.

98. Steinbrecht RA, Mohren W, Pulker HK, Schneider D. Cuticular Interference Reflectors in the Golden Pupae of Danaine Butterflies. Proc R Soc London B Biol Sci. 1985;226(1244):367–90.

99. Ingram AL, Lousse V, Parker AR, Vigneron JP. Dual gratings interspersed on a single butterfly scale. J R Soc Interface. 2008;5(28):1387–90.

100. Izumi M, Sweeney AM, DeMartini DG, Weaver JC, Powers ML, Tao A, et al. Changes in reflectin protein phosphorylation are associated with dynamic iridescence in squid. J R Soc Interface. 2010;7(44):549–60.

101. Welch V, Vigneron JP, Lousse V, Parker A. Optical properties of the iridescent organ of the comb-jellyfish Beroë cucumis (Ctenophora). Phys Rev E. American Physical Society; 2006 Apr 14;73(4):41916.

102. England G, Kolle M, Kim P, Khan M, Muñoz P, Mazur E, et al. Bioinspired micrograting arrays mimicking the reverse color diffraction elements evolved by the butterfly Pierella luna. Proc Natl Acad Sci U S A. 2014;111(44):15630–4.

103. Michielsen K, Stavenga D. Gyroid cuticular structures in butterfly wing scales: biological photonic crystals. J R Soc Interface. 2008 Jan 6;5(18):85–94.

104. Ghiradella HT, Radigan W. Development of Butterfly Scales II. Struts, lattices, and surface tension. J Morphol. 1976;150:279–98.

105. Price JS, Burton JL, Shuster S, Wolff K. Control of scrotal colour in the vervet monkey. J Med Primatol. 1976;5(5):296–304.

106. Prum RO, Torres RH. Structural colouration of mammalian skin: convergent evolution of coherently scattering dermal collagen arrays. J Exp Biol. 2004 May;207(Pt 12):2157–72.

107. Prum RO, Torres R. Structural colouration of avian skin: convergent evolution of coherently scattering dermal collagen arrays. J Exp Biol. 2003;206(14).

108. Prum RO. Blue integumentary structural colours in dragonflies (Odonata) are not produced by incoherent Tyndall scattering. J Exp Biol. 2004 Oct 15;207(22):3999–4009.

109. Nijhout HF. The Development and Evolution of Butterfly Wing Patterns. Washington: Smithsonian Institution Press; 1991. 297 p.

110. Ghiradella H. Light and color on the wing: structural colors in butterflies and moths. Vol. 30, Applied optics. 1991. p. 3492–500.

111. Mallet J. Hybrid zones of Heliconius butterflies in Panama and the stability and movement of warning colour clines. Heredity (Edinb). 1986;56:191–202.

112. Harvey PH, Bull J, Pemberton M, Paxton RJ. The Evolution of Aposematic Coloration in Distasteful Prey: A Family Model. Am Nat. 1982;119(5):710–9.

113. Nijhout HF. Ontogeny of the Color Pattern on the Wings of Precis coenia (Lepidoptera: Nymphalidae). Dev Biol. 1980;80(2):275–88.

114. Terenius O, Papanicolaou A, Garbutt JS, Eleftherianos I, Huvenne H, Kanginakudru S, et al. RNA interference in Lepidoptera: An overview of successful and unsuccessful studies and implications for experimental design. J Insect Physiol. 2011 Feb;57(2):231–45.

115. Ando T, Fujiwara H. Electroporation-mediated somatic transgenesis for rapid functional analysis in insects. Development. 2013 Jan 15;140(2):454–8.

116. Hung R-J, Yazdani U, Yoon J, Wu H, Yang T, Gupta N, et al. Mical links semaphorins to F-actin disassembly. Nature. 2010 Feb 11;463(7282):823–7.

117. Keil TA. Functional Morphology of Insect Mechanoreceptors. Microsc Res Tech. 1997;39:506–31.

118. Golubyatnikov VP, Bukharina TA, Furman DP. A model study of the morphogenesis of D. melanogaster mechanoreceptors: the central regulatory circuit. J Bioinform Comput Biol. 2015 Feb;13(1):1540006.

119. Furman DP, Bukharina TA. Morphogenesis of Drosophila melanogaster macrochaetes: cell fate determination for bristle organ. J Stem Cells. 2012;7(1):19–41.

120. Guild GM, Connelly PS, Ruggiero L, Vranich KA, Tilney LG. Actin filament bundles in Drosophila wing hairs: hairs and bristles use different strategies for assembly. Mol Biol Cell. 2005 Aug;16(8):3620–31.

121. Stossberg M. Die Zellvorgange bei der entwicklung der flugelschuppen von Ephestia kuhniella Z. Zeitschrift fur Morphol und Okol der Tiere. 1938;34(2):173–206.

122. Galant R, Skeath JB, Paddock S, Lewis DL, Carroll SB. Expression pattern of a butterfly achaete-scute homolog reveals the homology of butterfly wing scales and insect sensory bristles. Curr Biol. 1998;8:807–13.

123. Tilney LG, DeRosier DJ. How to make a curved Drosophila bristle using straight actin bundles. Proc Natl Acad Sci U S A. 2005 Dec 27;102(52):18785–92.

124. Dinwiddie A, Null RW, Pizzano M, Chuong L, Krup AL, Tan HE, et al. Dynamics of F-actin prefigure the structure of butterfly wing scales. Dev Biol. 2014;392(2):404–18.

125. Ghiradella HT. Structure of butterfly scales: Patterning in an insect cuticle. Microsc Res Tech. 1994;27(5):429–38.

126. Overton J. Microtubules and microfibrils in morphogenesis of the scale cells of Ephestia kühniella. J Cell Biol. The Rockefeller University Press; 1966 May;29(2):293–305.

127. Tong XL, Dai FY, Su MK, Ma Y, Tan D, Zhang Z, et al. Identification and expression of the achaete-scute complex in the silkworm, Bombyx mori. Insect Mol Biol. 2008;17(4):395–404.

128. Reed RD. Evidence for Notch-mediated lateral inhibition in organizing butterfly wing scales. Dev Genes Evol. 2004;214(1):43–6.

129. Zhou QX, Li YN, Shen XJ, Yi YZ, Zhang YZ, Zhang ZF. The scaleless wings mutant in Bombyx mori is associated with a lack of scale precursor cell differentiation followed by excessive apoptosis. Dev Genes Evol. 2006;216(11):721–6.

130. Saranathan V, Osuji CO, Mochrie SGJ, Noh H, Narayanan S, Sandy A, et al. Structure, function, and self-assembly of single network gyroid (I4132) photonic crystals in butterfly wing scales. Proc Natl Acad Sci. 2010;107(26):11676–81.

131. Koch PB, Keys DN, Rocheleau T, Aronstein K, Blackburn M, Carroll SB, et al. Regulation of dopa decarboxylase expression during colour pattern formation in wild-type and melanic tiger swallowtail butterflies. Development. 1998;125(12):2303–13.

132. Reed RD, Nagy LM. Evolutionary redeployment of a biosynthetic module: expression of eye pigment genes vermilion, cinnabar, and white in butterfly wing development. Evol <html_ent glyph="@amp;" ascii="&"/> Dev. 2005 Jul;7(4):301–11.

133. Reed RD, McMillan WO, Nagy LM. Gene expression underlying adaptive variation in Heliconius wing patterns: non-modular regulation of overlapping cinnabar and vermilion prepatterns. Proc Biol Sci. 2008;275(1630):37–45.

134. Hines HM, Papa R, Ruiz M, Papanicolaou A, Wang C, Nijhout HF, et al. Transcriptome analysis reveals novel patterning and pigmentation genes underlying *Heliconius* butterfly wing pattern variation. BMC Genomics. BMC Genomics; 2012;13(1):288.

135. Ferguson LC, Jiggins CD. Shared and divergent expression domains on mimetic Heliconius wings. Evol Dev. 2009;11(5):498–512.

136. Morgan TH, Bridges CB. Sex-linked inheritance in Drosophila. Washington D.C.: Carnegie Institution of Washington; 1916. 98 p.

137. Overton J. The fine structure of developing bristles in wild type and mutant Drosophila melanogaster. J Morphol. 1967 Aug;122(4):367–79.

138. Tilney LG, Tilney MS, Guild GM. F actin bundles in Drosophila bristles. I. Two filament cross-links are involved in bundling. J Cell Biol. 1995 Aug;130(3):629–38.

139. Petersen NS, Lankenau DH, Mitchell HK, Young P, Corces VG. forked proteins are components of fiber bundles present in developing bristles of Drosophila melanogaster. Genetics. 1994;136(1).

140. Tilney LG, Connelly PS, Vranich KA, Shaw MK, Guild GM. Regulation of actin filament cross-linking and bundle shape in Drosophila bristles. J Cell Biol. 2000 Jan 10;148(1):87–100.

141. Kohler W, Feldotto W. Morphologische und experimentelle untersuchungen uber farbe, form und struktur der schuppen von Vanessa urticae und ihre gegenseitigen beziehungen. Arch für Entwicklungsmechanik der Org. 1937;(136):313–99.

142. Ohno Y, Otaki JM. Spontaneous long-range calcium waves in developing butterfly wings. BMC Dev Biol. BioMed Central; 2015;15(17).

143. Bitan A, Guild GM, Bar-Dubin D, Abdu U. Asymmetric microtubule function is an essential requirement for polarized organization of the Drosophila bristle. Mol Cell Biol. 2010 Jan 15;30(2):496–507.

144. Otani T, Oshima K, Onishi S, Takeda M, Shinmyozu K, Yonemura S, et al. IKKε

regulates cell elongation through recycling endosome shuttling. Dev Cell. 2011 Feb 15;20(2):219–32.

145. Bitan A, Rosenbaum I, Abdu U. Stable and dynamic microtubules coordinately determine and maintain Drosophila bristle shape. Development. 2012 Jun;139(11):1987–96.

146. Melkov A, Simchoni Y, Alcalay Y, Abdu U. Dynamic microtubule organization and mitochondrial transport are regulated by distinct Kinesin-1 pathways. Biol Open. 2015;4(12):1696–706.

147. Melkov A, Baskar R, Alcalay Y, Abdu U. A new mode of mitochondrial transport and polarized sorting regulated by Dynein, Milton and Miro. Development. 2016 Nov 15;143(22):4203–13.

148. Reed RD, Papa R, Martin A, Hines HM, Counterman BA, Pardo-Diaz C, et al. optix Drives the Repeated Convergent Evolution of Butterfly Wing Pattern Mimicry. Science (80-). 2011 Aug 26;333(6046):1137–41.

149. The Heliconius Genome Consortium, Dasmahapatra KK, Walters JR, Briscoe AD, Davey JW, Whibley A, et al. Butterfly genome reveals promiscuous exchange of mimicry adaptations among species. Nature. Nature Publishing Group; 2012;487(7405):94–8.

150. Zhan S, Zhang W, Niitepõld K, Hsu J, Haeger JF, Zalucki MP, et al. The genetics of monarch butterfly migration and warning colouration. Nature. 2014 Oct 16;514(7522):317–21.

151. Hume AN. Myosin - a monarch of pigment transport? Pigment Cell Melanoma Res. 2015 Mar;28(2):126–7.

152. Perry M, Kinoshita M, Saldi G, Huo L, Arikawa K, Desplan C. Molecular logic behind the three-way stochastic choices that expand butterfly colour vision. Nature. 2016 Jul 6;535(7611):280–4.

153. Brendza RP, Sheehan KB, Turner FR, Saxton WM. Clonal tests of conventional kinesin function during cell proliferation and differentiation. Mol Biol Cell. 2000 Apr;11(4):1329–43.

154. Hopmann R, Cooper JA, Miller KG. Actin organization, bristle morphology, and viability are affected by actin capping protein mutations in Drosophila. J Cell Biol. 1996 Jun;133(6):1293–305.

155. Wahlström G, Vartiainen M, Yamamoto L, Mattila PK, Lappalainen P, Heino TI. Twinfilin is required for actin-dependent developmental processes in Drosophila. J Cell Biol. 2001 Nov 26;155(5):787–96.

156. Otani T, Ogura Y, Misaki K, Maeda T, Kimpara A, Yonemura S, et al. IKKε inhibits PKC to promote Fascin-dependent actin bundling. Development. 2016;143(20).

157. Yoshioka S, Nakano T, Nozue Y, Kinoshita S. Coloration using higher order optical interference in the wing pattern of the Madagascan sunset moth. J R Soc

Interface. 2008;5(21):457–64.

158. Kishimoto S, Wang Q, Xie H, Zhao Y. Study of the surface structure of butterfly wings using the scanning electron microscopic moiré method. Appl Opt. 2007;46:7026–34.

159. Neville AC, Luke BM. A biological system producing a self-assembled cholesteric protein liquid crystal. J Cell Sci. 1971;8:93–109.

160. Lotan T, Chalifa-Caspi V, Ziv T, Brekhman V, Gordon MM, Admon A, et al. Evolutionary conservation of the mature oocyte proteome. EuPA Open Proteomics. 2014;3:27–36.

161. Plaza S, Chanut-Delalande H, Fernandes I, Wassarman PM, Payre F. From A to Z: apical structures and zona pellucida-domain proteins. Trends Cell Biol. Elsevier; 2010 Sep;20(9):524–32.

162. Jovine L, Darie CC, Litscher ES, Wassarman PM. Zona Pellucida Domain Proteins. Annu Rev Biochem. Annual Reviews; 2005 Jun;74(1):83–114.

163. Sapio MR, Hilliard MA, Cermola M, Favre R, Bazzicalupo P. The Zona Pellucida domain containing proteins, CUT-1, CUT-3 and CUT-5, play essential roles in the development of the larval alae in Caenorhabditis elegans. Dev Biol. 2005 Jun 1;282(1):231–45.

164. Singh RN, Sulston JE. Some Observations On Moulting in Caenorhabditis Elegans. Nematologica. Brill; 1978 Jan 1;24(1):63–71.

165. Fernandes I, Chanut-Delalande H, Ferrer P, Latapie Y, Waltzer L, Affolter M, et al. Zona Pellucida Domain Proteins Remodel the Apical Compartment for Localized Cell Shape Changes. Dev Cell. 2010 Jan;18(1):64–76.

166. Jaźwińska A, Ribeiro C, Affolter M. Epithelial tube morphogenesis during Drosophila tracheal development requires Piopio, a luminal ZP protein. Nat Cell Biol. 2003 Oct 14;5(10):895–901.

167. Sakaidani Y, Nomura T, Matsuura A, Ito M, Suzuki E, Murakami K, et al. O-linked-N-acetylglucosamine on extracellular protein domains mediates epithelial cell-matrix interactions. Nat Commun. Nature Publishing Group; 2011;2:583.

168. Nagaraj R, Adler PN. Dusky-like functions as a Rab11 effector for the deposition of cuticle during Drosophila bristle development. Development. 2012 Mar;139(5):906–16.

169. Adler PN, Sobala LF, Thom D, Nagaraj R. dusky-like is required to maintain the integrity and planar cell polarity of hairs during the development of the Drosophila wing. Dev Biol. 2013 Jul;379(1):76–91.

170. Li C, Yun X, Li B. Dusky-like is required for epidermal pigmentation and metamorphosis in Tribolium castaneum. Sci Rep. Nature Publishing Group; 2016;6:20102.

171. Sheue C-R, Sarafis V, Kiew R, Liu H-Y, Salino A, Kuo-Huang L-L, et al. Bizonoplast, a unique chloroplast in the epidermal cells of microphylls in the shade plant Selaginella erythropus (Selaginellaceae). Am J Bot. 2007 Dec 1;94(12):1922–9.

172. NASRULHAQ-BOYCE A, DUCKETT JG. Dimorphic epidermal cell chloroplasts in the mesophyll-less leaves of an extreme-shade tropical fern, Teratophyllum rotundifoliatum (R. Bonap.) Holtt.: a light and electron microscope study. New Phytol. Blackwell Publishing Ltd; 1991 Nov;119(3):433–44.

173. Graham RM, Lee DW, Norstog K. Physical and Ultrastructural Basis of Blue Leaf Iridescence in Two Neotropical Ferns. Am J Bot. 1993 Feb;80(2):198.

174. Knoll A, Horvat A, Lyakhova KS, Krausch G, Sevink GJA, Zvelindovsky A V., et al. Phase Behavior in Thin Films of Cylinder-Forming Block Copolymers. Phys Rev Lett. 2002 Jun 27;89(3):35501.

175. Özbek S. The cnidarian nematocyst: a miniature extracellular matrix within a secretory vesicle. Protoplasma. 2011 Oct 19;248(4):635–40.

176. Özbek S, Pokidysheva E, Schwager M, Schulthess T, Tariq N, Barth D, et al. The Glycoprotein NOWA and Minicollagens Are Part of a Disulfidelinked Polymer That Forms the Cnidarian Nematocyst Wall. J Biol Chem. 2004 Dec 10;279(50):52016–23.

177. Adamczyk P, Meier S, Gross T, Hobmayer B, Grzesiek S, Bächinger HP, et al. Minicollagen-15, a Novel Minicollagen Isolated from Hydra, Forms Tubule Structures in Nematocysts. J Mol Biol. 2008 Feb 29;376(4):1008–20.

178. Tursch A, Mercadante D, Tennigkeit J, Gräter F, Özbek S. Minicollagen cysteine-rich domains encode distinct modes of polymerization to form stable nematocyst capsules. Sci Rep. 2016 Sep 11;6(1):25709.

179. Beckmann A, Özbek S. The Nematocyst: a molecular map of the Cnidarian stinging organelle. Int J Dev Biol. 2012;56(6-7–8):577–82.

180. Pfeffer SR. Rab GTPases: master regulators of membrane trafficking. Curr Opin Cell Biol. 1994 Aug;6(4):522–6.

181. Dunst S, Kazimiers T, von Zadow F, Jambor H, Sagner A, Brankatschk B, et al. Endogenously tagged rab proteins: a resource to study membrane trafficking in Drosophila. Dev Cell. 2015 May 4;33(3):351–65.

182. Zhang J, Schulze KL, Hiesinger PR, Suyama K, Wang S, Fish M, et al. Thirty-One Flavors of Drosophila Rab Proteins. Genetics. 2006 Dec 6;176(2):1307–22.

183. Zhang J, Fonovic M, Suyama K, Bogyo M, Scott MP. Rab35 controls actin bundling by recruiting fascin as an effector protein. Science. 2009 Sep 4;325(5945):1250–4.

184. Purcell K, Artavanis-Tsakonas S. The developmental role of warthog, the notch modifier encoding Drab6. J Cell Biol. 1999 Aug 23;146(4):731–40.

185. Storrie B, Micaroni M, Morgan GP, Jones N, Kamykowski JA, Wilkins N, et al. Electron Tomography Reveals Rab6 Is Essential to the Trafficking of trans-Golgi Clathrin and COPI-Coated Vesicles and the Maintenance of Golgi Cisternal Number. Traffic. 2012 May;13(5):727–44.

186. Wassmer T, Attar N, Harterink M, van Weering JRT, Traer CJ, Oakley J, et al. The Retromer Coat Complex Coordinates Endosomal Sorting and Dynein-Mediated Transport, with Carrier Recognition by the trans-Golgi Network. Dev Cell. 2009 Jul;17(1):110–22.

187. Blaumueller CM, Qi H, Zagouras P, Artavanis-Tsakonas S. Intracellular cleavage of Notch leads to a heterodimeric receptor on the plasma membrane. Cell. 1997 Jul 25;90(2):281–91.

188. Logeat F, Bessia C, Brou C, LeBail O, Jarriault S, Seidah NG, et al. The Notch1 receptor is cleaved constitutively by a furin-like convertase. Proc Natl Acad Sci U S A. 1998 Jul 7;95(14):8108–12.

189. McConlogue L, Castellano F, deWit C, Schenk D, Maltese WA. Differential effects of a Rab6 mutant on secretory versus amyloidogenic processing of Alzheimer's beta-amyloid precursor protein. J Biol Chem. 1996 Jan 19;271(3):1343–8.

190. Verheyen EM, Purcell KJ, Fortini ME, Artavanis-Tsakonas S. Analysis of dominant enhancers and suppressors of activated Notch in Drosophila. Genetics. 1996 Nov;144(3):1127–41.

191. Zelazny B, Neville AC. Endocuticle layer formation controlled by non-circadian clocks in beetles. J Insect Physiol. 1972 Oct;18(10):1967–79.

192. Ito C, Goto SG, Shiga S, Tomioka K, Numata H. Peripheral circadian clock for the cuticle deposition rhythm in Drosophila melanogaster. Proc Natl Acad Sci. 2008 Jun 17;105(24):8446–51.

193. Ito C, Goto SG, Tomioka K, Numata H. Temperature Entrainment of the Circadian Cuticle Deposition Rhythm in Drosophila melanogaster. J Biol Rhythms. 2011 Feb;26(1):14–23.

194. Neville AC, Parry DA, Woodhead-Galloway J. The chitin crystallite in arthropod cuticle. J Cell Sci. 1976 Jun;21(1):73–82.

195. Neville AC. Biology of fibrous composites: development beyond the cell membrane. 1st ed. Cambridge: Press Syndicate of the University of Cambridge; 1993. 214 p.

196. Brady P, Cummings M. Differential response to circularly polarized light by the jewel scarab beetle Chrysina gloriosa. Am Nat. 2010;175(5):614–20.

197. Abouchar L, Petkova MD, Steinhardt CR, Gregor T. Fly wing vein patterns have spatial reproducibility of a single cell. J R Soc Interface. The Royal Society; 2014 Aug 6;11(97):20140443.

198. Ingram AL, Deparis O, Boulenguez J, Kennaway G, Berthier S, Parker AR.

Structural origin of the green iridescence on the chelicerae of the red-backed jumping spider, Phidippus johnsoni (Salticidae: Araneae). Arthropod Struct Dev. 2011;40(1):21–5.

199. Truebestein L, Elsner DJ, Fuchs E, Leonard TA. A molecular ruler regulates cytoskeletal remodelling by the Rho kinases. Nat Commun. 2015 Dec 1;6:10029.

200. Oda T, Yanagisawa H, Kamiya R, Kikkawa M. A molecular ruler determines the repeat length in eukaryotic cilia and flagella. Science (80-). 2014;346(6211):857–60.

201. Shyer AE, Tallinen T, Nerurkar NL, Wei Z, Gil ES, Kaplan DL, et al. Villification: How the Gut Gets Its Villi. Science (80-). 2013 Oct 11;342(6155):212–8.

202. Hissa B, Pontes B, Roma PMS, Alves AP, Rocha CD, Valverde TM, et al. Membrane Cholesterol Removal Changes Mechanical Properties of Cells and Induces Secretion of a Specific Pool of Lysosomes. Seaman M, editor. PLoS One. Public Library of Science; 2013 Dec 20;8(12):e82988.

203. Takei T, Yaguchi T, Fujii T, Nomoto T, Toyota T, Fujinami M. Measurement of membrane tension of free standing lipid bilayers via laser-induced surface deformation spectroscopy. Soft Matter. 2015 Nov 28;11(44):8641–7.

204. Hussain N, Siegel A, Johnson M, Naumann C. Cholesterol-Induced Buckling in Physisorbed Polymer-Tethered Lipid Monolayers. Polymers (Basel). 2013 Apr 26;5(2):404–17.

205. Gov NS, Gopinathan A. Dynamics of membranes driven by actin polymerization. Biophys J. The Biophysical Society; 2006 Jan 15;90(2):454–69.

206. Wallace AR. XVIII.— On the law which has regulated the introduction of new species. Ann Mag Nat Hist. 1855;16(93):184–96.

207. Darwin C. The Descent of Man, and Selection in Relation to Sex. 1st ed. London: John Murray; 1871.

208. Kettlewell HBD. Selection experiments on industrial melanism in the Lepidoptera. Heredity (Edinb). 1955;9:323–42.

209. Koch PB, Behnecke B, Ffrench-Constant RH. The molecular basis of melanism and mimicry in a swallowtail butterfly. Curr Biol. 2000 May;10(10):591–4.

210. Reed RD, Serfas MS. Butterfly Wing Pattern Evolution Is Associated with Changes in a Notch/Distal-less Temporal Pattern Formation Process. Curr Biol. 2004 Jul 13;14(13):1159–66.

211. Suzuki Y, Nijhout HF. Evolution of a Polyphenism by Genetic Accommodation. Science (80-). 2006 Feb 3;311(5761):650–2.

212. Nishikawa H, Iijima T, Kajitani R, Yamaguchi J, Ando T, Suzuki Y, et al. A genetic mechanism for female-limited Batesian mimicry in Papilio butterfly. Nat Genet. 2015 Mar 9;47(4):405–9.

213. Martin A, Reed RD. wingless and aristaless2 Define a Developmental Ground Plan for Moth and Butterfly Wing Pattern Evolution. Mol Biol Evol. 2010 Dec 1;27(12):2864–78.

214. Suzuki TK, Tomita S, Sezutsu H. Gradual and contingent evolutionary emergence of leaf mimicry in butterfly wing patterns. BMC Evol Biol. 2014;14(229):1–13.

215. ROTHSCHILD M, MUMMERY R. Carotenoids and bile pigments in Danaid and swallowtail butterflies. Biol J Linn Soc. Blackwell Publishing Ltd; 1985 Jan;24(1):1–14.

216. Stavenga DG, Giraldo M a, Leertouwer HL. Butterfly wing colors: glass scales of Graphium sarpedon cause polarized iridescence and enhance blue/green pigment coloration of the wing membrane. J Exp Biol. 2010;213(Pt 10):1731–9.

217. Vukusic P, Stavenga DG. Physical methods for investigating structural colours in biological systems. J R Soc Interface. 2009;6(Suppl 2):S133–48.

218. Berthier S. Photonique des Morphos. Paris: Springer Paris; 2010. 248 p.

219. Chazot N, Panara S, Zilbermann N, Blandin P, Le Poul Y, Cornette R, et al. Morpho morphometrics: Shared ancestry and selection drive the evolution of wing size and shape in Morpho butterflies. Evolution (N Y). 2016 Jan;70(1):181–94.

220. Berthier S, Charron E, Boulenguez J. Morphological structure and optical properties of the wings of Morphidae. Insect Sci. 2006;13:145–58.

221. Pandurangan V. Colours in posters since 1914 [Internet]. 2012. Available from: www.vijayp.ca/blog/2012/06/colours-in-movie-posters-since-1914/

222. Koch PB, Kaufmann N. Pattern specific melanin synthesis and DOPA decarboxylase activity in a butterfly wing of Precis coenia Hübner. Insect Biochem Mol Biol. 1995 Jan;25(1):73–82.

223. Koch PB. Colour pattern specific melanin synthesis is controlled by ecdysteroids via dopa decarboxylase in wings of Precis coenia (Lepidoptera: Nymphalidae). Eur J Entomol. 1995;92:161–7.

224. Koch PB. Wings of the Butterfly Precis coenia Synthesize Dopamine Melanin by Selective Enzyme Activity of Dopadecarboxylase. Naturwissenschaften. Springer-Verlag; 1994;81:36–8.

225. Vukusic P, Sambles JR, Lawrence CR, Wootton RJ. Quantified interference and diffraction in single Morpho butterfly scales. Proc R Soc London Ser B Biol Sci. The Royal Society; 1999 Jul 22;266(1427):1403–11.

226. Blandin P, Purser B. Evolution and diversification of Neotropical butterflies: Insights from the biogeography and phylogeny of the genus Morpho Fabricius, 1807 (Nymphalidae: Morphinae), with a review of the geodynamics of South America. Trop Lepid Res. 2013;23(2):62–85.

227. Ding Y, Xu S, Wang ZL. Structural colors from Morpho peleides butterfly wing

scales. J Appl Phys. 2009 Oct;106(7):74702.

228. Vukusic P, Kelly R, Hooper I. A biological sub-micron thickness optical broadband reflector characterized using both light and microwaves. J R Soc Interface. The Royal Society; 2009 Apr 6;6 Suppl 2(Suppl 2):S193-201.

229. Hsiung B-K, Blackledge TA, Shawkey MD. Spiders do have melanin after all. J Exp Biol. 2015 Nov 1;218(22):3632–5.

230. Ito K, Yoshikawa M, Fujii T, Tabunoki H, Yokoyama T. Melanin pigmentation gives rise to black spots on the wings of the silkworm Bombyx mori. J Insect Physiol. 2016 Aug;91–92:100–6.

231. Liu S, Wang M, Li X. Overexpression of Tyrosine hydroxylase and Dopa decarboxylase associated with pupal melanization in Spodoptera exigua. Sci Rep. 2015 Jun 18;5(1):11273.

232. Iwata M, Ohno Y, Otaki JM. Real-Time In Vivo Imaging of Butterfly Wing Development: Revealing the Cellular Dynamics of the Pupal Wing Tissue. Benoit JB, editor. PLoS One. Public Library of Science; 2014 Feb 21;9(2):e89500.

233. Futahashi R, Banno Y, Fujiwara H. Caterpillar color patterns are determined by a two-phase melanin gene prepatterning process: new evidence from tan and laccase2. Evol Dev. Blackwell Publishing Inc; 2010 Mar 17;12(2):157–67.

234. Futahashi R, Fujiwara H. Melanin-synthesis enzymes coregulate stage-specific larval cuticular markings in the swallowtail butterfly, Papilio xuthus. Dev Genes Evol. Springer-Verlag; 2005 Oct 25;215(10):519–29.

235. Wittkopp PJ, True JR, Carroll SB. Reciprocal functions of the Drosophila yellow and ebony proteins in the development and evolution of pigment patterns. Development. 2002 Apr;129(8):1849–58.

236. Ishizaki Y, Umebachi Y. Level changes of beta-alanine, dopamine, and N-beta-alanyldopamine during the pupal stage of Papilio xuthus (Lepidoptera:Papilionidae). Comp Biochem Physiol. Pergamon Press; 1988;90C(1):83–7.

237. Ishizaki Y, Umebachi Y. Further studies on dopamine and during the pupal stage of Papilio xuthus (Lepidoptera: Papilionidae). Comp Biochem Physiol Part B Comp Biochem. 1990 Jan;97(3):563–7.

238. Stathakis DG, Burton DY, McIvor WE, Krishnakumar S, Wright TR, O'Donnell JM. The catecholamines up (Catsup) protein of Drosophila melanogaster functions as a negative regulator of tyrosine hydroxylase activity. Genetics. 1999 Sep;153(1):361–82.

239. Hiruma K, Riddiford LM, Hopkins TL, Morgan TD. Roles of dopa decarboxylase and phenoloxidase in the melanization of the tobacco hornworm and their control by 20-hydroxyecdysone. J Comp Physiol B. 1985;155(6):659–69.

240. Hiruma K, Riddiford LM. Regulation of melanization of tobacco hornworm larval

cuticle in vitro. J Exp Zool. 1984 Jun;230(3):393–403.

241. Ninomiya Y, Tanaka K, Hayakawa Y. Mechanisms of black and white stripe pattern formation in the cuticles of insect larvae. J Insect Physiol. 2006 Jun;52(6):638–45.

242. Koch PB, Keys DN, Rocheleau T, Aronstein K, Blackburn M, Carroll SB, et al. Regulation of dopa decarboxylase expression during colour pattern formation in wild-type and melanic tiger swallowtail butterflies. Development. The Company of Biologists Ltd; 1998 Jun;125(12):2303–13.

243. MATĚJKOVÁ-PLSKOVA J, SHIOJIRI S, SHIOJIRI M. Fine structures of wing scales in Sasakia charonda butterflies as photonic crystals. J Microsc. Blackwell Publishing Ltd; 2009 Nov;236(2):88–93.

244. Han Z, Wu L, Qiu Z, Ren L. Microstructure and structural color in wing scales of butterfly Thaumantis diores. Chinese Sci Bull. SP Science in China Press; 2009 Feb 12;54(4):535–40.

245. Han Z, Wu L, Qiu Z, Guan H, Ren L. Structural Colour in Butterfly Apatura ilia Scales and the Microstructure Simulation of Photonic Crystal. J Bionic Eng. 2008 Sep;5:14–9.

246. Ghiradella HT, Aneshansley D, Eisner T, Silberglied RE, Hinton HE. Ultraviolet Reflection of a Male Butterfly: Interference Color Caused by Thin-Layer Elaboration of Wing Scales. Science (80-). 1972 Dec 15;178(4066):1214–7.

247. Lamason RL, Manzoor-Ali PKM, Mest JR, Wong AC, Norton HL, Aros MC, et al. SLC24A5, a Putative Cation Exchanger, Affects Pigmentation in Zebrafish and Humans. Science (80-). 2005;310(5755):1782–6.

248. Daniels E V, Murad R, Mortazavi A, Reed RD. Extensive transcriptional response associated with seasonal plasticity of butterfly wing patterns. Mol Ecol. 2014 Dec;23(24):6123–34.

249. Koch PB, Merk R, Reinhardt R, Weber P. Localization of ecdysone receptor protein during colour pattern formation in wings of the butterfly Precis coenia (Lepidoptera: Nymphalidae) and co-expression with Distal-less protein. Dev Genes Evol. 2003;212(12):571–84.

250. True JR, Edwards KA, Yamamoto D, Carroll SB. Drosophila wing melanin patterns form by vein-dependent elaboration of enzymatic prepatterns. Curr Biol. 1999 Dec 2;9(23):1382–91.

251. Futahashi R, Fujiwara H. Regulation of 20-hydroxyecdysone on the larval pigmentation and the expression of melanin synthesis enzymes and yellow gene of the swallowtail butterfly, Papilio xuthus. Insect Biochem Mol Biol. 2007 Aug;37(8):855–64.

252. Koch PB, Behnecke B, Weigmann-Lenz M, Ffrench-Constant RH. Insect pigmentation: activities of β-alanyldopamine synthase in wing color patterns of wild-type and melanic mutant swallowtail butterfly Papilio glaucus. Pigment Cell

Res. 2000;13:54–8.

253. Ferguson LC, Maroja LS, Jiggins CD. Convergent, modular expression of ebony and tan in the mimetic wing patterns of Heliconius butterflies. Dev Genes Evol. 2011;221(5–6):297–308.

254. Piskur J, Kolbak D, Søndergaard L, Pedersen MB. The dominant mutation Suppressor of black indicates that de novo pyrimidine biosynthesis is involved in the Drosophila tan pigmentation pathway. Mol Gen Genet. 1993;241(3–4):335–40.

255. Futahashi R, Sato J, Meng Y, Okamoto S, Daimon T, Yamamoto K, et al. yellow and ebony are the responsible genes for the larval color mutants of the silkworm Bombyx mori. Genetics. 2008;180(4):1995–2005.

256. Leertouwer HL, Wilts BD, Stavenga DG. Refractive index and dispersion of butterfly chitin and bird keratin measured by polarizing interference microscopy. Opt Express. 2011 Nov 21;19(24):24061.

257. Stavenga DG, Leertouwer HL, Wilts BD. Quantifying the refractive index dispersion of a pigmented biological tissue using Jamin–Lebedeff interference microscopy. Light Sci Appl. 2013;2(9):e100.

258. Choussy M, Barbier M. Pigments biliaires des lépidoptères: Identification de la phorcabiline I et de la sarpédobiline chez diverses espèces. Biochem Syst Ecol. 1973 Dec;1(4):199–201.

259. Condamine FL, Toussaint EFA, Cotton AM, Genson GS, Sperling FAH, Kergoat GJ. Fine-scale biogeographical and temporal diversification processes of peacock swallowtails (Papilio subgenus Achillides) in the Indo-Australian Archipelago. Cladistics. 2013;29(1):88–111.

260. Cassildé C, Blandin P, Silvain J. Phylogeny of the genus Morpho Fabricius 1807: insights from two mitochondrial genes (Lepidoptera: Nymphalidae). Ann la Société Entomol Fr. 2012;48(1–2):173–88.

261. Yoshioka S, Kinoshita S. Polarization-sensitive color mixing in the wing of the Madagascan sunset moth. Opt Express. 2007;15(5):2691–701.

262. Kolle M, Salgard-Cunha PM, Scherer MRJ, Huang F, Vukusic P, Mahajan S, et al. Mimicking the colourful wing scale structure of the Papilio blumei butterfly. Nat Nanotechnol. Nature Publishing Group; 2010;5(7):511–5.

263. Tilney LG, Connelly PS, Smith S, Guild GM. F-actin bundles in Drosophila bristles are assembled from modules composed of short filaments. J Cell Biol. 1996 Dec;135(5):1291–308.

264. Tilney LG, Connelly PS, Guild GM. Microvilli appear to represent the first step in actin bundle formation in Drosophila bristles. J Cell Sci. 2004 Jul 15;117(Pt 16):3531–8.

265. Guild GM, Connelly PS, Ruggiero L, Vranich KA, Tilney LG. Long continuous

actin bundles in Drosophila bristles are constructed by overlapping short filaments. J Cell Biol. 2003 Sep 15;162(6):1069–77.

266. Futahashi R, Kurita R, Mano H, Fukatsu T. Redox alters yellow dragonflies into red. Proc Natl Acad Sci U S A. National Academy of Sciences; 2012 Jul 31;109(31):12626–31.

267. Singert SJ. Tyrosine phosphorylation accompanying the cellularization of the syncytial blastoderm of Drosophila. 1995;92(August):8154–7.

268. Mazumdar A, Mazumdar M. How one becomes many: Blastoderm cellularization in Drosophila melanogaster. BioEssays. 2002;24(11):1012–22.

269. Loncar D, Singer SJ. Cell membrane formation during the cellularization of the syncytial blastoderm of Drosophila. Proc Natl Acad Sci U S A. 1995;92(6):2199–203.

270. Mavrakis M, Azou-Gros Y, Tsai F-C, Alvarado J, Bertin A, Iv F, et al. Septins promote F-actin ring formation by crosslinking actin filaments into curved bundles. Nat Cell Biol. 2014;16(4):322–34.

271. Paschinger K, Rendić D, Wilson IBH. Revealing the anti-HRP epitope in Drosophila and Caenorhabditis. Glycoconj J. Springer US; 2009 Apr 26;26(3):385–95.

272. Tilney LG, Connelly PS, Vranich KA, Shaw MK, Guild GM. Actin filaments and microtubules play different roles during bristle elongation in Drosophila. J Cell Sci. 2000 Apr;1255–65.

273. Frank DJ, Hopmann R, Lenartowska M, Miller KG. Capping protein and the Arp2/3 complex regulate nonbundle actin filament assembly to indirectly control actin bundle positioning during Drosophila melanogaster bristle development. Mol Biol Cell. 2006 Sep;17(9):3930–9.

274. Hopmann R, Miller KG. A balance of capping protein and profilin functions is required to regulate actin polymerization in Drosophila bristle. Mol Biol Cell. 2003 Jan;14(1):118–28.

275. Appel LF, Prout M, Abu-Shumays R, Hammonds AS, Garbe JC, Fristrom D, et al. The Drosophila Stubble-stubbloid gene encodes an apparent transmembrane serine protease required for epithelial morphogenesis. Proc Natl Acad Sci U S A. 1993 Jun 1;90(11):4937–41.

276. Bayer CA, Halsell SR, Fristrom JW, Kiehart DP, von Kalm L. Genetic interactions between the RhoA and Stubble-stubbloid loci suggest a role for a type II transmembrane serine protease in intracellular signaling during Drosophila imaginal disc morphogenesis. Genetics. 2003 Nov;165(3):1417–32.

277. Hammonds AS, Fristrom JW. Mutational analysis of Stubble-stubbloid gene structure and function in Drosophila leg and bristle morphogenesis. Genetics. 2006 Mar;172(3):1577–93.

278. Yong E. 3-D Scans Reveal Caterpillars Turning Into Butterflies [Internet]. National Geographic: Not Exactly Rocket Science Blog. 2013. Available from: http://phenomena.nationalgeographic.com/2013/05/14/3-d-scans-caterpillars-transforming-butterflies-metamorphosis/

279. Lowe T, Garwood RJ, Simonsen TJ, Bradley RS, Withers PJ. Metamorphosis revealed: time-lapse three-dimensional imaging inside a living chrysalis. J R Soc Interface. 2013;10(84).

280. Ohno Y, Otaki JM. Live Cell Imaging of Butterfly Pupal and Larval Wings In Vivo. Breuker C, editor. PLoS One. Public Library of Science; 2015 Jun 24;10(6):e0128332.

281. Marcus JM, Ramos DM, Monteiro A. Germline transformation of the butterfly Bicyclus anynana. Proc R Soc B Biol Sci. 2004;271(Suppl_5):S263–5.

282. Uhlirova M, Asahina M, Riddiford LM, Jindra M. Heat-inducible transgenic expression in the silkmoth Bombyx mori. Dev Genes Evol. 2002;212(3):145–51.

283. Pierre C, Toshiki T, Chantal T, Corinne R, Toshio K, Eappen A, et al. Germline transformation of the silkworm Bombyx mori L. using a piggyBac transposon-derived vector. Nat Biotechnol. 2000 Jan 1;18(1):81–4.

284. Lewis DL, Brunetti CR. Ectopic transgene expression in butterfly imaginal wing discs using vaccinia virus. Biotechniques. 2006;40(1):48–54.

285. Uhlirova M, Foy BD, Beaty BJ, Olson KE, Riddiford LM, Jindra M. Use of Sindbis virus-mediated RNA interference to demonstrate a conserved role of Broad-Complex in insect metamorphosis. Proc Natl Acad Sci U S A. 2003;100(26):15607–12.

286. Lewis DL, DeCamillis MA, Brunetti CR, Halder G, Kassner VA, Selegue JE, et al. Ectopic gene expression and homeotic transformations in arthropods using recombinant Sindbis viruses. Curr Biol. 1999 Nov 18;9(22):1279–87.

287. Dhungel B, Ohno Y, Matayoshi R, Otaki JM. Baculovirus-mediated gene transfer in butterfly wings in vivo: an efficient expression system with an anti-gp64 antibody. BMC Biotechnol. 2013 Mar 25;13(1):27.

288. Osanai-Futahashi M, Ohde T, Hirata J, Uchino K, Futahashi R, Tamura T, et al. A visible dominant marker for insect transgenesis. Nat Commun. Nature Publishing Group; 2012;3:1295.

289. Adachi T, Tomita M, Shimizu K, Ogawa S, Yoshizato K. Generation of hybrid transgenic silkworms that express Bombyx mori prolyl-hydroxylase α-subunits and human collagens in posterior silk glands: Production of cocoons that contained collagens with hydroxylated proline residues. J Biotechnol. 2006;126(2):205–19.

290. Tomita M, Munetsuna H, Sato T, Adachi T, Hino R, Hayashi M, et al. Transgenic silkworms produce recombinant human type III procollagen in cocoons. Nat Biotechnol. Nature Publishing Group; 2002 Dec 16;21(1):52–6.

291. Ogawa S, Tomita M, Shimizu K, Yoshizato K. Generation of a transgenic silkworm that secretes recombinant proteins in the sericin layer of cocoon: Production of recombinant human serum albumin. J Biotechnol. 2007;128(3):531–44.

292. Ramos DM, Kamal F, Wimmer E a, Cartwright AN, Monteiro A. Temporal and spatial control of transgene expression using laser induction of the hsp70 promoter. BMC Dev Biol. 2006;6:55.

293. Moto K, Abdel Salam SE, Sakurai S, Iwami M. Gene transfer into insect brain and cell-specific expression of bombyxin gene. Dev Genes Evol. 1999;209(7):447–50.

294. Golden K, Sagi V, Markwarth N, Chen B, Monteiro A. In vivo electroporation of DNA into the wing epidermis of the butterfly, Bicyclus anynana. J Insect Sci. 2007;7(53):1–8.

295. Zhou F, Gao Z, Lv Z, Chen J, Hong Y, Yu W, et al. Construction of the ie1-Bacmid expression system and its use to express EGFP and BmAGO2 in BmN cells. Appl Biochem Biotechnol. 2013;169(8):2237–47.

296. del Valle Rodríguez A, Didiano D, Desplan C. Power tools for gene expression and clonal analysis in Drosophila. Nat Methods. NIH Public Access; 2011 Dec 28;9(1):47–55.

297. Luan H, Peabody NC, Vinson CR, White BH. Refined spatial manipulation of neuronal function by combinatorial restriction of transgene expression. Neuron. NIH Public Access; 2006 Nov 9;52(3):425–36.

298. Kojima K, Oritani K, Nakatsukasa T, Asano S, Sahara K, Bando H. Ecdysone response element in a baculovirus immediate-early gene, ie1, promoter. Virus Res. 2007;130(1):202–9.

299. Diao F, White BH. A novel approach for directing transgene expression in Drosophila: T2A-Gal4 in-frame fusion. Genetics. 2012;190(3):1139–44.

300. Riedl J, Crevenna AH, Kessenbrock K, Yu JH, Neukirchen D, Bista M, et al. Lifeact: a versatile marker to visualize F-actin. Nat Methods. NIH Public Access; 2008 Jul;5(7):605–7.

301. Lees AD, Picken LER. Shape in Relation to Fine Structure in the Bristles of Drosophila melanogaster. Proc R Soc London B Biol Sci. 1945;132(869):396–423.

302. Zhang M, Chang H, Zhang Y, Yu J, Wu L, Ji W, et al. Rational design of true monomeric and bright photoactivatable fluorescent proteins. Nat Methods. 2012 May 13;9(7):727–9.

303. Shcherbakova DM, Sengupta P, Lippincott-Schwartz J, Verkhusha V V. Photocontrollable fluorescent proteins for superresolution imaging. Annu Rev Biophys. NIH Public Access; 2014;43:303–29.

304. Wu YI, Frey D, Lungu OI, Jaehrig A, Schlichting I, Kuhlman B, et al. A genetically encoded photoactivatable Rac controls the motility of living cells. Nature. 2009

Sep 3;461(7260):104–8.

305. Pudasaini A, El-Arab KK, Zoltowski BD. LOV-based optogenetic devices: light-driven modules to impart photoregulated control of cellular signaling. Front Mol Biosci. 2015;2:18.

306. Dubin-Bar D, Bitan A, Bakhrat A, Kaiden-Hasson R, Etzion S, Shaanan B, et al. The Drosophila IKK-related kinase (Ik2) and Spindle-F proteins are part of a complex that regulates cytoskeleton organization during oogenesis. BMC Cell Biol. 2008 Sep 17;9(1):51.

307. Koch N, Dharmalingam E, Westermann M, Qualmann B, Thomas U, Kessels MM. Abp1 utilizes the Arp2/3 complex activator Scar/WAVE in bristle development. J Cell Sci. 2012;125(15):3578–89.

308. Niopek D, Wehler P, Roensch J, Eils R, Di Ventura B. Optogenetic control of nuclear protein export. Nat Commun. Nature Publishing Group; 2016 Feb 8;7:10624.

309. Niopek D, Benzinger D, Roensch J, Draebing T, Wehler P, Eils R, et al. Engineering light-inducible nuclear localization signals for precise spatiotemporal control of protein dynamics in living cells. Nat Commun. Nature Publishing Group; 2014 Jul 14;5:27–41.

310. Moussian B, Letizia A, Martínez-Corrales G, Rotstein B, Casali A, Llimargas M. Deciphering the genetic programme triggering timely and spatially-regulated chitin deposition. PLoS Genet. 2015 Jan;11(1):e1004939.

311. Yusa K, Zhou L, Li MA, Bradley A, Craig NL. A hyperactive piggyBac transposase for mammalian applications. Proc Natl Acad Sci U S A. National Academy of Sciences; 2011 Jan 25;108(4):1531–6.

312. Wilson MH, Coates CJ, George AL. PiggyBac Transposon-mediated Gene Transfer in Human Cells. Mol Ther. 2007 Jan;15(1):139–45.

313. Adey A, Morrison HG, Asan, Xun X, Kitzman JO, Turner EH, et al. Rapid, low-input, low-bias construction of shotgun fragment libraries by high-density in vitro transposition. Genome Biol. BioMed Central; 2010;11(12):R119.

314. Tilney LG, Connelly PS, Ruggiero L, Vranich KA, Guild GM. Actin filament turnover regulated by cross-linking accounts for the size, shape, location, and number of actin bundles in Drosophila bristles. Mol Biol Cell. 2003 Oct;14(10):3953–66.

315. Shapira S, Bakhrat A, Bitan A, Abdu U. The Drosophila javelin Gene Encodes a Novel Actin-Associated Protein Required for Actin Assembly in the Bristle. Mol Cell Biol. 2011 Nov 15;31(22):4582–92.

316. Nappi AJ, Christensen BM. Melanogenesis and associated cytotoxic reactions: Applications to insect innate immunity. Insect Biochem Mol Biol. 2005;35(5):443–59.

317. Serfas MS, Carroll SB. Pharmacologic approaches to butterfly wing patterning: sulfated polysaccharides mimic or antagonize cold shock and alter the interpretation of gradients of positional information. Dev Biol. 2005 Nov 15;287(2):416–24.

318. De Prins J, Saitoh K. Karyology and Sex Determination. In: Kristensen NP, editor. Handbook of Zoology Lepidoptera, Moths and Butterflies, Vol 2. de Gruyter; 2003. p. 449–68.

319. Marshall WS. Development of the frenulum of the wax moth, Galleria mellonella, Linn. Trans Wisconsin Acad Sci Arts, Lett. 1921;20:199–204.

320. Cho EH, Nijhout HF. Development of polyploidy of scale-building cells in the wings of Manduca sexta. Arthropod Struct Dev. Elsevier Ltd; 2013;42(1):37–46.

321. Hassan BA, Prokopenko SN, Breuer S, Zhang B, Paululat A, Bellen HJ. skittles, a Drosophila phosphatidylinositol 4-phosphate 5-kinase, is required for cell viability, germline development and bristle morphology, but not for neurotransmitter release. Genetics. 1998 Dec;150(4):1527–37.

322. Verheyen EM, Cooley L. Profilin mutations disrupt multiple actin-dependent processes during Drosophila development. Development. 1994 Apr;120(4):717–28.

323. Cant K, Cooley L. Single amino acid mutations in Drosophila fascin disrupt actin bundling function in vivo. Genetics. 1996 May;143(1):249–58.

324. Gervais L, Claret S, Januschke J, Roth S, Guichet A. PIP5K-dependent production of PIP2 sustains microtubule organization to establish polarized transport in the Drosophila oocyte. Development. 2008 Dec 23;135(23):3829–38.

325. Zhang L, Mao YS, Janmey PA, Yin HL. Phosphatidylinositol 4, 5 Bisphosphate and the Actin Cytoskeleton. In: Sub-cellular biochemistry. 2012. p. 177–215.

326. Kakumoto T, Nakata T, Bewick G, Hope T, Bamburg J. Optogenetic Control of PIP3: PIP3 Is Sufficient to Induce the Actin-Based Active Part of Growth Cones and Is Regulated via Endocytosis. Datta PK, editor. PLoS One. Public Library of Science; 2013 Aug 7;8(8):e70861.

327. Dechkrong P, Jiwajinda S, Dokchan P, Kongtungmon M, Chomsaeng N, Chairuangsri T, et al. Fine structure of wing scales of butterflies, Euploea mulciber and Troides aeacus. J Struct Biol. Elsevier Inc.; 2011;176(1):75–82.

328. Anderson TF, Richards AG. An electron microscope study of some structural colors of insects. J Appl Phys. 1942;13(12):748–58.

329. Yoshioka S, Kinoshita S. Wavelength-selective and anisotropic light-diffusing scale on the wing of the Morpho butterfly. Proc Biol Sci. 2004;271(1539):581–7.

330. Xu K, Zhong G, Zhuang X. Actin, spectrin, and associated proteins form a periodic cytoskeletal structure in axons. Science. 2013 Jan 25;339(6118):452–6.

331. Hannezo E, Dong B, Recho P, Joanny J-F, Hayashi S. Cortical instability drives periodic supracellular actin pattern formation in epithelial tubes. Proc Natl Acad Sci. 2015 Jul 14;112(28):8620–5.

332. Franke JD, Montague RA, Kiehart DP. Nonmuscle myosin II is required for cell proliferation, cell sheet adhesion and wing hair morphology during wing morphogenesis. Dev Biol. 2010 Sep;345(2):117–32.

333. Locke M. The Formation of Tracheae and Tracheoles in Rhodnius prolixus. J Cell Sci. 1958;s3-99(45).

334. Dubin-Bar D, Bitan A, Bakhrat A, Amsalem S, Abdu U. Drosophila javelin-like encodes a novel microtubule-associated protein and is required for mRNA localization during oogenesis. Development. 2011 Nov 1;138(21):4661–71.

335. Guild GM, Connelly PS, Vranich KA, Shaw MK, Tilney LG. Actin filament turnover removes bundles from Drosophila bristle cells. J Cell Sci. 2002;115(3).

336. Deng H, Lee JK, Goldstein LSB, Branton D. Drosophila Development Requires Spectrin Network Formation. J Cell Biol. 1995;128(1–2):71–9.

337. Liem RKH. Cytoskeletal Integrators: The Spectrin Superfamily. Cold Spring Harb Perspect Biol. 2016 Oct 3;8(10):a018259.

338. Pollard TD. Actin and Actin-Binding Proteins. Cold Spring Harb Perspect Biol. 2016 Aug 1;8(8):a018226.

339. Mummery-Widmer JL, Yamazaki M, Stoeger T, Novatchkova M, Bhalerao S, Chen D, et al. Genome-wide analysis of Notch signalling in Drosophila by transgenic RNAi. Nature. 2009 Apr 23;458(7241):987–92.

340. Craig DH, Haimovich B, Basson MD. alpha-Actinin-1 phosphorylation modulates pressure-induced colon cancer cell adhesion through regulation of focal adhesion kinase-Src interaction. AJP Cell Physiol. 2007 Oct 3;293(6):C1862–74.

341. Shao H, Wu C, Wells A. Phosphorylation of alpha-Actinin 4 upon Epidermal Growth Factor Exposure Regulates Its Interaction with Actin. J Biol Chem. 2010 Jan 22;285(4):2591–600.

342. Hudson AM, Cooley L. A subset of dynamic actin rearrangements in Drosophila requires the Arp2/3 complex. J Cell Biol. 2002 Feb 18;156(4):677–87.

343. Callan-Jones A, Sorre B, Bassereau P. Curvature-driven lipid sorting in biomembranes. Cold Spring Harb Perspect Biol. Cold Spring Harbor Laboratory Press; 2011 Feb 1;3(2).

344. Balcer HI, Daugherty-Clarke K, Goode BL. The p40/ARPC1 Subunit of Arp2/3 Complex Performs Multiple Essential Roles in WASp-regulated Actin Nucleation. J Biol Chem. 2010 Mar 12;285(11):8481–91.

345. Boseman A, Nowlin K, Ashraf S, Yang J, Lajeunesse D. Ultrastructural analysis of wild type and mutant Drosophila melanogaster using helium ion microscopy.

Micron. 2013 Aug;51:26–35.

346. Cox GN, Kusch M, Edgar RS. Cuticle of Caenorhabditis elegans: its isolation and partial characterization. J Cell Biol. 1981 Jul;90(1):7–17.

347. Cox GN, Staprans S, Edgar RS. The cuticle of Caenorhabditis elegans. II. Stage-specific changes in ultrastructure and protein composition during postembryonic development. Dev Biol. 1981 Sep;86(2):456–70.

348. Costa M, Draper BW, Priess JR. The role of actin filaments in patterning the Caenorhabditis elegans cuticle. Dev Biol. 1997 Apr 15;184(2):373–84.

349. Broday L, Kolotuev I, Didier C, Bhoumik A, Podbilewicz B, Ronai Z. The LIM domain protein UNC-95 is required for the assembly of muscle attachment structures and is regulated by the RING finger protein RNF-5 in *C. elegans*. J Cell Biol. 2004 Jun 21;165(6):857–67.

350. Broday L, Hauser CA, Kolotuev I, Ronai Z. Muscle–epidermis interactions affect exoskeleton patterning in Caenorhabditis elegans. Dev Dyn. Wiley-Liss, Inc.; 2007 Nov;236(11):3129–36.

351. Campos-Fernández C, Azofeifa DE, Hernández-Jiménez M, Ruiz-Ruiz A, Vargas WE. Visible light reflection spectra from cuticle layered materials. Opt Mater Express. Optical Society of America; 2011 May 1;1(1):85.

352. Ray RP, Matamoro-Vidal A, Ribeiro PS, Tapon N, Houle D, Salazar-Ciudad I, et al. Patterned Anchorage to the Apical Extracellular Matrix Defines Tissue Shape in the Developing Appendages of Drosophila. Dev Cell. 2015 Aug;34(3):310–22.

353. Tilney LG, Connelly PS, Ruggiero L, Vranich KA, Guild GM, DeRosier DJ. The Role Actin Filaments Play in Providing the Characteristic Curved Form of Drosophila Bristles. Mol Biol Cell. 2004 Sep 22;15(12):5481–91.

354. Yan J, Huen D, Morely T, Johnson G, Gubb D, Roote J, et al. The multiple-wing-hairs gene encodes a novel GBD-FH3 domain-containing protein that functions both prior to and after wing hair initiation. Genetics. Genetics Society of America; 2008 Sep;180(1):219–28.

355. Aigouy B, Farhadifar R, Staple DB, Sagner A, Röper J-C, Jülicher F, et al. Cell Flow Reorients the Axis of Planar Polarity in the Wing Epithelium of Drosophila. Cell. 2010 Sep;142(5):773–86.

356. Siddique RH, Gomard G, Hölscher H, Arikawa K, Vigneron JP. The role of random nanostructures for the omnidirectional anti-reflection properties of the glasswing butterfly. Nat Commun. Nature Publishing Group; 2015 Apr 22;6:6909.

357. Stavenga D., Foletti S, Palasantzas G, Arikawa K. Light on the moth-eye corneal nipple array of butterflies. Proc R Soc B Biol Sci. 2006 Mar 22;273(1587):661–7.

358. Perez Goodwyn P, Maezono Y, Hosoda N, Fujisaki K. Waterproof and translucent wings at the same time: Problems and solutions in butterflies. Naturwissenschaften. 2009;96(7):781–7.

359. Kryuchkov M, Katanaev VL, Enin GA, Sergeev A, Timchenko AA, Serdyuk IN. Analysis of Micro- and Nano-Structures of the Corneal Surface of Drosophila and Its Mutants by Atomic Force Microscopy and Optical Diffraction. Uversky VN, editor. PLoS One. IRL Press; 2011 Jul 21;6(7):e22237.

360. Ren N, He B, Stone D, Kirakodu S, Adler PN. The shavenoid Gene of Drosophila Encodes a Novel Actin Cytoskeleton Interacting Protein That Promotes Wing Hair Morphogenesis. Genetics. 2005 Dec 30;172(3):1643–53.

361. Marygold SJ, Roote J, Reuter G, Lambertsson A, Ashburner M, Millburn GH, et al. The ribosomal protein genes and Minute loci of Drosophila melanogaster. Genome Biol. BioMed Central; 2007;8(10):R216.

362. Chanut-Delalande H, Fernandes I, Roch F, Payre F, Plaza S. Shavenbaby Couples Patterning to Epidermal Cell Shape Control. Martinez Arias A, editor. PLoS Biol. Cold Spring Harbor Laboratory Press; 2006 Aug 22;4(9):e290.

Appendix 1

Lepidopteran Scale Development Candidate Identification based on Mummery-Widmer Bristle RNAi Screen

Introduction

Drosophila melanogaster is a model insect that has many advantages for research studies. Among these are the ability to express constructs in a cell specific manner. Though lacking structurally colored scales homologous to butterflies, Drosophila do produce mechanosensory bristles, which are born from a homologous cell type, the sensory organ precursor (SOP). In 2009, Jennifer Mummery-Widmer and her collaborators published the results of an RNAi screen directed at knocking down 82.2% of the protein coding genes in the pupal notum of *Drosophila* (348). The results of their screening (20,262 RNAi lines driven by the dorsal notum driver *pnr:*Gal4) were also published online along with their scoring of a handful of categories including macrochaete morphogenesis. The published paper focused upon defects similar to Notch signaling – not on morphogenesis. We believe that screens like this could prove very useful for identifying and testing candidates of scale development.

Methods

From the Knoblich lab's website (http://bristlescreen.imba.oeaw.ac.at), we pulled all genes with an attributed morphological defect. It is worth mentioning that the metric by which they scored their data was percent of notum with a defect, not magnitude of a defect – thus a 10 represents the largest area of defects seen not the most dramatic of defect morphologically. Further it is worth mentioning that the driver chosen (pnr:Gal4) is a pan-dorsal notum driver, not a driver specific to the SOPs. This means that some defects may be non-cell autonomously derived.

Once the genes with morphological function were collected, we then used Flybase to obtain GO Term, Cellular, and molecular function data for the genes. Since we had an interest in scale morphogenesis, we came up with a set of search terms associated with morphogenesis. We searched the Flybase data for these keywords and characterized genes based on these interests.

Results

From 593 genes assigned some morphological phenotype, 70 had no GO Term of interest (GOTOI). 175 genes had at least one "Membrane" classed GO Term, 85 had at least one "Actin" classed GO Term, 68 "Tubulin", 21 "ER", 4 "Golgi", 68 "Chitin/ECM", 192 "Ploidy/Growth/Size", 81 with "Planar Cell Polarity (PCP)", 277 with "Morphogenesis/Chaete", 223 "Signal Transduction", and 219 with "Transcription/Translation". Within each of these we ranked the individual search terms and found sometimes surprising results such as "Microtubule" was found in 100% of "Microtubule" class genes, but "Tubulin" was found in only ~6%. Similarly, "Transcription"

was found in 84% of the “Transcription/Translation” class but the term “Translation” was found only in ~17%. This extreme bias was not found in all classes of terms, Chitin/ECM and PCP classes both feature flatter distributions among their search terms. Whether these biases reflect biologically relevant differences among developing bristles or whether they appear as a function of GO Term encoding/searching is unclear.

Wingless returned the single highest number of GO Term classes represented by a gene at 9 (Membrane, Actin, ER, Chitin/ECM, Ploidy/Growth/Size, PCP, Morphogenesis, Signal/Transduction, and Txn/Tln), while 108 genes (18.2%) had only a single GO Term Class represented.

We also found 12 genes that have morphological phenotypes according to Mummery-Widmer’s data that have been assigned CG numbers by Flybase but have not been further characterized. Among these there were 3 with GO Terms of interest, specifically “Membrane”, “Ploidy”, “Morphogenesis”, and “Signal Transduction”. CG32301 has sequence indicating nucleotide cyclase activity and as such may be regulated by g protein signaling pathways. CG42235 has sequence suggesting a sodium/solute transporter function. While CG4747 has sequence suggesting NAD binding and phosphogluconate dehydrogenase activity, thus potentially involved in central metabolism and NADH/NADPH production.

Finally, we asked whether any of the screened RNAi lines transform bristles toward scale-like phenotypes with the interest of knowing if the transition between the two cell types could be mediated by a single loss of function. However, after looking through all of the posted images for the 593 genes tested, we found no evidence of a single gene that mediates such a transition.

Conclusions

I believe the screening ability of *Drosophila* can provide a vital resource to our understanding of Lep scale development, both for comparative and discovery purposes. While this single study has its caveats (such as confounding effects of choosing a broadly expressed driver, the fact that a low power dissecting scope was (necessarily) used to screen, and RNAi likely produces only partial knockdowns) its broad scope targeting 82% of coding genes provides an excellent starting point for developing hypotheses. This combined with the vast data resources available on Flybase should provide a valuable resource to those interested in scale biology. Further this GO Term based search is useful for identifying prime candidates for manipulation, which can be validated by literature search. For instance if one was interested in the intersection of signaling, morphogenesis, actin, and microtubules, one would stumble upon the genes IKK epsilon and Rab11 which have been shown to be very important in *Drosophila* bristle development and may be great genes of interest to lep scale development (161,173,316,366,317). The only hurdle remaining seems to be a method of knockdown in leps that avoids pleiotropy. It seems reasonable that the technologies mentioned in previous chapters will allow researchers to begin testing butterfly homologs soon.

Acknowledgement

This survey was done almost entirely by Jerry Lo. Without his dedicated work this would not have been possible.

Figure A1.1 Plots of GO Term Classes for genes giving morphological phenotype from Mummery-Widmer screen

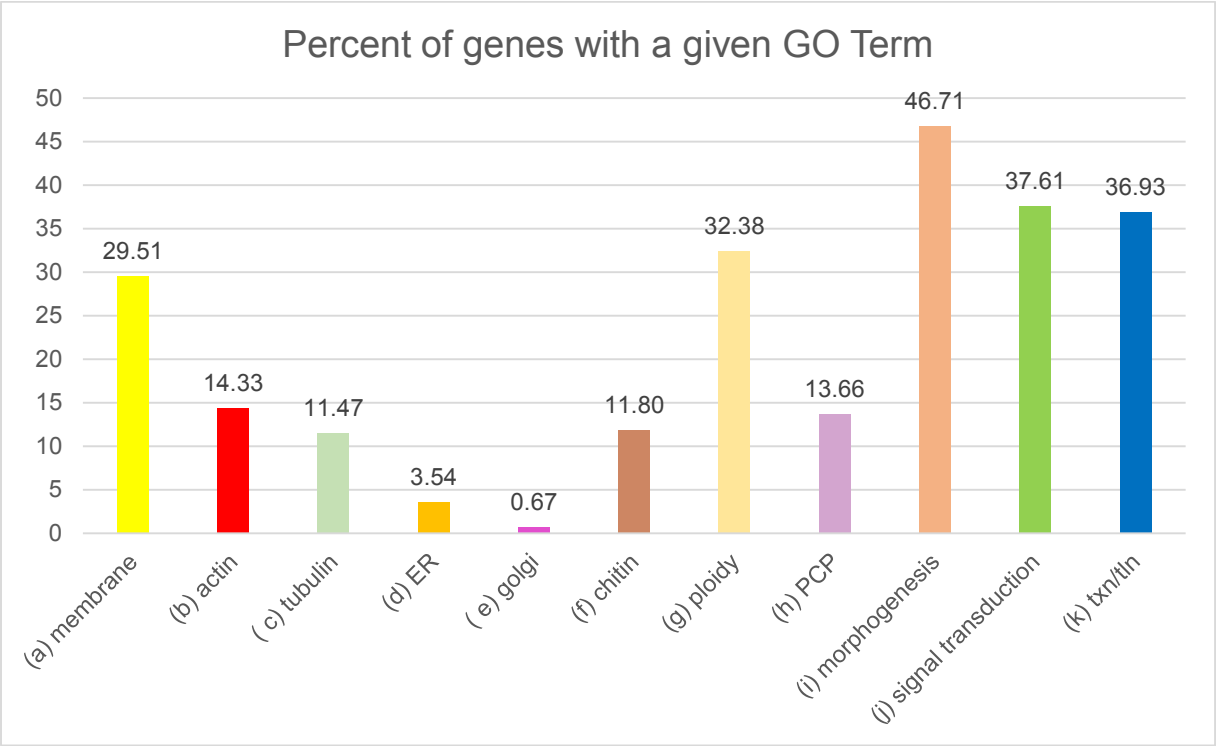

Breakdown of percent of genes featuring a class of GO Term search terms (total genes in a class/total number of genes with morphological defect). The sum of the percentages is more than 100% as many genes contained more than one search class.

Figure A1.2 Breakdown of genes/search term within GO Term Classes

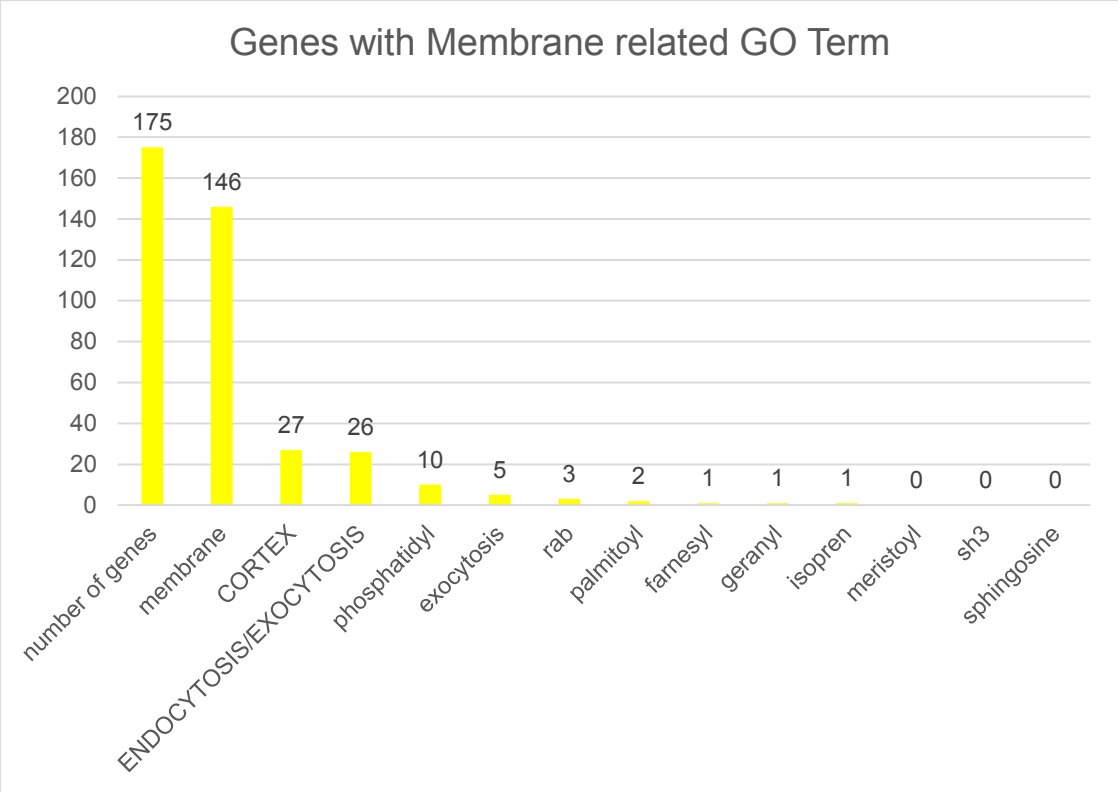

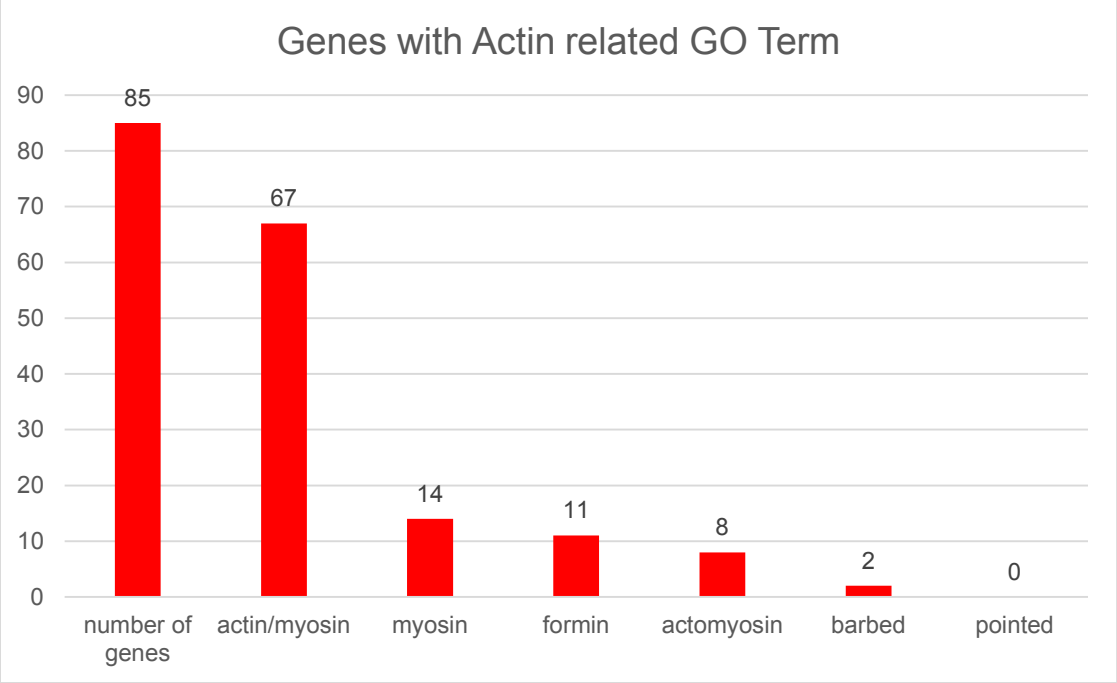

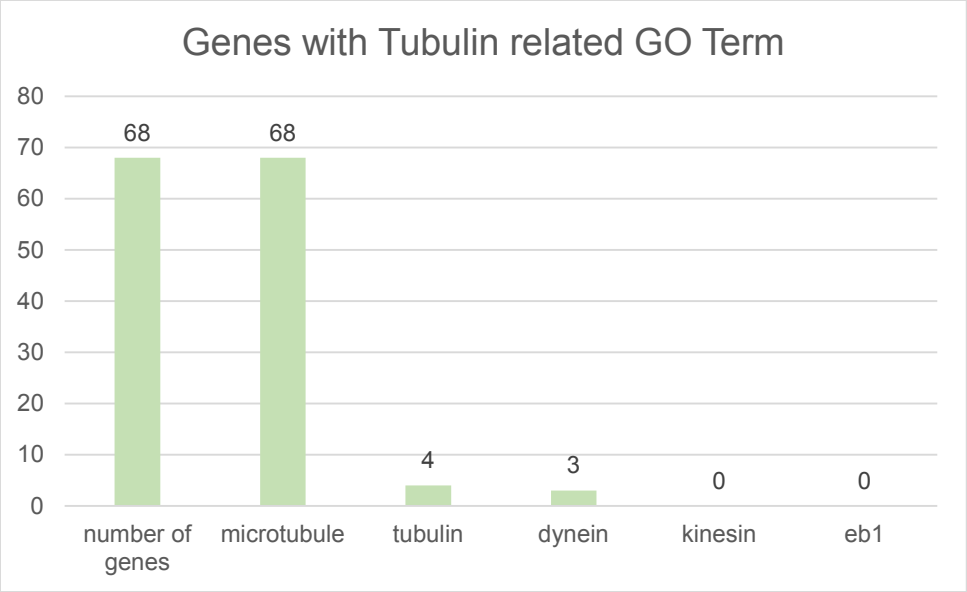
Genes with Tubulin related GO Term
80
70
60
50
40
30
20
10
0
68
68
4
3
0
0
number of genes
microtubule
tubulin
dynein
kinesin
eb1

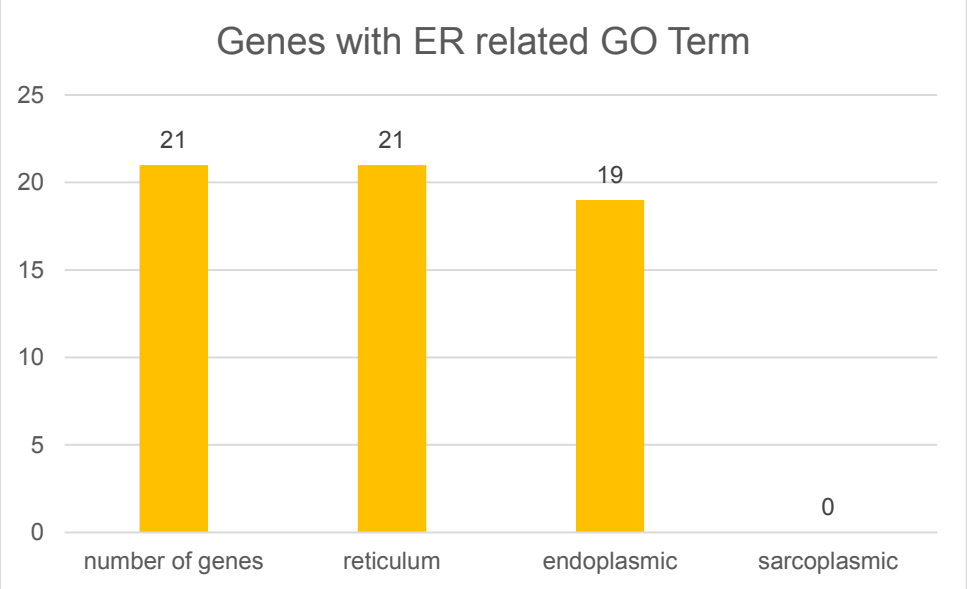
Genes with ER related GO Term
25
20
15
10
5
0
21
21
19
0
number of genes
reticulum
endoplasmic
sarcoplasmic

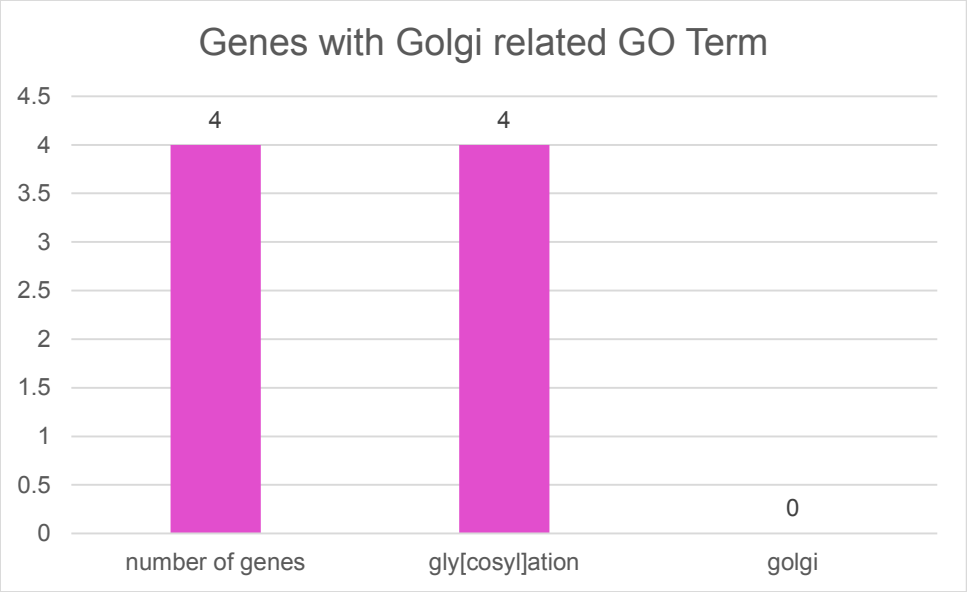
Genes with Golgi related GO Term
4.5
4
3.5
3
2.5
2
1.5
1
0.5
0
4
4
0
number of genes
gly[cosyl]ation
golgi

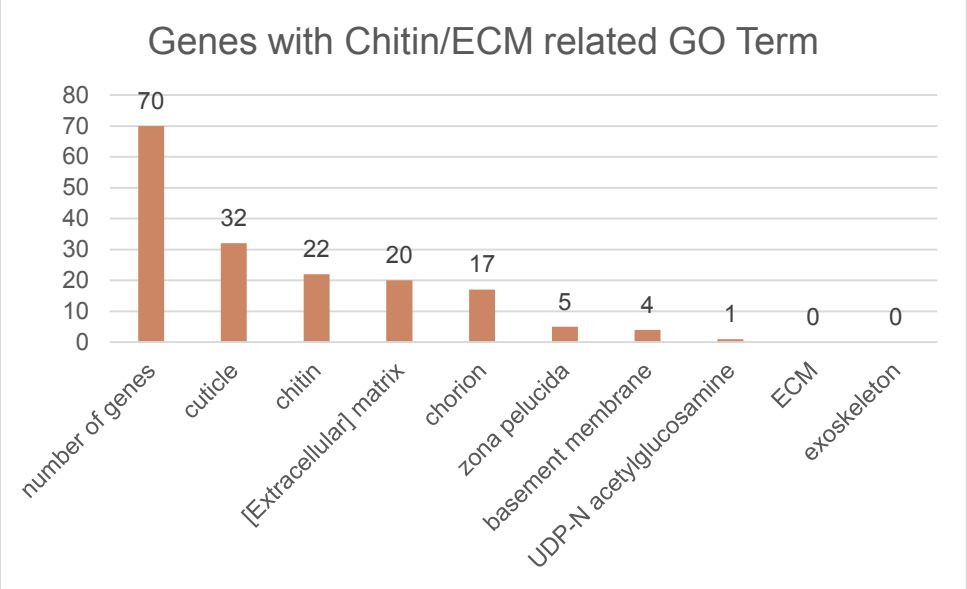
Genes with Chitin/ECM related GO Term
80
70
60
50
40
30
20
10
0
70
32
22
20
17
5
4
1
0
0
number of genes
cuticle
chitin
[Extracellular] matrix
chorion
zona pelucida
basement membrane
UDP-N acetylglucosamine
ECM
exoskeleton

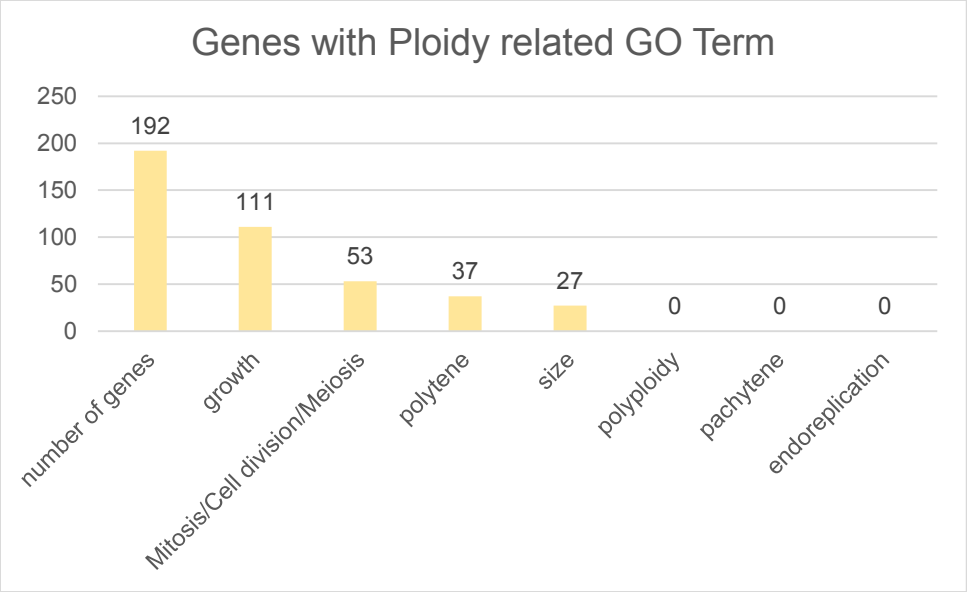
Genes with Ploidy related GO Term
250
200
150
100
50
0
192
111
53
37
27
0
0
0
number of genes
growth
Mitosis/Cell division/Meiosis
polytene
size
polyploidy
pachytene
endoreplication

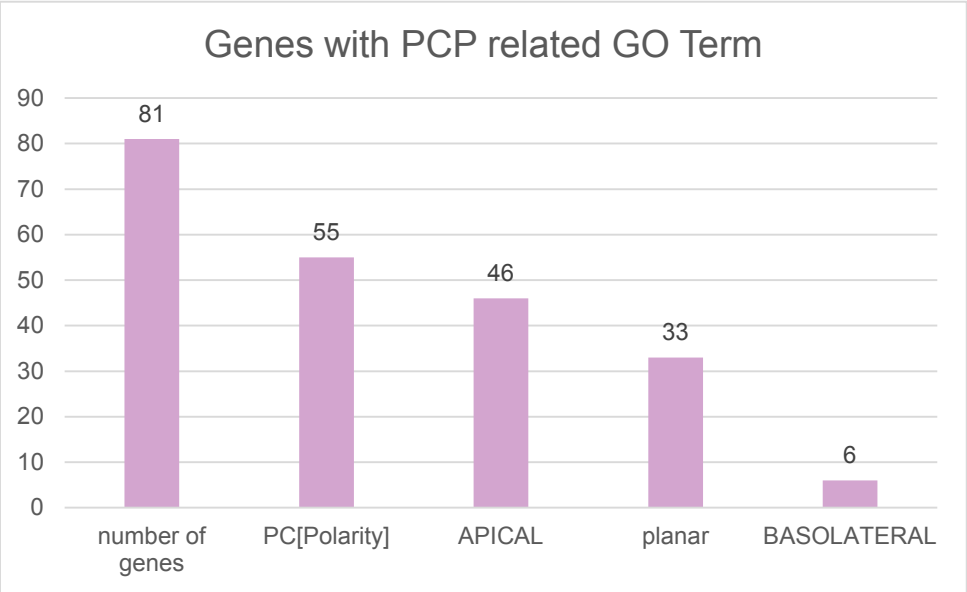
Genes with PCP related GO Term
90
80
70
60
50
40
30
20
10
0
81
55
46
33
6
number of genes
PC[Polarity]
APICAL
planar
BASOLATERAL

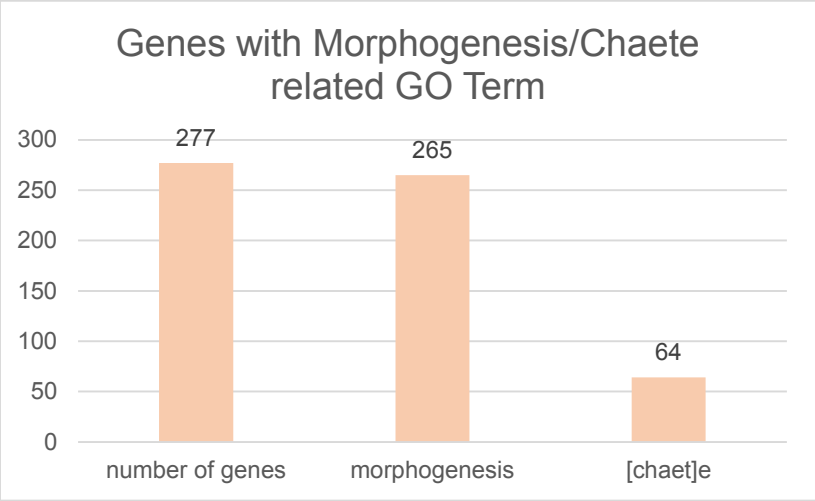
Genes with Morphogenesis/Chaete related GO Term
300
250
200
150
100
50
0
277
265
64
number of genes
morphogenesis
[chaet]e

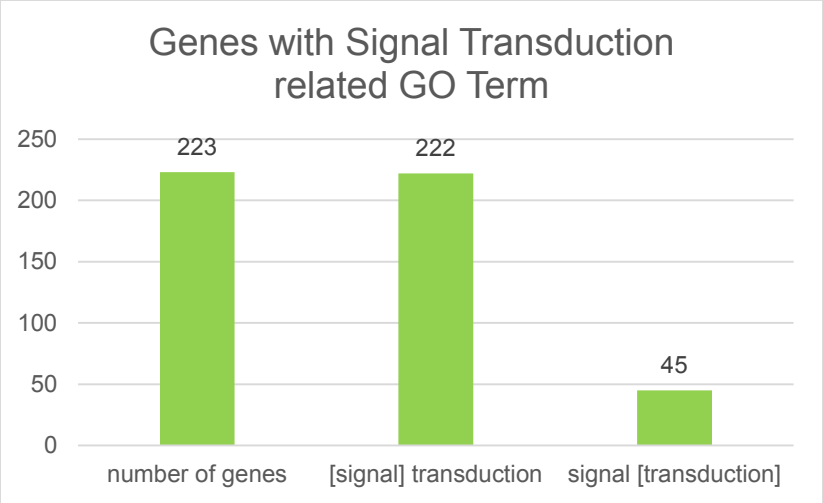

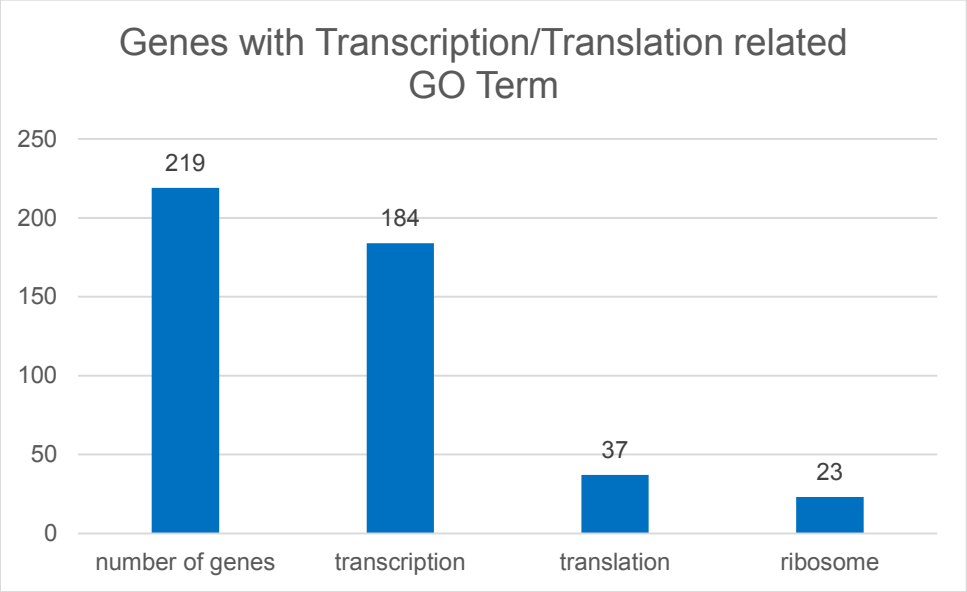

Total number of all genes with at least one GO Term keyword, remaining bars show breakdown of genes with a given search term listed above. Total number of genes may be less than the sum of genes featuring individual search terms as some genes may have more than one search term.

Figure A1.3 Breakdown of GO Term Classes per uncharacterized genes

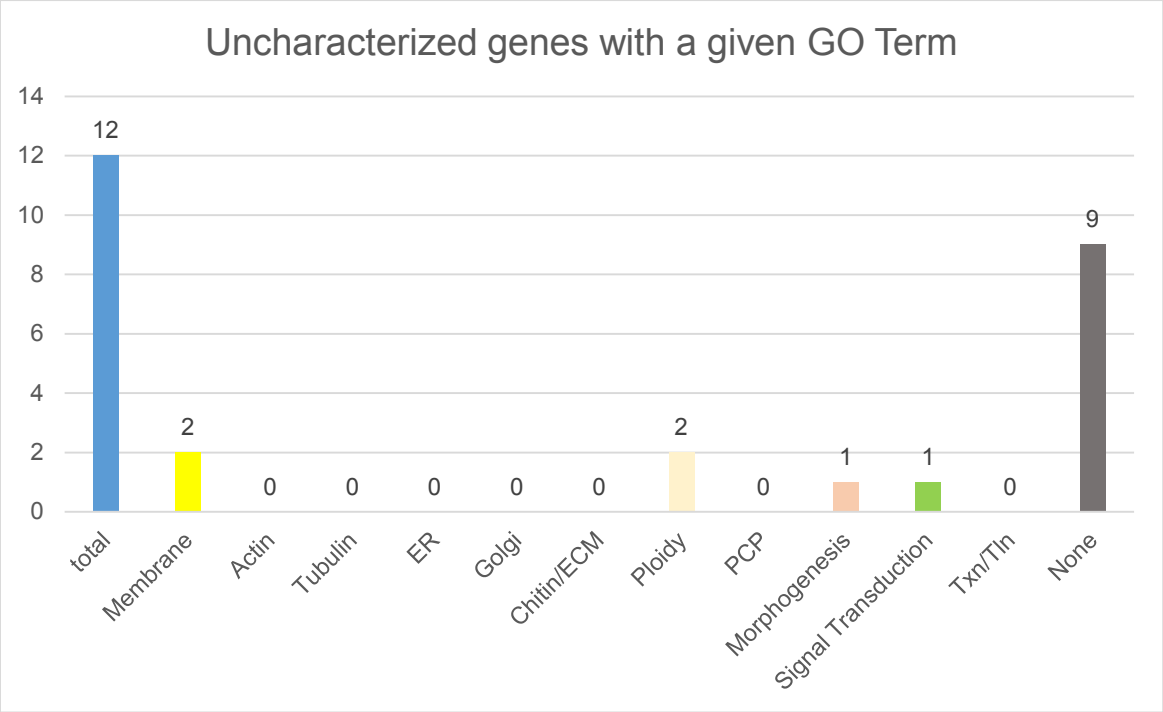

Total number of uncharacterized genes (CG number alone), remaining bars show breakdown of genes with a given search term listed above. Total number of genes may be less than the sum of genes featuring individual search terms as some genes may have more than one search term.

Table A1.1 Alphabetical listing of represented GO Term class types

Class Type	Total GO Terms	Genes with this set of GO Terms	% total
a	1	11	1.855
ab	2	1	0.1686
abcfh	5	1	0.1686
abcfhi	6	1	0.1686
abcfij	6	1	0.1686
abcg	4	1	0.1686
abcgh	5	1	0.1686
abcghi	6	1	0.1686
abchi	5	1	0.1686
abchij	6	1	0.1686
abcij	5	1	0.1686
abdfghijk	9	1	0.1686
abfh	4	1	0.1686
abfhi	5	4	0.6745
abfhjk	6	1	0.1686
abfij	5	2	0.3373
abfijk	6	1	0.1686
abghij	6	1	0.1686
abgij	5	2	0.3373
abgj	4	1	0.1686
abhi	4	1	0.1686
abhij	5	3	0.5059
abhijk	6	1	0.1686
abi	3	7	1.1804
abij	4	7	1.1804
abj	3	2	0.3373
ac	2	3	0.5059
acdfg	5	1	0.1686
acdg	4	1	0.1686
acdi	4	2	0.3373
acgh	4	1	0.1686
acghi	5	1	0.1686
acghij	6	2	0.3373
ach	3	1	0.1686
achi	4	1	0.1686
acij	4	1	0.1686
acijk	5	1	0.1686
ad	2	1	0.1686
adefgij	7	1	0.1686
adegj	5	1	0.1686
adfi	4	1	0.1686
adfij	5	1	0.1686
adghi	5	1	0.1686
adghj	5	1	0.1686
adhi	4	1	0.1686

adij	4	1	0.1686
adj	3	1	0.1686
aej	3	1	0.1686
af	2	1	0.1686
afhi	4	1	0.1686
afhij	5	3	0.5059
afhijk	6	4	0.6745
afi	3	2	0.3373
afij	4	2	0.3373
afj	3	2	0.3373
ag	2	5	0.8432
agh	3	2	0.3373
aghi	4	1	0.1686
aghij	5	3	0.5059
aghijk	6	1	0.1686
aghj	4	2	0.3373
agi	3	3	0.5059
agij	4	8	1.3491
agj	3	6	1.0118
ah	2	4	0.6745
ahi	3	2	0.3373
ahij	4	4	0.6745
ahijk	5	1	0.1686
ahj	3	2	0.3373
ahjk	4	1	0.1686
ai	2	3	0.5059
aij	3	12	2.0236
aijk	4	3	0.5059
aik	3	1	0.1686
aj	2	14	2.3609
b	1	2	0.3373
bc	2	2	0.3373
bcfgj	5	1	0.1686
bcg	3	2	0.3373
bcghi	5	1	0.1686
bcgi	4	1	0.1686
bch	3	1	0.1686
bchi	4	1	0.1686
bci	3	4	0.6745
bcij	4	2	0.3373
bdfhij	6	1	0.1686
bdi	3	1	0.1686
bfghj	5	1	0.1686
bfhi	4	1	0.1686
bfi	3	1	0.1686
bfij	4	1	0.1686
bg	2	2	0.3373
bgi	3	2	0.3373

bgij	4	1	0.1686
bgijk	5	2	0.3373
bhi	3	1	0.1686
bhj	3	1	0.1686
bi	2	3	0.5059
bij	3	1	0.1686
bijk	4	3	0.5059
bik	3	1	0.1686
c	1	5	0.8432
cd	2	1	0.1686
cdfi	4	1	0.1686
cek	3	1	0.1686
cf	2	1	0.1686
cg	2	4	0.6745
cgi	3	1	0.1686
cgijk	5	1	0.1686
cgj	3	1	0.1686
cgk	3	2	0.3373
chj	3	1	0.1686
ci	2	2	0.3373
cij	3	1	0.1686
cik	3	1	0.1686
cj	2	1	0.1686
ck	2	5	0.8432
d	1	1	0.1686
dik	3	1	0.1686
f	1	7	1.1804
fg	2	1	0.1686
fgijk	5	1	0.1686
fgik	4	2	0.3373
fgjk	4	1	0.1686
fgk	3	1	0.1686
fhij	4	1	0.1686
fhijk	5	1	0.1686
fhk	3	1	0.1686
fi	2	4	0.6745
fij	3	2	0.3373
fik	3	2	0.3373
fj	2	3	0.5059
fjk	3	2	0.3373
fk	2	1	0.1686
g	1	24	4.0472
ghijk	5	1	0.1686
ghj	3	1	0.1686
ghk	3	1	0.1686
gi	2	6	1.0118
gij	3	5	0.8432
gijk	4	18	3.0354

gik	3	26	4.3845
gj	2	6	1.0118
gjk	3	2	0.3373
gk	2	25	4.2159
h	1	2	0.3373
hij	3	2	0.3373
hijk	4	1	0.1686
hik	3	1	0.1686
hk	2	1	0.1686
i	1	5	0.8432
ij	2	5	0.8432
ijk	3	20	3.3727
ik	2	34	5.7336
j	1	17	2.8668
jk	2	11	1.855
k	1	33	5.5649
none	0	70	11.804
# Categories	**Avg # GO Terms**	**# Total Genes**	
158	2.382799325	593	

Categories of genes showing morphological defect based upon attributed GO Terms in search classes of interest (a-k). All unique combinations of search classes found are listed, ranked in alphabetical order. Number of classes of search terms is indicated in the second column (e.g. if a set of genes have "Membrane" and "Actin" search classes within their GO Terms, they will be listed under "ab" and have a 2 in their "Total GO Terms" column). The number of genes causing a morphological defect for each particular grouping of GO Term is found in the third column, and the percent of the total number of morphological defect causing GO Term groups are indicated in the 4th column. Classes of GO Terms: **a** Membrane, **b** Actin, **c** Tubulin, **d** ER, **e** Golgi, **f** chitin, **g** Ploidy, **h** PCP, **i** Morphogenesis, **j** Signal Transduction, **k** Txn/Tln

Table A1.2 Genes per GO Term class types

Class Type	Total GO Terms	Genes with this set of GO Terms	% total
none	0	70	11.804
ik	2	34	5.7336
k	1	33	5.5649
gik	3	26	4.3845
gk	2	25	4.2159
g	1	24	4.0472
ijk	3	20	3.3727
gijk	4	18	3.0354
j	1	17	2.8668
aj	2	14	2.3609
aij	3	12	2.0236
a	1	11	1.855
jk	2	11	1.855
agij	4	8	1.3491
abi	3	7	1.1804
abij	4	7	1.1804
f	1	7	1.1804
agj	3	6	1.0118
gi	2	6	1.0118
gj	2	6	1.0118
ag	2	5	0.8432
c	1	5	0.8432
ck	2	5	0.8432
gij	3	5	0.8432
i	1	5	0.8432
ij	2	5	0.8432
abfhi	5	4	0.6745
afhijk	6	4	0.6745
ah	2	4	0.6745
ahij	4	4	0.6745
bci	3	4	0.6745
cg	2	4	0.6745
fi	2	4	0.6745
abhij	5	3	0.5059
ac	2	3	0.5059
afhij	5	3	0.5059
aghij	5	3	0.5059
agi	3	3	0.5059
ai	2	3	0.5059
aijk	4	3	0.5059
bi	2	3	0.5059
bijk	4	3	0.5059
fj	2	3	0.5059

abfij	5	2	0.3373
abgij	5	2	0.3373
abj	3	2	0.3373
acdi	4	2	0.3373
acghij	6	2	0.3373
afi	3	2	0.3373
afij	4	2	0.3373
afj	3	2	0.3373
agh	3	2	0.3373
aghj	4	2	0.3373
ahi	3	2	0.3373
ahj	3	2	0.3373
b	1	2	0.3373
bc	2	2	0.3373
bcg	3	2	0.3373
bcij	4	2	0.3373
bg	2	2	0.3373
bgi	3	2	0.3373
bgijk	5	2	0.3373
cgk	3	2	0.3373
ci	2	2	0.3373
fgik	4	2	0.3373
fij	3	2	0.3373
fik	3	2	0.3373
fjk	3	2	0.3373
gjk	3	2	0.3373
h	1	2	0.3373
hij	3	2	0.3373
ab	2	1	0.1686
abcfh	5	1	0.1686
abcfhi	6	1	0.1686
abcfij	6	1	0.1686
abcg	4	1	0.1686
abcgh	5	1	0.1686
abcghi	6	1	0.1686
abchi	5	1	0.1686
abchij	6	1	0.1686
abcij	5	1	0.1686
abdfghijk	9	1	0.1686
abfh	4	1	0.1686
abfhjk	6	1	0.1686
abfijk	6	1	0.1686
abghij	6	1	0.1686
abgj	4	1	0.1686
abhi	4	1	0.1686
abhijk	6	1	0.1686

acdfg	5	1	0.1686
acdg	4	1	0.1686
acgh	4	1	0.1686
acghi	5	1	0.1686
ach	3	1	0.1686
achi	4	1	0.1686
acij	4	1	0.1686
acijk	5	1	0.1686
ad	2	1	0.1686
adefgij	7	1	0.1686
adegj	5	1	0.1686
adfi	4	1	0.1686
adfij	5	1	0.1686
adghi	5	1	0.1686
adghj	5	1	0.1686
adhi	4	1	0.1686
adij	4	1	0.1686
adj	3	1	0.1686
aej	3	1	0.1686
af	2	1	0.1686
afhi	4	1	0.1686
aghi	4	1	0.1686
aghijk	6	1	0.1686
ahijk	5	1	0.1686
ahjk	4	1	0.1686
aik	3	1	0.1686
bcfgj	5	1	0.1686
bcghi	5	1	0.1686
bcgi	4	1	0.1686
bch	3	1	0.1686
bchi	4	1	0.1686
bdfhij	6	1	0.1686
bdi	3	1	0.1686
bfghj	5	1	0.1686
bfhi	4	1	0.1686
bfi	3	1	0.1686
bfij	4	1	0.1686
bgij	4	1	0.1686
bhi	3	1	0.1686
bhj	3	1	0.1686
bij	3	1	0.1686
bik	3	1	0.1686
cd	2	1	0.1686
cdfi	4	1	0.1686
cek	3	1	0.1686
cf	2	1	0.1686

cgi	3	1	0.1686
cgijk	5	1	0.1686
cgj	3	1	0.1686
chj	3	1	0.1686
cij	3	1	0.1686
cik	3	1	0.1686
cj	2	1	0.1686
d	1	1	0.1686
dik	3	1	0.1686
fg	2	1	0.1686
fgijk	5	1	0.1686
fgjk	4	1	0.1686
fgk	3	1	0.1686
fhij	4	1	0.1686
fhijk	5	1	0.1686
fhk	3	1	0.1686
fk	2	1	0.1686
ghijk	5	1	0.1686
ghj	3	1	0.1686
ghk	3	1	0.1686
hijk	4	1	0.1686
hik	3	1	0.1686
hk	2	1	0.1686

Same as above sorted on the most number of genes per class type. Classes of GO Terms: **a** Membrane, **b** Actin, **c** Tubulin, **d** ER, **e** Golgi, **f** chitin, **g** Ploidy, **h** PCP, **i** Morphogenesis, **j** Signal Transduction, **k** Txn/Tln

Table A1.3
All genes with a morphological defect and their associated GO Term class

Flybase #	Gene Symbol	GO Term Classes	Total Classes
FBgn0004364	18w	aij	3
FBgn0000008	a	ah	2
FBgn0086443	Aats-asn	-	0
FBgn0027080	Aats-tyr	-	0
FBgn0264442	ab	ik	2
FBgn0000015	Abd-B	ik	2
FBgn0020510	Abi	abij	4
FBgn0036372	Abp1	abi	3
FBgn0000022	ac	ik	2
FBgn0000042	Act5C	bcg	3
FBgn0000052	ade2	-	0
FBgn0000053	ade3	-	0
FBgn0000054	Adf1	gik	3
FBgn0039747	AdoR	aj	2
FBgn0262739	AGO1	ghk	3
FBgn0000061	al	ijk	3
FBgn0003270	amos	gik	3
FBgn0027356	Amph	a	1
FBgn0030328	Amun	i	1
FBgn0260642	Antp	gk	2
FBgn0000097	aop	aghijk	6
FBgn0004569	aos	fhij	4
FBgn0267978	ap	ik	2
FBgn0264855	AP-2alpha	ag	2
FBgn0031458	aph-1	agj	3
FBgn0260941	app	adghi	5
FBgn0261112	APP-BP1	-	0
FBgn0000108	Appl	afi	3
FBgn0015903	apt	k	1
FBgn0015904	ara	ik	2
FBgn0017418	ari-1	d	1
FBgn0000117	arm	afhijk	6
FBgn0011742	Arp2	bi	2
FBgn0262716	Arp3	abij	4
FBgn0001961	Arpc1	bij	3
FBgn0000119	arr	aij	3
FBgn0000137	ase	ik	2
FBgn0029094	asf1	gijk	4
FBgn0000139	ash2	gik	3
FBgn0000140	asp	bci	3
FBgn0260945	Atg1	aj	2
FBgn0010433	ato	ijk	3
FBgn0030343	ATP7	af	2
FBgn0000147	aurA	cg	2
FBgn0037218	aux	ij	2

FBgn0013751	Awh	gk	2
FBgn0026597	Axn	agij	4
FBgn0004587	B52	gk	2
FBgn0004870	bab1	ik	2
FBgn0262451	ban	jk	2
FBgn0000163	baz	acghi	5
FBgn0043362	bchs	i	1
FBgn0250788	beta-Spec	abcg	4
FBgn0263107	bft	gi	2
FBgn0000180	bib	agj	3
FBgn0014133	bif	bcgi	4
FBgn0040487	BobA	j	1
FBgn0004132	boca	adghj	5
FBgn0283451	br	gik	3
FBgn0000216	Brd	j	1
FBgn0086694	Bre1	-	0
FBgn0000212	brm	gijk	4
FBgn0004101	bs	ik	2
FBgn0014949	btn	gk	2
FBgn0266756	btsz	abhi	4
FBgn0038901	Burs	fi	2
FBgn0265598	Bx	ik	2
FBgn0004856	Bx42	-	0
FBgn0004863	C15	ijk	3
FBgn0005585	Calr	adfi	4
FBgn0262166	calypso	-	0
FBgn0023095	caps	ai	2
FBgn0022213	Cas	j	1
FBgn0004878	cas	k	1
FBgn0024249	cato	k	1
FBgn0002022	Catsup	ad	2
FBgn0015919	caup	ik	2
FBgn0043364	cbt	ghijk	5
FBgn0004876	cdi	bhj	3
FBgn0000289	cg	ik	2
FBgn0037021	CG11399	-	0
FBgn0043458	CG12084	-	0
FBgn0022349	CG1910	-	0
FBgn0052301	CG32301	agij	4
FBgn0031622	CG3251	-	0
FBgn0250757	CG42235	a	1
FBgn0261674	CG42709	-	0
FBgn0264090	CG43759	-	0
FBgn0028506	CG4455	-	0
FBgn0043456	CG4747	g	1
FBgn0043457	CG5180	-	0
FBgn0043455	CG5986	-	0
FBgn0021760	chb	cj	2
FBgn0013764	Chi	gik	3

FBgn0000308	chic	abi	3
FBgn0000307	chif	f	1
FBgn0015371	chn	ik	2
FBgn0004859	ci	afhijk	6
FBgn0027598	cindr	abi	3
FBgn0000317	ck	abfhi	5
FBgn0264492	CkIIalpha	ijk	3
FBgn0000339	cni	agj	3
FBgn0010434	cora	abfhi	5
FBgn0259173	corn	acgh	4
FBgn0010313	corto	g	1
FBgn0034577	cpa	abchi	5
FBgn0011570	cpb	bci	3
FBgn0000370	crc	fk	2
FBgn0000376	crm	k	1
FBgn0020309	crol	gijk	4
FBgn0028837	CSN6	gj	2
FBgn0004198	ct	ijk	3
FBgn0020496	CtBP	bgijk	5
FBgn0011760	ctp	bci	3
FBgn0261808	cu	-	0
FBgn0261268	Cul3	i	1
FBgn0039632	Cul5	-	0
FBgn0015376	cutlet	-	0
FBgn0000405	CycB	cg	2
FBgn0010382	CycE	fi	2
FBgn0001992	Cyp303a1	ab	2
FBgn0015031	cype	-	0
FBgn0086907	Cyt-c-d	a	1
FBgn0262029	d	bhi	3
FBgn0000411	D	ik	2
FBgn0267821	da	ik	2
FBgn0020493	Dad	bijk	4
FBgn0263930	dally	abfij	5
FBgn0010316	dap	i	1
FBgn0023388	Dap160	aghj	4
FBgn0263864	Dark	ij	2
FBgn0067779	dbr	-	0
FBgn0002413	dco	aghj	4
FBgn0001108	DCTN1-p150	bcghi	5
FBgn0040228	DCTN5-p25	bc	2
FBgn0000422	Ddc	f	1
FBgn0013799	Deaf1	gk	2
FBgn0029131	Debcl	aij	3
FBgn0036038	defl	-	0
FBgn0000439	Dfd	ik	2
FBgn0260635	Diap1	gij	3
FBgn0015247	Diap2	gj	2
FBgn0011274	Dif	jk	2

FBgn0000463	Dl	abhij	5
FBgn0260632	dl	jk	2
FBgn0001624	dlg1	adhi	4
FBgn0000157	Dll	gik	3
FBgn0265998	Doa	cdfi	4
FBgn0029944	Dok	aij	3
FBgn0011763	Dp	fjk	3
FBgn0010109	dpn	gijk	4
FBgn0000490	dpp	bfij	4
FBgn0053196	dpy	f	1
FBgn0000492	Dr	ik	2
FBgn0020381	Dredd	gj	2
FBgn0015664	Dref	gik	3
FBgn0004638	drk	abij	4
FBgn0026404	Dronc	gij	3
FBgn0000497	ds	acghij	6
FBgn0000499	dsh	abhij	5
FBgn0012893	Dsim\sc	-	0
FBgn0000504	dsx	gik	3
FBgn0013139	Dvir\sc	-	0
FBgn0015690	Dvir\y	-	0
FBgn0000520	dwg	gk	2
FBgn0000524	dx	agij	4
FBgn0002592	E(spl)m2-BFM	j	1
FBgn0002609	E(spl)m3-HLH	jk	2
FBgn0002629	E(spl)m4-BFM	j	1
FBgn0002631	E(spl)m5-HLH	gk	2
FBgn0002632	E(spl)m6-BFM	j	1
FBgn0002633	E(spl)m7-HLH	gik	3
FBgn0000591	E(spl)m8-HLH	gijk	4
FBgn0002732	E(spl)malpha-BFM	j	1
FBgn0002733	E(spl)mbeta-HLH	jk	2
FBgn0002734	E(spl)mdelta-HLH	jk	2
FBgn0002735	E(spl)mgamma-HLH	jk	2
FBgn0000617	e(y)1	gk	2
FBgn0000618	e(y)2	k	1
FBgn0087008	e(y)3	gik	3
FBgn0011766	E2f1	fik	3
FBgn0027066	Eb1	bch	3
FBgn0263933	ebi	gijk	4
FBgn0000542	ec	-	0
FBgn0000546	EcR	fgijk	5
FBgn0000547	ed	abij	4
FBgn0028737	Ef1beta	k	1
FBgn0029176	Ef1gamma	cgk	3
FBgn0011217	eff	cgi	3
FBgn0003731	Egfr	afhij	5
FBgn0001404	egh	achi	4
FBgn0261609	eIF-2alpha	ck	2

FBgn0034967	eIF-5A	gk	2
FBgn0004858	elB	j	1
FBgn0036574	elg1	-	0
FBgn0000575	emc	fgik	4
FBgn0000578	ena	bdi	3
FBgn0031250	Ent1	ag	2
FBgn0035060	Eps-15	abj	3
FBgn0036974	eRF1	jk	2
FBgn0001981	esg	k	1
FBgn0004583	ex	ahijk	5
FBgn0005558	ey	gijk	4
FBgn0000320	eya	ik	2
FBgn0000625	eyg	ik	2
FBgn0262111	f	bfi	3
FBgn0005632	faf	a	1
FBgn0000635	Fas2	agij	4
FBgn0011205	fbl	ai	2
FBgn0030241	feo	bcg	3
FBgn0000658	fj	ahij	4
FBgn0264078	Flo2	a	1
FBgn0260049	flr	b	1
FBgn0000711	flw	bi	2
FBgn0011591	fng	adefgij	7
FBgn0042641	frc	afhi	4
FBgn0051774	fred	fij	3
FBgn0086698	frtz	h	1
FBgn0004652	fru	gik	3
FBgn0001075	ft	acghij	6
FBgn0001078	ftz-f1	ijk	3
FBgn0001079	fu	ahjk	4
FBgn0001083	fw	ahi	3
FBgn0001084	fy	h	1
FBgn0001085	fz	abghij	6
FBgn0016797	fz2	agij	4
FBgn0001122	Galphao	abgij	5
FBgn0001123	Galphas	afij	4
FBgn0024234	gbb	abfij	5
FBgn0014179	gcm	ik	2
FBgn0005198	gig	j	1
FBgn0015229	glec	a	1
FBgn0001987	Gli	ai	2
FBgn0013272	Gp150	aj	2
FBgn0015946	grim	j	1
FBgn0026431	Grip75	c	1
FBgn0001612	Grip91	c	1
FBgn0001139	gro	bijk	4
FBgn0261278	grp	-	0
FBgn0010226	GstS1	-	0
FBgn0260399	gwl	g	1

FBgn0001168	h	aik	3
FBgn0001169	H	ijk	3
FBgn0001179	hay	k	1
FBgn0039904	Hcf	gk	2
FBgn0015805	HDAC1	gijk	4
FBgn0011771	Hem	abi	3
FBgn0010303	hep	abfhjk	6
FBgn0011224	heph	cgijk	5
FBgn0004644	hh	afhijk	6
FBgn0003997	hid	gij	3
FBgn0267791	HnRNP-K	ik	2
FBgn0032250	holn1	ij	2
FBgn0001202	hook	ac	2
FBgn0261239	Hr39	ijk	3
FBgn0264562	Hr4	jk	2
FBgn0000448	Hr46	gjk	3
FBgn0004838	Hrb27C	k	1
FBgn0031005	Hs3st-B	ij	2
FBgn0266599	Hsc70-4	ac	2
FBgn0031728	Hsp60C	g	1
FBgn0001233	Hsp83	abgj	4
FBgn0001235	hth	gijk	4
FBgn0037657	hyx	ijk	3
FBgn0263133	ico	k	1
FBgn0086657	IKKepsilon	bcij	4
FBgn0262735	Imp	g	1
FBgn0001259	in	ah	2
FBgn0034224	insb	j	1
FBgn0011674	insc	ah	2
FBgn0031434	insv	jk	2
FBgn0011774	Irbp	-	0
FBgn0011604	Iswi	gijk	4
FBgn0037374	jagn	acdi	4
FBgn0015396	jumu	gik	3
FBgn0263973	jv	bgi	3
FBgn0263929	jvl	bci	3
FBgn0031016	kek5	aj	2
FBgn0001308	Khc	bchi	4
FBgn0266557	kis	cik	3
FBgn0037978	KLHL18	b	1
FBgn0013469	klu	j	1
FBgn0001319	kn	hik	3
FBgn0266450	Kr-h1	k	1
FBgn0040206	krz	fj	2
FBgn0004167	kst	abcgh	5
FBgn0259984	kuz	agij	4
FBgn0001341	l(1)1Bi	gk	2
FBgn0026713	l(1)G0007	gi	2
FBgn0002561	l(1)sc	ik	2

FBgn0010549	l(2)03659	a	1
FBgn0001986	l(2)35Df	-	0
FBgn0002031	l(2)37Cc	ac	2
FBgn0086445	l(2)37Cd	-	0
FBgn0261983	l(2)gd1	aghij	5
FBgn0002354	l(3)87Df	-	0
FBgn0002522	lab	ijk	3
FBgn0002524	lace	aj	2
FBgn0002526	LanA	afi	3
FBgn0011640	lark	bg	2
FBgn0261618	larp	-	0
FBgn0262976	lawc	g	1
FBgn0031759	lid	bg	2
FBgn0026411	Lim1	ik	2
FBgn0283521	lola	ik	2
FBgn0022238	lolal	ik	2
FBgn0028582	lqf	aj	2
FBgn0261279	lqfR	aj	2
FBgn0002577	m	abfhi	5
FBgn0034590	Magi	a	1
FBgn0002643	mam	gijk	4
FBgn0017578	Max	k	1
FBgn0025743	mbt	agj	3
FBgn0086384	Mer	abhij	5
FBgn0034240	MESR4	j	1
FBgn0264694	mgr	c	1
FBgn0025814	Mgstl	ag	2
FBgn0261786	mi	-	0
FBgn0263601	mib1	aghij	5
FBgn0053208	Mical	abi	3
FBgn0261963	mid	fhk	3
FBgn0262379	mir-1012	g	1
FBgn0262403	mir-278	-	0
FBgn0262390	mir-303	-	0
FBgn0262370	mir-7	fgjk	4
FBgn0262302	mir-954	-	0
FBgn0262317	mir-966	-	0
FBgn0262203	mir-967	g	1
FBgn0262181	mir-972	g	1
FBgn0262301	mir-979	-	0
FBgn0262339	mir-982	-	0
FBgn0262235	mir-983-1	-	0
FBgn0262282	mir-984	-	0
FBgn0262307	mir-990	-	0
FBgn0262373	mir-9a	ij	2
FBgn0014343	mirr	ijk	3
FBgn0036844	Mkp3	-	0
FBgn0034051	Mlf	gik	3
FBgn0002780	mod	-	0

FBgn0002783	mor	gik	3
FBgn0002791	mr	-	0
FBgn0027948	msps	cd	2
FBgn0002873	mud	ach	3
FBgn0002876	mul	g	1
FBgn0002877	mur	g	1
FBgn0002901	mus304	-	0
FBgn0002914	Myb	fgk	3
FBgn0262656	Myc	gjk	3
FBgn0004647	N	abhijk	6
FBgn0028471	Nab2	-	0
FBgn0010488	NAT1	gik	3
FBgn0261530	nbs	gj	2
FBgn0004374	neb	c	1
FBgn0261617	nej	gijk	4
FBgn0002932	neur	aij	3
FBgn0030505	NFAT	aijk	4
FBgn0011817	nmo	hij	3
FBgn0005771	noc	k	1
FBgn0016047	nompA	fi	2
FBgn0016919	nompB	i	1
FBgn0016920	nompC	ag	2
FBgn0013717	not	k	1
FBgn0044028	Notum	fj	2
FBgn0265011	Np	-	0
FBgn0013718	nuf	abcghi	6
FBgn0002973	numb	aj	2
FBgn0004102	oc	ik	2
FBgn0033901	O-fut1	adegj	5
FBgn0003002	opa	gijk	4
FBgn0021767	org-1	gk	2
FBgn0261885	osa	ijk	3
FBgn0003028	ovo	fik	3
FBgn0038418	pad	gik	3
FBgn0060296	pain	ag	2
FBgn0023216	Parg	-	0
FBgn0051481	pb	k	1
FBgn0003041	pbl	abij	4
FBgn0003042	Pc	k	1
FBgn0005655	PCNA	cf	2
FBgn0020386	Pdk1	aij	3
FBgn0004860	ph-d	gk	2
FBgn0013725	phyl	j	1
FBgn0015278	Pi3K68D	abj	3
FBgn0260962	pic	f	1
FBgn0086706	pix	k	1
FBgn0000273	Pka-C1	acijk	5
FBgn0259243	Pka-R1	bcfgj	5
FBgn0005626	ple	f	1

FBgn0025741	PlexA	aj	2
FBgn0010441	pll	agj	3
FBgn0003117	pnr	bijk	4
FBgn0003118	pnt	aijk	4
FBgn0283467	Pol32	g	1
FBgn0003124	polo	bc	2
FBgn0040294	POSH	cgj	3
FBgn0003130	Poxn	gik	3
FBgn0261285	Ppcs	bgi	3
FBgn0014269	prod	g	1
FBgn0023174	Prosbeta2	g	1
FBgn0002284	Prosbeta6	-	0
FBgn0033688	Prp8	-	0
FBgn0005624	Psc	g	1
FBgn0019947	Psn	aghij	5
FBgn0263102	psq	gi	2
FBgn0003892	ptc	aij	3
FBgn0004370	Ptp10D	ahj	3
FBgn0003162	Pu	f	1
FBgn0243512	puc	bdfhij	6
FBgn0039214	puf	jk	2
FBgn0028577	pUf68	g	1
FBgn0003165	pum	ijk	3
FBgn0003169	put	abij	4
FBgn0003174	pwn	gij	3
FBgn0053207	pxb	gj	2
FBgn0262614	pyd	ahij	4
FBgn0043900	pygo	ijk	3
FBgn0019662	qm	a	1
FBgn0028622	qsm	fi	2
FBgn0015790	Rab11	abcij	5
FBgn0014010	Rab5	ahij	4
FBgn0015797	Rab6	acij	4
FBgn0010333	Rac1	abchij	6
FBgn0014011	Rac2	bcij	4
FBgn0003079	Raf	aij	3
FBgn0015286	Rala	agij	4
FBgn0003204	ras	g	1
FBgn0003206	Ras64B	aj	2
FBgn0003205	Ras85D	afhij	5
FBgn0015799	Rbf	fjk	3
FBgn0014018	Rel	gijk	4
FBgn0020379	Rfx	gik	3
FBgn0026376	Rgl	j	1
FBgn0003255	rk	afj	3
FBgn0003256	rl	aijk	4
FBgn0003261	Rm62	cg	2
FBgn0003267	ro	hk	2
FBgn0024196	robl	ci	2

FBgn0005631	robo1	aij	3
FBgn0037351	RpL13A	ijk	3
FBgn0017579	RpL14	k	1
FBgn0028697	RpL15	k	1
FBgn0002607	RpL19	gk	2
FBgn0261606	RpL27A	gk	2
FBgn0002579	RpL36	gk	2
FBgn0261608	RpL37A	k	1
FBgn0064225	RpL5	gk	2
FBgn0015756	RpL9	gk	2
FBgn0002593	RpLP1	k	1
FBgn0011706	rpr	aij	3
FBgn0261593	RpS10b	ck	2
FBgn0010265	RpS13	gk	2
FBgn0005533	RpS17	k	1
FBgn0004867	RpS2	gk	2
FBgn0015521	RpS21	k	1
FBgn0003942	RpS27A	ck	2
FBgn0039739	RpS28a	gk	2
FBgn0002622	RpS3	cek	3
FBgn0017545	RpS3A	k	1
FBgn0002590	RpS5a	k	1
FBgn0011305	Rsf1	k	1
FBgn0003285	rst	aghi	4
FBgn0003301	rut	afj	3
FBgn0003310	S	adij	4
FBgn0261648	salm	gik	3
FBgn0000287	salr	ik	2
FBgn0019932	SamDC	-	0
FBgn0005278	Sam-S	gi	2
FBgn0034408	sano	agh	3
FBgn0003319	Sb	abi	3
FBgn0010575	sbb	ijk	3
FBgn0003321	sbr	a	1
FBgn0004170	sc	ik	2
FBgn0003326	sca	fij	3
FBgn0260936	scny	fg	2
FBgn0003339	Scr	k	1
FBgn0263289	scrib	ahi	3
FBgn0004880	scrt	ik	2
FBgn0003345	sd	ijk	3
FBgn0267376	SelR	bi	2
FBgn0002573	sens	gijk	4
FBgn0004197	Ser	afhij	5
FBgn0011474	Set8	g	1
FBgn0003371	sgg	fhijk	5
FBgn0261445	sgl	hij	3
FBgn0003390	shf	fj	2
FBgn0003392	shi	abcfij	6

FBgn0003396	shn	bgijk	5
FBgn0010762	simj	k	1
FBgn0003410	sina	-	0
FBgn0016984	sktl	abcfh	5
FBgn0283468	slmb	bfghj	5
FBgn0030018	slpr	agi	3
FBgn0003435	sm	-	0
FBgn0265523	Smr	gijk	4
FBgn0264922	smt3	bgij	4
FBgn0003447	sn	bfhi	4
FBgn0003448	sna	ik	2
FBgn0264357	SNF4Agamma	-	0
FBgn0265630	sno	ijk	3
FBgn0003463	sog	abgij	5
FBgn0001965	Sos	abij	4
FBgn0087021	Spc25	-	0
FBgn0260440	spdo	agij	4
FBgn0016977	spen	hijk	4
FBgn0005672	spi	adfij	5
FBgn0086362	spn-F	ci	2
FBgn0003499	sr	k	1
FBgn0003507	srp	gik	3
FBgn0003513	ss	gik	3
FBgn0011481	Ssdp	gik	3
FBgn0003517	sta	ck	2
FBgn0024836	stan	ahij	4
FBgn0003525	stg	agi	3
FBgn0003557	Su(dx)	aij	3
FBgn0003559	su(f)	g	1
FBgn0004837	Su(H)	gijk	4
FBgn0014037	Su(Tpl)	gk	2
FBgn0003598	Su(var)3-7	g	1
FBgn0265623	Su(z)2	-	0
FBgn0003545	sub	c	1
FBgn0005561	sv	gik	3
FBgn0003651	svp	ijk	3
FBgn0034135	Syn2	g	1
FBgn0010355	Taf1	k	1
FBgn0004406	tam	-	0
FBgn0028980	tant	-	0
FBgn0040071	tara	k	1
FBgn0025790	TBPH	cij	3
FBgn0045035	tefu	-	0
FBgn0261014	TER94	acdi	4
FBgn0261953	TfAP-2	gik	3
FBgn0264075	tgo	bik	3
FBgn0031390	tho2	-	0
FBgn0003714	tko	gk	2
FBgn0003716	tkv	abfijk	6

FBgn0086899	Tlk	g	1
FBgn0036494	Toll-6	aj	2
FBgn0034476	Toll-7	aj	2
FBgn0029114	Tollo	aej	3
FBgn0026320	Tom	ghj	3
FBgn0033636	tou	gk	2
FBgn0028978	trbl	j	1
FBgn0003744	trc	aij	3
FBgn0046687	Tre1	aj	2
FBgn0261793	Trf2	gik	3
FBgn0013263	Trl	gik	3
FBgn0003862	trx	cgk	3
FBgn0026317	Tsc1	gij	3
FBgn0003866	tsh	ik	2
FBgn0003870	ttk	fgik	4
FBgn0250874	ttm50	a	1
FBgn0265974	ttv	adj	3
FBgn0003896	tup	ijk	3
FBgn0002673	twe	-	0
FBgn0038206	twf	abi	3
FBgn0262801	twr	aj	2
FBgn0004889	tws	chj	3
FBgn0029128	tyn	abfh	4
FBgn0017457	U2af38	-	0
FBgn0023143	Uba1	agj	3
FBgn0015320	Ubc2	-	0
FBgn0003944	Ubx	ik	2
FBgn0262124	uex	-	0
FBgn0003950	unc	-	0
FBgn0004395	unk	gi	2
FBgn0003963	ush	gijk	4
FBgn0052479	Usp10	j	1
FBgn0030969	Usp39	-	0
FBgn0035402	Usp5	gi	2
FBgn0030366	Usp7	gk	2
FBgn0029687	Vap-33A	acdfg	5
FBgn0259789	vfl	k	1
FBgn0003975	vg	ik	2
FBgn0262736	Vha16-1	agi	3
FBgn0037671	VhaM8.9	ahj	3
FBgn0003984	vn	afij	4
FBgn0016076	vri	ik	2
FBgn0260987	vtd	g	1
FBgn0086680	vvl	ik	2
FBgn0035120	wac	cg	2
FBgn0004655	wapl	g	1
FBgn0024273	WASp	abcfhi	6
FBgn0005642	wdn	k	1
FBgn0040066	wds	ck	2

FBgn0004009	wg	abdfghijk	9
FBgn0037098	Wnk	gj	2
FBgn0010453	Wnt4	afhijk	6
FBgn0021872	Xbp1	dik	3
FBgn0004034	y	f	1
FBgn0004049	yrt	ah	2
FBgn0265434	zip	abfhi	5
FBgn0051860	ZnT33D	agh	3
FBgn0004643	Zw10	acdg	4

Genes identified from Mummery-Widmer RNAi screen having some morphological phenotype. **1st column** – Flybase identifier, **2nd Column** – gene shorthand, **3rd column** – our assignment of GO Term class, **4th column** – number of GO Term classes associated with the gene. Classes of GO Terms: **a** Membrane, **b** Actin, **c** Tubulin, **d** ER, **e** Golgi, **f** chitin, **g** Ploidy, **h** PCP, **i** Morphogenesis, **j** Signal Transduction, **k** Txn/Tln

Appendix 2
Data Contributing to *Morpho* Survey

Figure A2.1 Wings of butterflies surveyed and not shown in main text

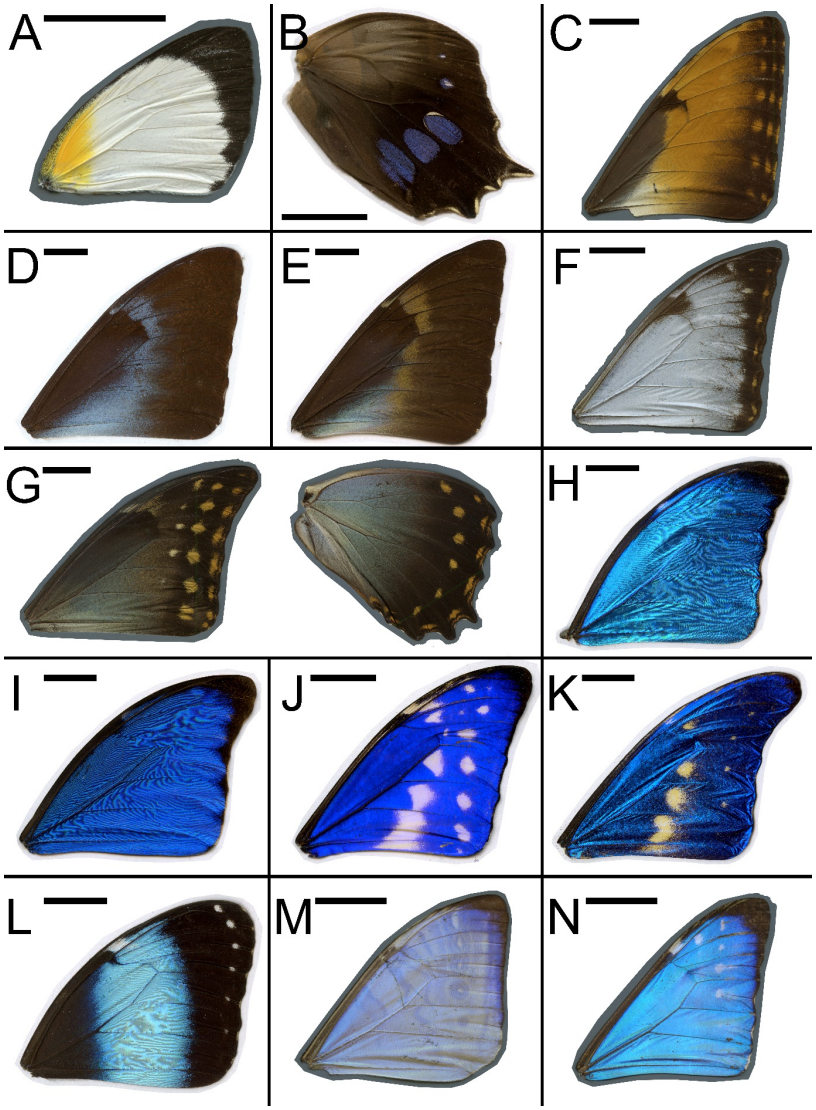

A *Appias sylvia* (Pieridae) male forewing **B** *Antirrhea philoctetes avernus* (Nymphalidae:Morphini) male hindwing **C** *Morpho hecuba* (Nymphalidae:Morphini) male forewing **D** *Morpho cisseis gahua* – blue form (Nymphalidae:Morphini) male forewing **E** *Morpho cisseis gahua* – orange form (Nymphalidae:Morphini) male forewing **F** *Morpho theseus* (Nymphalidae:Morphini) male forewing **G** *Morpho amphitryon* (Nymphalidae:Morphini) male fore and hindwing **H** *Morpho amathonte* (Nymphalidae:Morphini) male forewing **I** *Morpho anaxibia* (Nymphalidae:Morphini) male forewing **J** *Morpho cypris* (Nymphalidae:Morphini) male forewing **K** *Morpho rhetenor helena* (Nymphalidae:Morphini) male forewing **L** *Morpho achilles* (Nymphalidae:Morphini) male forewing **M** *Morpho sulkowskyi* (Nymphalidae:Morphini) male forewing **N** *Morpho zephyritis* (Nymphalidae:Morphini) male forewing **Scale bars** 1.5cm

Figure A2.2 Reflected light images of wings from butterflies not shown in main text

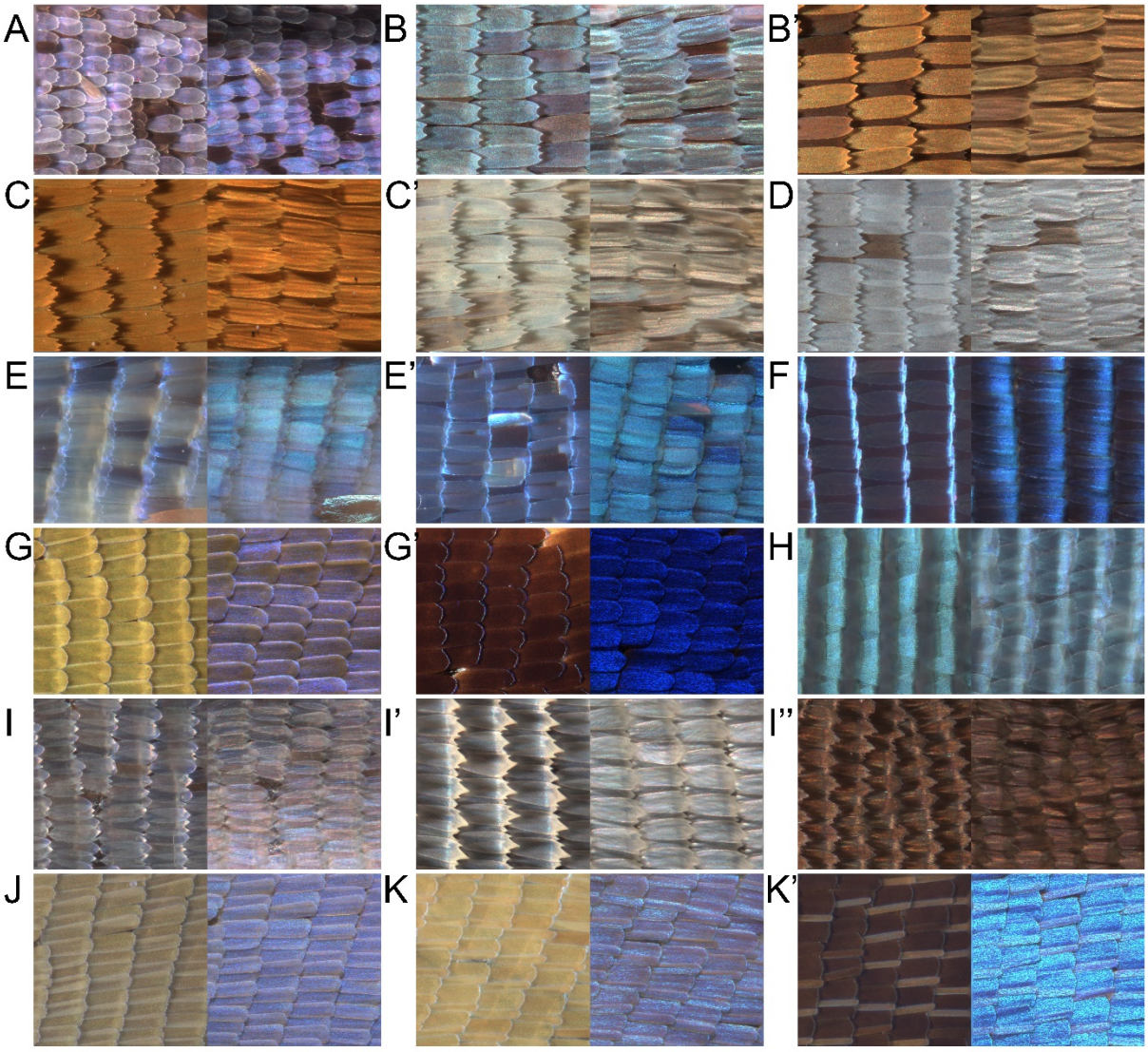

In all image pairs, angle of incidence is at 45° with azimuth parallel to scale length in left image and perpendicular to scale length in right image. **A** *Antirrhea philoctetes avernus* blue spot on hindwing **B,B'** *Morpho cisseis gahua* – orange form blue region, orange region respectively **C,C'** *Morpho hecuba* orange and white regions respectively **D** *Morpho theseus* white region **G** *Morpho amphitryon* male fore and hindwing **H** *Morpho amathonte* (Nymphalidae:Morphini) male forewing **I** *Morpho anaxibia* (Nymphalidae:Morphini) male forewing **J** *Morpho cypris* (Nymphalidae:Morphini) male forewing **K** *Morpho rhetenor helena* (Nymphalidae:Morphini) male forewing **L** *Morpho achilles* (Nymphalidae:Morphini) male forewing **M** *Morpho sulkowskyi* (Nymphalidae:Morphini) male forewing **N** *Morpho zephyritis* (Nymphalidae:Morphini) male forewing **Scale bars** 1.5cm

Figure A2.3 Reflected light single scale abwing color analysis

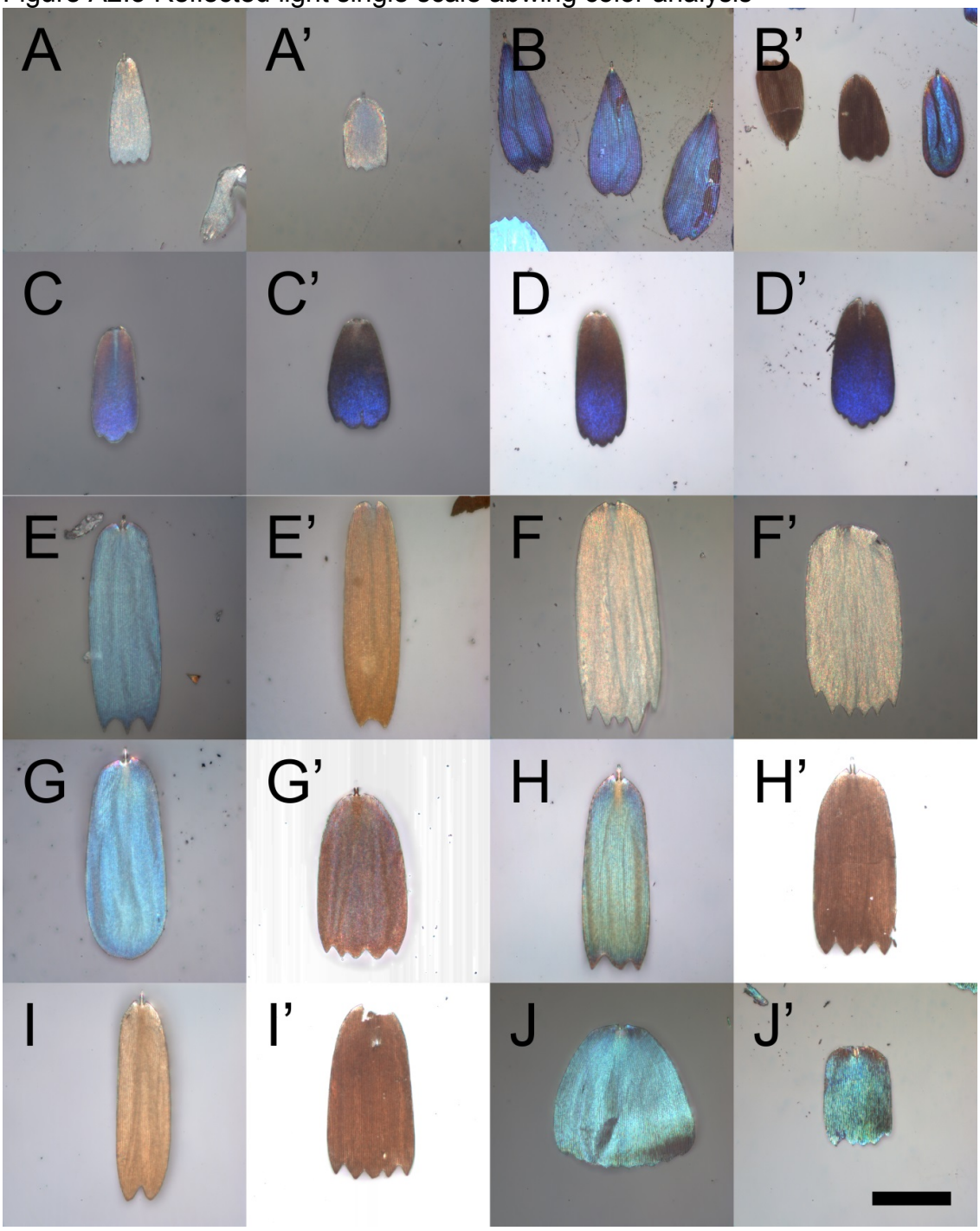

Reflected light images of cover scales (X) and ground scales (X'), except E,E' which are both cover scales. **A,A'** – *Appias sylvia,* **B,B'** – *Antirrhea phlioctetes avernus* **C,C',D,D'** – *Caligo* light and dark blue respectively **E,E'** – Cover scales of *M. cisseis gahua* blue and orange, **F,F'** *M. hecuba* white scales cover & ground **G,G'** *M. amphitryon* cover and ground from blue region, **H,H'** from green region, and **I,I'** from orange region. **J,J'** *M. achilles* from green band cover and ground. Scale bar 100um.

Figure A2.4 Outgroup adwing scale reflectance

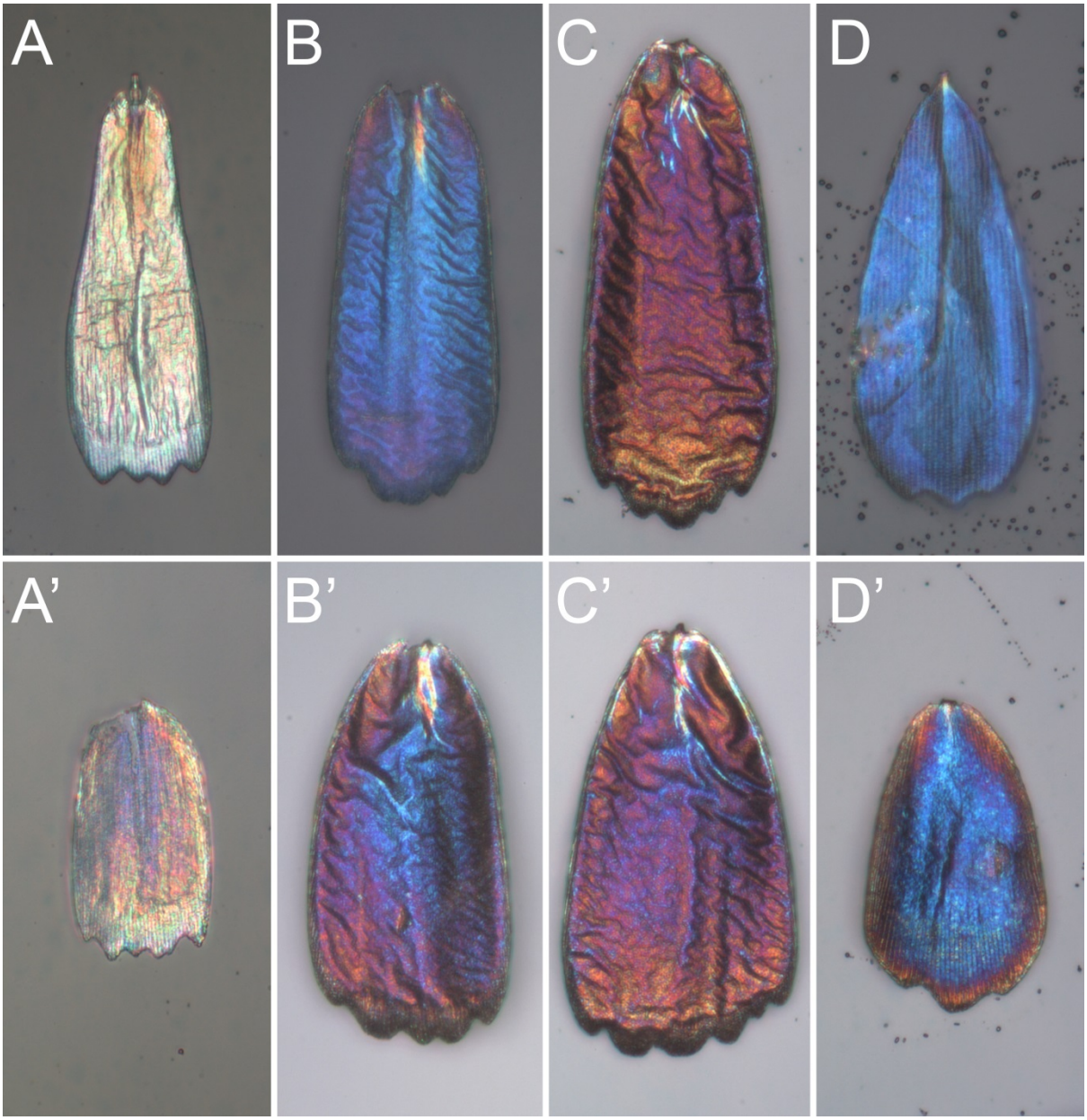

A – Cover scale from *Appias sylvia* forewing. **A' –** Ground scale from *Appias sylvia* forewing. **B,B' –** Cover and ground scale from the white field of *Caligo*. **C,C' –** Cover and ground scale from the dark blue field of the same *Caligo*. **D,D' –** Cover and Ground scale from the blue spot of *Antirrhea philoctetes avernus* hindwing.

Figure A2.5 Adwing reflectance of scales from the blue regions of *M. marcus*

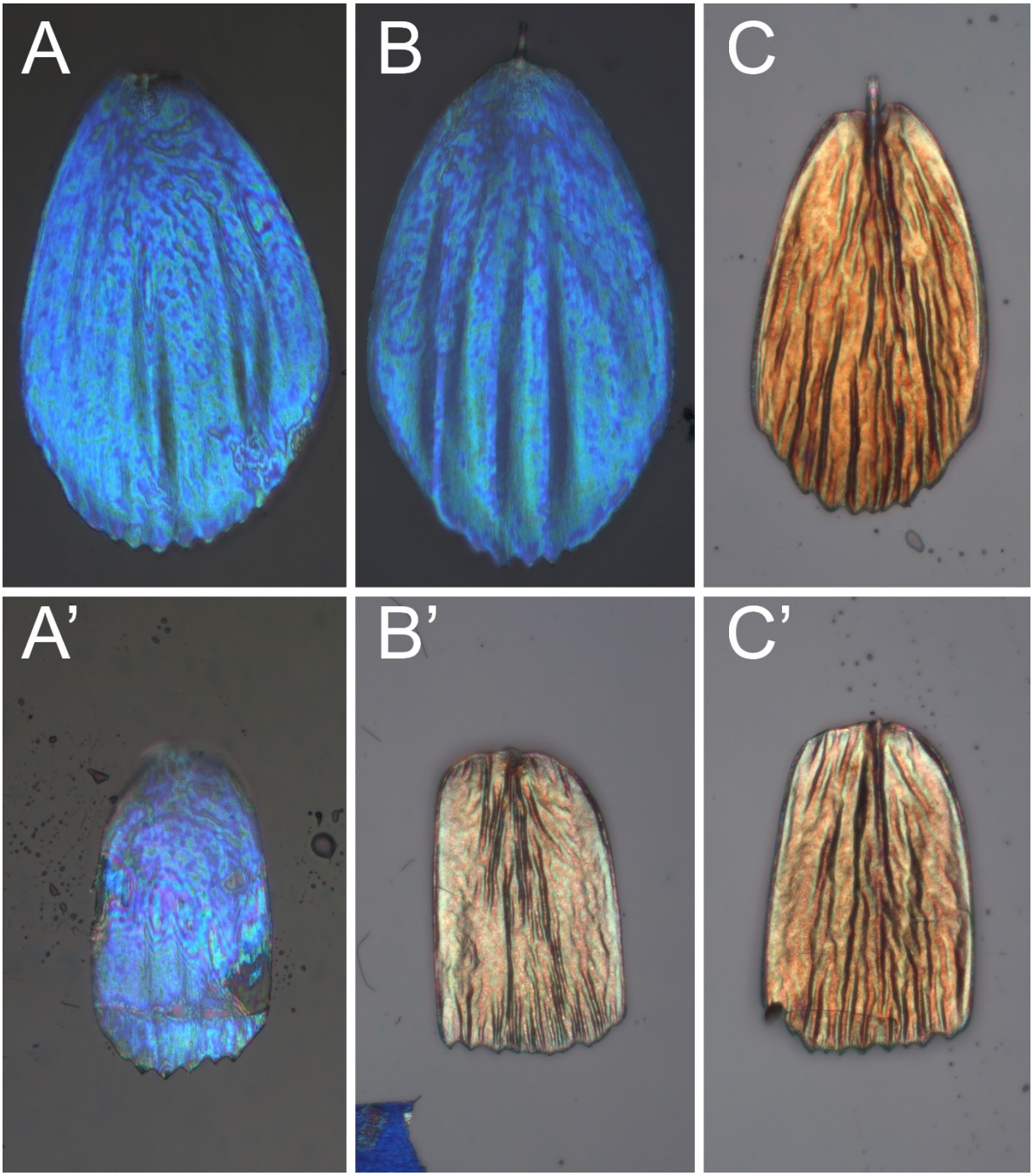

Pigmented scales of *Morpho marcus* have golden adwing reflectance. It is possible that in addition to increasing saturation by absorbing backscatter, the melanin may extinguish contaminating lower lamina thin-film reflectance. **A –** Cover scale from white spot of *M. marcus* forewing. **A' –** Ground scale from white spot of *M. marcus* forewing. **B –** Cover scale from the main blue field of M. marcus forewing. **B' –** Ground scale from the main blue field of *M. marcus* forewing. **C –** Cover scale from the distal dark blue tip of *M. marcus* forewing. **C' –** Ground scale from the distal dark blue tip of *M. marcus* forewing.

Figure A2.6 Denuding bright blue region of *M. marcus* reveals dark blue reflectance

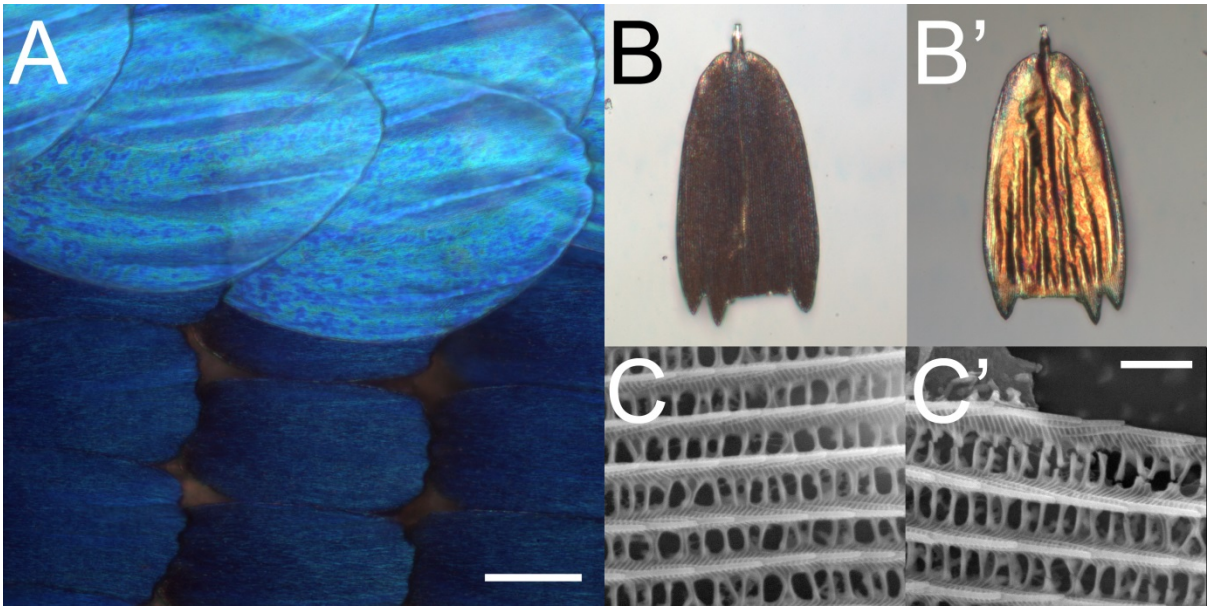

A Region of main blue region from *M. marcus* denuded of cover scales uncovers a dark blue similar to the distal dark blue tip. **B,B'** Representative, rarely occurring non-structural ground scales of distal dark blue region, seen from ab- and adwing reflectance perspectives respectively. **C,C'** Two views of the ridges from a scale like that of **B** showing difference in ridge structure versus that of the "railroad track" ridge seen in blue scales (Fig2.2F, J, &N).

Figure A2.7
Reflected light from adwing surface of *M. cisseis, amphitryon, hecuba* and *theseus*

A-A'' *M. cisseis gahua* (orange form) scales ground, blue cover, orange cover. **B-B''** *M. hecuba* orange cover scale, white cover scale, white ground scale. **C-F** *M. amphitryon* blue cover, blue ground, green cover, green ground, orange cover, orange ground, light orange cover scale. **G** *M. theseus* white ground scale

Figure A2.8 Reflected light analysis of adwing scale face from *M. amathonte* and *godartii* subspecies.

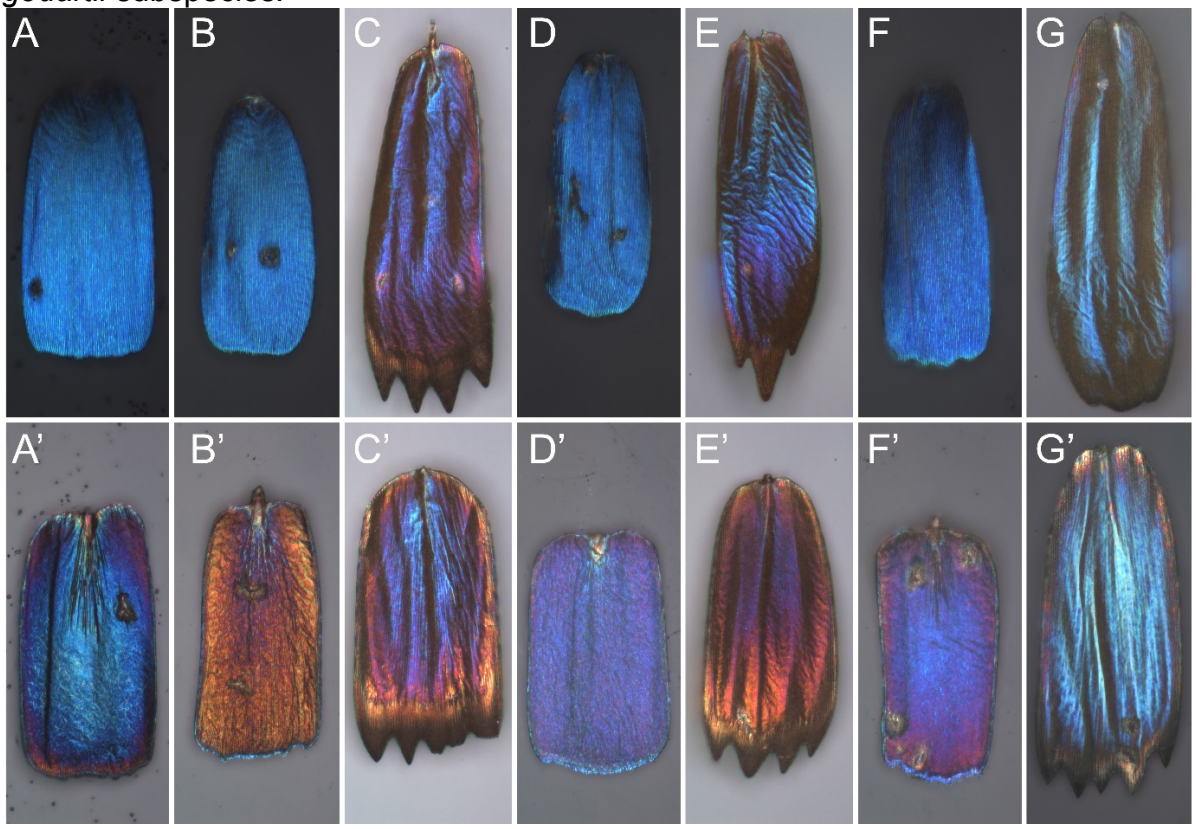

A – *M. amathonte* dorsal cover, **A' –** *M. amathonte* dorsal ground scale, **B –** *M. godartii didius* dorsal cover, **B' –** *M. godartii didius* dorsal ground scale, **C –** *M. godartii didius* ventral cover, **C' –** *M. godartii didius* ventral ground scale, **D –** *M. godartii assarpai* Dark form dorsal cover, **D' –** *M. godartii assarpai* Dark form dorsal ground scale, **E –** *M. godartii assarpai* Dark form ventral cover, **E' –** *M. godartii assarpai* Dark form ventral ground scale, **F –** *M. godartii assarpai* Light form dorsal cover, **F' –** *M. godartii assarpai* Light form dorsal ground scale, **G –** *M. godartii assarpai* Light form ventral cover, **G' –** *M. godartii assarpai* Light form ventral ground scale

Figure A2.9 Reflected light analysis of *M. polyphemus, epistrophus, helenor peleides,* and *achilles* scales from adwing side

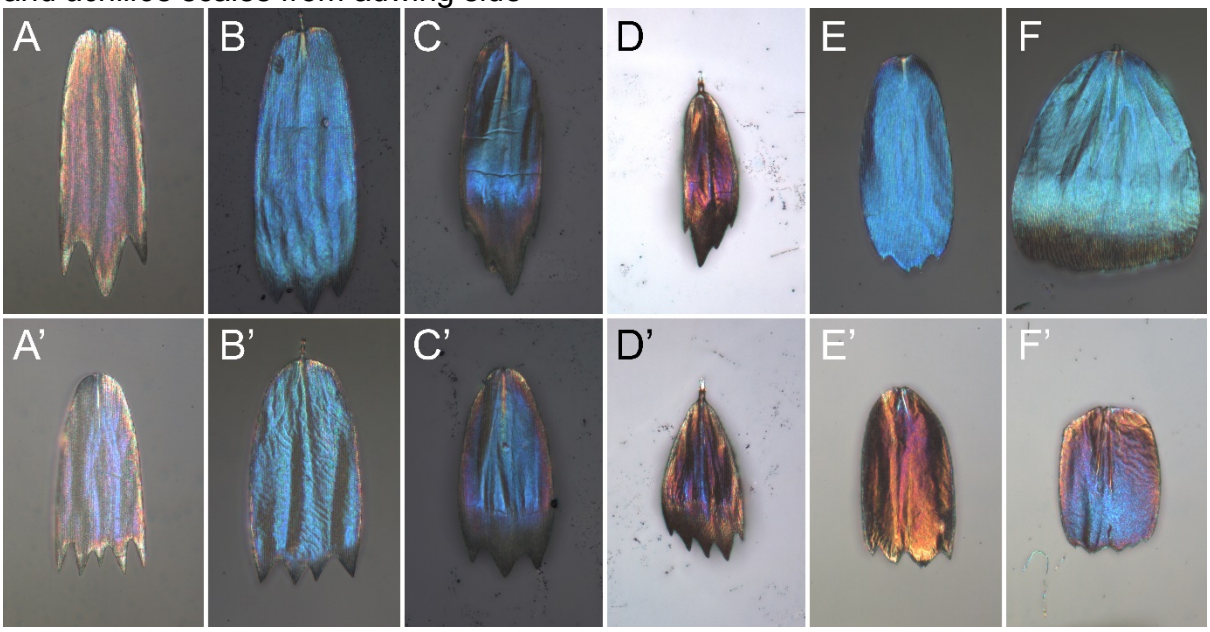

A,A' *M. polyphemus* cover and ground. **B,B'** *M. epistrophus catenarius* cover and ground. **C,C'** *M.h. peleides* ventral white scales cover and ground. **D,D'** *M.h. peleides* distal dorsal black scales cover and ground. **E,E'** *M.h.peleides* dorsal blue scales cover and ground. **F,F'** *M. Achilles* green band cover and ground

Figure A2.10 Whole wing reflectance data for species not shown in main text

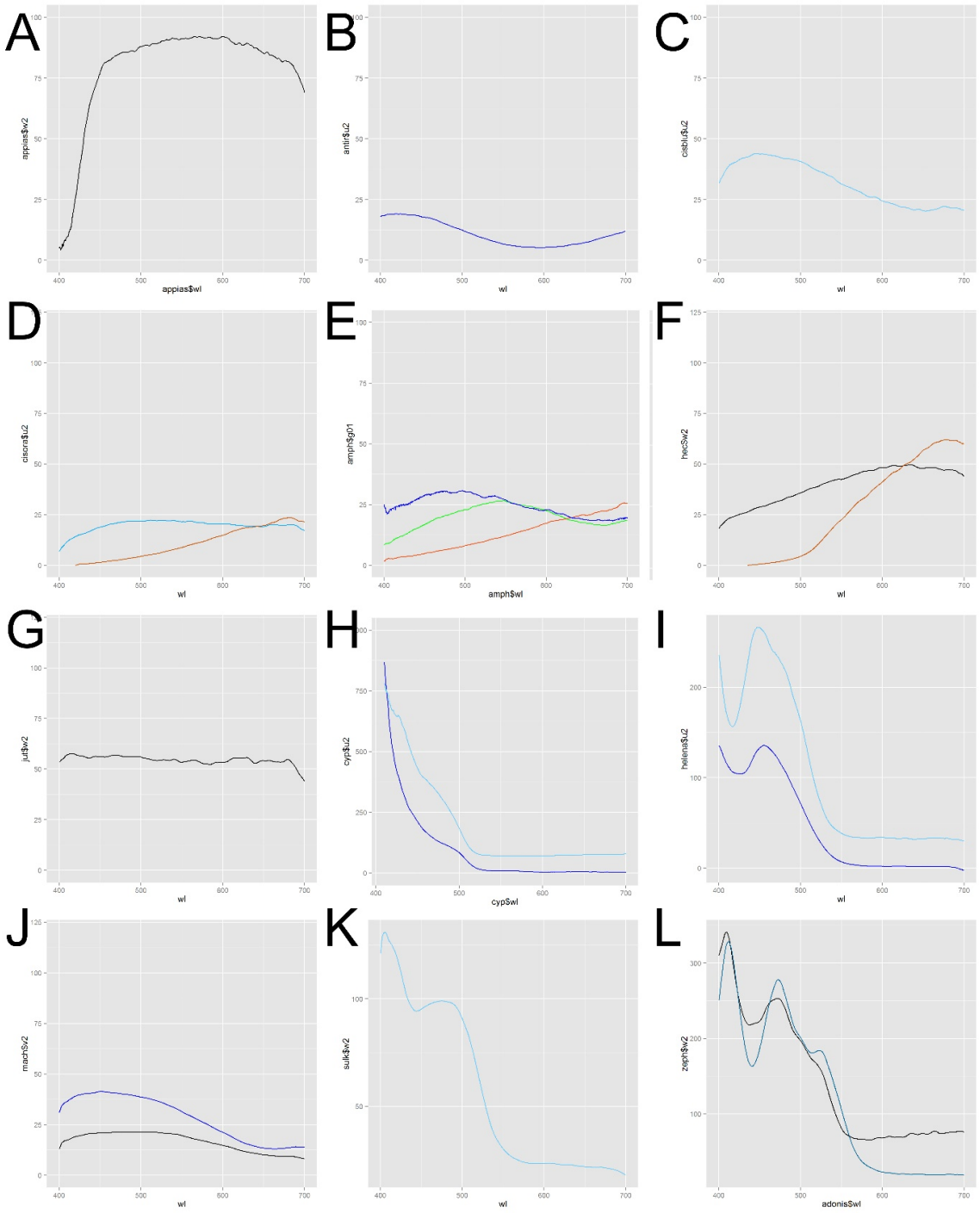

A *Appias sylvia* dorsal white **B** *Antirrhea phlioctetes avernus* hindwing blue spot **C** *M. cisseis gahua* blue form blue region **D** *M. cisseis gahua* orange form, blue line from blue region, orange line from orange region **E** *M. amphitryon*, blue line from blue region, green from green region, orange from orange region **F** *M. hecuba*, black line is white region, orange line orange region **G** *M. theseus* white region **H** *M. cypris* dark blue line blue region, light blue white stripe. Due to extremely high peak at 400nm, we only show data from 410nm to 700nm to highlight the sub peaks found in the spectra. **I** *M. rhetenor helena* dark blue line is blue region reflectance, light blue is white spot **J** *M. achilles* blue - blue green band, black line white spot. **K** *M. sulkowskyi* white region **L** *M. zephyritis* blue line – blue region, black line white spot.

Figure A2.11 Transmitted light analysis of single scales

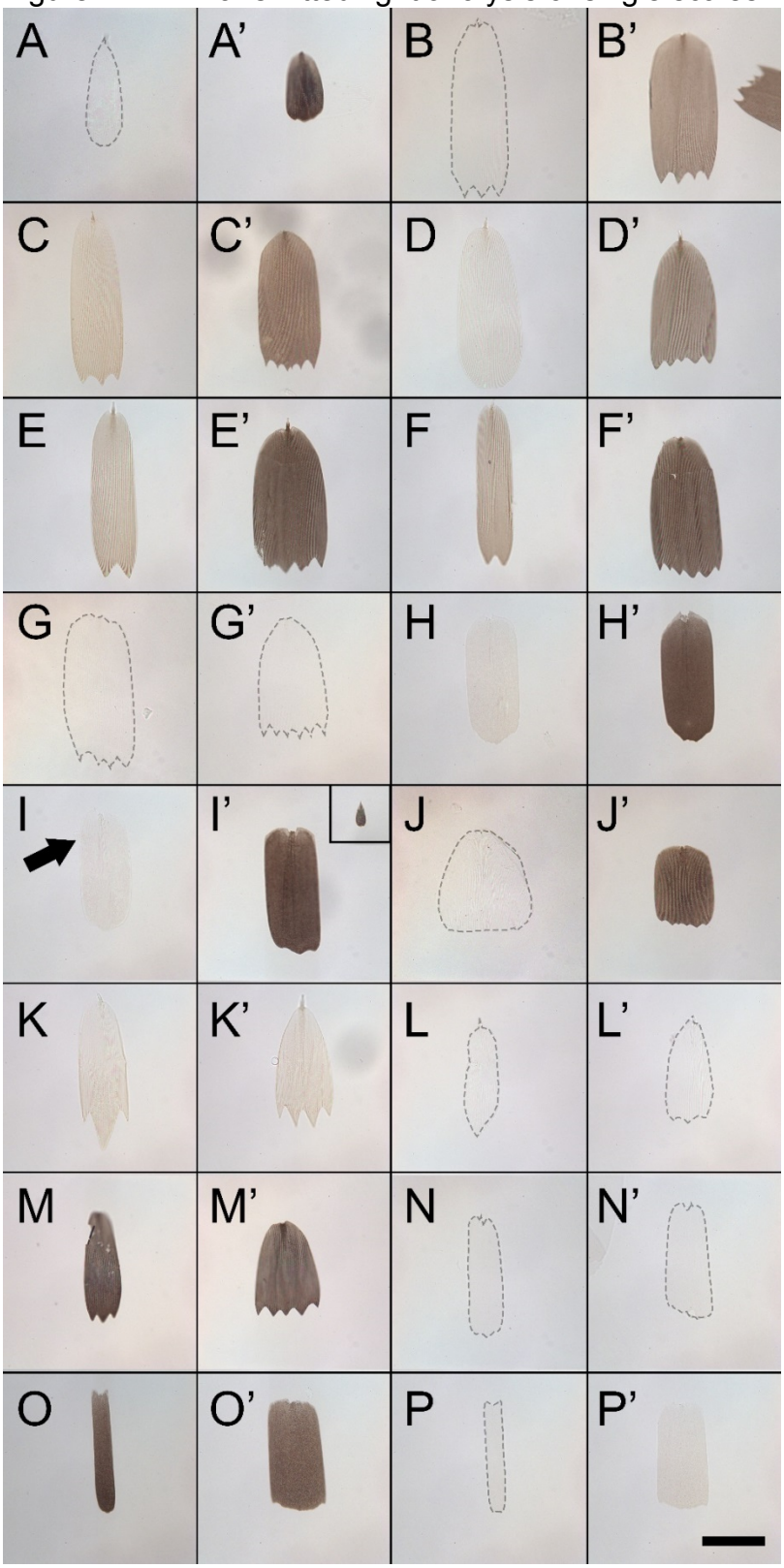

A,A' *Antirrhea philoctetes avernus* cover and ground **B,B'** *M. cisseis* orange region **C,C'** *M. cisseis* blue region **D,D'** *M. amphitryon* blue region **E,E'** *M. amphitryon* green region **F,F'** *M. amphitryon* orange region **G,G'** *M. theseus* white region **H,H'** *M. cypris* ground scales white and blue regions **I,I'** *M. rhetenor helena* ground scale **I,I' arrow,inset** cover scales **J,J'** *M. achilles* green band **K,K'** *M.h. peleides* ventral white region **L,L'** *M.h. peleides* dorsal white spot **M,M'** *M.h. peleides* dorsal black region **N,N'** *M. sulkowskyi* main desaturated blue **O,O'** *M. zephyritis* blue region **P,P'** *M. zephyritis* white spot

Scale bar 100um

Scales in immersion oil matching the cuticle refractive index and visualized in transmission.

Boundaries of unpigmented scales have been shown by dashed line.

Figure A2.12 Single scale transmission data for species not shown in main text

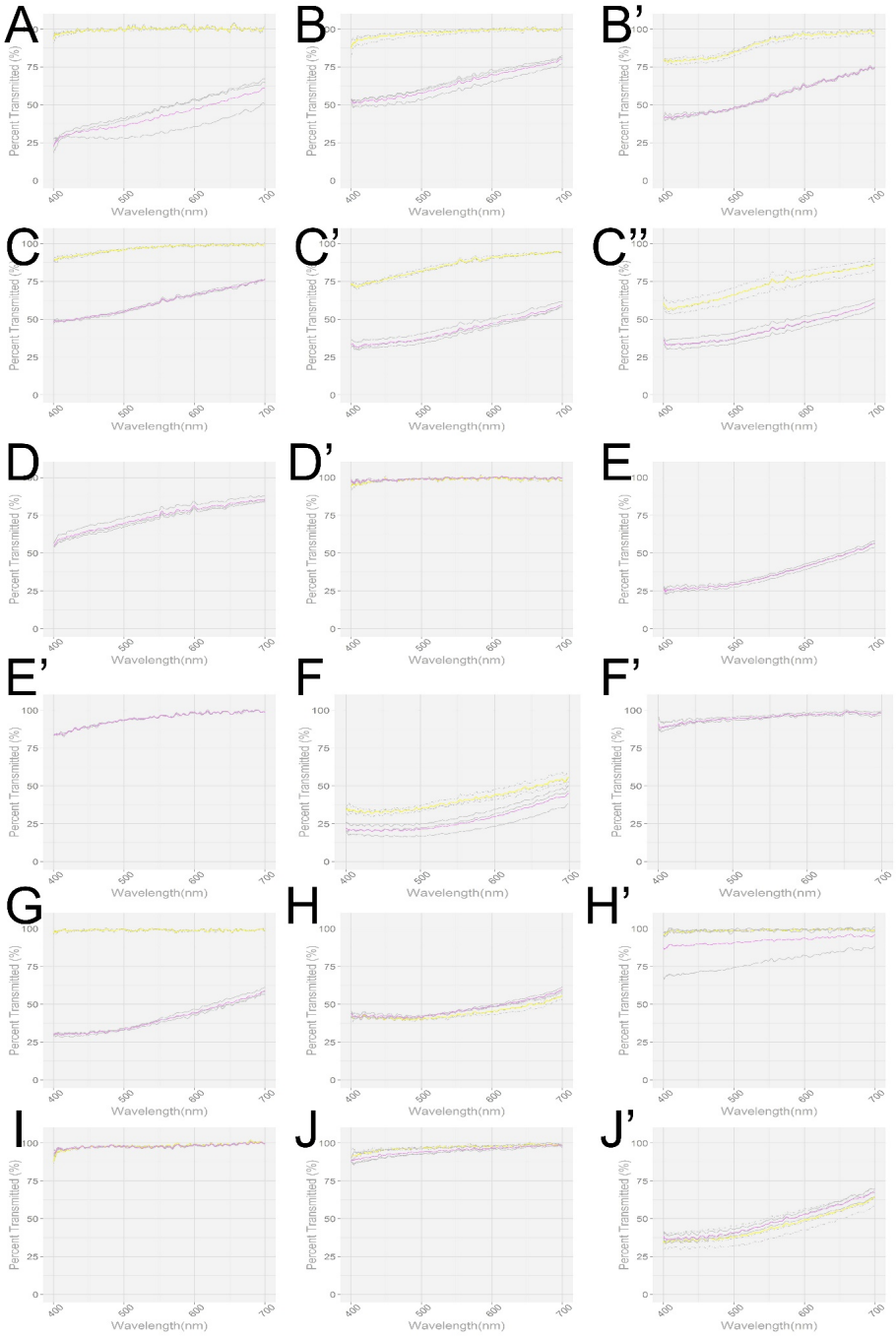

For all spectra, yellow line indicates the average of 3 cover scales, purple line indicates average of 3 ground scales. Dashed grey lines are the individual readings of the cover scales. Solid grey lines are individual readings for the ground scales. **A** *Antirrhea phlioctetes avernus* hindwing blue spot **B** *M. cisseis gahua* orange form from blue region, **B'** *M. cisseis gahua* orange form from orange region **C** *M. amphitryon* from blue region **C'** *M. amphitryon* from green region **C''** *M. amphitryon* from orange region **D** *M. theseus* brown border region (ground scales only) **D'** *M. theseus* white region **E** *M. cypris* blue ground scales (cover not measured) **E'** *M. cypris* white ground scales (cover not measured) **F** *M. rhetenor helena* blue region **F'** *M. rhetenor helena* white region (cover scales not measured) **G** *Morpho achilles* blue-green region **H** *Morpho peleides* distal black region **H'** *Morpho peleides* white spot on dorsal surface **I** *Morpho sulkowskyi* white scales **J** *Morpho zephyritis* dorsal white spot **J'** *Morpho zephyritis* blue region

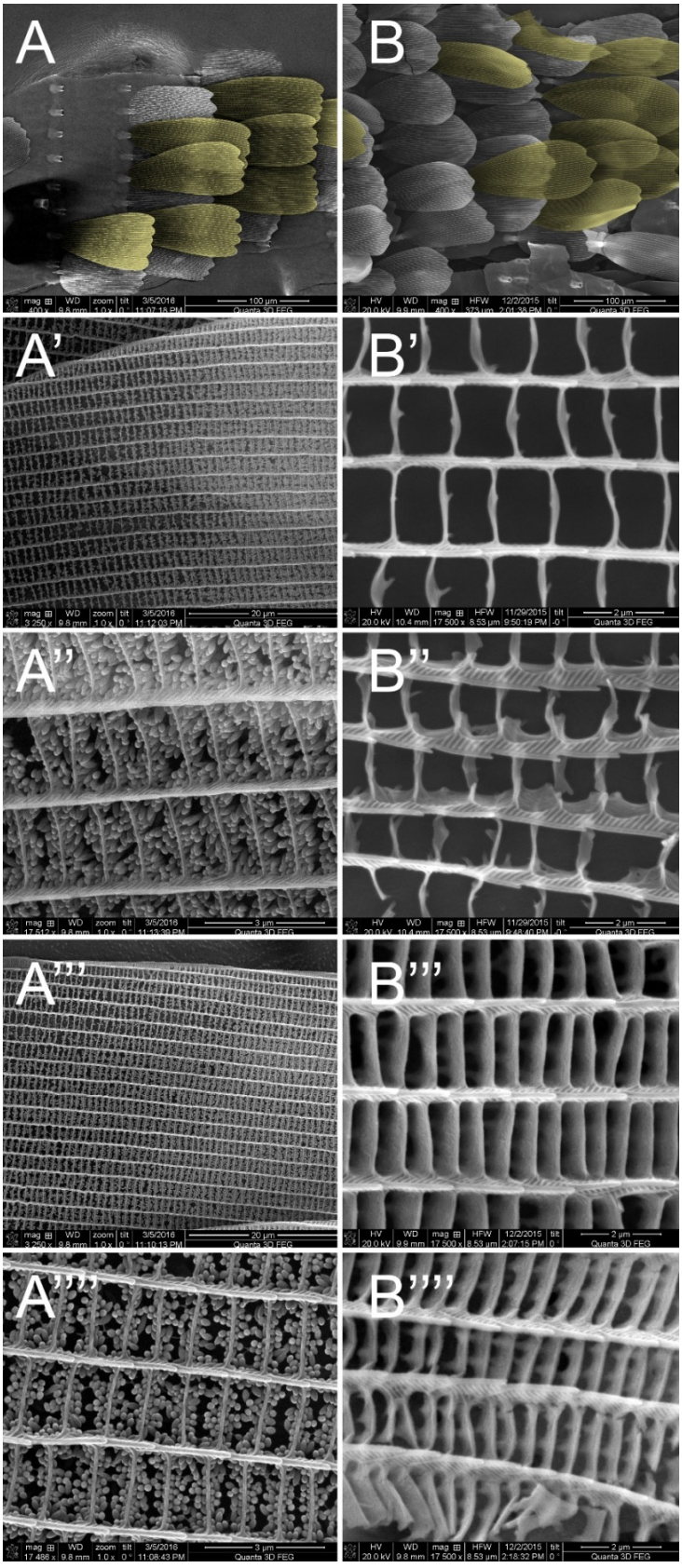

Figure A2.13
SEM analysis of *Appias sylvia* and *Antirrhea philoctetes avernus* ground and cover scales

Top row – views of scales on dorsal wing, yellow pseudocolor indicates cover scale. **X',X''** rows cover scale ridges from above and oblique view **X''',X'''' rows** ground scale ridges from above and oblique view **Scale bars** as indicated in image

A-A'''' *Appias sylvia* **B-B''''** *Antirrhea philoctetes avernus* blue spot

Figure A2.14 SEM analysis of *M. marcus* scales

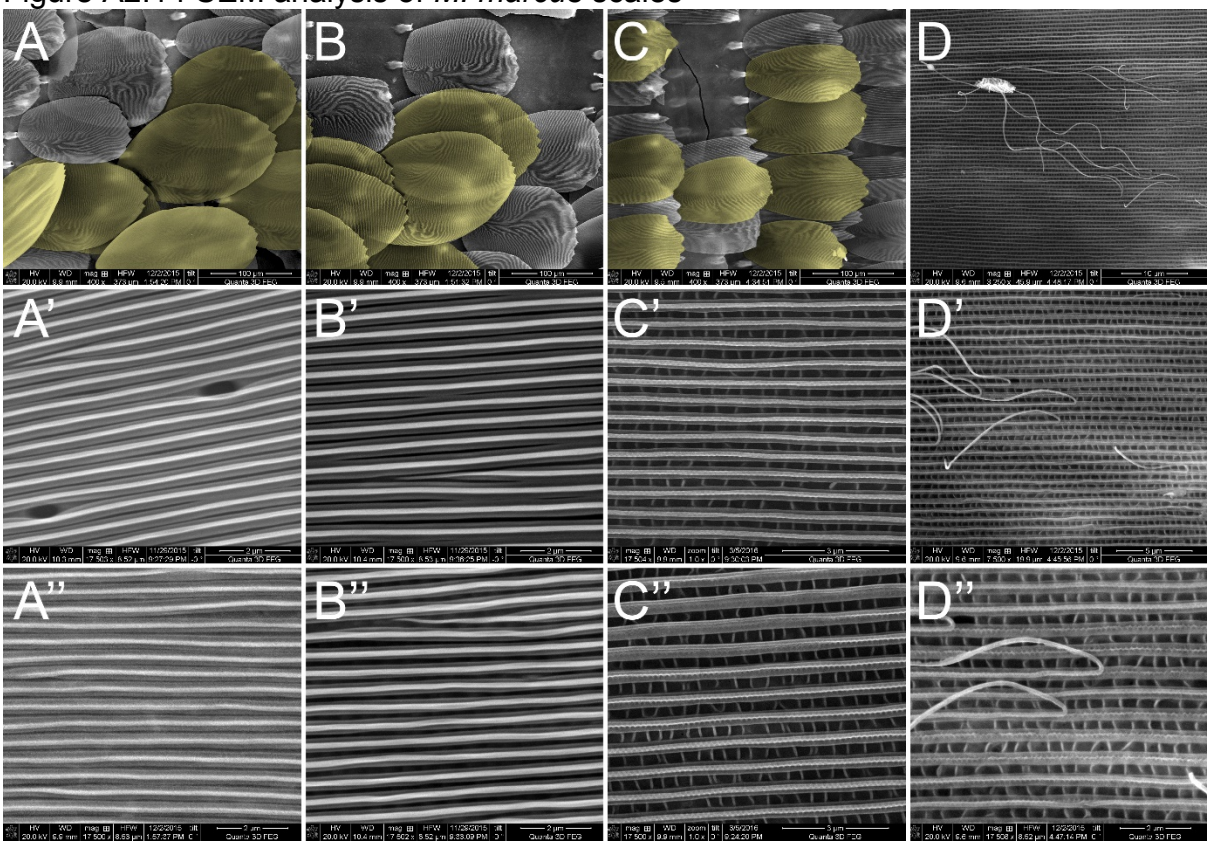

A-C Top row – views of scales on dorsal wing, yellow pseudocolor indicates cover scale. **A'-C' row** Magnification of cover scale ridges from above **A''-C'' row** Magnification of ground scale ridges from above **Scale bars** as indicated in image

A-A'' *M. marcus* main blue **B-B''** *M. marcus* dorsal white spot **C-C''** *M. marcus* distal dark blue **D-D''** Multiple magnifications of a peeled off "traintrack" lamella from dark blue scale.

Figure A2.15 SEM analysis of *M.cisseis, hecuba, theseus, and amphitryon* scales

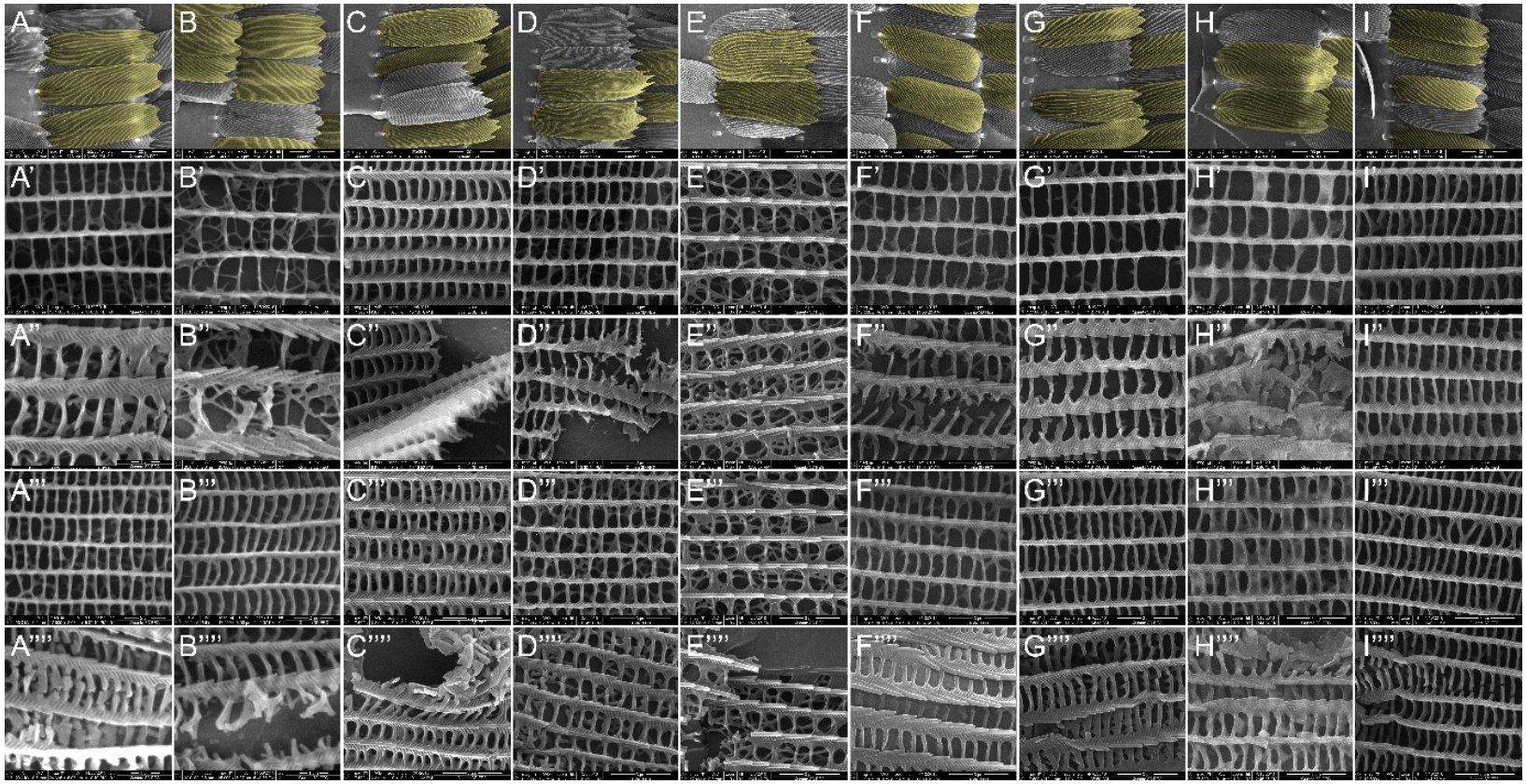

Top row – views of scales on dorsal wing, yellow pseudocolor indicates cover scale. **X',X''** rows cover scale ridges from above and oblique view **X''',X'''' rows** ground scale ridges from above and oblique view **Scale bars** as indicated in image

A-A'''' *M. cisseis gahua* orange region **B-B''''** *M. cisseis gahua* blue region **C-C''''** *M. hecuba* orange region **D-D''''** *M. hecuba* white region **E-E''''** *M. theseus white* region **F-F''''** *M. amphitryon* blue region **G-G''''** *M. amphitryon* green region **H-H''''** *M. amphitryon* yellow region **I-I''''** *M. amphitryon* orange region

Figure A2.16 SEM analysis of *M. amathonte* and *godartii subspecies* scales

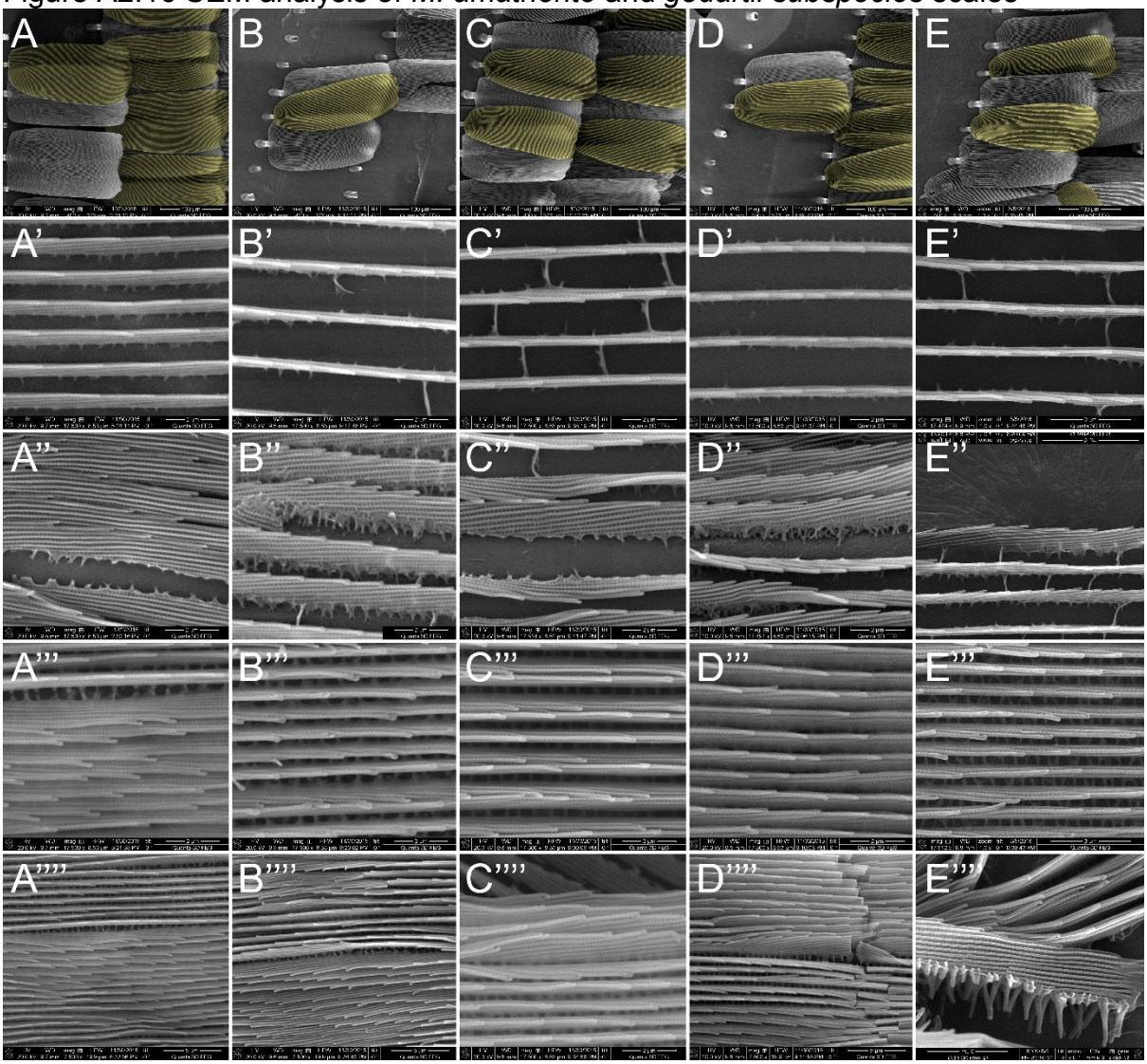

Top row – views of scales on dorsal wing, yellow pseudocolor indicates cover scale. **X',X''** rows cover scale ridges from above and oblique view **X''',X'''' rows** ground scale ridges from above and oblique view **Scale bars** as indicated in image

A-A'''' *M. amathonte* **B-B''''** *M. godartii julansthicus* **C-C''''** *M. godartii didius* **D-D''''** *M. godartii assarpai* Dark form **E-E''''** *M. godartii assarpai* light form

Figure A2.17
SEM analysis of scales of *M.polyphemus, M. epistrophus, M. achilles* and *M.h. peledies*

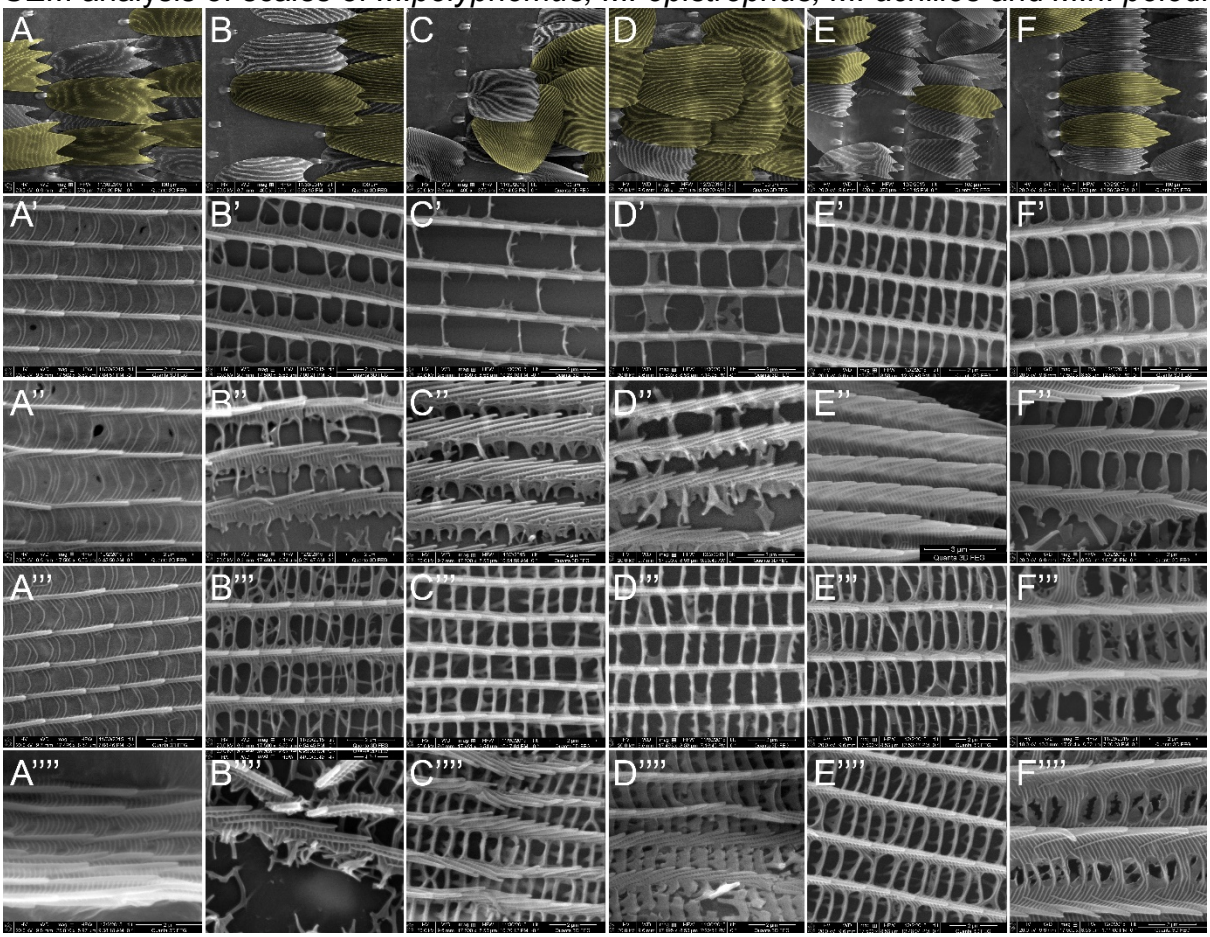

Top row – views of scales on dorsal wing, yellow pseudocolor indicates cover scale. **X',X''** rows cover scale ridges from above and oblique view **X''',X'''' rows** ground scale ridges from above and oblique view **Scale bars** as indicated in image

A-A'''' *M. polyphemus* **B-B''''** *M. epistrophus catenarius* **C-C''''** *M. achilles* **D-D''''** *M.h.peleides* dorsal blue **E-E''''** *M.h.peleides* dorsal black **F-F''''** *M.h.peleide* ventral white

Figure A2.18 SEM analysis of *M. anaxibia* and *M. cypris* scales

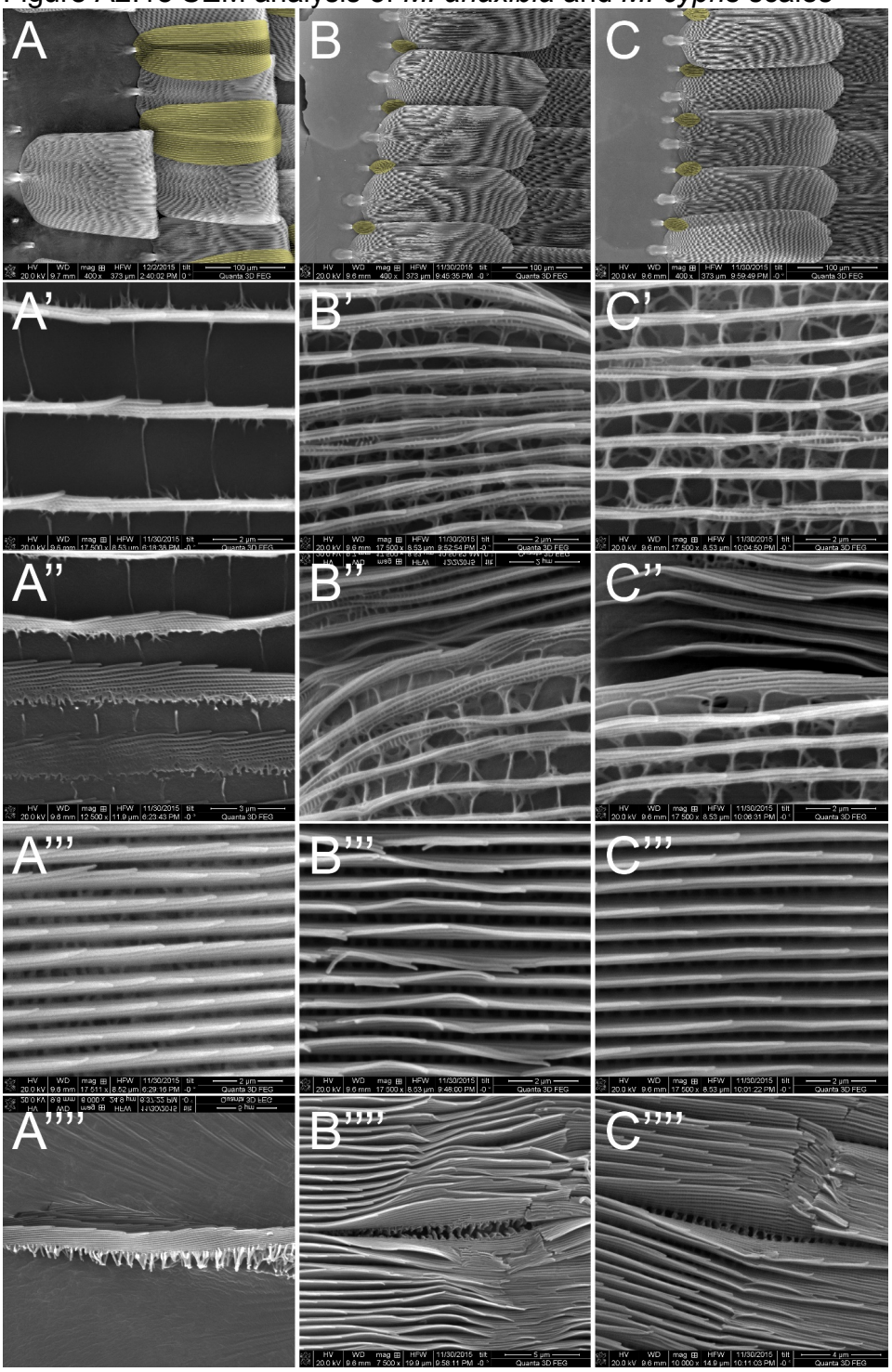

Top row – views of scales on dorsal wing, yellow pseudocolor indicates cover scale. **X',X''** rows cover scale ridges from above and oblique view **X''',X'''' rows** ground scale ridges from above and oblique view **Scale bars** as indicated in image

A-A'''' *M. anaxibia* **B-B''''** *M. cypris* blue region **C-C''''** *M. cypris* white stripe

Figure A2.19 SEM analysis of *M. sulkowskyi and M. zephyritis* scales

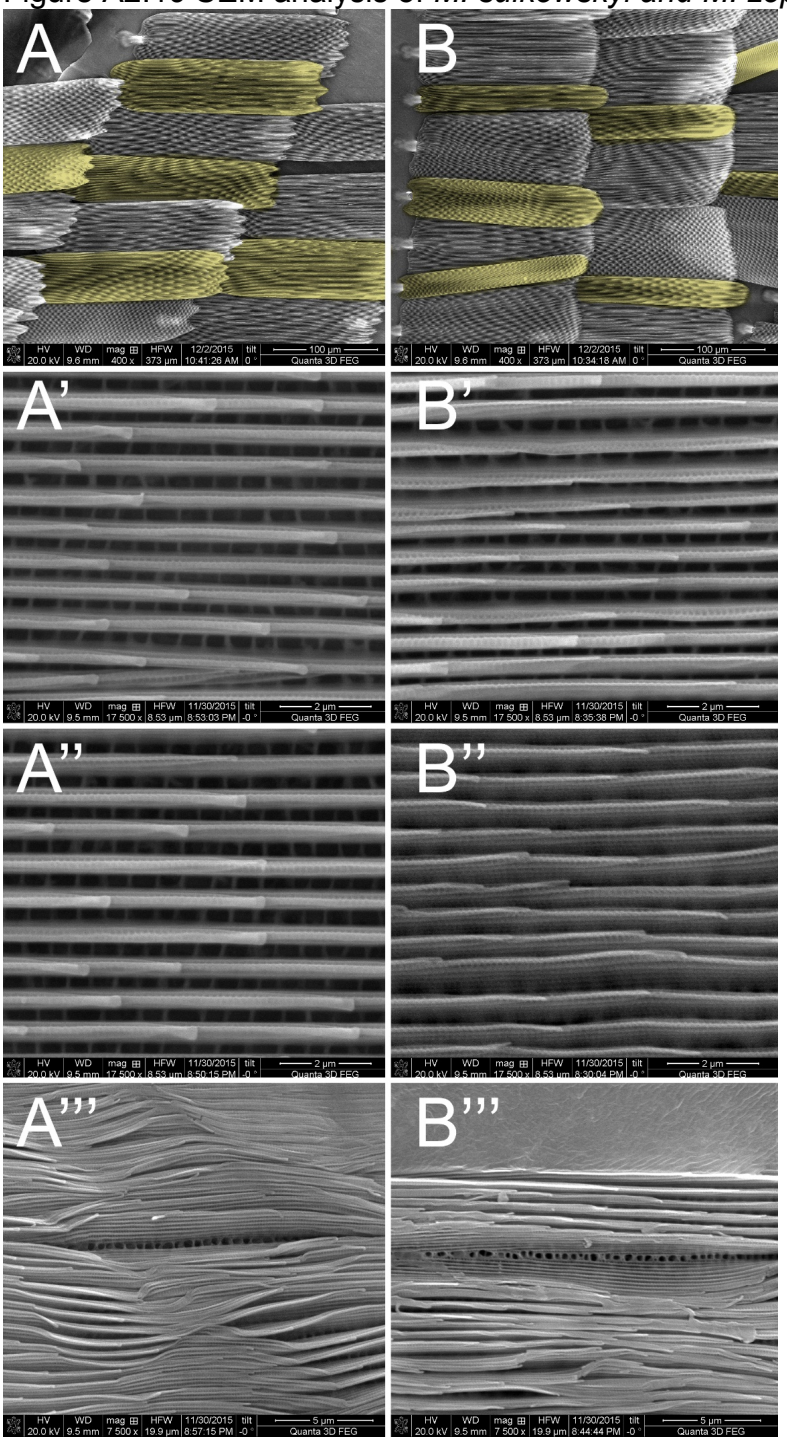

Top row – views of scales on dorsal wing, yellow pseudocolor indicates cover scale. **X',X'''** rows cover scale ridges from above and of damaged cover scales to give an oblique ridge view **X'' row** ground scale ridges from above and oblique view **Scale bars** as indicated in image

A-A''' *M. sulkowskyi* **B-B'''** *M. zephyritis* blue

Figure A2.20 SEM analysis of 3IT *ex vivo* cultured wing disc scales

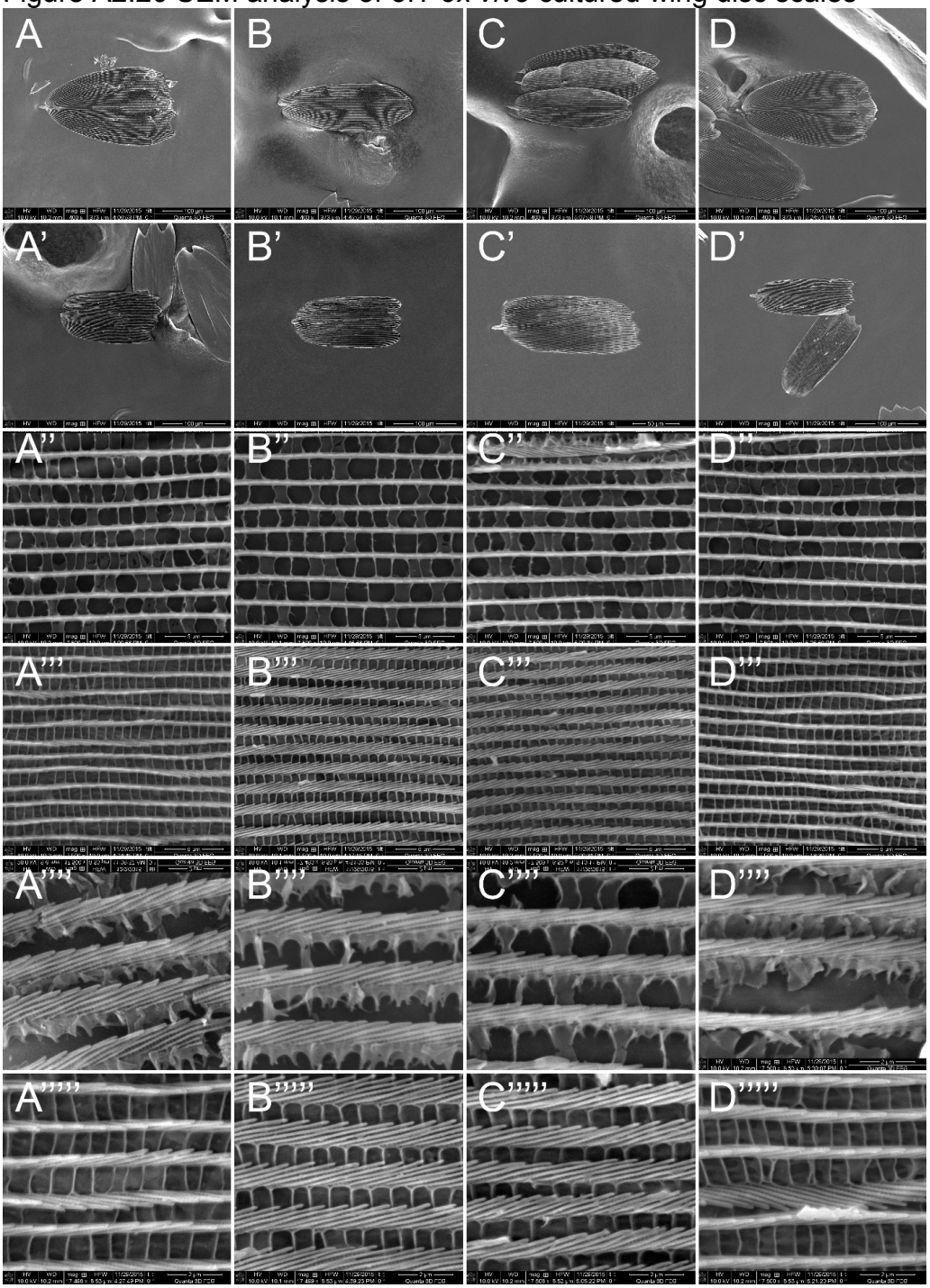

A-A''''' – Scales from STD culture medium cultured wing discs. **B-B''''' –** Scales from STD+3IT culture medium cultured wing discs. **C-C''''' –** Scales from STD+3IT+Tyrosine culture medium cultured wing discs. **D-D''''' –** Scales from STD+3IT+DOPA culture medium cultured wing discs. **X,X'',X'''' = Cover scale; X',X''',X''''' = Ground scale**

Figure A2.21 SEM analysis of scales from masking *ex vivo* experiment

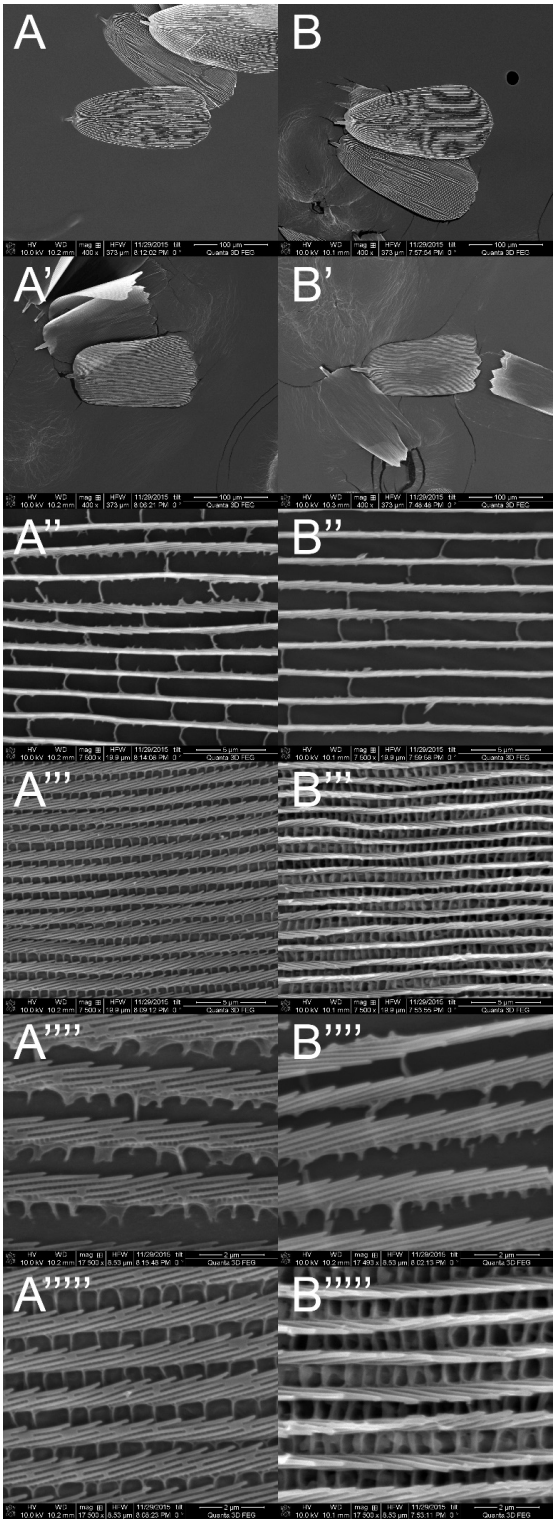

A-A''''' – Scales from masked (naïve) portion of a wing STD+L-DOPA culture medium cultured wing discs. **B-B''''' –** Scales from an exposed region on the same cultured wing. **X,X'',X'''' = Cover scale; X',X''',X''''' = Ground scale**

Figure A2.22 SEM analysis of *in vivo* 3IT-injected *M.h.peleides* scales

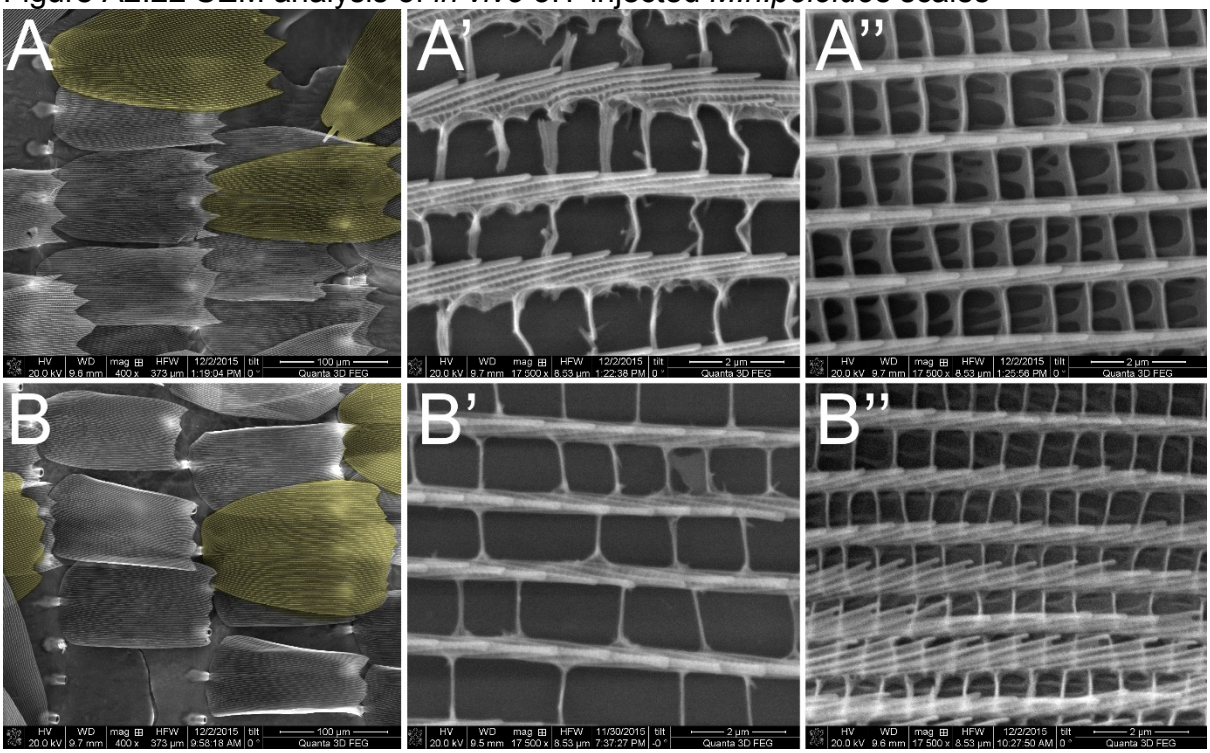

A-A'' Scales from butterfly injected with 60mM 3IT as a pupa. **A** view of the wing with cover scales pseudocolored yellow. **A'** Close up of the cover scale from oblique angle to show ridges. **A''** Close up of the ground scale ridges **B-B''** Scales from butterfly injected with 140mM 3IT as a pupa. **B** view of the wing with cover scales pseudocolored yellow, taco-ing of the ground scales is obvious here. **B'** Close up of the cover scale. **A''** Close up of the ground scale ridges seen from oblique viewing angle to see ridge lamellae.

Appendix 3
Genetic Constructs and Clones

Sequence A3.1 piEx-4:LifeAct:eGFP (AmpR)

```
TITLE       pIELAG (4579bp)
FEATURES             Location/Qualifiers
     misc_feature    1084..1086
                     /note="TLN Start Codon"
     CDS             1177..1248
                     /note="Abp140p Actin binding domain"
     CDS             1249..1968
                     /note="eGFP"
ORIGIN

        1 cgcgtaaaac acaatcaagt atgagtcata agctgatgtc atgttttgca cacggctcat
       61 aaccgaactg gctttacgag tagaattcta cttgtaacgc acgatcagtg gatgatgtca
      121 tttgtttttc aaatcgagat gatgtcatgt tttgcacacg gctcataaac tcgctttacg
      181 agtagaattc tacgtgtaac gcacgatcga ttgatgagtc atttgttttg caatatgata
      241 tcatacaata tgactcattt gtttttcaaa accgaacttg atttacgggt agaattctac
      301 ttgtaaagca caatcaaaaa gatgatgtca tttgtttttc aaaactgaac tcgctttacg
      361 agtagaattc tacgtgtaaa acacaatcaa gaaatgatgt catttgttat aaaaataaaa
      421 gctgatgtca tgttttgcac atggctcata actaaactcg ctttacgggt agaattctac
      481 gcgcgtcgat gtctttgtga tgcgcgcgac atttttgtag gttattgata aaatgaacgg
      541 atacgttgcc cgacattatc attaaatcct tggcgtagaa tttgtcgggt ccattgtccg
      601 tgtgcgctag catgcccgta acggacctcg tacttttggc ttcaaaggtt ttgcgcacag
      661 acaaaatgtg ccacacttgc agctctgcat gtgtgcgcgt taccacaaat cccaacggcg
      721 cagtgtactt gttgtatgca aataaatctc gataaaggcg cggcgcgcga atgcagctga
      781 tcacgtacgc tcctcgtgtt ccgttcaagg acggtgttat cgacctcaga ttaatgttta
      841 tcggccgact gttttcgtat ccgctcacca aacgcgtttt tgcattaaca ttgtatgtcg
      901 gcggatgttc tatatctaat ttgaataaat aaacgataac cgcgttggtt ttagagggca
```

961 taataaaaga aatattgtta tcgtgttcgc cattagggca gtataaattg acgttcatgt
1021 tggatattgt ttcagttgca agttgacact ggcggcgaca agatcgtgaa caaccaagtg
1081 accatggcat cgttaacacg tcaagagctc gcggatccca attggcAGAT CTCGAGCTCA
1141 AGCTTCGAAT TCTGCAGTCG ACGGTACCGC GGGCCcATGG GTGTCGCAGA TTTGATCAAG
1201 AAATTCGAAA GCATCTCAAA GGAAGAActg GATCCACCGG TCGCCACCAT GGTGAGCAAG
1261 GGCGAGGAGC TGTTCACCGG GGTGGTGCCC ATCCTGGTCG AGCTGGACGG CGACGTAAAC
1321 GGCCACAAGT TCAGCGTGTC CGGCGAGGGC GAGGGCGATG CCACCTACGG CAAGCTGACC
1381 CTGAAGTTCA TCTGCACCAC CGGCAAGCTG CCCGTGCCCT GGCCCACCCT CGTGACCACC
1441 CTGACCTACG GCGTGCAGTG CTTCAGCCGC TACCCCGACC ACATGAAGCA GCACGACTTC
1501 TTCAAGTCCG CCATGCCCGA AGGCTACGTC CAGGAGCGCA CCATCTTCTT CAAGGACGAC
1561 GGCAACTACA AGACCCGCGC CGAGGTGAAG TTCGAGGGCG ACACCCTGGT GAACCGCATC
1621 GAGCTGAAGG GCATCGACTT CAAGGAGGAC GGCAACATCC TGGGGCACAA GCTGGAGTAC
1681 AACTACAACA GCCACAACGT CTATATCATG GCCGACAAGC AGAAGAACGG CATCAAGGTG
1741 AACTTCAAGA TCCGCCACAA CATCGAGGAC GGCAGCGTGC AGCTCGCCGA CCACTACCAG
1801 CAGAACACCC CCATCGGCGA CGGCCCCGTG CTGCTGCCCG ACAACCACTA CCTGAGCACC
1861 CAGTCCGCCC TGAGCAAAGA CCCCAACGAG AAGCGCGATC ACATGGTCCT GCTGGAGTTC
1921 GTGACCGCCG CCGGGATCAC TCTCGGCATG GACGAGCTGT ACAAGTAAAG CGGCCGCatc
1981 ttctggtaaa gaaaccgctg ctgcgaaatt tgaacgccag cacatggact cgccaccgcc
2041 ttctggcctc gagcaccacc atcaccatca ccatcactaa gtgattaacc tcaggttata
2101 catatatttt gaatttaatt aattatacat atattttata ttatttttgt cttttattat
2161 cgaggggccg ttgttggtgt ggggttttgc atagaaataa caatgggagt tggcgacgtt
2221 gctgcgccaa caccacctcc cttccctcct ttcatcatgt atctgtagat aaaataaaat
2281 attaaaccta aaaacaagac cgcgcctatc aacaaaatga taggcattaa cttgccgctg
2341 acgctgtcac taacgttgga cgatttgccg actaaacctt catcgcccag taaccaatct
2401 agacgtcagg tggcactttt cggggaaatg tgcgcggaac ccctatttgt ttatttttct
2461 aaatacattc aaatatgtat ccgctcatga gacaataacc ctgataaatg cttcaataat
2521 attgaaaaag gaagagtatg agtattcaac atttccgtgt cgcccttatt ccctttttg
2581 cggcattttg ccttcctgtt tttgctcacc cagaaacgct ggtgaaagta aaagatgctg
2641 aagatcagtt gggtgcacga gtgggttaca tcgaactgga tctcaacagc ggtaagatcc
2701 ttgagagttt tcgccccgaa gaacgttttc caatgatgag cacttttaaa gttctgctat
2761 gtggcgcggt attatcccgt attgacgccg ggcaagagca actcggtcgc cgcatacact
2821 attctcagaa tgacttggtt gagtactcac cagtcacaga aaagcatctt acggatggca

2881 tgacagtaag agaattatgc agtgctgcca taaccatgag tgataacact gcggccaact

2941 tacttctgac aacgatcgga ggaccgaagg agctaaccgc ttttttgcac aacatggggg

3001 atcatgtaac tcgccttgat cgttgggaac cggagctgaa tgaagccata ccaaacgacg

3061 agcgtgacac cacgatgcct gtagcaatgg caacaacgtt gcgcaaacta ttaactggcg

3121 aactacttac tctagcttcc cggcaacaat taatagactg gatggaggcg gataaagttg

3181 caggaccact tctgcgctcg gcccttccgg ctggctggtt tattgctgat aaatctggag

3241 ccggtgagcg tgggtctcgc ggtatcattg cagcactggg gccagatggt aagccctccc

3301 gtatcgtagt tatctacacg acggggagtc aggcaactat ggatgaacga aatagacaga

3361 tcgctgagat aggtgcctca ctgattaagc attggtaact gtcagaccaa gtttactcat

3421 atatacttta gattgattta aaacttcatt tttaatttaa aaggatctag gtgaagatcc

3481 tttttgataa tctcatgacc aaaatccctt aacgtgagtt ttcgttccac tgagcgtcag

3541 accccgtaga aaagatcaaa ggatcttctt gagatccttt ttttctgcgc gtaatctgct

3601 gcttgcaaac aaaaaaacca ccgctaccag cggtggtttg tttgccggat caagagctac

3661 caactctttt tccgaaggta actggcttca gcagagcgca gataccaaat actgtccttc

3721 tagtgtagcc gtagttaggc caccacttca agaactctgt agcaccgcct acatacctcg

3781 ctctgctaat cctgttacca gtggctgctg ccagtggcga taagtcgtgt cttaccgggt

3841 tggactcaag acgatagtta ccggataagg cgcagcggtc gggctgaacg gggggttcgt

3901 gcacacagcc cagcttggag cgaacgacct acaccgaact gagataccta cagcgtgagc

3961 tatgagaaag cgccacgctt cccgaaggga gaaaggcgga caggtatccg gtaagcggca

4021 gggtcggaac aggagagcgc acgagggagc ttccaggggg aaacgcctgg tatctttata

4081 gtcctgtcgg gtttcgccac ctctgacttg agcgtcgatt tttgtgatgc tcgtcagggg

4141 ggcggagcct atggaaaaac gccagcaacg cggccttttt acggttcctg gccttttgct

4201 ggccttttgc tcacatgttc tttcctgcgt tatcccctga ttctgtggat aaccgtatta

4261 ccgcctttga gtgagctgat accgctcgcc gcagccgaac gaccgagcgc agcgagtcag

4321 tgagcgagga agcggaagag cgcccaatac gcaaaccgcc tctccccgcg cgttggccga

4381 ttcattaatg cagctggcac gacaggtttc ccgactggaa agcgggcagt gagcgcaacg

4441 caattaatgt gagttagctc actcattagg caccccaggc tttacacttt atgcttccgg

4501 ctcgtatgtt gtgtggaatt gtgagcggat aacaatttca cacaggaaac agctatgacc

4561 atgattacga attcccggg

//

A gift of Henk Roelink's lab, LifeAct:eGFP was subcloned from a CMV:LifeAct:eGFP:N1 plasmid, digested using NEB restriction enzymes BglII and NotI and ligated into Novagen's pIEx-4 plasmid cut using the same enzymes. Plasmid constructed by Jessica Poon.

Sequence A3.2 pIEx-4:LifeAct:mCherry (AmpR)

```
TITLE       pIEx:LA:mCherry  (4404bp)
FEATURES             Location/Qualifiers
     misc_feature    1084..1086
                     /note="TLN Start Codon"
     misc_recomb     1092..1097
                     /note="HpaI site"
     CDS             1099..1149
                     /note="Abp140p Actin Binding Domain"
     CDS             1162..1872
                     /note="mCherry coding"
     misc_recomb     1873..1878
                     /note="XhoI cut site"
ORIGIN

        1 cgcgtaaaac acaatcaagt atgagtcata agctgatgtc atgttttgca cacggctcat
       61 aaccgaactg gctttacgag tagaattcta cttgtaacgc acgatcagtg gatgatgtca
      121 tttgtttttc aaatcgagat gatgtcatgt tttgcacacg gctcataaac tcgctttacg
      181 agtagaattc tacgtgtaac gcacgatcga ttgatgagtc atttgttttg caatatgata
      241 tcatacaata tgactcattt gtttttcaaa accgaacttg atttacgggt agaattctac
      301 ttgtaaagca caatcaaaaa gatgatgtca tttgtttttc aaaactgaac tcgctttacg
      361 agtagaattc tacgtgtaaa acacaatcaa gaaatgatgt catttgttat aaaaataaaa
      421 gctgatgtca tgttttgcac atggctcata actaaactcg ctttacgggt agaattctac
      481 gcgcgtcgat gtctttgtga tgcgcgcgac atttttgtag gttattgata aaatgaacgg
      541 atacgttgcc cgacattatc attaaatcct tggcgtagaa tttgtcgggt ccattgtccg
      601 tgtgcgctag catgcccgta acggacctcg tacttttggc ttcaaaggtt ttgcgcacag
      661 acaaaatgtg ccacacttgc agctctgcat gtgtgcgcgt taccacaaat cccaacggcg
      721 cagtgtactt gttgtatgca aataaatctc gataaaggcg cggcgcgcga atgcagctga
      781 tcacgtacgc tcctcgtgtt ccgttcaagg acggtgttat cgacctcaga ttaatgttta
      841 tcggccgact gttttcgtat ccgctcacca aacgcgtttt tgcattaaca ttgtatgtcg
      901 gcggatgttc tatatctaat ttgaataaat aaacgataac cgcgttggtt ttagagggca
```

961 taataaaaga aatattgtta tcgtgttcgc cattagggca gtataaattg acgttcatgt
1021 tggatattgt ttcagttgca agttgacact ggcggcgaca agatcgtgaa caaccaagtg
1081 accATGgcat cgttaactAT GGGTGTCGCA GATTTGATCA AGAAATTCGA AAGCATCTCA
1141 AAGGAAGAAC TGGATCCTAG AATGGTGAGC AAGGGCGAGG AGGATAACAT GGCCATCATC
1201 AAGGAGTTCA TGCGCTTCAA GGTGCACATG GAGGGCTCCG TGAACGGCCA CGAGTTCGAG
1261 ATCGAGGGCG AGGGCGAGGG CCGCCCCTAC GAGGGCACCC AGACCGCCAA GCTGAAGGTG
1321 ACCAAGGGTG GCCCCCTGCC CTTCGCCTGG GACATCCTGT CCCCTCAGTT CATGTACGGC
1381 TCCAAGGCCT ACGTGAAGCA CCCCGCCGAC ATCCCCGACT ACTTGAAGCT GTCCTTCCCC
1441 GAGGGCTTCA AGTGGGAGCG CGTGATGAAC TTCGAGGACG GCGGCGTGGT GACCGTGACC
1501 CAGGACTCCT CCCTGCAGGA CGGCGAGTTC ATCTACAAGG TGAAGCTGCG CGGCACCAAC
1561 TTCCCCTCCG ACGGCCCCGT AATGCAGAAG AAGACCATGG GCTGGGAGGC CTCCTCCGAG
1621 CGGATGTACC CCGAGGACGG CGCCCTGAAG GGCGAGATCA AGCAGAGGCT GAAGCTGAAG
1681 GACGGCGGCC ACTACGACGC TGAGGTCAAG ACCACCTACA AGGCCAAGAA GCCCGTGCAG
1741 CTGCCCGGCG CCTACAACGT CAACATCAAG TTGGACATCA CCTCCCACAA CGAGGACTAC
1801 ACCATCGTGG AACAGTACGA ACGCGCCGAG GGCCGCCACT CCACCGGCGG CATGGACGAG
1861 CTGTACAAGT GActcgagca ccaccatcac catcaccatc actaagtgat taacctcagg
1921 ttatacatat attttgaatt taattaatta tacatatatt ttatattatt tttgtctttt
1981 attatcgagg ggccgttgtt ggtgtggggt tttgcataga aataacaatg ggagttggcg
2041 acgttgctgc gccaacacca cctcccttcc ctcctttcat catgtatctg tagataaaat
2101 aaaatattaa acctaaaaac aagaccgcgc ctatcaacaa aatgataggc attaacttgc
2161 cgctgacgct gtcactaacg ttggacgatt tgccgactaa accttcatcg cccagtaacc
2221 aatctagacg tcaggtggca cttttcgggg aaatgtgcgc ggaaccccta tttgtttatt
2281 tttctaaata cattcaaata tgtatccgct catgagacaa taaccctgat aaatgcttca
2341 ataatattga aaaaggaaga gtatgagtat tcaacatttc cgtgtcgccc ttattccctt
2401 ttttgcggca ttttgccttc ctgtttttgc tcacccagaa acgctggtga aagtaaaaga
2461 tgctgaagat cagttgggtg cacgagtggg ttacatcgaa ctggatctca acagcggtaa
2521 gatccttgag agttttcgcc ccgaagaacg ttttccaatg atgagcactt ttaaagttct
2581 gctatgtggc gcggtattat cccgtattga cgccgggcaa gagcaactcg gtcgccgcat
2641 acactattct cagaatgact tggttgagta ctcaccagtc acagaaaagc atcttacgga
2701 tggcatgaca gtaagagaat tatgcagtgc tgccataacc atgagtgata acactgcggc
2761 caacttactt ctgacaacga tcggaggacc gaaggagcta accgcttttt tgcacaacat
2821 gggggatcat gtaactcgcc ttgatcgttg ggaaccggag ctgaatgaag ccataccaaa

```
2881 cgacgagcgt gacaccacga tgcctgtagc aatggcaaca acgttgcgca aactattaac
2941 tggcgaacta cttactctag cttcccggca acaattaata gactggatgg aggcggataa
3001 agttgcagga ccacttctgc gctcggccct tccggctggc tggtttattg ctgataaatc
3061 tggagccggt gagcgtgggt ctcgcggtat cattgcagca ctggggccag atggtaagcc
3121 ctcccgtatc gtagttatct acacgacggg gagtcaggca actatggatg aacgaaatag
3181 acagatcgct gagataggtg cctcactgat taagcattgg taactgtcag accaagttta
3241 ctcatatata ctttagattg atttaaaact tcatttttaa tttaaaagga tctaggtgaa
3301 gatccttttt gataatctca tgaccaaaat cccttaacgt gagttttcgt tccactgagc
3361 gtcagacccc gtagaaaaga tcaaaggatc ttcttgagat cctttttttc tgcgcgtaat
3421 ctgctgcttg caaacaaaaa aaccaccgct accagcggtg gtttgtttgc cggatcaaga
3481 gctaccaact ctttttccga aggtaactgg cttcagcaga gcgcagatac caaatactgt
3541 ccttctagtg tagccgtagt taggccacca cttcaagaac tctgtagcac cgcctacata
3601 cctcgctctg ctaatcctgt taccagtggc tgctgccagt ggcgataagt cgtgtcttac
3661 cgggttggac tcaagacgat agttaccgga taaggcgcag cggtcgggct gaacgggggg
3721 ttcgtgcaca cagcccagct tggagcgaac gacctacacc gaactgagat acctacagcg
3781 tgagctatga gaaagcgcca cgcttcccga agggagaaag gcggacaggt atccggtaag
3841 cggcagggtc ggaacaggag agcgcacgag ggagcttcca gggggaaacg cctggtatct
3901 ttatagtcct gtcgggtttc gccacctctg acttgagcgt cgatttttgt gatgctcgtc
3961 aggggggcgg agcctatgga aaaacgccag caacgcggcc tttttacggt tcctggcctt
4021 ttgctggcct tttgctcaca tgttctttcc tgcgttatcc cctgattctg tggataaccg
4081 tattaccgcc tttgagtgag ctgataccgc tcgccgcagc cgaacgaccg agcgcagcga
4141 gtcagtgagc gaggaagcgg aagagcgccc aatacgcaaa ccgcctctcc ccgcgcgttg
4201 gccgattcat taatgcagct ggcacgacag gtttcccgac tggaaagcgg gcagtgagcg
4261 caacgcaatt aatgtgagtt agctcactca ttaggcaccc caggctttac actttatgct
4321 tccggctcgt atgttgtgtg gaattgtgag cggataacaa tttcacacag gaaacagcta
4381 tgaccatgat tacgaattcc cggg
```

//

A gift of Henk Roelink's lab, LifeAct:mCherry was subcloned from a CMV:LifeAct:mCherry:N1 plasmid by PCR amplification using the primers RWN021: aaaGTTAACtATGGGTGTCGCAGATTTGA and RWN022: aatCTCGAGTCACTTGTACAGCTCGTCCATG. The purified fragment was digested using NEB restriction enzymes HpaI and XhoI and ligated into Novagen's pIEx-4 plasmid cut with the same enzymes.

Sequence A3.3 “pfIErfly” → pSLfa1180fa[IEx] (AmpR)

```
TITLE       pfIErfly --> pSLfa180fa[HpaI/Xba1] + piex[EcoRV/Xba1] (4813bp)
            -> Use FseI to subclone into pBac,pHer,pMos
            --> FseI is terrible, use this plasmid only as a control
            ---> HpaI, BmgBI, BspMI, SbfI, AgeI, KpnI, PflMI single cut
      within MCS of pIEx fragment


FEATURES             Location/Qualifiers
     misc_recomb     2882..2889
                 /note="FseI - North site"
     misc_recomb     3306..4423
                     /note="pIEx HR5/IE:MCS:Terminator"
     misc_recomb     3911..3916
                     /note="HpaI"
     misc_feature    3903..3905
                     /note="TLN Start Codon"
     misc_recomb     4563..4570
                 /note="FseI - South site"
ORIGIN

        1 TCTTCCGCTT CCTCGCTCAC TGACTCGCTG CGCTCGGTCG TTCGGCTGCG GCGAGCGGTA
       61 TCAGCTCACT CAAAGGCGGT AATACGGTTA TCCACAGAAT CAGGGGATAA CGCAGGAAAG
      121 AACATGTGAG CAAAAGGCCA GCAAAAGGCC AGGAACCGTA AAAAGGCCGC GTTGCTGGCG
      181 TTTTTCCATA GGCTCCGCCC CCCTGACGAG CATCACAAAA ATCGACGCTC AAGTCAGAGG
      241 TGGCGAAACC CGACAGGACT ATAAAGATAC CAGGCGTTTC CCCCTGGAAG CTCCCTCGTG
      301 CGCTCTCCTG TTCCGACCCT GCCGCTTACC GGATACCTGT CCGCCTTTCT CCCTTCGGGA
      361 AGCGTGGCGC TTTCTCATAG CTCACGCTGT AGGTATCTCA GTTCGGTGTA GGTCGTTCGC
      421 TCCAAGCTGG GCTGTGTGCA CGAACCCCCC GTTCAGCCCG ACCGCTGCGC CTTATCCGGT
      481 AACTATCGTC TTGAGTCCAA CCCGGTAAGA CACGACTTAT CGCCACTGGC AGCAGCCACT
      541 GGTAACAGGA TTAGCAGAGC GAGGTATGTA GGCGGTGCTA CAGAGTTCTT GAAGTGGTGG
      601 CCTAACTACG GCTACACTAG AAGAACAGTA TTTGGTATCT GCGCTCTGCT GAAGCCAGTT
```

661 ACCTTCGGAA AAAGAGTTGG TAGCTCTTGA TCCGGCAAAC AAACCACCGC TGGTAGCGGT

721 GGTTTTTTTG TTTGCAAGCA GCAGATTACG CGCAGAAAAA AAGGATCTCA AGAAGATCCT

781 TTGATCTTTT CTACGGGGTC TGACGCTCAG TGGAACGAAA ACTCACGTTA AGGGATTTTG

841 GTCATGAGAT TATCAAAAAG GATCTTCACC TAGATCCTTT TAAATTAAAA ATGAAGTTTT

901 AAATCAATCT AAAGTATATA TGAGTAAACT TGGTCTGACA GTTACCAATG CTTAATCAGT

961 GAGGCACCTA TCTCAGCGAT CTGTCTATTT CGTTCATCCA TAGTTGCCTG ACTCCCCGTC

1021 GTGTAGATAA CTACGATACG GGAGGGCTTA CCATCTGGCC CCAGTGCTGC AATGATACCG

1081 CGAGACCCAC GCTCACCGGC TCCAGATTTA TCAGCAATAA ACCAGCCAGC CGGAAGGGCC

1141 GAGCGCAGAA GTGGTCCTGC AACTTTATCC GCCTCCATCC AGTCTATTAA TTGTTGCCGG

1201 GAAGCTAGAG TAAGTAGTTC GCCAGTTAAT AGTTTGCGCA ACGTTGTTGC CATTGCTACA

1261 GGCATCGTGG TGTCACGCTC GTCGTTTGGT ATGGCTTCAT TCAGCTCCGG TTCCCAACGA

1321 TCAAGGCGAG TTACATGATC CCCCATGTTG TGCAAAAAAG CGGTTAGCTC CTTCGGTCCT

1381 CCGATCGTTG TCAGAAGTAA GTTGGCCGCA GTGTTATCAC TCATGGTTAT GGCAGCACTG

1441 CATAATTCTC TTACTGTCAT GCCATCCGTA AGATGCTTTT CTGTGACTGG TGAGTACTCA

1501 ACCAAGTCAT TCTGAGAATA GTGTATGCGG CGACCGAGTT GCTCTTGCCC GGCGTCAATA

1561 CGGGATAATA CCGCGCCACA TAGCAGAACT TTAAAAGTGC TCATCATTGG AAAACGTTCT

1621 TCGGGGCGAA AACTCTCAAG GATCTTACCG CTGTTGAGAT CCAGTTCGAT GTAACCCACT

1681 CGTGCACCCA ACTGATCTTC AGCATCTTTT ACTTTCACCA GCGTTTCTGG GTGAGCAAAA

1741 ACAGGAAGGC AAAATGCCGC AAAAAAGGGA ATAAGGGCGA CACGGAAATG TTGAATACTC

1801 ATACTCTTCC TTTTTCAATA TTATTGAAGC ATTTATCAGG GTTATTGTCT CATGAGCGGA

1861 TACATATTTG AATGTATTTA GAAAAATAAA CAAATAGGGG TTCCGCGCAC ATTTCCCCGA

1921 AAAGTGCCAC CTGACGTCTA AGAAACCATT ATTATCATGA CATTAACCTA TAAAAATAGG

1981 CGTATCACGA GGCCCTTTCG TCTCGCGCGT TTCGGTGATG ACGGTGAAAA CCTCTGACAC

2041 ATGCAGCTCC CGGAGACGGT CACAGCTTGT CTGTAAGCGG ATGCCGGGAG CAGACAAGCC

2101 CGTCAGGGCG CGTCAGCGGG TGTTGGCGGG TGTCGGGGCT GGCTTAACTA TGCGGCATCA

2161 GAGCAGATTG TACTGAGAGT GCACCATAAA ATTGTAAACG TTAATATTTT GTTAAAATTC

2221 GCGTTAAATT TTTGTTAAAT CAGCTCATTT TTTAACCAAT AGGCCGAAAT CGGCAAAATC

2281 CCTTATAAAT CAAAAGAATA GCCCGAGATA GGGTTGAGTG TTGTTCCAGT TTGGAACAAG

2341 AGTCCACTAT TAAAGAACGT GGACTCCAAC GTCAAAGGGC GAAAAACCGT CTATCAGGGC

2401 GATGGCCCAC TACGTGAACC ATCACCCAAA TCAAGTTTTT TGGGGTCGAG GTGCCGTAAA

2461 GCACTAAATC GGAACCCTAA AGGGAGCCCC CGATTTAGAG CTTGACGGGG AAAGCCGGCG

2521 AACGTGGCGA GAAAGGAAGG GAAGAAAGCG AAAGGAGCGG GCGCTAGGGC GCTGGCAAGT

2581 GTAGCGGTCA CGCTGCGCGT AACCACCACA CCCGCCGCGC TTAATGCGCC GCTACAGGGC

2641 GCGTACTATG GTTGCTTTGA CGTATGCGGT GTGAAATACC GCACAGATGC GTAAGGAGAA

2701 AATACCGCAT CAGGCGCCAT TCGCCATTCA GGCTGCGCAA CTGTTGGGAA GGGCGATCGG

2761 TGCGGGCCTC TTCGCTATTA CGCCAGCTGG CGAAAGGGGG ATGTGCTGCA AGGCGATTAA

2821 GTTGGGTAAC GCCAGGGTTT TCCCAGTCAC GACGTTGTAA AACGACGGCC AGTGCCAAGC

2881 TGGCCGGCCT AGGCGCGCCA AGCTTAAGGT GCACGGCCCA CGTGGCCACT AGTACTTCTC

2941 GAGCTCTGTA CATGTCCGCG GTCGCGACGT ACGCGTATCG ATGGCGCCAG CTGCAGGCGG

3001 CCGCCATATG CATCCTAGGC CTATTAATAT TCCGGAGTAT ACGTAGCCGG CTAACGTTat

3061 catacaatat gactcatttg tttttcaaaa ccgaacttga tttacgggta gaattctact

3121 tgtaaagcac aatcaaaaag atgatgtcat ttgtttttca aaactgaact cgctttacga

3181 gtagaattct acgtgtaaaa cacaatcaag aaatgatgtc atttgttata aaaataaaag

3241 ctgatgtcat gttttgcaca tggctcataa ctaaactcgc tttacgggta gaattctacg

3301 cgcgtcgatg tctttgtgat gcgcgcgaca tttttgtagg ttattgataa aatgaacgga

3361 tacgttgccc gacattatca ttaaatcctt ggcgtagaat ttgtcgggtc cattgtccgt

3421 gtgcgctagc atgcccgtaa cggacctcgt acttttggct tcaaaggttt tgcgcacaga

3481 caaaatgtgc cacacttgca gctctgcatg tgtgcgcgtt accacaaatc ccaacggcgc

3541 agtgtacttg ttgtatgcaa ataaatctcg ataaaggcgc ggcgcgcgaa tgcagctgat

3601 cacgtacgct cctcgtgttc cgttcaagga cggtgttatc gacctcagat taatgtttat

3661 cggccgactg ttttcgtatc cgctcaccaa acgcgttttt gcattaacat tgtatgtcgg

3721 cggatgttct atatctaatt tgaataaata aacgataacc gcgttggttt tagagggcat

3781 aataaaagaa atattgttat cgtgttcgcc attagggcag tataaattga cgttcatgtt

3841 ggatattgtt tcagttgcaa gttgacactg gcggcgacaa gatcgtgaac aaccaagtga

3901 ccatggcatc gttaacacgt caagagctcg cggatcccaa ttggcagatc tcggcgcgcc

3961 tgcaggtcga cggtaccggt tcgaagcttg cggccgcatc ttctggtaaa gaaaccgctg

4021 ctgcgaaatt tgaacgccag cacatggact cgccaccgcc ttctggcctc gagcaccacc

4081 atcaccatca ccatcactaa gtgattaacc tcaggttata catatatttt gaatttaatt

4141 aattatacat atattttata ttatttttgt cttttattat cgaggggccg ttgttggtgt

4201 ggggttttgc atagaaataa caatgggagt tggcgacgtt gctgcgccaa caccacctcc

4261 cttccctcct ttcatcatgt atctgtagat aaaataaaat attaaaccta aaaacaagac

4321 cgcgcctatc aacaaaatga taggcattaa cttgccgctg acgctgtcac taacgttgga

4381 cgatttgccg actaaacctt catcgcccag taaccaatct agaACTATAG CTAGCATGCG

4441 CAAATTTAAA GCGCTGATAT CGATCGCGCG CAGATCTGTC ATGATGATCA TTGCAATTGG

```
4501 ATCCATATAT AGGGCCCGGG TTATAATTAC CTCAGGTCGA CGTCCCATGG CCATTCGAAT
4561 TCGGCCGGCC TAGGCGCGCC AATTCGTAAT CATGTCATAG CTGTTTCCTG TGTGAAATTG
4621 TTATCCGCTC ACAATTCCAC ACAACATACG AGCCGGAAGC ATAAAGTGTA AAGCCTGGGG
4681 TGCCTAATGA GTGAGCTAAC TCACATTAAT TGCGTTGCGC TCACTGCCCG CTTTCCAGTC
4741 GGGAAACCTG TCGTGCCAGC TGCATTAATG AATCGGCCAA CGCGCGGGGA GAGGCGGTTT
4801 GCGTATTGGG CGC
//
```

A gift Carsten Horn and Ernst Wimmer, pSLfa1180fa was digested using NEB restriction enzymes HpaI and XbaI. The linearized fragment was ligated to a fragment of pIEx-4 containing the HR5:IE1 enhancer/promoter, MCS, and IE1 terminator following digestion of Novagen's pIEx-4 using EcoRV and XbaI. The ligation results in pSLfa1180fa having an HpaI scar but retains pIEx-4's HpaI for convenient cloning near the translation start site. This plasmid was intended to be an easy shuttle vector into pBac[3xP3:eGFP]afm (or the other Horn/Wimmer transposition plasmids) – however, the only enzyme capable of prepping it for shuttling is FseI, which is woefully inefficient at cutting. As such I discourage the use of this plasmid other than as a negative control for expression without transposon mediated integration.

Sequence A3.4 “pBacIE” → pBac[3xP3:eGFP;IEx] (AmpR)

```
TITLE       "pBacIE" --> pBAC[3xP3eGFPafm] HpaI/AvrII + pFIERFLY smai/spei
FEATURES             Location/Qualifiers
     protein_bind    696..923
                     /note="pBac Right Arm"
     CDS             2031..2750
                     /note="eGFP"
     misc_recomb     2874..4462
                     /note="pfIErfly SmaI/SpeI fragment"
     misc_recomb     3475..3480
                     /note="HpaI"
     misc_feature    3486..3488
                     /note="TLN Start Codon"
     protein_bind    4559..5237
                     /note="pBac Left Arm"
ORIGIN

        1 GTGCCAAGCT TTGTTTAAAA ATATAACAAA ATTGTGATCC CACAAAATGA AGTGGGGCAA
       61 AATCAAATAA TTAATAGTGT CCGTAAACTT GTTGGTCTTC AACTTTTTGA GGAACACGTT
      121 GGACGGCAAA TCCGTGACTA TAACACAAGT TGATTTAATA ANTTTAGCCA ACACGTCGGG
      181 CTGCGTGTTT TTTGCCGACG CGTCTGTGTA CACGTTGATT AACTGGTCGA TTAAACTGTT
      241 GAAATAATTT AATTTTTGGT TCTTCTTTAA ATCTGTGATG AAATTTTTTA AAATAACTTT
      301 AAATTCTTCA TTGGTAAAAA ATGCCACGTT TTGCAACTTG TGAGGGTCTA ATATGAGGTC
      361 AAACTCAGTA GGAGTTTTAT CCAAAAAAGA AAACATGATT ACGTCTGTAC ACGAACGCGT
      421 ATTAACGCAG AGTGCAAAGT ATAAGAGGGT TAAAAAATAT ATTTTACGCA CCATATACGC
      481 ATCGGGTTGA TATCGTTAAT ATGGATCAAT TTGAACAGTT GATTAACGTG TCTCTGCTCA
      541 AGTCTTTGAT CAAAACGCAA ATCGACGAAA ATGTGTCGGA CAATATCAAG TCGATGAGCG
      601 AAAAACTAAA AAGGCTAGAA TACGACAATC TCACAGACAG CGTTGAGATA TACGGTATTC
      661 ACGACAGCAG GCTGAATAAT AAAAAAATTA GAAACTATTA TTTAACCCTA GAAAGATAAT
      721 CATATTGTGA CGTACGTTAA AGATAATCAT GCGTAAAATT GACGCATGTG TTTTATCGGT
      781 CTGTATATCG AGGTTTATTT ATTAATTTGA ATAGATATTA AGTTTTATTA TATTTACACT
```

841 TACATACTAA TAATAAATTC AACAAACAAT TTATTTATGT TTATTTATTT ATTAAAAAAA

901 AACAAAAACT CAAAATTTCT TCTATAAAGT AACAAAACTT TTAAACATTC TCTCTTTTAC

961 AAAAATAAAC TTATTTTGTA CTTTAAAAAC AGTCATGTTG TATTATAAAA TAAGTAATTA

1021 GCTTAACTTA TACATAATAG AAACAAATTA TACTTATTAG TCAGTCAGAA ACAACTTTGG

1081 CACATATCAA TATTATGCTC TCGACAAATA ACTTTTTTGC ANTTTTTGCA CGATGCATTT

1141 GCCTTTCGCC TTATTTTAGA GGGGCAGTAA GTACAGTAAG TACGTTTTTT CATTACTGGC

1201 TCTTCAGTAC TGTCATCTGA TGTACCAGGC ACTTCATTTG GCAAAATATT AGAGATATTA

1261 TCGCGCAAAT ATCTCTTCAA AGTAGGAGCT TCTAAACGCT TACGCATAAA CGATGACGTC

1321 AGGCTCATGT AAAGGTTTCT CATAAANTTT TTGCGACTTT GAACCTTTTC TCCCTTGCTA

1381 CTGACATTAT GGCTGTATAT AATAAAAGAA TTTATGCAGG CAATGTTTAT CATTCCGTAC

1441 AATAATGCCA TAGGCCACCT ATTCGTCTTC CTACTGCAGG TCATCACAGA ACACATTTGG

1501 TCTAGCGTGT CCACTCCGCC TTTAGTTTGA TTATAATACA TAACCATTTG CGGTTTACCG

1561 GTACTTTCGT TGATAGAAGC ATCCTCATCA CAAGATGATA ATAAGTATAC CATCTTAGCT

1621 GGCTTCGGTT TATATGAGAC GAGAGTAAGG GGTCCGTCAA AACAAAACAT CGATGTTCCC

1681 ACTGGCCTGG AGCGACTGTT TTTCAGTACT TCCGGTATCT CGCGTTTGTT TGATCGCACG

1741 GTTCCCACAA TGGTTAATTC GAGCTCGCCC GGGGATCTAA TTCAATTAGA GACTAATTCA

1801 ATTAGAGCTA ATTCAATTAG GATCCAAGCT TATCGATTTC GAACCCTCGA CCGCCGGAGT

1861 ATAAATAGAG GCGCTTCGTC TACGGAGCGA CAATTCAATT CAAACAAGCA AAGTGAACAC

1921 GTCGCTAAGC GAAAGCTAAG CAAATAAACA AGCGCAGCTG AACAAGCTAA ACAATCGGGG

1981 TACCGCTAGA GTCGACGGTA CCGCGGGCCC GGGATCCACC GGTCGCCACC ATGGTGAGCA

2041 AGGGCGAGGA GCTGTTCACC GGGGTGGTGC CCATCCTGGT CGAGCTGGAC GGCGACGTAA

2101 ACGGCCACAA GTTCAGCGTG TCCGGCGAGG GCGAGGGCGA TGCCACCTAC GGCAAGCTGA

2161 CCCTGAAGTT CATCTGCACC ACCGGCAAGC TGCCCGTGCC CTGGCCCACC CTCGTGACCA

2221 CCCTGACCTA CGGCGTGCAG TGCTTCAGCC GCTACCCCGA CCACATGAAG CAGCACGACT

2281 TCTTCAAGTC CGCCATGCCC GAAGGCTACG TCCAGGAGCG CACCATCTTC TTCAAGGACG

2341 ACGGCAACTA CAAGACCCGC GCCGAGGTGA AGTTCGAGGG CGACACCCTG GTGAACCGCA

2401 TCGAGCTGAA GGGCATCGAC TTCAAGGAGG ACGGCAACAT CCTGGGGCAC AAGCTGGAGT

2461 ACAACTACAA CAGCCACAAC GTCTATATCA TGGCCGACAA GCAGAAGAAC GGCATCAAGG

2521 TGAACTTCAA GATCCGCCAC AACATCGAGG ACGGCAGCGT GCAGCTCGCC GACCACTACC

2581 AGCAGAACAC CCCCATCGGC GACGGCCCCG TGCTGCTGCC CGACAACCAC TACCTGAGCA

2641 CCCAGTCCGC CCTGAGCAAA GACCCCAACG AGAAGCGCGA TCACATGGTC CTGCTGGAGT

2701 TCGTGACCGC CGCCGGGATC ACTCTCGGCA TGGACGAGCT GTACAAGTAA AGCGGCCGCG

2761 ACTCTAGATC ATAATCAGCC ATACCACATT TGTAGAGGTT TTACTTGCTT TAAAAAACCT

2821 CCCCACACCT CCCCCTGAAC CTGAAACATA AAATGAATGC AATTGTTGTT GTTGGGCCCT

2881 ATATATGGAT CCAATTGCAA TGATCATCAT GACAGATCTG CGCGCGATCG ATATCAGCGC

2941 TTTAAATTTG CGCATGCTAG CTATAGTtct agattggtta ctgggcgatg aaggtttagt

3001 cggcaaatcg tccaacgtta gtgacagcgt cagcggcaag ttaatgccta tcattttgtt

3061 gataggcgcg gtcttgtttt taggtttaat attttatttt atctacagat acatgatgaa

3121 aggagggaag ggaggtggtg ttggcgcagc aacgtcgcca actcccattg ttatttctat

3181 gcaaaacccc acaccaacaa cggcccctcg ataataaaag acaaaaataa tataaaatat

3241 atgtataatt aattaaattc aaaatatatg tataacctga ggttaatcac ttagtgatgg

3301 tgatggtgat ggtggtgctc gaggccagaa ggcggtggcg agtccatgtg ctggcgttca

3361 aatttcgcag cagcggtttc tttaccagaa gatgcggccg caagcttcga accggtaccg

3421 tcgacctgca ggcgcgccga gatctgccaa ttgggatccg cgagctcttg acgtgttaac

3481 gatgccatgg tcacttggtt gttcacgatc ttgtcgccgc cagtgtcaac ttgcaactga

3541 aacaatatcc aacatgaacg tcaatttata ctgccctaat ggcgaacacg ataacaatat

3601 ttcttttatt atgccctcta aaaccaacgc ggttatcgtt tatttattca aattagatat

3661 agaacatccg ccgacataca atgttaatgc aaaaacgcgt ttggtgagcg gatacgaaaa

3721 cagtcggccg ataaacatta atctgaggtc gataacaccg tccttgaacg gaacacgagg

3781 agcgtacgtg atcagctgca ttcgcgcgcc gcgcctttat cgagatttat ttgcatacaa

3841 caagtacact gcgccgttgg gatttgtggt aacgcgcaca catgcagagc tgcaagtgtg

3901 gcacattttg tctgtgcgca aaacctttga agccaaaagt acgaggtccg ttacgggcat

3961 gctagcgcac acggacaatg gacccgacaa attctacgcc aaggatttaa tgataatgtc

4021 gggcaacgta tccgttcatt ttatcaataa cctacaaaaa tgtcgcgcgc atcacaaaga

4081 catcgacgcg cgtagaattc tacccgtaaa gcgagtttag ttatgagcca tgtgcaaaac

4141 atgacatcag cttttatttt tataacaaat gacatcattt cttgattgtg ttttacacgt

4201 agaattctac tcgtaaagcg agttcagttt tgaaaaacaa atgacatcat ctttttgatt

4261 gtgctttaca agtagaattc tacccgtaaa tcaagttcgg ttttgaaaaa caaatgagtc

4321 atattgtatg atAACGTTAG CCGGCTACGT ATACTCCGGA ATATTAATAG GCCTAGGATG

4381 CATATGGCGG CCGCCTGCAG CTGGCGCCAT CGATACGCGT ACGTCGCGAC CGCGGACATG

4441 TACAGAGCTC GAGAAGTACT AGCTAggccg gccGAATTCG AATGGCCATG GGACGTCGAC

4501 CTGAGGTAAT TATAACCCGG GCCCTATATA TGGATCCAAT TGCAATGATC ATCATGACAG

4561 ATCTGACAAT GTTCAGTGCA GAGACTCGGC TACGCCTCGT GGACTTTGAA GTTGACCAAC

4621 AATGTTTATT CTTACCTCTA ATAGTCCTCT GTGGCAAGGT CAAGATTCTG TTAGAAGCCA

4681 ATGAAGAACC TGGTTGTTCA ATAACATTTT GTTCGTCTAA TATTTCACTA CCGCTTGACG

4741 TTGGCTGCAC TTCATGTACC TCATCTATAA ACGCTTCTTC TGTATCGCTC TGGACGTCAT

4801 CTTCACTTAC GTGATCTGAT ATTTCACTGT CAGAATCCTC ACCAACAAGC TCGTCATCGC

4861 TTTGCAGAAG AGCAGAGAGG ATATGCTCAT CGTCTAAAGA ACTACCCATT TTATTATATA

4921 TTAGTCACGA TATCTATAAC AAGAAAATAT ATATATAATA AGTTATCACG TAAGTAGAAC

4981 ATGAAATAAC AATATAATTA TCGTATGAGT TAAATCTTAA AAGTCACGTA AAAGATAATC

5041 ATGCGTCATT TTGACTCACG CGGTCGTTAT AGTTCAAAAT CAGTGACACT TACCGCATTG

5101 ACAAGCACGC CTCACGGGAG CTCCAAGCGG CGACTGAGAT GTCCTAAATG CACAGCGACG

5161 GATTCGCGCT ATTTAGAAAG AGAGAGCAAT ATTTCAAGAA TGCATGCGTC AATTTTACGC

5221 AGACTATCTT TCTAGGGTTA AAAAAGATTT GCGCTTTACT CGACCTAAAC TTTAAACACG

5281 TCATAGAATC TTCGTTTGAC AAAAACCACA TTGTGGCCAA GCTGTGTGAC GCGACGCGCG

5341 CTAAAGAATG GCAAACCAAG TCGCGCGAGC GTCGACTCTA GAGGATCCCC GGGTACCGAG

5401 CTCGAATTCG TAATCATGTC ATAGCTGTTT CCTGTGTGAA ATTGTTATCC GCTCACAATT

5461 CCACACAACA TACGAGCCGG AAGCATAAAG TGTAAAGCCT GGGGTGCCTA ATGAGTGAGC

5521 TAACTCACAT TAATTGCGTT GCGCTCACTG CCCGCTTTCC AGTCGGGAAA CCTGTCGTGC

5581 CAGCTGCATT AATGAATCGG CCAACGCGCG GGGAGAGGCG GTTTGCGTAT TGGGCGCTCT

5641 TCCGCTTCCT CGCTCACTGA CTCGCTGCGC TCGGTCGTTC GGCTGCGGCG AGCGGTATCA

5701 GCTCACTCAA AGGCGGTAAT ACGGTTATCC ACAGAATCAG GGGATAACGC AGGAAAGAAC

5761 ATGTGAGCAA AAGGCCAGCA AAAGGCCAGG AACCGTAAAA AGGCCGCGTT GCTGGCGTTT

5821 TTCCATAGGC TCCGCCCCCC TGACGAGCAT CACAAAAATC GACGCTCAAG TCAGAGGTGG

5881 CGAAACCCGA CAGGACTATA AAGATACCAG GCGTTTCCCC CTGGAAGCTC CCTCGTGCGC

5941 TCTCCTGTTC CGACCCTGCC GCTTACCGGA TACCTGTCCG CCTTTCTCCC TTCGGGAAGC

6001 GTGGCGCTTT CTCATAGCTC ACGCTGTAGG TATCTCAGTT CGGTGTAGGT CGTTCGCTCC

6061 AAGCTGGGCT GTGTGCACGA ACCCCCCGTT CAGCCCGACC GCTGCGCCTT ATCCGGTAAC

6121 TATCGTCTTG AGTCCAACCC GGTAAGACAC GACTTATCGC CACTGGCAGC AGCCACTGGT

6181 AACAGGATTA GCAGAGCGAG GTATGTAGGC GGTGCTACAG AGTTCTTGAA GTGGTGGCCT

6241 AACTACGGCT ACACTAGAAG AACAGTATTT GGTATCTGCG CTCTGCTGAA GCCAGTTACC

6301 TTCGGAAAAA GAGTTGGTAG CTCTTGATCC GGCAAACAAA CCACCGCTGG TAGCGGTGGT

6361 TTTTTTGTTT GCAAGCAGCA GATTACGCGC AGAAAAAAAG GATCTCAAGA AGATCCTTTG

6421 ATCTTTTCTA CGGGGTCTGA CGCTCAGTGG AACGAAANCT CACGTTAAGG GATTTTGGTC

6481 ATGAGATTAT CAAAAAGGAT CTTCACCTAG ATCCTTTTAA NTTAAAAATG AAGTTTTAAA

6541 TCAATCTAAA GTATATATGA GTAAACTTGG TCTGACAGTT ACCAATGCTT AATCAGTGAG

```
6601 GCACCTATCT CAGCGATCTG TCTATTTCGT TCATCCATAG TTGCCTGACT CCCCGTCGTG
6661 TAGATAACTA CGATACGGGA GGGCTTACCA TCTGGCCCCA GTGCTGCAAT GATACCGCGA
6721 GACCCACGCT CACCGGCTCC AGATTTATCA GCAATAAACC AGCCAGCCGG AAGGGCCGAG
6781 CGCAGAAGTG GTCCTGCAAC TTTATCCGCC TCCATCCAGT CTATTAATTG TTGCCGGGAA
6841 GCTAGAGTAA GTAGTTCGCC AGTTAATAGT TTGCGCAACG TTGTTGCCAT TGCTACAGGC
6901 ATCGGNNTGt cacgctcgtc gtttggtanG GCTTCATTCA GTTCCGGTTC CCAACGATCA
6961 AGGCGAGTTA CATGATCCCC CCATGTTGTG CAAAAAAGCG GTTAGCTCCT TCGGTCCTCC
7021 GATCGTTGTC AGAAGTAAGT TGGCCGCAGT GTTATCACTC ATGGTTATGG CAGCACTGCA
7081 TAATTCTCTT ACTGTCATGC CATCCGTAAG ATGCTTTTCT GTGACTGGTG AGTACTCAAC
7141 CAAGTCATTC TGAGAATAGT GTATGCGGCG ACCGAGTTGC TCTTGCCCGG CGTCAATACG
7201 GGATAATACC GCGCCACATA GCAGAACTTT AAAAGTGCTC ATCATTGGAA AACGTTCTTC
7261 GGGGCGAAAA CTCTCAAGGA TCTTACCGCT GTTGAGATCC AGTTCGATGT AACCCACTCG
7321 TGCACCCAAC TGATCTTCAG CATCTTTTAC TTTCACCAGC GTTTCTGGGT GAGCAAAAAC
7381 AGGAAGGCAA AATGCCGCAA AAAAGGGAAT AAGGGCGACA CGGAAATGTT GAATACTCAT
7441 ACTCTTCCTT TTTCAATATT ATTGAAGCAT TTATCAGGGT TATTGTCTCA TGAGCGGATA
7501 CATATTTGAA TGTATTTAGA AAAATAAACA AATAGGGGTT CCGCGCACAT TTCCCCGAAA
7561 AGTGCCACCT GACGTCTAAG AAACCATTAT TATCATGACA TTAACCTATA AAAATAGGCG
7621 TATCACGAGG CCCTTTCGTC TCGCGCGTTT CGGTGATGAC GGTGAAAACC TCTGACACAT
7681 GCAGCTCCCG GAGACGGTCA CAGCTTGTCT GTAAGCGGAT GCCGGGAGCA GACAAGCCCG
7741 TCAGGGCGCG TCAGCGGGTG TTGGCGGGTG TCGGGGCTGG CTTAACTATG CGGCATCAGA
7801 GCAGATTGTA CTGAGAGTGC ACCATATGCG GTGTGAAATA CCGCACAGAT GCGTAAGGAG
7861 AAAATACCGC ATCAGGCGCC ATTCGCCATT CAGGCTGCGC AACTGTTGGG AAGGGCGATC
7921 GGTGCGGGCC TCTTCGCTAT TACGCCAGCT GGCGAAAGGG GGATGTGCTG CAAGGCGATT
7981 AAGTTGGGTA ACGCCAGGGT TTTCCCAGTC ACGACGTTGT AAAACGACGG CCA
```

//

Since pfIErfly was poor at shuttling, I built pBacIE, a plasmid containing the 3xP3 reporter, the HR5/IE1 RNA polII enhancer/promoter and terminator from pIEx-4 with the MCS as well. A gift Carsten Horn and Ernst Wimmer, pBac[3xP3:eGFP]afm was digested using NEB restriction enzymes HpaI and AvrII. The fragment containing both pBac transposition arms, 3xP3:eGFP, and the Ampicillin resistance cassette was retained and ligated to a fragment of pIEx-4 containing the HR5:IE1 enhancer/promoter, MCS, and IE1 terminator following digestion of IE1 using SmaI and SpeI. Cutting pBac[3xP3:eGFP]afm with HpaI and ligating it to the blunt SmaI produced a scar destroying both sites. This is important as it leaves only a single HpaI site near the translation start site of the HR5/IE1 promoter.

Sequence A3.5 pBacIE[3xP3:eGFP;LifeAct:mEos3.2] (AmpR)

```
TITLE       pBacIE[3xP3:eGFP;LA:mEos3.2] (8787bp)
FEATURES             Location/Qualifiers
     protein_bind    3475..3221
                     /note="pBac Left Arm"
     misc_feature    4548..4546
                     /note="TLN Start Codon"
     CDS             4558..4629
                     /note="LifeAct"
     CDS             4630..4884
                     /note="mEos3.2"
     CDS             6757..6503
                     /note="eGFP"
     promoter        7032..6778
                     /note="3xP3 promoter"
     protein_bind    8092..7865
                     /note="pBac right arm"
ORIGIN

        1 TGGCCGTCGT TTTACAACGT CGTGACTGGG AAAACCCTGG CGTTACCCAA CTTAATCGCC
       61 TTGCAGCACA TCCCCCTTTC GCCAGCTGGC GTAATAGCGA AGAGGCCCGC ACCGATCGCC
      121 CTTCCCAACA GTTGCGCAGC CTGAATGGCG AATGGCGCCT GATGCGGTAT TTTCTCCTTA
      181 CGCATCTGTG CGGTATTTCA CACCGCATAT GGTGCACTCT CAGTACAATC TGCTCTGATG
      241 CCGCATAGTT AAGCCAGCCC CGACACCCGC CAACACCCGC TGACGCGCCC TGACGGGCTT
      301 GTCTGCTCCC GGCATCCGCT TACAGACAAG CTGTGACCGT CTCCGGGAGC TGCATGTGTC
      361 AGAGGTTTTC ACCGTCATCA CCGAAACGCG CGAGACGAAA GGGCCTCGTG ATACGCCTAT
      421 TTTTATAGGT TAATGTCATG ATAATAATGG TTTCTTAGAC GTCAGGTGGC ACTTTTCGGG
      481 GAAATGTGCG CGGAACCCCT ATTTGTTTAT TTTTCTAAAT ACATTCAAAT ATGTATCCGC
      541 TCATGAGACA ATAACCCTGA TAAATGCTTC AATAATATTG AAAAAGGAAG AGTATGAGTA
      601 TTCAACATTT CCGTGTCGCC CTTATTCCCT TTTTTGCGGC ATTTTGCCTT CCTGTTTTTG
      661 CTCACCCAGA AACGCTGGTG AAAGTAAAAG ATGCTGAAGA TCAGTTGGGT GCACGAGTGG
```

721 GTTACATCGA ACTGGATCTC AACAGCGGTA AGATCCTTGA GAGTTTTCGC CCCGAAGAAC

781 GTTTTCCAAT GATGAGCACT TTTAAAGTTC TGCTATGTGG CGCGGTATTA TCCCGTATTG

841 ACGCCGGGCA AGAGCAACTC GGTCGCCGCA TACACTATTC TCAGAATGAC TTGGTTGAGT

901 ACTCACCAGT CACAGAAAAG CATCTTACGG ATGGCATGAC AGTAAGAGAA TTATGCAGTG

961 CTGCCATAAC CATGAGTGAT AACACTGCGG CCAACTTACT TCTGACAACG ATCGGAGGAC

1021 CGAAGGAGCT AACCGCTTTT TTGCACAACA TGGGGGGATC ATGTAACTCG CCTTGATCGT

1081 TGGGAACCGG AACTGAATGA AGCCntacca aacgacgagc gtgaCANNCC GATGCCTGTA

1141 GCAATGGCAA CAACGTTGCG CAAACTATTA ACTGGCGAAC TACTTACTCT AGCTTCCCGG

1201 CAACAATTAA TAGACTGGAT GGAGGCGGAT AAAGTTGCAG GACCACTTCT GCGCTCGGCC

1261 CTTCCGGCTG GCTGGTTTAT TGCTGATAAA TCTGGAGCCG GTGAGCGTGG GTCTCGCGGT

1321 ATCATTGCAG CACTGGGGCC AGATGGTAAG CCCTCCCGTA TCGTAGTTAT CTACACGACG

1381 GGGAGTCAGG CAACTATGGA TGAACGAAAT AGACAGATCG CTGAGATAGG TGCCTCACTG

1441 ATTAAGCATT GGTAACTGTC AGACCAAGTT TACTCATATA TACTTTAGAT TGATTTAAAA

1501 CTTCATTTTT AANTTAAAAG GATCTAGGTG AAGATCCTTT TTGATAATCT CATGACCAAA

1561 ATCCCTTAAC GTGAGNTTTC GTTCCACTGA GCGTCAGACC CCGTAGAAAA GATCAAAGGA

1621 TCTTCTTGAG ATCCTTTTTT TCTGCGCGTA ATCTGCTGCT TGCAAACAAA AAAACCACCG

1681 CTACCAGCGG TGGTTTGTTT GCCGGATCAA GAGCTACCAA CTCTTTTTCC GAAGGTAACT

1741 GGCTTCAGCA GAGCGCAGAT ACCAAATACT GTTCTTCTAG TGTAGCCGTA GTTAGGCCAC

1801 CACTTCAAGA ACTCTGTAGC ACCGCCTACA TACCTCGCTC TGCTAATCCT GTTACCAGTG

1861 GCTGCTGCCA GTGGCGATAA GTCGTGTCTT ACCGGGTTGG ACTCAAGACG ATAGTTACCG

1921 GATAAGGCGC AGCGGTCGGG CTGAACGGGG GGTTCGTGCA CACAGCCCAG CTTGGAGCGA

1981 ACGACCTACA CCGAACTGAG ATACCTACAG CGTGAGCTAT GAGAAAGCGC CACGCTTCCC

2041 GAAGGGAGAA AGGCGGACAG GTATCCGGTA AGCGGCAGGG TCGGAACAGG AGAGCGCACG

2101 AGGGAGCTTC CAGGGGGAAA CGCCTGGTAT CTTTATAGTC CTGTCGGGTT TCGCCACCTC

2161 TGACTTGAGC GTCGATTTTT GTGATGCTCG TCAGGGGGGC GGAGCCTATG GAAAAACGCC

2221 AGCAACGCGG CCTTTTTACG GTTCCTGGCC TTTTGCTGGC CTTTTGCTCA CATGTTCTTT

2281 CCTGCGTTAT CCCCTGATTC TGTGGATAAC CGTATTACCG CCTTTGAGTG AGCTGATACC

2341 GCTCGCCGCA GCCGAACGAC CGAGCGCAGC GAGTCAGTGA GCGAGGAAGC GGAAGAGCGC

2401 CCAATACGCA AACCGCCTCT CCCCGCGCGT TGGCCGATTC ATTAATGCAG CTGGCACGAC

2461 AGGTTTCCCG ACTGGAAAGC GGGCAGTGAG CGCAACGCAA TTAATGTGAG TTAGCTCACT

2521 CATTAGGCAC CCCAGGCTTT ACACTTTATG CTTCCGGCTC GTATGTTGTG TGGAATTGTG

2581 AGCGGATAAC AATTTCACAC AGGAAACAGC TATGACATGA TTACGAATTC GAGCTCGGTA

2641 CCCGGGGATC CTCTAGAGTC GACGCTCGCG CGACTTGGTT TGCCATTCTT TAGCGCGCGT

2701 CGCGTCACAC AGCTTGGCCA CAATGTGGTT TTTGTCAAAC GAAGATTCTA TGACGTGTTT

2761 AAAGTTTAGG TCGAGTAAAG CGCAAATCTT TTTTAACCCT AGAAAGATAG TCTGCGTAAA

2821 ATTGACGCAT GCATTCTTGA AATATTGCTC TCTCTTTCTA AATAGCGCGA ATCCGTCGCT

2881 GTGCATTTAG GACATCTCAG TCGCCGCTTG GAGCTCCCGT GAGGCGTGCT TGTCAATGCG

2941 GTAAGTGTCA CTGATTTTGA ACTATAACGA CCGCGTGAGT CAAAATGACG CATGATTATC

3001 TTTTACGTGA CTTTTAAGAT TTAACTCATA CGATAATTAT ATTGTTATTT CATGTTCTAC

3061 TTACGTGATA ACTTATTATA TATATATTTT CTTGTTATAG ATATCGTGAC TAATATATAA

3121 TAAAATGGGT AGTTCTTTAG ACGATGAGCA TATCCTCTCT GCTCTTCTGC AAAGCGATGA

3181 CGAGCTTGTT GGTGAGGATT CTGACAGTGA AATATCAGAT CACGTAAGTG AAGATGACGT

3241 CCAGAGCGAT ACAGAAGAAG CGTTTATAGA TGAGGTACAT GAAGTGCAGC CAACGTCAAG

3301 CGGTAGTGAA ATATTAGACG AACAAAATGT TATTGAACAA CCAGGTTCTT CATTGGCTTC

3361 TAACAGAATC TTGACCTTGC CACAGAGGAC TATTAGAGGT AAGAATAAAC ATTGTTGGTC

3421 AACTTCAAAG TCCACGAGGC GTAGCCGAGT CTCTGCACTG AACATTGTCA GATCTGTCAT

3481 GATGATCATT GCAATTGGAT CCATATATAG GGCCCGGGTT ATAATTACCT CAGGTCGACG

3541 TCCCATGGCC ATTCGAATTC ggccggccTA GCTAGTACTT CTCGAGCTCT GTACATGTCC

3601 GCGGTCGCGA CGTACGCGTA TCGATGGCGC CAGCTGCAGG CGGCCGCCAT ATGCATCCTA

3661 GGCCTATTAA TATTCCGGAG TATACGTAGC CGGCTAACGT Tatcatacaa tatgactcat

3721 ttgtttttca aaaccgaact tgatttacgg gtagaattct acttgtaaag cacaatcaaa

3781 aagatgatgt catttgtttt tcaaaactga actcgcttta cgagtagaat tctacgtgta

3841 aaacacaatc aagaaatgat gtcatttgtt ataaaaataa aagctgatgt catgttttgc

3901 acatggctca taactaaact cgctttacgg gtagaattct acgcgcgtcg atgtctttgt

3961 gatgcgcgcg acatttttgt aggttattga taaaatgaac ggatacgttg cccgacatta

4021 tcattaaatc cttggcgtag aatttgtcgg gtccattgtc cgtgtgcgct agcatgcccg

4081 taacggacct cgtacttttg gcttcaaagg ttttgcgcac agacaaaatg tgccacactt

4141 gcagctctgc atgtgtgcgc gttaccacaa atcccaacgg cgcagtgtac ttgttgtatg

4201 caaataaatc tcgataaagg cgcggcgcgc gaatgcagct gatcacgtac gctcctcgtg

4261 ttccgttcaa ggacggtgtt atcgacctca gattaatgtt tatcggccga ctgttttcgt

4321 atccgctcac caaacgcgtt tttgcattaa cattgtatgt cggcggatgt tctatatcta

4381 atttgaataa ataaacgata accgcgttgg ttttagaggg cataataaaa gaaatattgt

4441 tatcgtgttc gccattaggg cagtataaat tgacgttcat gttggatatt gtttcagttg

4501 caagttgaca ctggcggcga caagatcgtg aacaaccaag tgaccATGgc atcgttAATG

4561 GGCGTGGCCG ACTTGATCAA GAAGTTCGAG TCCATCTCCA AGGAGGAGGG GGATCCACCG

4621 GTCGCCACCA TGAGTGCGAT TAAGCCAGAC ATGAAGATCA AACTCCGTAT GGAAGGCAAC

4681 GTAAACGGGC ACCACTTTGT GATCGACGGA GATGGTACAG GCAAGCCTTT TGAGGGAAAA

4741 CAGAGTATGG ATCTTGAAGT CAAAGAGGGC GGACCTCTGC CTTTTGCCTT TGATATCCTG

4801 ACCACTGCAT TCCATTACGG CAACAGGGTA TTCGCCAAAT ATCCAGACAA CATACAAGAC

4861 TATTTTAAGC AGTCGTTTCC TAAGGGGTAT TCGTGGGAAC GAAGCTTGAC TTTCGAAGAC

4921 GGGGGCATTT GCAACGCCAG AAACGACATA ACAATGGAAG GGGACACTTT CTATAATAAA

4981 GTTCGATTTT ATGGTACCAA CTTTCCCGCC AATGGTCCAG TTATGCAGAA GAAGACGCTG

5041 AAATGGGAGC CCTCCACTGA GAAAATGTAT GTGCGTGATG GAGTGCTGAC GGGTGATATT

5101 GAGATGGCTT TGTTGCTTGA AGGAAATGCC CATTACCGAT GTGACTTCAG AACTACTTAC

5161 AAAGCTAAGG AGAAGGGTGT CAAGTTACCA GGCGCCCACT TTGTGGACCA CTGCATTGAG

5221 ATTTTAAGCC ATGACAAAGA TTACAACAAG GTTAAGCTGT ATGAGCATGC TGTTGCTCAT

5281 TCTGGATTGC CTGACAATGC CAGACGATAA aacacgtcaa gagctcgcgg atcccaattg

5341 gcagatctcg gcgcgcctgc aggtcgacgg taccggttcg aagcttgcgg ccgcatcttc

5401 tggtaaagaa accgctgctg cgaaatttga acgccagcac atggactcgc caccgccttc

5461 tggcctcgag caccaccatc accatcacca tcactaagtg attaacctca ggttatacat

5521 atattttgaa tttaattaat tatacatata ttttatatta tttttgtctt ttattatcga

5581 ggggccgttg ttggtgtggg gttttgcata gaaataacaa tgggagttgg cgacgttgct

5641 gcgccaacac cacctccctt ccctcctttc atcatgtatc tgtagataaa ataaaatatt

5701 aaacctaaaa acaagaccgc gcctatcaac aaaatgatag gcattaactt gccgctgacg

5761 ctgtcactaa cgttggacga tttgccgact aaaccttcat cgcccagtaa ccaatctaga

5821 ACTATAGCTA GCATGCGCAA ATTTAAAGCG CTGATATCGA TCGCGCGCAG ATCTGTCATG

5881 ATGATCATTG CAATTGGATC CATATATAGG GCCCAACAAC AACAATTGCA TTCATTTTAT

5941 GTTTCAGGTT CAGGGGGAGG TGTGGGGAGG TTTTTTAAAG CAAGTAAAAC CTCTACAAAT

6001 GTGGTATGGC TGATTATGAT CTAGAGTCGC GGCCGCTTTA CTTGTACAGC TCGTCCATGC

6061 CGAGAGTGAT CCCGGCGGCG GTCACGAACT CCAGCAGGAC CATGTGATCG CGCTTCTCGT

6121 TGGGGTCTTT GCTCAGGGCG GACTGGGTGC TCAGGTAGTG GTTGTCGGGC AGCAGCACGG

6181 GGCCGTCGCC GATGGGGGTG TTCTGCTGGT AGTGGTCGGC GAGCTGCACG CTGCCGTCCT

6241 CGATGTTGTG GCGGATCTTG AAGTTCACCT TGATGCCGTT CTTCTGCTTG TCGGCCATGA

6301 TATAGACGTT GTGGCTGTTG TAGTTGTACT CCAGCTTGTG CCCCAGGATG TTGCCGTCCT

6361 CCTTGAAGTC GATGCCCTTC AGCTCGATGC GGTTCACCAG GGTGTCGCCC TCGAACTTCA

6421 CCTCGGCGCG GGTCTTGTAG TTGCCGTCGT CCTTGAAGAA GATGGTGCGC TCCTGGACGT

6481 AGCCTTCGGG CATGGCGGAC TTGAAGAAGT CGTGCTGCTT CATGTGGTCG GGGTAGCGGC

6541 TGAAGCACTG CACGCCGTAG GTCAGGGTGG TCACGAGGGT GGGCCAGGGC ACGGGCAGCT

6601 TGCCGGTGGT GCAGATGAAC TTCAGGGTCA GCTTGCCGTA GGTGGCATCG CCCTCGCCCT

6661 CGCCGGACAC GCTGAACTTG TGGCCGTTTA CGTCGCCGTC CAGCTCGACC AGGATGGGCA

6721 CCACCCCGGT GAACAGCTCC TCGCCCTTGC TCACCATGGT GGCGACCGGT GGATCCCGGG

6781 CCCGCGGTAC CGTCGACTCT AGCGGTACCC CGATTGTTTA GCTTGTTCAG CTGCGCTTGT

6841 TTATTTGCTT AGCTTTCGCT TAGCGACGTG TTCACTTTGC TTGTTTGAAT TGAATTGTCG

6901 CTCCGTAGAC GAAGCGCCTC TATTTATACT CCGGCGGTCG AGGGTTCGAA ATCGATAAGC

6961 TTGGATCCTA ATTGAATTAG CTCTAATTGA ATTAGTCTCT AATTGAATTA GATCCCCGGG

7021 CGAGCTCGAA TTAACCATTG TGGGAACCGT GCGATCAAAC AAACGCGAGA TACCGGAAGT

7081 ACTGAAAAAC AGTCGCTCCA GGCCAGTGGG AACATCGATG TTTTGTTTTG ACGGACCCCT

7141 TACTCTCGTC TCATATAAAC CGAAGCCAGC TAAGATGGTA TACTTATTAT CATCTTGTGA

7201 TGAGGATGCT TCTATCAACG AAAGTACCGG TAAACCGCAA ATGGTTATGT ATTATAATCA

7261 AACTAAAGGC GGAGTGGACA CGCTAGACCA AATGTGTTCT GTGATGACCT GCAGTAGGAA

7321 GACGAATAGG TGGCCTATGG CATTATTGTA CGGAATGATA AACATTGCCT GCATAAATTC

7381 TTTTATTATA TACAGCCATA ATGTCAGTAG CAAGGGAGAA AAGGTTCAAA GTCGCAAAAA

7441 NTTTATGAGA AACCTTTACA TGAGCCTGAC GTCATCGTTT ATGCGTAAGC GTTTAGAAGC

7501 TCCTACTTTG AAGAGATATT TGCGCGATAA TATCTCTAAT ATTTTGCCAA ATGAAGTGCC

7561 TGGTACATCA GATGACAGTA CTGAAGAGCC AGTAATGAAA AAACGTACTT ACTGTACTTA

7621 CTGCCCCTCT AAAATAAGGC GAAAGGCAAA TGCATCGTGC AAAAANTGCA AAAAAGTTAT

7681 TTGTCGAGAG CATAATATTG ATATGTGCCA AAGTTGTTTC TGACTGACTA ATAAGTATAA

7741 TTTGTTTCTA TTATGTATAA GTTAAGCTAA TTACTTATTT TATAATACAA CATGACTGTT

7801 TTTAAAGTAC AAAATAAGTT TATTTTTGTA AAAGAGAGAA TGTTTAAAAG TTTTGTTACT

7861 TTATAGAAGA AATTTTGAGT TTTTGTTTTT TTTTAATAAA TAAATAAACA TAAATAAATT

7921 GTTTGTTGAA TTTATTATTA GTATGTAAGT GTAAATATAA TAAAACTTAA TATCTATTCA

7981 AATTAATAAA TAAACCTCGA TATACAGACC GATAAAACAC ATGCGTCAAT TTTACGCATG

8041 ATTATCTTTA ACGTACGTCA CAATATGATT ATCTTTCTAG GGTTAAATAA TAGTTTCTAA

8101 TTTTTTTATT ATTCAGCCTG CTGTCGTGAA TACCGTATAT CTCAACGCTG TCTGTGAGAT

8161 TGTCGTATTC TAGCCTTTTT AGTTTTTCGC TCATCGACTT GATATTGTCC GACACATTTT

8221 CGTCGATTTG CGTTTTGATC AAAGACTTGA GCAGAGACAC GTTAATCAAC TGTTCAAATT

8281 GATCCATATT AACGATATCA ACCCGATGCG TATATGGTGC GTAAAATATA TTTTTTAACC

8341 CTCTTATACT TTGCACTCTG CGTTAATACG CGTTCGTGTA CAGACGTAAT CATGTTTTCT

```
8401 TTTTTGGATA AAACTCCTAC TGAGTTTGAC CTCATATTAG ACCCTCACAA GTTGCAAAAC
8461 GTGGCATTTT TTACCAATGA AGAATTTAAA GTTATTTTAA AAAATTTCAT CACAGATTTA
8521 AAGAAGAACC AAAAATTAAA TTATTTCAAC AGTTTAATCG ACCAGTTAAT CAACGTGTAC
8581 ACAGACGCGT CGGCAAAAAA CACGCAGCCC GACGTGTTGG CTAAANTTAT TAAATCAACT
8641 TGTGTTATAG TCACGGATTT GCCGTCCAAC GTGTTCCTCA AAAAGTTGAA GACCAACAAG
8701 TTTACGGACA CTATTAATTA TTTGATTTTG CCCCACTTCA TTTTGTGGGA TCACAATTTT
8761 GTTATATTTT TAAACAAAGC TTGGCAC
//
```

The plasmid from A3.4, pBacIE, was digested using restriction enzyme HpaI. A gift of Michael Davidson – Addgene: 54696, the plasmid mEos3.2:LifeAct-7 (KanR) was PCR amplified using the primers

RWN100: tgaccatggcatcgttAATGGGCGTGGCCGACTT and

RWN101: gagctcttgacgtgttTTATCGTCTGGCATTGTCAGGC.

The purified fragments were then ligated via Gibson Assembly. The promoters 3xP3 and HR5/IE1 point toward one another.

Sequence A3.6 pflErfly[H_2A:mCherry:F2A:eGFP:CAAX] (AmpR)

TITLE pflErfly[mCherry:DreH2A.V:F2A:eGFP:CAAX] (6783bp)

FEATURES	Location/Qualifiers
misc_feature	3903..3905
	/note="TLN Start Codon"
misc_recomb	3911..3916
	/note="HpaI Scar"
CDS	4305..4559
	/note="*Danio rerio* Histone H2A.V"
CDS	4305..4559
	/note="mCherry"
CDS	5046..5084
	/note="F2A Ribosomal Skip Site"
CDS	5085..5339
	/note="eGFP"
CDS	5810..5883
	/note="H-Ras CAAX Box"

ORIGIN

```
        1 TCTTCCGCTT CCTCGCTCAC TGACTCGCTG CGCTCGGTCG TTCGGCTGCG GCGAGCGGTA
       61 TCAGCTCACT CAAAGGCGGT AATACGGTTA TCCACAGAAT CAGGGGATAA CGCAGGAAAG
      121 AACATGTGAG CAAAAGGCCA GCAAAAGGCC AGGAACCGTA AAAAGGCCGC GTTGCTGGCG
      181 TTTTTCCATA GGCTCCGCCC CCCTGACGAG CATCACAAAA ATCGACGCTC AAGTCAGAGG
      241 TGGCGAAACC CGACAGGACT ATAAAGATAC CAGGCGTTTC CCCCTGGAAG CTCCCTCGTG
      301 CGCTCTCCTG TTCCGACCCT GCCGCTTACC GGATACCTGT CCGCCTTTCT CCCTTCGGGA
      361 AGCGTGGCGC TTTCTCATAG CTCACGCTGT AGGTATCTCA GTTCGGTGTA GGTCGTTCGC
      421 TCCAAGCTGG GCTGTGTGCA CGAACCCCCC GTTCAGCCCG ACCGCTGCGC CTTATCCGGT
      481 AACTATCGTC TTGAGTCCAA CCCGGTAAGA CACGACTTAT CGCCACTGGC AGCAGCCACT
      541 GGTAACAGGA TTAGCAGAGC GAGGTATGTA GGCGGTGCTA CAGAGTTCTT GAAGTGGTGG
      601 CCTAACTACG GCTACACTAG AAGAACAGTA TTTGGTATCT GCGCTCTGCT GAAGCCAGTT
      661 ACCTTCGGAA AAAGAGTTGG TAGCTCTTGA TCCGGCAAAC AAACCACCGC TGGTAGCGGT
```

721 GGTTTTTTTG TTTGCAAGCA GCAGATTACG CGCAGAAAAA AAGGATCTCA AGAAGATCCT

781 TTGATCTTTT CTACGGGGTC TGACGCTCAG TGGAACGAAA ACTCACGTTA AGGGATTTTG

841 GTCATGAGAT TATCAAAAAG GATCTTCACC TAGATCCTTT TAAATTAAAA ATGAAGTTTT

901 AAATCAATCT AAAGTATATA TGAGTAAACT TGGTCTGACA GTTACCAATG CTTAATCAGT

961 GAGGCACCTA TCTCAGCGAT CTGTCTATTT CGTTCATCCA TAGTTGCCTG ACTCCCCGTC

1021 GTGTAGATAA CTACGATACG GGAGGGCTTA CCATCTGGCC CCAGTGCTGC AATGATACCG

1081 CGAGACCCAC GCTCACCGGC TCCAGATTTA TCAGCAATAA ACCAGCCAGC CGGAAGGGCC

1141 GAGCGCAGAA GTGGTCCTGC AACTTTATCC GCCTCCATCC AGTCTATTAA TTGTTGCCGG

1201 GAAGCTAGAG TAAGTAGTTC GCCAGTTAAT AGTTTGCGCA ACGTTGTTGC CATTGCTACA

1261 GGCATCGTGG TGTCACGCTC GTCGTTTGGT ATGGCTTCAT TCAGCTCCGG TTCCCAACGA

1321 TCAAGGCGAG TTACATGATC CCCCATGTTG TGCAAAAAAG CGGTTAGCTC CTTCGGTCCT

1381 CCGATCGTTG TCAGAAGTAA GTTGGCCGCA GTGTTATCAC TCATGGTTAT GGCAGCACTG

1441 CATAATTCTC TTACTGTCAT GCCATCCGTA AGATGCTTTT CTGTGACTGG TGAGTACTCA

1501 ACCAAGTCAT TCTGAGAATA GTGTATGCGG CGACCGAGTT GCTCTTGCCC GGCGTCAATA

1561 CGGGATAATA CCGCGCCACA TAGCAGAACT TTAAAAGTGC TCATCATTGG AAAACGTTCT

1621 TCGGGGCGAA AACTCTCAAG GATCTTACCG CTGTTGAGAT CCAGTTCGAT GTAACCCACT

1681 CGTGCACCCA ACTGATCTTC AGCATCTTTT ACTTTCACCA GCGTTTCTGG GTGAGCAAAA

1741 ACAGGAAGGC AAAATGCCGC AAAAAAGGGA ATAAGGGCGA CACGGAAATG TTGAATACTC

1801 ATACTCTTCC TTTTTCAATA TTATTGAAGC ATTTATCAGG GTTATTGTCT CATGAGCGGA

1861 TACATATTTG AATGTATTTA GAAAAATAAA CAAATAGGGG TTCCGCGCAC ATTTCCCCGA

1921 AAAGTGCCAC CTGACGTCTA AGAAACCATT ATTATCATGA CATTAACCTA TAAAAATAGG

1981 CGTATCACGA GGCCCTTTCG TCTCGCGCGT TTCGGTGATG ACGGTGAAAA CCTCTGACAC

2041 ATGCAGCTCC CGGAGACGGT CACAGCTTGT CTGTAAGCGG ATGCCGGGAG CAGACAAGCC

2101 CGTCAGGGCG CGTCAGCGGG TGTTGGCGGG TGTCGGGGCT GGCTTAACTA TGCGGCATCA

2161 GAGCAGATTG TACTGAGAGT GCACCATAAA ATTGTAAACG TTAATATTTT GTTAAAATTC

2221 GCGTTAAATT TTTGTTAAAT CAGCTCATTT TTTAACCAAT AGGCCGAAAT CGGCAAAATC

2281 CCTTATAAAT CAAAAGAATA GCCCGAGATA GGGTTGAGTG TTGTTCCAGT TTGGAACAAG

2341 AGTCCACTAT TAAAGAACGT GGACTCCAAC GTCAAAGGGC GAAAAACCGT CTATCAGGGC

2401 GATGGCCCAC TACGTGAACC ATCACCCAAA TCAAGTTTTT TGGGGTCGAG GTGCCGTAAA

2461 GCACTAAATC GGAACCCTAA AGGGAGCCCC CGATTTAGAG CTTGACGGGG AAAGCCGGCG

2521 AACGTGGCGA GAAAGGAAGG GAAGAAAGCG AAAGGAGCGG GCGCTAGGGC GCTGGCAAGT

2581 GTAGCGGTCA CGCTGCGCGT AACCACCACA CCCGCCGCGC TTAATGCGCC GCTACAGGGC

2641 GCGTACTATG GTTGCTTTGA CGTATGCGGT GTGAAATACC GCACAGATGC GTAAGGAGAA

2701 AATACCGCAT CAGGCGCCAT TCGCCATTCA GGCTGCGCAA CTGTTGGGAA GGGCGATCGG

2761 TGCGGGCCTC TTCGCTATTA CGCCAGCTGG CGAAAGGGGG ATGTGCTGCA AGGCGATTAA

2821 GTTGGGTAAC GCCAGGGTTT TCCCAGTCAC GACGTTGTAA AACGACGGCC AGTGCCAAGC

2881 TGGCCGGCCT AGGCGCGCCA AGCTTAAGGT GCACGGCCCA CGTGGCCACT AGTACTTCTC

2941 GAGCTCTGTA CATGTCCGCG GTCGCGACGT ACGCGTATCG ATGGCGCCAG CTGCAGGCGG

3001 CCGCCATATG CATCCTAGGC CTATTAATAT TCCGGAGTAT ACGTAGCCGG CTAACGTTAT

3061 CATACAATAT GACTCATTTG TTTTTCAAAA CCGAACTTGA TTTACGGGTA GAATTCTACT

3121 TGTAAAGCAC AATCAAAAAG ATGATGTCAT TTGTTTTTCA AAACTGAACT CGCTTTACGA

3181 GTAGAATTCT ACGTGTAAAA CACAATCAAG AAATGATGTC ATTTGTTATA AAAATAAAAG

3241 CTGATGTCAT GTTTTGCACA TGGCTCATAA CTAAACTCGC TTTACGGGTA GAATTCTACG

3301 CGCGTCGATG TCTTTGTGAT GCGCGCGACA TTTTTGTAGG TTATTGATAA AATGAACGGA

3361 TACGTTGCCC GACATTATCA TTAAATCCTT GGCGTAGAAT TTGTCGGGTC CATTGTCCGT

3421 GTGCGCTAGC ATGCCCGTAA CGGACCTCGT ACTTTTGGCT TCAAAGGTTT TGCGCACAGA

3481 CAAAATGTGC CACACTTGCA GCTCTGCATG TGTGCGCGTT ACCACAAATC CCAACGGCGC

3541 AGTGTACTTG TTGTATGCAA ATAAATCTCG ATAAAGGCGC GGCGCGCGAA TGCAGCTGAT

3601 CACGTACGCT CCTCGTGTTC CGTTCAAGGA CGGTGTTATC GACCTCAGAT TAATGTTTAT

3661 CGGCCGACTG TTTTCGTATC CGCTCACCAA ACGCGTTTTT GCATTAACAT TGTATGTCGG

3721 CGGATGTTCT ATATCTAATT TGAATAAATA AACGATAACC GCGTTGGTTT TAGAGGGCAT

3781 AATAAAAGAA ATATTGTTAT CGTGTTCGCC ATTAGGGCAG TATAAATTGA CGTTCATGTT

3841 GGATATTGTT TCAGTTGCAA GTTGACACTG GCGGCGACAA GATCGTGAAC AACCAAGTGA

3901 CCATGGCATC GTTAATGGCA GGTGGAAAAG CAGGTAAAGA CAGTGGCAAA GCCAAGGCGA

3961 AAGCAGTGTC TCGCTCGCAA AGAGCTGGTC TTCAGTTTCC AGTGGGACGA ATCCACAGGC

4021 ACTTGAAGAC ACGCACTACA AGCCATGGTC GAGTAGGAGC AACAGCAGCC GTTTACAGCG

4081 CAGCCATTCT TGAATATCTC ACAGCTGAAG TTTTGGAGTT GGCGGGAAAT GCTTCAAAAG

4141 ACCTGAAGGT GAAGCGCATC ACTCCTCGAC ATTTACAGCT GGCCATTCGA GGAGATGAGG

4201 AGCTCGATTC CCTTATCAAG GCCACTATTG CTGGAGGAGG TGTGATTCCA CACATCCACA

4261 AGTCTCTGAT TGGTAAGAAG GGCCAGCAGA AAACCGCAGG GGGGATGGTG AGCAAGGGCG

4321 AGGAGGACAA CATGGCCATC ATCAAGGAGT TCATGCGCTT CAAGGTGCAC ATGGAGGGCT

4381 CCGTGAACGG CCACGAGTTC GAGATCGAGG GCGAGGGCGA GGGCCGCCCC TACGAGGGCA

4441 CCCAGACCGC CAAGCTGAAG GTGACCAAGG GCGGCCCCCT GCCCTTCGCC TGGGACATCC

4501 TGTCCCCTCA GTTCATGTAC GGCTCCAAGG CCTACGTGAA GCACCCCGCC GACATCCCCG

4561 ACTACTTGAA GCTGTCCTTC CCCGAGGGCT TCAAGTGGGA GCGCGTGATG AACTTCGAGG

4621 ACGGCGGCGT GGTGACCGTG ACCCAGGACT CCTCCCTGCA GGACGGCGAG TTCATCTACA

4681 AGGTGAAGCT GCGCGGCACC AACTTCCCCT CCGACGGCCC CGTAATGCAG AAGAAGACCA

4741 TGGGCTGGGA GGCCTCCTCC GAGCGGATGT ACCCCGAGGA CGGCGCCCTG AAGGGCGAGA

4801 TCAAGCAGAG GCTGAAGCTG AAGGACGGCG GCCACTACGA CGCCGAGGTC AAGACCACCT

4861 ACAAGGCCAA GAAGCCCGTG CAGCTGCCCG GCGCCTACAA CGTCAACATC AAGCTGGACA

4921 TCACCTCCCA CAACGAGGAC TACACCATCG TGGAACAGTA CGAGCGCGCC GAGGGCCGCC

4981 ACTCCACCGG CGGCATGGAC GAGCTGTACA AGGTGAAACA GACTTTGAAT TTTGACCTTC

5041 TCAAGTTGGC GGGAGACGTG GAGTCCAACC CAGGGCCCAA GCTTATGGTG AGCAAGGGCG

5101 AGGAGCTGTT CACCGGGGTG GTGCCCATCC TGGTCGAGCT GGACGGCGAC GTAAACGGCC

5161 ACAAGTTCAG CGTGTCCGGC GAGGGCGAGG GCGATGCCAC CTACGGCAAG CTGACCCTGA

5221 AGTTCATCTG CACCACCGGC AAGCTGCCCG TGCCCTGGCC CACCCTCGTG ACCACCCTGA

5281 CCTACGGCGT GCAGTGCTTC AGCCGCTACC CCGACCACAT GAAGCAGCAC GACTTCTTCA

5341 AGTCCGCCAT GCCCGAAGGC TACGTCCAGG AGCGCACCAT CTTCTTCAAG GACGACGGCA

5401 ACTACAAGAC CCGCGCCGAG GTGAAGTTCG AGGGCGACAC CCTGGTGAAC CGCATCGAGC

5461 TGAAGGGCAT CGACTTCAAG GAGGACGGCA ACATCCTGGG GCACAAGCTG GAGTACAACT

5521 ACAACAGCCA CAACGTCTAT ATCATGGCCG ACAAGCAGAA GAACGGCATC AAGGTGAACT

5581 TCAAGATCCG CCACAACATC GAGGACGGCA GCGTGCAGCT CGCCGACCAC TACCAGCAGA

5641 ACACCCCCAT CGGCGACGGC CCCGTGCTGC TGCCCGACAA CCACTACCTG AGCACCCAGT

5701 CCGCCCTGAG CAAAGACCCC AACGAGAAGC GCGATCACAT GGTCCTGCTG GAGTTCGTGA

5761 CCGCCGCCGG GATCACTCTC GGCATGGACG AGCTGTACAA GGGAGGAGGA AGATCTAAGC

5821 TGAACCCTCC TGATGAGAGT GGCCCCGGCT GCATGAGCTG CAAGTGTGTG CTCTCCTGAA

5881 TAAAACACGT CAAGAGCTCG CGGATCCCAA TTGGCAGATC TCGGCGCGCC TGCAGGTCGA

5941 CGGTACCGGT TCGAAGCTTG CGGCCGCATC TTCTGGTAAA GAAACCGCTG CTGCGAAATT

6001 TGAACGCCAG CACATGGACT CGCCACCGCC TTCTGGCCTC GAGCACCACC ATCACCATCA

6061 CCATCACTAA GTGATTAACC TCAGGTTATA CATATATTTT GAATTTAATT AATTATACAT

6121 ATATTTTATA TTATTTTTGT CTTTTATTAT CGAGGGGCCG TTGTTGGTGT GGGGTTTTGC

6181 ATAGAAATAA CAATGGGAGT TGGCGACGTT GCTGCGCCAA CACCACCTCC CTTCCCTCCT

6241 TTCATCATGT ATCTGTAGAT AAAATAAAAT ATTAAACCTA AAAACAAGAC CGCGCCTATC

6301 AACAAAATGA TAGGCATTAA CTTGCCGCTG ACGCTGTCAC TAACGTTGGA CGATTTGCCG

6361 ACTAAACCTT CATCGCCCAG TAACCAATCT AGAACTATAG CTAGCATGCG CAAATTTAAA

6421 GCGCTGATAT CGATCGCGCG CAGATCTGTC ATGATGATCA TTGCAATTGG ATCCATATAT

```
6481 AGGGCCCGGG TTATAATTAC CTCAGGTCGA CGTCCCATGG CCATTCGAAT TCGGCCGGCC
6541 TAGGCGCGCC AATTCGTAAT CATGTCATAG CTGTTTCCTG TGTGAAATTG TTATCCGCTC
6601 ACAATTCCAC ACAACATACG AGCCGGAAGC ATAAAGTGTA AAGCCTGGGG TGCCTAATGA
6661 GTGAGCTAAC TCACATTAAT TGCGTTGCGC TCACTGCCCG CTTTCCAGTC GGGAAACCTG
6721 TCGTGCCAGC TGCATTAATG AATCGGCCAA CGCGCGGGGA GAGGCGGTTT GCGTATTGGG
6781 CGC
//
```

The plasmid from figure A3.3, pfIErfly,was digested using restriction enzyme HpaI. A fragment containing H_2A:mCherry:F2A:eGFP:CAAX (plasmid template a gift of Duygu Özpolat) was PCR amplified using primers:

5’-GAACAACCAAGTGACCATGGCATCGTTAATGGCAGGTGGAAAAGCAGGTAAA-3’ and

5’- TTGGGATCCGCGAGCTCTTGACGTGTTTTATTCAGGAGAGCACACACTTGCAG-3’.

The fragment was then Gibson cloned into the linearized pfIErfly fragment with the help of Jose Breton-Arias.

Sequence A3.7 *Morpho peleides* Tyrosine hydroxylase mRNA (*pale*)

LOCUS *Morpho peleides pale* mRNA sequence
DEFINITION *Morpho peleides pale* mRNA sequence
TITLE *Morpho peleides pale* mRNA sequence

FEATURES Location/Qualifiers

Undefined 1..113
/note="Morpho peleides Tyrosine hydroxylase 5' UTR"

Undefined 114..1784
/note="Morpho peleides Tyrosine hydroxylase ORF"

Undefined 1785..1893
/note="Morpho peleides Tyrosine hydroxylase 3' UTR"

ORIGIN

```
       1 AGACAGGCTT CAGCCCGTGG TCGAGACATA AGGCTCTCGC AGACGTACGC TAGCTAAACG
      61 CGCAGTGAAC TCCCGTTCAG GCTTCAACTT TTCAAGTGGT GTGTCGTGAA GAAATGGCCG
     121 TAGCCGCAGC ACAAAAGAAC CGCGAAATGT TCGCCATCAA GAAATCCTAC AGCATTGAGA
     181 ACGGTTATCC ATCACGCCGT CGCTCGCTTG TAGACGACGC CCGCTTCGAA ACTCTTGTTG
     241 TCAAACAGAC CAAGCAAAGT GTGCTTGAAG AGGCTCGTGC TCGTGCCAAT GACTCTGGCT
     301 TGGAATCAGA CTTTATCCAA GACGCCGCTC AACTTGGCGA AGGCGAGAAA TATGAAGATG
     361 GCACCCTACC TGATGATAAC AAAAATGCTA CTTCTGATGC TGATCCTACC GATGGTGGAG
     421 CAAAATCAGA TGAAGATTAC ACTCTTACTG AAGAGGAGAT AATTCTACAA AACGCTGCAA
     481 GCGAGAGCCC AGAGGCCGAA CAAGCGATTC AAAAGGCCGC TCTACTCCTT CGTATGCGCG
     541 AAGGCATGGG AGCTCTTGCT CGCATTCTCA AAACTATTGA CAACTATAAG GGCTGTGTAG
     601 AACATCTCGA AACTCGTCCC TCTCAAGTCT CTGGTATCCA ATTCGATGCT CTTGTAAAAG
     661 TCAGCATGTC GCGCATCAAC TTGCTGCAAC TCATCAGATC TCTTCGCCAA TCAACTTCCT
     721 TCGCTGGCGC AAGTCTGTTC TCCGACAACA TTTCTAACAA AACTCCGTGG TTCCCCCGTC
     781 ACGCATCCGA TCTCGACAAT TGCAATCACC TGATGACCAA ATACGAGCCT GAACTCGACA
     841 TGAATCACCC AGGTTTCGCT GATAAGGAAT ATCGTGAACG CAGAAAGGAA ATTGCCGAAA
     901 TTGCTTTCGC TTACAAATAT GGTGACGCTA TCCCATCGAT TACCTACACT GAAACTGAGA
     961 ACGCAACCTG GCAACGAGTT TTTAACACCG TGGTCGATCT TATGCCCAAA CATGCTTGCA
    1021 AAGAATACAA GGCAGCATTC GGCAAGCTGC AAGCTGCTGA TATCTTCGTG CCTCACCGCA
    1081 TCCCACAGTT GGAAGACGTG AGCACTTTCC TTCGCAAGCA CACCGGTTTC ACTCTTCGTC
    1141 CAGCAGCTGG GCTGCTCACA GCTCGCGACT TCCTCGCTTC CCTGGCTTTC CGTGTGTTCC
    1201 AGTCTACACA GTACGTGCGT CATGCCAACT CACCCTTCCA CACACCTGAA CCAGATTGTA
    1261 TCCATGAGCT GCTCGGACAT ATTCCTCTTT TGGCTGACCC GAGTTTTGCC CAGTTCTCTC
    1321 AAGAAATCGG CCTCGCTTCA CTTGGCGCTT CAGATTCTGA AATCGAAAAA TTGTCCACTG
    1381 TATACTGGTT CACCGTTGAA TTCGGTTTAT GCAAAGAAAA CCAACAACTG AAGGCATATG
    1441 GCGCTGCTCT GCTGTCTTCC ATTGGAGAAT TGCTTCACGC TCTCAGTGAC AAACCTGAAC
    1501 TTAGACCTTT TGAGCCTGCT TCCACATCTC TGCAACCGTA TCAGGACCAA GAATATCAAC
    1561 CTATTTATTA CGTGGCTGAA AGCTTCGAAG ATGCCAAAGA TAAATTCAGA CGCTGGGTGT
    1621 CCACCATGTC GCGACCTTTC GAGGTCCGCT TTAACCCGCA CACTGAGCGC GTCGAGGTCC
    1681 TTGACTCGGT CGACAAATTG GAGACCATCA TCTGGCAACT GAACACAGAG ATGCTTCATC
    1741 TCACTAACGC CATTAGCAAG CTCAGGGGAT CAAACTTCGA GTGAACCGGT TACCTGCATC
    1801 CTACAACCAG ACCAGACGCG GCCTCGCCGT ATCTTGTATA GCTAGTGATA TTATAGACGT
    1861 AAGATTGTTG TCGTGTTGAG CGTGTGTGCG TGT
```

//

Morpho peleides pale was cloned from cDNA made from pupal wing tissue. Cloning was achieved by touchdown PCR amplification using the degenerate primers 5'-CYGTTTGCAATCCAAAGTTTAGTT-3' and 5'-AGCTTCTTGACGGCRTTG-3'.

Sequence A3.8 Alignment of translated *pale* mRNA from *Morpho peleides*

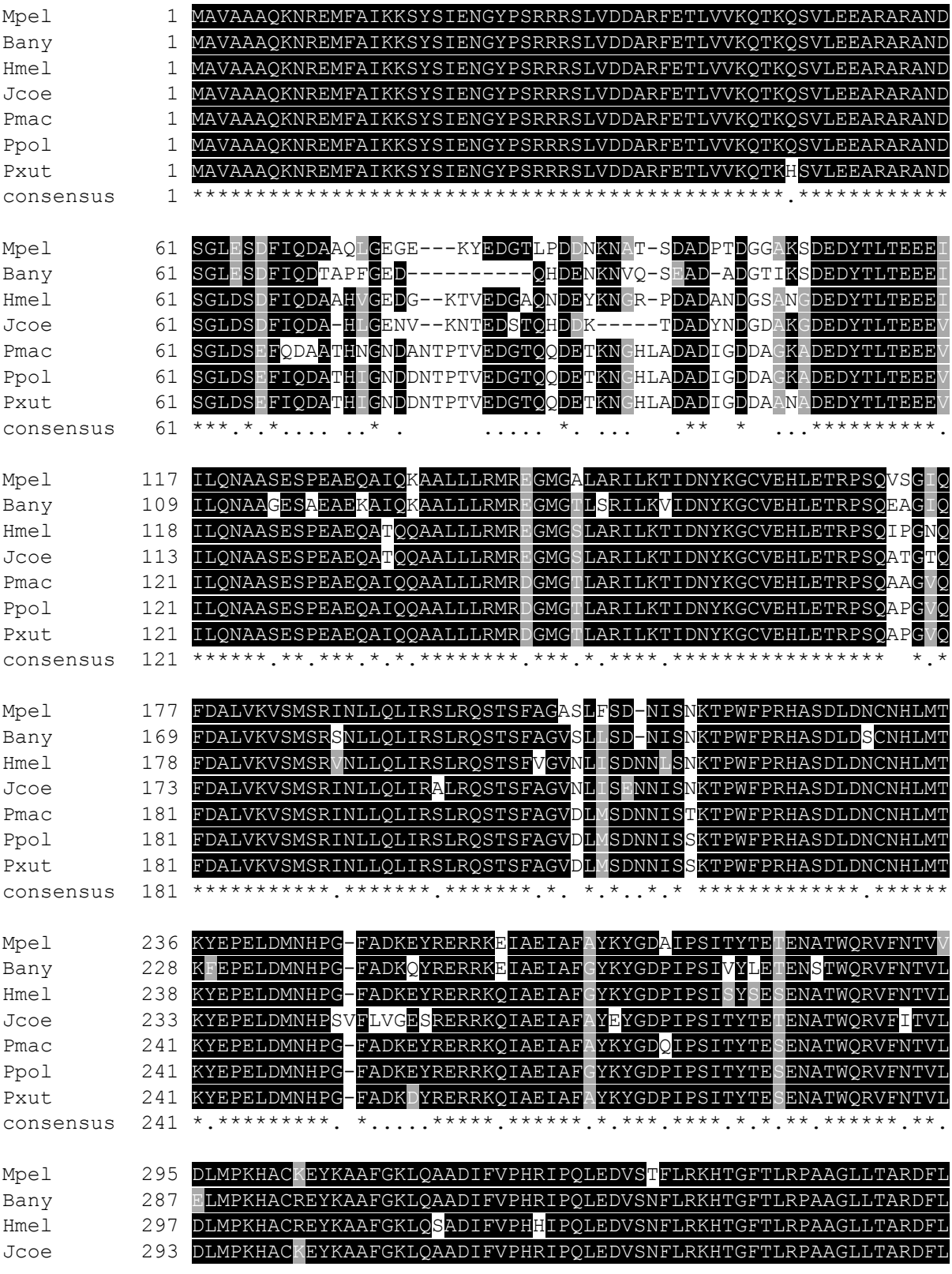

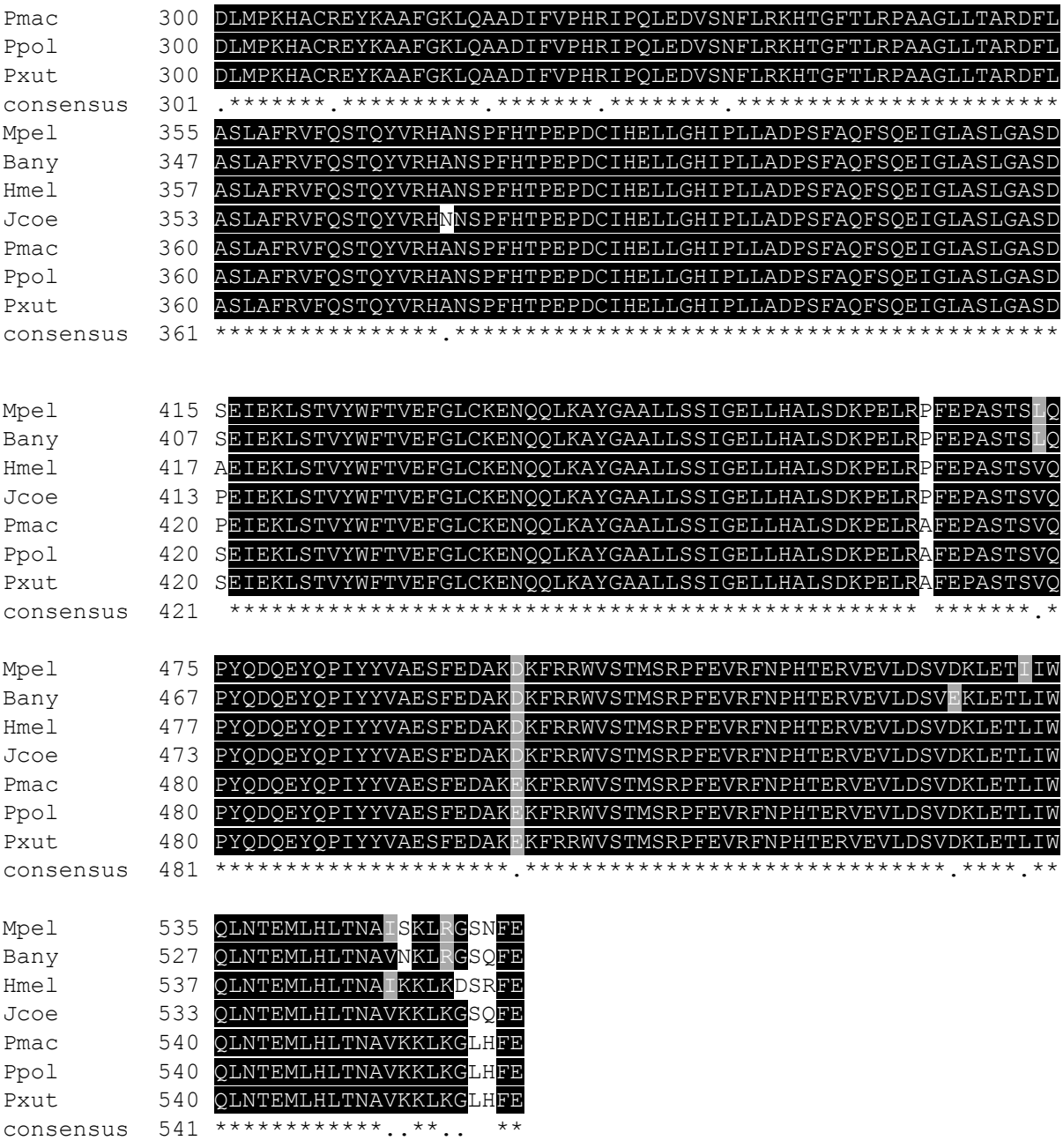

Mpel – *Morpho peleides*, Bany – *Bicyclus anynana*, Hmel – *Heliconius melpomene*, Jcoe – *Junonia coenia*, Pmac – *Papilio machaon*, Ppol – *Papilio polytes*, Pxut – *Papilio xuthus*

Alignment was performed using “T-Coffee alignment” (http://tcoffee.crg.cat/apps/tcoffee/do:regular) with the following settings: fasta_aln, clustalw_aln, phylip. The figure was made using the online program “Box Shade” (http://www.ch.embnet.org/cgi-bin/BOX_form_parser) with the following settings: FastA_Aln from tcoffee as input, output: rtf_new, font size: 10, consensus with symbols, fraction of sequences: 0.7, input sequence format: ALN

Appendix 4
Computer Script for Image Analysis

Introduction

These scripts were written utilizing Python2.7 and R3.1.3. For the Python scripts to work, the libraries PIL and Pandas were added, and the OS and CSV libraries were called. For the R portion of the scripts, the library ggplot2 was added. Further, the scripts expect 4 unique directory locations – a folder where the images for analysis are to be found, a location for where the tabulated CSV files can be saved, a location for the generated R script to be saved, and a location to which R can output the final plots. Here I provide the script as well as examples of the input and outputs of the script.

Figure A4.1 Graphical flowchart representation of custom Python/R scripts

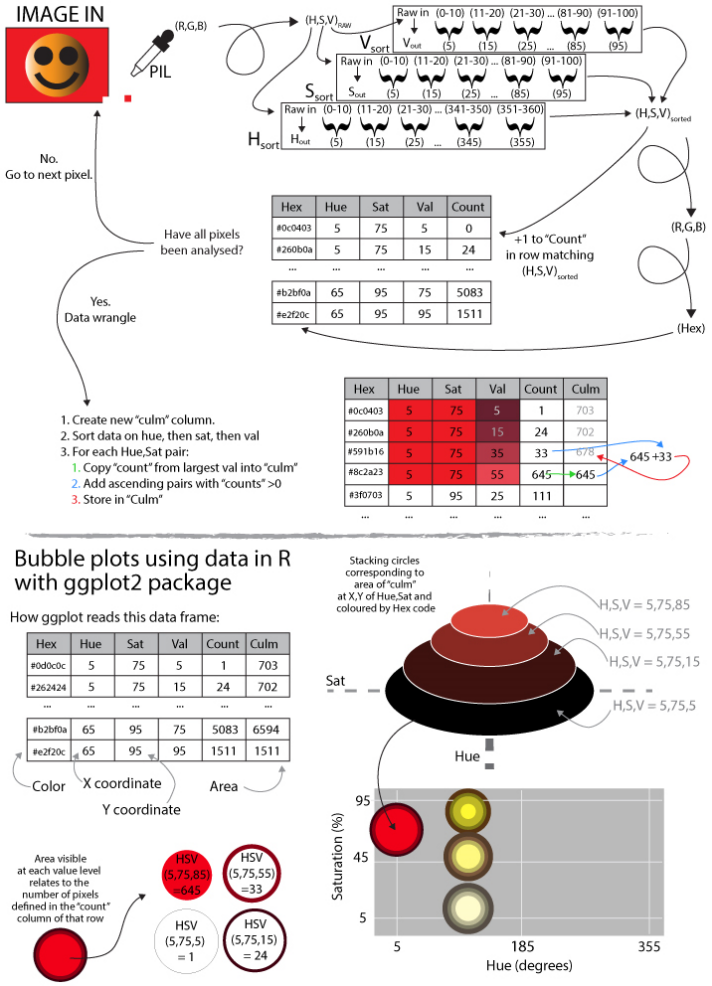

RGB values for a picture or region of interest (ROI) are read pixel-by-pixel by the Python script. These values are converted into the more intuitive color space HSV and then binned into values of 10 to reduce the color space to one of 3600 colors defined combinatorially by 36 hues (5-355 degrees, red to magenta), 10 saturation values (5-95%, least pure to purest), and 10 value values (5-95%, darkest to lightest). This new HSV value is then converted back to RGB so that the hexadecimal color code can be computed for use later in plotting. A dictionary is then queried for the existence of an entry with the binned HSV value computed following the binning. If already existing the dictionary updates the count for that HSV value by adding 1. If the entry is not in existence, a new entry with the HSV values computed is created with a count of 1 and the hex code for that HSV combination will be stored with the new entry. With operations complete on this pixel, the algorithm moves to the next pixel in the input image/ROI. When all pixels have been analyzed for the image, the algorithm then sorts the dictionary by “Hue”, then “Sat”, then “Val”. For entries with the same hue and saturation, the program first duplicates the pixel count of the entry with the highest “Val” into the “cumulative counts” column for that entry. Next it adds the pixel counts of the second highest “Val” entry to the first’s “Cumulative”, entering the sum into the second highest “Val” entry’s cumulative counts column. This is repeated for all descending pairs of “Val” in every Hue,Sat pair. Plotting is done in R using the ggplot2 package by layering circles of sizes corresponding to the cumulative pixel totals of each Val, using Hue and Sat as the X and Y coordinates respectively. When viewing the plot concentric circles of decreasing value can be seen expanding out from the Hue,Sat coordinates on the graph. Visible area indicates the original counts made by the algorithm – this is why the program finds the cumulative count: the largest Val entry has an area that obscures the same amount of area from the next value. By adding the counts of consecutive values in a cumulative manner, the resulting visible area corresponds to only that of the original count and is not obscured by the overlain bubbles of previous counts.

Script A4.1 Image to Hue, Saturation, Value plot (run in Python 2.7)

```
## Calling necessary Python 2.7 libraries

import os

import csv

from PIL import Image

import pandas


##########Interactive command line option for setting directory

base1=raw_input("What would you like the R file to be called? File name
will look like: (your text).R ")    ## splits the file name into its
component name and extension so the name can be reused for output files


########## Hard coding for entering the directories

rawim="C:/…/001imagesin" ## where are your images?

csvdata="C:/…/002dataout" ## where do you want the csv?

rcode="C:/…/003Rscriptout" ## Where do you want the R code?

plotout="C:/…/004plotsout" ## Where do you want the plots?

bub=str(25) ## setting bubble ratios for bubble plots

ratio=str(1.8) ## XY ratio for plot outputs


## Warning display and program trigger

raw_input("Please make sure your image names have no whitespaces, non-
alphanumeric characters, do not start with a number, and are not in
.png, .tif, or .raw format. This will take about 1 minute per 50k
pixels of image, please hang on. Press enter to start.") # just warning
folks of the time


## Program subroutines

    ## conversion of RGB to HSV

def rgbtohsv(R,G,B): ## taken from ActiveState Code Recipes 576919 rgb
and hsv conversion

    varR=(R)

    varG=(G)

    varB=(B)

    mn=min(varR,varG,varB)
```

```
    mx=max(varR,varG,varB)
    df=mx-mn
    if mx==mn:
        h=0
    elif mx==varR:
        h=(60*((varG-varB)/df)+360)%360
    elif mx==varG:
        h=(60*((varB-varR)/df)+120)%360
    elif mx==varB:
        h=(60*((varR-varG)/df)+240)%360
    if mx==0:
        s=0
    else:
        s=df/mx
    v=mx
    h=h/360.0
    return h,s,v

    ##conversion of HSV to RGB
def hsvtorgb(H,S,V):
    if (S == 0):                        #HSV from 0 to 1
        R = V*255
        G = V*255
        B = V*255
        return R,G,B
    else:
        varh = H*6
        if varh==6:
            varh=0      #H must be < 1
        vari=int(varh)              #Or ... var_i = floor( var_h )
        var1=V*(1-S)
        var2=V*(1-S*(varh-vari))
```

```
        var3=V*(1-S*(1-(varh-vari)))
        if vari==0:
            varr=V
            varg=var3
            varb=var1
        elif vari==1:
            varr=var2
            varg=V
            varb=var1
        elif vari==2:
            varr=var1
            varg=V
            varb=var3
        elif vari==3:
            varr=var1
            varg=var2
            varb=V
        elif vari==4:
            varr=var3
            varg=var1
            varb=V
        else:
            varr=V
            varg=var1
            varb=var2
        R=varr*255                  ##RGB results from 0 to 255
        G=varg*255
        B=varb*255
        return R,G,B


    ## code to make a function for generating Hex from RGB values found
on internet
```

```
def tohex(R,G,B):
      hexchars = "0123456789ABCDEF"
      calcr1=hexchars[int(R / 16.000000000000000000000000000000)]
      calcr2=hexchars[int(R % 16.000000000000000000000000000000)]
      calcg1=hexchars[int(G / 16.000000000000000000000000000000)]
      calcg2=hexchars[int(G % 16.000000000000000000000000000000)]
      calcb1=hexchars[int(B / 16.000000000000000000000000000000)]
      calcb2=hexchars[int(B % 16.000000000000000000000000000000)]
      return "#"+calcr1+calcr2+calcg1+calcg2+calcb1+calcb2


    ### This function evaluates an input s or l value (SL) and compares
the input to the cutoff value in the first position of each pair
(cutoff, value), it then returns the second of the numbers
def slbin(SV):
      sv=SV
      cutoffs=[
            (0.100, 0.05),
            (0.200, 0.15),
            (0.300, 0.25),
            (0.400, 0.35),
            (0.500, 0.45),
            (0.600, 0.55),
            (0.700, 0.65),
            (0.800, 0.75),
            (0.900, 0.85),
            (1.200, 0.95)
      ]
      for cutoff, value in cutoffs:
            if sv<=cutoff:
                  return value


    ### This function evaluates an input h value (H) and compares the
input to the cutoff value in the first position of each pair (cutoff,
value), it then returns the second of the numbers
```

```
def hbin(H):
      X=H
      cutoffs=[
        (0.027777777777777777777777777777, 5.0),
            (0.055555555555555555555555555555, 15.0),
            (0.083333333333333333333333333333, 25.0),
            (0.11111111111111111111111111111, 35.0),
            (0.13888888888888888888888888888, 45.0),
            (0.16666666666666666666666666667, 55.0),
            (0.19444444444444444444444444444, 65.0),
            (0.22222222222222222222222222222, 75.0),
            (0.25, 85.0),
            (0.27777777777777777777777777778, 95.0),
            (0.30555555555555555555555555556, 105.0),
            (0.33333333333333333333333333333, 115.0),
            (0.36111111111111111111111111111, 125.0),
            (0.38888888888888888888888888889, 135.0),
            (0.41666666666666666666666666667, 145.0),
            (0.44444444444444444444444444444, 155.0),
            (0.47222222222222222222222222222, 165.0),
            (0.50, 175.0),
            (0.52777777777777777777777777778, 185.0),
            (0.55555555555555555555555555556, 195.0),
            (0.58333333333333333333333333333, 205.0),
            (0.61111111111111111111111111111, 215.0),
            (0.63888888888888888888888888888, 225.0),
            (0.66666666666666666666666666667, 235.0),
            (0.69444444444444444444444444444, 245.0),
            (0.72222222222222222222222222222, 255.0),
            (0.75, 265.0),
            (0.77777777777777777777777777778, 275.0),
            (0.80555555555555555555555555556, 285.0),
```

```
            (0.83333333333333333333333333333, 295.0),
            (0.86111111111111111111111111111, 305.0),
            (0.88888888888888888888888888889, 315.0),
            (0.91666666666666666666666666667, 325.0),
            (0.94444444444444444444444444444, 335.0),
            (0.97222222222222222222222222222, 345.0),
            (1.00000000000000000000000000000, 355.0)
             ]
      for cutoff, value in cutoffs:
            if float(X)<=cutoff:
                  return value


## --- END SUBROUTINES ---- ####

### Starting pixel to HSV+HEX for CSV creation
os.chdir(rawim)  ## Reading in images from directory
for pics in os.listdir(rawim):
    im=Image.open(pics)
    pix=im.load()
    pixels=list(im.getdata())
    width, height=im.size
    dicpixr={}  ## Creating dictionaries for storing pixel data
    q=0
    p=0
    y=[]
    hex={}
    for i in pixels:
        p+=1
        H=0
        V=0
        S=0
```

```
        dicpixr[q]=pixels[q]

        R=(dicpixr[q][0])/255.0

        G=(dicpixr[q][1])/255.0

        B=(dicpixr[q][2])/255.0

        hsv=rgbtohsv(R,G,B)

        h1=hbin(hsv[0]) #this transforms the float to a 5 decimal place
"integer"

        s1=slbin(hsv[1])

        v1=slbin(hsv[2])

        rgb=hsvtorgb(h1/360.0,s1,v1) #once a single combination of Hsv
have been created by the for loop

        r1=int(rgb[0]) ## these take the output of hlstorgb (a tuple)
and pull out integers from each that "tohex" can comprehend

        g1=int(rgb[1])

        b1=int(rgb[2])

        T=tohex(r1,g1,b1)    ## T is a variable that stores the value
output by the to hex function

        hex[p]=h1,s1,v1,T  ## creating a new entry in the dictionary

        y.append(hex[p]) ## THIS MOST RECENT ENTRY WILL BE APPENDED TO
THE LIST Y

        q+=1


    ### COUNTING LOOP

    d=dict()        ## YET ANOTHER DICTIONARY

    for a in y:     ## THIS FOR LOOP RUNS THROUGH ALL THE ENTRIES IN
THE LIST Y

        if a in d:  ## ASKING IF A IS ALREADY IN THE DICTIONARY

            d[a]+=1     ## YES? INCREASE COUNTER BY ONE WITH VALUE OF Y
AS THE KEY

        else:           ## NO?

            d[a]=d.get(a,1)    ##INITIALIZE "A" AS A KEY WITH THE VALUE
OF 1


    ## the following code organizes the data in d as a pandas
dataframe, it then sorts on H and S, slices data into pieces based on
```

```
h&S, creates a new column called culm, then stitches everything back
together into a single data frame

    i=0

    df=pandas.DataFrame(columns=list("xhsvcu")) ## creates an empty
data frame with header x, h, s, v, c

    if i <= len(d):                             ## this says that if
the counter i is less than the length of the dictionary to continue
cycling

        for key, value in d.items():            ## for entries in
dictionary d with key and value


df.loc[i]=([key[3],int(key[0]),int(key[1]*100),int(key[2]*100),value,0]
) ## make an entry into the data frame at i, with these values from d

            i+=1                                                ## increase
i by one

    df.loc[:,('u')]=df.loc[:,('c')]



    ## creating new data frames from old slicing on h and s


hue=[0,10,20,30,40,50,60,70,80,90,100,110,120,130,140,150,160,170,180,1
90,200,210,220,230,240,250,260,270,280,290,300,310,320,330,340,350,360]

    sv=[0,10,20,30,40,50,60,70,80,90,100]

    dn={}

    a=1

    while a < len(hue):

        b=1

        while b < len(sv):

            name="hs"+str(hue[a])+str(sv[b])

            dfsub = pandas.DataFrame(df.loc[(df.h <=int(hue[a])) &
(df.h >= int(hue[a-1])) & (df.s <= int(sv[b])) & (df.s>=int(sv[b-1]))])

            dfsub=dfsub.sort(['v'], ascending=[0])

            dfsub=dfsub.reset_index()

            listc=dfsub['u'].tolist()

            listi=dfsub['index'].tolist()

            j=1

            if len(listc) >= 2:
```

```
                while j < len(listc):
                    uent=listc[j]+listc[j-1]
                    listc[j]=uent
                    ind=listi[j]
                    df.u[ind]=uent
                    j+=1
            b+=1
        a+=1


    ## transforming the data frame into something that can be iterated
over for writing
    df=df.sort(['h','s','v'])                                ## recreate
the dataframe sorted on h, then s, then l
    dfx=df['x'].tolist()                                  ## these
following commands create lists from columns in the dataframe
    dfh=df['h'].tolist()
    dfs=df['s'].tolist()
    dfv=df['v'].tolist()
    dfc=df['c'].tolist()
    dfu=df['u'].tolist()


    ## CREATING CSV OUTPUT FILES FROM THE DATA
    base,ext=os.path.splitext(pics)    ## splits the file name into its
component name and extension so the name can be reused for output files
    out=os.path.join(csvdata,base)



    ## Writing counts to csv
    with open(out+'count.csv', 'wb') as outfile:
        writer = csv.writer(outfile)
        writer.writerow(["hex","h","s","v","count","culm"]) ## header
row for data
        i=0                                          ## creating a
counter
```

```
        while i < len(dfx):                          ## making a loop
that runs for the length of the list


writer.writerow([dfx[i],dfh[i],dfs[i],dfv[i],dfc[i],dfu[i]])

            i+=1


print "Done making CSVs! Check",csvdata,"to see if your files are
successful."


########

## Taking CSV and producing executable R file


dic={}                           ## this creates the command dictionary
where each command will be stored

dicount=0


dic[dicount]="setwd('"+csvdata+"')"        ## This creates the command
for storing the working directory so R knows where to find the raw data

dicount+=1

dic[dicount]="library(ggplot2)"         ## this imports ggplot2 library
to create the plots

dicount+=1


                      ## this is the key generator for storing unique
lines of code in the dictionary


## creating an R function to eliminate most of the repetitive chunks of
this code

deg=(5,15,25,35,45,55,65,75,85,95,105,115,125,135,145,155,165,175,185,1
95,205,215,225,235,245,255,265,275,285,295,305,315,325,335,345,355)

dic[dicount]="x=c"+str(deg)

dicount+=1

dic[dicount]="binfx<-function(dataframe) {"

dicount+=1

dic[dicount]="dataframe=dataframe"

dicount+=1
```

```
i=1

while i<len(deg):

    for i in deg:

      dic[dicount]="
h"+str(i)+"=subset(dataframe,h<="+str(i)+"&h>"+str(i-
10)+",select=c(count))"

      dicount+=1

      dic[dicount]="     sum"+str(i)+"=sum(h"+str(i)+"$count)"

      dicount+=1

      i+=1

dic[dicount]="
d=c(sum5,sum15,sum25,sum35,sum45,sum55,sum65,sum75,sum85,sum95,sum105,s
um115,sum125,sum135,sum145,sum155,sum165,sum175,sum185,sum195,sum205,su
m215,sum225,sum235,sum245,sum255,sum265,sum275,sum285,sum295,sum305,sum
315,sum325,sum335,sum345,sum355)"

dicount+=1

dic[dicount]="     dx=data.frame(d,x)"

dicount+=1

dic[dicount]="     total=sum(dx$d)"

dicount+=1

dic[dicount]="     dx$norm=(dx$d/total*30)+100"

dicount+=1

dic[dicount]="     return(dx)"

dicount+=1

dic[dicount]="}"

dicount+=1


### Loop for reading in all csv files in a folder

for files in os.listdir(csvdata):          ## For loop to read in all
the files within the raw data folder - this is used to create specific
lines of code referencing the files

    store,ext=os.path.splitext(files)   ## this removes the extension
information from the file

    dic[dicount]=store+'=read.csv("'+store+'.csv",header=TRUE)'  ##
creating a command to open the file in R under a variable name

    dicount+=1
```

```
dic[dicount]=store+"1="+store+"[order("+store+"$v,"+store+"$h,"+store+"
$s),]"  ## this command sorts the data on lightness then hue then
saturation -- this is important so that the concentric circles can be
made

    dicount+=1

    ##### This next line creates a new data frame from which tile plots
can be made where the first tile is the largest proportion of the
pixels and the last the least

    #dic[dicount]=store+"tile="+store+"[order(-
"+store+"$count,"+store+"$h,"+store+"$s),]"  ## this command sorts the
data on lightness then hue then saturation -- this is important so that
the concentric circles can be made

    #dicount+=1

    #Creating a variable == total number of pixels for scaling y axis
of line graph

    dic[dicount]="total=sum("+store+"$count)"  ## this command sorts
the data on lightness then hue then saturation -- this is important so
that the concentric circles can be made

    dicount+=1

    dic[dicount]="rm("+store+")" ## since the code stores the sorted
dataframe as a new variable, this tells R to remove the original
dataframe

    dicount+=1



    ##### Creating code for an XY bubble chart

    dic[dicount]="ggplot(NULL)+geom_point(data="+store+"1,
aes(x=h,y=s,size=culm,colour=hex))+"  ## This line tells R/ggplot where
to find the data, what values to use for X,Y plotting, to use "culm" as
the size of the bubble, and to use "hex" to infer color (important
though that without the data in the following line hex will not be used
as a color directly but as a category to color by --eg. a hex for a
green color will be read as a category not a green color command)

    dicount+=1


dic[dicount]="scale_size_area(max_size="+bub+")+scale_colour_identity()
+scale_x_continuous(minor_breaks=seq(0,360,30),breaks=seq(0,360,60),lim
its=c(0,360))+scale_y_continuous(limits=c(0,100))+xlab('Hue
(degrees)')+ylab('Saturation
(%)')+theme(panel.background=element_rect(fill='grey95'),panel.grid.maj
or=element_line(color='grey85'),
panel.grid.minor=element_line(color='grey90'),text =
element_text(size=20,colour='grey65'),
```

```
axis.text.x=element_text(angle=45,vjust=0.75),legend.position='none')+c
oord_fixed(ratio="+ratio+")+ggsave(filename='bubble"+store+".png',path=
'"+plotout+"',scale=1)"

    dicount+=1

out=os.path.join(rcode,base1)

with open(out+'.R', 'w') as outfile:

    for key,value in dic.iteritems():

        outfile.write("%s\n" % (str(value)))


print "All done! You can find your files in "+rcode+"!"
```

Figure A4.2 Test images used to verify function of script

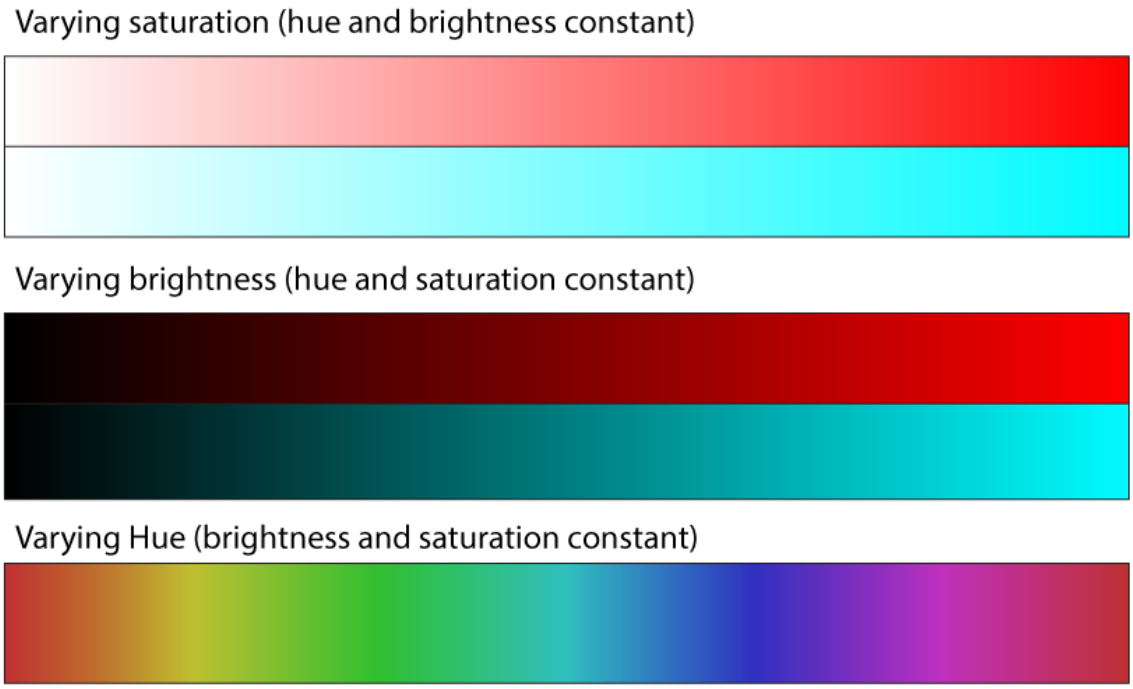

Figure A4.3 Hue and Value held constant with varying saturation

INPUT:

OUTPUT:

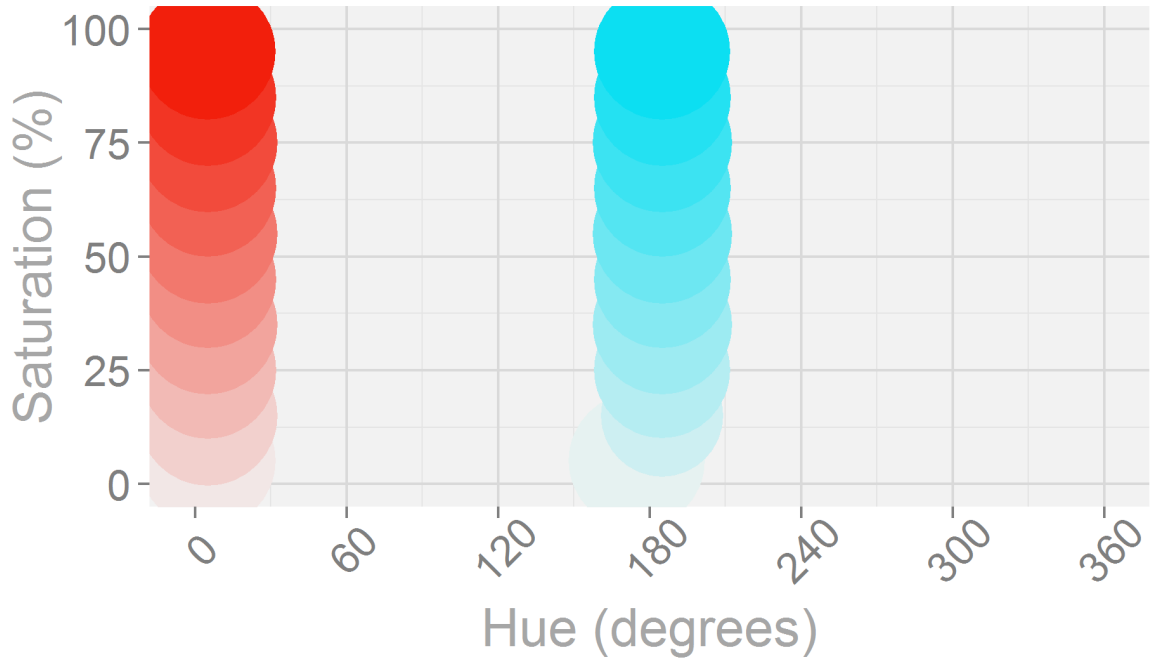

Figure A4.4 Hue and saturation held constant with varying value

INPUT:

OUTPUT:

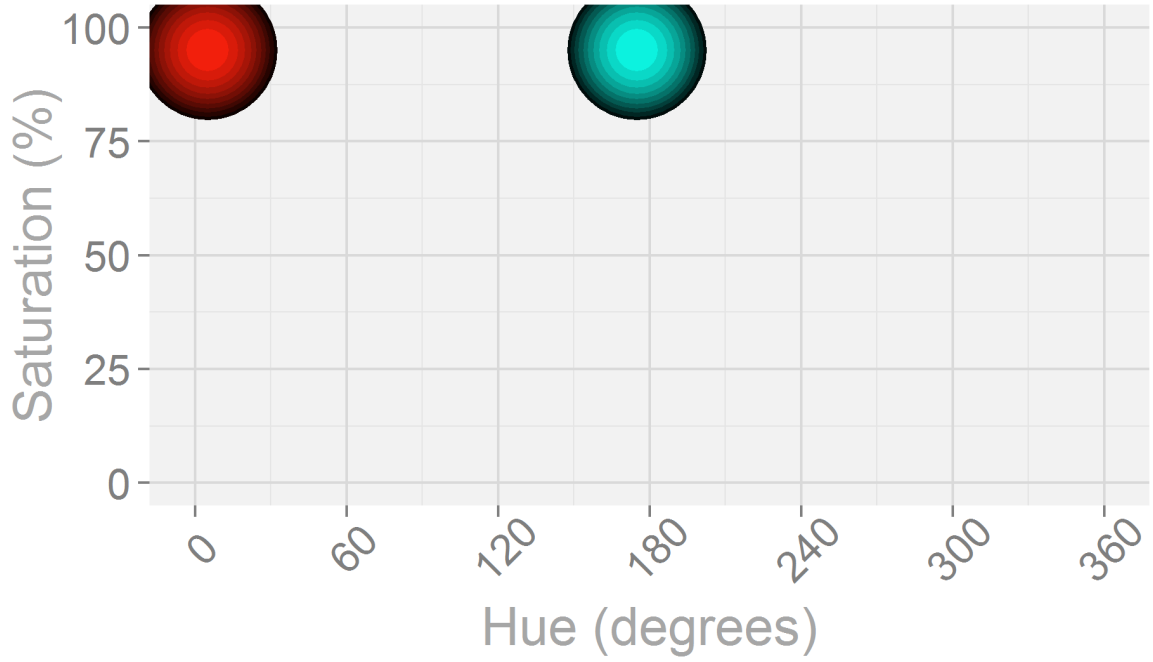

Figure A4.5 Saturation and Value held constant with varying Hue

INPUT:

OUTPUT:

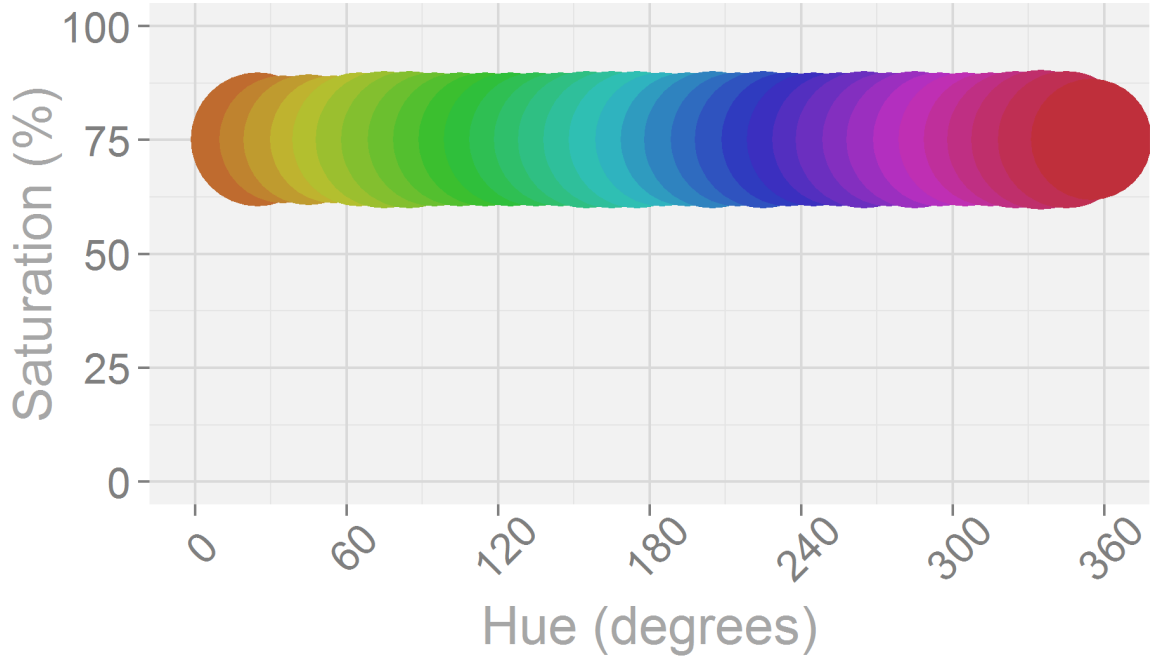

Figure A4.6 Result of script running on a complex input